FINAL REPORT

U.F. Project No: 00117134
FDOT Project No: BDV31-977-30

IMPROVED ANALYSIS TOOL FOR CONCRETE PAVEMENT

Mang Tia
Kukjoo Kim
Sangyoung Han

September 2017

Department of Civil and Coastal Engineering
Engineering School of Sustainable Infrastructure and Environment
College of Engineering
University of Florida
Gainesville, Florida 32611-6580

DISCLAIMER

The opinions, findings, and conclusions expressed in this publication are those of the authors and not necessarily those of the State of Florida Department of Transportation or the U.S. Department of Transportation.

Prepared in cooperation with the State of Florida Department of Transportation and the U.S. Department of Transportation.

SI (MODERN METRIC) CONVERSION FACTORS (from FHWA)

APPROXIMATE CONVERSIONS TO SI UNITS

SYMBOL	WHEN YOU KNOW	MULTIPLY BY	TO FIND	SYMBOL
LENGTH				
in	inches	25.4	millimeters	mm
ft	feet	0.305	meters	m
yd	yards	0.914	meters	m
mi	miles	1.61	kilometers	km

SYMBOL	WHEN YOU KNOW	MULTIPLY BY	TO FIND	SYMBOL
AREA				
in^2	square inches	645.2	square millimeters	mm^2
ft^2	square feet	0.093	square meters	m^2
yd^2	square yard	0.836	square meters	m^2
ac	acres	0.405	hectares	ha
mi^2	square miles	2.59	square kilometers	km^2

SYMBOL	WHEN YOU KNOW	MULTIPLY BY	TO FIND	SYMBOL
VOLUME				
fl oz	fluid ounces	29.57	milliliters	mL
gal	gallons	3.785	liters	L
ft^3	cubic feet	0.028	cubic meters	m^3
yd^3	cubic yards	0.765	cubic meters	m^3
NOTE: volumes greater than 1000 L shall be shown in m^3				

SYMBOL	WHEN YOU KNOW	MULTIPLY BY	TO FIND	SYMBOL
MASS				
oz	ounces	28.35	grams	g
lb	pounds	0.454	kilograms	kg
T	short tons (2000 lb)	0.907	megagrams (or "metric ton")	Mg (or "t")

SYMBOL	WHEN YOU KNOW	MULTIPLY BY	TO FIND	SYMBOL
TEMPERATURE (exact degrees)				
ºF	Fahrenheit	5 (F-32)/9 or (F-32)/1.8	Celsius	ºC

SYMBOL	WHEN YOU KNOW	MULTIPLY BY	TO FIND	SYMBOL
ILLUMINATION				
fc	foot-candles	10.76	lux	lx
fl	foot-Lamberts	3.426	candela/m^2	cd/m^2

SYMBOL	WHEN YOU KNOW	MULTIPLY BY	TO FIND	SYMBOL
FORCE and PRESSURE or STRESS				
lbf	poundforce	4.45	newtons	N
kip	kilo poundforce	4.45	kilo newtons	kN
lbf/in^2	poundforce per square inch	6.89	kilopascals	kPa

APPROXIMATE CONVERSIONS TO SI UNITS

SYMBOL	WHEN YOU KNOW	MULTIPLY BY	TO FIND	SYMBOL
LENGTH				
mm	millimeters	0.039	inches	in
m	meters	3.28	feet	ft
m	meters	1.09	yards	yd
km	kilometers	0.621	miles	mi

SYMBOL	WHEN YOU KNOW	MULTIPLY BY	TO FIND	SYMBOL
AREA				
mm^2	square millimeters	0.0016	square inches	in^2
m^2	square meters	10.764	square feet	ft^2
m^2	square meters	1.195	square yards	yd^2
ha	hectares	2.47	acres	ac
km^2	square kilometers	0.386	square miles	mi^2

SYMBOL	WHEN YOU KNOW	MULTIPLY BY	TO FIND	SYMBOL
VOLUME				
mL	milliliters	0.034	fluid ounces	fl oz
L	liters	0.264	gallons	gal
m^3	cubic meters	35.314	cubic feet	ft^3
m^3	cubic meters	1.307	cubic yards	yd^3

SYMBOL	WHEN YOU KNOW	MULTIPLY BY	TO FIND	SYMBOL
MASS				
g	grams	0.035	ounces	oz
kg	kilograms	2.202	pounds	lb
Mg (or "t")	megagrams (or "metric ton")	1.103	short tons (2000 lb)	T

SYMBOL	WHEN YOU KNOW	MULTIPLY BY	TO FIND	SYMBOL
TEMPERATURE (exact degrees)				
ºC	Celsius	1.8C+32	Fahrenheit	ºF

SYMBOL	WHEN YOU KNOW	MULTIPLY BY	TO FIND	SYMBOL
ILLUMINATION				
lx	lux	0.0929	foot-candles	fc
cd/m^2	candela/m^2	0.2919	foot-Lamberts	fl

SYMBOL	WHEN YOU KNOW	MULTIPLY BY	TO FIND	SYMBOL
FORCE and PRESSURE or STRESS				
N	newtons	0.225	poundforce	lbf
kPa	kilopascals	0.145	poundforce per square inch	lbf/in^2

*SI is the symbol for International System of Units. Appropriate rounding should be made to comply with Section 4 of ASTM E380.
(Revised March 2003)

TECHNICAL REPORT DOCUMENTATION PAGE

1. Report No.	2. Government Accession No.	3. Recipient's Catalog No.

4. Title and Subtitle	5. Report Date
Improved Analysis Tool For Concrete Pavement	August 2017
	6. Performing Organization Code
7. Author(s)	8. Performing Organization Report No.
Mang Tia, Kukjoo Kim, and Sangyoung Han	00117134
9. Performing Organization Name and Address	10. Work Unit No. (TRAIS)
Department of Civil and Coastal Engineering Engineering School of Sustainable Infrastructure & Environment University of Florida 365 Weil Hall – P.O. Box 116580 Gainesville, FL 32611-6580	11. Contract or Grant No. BDV31-977-30
12. Sponsoring Agency Name and Address	13. Type of Report and Period Covered
Florida Department of Transportation 605 Suwannee Street, MS 30 Tallahassee, FL 32399	Final Report 10/15/14 – 9/31/17
	14. Sponsoring Agency Code

15. Supplementary Notes

Prepared in cooperation with the U.S. Department of Transportation and the Federal Highway Administration

16. Abstract

Improved 3-D finite element (FE) models were developed for analysis of (1) precast prestressed concrete pavement (PPCP) with consideration of the effects of longitudinal and transverse prestress forces, (2) jointed plain concrete pavement (JPCP) containing RAP with incorporation of the actual stress-strain characteristics of the concrete, (3) JPCP, which models dowel bars with actual bar dimensions and properties, and (4) continuously reinforced concrete pavement (CRCP), which analyzes the horizontal cracking potential under environmental and traffic loading conditions. Verification of the FE models was accomplished through comparison with measured falling weight deflectometer (FWD) deflection basins and strain data from test slabs. Parametric analyses on the effects of various design parameters on the potential performance of the concrete pavements were also conducted.

A user-friendly interface software which prompts for user inputs and generates an input file for the developed software was developed for use in the analysis of JPCP. User-friendly guides were also developed for input files for analysis of PPCP, JPCP, CRCP, and JPCP with dowel joints.

Various strain sensors were evaluated in the laboratory and also in full-size concrete test slabs subjected to HVS loading. The developed FE models were validated and recommended for use. Fiber optic and electrical resistance strain gauge can be used to measure dynamic strains in concrete slabs. Fiber optic and vibrating wire strain gauge can be used to measure static and long-term strains in concrete slabs. It is recommended that a series of 5 to 7 uniformly spaced strain gauges be placed at and around the wheel path on the test slab in order to be able to capture the location of the applied load and the maximum strain caused by the applied load. The use of the critical stress-analysis and the computed maximum stress-to-strength ratio to assess the potential performance of concrete pavement slabs is recommended.

17. Key Words	18. Distribution Statement
3-D finite-element model; Precast prestressed concrete pavement (PPCP); Concrete containing RAP; Continuously reinforced concrete pavement (CRCP); Fiber optic sensor; Strain gauge.	No restrictions.

19. Security Classif. (of this report)	20. Security Classif. (of this page)	21. No. of Pages	22. Price
Unclassified	Unclassified	541	

Form DOT F 1700.7 (8-72) Reproduction of completed page authorized

ACKNOWLEDGMENTS

The Florida Department of Transportation (FDOT) is gratefully acknowledged for providing the financial support for this study. A compilation of this nature could not have been completed without the help and support of others. The FDOT Materials Office provided the additional testing equipment, materials, and personnel needed for this investigation. Sincere thanks go to the project manager, Mr. James Greene, for providing his technical coordination and advice throughout the project. Sincere gratitude is extended to Messrs. Wayne Allick Jr., Abdenour Nazef, Alex Vuotto, Jacob McDonald, Michael Bergin, and Harvey DeFord of the FDOT Materials Office for their invaluable expert advice and help on this project.

EXECUTIVE SUMMARY

Background and Research Needs

There are many finite-element-based programs which have been developed specifically for analysis of concrete pavement. Examples of such programs include FEACONS, KENSLABS, WESLIQID, J-SLAB, and ISLAB2000. These programs typically model the concrete pavement by 2-D elements. The concrete slabs are modeled by plate elements, and dowel bars are modeled as either bar elements or spring elements. Due to the limitations of 2-D analysis (as compared with 3-D analysis) and the simplified elements used, the behavior of the concrete pavement cannot be accurately modeled. Difficulties in matching analytical falling weight deflectometer (FWD) deflection basins with the measured FWD deflection basins were often encountered especially for composite pavements and at locations near doweled joints and edges of slabs. Since these programs model concrete as a linear elastic material, a ductile concrete such as one made with reclaimed asphalt pavement (RAP) aggregate cannot be accurately modeled without modification of these existing programs.

This study was conducted to address the need to develop improved finite element (FE) models of concrete pavements, especially for precast prestressed concrete pavement (PPCP), concrete pavement containing RAP, and continuously reinforced concrete pavement (CRCP) with the capability of analyzing the horizontal cracking potential under environmental and traffic loading conditions. The developed models permit the analysis of complicated stress states in concrete pavement using RAP concrete, which has a non-linear stress-strain behavior, prestress forces in PPCP, and effects of reinforcement on horizontal cracking.

Another critical need of FDOT is the development of an effective instrumentation plan for the monitoring and evaluation of the US-301 Concrete Test Road which will be started in 2018. A recently completed research project recommended the use of a 'hybrid' instrumentation

plan, which included the use of fiber optic strain gauges coupled with electrical resistance strain gauges and moisture sensors. The 'hybrid' system would minimize issues with long cable lengths and electromagnetic noise through the use of fiber optic strain gauges while supplementing these sensors with less expensive electrical resistance sensors. Further study is needed to determine the most effective configuration for these sensors, the most effective installation procedures to be adopted, and to optimize the gauge length and geometry of the fiber optic sensors.

Scope of Study

Improved finite element models using the commercially available ADINA software package were developed for analyzing concrete pavements. The developed analysis tools include (1) a FE model to properly consider the effects of longitudinal and transverse prestress forces in precast prestressed concrete pavement (PPCP), (2) for analysis of jointed plain concrete pavement (JPCP) containing RAP, a FE model that incorporates the actual stress-strain characteristics of the concrete instead of assuming a linear elastic behavior, (3) a FE model for JPCP which models dowel bars with actual bar dimensions and properties, and (4) an improved analysis model for continuously reinforced concrete pavement (CRCP) to analyze the horizontal cracking potential under environmental and traffic loading conditions. To improve model accuracy, verification of the FE models was accomplished through comparison with measured FWD deflection basins and strain data from test slabs. Using the developed and validated models, parametric analyses of the effects of various design parameters on the potential performance of the concrete pavements were also conducted.

A user-friendly interface software, named AIFG (ADINA Input File Generator), which prompts for user inputs and generate an input file for the developed software was developed for

use in the analysis of JPCP. User-friendly guides were also developed for ADINA input files for analysis of PPCP, JPCP, CRCP, and JPCP with doweled joints.

Various selected strain sensors were evaluated in the laboratory to assess their behavior and performance in concrete cylinders under known static and dynamic strain conditions. Various selected strain sensors were also evaluated in full-size concrete test slabs subjected to HVS loading. The responses of the strain sensors in the concrete test slabs under different loading configurations were studied in order to develop an effective instrumentation and analysis methodology for evaluation of concrete test pavements.

Main Findings

Modeling of PPCP

A 3-D finite element model was developed to analyze the structural response of PPCP under typical Florida conditions. The model was calibrated using the measured FWD deflection data from a PPCP test section in Florida. The model was then used to perform a parametric analysis to determine the effects of a few important pavement parameters on the maximum induced stresses in PPCP. The main findings are summarized as follows:

(1) The maximum computed stress in the concrete slab under critical loading conditions increases significantly as the concrete modulus increases. However, the stress-to-strength ratio decreases due to increase of flexural strength as the concrete modulus increases.

(2) The maximum computed stress in the concrete slab increases as the coefficient of thermal expansion increases.

(3) The PPCP system evaluated appeared to have a good predictive performance with computed stress-to-strength ratio of less than 0.5 up to a loss of 20 % of prestress force in the longitudinal and transverse directions.

(4) The maximum computed stress decreases with an increase of subgrade stiffness. However, the effects of the subgrade stiffness are relatively small as compared with the effects of other parameters.

Modeling of JPCP Using RAP Concrete

A non-linear FE model which incorporated the actual stress-strain behavior of the RAP concrete obtained from the flexural strength test was developed to evaluate the effects of the non-linear stress-strain behavior of the RAP concrete in a JPCP. The analytical results from the FE model incorporating the actual stress-strain behavior of the RAP concrete were compared with the corresponding results from the linear elastic FE model. It was observed that the maximum computed tensile stresses in the concrete using the linear elastic model tend to overestimate the induced stresses at high stress level. Thus, the non-linear model using the actual stress-strain characteristics of the RAP concrete should be used in order to obtain more accurate estimation of stresses in the concrete slabs.

Modeling of Dowel Bars

A 3-D FE model was developed to model the behavior of dowel bars in JPCP by using the actual dimensions and properties of the dowel bars. The developed FE model was validated by matching the measured FWD deflection basins with analytical deflection basins. The main findings are summarized as follow:

(1) The load transfer mechanism across the doweled joint can be modeled well by using the contact sliding surface between the concrete and dowel bars.

(2) For modeling the dowel sleeve and dowel bar, very fine mesh size less than 2/5 in. was required to accurately capture the bearing stresses in the concrete.

(3) The developed 3-D FE model can be used to study the behavior of dowel bars under combined temperature-load conditions as well as the effects of various special dowel bar configurations, including the maximum dowel deflection, the bearing stress on dowel-concrete interface, and shear force transfer.

Modeling of CRCP

A 3-D finite element model was developed to analyze the structural response of CRCP under typical Florida conditions. This model can be used to calculate the maximum vertical

tensile stress in a CRCP. When the vertical tensile stress is excessive, it can cause the formation of horizontal cracking at mid-depth of the CRCP slab. Once this horizontal cracking occurs, the upper thin slab would easily crack under combined temperature and load effects. The developed model was used to perform a parametric analysis to determine the effects of important pavement parameters on the maximum induced vertical tensile stresses for estimating the horizontal cracking potential. The main findings are summarized as follows:

(1) The critical load position is at the corner of a slab formed by transverse cracks when the concrete slab has a positive temperature differential.

(2) The maximum vertical tensile stresses under the critical temperature-load condition are affected little by the coefficient of thermal expansion of the concrete.

(3) The maximum stress-to-strength ratio decreases as the concrete's flexural strength increases.

(4) The maximum vertical tensile stresses decrease as the base modulus increases under the critical temperature-load condition.

(5) The maximum tensile stresses decrease as the base friction increases under the critical temperature-load condition.

(6) Increasing slab thickness reduces the vertical tensile stress at the depth of steel.

(7) The critical vertical stresses decrease slightly when the transverse crack spacing increases.

(8) The vertical tensile stresses are significantly reduced when the steel spacing is reduced. In addition, the vertical tensile stress in the region far away from the tire load is affected little by the longitudinal steel spacing. From this result, the use of varying longitudinal steel spacing (i.e., small steel spacing under wheel path and wide steel spacing for other region) may be one of the ways to reduce the horizontal cracking potential in CRCP.

Laboratory Evaluation of Strain Sensors

An experimental testing program was conducted to evaluate the performance characteristics of fiber optic, vibrating wire, and electrical resistance strain gauges in measuring strains in concrete due to load and drying shrinkage. The different sensors were evaluated in

terms of accuracy, repeatability, and reproducibility. The main findings are summarized as follows:

(1) When compared with the strains measured by a calibrated extensometer in a compression test where the strains varied from 0 to around 450 με, the fiber optic strain sensor (FOS) showed an average error of 2.7 με, as compared with average errors of 5.7 με and 5.6 με for an electrical resistance strain gauge and a vibrating wire strain gauge (VWSG), respectively. However, their differences in error were found to be statistically insignificant at 95% confidence level.

(2) The repeatability of the strain measurements by the FOS in terms of coefficient of variation (COV) was 7.5 % as compared with COVs of 4.4, 5.6, and 9.6% for the three different electrical resistance strain gauges.

(3) The reproducibility of the strain measurements by the FOS in terms of COV was 9.8% as compared with COVs of 5.4, 5.7, and 10.1 % for the three different electrical resistance strain gauges.

(4) When compared with the strains measured by a calibrated linear variable differential transformer (LVDT) in a concrete drying shrinkage test where the strains varied from 0 to around 250 με, the FOS showed an average difference of 30.37 με, while the VWSG showed an average difference of 34.04 με. The difference in strain measurements by the different gauges was statistically insignificant at 95% confidence level.

Field Evaluation of Strain Sensors and Analysis Methodology

Various strain sensors were evaluated in full-size concrete pavement slabs subjected to actual outside environment and realistic wheel loads by a Heavy Vehicle Simulator (HVS). This field testing program was also conducted to assess the validity of the analysis results from the finite element (FE) model for jointed plain concrete pavement which has been developed for this study.

The main findings of the field testing program are as follows:

(1) The developed FE model for JPCP can predict load-induced deflections and strains on the concrete pavement slabs fairly accurately. The results of FWD tests on the concrete slabs can be used to calibrate the FE model parameters for the concrete slabs.

(2) The use of critical stress-analysis and the computed maximum stress-to-strength ratio have been shown to be effective in assessing the potential performance of concrete pavement slabs.

(3) The arrangement of a series of uniformly spaced strain gauges placed at and around the wheel path can be used to capture the location of the applied load and the maximum strains caused by the applied load.

(4) The FOS and the Kyowa electrical resistance strain gauge were observed to record dynamic load-induced strains fairly accurately. The shorter FOS (with gauge length of 4.3 in.) was observed to record more accurate strains in the concrete test slabs than the longer FOS (with gauge length of 9.8 in.).

(5) The total environmental strains measured by the VWSG were observed to be equal to the thermal strain as measured by the fiber optic sensors.

Recommendations

Based on the findings from this study, the following recommendations are made:

(1) The developed 3-D FE model for PPCP is recommended for use in evaluation of structural behavior and performance of PPCP systems under Florida conditions. In the design of PPCP, correct values of concrete properties and design parameters should be employed in an appropriate analytical model rather than the use of the stress equivalency concept or the strength equivalency concept to evaluate the response of the PPCP.

(2) The developed non-linear 3-D FE model incorporating the actual stress-strain characteristics of the concrete is recommended for use for analysis of JPCP using RAP concrete. In the analysis of the concrete pavement containing RAP, an analytical model using the actual stress-strain characteristics, instead of the assumption of the concrete as a linear elastic material, should be employed to calculate the maximum stresses in the concrete.

(3) The developed 3-D FE model which models dowel bars using its actual dimensions is recommended for use. It can be used to study the behavior of dowel bars under combined temperature-load conditions, and the effects of various special dowel bar configurations including the maximum dowel deflection, the bearing stress on dowel-concrete interface, and shear force transfer.

(4) The developed 3-D FE model for CRCP is recommended for use in determining the maximum vertical tensile stresses in CRCP. When the vertical tensile stresses are excessive, horizontal cracking at mid-depth of the slab will occur. The following procedures are recommended for analysis of CRCP to minimize horizontal cracking:

1. Analyze the maximum vertical tensile stress at the depth of the longitudinal steel under critical temperature-load condition.

2. Compare the maximum vertical tensile stress to flexural strength of the concrete used.
3. If maximum tensile stress is greater than 50% of the flexural strength of the concrete, try to reduce it to 50% or less by the following options:

    i) Reduce longitudinal steel spacing
    ii) Increase flexural strength of concrete
    iii) Increase base modulus
    iv) Increase slab thickness

(5) Fiber optic sensor and electrical resistance strain gauge have similar accuracy, can be used to measure dynamic strains in concrete slabs. Fiber optic sensor and vibrating wire strain gauge can be used to measure static and long-term strains in concrete slabs. The use of shorter fiber optic sensor (with gauge length of less than 5 in.) is recommended over the longer ones. A hybrid system with combination of fiber optic sensors, electrical resistance strain gauges, and VWSGs can be used. Fiber optic sensors are to be chosen for consideration of long-term durability, while electrical resistance strain gauge and VWSGs are to be chosen for cost consideration.

(6) It is recommended that a series of 5 to 7 uniformly spaced strain gauges be placed at and around the wheel path on the test slab in order to be able to capture the location of the applied load and the maximum strain caused by the applied load. At each location, one strain gauge is to be placed at 1 inch below the top of the concrete slab and one strain gauge is to be placed at 1 inch above the bottom of the slab.

(7) It is recommended that the critical stress-analysis and the computed maximum stress-to-strength ratio be used to assess the potential performance of concrete pavement slabs. A lower computed stress-to-strength ratio under critical loading condition would mean a better potential pavement performance.

TABLE OF CONTENTS

LIST OF TABLES

LIST OF FIGURES

CHAPTER 1
INTRODUCTION

1.1 Background and Research Needs

There are many finite-element-based programs which have been developed specifically for analysis of concrete pavement. Examples of such programs include FEACONS, KENSLABS, WESLIQID, J-SLAB, and ISLAB2000. These programs typically model the concrete pavement by 2-D elements. The concrete slabs are modeled by plate elements, and dowel bars are modeled as either bar elements or spring elements. Due to the limitations of 2-D analysis (as compared with 3-D analysis) and the simplified elements used, the behavior of the concrete pavement cannot be accurately modeled. Difficulties in matching analytical FWD deflection basins with the measured FWD deflection basins were often encountered especially for composite pavements and at locations near doweled joints and edges of slabs. Since these programs model concrete as a linear elastic material, a ductile concrete such as one made with Reclaimed Asphalt Pavement (RAP) aggregate cannot be accurately modeled without modification of these existing programs.

With the advancement of computational speed and computer memory capacity and the availability of comprehensive finite element programs for structural and thermal analysis (such as ADINA, DIANA and ABAQUS), 3-D modeling of concrete pavement can now be built readily by using the existing comprehensive finite-element programs, and without having to write the computer codes from scratch. Different finite elements can be tried out readily to determine the optimum ones to be used, without having to wait for the writing of the computer codes. Computational time and computer memory are no longer a big issue for running 3-D finite element programs.

Another critical need of FDOT is the development of an effective instrumentation plan for the monitoring and evaluation of the US-301 Concrete Test Road which will be started in 2018. A recently completed research project recommended the use of a 'hybrid' instrumentation plan which included the use of fiber optic strain gauges coupled with electrical resistance strain gauges and moisture sensors. The 'hybrid' system would minimize issues with long cable lengths and electromagnetic noise through the use of fiber optic strain gauges while supplementing these sensors with less expensive electrical resistance sensors. Further study is needed to determine the most effective configuration for these sensors, the most effective installation procedures to be adopted, and to optimize the gauge length and geometry of the fiber optic sensors.

1.2 Objectives of Research

The two main objectives of the research are (1) to develop improved analysis tools for concrete pavements using 3-D finite element modeling, and (2) to develop an effective instrumentation plan for the US-301 Concrete Test Road.

To accomplish the first main objective, an existing comprehensive finite element program ADINA was used to meet the first objective in order to speed up the time for the development of this analysis tool. The envisioned analysis tool was to have the following improvements as compared with the existing analysis tools for concrete pavements:

(1) Capability to model concrete with any stress-strain characteristics, including concrete containing RAP.

(2) Capability to model prestressed or post-tension concrete pavement.

(3) Capability to accurately model continuously reinforced concrete pavement.

(4) Modeling of dowel bars and tie bars with actual bar dimensions and properties.

(5) Capability to model base layers as bonded, unbonded, or partially bonded to the concrete slabs and subjected to any temperature or moisture distributions in the concrete pavement.

A user-friendly interface program, which prompts for user inputs and generate input files for the ADINA program, was developed as part of the work. The developed improved analysis tools will be used to aid the analysis of the experimental data from the US301 Concrete Test Road where various new concrete pavement designs will be evaluated, and the U.S. 92l/SR 600 Volusia County Test Road where precast prestressed concrete pavement (PPCP) system along with other concrete pavement rehabilitation techniques are to be evaluated.

To achieve the second main objective, investigations were made to answer the following questions:

(1) What are the most effective strain sensors to be used for concrete test road?

(2) What are the most effective locations for the sensors to be placed, for environmental responses and for dynamic responses? At what depths should the sensors for strain measurement be located? At what depths and locations within the slab should the thermocouples be placed to adequately measure a non-linear temperature gradient?

(3) What are the most effective procedures for installation of the strain and temperature sensors to be adopted?

(4) How should the collected strain and temperature data be analyzed to assess the behavior and performance of the test slabs?

1.3 Approach and Scope of Research

This research mainly focused on the development of improved analysis tools using finite element models for non-conventional concrete pavements including ductile concrete slabs made with RAP, PPCP, and CRCP. The developed 3-D FE models were calibrated using FWD deflection data and dynamic strains induced by HVS loads and measured by embedded gauges. The developed models were also used to perform parametric analyses to evaluate the effects of concrete properties, slab thickness, modulus of subgrade reaction, and other pavement design parameters on pavement structural behavior.

In addition, in order to develop an effective instrumentation plan, various selected strain sensors were evaluated to assess their performance in concrete cylinders under known static and dynamic strain conditions. Various selected strain sensors were also evaluated in full-size concrete test slabs subjected to HVS loading. The responses of the strain sensors in the concrete test slabs under different loading configurations were studied in order to develop an effective instrumentation and analysis methodology for evaluation of concrete test pavements. The overall research approach is presented in a flow chart in Figure 1, and details for each phase of this research are described in the following sections.

The research work includes the following tasks:

- Literature Review on the Finite Element Method
  - Overview the current state-of-the-art models of concrete pavement systems.
  - Identify what specific modeling strategies are needed.
  - Identify the factors influencing performance of the specific concrete pavements.
- Development of a finite element model for PPCP
  - Incorporate prestressing forces in the longitudinal and transverse directions in the FE model.
  - Calibrate the model using FWD data from test road implemented on SR-600, FL.
  - Evaluate the effects of loading location on the critical stresses.
  - Evaluate the effects of concrete properties on response of PPCP under combined environmental and traffic loading.
  - Quantify the effects of transverse prestressing and longitudinal post-tensioning forces on performance in terms of stress-to-strength ratio.
  - Evaluate the effect of the stiffness of the base material to the performance of the PPCP.
- Development of a finite element model for analysis of JPCP with the following capabilities:
  - Modeling a ductile concrete such as concrete containing RAP.

- Interface bonding conditions (i.e., fully bonding, partially bonding, and unbonding) between the base layer and the concrete slab.

- Modeling dowel bars and tie bars with actual bar dimensions and properties.

- Development of a finite element model for analysis of CRCP

  - Identify the major distress mode and mechanism (horizontal cracking) in CRCP

  - Develop the finite element model to evaluate the horizontal cracking mechanism.

  - Evaluate the design parameters influencing horizontal cracking potential in CRCP under combined environmental and traffic loads.

- Development of a user-friendly interface program, which will prompt for user inputs and generate input file for the ADINA program for the running of the finite element models.

  - Develop the computer program for generating inputs to the ADINA software for analysis of JPCP with/ without RAP concrete.

- Laboratory study on performance characteristics of concrete pavement strain sensors including fiber optic, vibrating wire, and conventional electrical resistance strain gauges.

  - Assess the performance under known static and dynamic strain conditions in terms of accuracy, repeatability, and reproducibility.

  - Evaluate the responses of fiber optic and vibrating wire strain sensor due to concrete drying shrinkage.

- Full-scale field test for evaluating the performance characteristics of concrete pavement strain sensors and developing an effective instrumentation plan for evaluation of concrete test pavements.

  - Evaluate the performance characteristics of the embedded strain sensors in concrete test slabs under Accelerated Pavement Testing (APT) using a Heavy Vehicle Simulator (HVS).

  - Develop an effective instrumentation plan using strain sensors and data analysis methodology for evaluation of concrete test pavements.

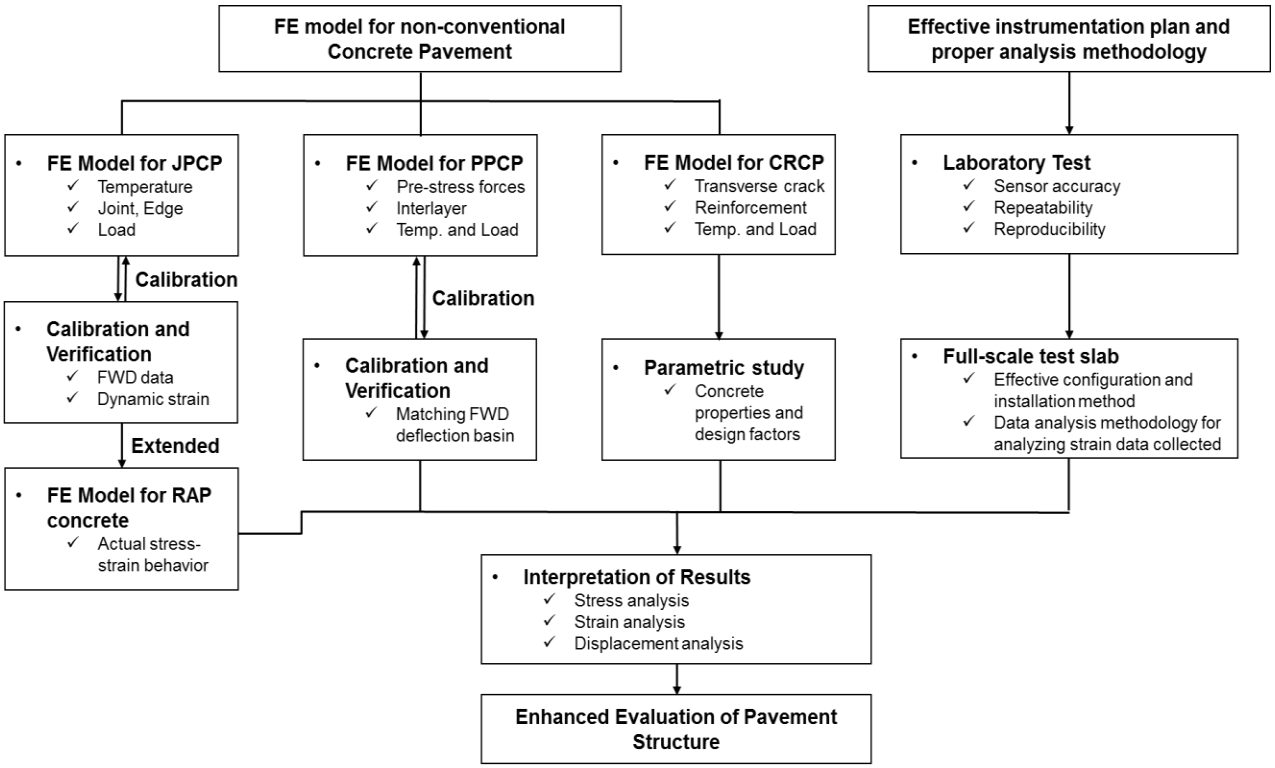

Figure 1-1. Research approach flow chart.

1.4 Outline of Report

Chapter 2 presents a literature review on the finite element modeling for analysis of concrete pavement behavior.

Chapters 3 presents the analysis results on the finite element modeling to determine the effects of critical loading location, concrete material properties, and loss of prestress force on the behavior of precast prestressed concrete pavement (PPCP).

Chapter 4 describes the development of the finite element models for ductile concrete pavement by incorporating actual stress-strain behavior of the RAP concrete and actual dowel bar dimensions. Modeling of dowel bars by using the actual dimension and properties of the dowel bars is also presented.

Chapter 5 presents the analysis results and recommendations to mitigate the horizontal cracking potential in continuously reinforced concrete pavement (CRCP) under critical temperature and load conditions.

Chapter 6 presents the development of computer program for generating inputs to the ADINA software for analysis of jointed plain concrete pavement (JPCP) with capabilities of analysis of RAP concrete and various interface bonding conditions.

Chapter 7 describes the laboratory test results on the performance characteristics of concrete pavement strain sensors including fiber optic, vibrating wire strain, and conventional electrical resistance strain gauges under know strain condition in terms of its accuracy, repeatability, and reproducibility.

Chapter 8 presents the field testing program, where full-size test slabs were instrumented and tested by the HVS, to determine an effective instrumentation plan and analysis methodology for concrete pavement evaluation.

Chapter 9 presents the findings and conclusions from this study, and recommendations for future research.

Users guides for the use of the developed software are presented in the Appendices.

CHAPTER 2
LITERATURE REVIEW ON FINITE ELEMENT MODELING OF CONCRETE PAVEMENT

A concrete pavement system consists of concrete slabs over one or more base layers. The response of a concrete slab under traffic loads is affected by slab size, the presence of different types of discontinuities (e.g., joints, cracks), load transfer mechanisms (e.g., dowel bar, aggregate interlocks), and the possible factors on environment (e.g., temperature curling, moisture warping). These concrete pavement behaviors make the analysis more complicated and challenging. Thus, appropriate levels of simplifications and recognizing the important factors are imperative in analysis of concrete pavements.

Numerous mechanistic response models have been developed with different levels of sophistication over the past decades, ranging from Westergaard's analytical solution, to multi-layer elastic theory, to finite element models. This chapter presents a literature review of the current concrete pavement response models and related research regarding concrete pavement performance analysis.

2.1 Analytical Response Model

Closed-form analytical solutions for calculating stresses and deflections due to thermal curling and traffic loading in rigid pavement had been developed by Westergaard based upon the theory of elasticity (Westergaard 1927). He assumed that the slab acts as a homogeneous, isotropic, elastic solid in equilibrium, and the reaction of the subgrade is only vertical and proportional to the deflection of the slab. The subgrade layer is characterized by the modulus of subgrade reaction or the *k* value, which is a measure of the stiffness of the subgrade in units of force per area per unit deflection or force/length^3. One of the important expression in Westergaard closed-form solution is the radius of relative stiffness, which quantifies the stiffness of the slab relative to that of the subgrade in the following equation:

$$\ell = 4\sqrt{\frac{Eh^3}{12(1-\nu^2)K}} \tag{2-1}$$

where, E= modulus of elasticity of concrete

h= thickness of slab

ν= Poisson's ratio of concrete

Westergaard solved the response of the slab by assuming that of a plate on a bed of springs (Winkler foundation) for the following three cases:

Wheel load close to the corner of a semi-infinite slab.

$$\sigma = \frac{3P}{h^2}\left[1-\left(\frac{\alpha\sqrt{2}}{\ell}\right)^{0.6}\right] \tag{2-2}$$

$$\Delta = \frac{P}{k\ell^2}\left[1.1-0.88\left(\frac{\alpha\sqrt{2}}{\ell}\right)\right] \tag{2-3}$$

where, σ = stress

Δ = deflection

ℓ = radius of relative stiffness

α = contact radius

p = concentrated load

h = thickness of the slab

k = modulus of subgrade reaction

Wheel load at the interior of an infinite slab.

$$\sigma = \frac{3(1+\nu)P}{2\pi h^2}\left(\ln\frac{\ell}{b}+0.6159\right) \tag{2-4}$$

$$\Delta = \frac{P}{8k\ell^2}\left\{1+\frac{1}{2\pi}\left[\ln\left(\frac{a}{2\ell}\right)-0.673\right]\left(\frac{\alpha}{\ell}\right)^2\right\} \quad (2\text{-}5)$$

where, $b = a$, when $a \geq 1.724h$

$b = \sqrt{1.6a^2 + h^2} - 0.675h$, when $a \leq 1.724h$

Wheel load at the edge of a semi-infinite slab.

$$\sigma = \frac{3(1+\nu)P}{\pi(3+\nu)h^2}\left[\ln\left(\frac{Eh^3}{100ka^4}\right)+1.84-\frac{4\nu}{3}+\frac{1-\nu}{2}+\frac{1.18(1+2\nu)a}{\ell}\right] \quad (2\text{-}6)$$

$$\Delta = \frac{\sqrt{2+1.2\nu P}}{\sqrt{Eh^3k}}\left[1-\frac{(0.76+0.4\nu)a}{\ell}\right] \quad (2\text{-}7)$$

Graphical influence charts that greatly simplified the determination of theoretical deflections and moments caused by multiple wheel loadings had been developed (Pickett and Ray 1951), and then extended to sixteen additional influence charts for deflection, moment, and reactive pressure under interior, edge, and center loadings on slab over liquid, elastic solid, and elastic layer subgrades. As a result of influence chart's simplicity, the FAA, U.S. Army, and U.S. Air Force adopted these charts to calculate the maximum tensile stress in concrete pavement systems. In addition, a few computerized versions of the influence chart had been also developed, including the programs H-51, H51-ES, and PDILB (commonly referred to as the PCA AIRPORT program). These programs are based upon Westergaard's theory and subjected to the limitation of its assumptions as follows:

- All pavement layers below the concrete slab must be represented by the modulus of subgrade reaction to give an equivalent response of several layers. However, multi-layer systems cannot be represented by a single parameter due to their complexity, including different stiffness, and bonded or unbonded condition.

- The foundation is linear elastic but most are nonlinear, stress dependent, and change with time and environment.
- The concrete slabs are always in full contact with the subgrade at all points. This assumption is limited to an analysis system where subgrade separation occurs due to curling and warping does not occur.
- The concrete slabs are considered as infinite (for the interior load case) or semi-infinite (for the edge and corner load case). In actual cases, rigid pavements tend to be relatively narrow and have joints.
- Load transfer cannot be considered. Edge stresses are reduced by load transfer achieved by aggregate interlock, mechanical load transfer devices such as dowel bars, or a combination of these.

2.2 Two-Dimensional Finite Element Models

Although closed-form analytical solutions are desirable to get some idea in routine pavement analysis and design, the assumptions of this methodology have resulted in many limitations. To overcome the limitations of analytical solutions, the finite element method has become a powerful numerical analysis technique since the early 1970s. A number of finite element models have been developed for concrete pavement analysis, such as ILLI-SLAB, JSLAB, KENSLABS, WESLIQID, FEACONS, KENLAYER, WESLAYER, and RIGMUL. All of the 2-D models used a 2-D medium-thick plate element and contain features such as mechanics of joint and interface condition between slab and base layer. Each node has three degrees of freedom with translation in the z-direction and rotations of the nodal *x*- and *y*- axes with the following assumptions:

- The plate element is assumed to be an elastic, homogeneous, and isotropic material.
- Transverse loads are carried by flexural force.
- Lines normal to the middle surface in the undeformed plate remain straight, unstretched, and always normal to the middle surface.
- Each lamina parallel to the middle surface is in a state of plane stress, and no axial or in-plane shear stress occurs during loading.

The subgrade model used by 2-D model was the dense liquid or Winkler foundation characterized by the modulus of subgrade reaction (k). This model represents the soil as a series of linear vertical springs with no shear interaction. Since the deflection in any nodal point depends not only on the force in this node but also on the deflection of the neighboring nodes, Winkler foundation has limitation due to its simplicity.

FEACONS (Finite Element Analysis of CONcrete Slab) (Tia et al. 1987) program was developed by the University of Florida to analyze concrete pavements for Florida Department of Transportation (FDOT). This program was modified several times to upgrade its capabilities. The latest version, FEACONS IV program can be used for analysis of jointed plane concrete pavement with the following capabilities: (1) modeling of interface condition between the concrete slab and base layer (bonded or unbonded), (2) modeling of effects of temperature differential between the top and bottom of the slab, (3) modeling of load transfer mechanism at joints using torsional and translational spring elements, (4) modeling of either a single or two layer concrete slab (slab and base or slab and overlay), and (5) modeling of effects of the weight of the slab in the analysis.

ILLI-SLAB programs was developed for the structural analysis of jointed concrete slabs consisting of one or two layers (Tabatabaie and Barenberg 1978). The concrete slab was modeled using a medium-thick elastic element over a Winkler foundation and dowel bars at joints were modeled as discrete bar elements. This program was extended to analyze jointed concrete pavements subjected to moving transient loads, and was renamed as DYNA-SLAB (Chatti et al. 1994).

WESLIQID program was developed by the U.S. Army Engineer Waterways Experimental Station to calculate stresses and deflections in jointed rigid pavements (Chou

1981). The WESLIQID was later extended to the KENSLABS computer program with the capability of modeling multiple slabs and various load transfer mechanisms. The subgrade was idealized as liquid, solid, or layer foundation (Huang 1974; Huang and Deng 1983).

A 2-D finite element program, called JSLAB, was developed. This program is essentially the same as ILLI-SLAB (e.g., medium-thick plate element and Winkler foundation) with a unique capability unlike ILLI-SLAB to consider noncircular load transfer devices (Tayabji and Colley 1986). To specify the noncircular dowels, the cross-section area and moment of inertia of the dowel must be considered as an input parameter.

2.3 Three-Dimensional Finite Element Models

There are two types of 3-D finite element programs available: general-purpose finite element program and finite element codes developed specifically for analysis of pavement systems. These 3-D finite element models can simulate more realistic pavement behaviors, such as a non-uniform load distribution, multi-wheel loads, pavement cracks, and nonlinear dynamic analysis. These finite element models are based on displacement formulations to capture the stresses and strains behavior. In the displacement-based finite elements model, the displacements at the nodes of the elements are calculated first as the primary variable and then the stresses and strains are calculated by numerical differential approximate solutions. However, the application of commercial finite element programs requires expertise in engineering mechanics, and demands a large amount of computation time.

Ioannides and Donnelly (1988) developed a 3-D finite element pavement model using an existing 3-D finite element program called GEOSYS. This study was conducted to provide an essential guide of the effective utilization of the 3-D finite element approach and to eliminate the need for conducting such preliminary and time-consuming studies (Ioannides and Donnelly, 1988). The main findings in this study are summarized as following:

- The subgrade should extend to a depth of about 10 l_e (or about 40 ft) to insure convergence of subgrade defections and strains. Where, l_e is radius of relative stiffness for elastic solid foundation ($l_e = \sqrt[3]{\{(1-\mu_s)D/G_s\}}$), D is slab flexural stiffness ($D = Eh^3/12(1-\mu^2)$), and G_s is shear modulus of elastic solid foundation ($G_s = E_s/2(1+\mu_s)$).

- The lateral subgrade extension beyond the slab edge should be about 7 l_e to 10 l_e (the range of 25 ~ 35 ft) to insure convergence of subgrade deflection.

- Both the horizontal and vertical subgrade boundaries should be on rollers to allow the subgrade elements to distribute loads by deforming.

- The slab should be modeled by two layers of 3-D brick elements. Very little increase in accuracy can be gained by increasing the number of layers in the slab, and linear bending stress distribution within its depth may be assumed.

- For the purpose of subdividing the subgrade into vertical direction, the subgrade may be divided into three regions: an upper, a middle, and a lower portion. The upper portion should be extended to about 1.0 l_e (or 4 ft) and should consist of layers no greater than 0.25 l_e to 0.5 l_e (or 1 to 2 ft). The middle portion, which is typically about 1.0 l_e to 4.0 l_e (4 ~ 15 ft), should be divided into at least two layers of elements. Finally, the lower portion may be divided into one or more layers of elements.

- The lateral extension of the subgrade beyond the slab edge should be divided into two or more elements.

Zaghloul et al. (1994) conducted a nonlinear and dynamic study of rigid pavements using ABAQUS, which is a general purpose, nonlinear, and dynamic finite element software. The subgrade and granular subgrade were modeled by 3-D eight-node brick elements with an elastic-plastic Drucker-Prager constitutive model, while the clay subgrade was modeled with a modified Cam-Clay constitutive model. Mohr-Coulomb friction was imposed between the slab and the subbase as an interface condition. Joints were modeled with gap elements which have an initial opening in the range of 0.9 to 1.9 cm, and dowel bars were modeled by bar elements at the mid-depth of the slab with zero bond stress on one side to allow horizontal movements. A 80-kN single axle load was applied with moving speed at 2.8 km/h. From this parametric study, it was

found that the dowel bars increase the joint efficiency and decrease the maximum vertical deflections. It also found that joint efficiency can be increased with closer dowel bar spacing.

Uddin et al. (1995) studied the effects of pavement discontinuities on surface deflections in a jointed plain concrete pavement using the general-purpose finite element program ABAQUS, when subjected to a standard falling weight deflectometer (FWD) load. The concrete slab, base, and subgrade layer were modeled by 3-D elastic brick elements. Cracks and transverse joints were modeled by gap elements, and dowel bars were modeled with beam elements. Back-calculation of the pavement layer moduli was carried out for an uncracked section, a section with cracked concrete slab, and a section with cracked concrete and cracked cement-treated base layer.

Kuo et al. (1995) developed a three-dimensional finite element model using ABAQUS to overcome many of the inherent limitation of two-dimensional finite element models. They investigated the various factors affecting rigid pavement support including base thickness and stiffness, interface bonding, slab curling and warping, and load transfer at the joints. The effect of loading conditions was also investigated such as interior loading and edge loading cases. The subgrade was modeled using ABAQUS "FOUNDATION" model, equivalent to the dense liquid or Winkler foundation, in which the user simply applies a spring coefficient to the face of an element. The aggregate interlocking was simply modeled by translational and rotational spring elements, while doweled joint was modeled by beam elements. The predicted pavement responses from the model had shown reasonable agreement with ILLI-SLAB results and full-scale field test data from the AASHTO Road Tests, PCA tests on cement-treated base, and the Arlington Road Tests.

Masad et al. (1996) also developed a three-dimensional finite element model using ABAQUS to examine the effects of temperature variation on plain concrete pavements. The slab and subgrade were modeled using eight-node brick elements assumed to be linear elastic materials. The model has the capability to determine the loss of contact between the slab and foundation due to linear and nonlinear temperature differentials. The results from the model were compared with those from existing 2-D finite element models KENSLABS, ILLI-SLAB, and JSLAB. The results of the parametric studies have shown reasonable agreement with other solutions.

EverFE program was developed by Davids et al. (1998) for simulating the response of jointed plain concrete pavement systems under axle loads and environmental effects. The slab and base layer were modeled using 20-node quadratic brick elements, and the sub-base layer was modeled with 8-node planar quadratic elements incorporated with dense liquid foundation below the bottom-most elastic layers. Interface condition between the slab and base was treated as either perfect bond or separation under tension. The modeling of temperature gradients through the depth of slab can be specified as linear, bi-linear, or tri-linear temperature changes with user specified coefficient of thermal expansion. The results from EverFE were compared with the measured values from scaled model tests of doweled rigid pavement in laboratory.

2.4 Summary

Several pavement response models have been developed since the early 1920s. These models can be characterized in two general categories: closed-form analytical solution and finite element models. The analytical solution based on the work of Westergaard are still used widely by field engineers to get insight of structural response under limited loading conditions. The finite element models have ability to model more realistic pavement behaviors. These finite

element programs are also classified into two types of model: (a) finite element code developed specifically for analysis of pavement systems, and (b) general-purpose finite elements programs.

With the development of the high-speed and high-memory computer, it is no longer a big issue applying a variety of problems in pavement analysis and running 3-D finite element programs. Table 2-1 presents an overview of the available finite element programs for analysis of rigid pavements as presented in the literature review.

Table 2-1. Summary of finite element models for rigid pavement analysis.

FE Program	Slab Model	Subgrade Model	Material Model
ILLI-SLAB	2-D medium thick plate	Winkler Boussinesq Nonlinear resilient	Linear elastic
JSLAB	2-D medium thick plate	Winkler	Linear elastic
WESLIQID and KENSLAB	2-D medium thick plate	Winkler	Linear elastic
FEACONS IV	2-D medium thick plate	Winkler (linear and nonlinear springs)	Linear elastic
GEOSYS	3-D brick element	Drucker-Prager	Linear elastic
ABAQUS	3-D brick element	3-D brick element with linear and nonlinear elastic, plastic, Constitutive model	Linear elastic viscoelastic
EverFE	3-D brick element	Winkler	Linear elastic

CHAPTER 3
DEVELOPMENT OF FINITE ELEMENT MODEL FOR ANALYSIS OF PRECAST PRESTRESSED CONCRETE PAVEMENT (PPCP)

3.1 Introduction

3.1.1 Background

The Florida Department of Transportation has implemented an initiative to evaluate precast prestressed concrete pavement (PPCP) as an effort toward minimizing disruption to the traveling public during pavement construction and rehabilitation. The use of PPCP for the replacement of deteriorated highways can give transportation agencies significant advantages in improving pavement performance, decreasing the time before opening to traffic, and minimizing user costs (Merritt et al. 2008; Merritt et al. 2002; Merritt and Tayabji 2009; Ye and Tayabji 2012). The unique feature of the PPCP is in the use of post-tension precast concrete slabs, which are compressed together with longitudinal and transverse post-tensioning of steel strands. Increasing the prestressing force helps the concrete panel to have an increased load carrying capacity like a thicker pavement due to induced compressive stresses in the slab. In addition, there will be voids under precast pavement slabs, and the prestressing forces will provide extra capacity to the panel to compensate for the non-uniformity in the subgrade and to control crack width by providing confinement. Panels can be cast and cured under more ideal condition in which high quality concrete slabs can be manufactured.

Previous research has indicated that the PPCP system provides both improved durability and minimal traffic disruption, and the contractor was satisfied with its constructability (Merritt et al. 2001). Also, well-documented design and construction guidelines have been developed (Tayabji et al. 2013). However, the current lack of understanding of the response of the PPCP under environmental and critical loading conditions is probably the great deficiency in the evaluation of the PPCP system. The response of PPCP under critical loading conditions has not

been well studied due to the complicated stress states caused by prestressing forces and loads. In addition, the main issues associated with the design and construction of this type of pavement system include (1) the effects of concrete properties including elastic modulus and coefficient of thermal expansion which are the most significant factors affecting the maximum stresses (Mallela et al. 2005; Tia et al. 1991), (2) the loss of prestressing due to concrete creep, strand relaxation, and/or strand cutting, and (3) the effect of preexisting pavement as a base layer for the new PPCP pavement system. A better understanding about how the PPCP system behaves under combined action of loads and prestress forces may help in the understanding of some of the existing problems and provide better guidelines for the design and construction of the PPCP system. Therefore, there is a need to develop improved PPCP model to accurately predict the behavior and performance of the PPCP system.

In this study, a three-dimensional (3-D) finite-element (FE) model was developed for analyzing a PPCP system. The 3-D model was used to calculate the response of PPCP under FWD loads and the analytical FWD deflections were compared with the actual measured FWD data. The validated 3-D model was then used to evaluate the effects of various design parameters on the performance of the PPCP.

3.1.2 Objectives

The analysis conducted herein was focused on the structural response of PPCP system under critical loading condition associated with FDOT's PPCP demonstration project. The primary objectives of this task are as follows:

- Evaluate the effects of loading location on the critical stresses in PPCP.
- Evaluate the effects of concrete properties on response of PPCP under combined environmental and traffic loading.
- Quantify the effects of transverse prestressing and longitudinal post-tensioning forces on performance in terms of stress-to-strength ratio.

- Evaluate the effects of the stiffness of the base material on the performance of the PPCP.

3.1.3 Scope

In this task, a 3-D finite element model was developed for stress analysis of PPCP under critical temperature-load conditions. The developed 3-D model was calibrated with measured deflection basins from FWD tests and then used to perform a parametric analysis to determine the effects of loading location, concrete material properties, loss of prestress force, and subgrade stiffness on the response of PPCP under critical temperature-load conditions.

3.2 Experience of the PPCP in Florida

The Florida PPCP pilot project was implemented on SR-600 in Volusia County. The project consisted of 792 ft (241 m) of PPCP designed for 30-year life. The test sections were part of a 6.5 mile (10 km) rehabilitation project completed in June of 2012. Each of the precast units was 24 ft × 12 ft and 9 in. thick (7.3 m × 3.7 m × 23 cm) and a total of 66 (60 interior and 6 end panels) panels were used. The panels were placed atop a 2 to 12 in. (5 to 30 cm) asphalt leveling course and a single-layer polyethylene sheet to reduce friction. Each panel was pretensioned in the transverse direction and post-tension in the longitudinal direction.

The Volusia PPCP test section was constructed over an existing concrete pavement (20-ft (6 m) slabs and untied) originally constructed in the 1940's. The westbound lanes were constructed in the 1940's and the eastbound lanes were added in the 1970's. The paved travel shoulders were constructed in 1997. The existing pavement showed significant distress and received no major rehabilitation except for localized slab replacement. The westbound lanes (MP 9.0 to MP 10.5) were flooded during a significant storm event in 2004 ~ 2005. The test section was located at MP 9.24.

The concrete mix for the slab was designed for a minimum 28-day compressive strength of 5,500 psi (38 MPa) and achieved an average 28-day strength of 10,602 psi (73 MPa). The

pretensioning tendons (in the transverse direction) were designed to be 0.5-in. (1.3 cm) diameter, grade 270 low-relaxation strands conforming to AASHTO 203. Theoretical values for area and modulus of elasticity were 0.153 in^2 (1 cm^2) and 28,500 ksi (197 GPa), respectively. The prestressing strands were assumed to be tensioned to 75% of the ultimate strength of the strand (270 ksi (1.9 GPa)) and a maximum jacking force of 31.0 kips (138 kN) per strand. The post-tensioning tendons are only different in that the diameter is 0.6 in. (1.5 cm) and the area is 0.217 in^2 (1.4 cm^2). The post-tensioning strands (in the longitudinal direction) were designed to be tensioned to 74% of the ultimate strength and a maximum jacking force of 43.4 kips (193 kN) per strand. In this project, the precast panels were pretensioned during fabrication using eight pretension strands which were spaced evenly above and below the post-tensioning ducts to minimize any prestress eccentricity, and twelve post-tension strands were used to provide permanent stress and load transfer between the panels. It must be noted that two tendons were installed in one sheath tube, and so in order to simplify the analysis, the two tendons were treated as one equivalent tendon which were modeled by an assemblage of 3-in. beam elements.

As part of an evaluation of the FDOT PPCP demonstration project, performance monitoring was conducted after it was open to traffic. For this condition survey, a distress map was developed and approximately 3% of panels (2 panels over total 66 panels) had transverse cracks at 3 years after construction. One panel had a 1 in. (2.54 cm) transverse crack and another had a 9 in. (22.86 cm) transverse crack. FDOT also conducted FWD deflection tests every year. Deflections were measured on both the “approach” and “leave” sides of each transverse joint. All of the LTE testing, as analyzed and provided by FDOT, showed very good load transfer, with most measuring greater than 90 percent (Long-Term Pavement Performance Program recommends 60 % as the threshold for load transfer restoration). From the FDOT initial survey,

it can be concluded that PPCP system shows good initial performance and anticipates better long-term performance.

3.3 Finite Element Modeling

3.3.1 FE Modeling of PPCP

The ADINA (version 9.0) finite element program was used to model the PPCP system. The eight-node isoparametric solid brick element was chosen for modeling the concrete slabs. The prestressing tendons were modeled as embedded beam elements specialized by ADINA. Perfect bond between concrete and tendons was assumed. The PPCP implemented on the test section consisted of sixty-six individual panels. However, only twenty-two panels were modeled in this task. Each panel had a dimension of 12 ft (3.7 m) in the longitudinal direction and 24 ft (7.3 m) in the transverse direction with 9 in. (23 cm) thickness. The thickness of the leveling asphalt layer was 2 in. (5 cm). The leveling course was placed over a 9-in (23 cm) existing concrete pavement. The subgrade was modeled as a layer with a thickness of 100 in. (254 cm). It was found that increasing the thickness of the subgrade layer to more than 100 in. (254 cm) had no significant effects on the computed stresses in the concrete slabs. The existing concrete, AC, and subgrade materials were modeled as isotropic and linearly elastic and characterized by their modulus of elasticity and Poisson's ratio. The contraction and expansion of the concrete panel due to temperature effects is also considered, and characterized by its coefficient of thermal expansion.

3.3.2 Modeling of Prestress

The prestress tendons were modeled as beam elements which were 3-in. (7.6 cm) long elements so that the length of the elements in the tendon would be consistent with the position of the nodes in the concrete-slab elements. The post-tension and pretension forces in the concrete in the longitudinal and transverse directions were modeled by the initial strains in the tendons

which were induced by these forces. The contact interface between the tendons and the concrete is assumed to be full bonding and there is no relative bond-slip.

When the initial strain is applied to the tendon elements, the tension stresses in the tendons were transferred as compression stresses in the concrete elements. The initial strain (ε) in the tendon was calculated by using the following equation.

$$\varepsilon = \frac{\sigma}{E} \tag{3.1}$$

Where, σ = prestress in the tendon

E = elastic modulus of the tendon

The modulus of elasticity of the tendons is 28,500 ksi (197 GPa). Therefore, the theoretical strain can be obtained if the applied stress is known. The applied stress in the tendon decided by the designer was 70% to 80% of the ultimate strength, f_{pu} of the steel. Table 3-1 presents the prestress force in each tendon and the applied initial strain used in the FE model.

Table 3-1. Prestress force and applied initial strain in each tendon

Strand	Pretension	Post-tension
Diameter (in)	0.5	0.6
Nominal Area (in^2)	0.153	0.217
Ultimate load (lbf)	41,300	58,600
75% of ultimate load (lbf)	30,950	43,950
$F_{jacking}$ (kip)	31.0	43.4
$\sigma_{jacking}$ (ksi)	202.5	200.0
$\varepsilon_{calculated}$	0.00710	0.00702

3.3.3 Modeling of Concrete-AC Interface

The PPCP slab contact with the AC leveling layer was maintained by applying the concrete self-weight and there was no external constraints. In addition, a polyethylene membrane was used to minimize prestress loss at the concrete panel-AC layer interface, which results in less interface friction. The PPCP panel-AC layer interface friction factor may range from 0.5 to 1.5 (Tayabji et al. 2013), while the AASHTO 93 Guide recommends a range of concrete-base friction of 0.9 to 2.2. In this modeling work, the sliding interface with frictional contact between the concrete panel and the AC layer was assumed ($\mu = 0.68$). The double symmetry of the geometry about x- and y- axes was utilized in the model in order to reduce computation time. The subgrade layer was fixed in the z-direction. Figure 3-1 shows the pavement structure modeled. Figure 3-2 shows the 3-D finite element model developed for the analysis of the PPCP system.

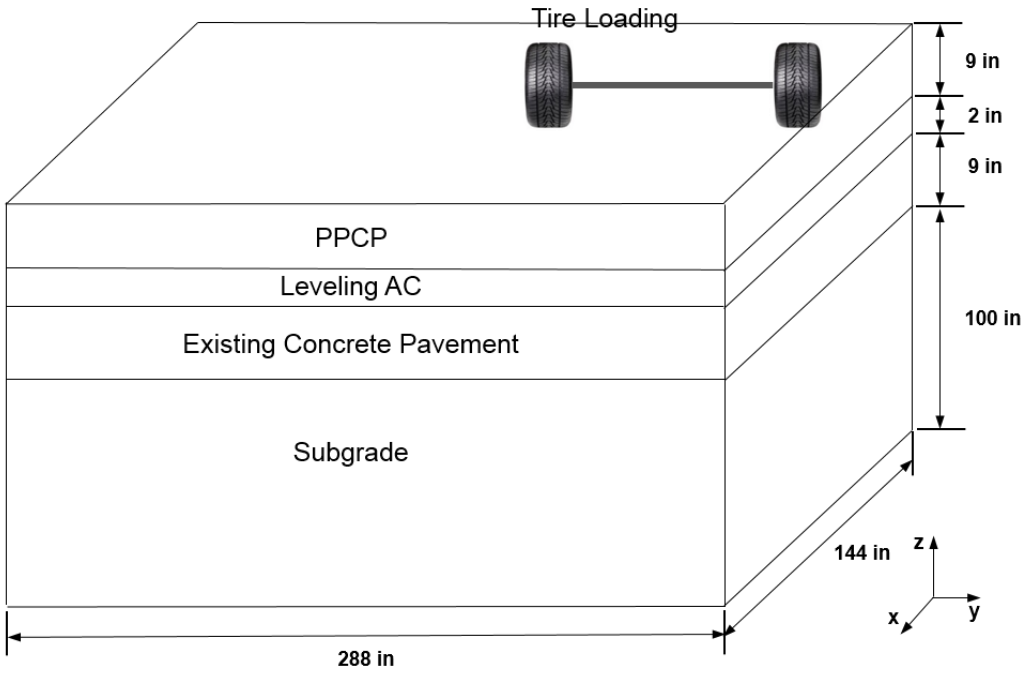

Figure 3-1. Pavement structure modeled

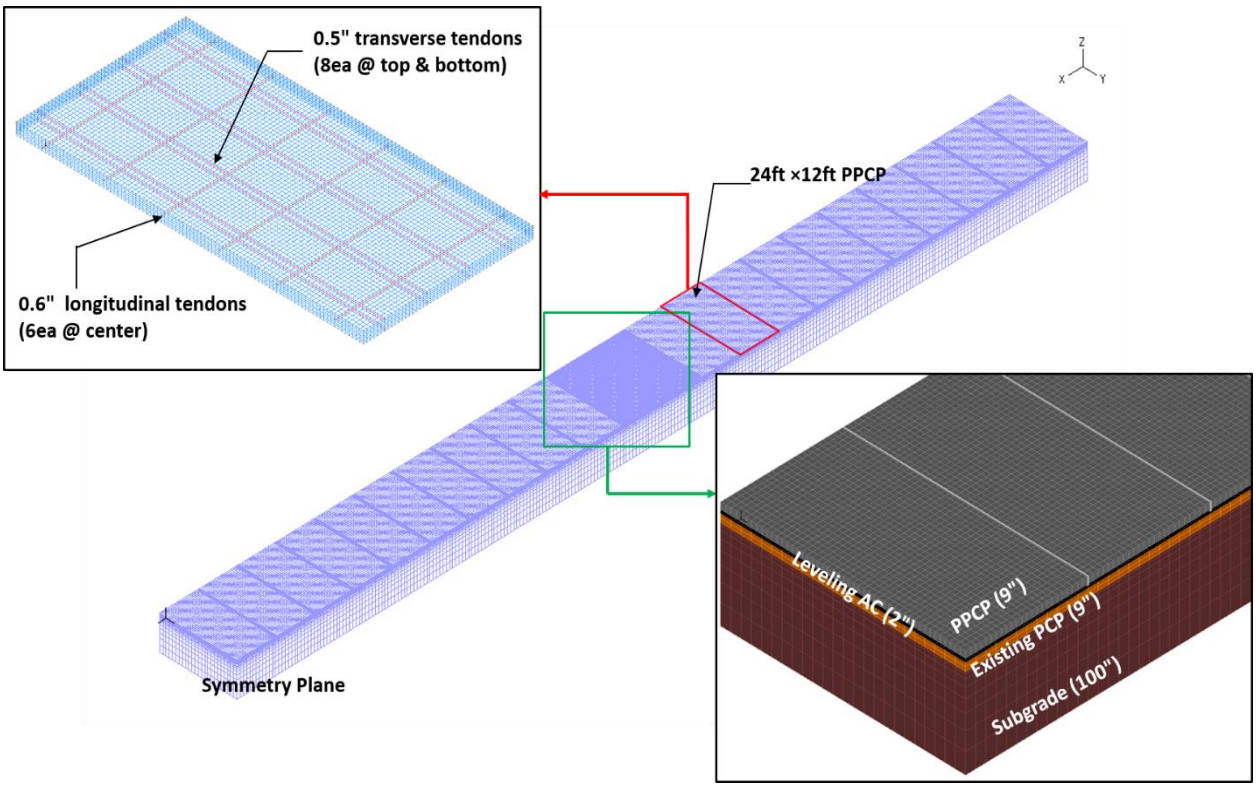

Figure 3-2. Finite element model developed

3.4 Calibration of FE Model and Determination of Model Parameters

In order for the 3-D finite element model to accurately analyze the behavior of PPCP system, it is necessary to have the correct properties of the pavement materials. The elastic moduli of the concrete were initially estimated from the results of laboratory tests in the design phase. The other material properties were adjusted by back-calculation method where analytical deflections were matched to the measured FWD deflections.

FWD tests were performed on the PPCP test section to estimate the elastic moduli of the other pavement materials. Pavement surface deflection basins caused by a 11-kip (49 kN) and 19-kip (85 kN) FWD load were used to estimate the elastic moduli of the pavement layers. FE model predicted deflection basin on the surface of the PPCP slab was compared with the FWD

test results. A twelve inch by twelve inch square loading area was used to model the loading area of the FWD which is a 12-inch (30.5 cm) diameter circular plate.

Figure 3-3 shows an example of matched deflection basin from the back-calculation process for estimating the elastic moduli of the asphalt, existing pavement, and subgrade materials. Using the estimated parameters, an appropriate match between the measured and the calculated deflection basin was achieved with the right properties of the pavement system. Table 3-2 presents material properties used in the FE model.

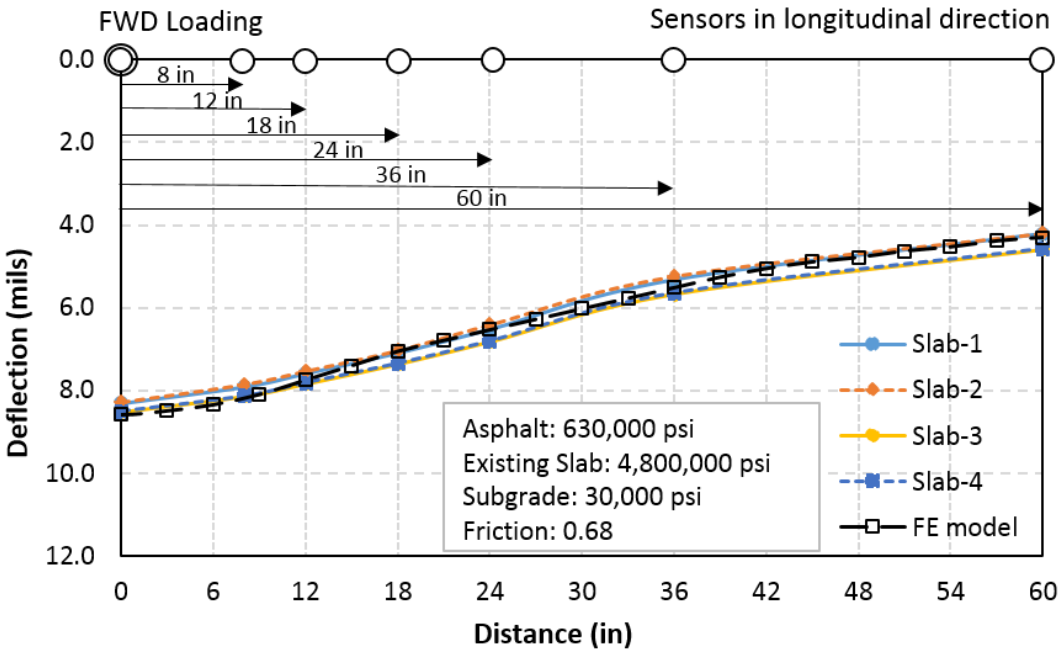

Figure 3-3. Matching of deflection basins in the longitudinal direction caused by a 19-kip (85 kN) FWD load applied to the center of a PPCP lane

Table 3-2. Material properties used in the FE model

Material	Modulus of Elasticity (psi)	Poisson's Ratio	CTE
PPCP	4,300,000	0.20	5.5×10^{-6}°F
AC layer	630,000	0.35	
Existing concrete	4,800,000	0.20	6.0×10^{-6}°F
Subgrade	30,000	0.40	

In order to evaluate the possibility for the concrete to crack at the various conditions, the maximum computed tensile stresses were divided by the flexural strength of concrete to obtain the stress-to-strength ratios. In this study, the flexural strength of concrete was not available, and it was first estimated from the compressive strength of the concrete by following equation (ACI 2002):

$$MR = 7.5 \times f_c^{0.5} \tag{3.2}$$

Where, MR = flexural strength, in psi

f_c = compressive strength, in psi

3.5 Results of Parametric Analysis

3.5.1 Effects of Loading Location on Critical Stresses

The critical loading condition had not been studied for PPCP system previously. Critical stress analysis was performed to determine the maximum tensile stresses in the slabs if they were subject to some critical load and temperature conditions. A 22-kip (98 kN) axle load, which represents the maximum legal load limit for single axle loads in Florida, was used as the applied load in the analysis. Analysis for the following two critical load-temperature conditions was performed: (1) A 22-kip (98 kN) axle load was applied to the mid-edge of the pavement slab with a temperature differential of ±20°F (±11.1°C), (2) A 22-kip (98 kN) axle load was applied to the corner of the pavement slab with a temperature differential of ±20°F (±11.1°C).

To find other possible critical loading conditions, analysis was also performed for the following load-temperature conditions: (1) A 22-kip (98 kN) axle load was applied to the inner middle of the slab with a temperature differential of ±20°F (±11.1°C), (2) A 22-kip (98 kN) axle load was applied to the inner corner of the lane with a temperature differential of ±20°F (±11.1°C), (3) Two 22-kip (98 kN) axle loads were applied to the center of the slab with a

temperature differential of ±20°F (±11.1°C), and (4) Two 22-kip (98 kN) axle loads were applied to the joint of center slab with a temperature differential of ±20°F (±11.1°C), as shown in Figure 3-4.

Table 3-3 shows the maximum computed tensile stresses in the longitudinal and transverse directions. It can be seen that the most critical loading condition was at mid-edge of the slab with +20°F (+11.1°C) temperature differential, which is the same as the critical loading condition for conventional concrete pavements. However, the transverse tensile stress was highest when the axial load was applied at the inner corner of the lane with a temperature differential of +20°F (+11.1°C). It also can be noted that the maximum tensile stresses when two single axles were placed simultaneously at the center of slab or at the joint of center slab were lower than the maximum stresses when one single axle load was placed at mid-edge.

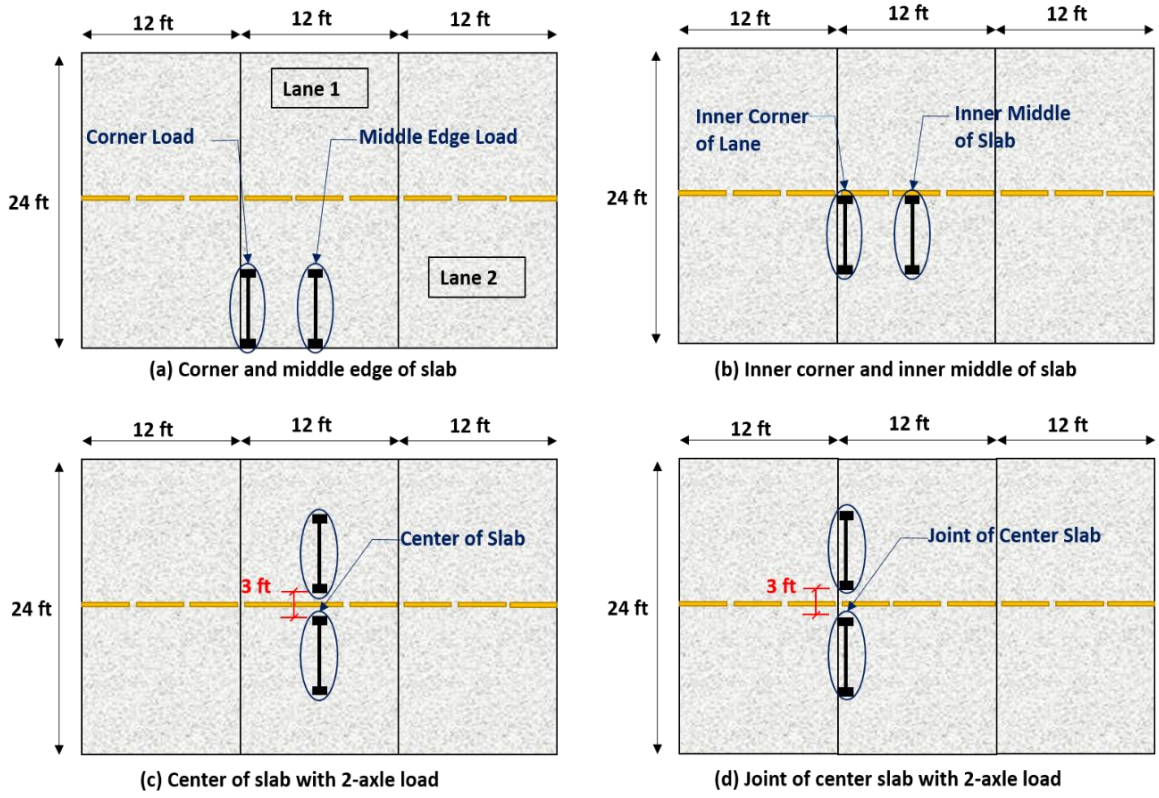

Figure 3-4. Illustration of critical loading conditions at slab corner and middle edge

Table 3-3. Computed maximum stresses in the PPCP system caused by a 22-kip axle load

Possible Critical Loading Conditions	Computed Maximum Tensile Stress (psi)					
	Corner	Middle Edge	Inner Corner	Inner Middle Edge	Inner Corner (2-axle)	Inner M-E (2-axle)
Temperature Differential of +20°F (+11.1°C) Between Top and Bottom						
Max. Longitudinal Stress (σ_{xx})	94.42	340.44	86.30	275.03	47.88	290.26
Max. Transverse Stress (σ_{yy})	132.34	130.76	314.79	154.44	274.40	134.67
Temperature Differential of -20°F (-11.1°C) Between Top and Bottom						
Max. Longitudinal Stress (σ_{xx})	264.95	90.13	168.21	80.45	203.32	49.34
Max. Transverse Stress (σ_{yy})	187.61	34.41	146.41	29.97	149.21	32.90

3.5.2 Effects of Concrete Modulus

The effects of elastic modulus of concrete on the maximum induced stresses were analyzed. The maximum longitudinal stresses in the slab caused by a 22-kip (98 kN) single axle load at the mid-edge with temperature differential of +20°F (+11.1°C) were computed. Figure 3-5 shows the maximum tensile stresses as a function of elastic modulus of concrete. It can be seen that the calculated maximum stress increases by around 40% when the elastic modulus increased from 3,800 to 6,000 ksi (26 to 41 GPa).

However, an increase in elastic modulus of the concrete is usually related to an increase in its flexural strength when the same aggregate is used. The flexural strength of the concrete can be related to its elastic modulus and unit weight by the following equation (ACI 2002):

$$MR = \frac{0.227E}{w^{1.5}} \tag{3.3}$$

Where, E = elastic modulus, in psi

MR = flexural strength, in psi

w = unit weight, in pcf

Using this equation and a unit weight of 140 pcf (2,243 kg/m^3), the concrete flexural strengths at various values of elastic modulus were calculated, and the stress-to-strength ratios were also plotted against the concrete elastic modulus in Figure 3-5. It can be noted that the maximum stress-to-strength ratio decreases as the concrete modulus increases.

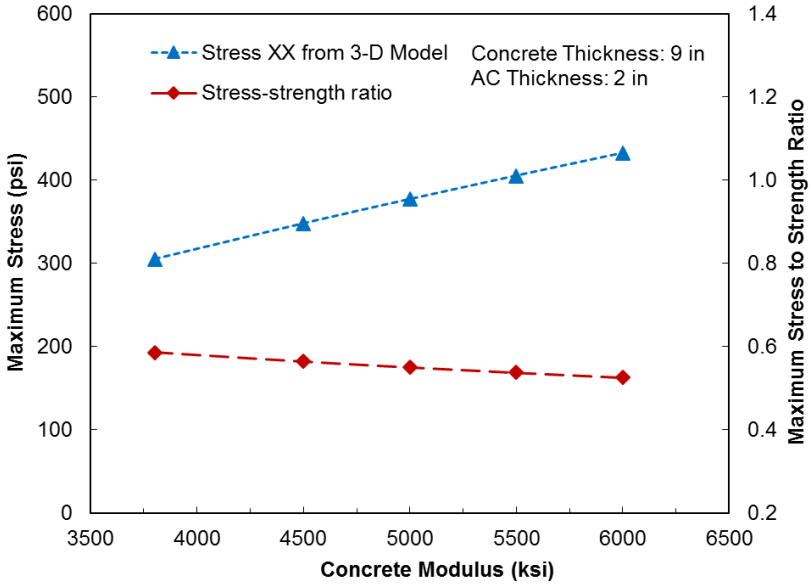

Figure 3-5. Effects of concrete modulus on maximum stress and stress ratio in PPCP

3.5.3 Effects of Coefficient of Thermal Expansion

The effect of the coefficient of thermal expansion of the pavement concrete ranging from 4.0 to 6.0 $\times 10^{-6}$°F (7.2 to 10.8 $\times 10^{-6}$°C) on the maximum induced stresses were analyzed. Using the different values of the coefficient of thermal expansion, the maximum stresses in PPCP under the critical loading conditions were calculated and presented in Figure 3-6. The calculated maximum tensile stresses increase by approximately 40% when the coefficient of thermal expansion increases from 4.0×10^{-6} to 6.5×10^{-6}°F (7.2 to 11.7 $\times 10^{-6}$°C).

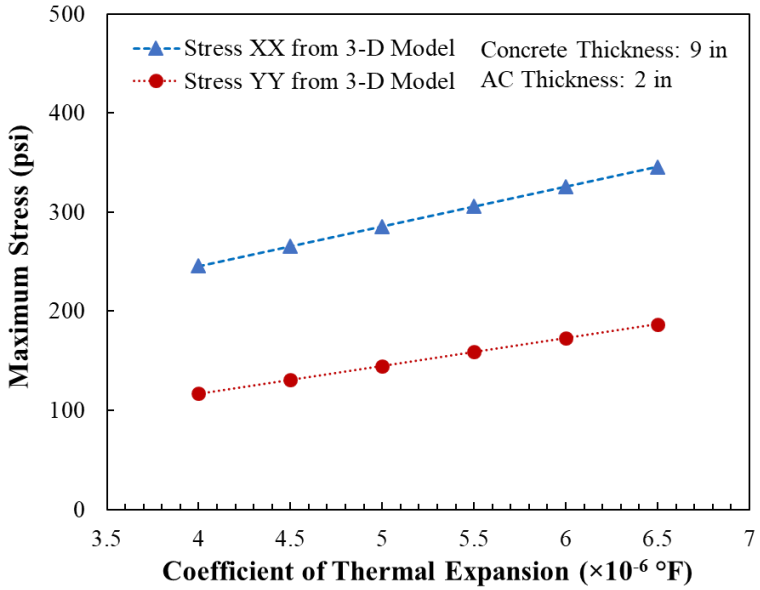

Figure 3-6. Effects of coefficient of thermal expansion on maximum stresses in PPCP

3.5.4 Effects of Prestress Force on Critical Stresses

The 3-D finite element model was also used to evaluate the effects of loss of transverse and longitudinal prestress force in terms of stress-to-strength ratio under critical loading conditions. In doing these computations, the flexural strength was calculated by equation (2), as presented earlier, and was equal to 772 psi (5.3 MPa) for this analysis. For long-term service life, approximately 40 % to 50 % losses of the applied prestress force were expected for a well-constructed PPCP (Tayabji et al. 2013). The maximum computed stresses in the concrete slabs were computed using the following two critical loading conditions, namely (1) a 22-kip (98 kN) axle load applied to the mid-edge of the slab with a temperature differential of +20°F (+11.1°C), which represents a typical severe condition in the daytime, and (2) a 22-kip (98 kN) axle load applied to the corner of the slab with a temperature differential of -20°F (-11.1°C), which represents a typical severe condition at night. Tables 3-4 and 3-5 present the maximum stresses and stress-strength ratio as a function of prestress force level. The maximum computed stresses

were divided by the flexural strength of the concrete panel to obtain the stress-to-strength ratios. According to fatigue theory (PCA 1984), the number of load repetitions to failure of concrete increases as the stress-to-strength ratio decreases. Thus, a lower computed stress-to-strength ratio would indicate a higher allowable number of load repetitions to failure and a better expected performance in service. When the stress-to-strength ratio is less than 0.5, the concrete is expected to be able to withstand an infinite number of stress cycles without fatigue failure (PCA 1984). The analysis results indicate that the maximum stresses increase as prestress force decrease. It shows the benefits of prestress force in PPCP. It can also be seen that the PPCP system evaluated appeared to have a good predicted pavement performance up to a loss of 20% of prestress force in the longitudinal and transverse directions with stress-strength ratio of less than 0.5.

Table 3-4. Effects of prestress on maximum stresses at +20°F temperature differential

Parameters	Prestress Force (kip)		Computed Stress (psi)		Stress Ratio	
	$F_{longitudinal}$	$F_{transverse}$	σ_{xx}	σ_{yy}	σ_{xx}/MR	σ_{yy}/MR
Transverse Pretension + Longitudinal Post-tension	43.4	31.0	340.44	314.79	0.44	0.41
	34.7	24.8	372.29	349.97	0.48	0.45
	26.0	18.6	404.15	385.16	0.52	0.50
	17.4	12.4	436.01	420.35	0.56	0.54
	8.7	6.2	467.86	455.54	0.61	0.59
	0	0	499.72	490.73	0.65	0.64
Transverse Pretension	43.4	24.8	347.67	363.40	0.45	0.47
	43.4	18.6	354.91	412.01	0.46	0.53
	43.4	12.4	362.14	460.62	0.47	0.60
	43.4	6.2	368.05	509.23	0.48	0.66
	43.4	0	376.61	557.83	0.49	0.72
Longitudinal Post-tension	34.7	31.0	365.06	301.36	0.47	0.39
	26.0	31.0	389.68	287.94	0.50	0.37
	17.4	31.0	414.30	274.52	0.54	0.36
	8.7	31.0	438.92	261.10	0.57	0.34
	0	31.0	463.54	247.68	0.60	0.32

Table 3-5. Effects of prestress on maximum stresses at -20°F temperature differential

Parameters	Prestress Force (kip)		Computed Stress (psi)		Stress Ratio	
	$F_{longitudinal}$	$F_{transverse}$	σ_{xx}	σ_{yy}	σ_{xx}/MR	σ_{yy}/MR
Transverse Pretension + Longitudinal Post-tension	43.4	31.0	264.95	187.61	0.34	0.24
	34.7	24.8	280.69	221.42	0.36	0.29
	26.0	18.6	301.04	256.01	0.39	0.33
	17.4	12.4	321.36	290.60	0.42	0.38
	8.7	6.2	341.71	325.19	0.44	0.42
	0	0	362.06	359.78	0.47	0.47
Transverse Pretension	43.4	24.8	260.14	231.78	0.34	0.30
	43.4	18.6	259.93	276.73	0.34	0.36
	43.4	12.4	259.72	321.68	0.34	0.42
	43.4	6.2	259.51	366.63	0.34	0.47
	43.4	0	259.30	411.59	0.34	0.53
Longitudinal Post-tension	34.7	31.0	280.90	176.47	0.36	0.23
	26.0	31.0	301.46	166.11	0.39	0.22
	17.4	31.0	322.00	155.75	0.42	0.20
	8.7	31.0	342.56	145.39	0.44	0.19
	0	31.0	363.12	135.03	0.47	0.17

3.5.5 Effects of Subgrade Stiffness

The effects of subgrade stiffness on maximum tensile stresses in PPCP were analyzed. The maximum computed stresses in the PPCP slabs were computed using the following two critical loading conditions, namely (1) a 22-kip (98 kN) axle load applied to the mid-edge of the slab with a temperature differential of +20°F (+11.1°C), and (2) a 22-kip (98 kN) axle load applied to the corner of the slab with a temperature differential of -20°F (-11.1°C). Also, the Winkler foundation was used in the FE model to study the effects of subgrade stiffness on maximum induced stresses. The subgrade stiffness was varied from 3.58 ksi/ft to 13.2 ksi/ft (81 MPa/m to 299 MPa/m).

Figures 3-7 and 8 show the plots of maximum tensile stresses in concrete as a function of subgrade stiffness. It is to be pointed out that the maximum stress decreases as the subgrade

stiffness increases. It can be explained by the fact that the PPCP system used in FE analysis has longer transverse dimension which may cause the settlement of mid-portion of slab and provide more uniform support. This agrees with previous findings that maximum stress decreases as subgrade modulus increases for a larger-dimension slab (Wu et al. 1993). Conversely, for concrete pavements of conventional size (12 ft × 15 ft (3.7 m × 4.6 m)) in Florida, the maximum tensile stress increases as the subgrade stiffness increases because the supporting area of the slab with the temperature differential varies depending on the stiffness of base layer. A higher subgrade stiffness may result in smaller supporting area and higher tensile stress, while a softer base may offer more uniform slab support than a rigid base resulting in lower tensile stress in the concrete slab.

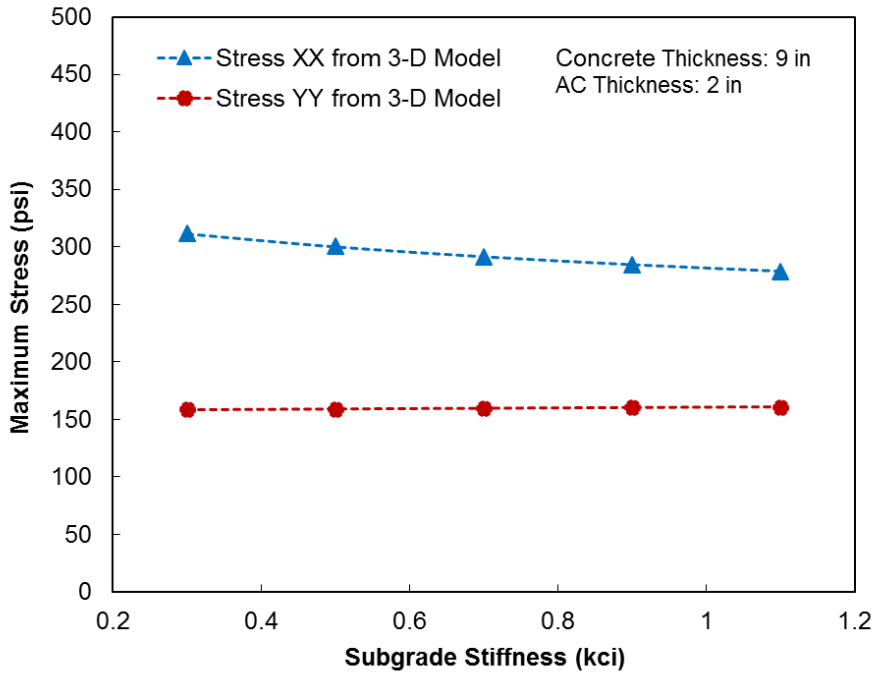

Figure 3-7. Effect of subgrade stiffness on critical stresses at +20°F temperature gradient

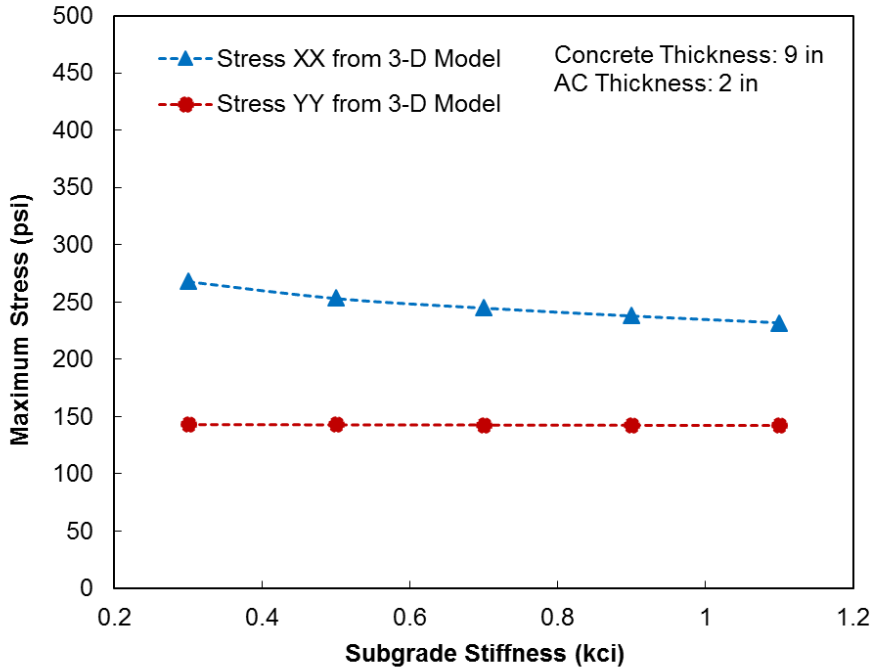

Figure 3-8. Effect of subgrade stiffness on critical stresses at -20°F temperature gradient

3.6 Summary of Findings

A 3-D finite elements model was developed to study the structural response of PPCP under typical Florida conditions. The model was calibrated using the measured FWD deflection data from a PPCP test section in Florida. The model was then used to perform a parametric analysis to determine the effects of a few important pavement parameters on the maximum induced stresses in PPCP. The main findings are summarized as follows:

- The critical loading condition was at the mid-edge of the slab with +20°F (+11.1°C) temperature differential for the longitudinal tensile stress. However, for the transverse tensile stress, the maximum tensile stress was highest when the load was applied at the inner corner of the lane with a temperature differential of +20°F (+11.1°C).

- Results from the parametric analysis indicated that the maximum stress in the concrete slab increases significantly as the concrete modulus increases. However, the stress-to-strength ratio decreases due to increase of flexural strength as the concrete modulus increases.

- The maximum stress in the concrete slab increases as the coefficient of thermal expansion increases.

- Based on the fact that a lower stress-to-strength ratio was related to better observed pavement performance, the PPCP system evaluated appeared to have a good predicted performance with computed stress-to-strength ratio of less than 0.5 up to a loss of 20 % of prestress force in the longitudinal and transverse directions.

- The maximum stress decreases with an increase of subgrade stiffness. However, the effects of the subgrade stiffness are relatively small as compared with the effects of other parameters.

The results of the parametric analysis show the significant effects of various concrete properties and design parameters on the behavior and performance of PPCP system under Florida conditions. Thus, in the design of the PPCP, the correct values of concrete properties and design parameters should be employed in an appropriate analytical model to evaluate the response of the PPCP. The 3-D FE model presented in this report can be used to evaluate structural behavior and performance of PPCP systems under Florida conditions.

CHAPTER 4
DEVELOPMENT OF SOFTWARE FOR ANALYSIS OF JOINTED PLAIN CONCRETE PAVEMENT (JPCP)

4.1 Introduction

4.1.1 Background

There are many finite-element-based programs which have been developed specifically for analysis of concrete pavement. Examples of such programs include FEACONS, KENSLABS, WESLIQID, J-SLAB, and ISLAB2000. These programs typically model the concrete pavement by 2-D elements. The concrete slabs are modeled by plate elements and dowel bars are modeled as either bar elements or spring elements. Due to the limitations of 2-D analysis (as compared with 3-D analysis) and the simplified elements used, the behavior of the concrete pavement cannot be accurately modeled. Difficulties in matching analytical strain and FWD deflection basins with the measured strain and FWD deflection basins were often encountered especially at locations near the joints and edges of slabs. Since these programs model concrete as a linear elastic material, a ductile concrete such as one made with Reclaimed Asphalt Pavement (RAP) aggregate cannot be accurately modeled without modification of these existing programs.

With the advancement of computational speed and computer memory capacity, and the availability of comprehensive finite element programs for structural and thermal analysis (such as ADINA, DIANA and ABAQUS), 3-D modeling of concrete pavement can now be built readily (by using the existing comprehensive finite-element programs, and without having to write the computer codes from scratch). Different finite elements can be tried out readily to determine the optimum ones to be used, without having to wait for the writing of the computer codes. Computational time and computer memory are no longer a big issue for running 3-D finite element programs.

4.1.2 Objectives and Scope

The main objective of this task of the research project was to develop a 3-D finite element model for analysis of jointed plain concrete pavement (JPCP) with improved capability of modeling the actual stress-strain characteristics of a ductile concrete such as concrete containing RAP, and modeling dowel bars with actual bar dimensions and properties. This report presents the development of the 3-D finite element model for JPCP with the aforementioned capabilities using the ADINA software.

4.2 Modeling of JPCP Using ADINA

4.2.1 Concrete Slab

Most of the existing FE models for analysis of concrete pavement consider the concrete slab as a linear elastic material. This elastic analysis requires the inputs of concrete properties including (1) modulus of elasticity, (2) Poisson's ratio, (3) density, and (4) coefficient of thermal expansion. However, more recently, the used of Reclaimed Asphalt Pavement (RAP) materials in Portland cement concrete (PCC) pavement has been shown to be feasible. This RAP concrete has a more non-linear stress-strain behavior and fails at a higher strain level (Al-Oraimi et al. 2009; Hassan et al. 2000; Huang et al. 2006; Huang et al. 2005; Tia et al. 2012; Tia et al. 2009). For more realistic and effective modeling of the RAP concrete behavior, the actual stress-strain characteristics of the concrete needs to be incorporated in the FE model.

The concrete slab was modeled by an assemblage of hexahedron elements defined by 8, 20, 21, or 27 nodes to capture the full three-dimensional stress, strain, and displacement of the concrete under combined load-temperature effects. Figure 4-1 shows the available element types which can be used. These elements have different integration points and number of nodes. In this study, the eight-node brick element was used. To choose the adequate mesh size and

element types, convergence studies were conducted, and it was found that using an element size of less than 3 inches was needed in order to capture the concrete responses accurately.

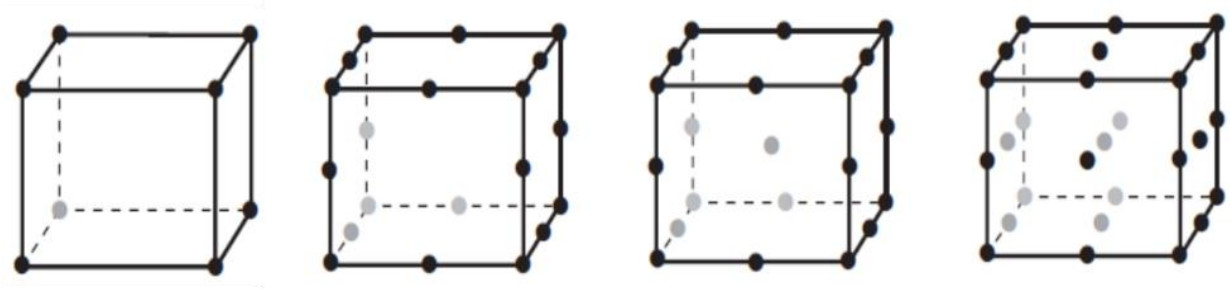

Figure 4-1. 8-, 20-, 21- & 27-node elements

4.2.2 Subgrade Layer

Subgrade layer is the foundation which provides the support under the concrete slab. In FE modeling using ADINA software, various subgrade models including Winkler or dense liquid, elastic solid, and Drucker-Prager model are available in its material library. The Winker or dense liquid foundation is the simplest model for an idealized soil behavior using a series of independent vertical springs characterized by the modulus of subgrade reaction (k). This model has no shear interaction as shown in Figure 4-2. Since the deflection in any nodal point depends not only on the force in this node but also on the deflection of the neighboring nodes, the Winkler foundation, where deflection is dependent only on the applied load at the node, can be seen to have limitation due to its simplicity.

The elastic solid foundation (base, subbase and subgrade) can be modeled as isotropic and linearly elastic, and is characterized by their elastic modulus, and Poisson's ratio. The elastic solid foundation can capture the more realistic response under applied loads.

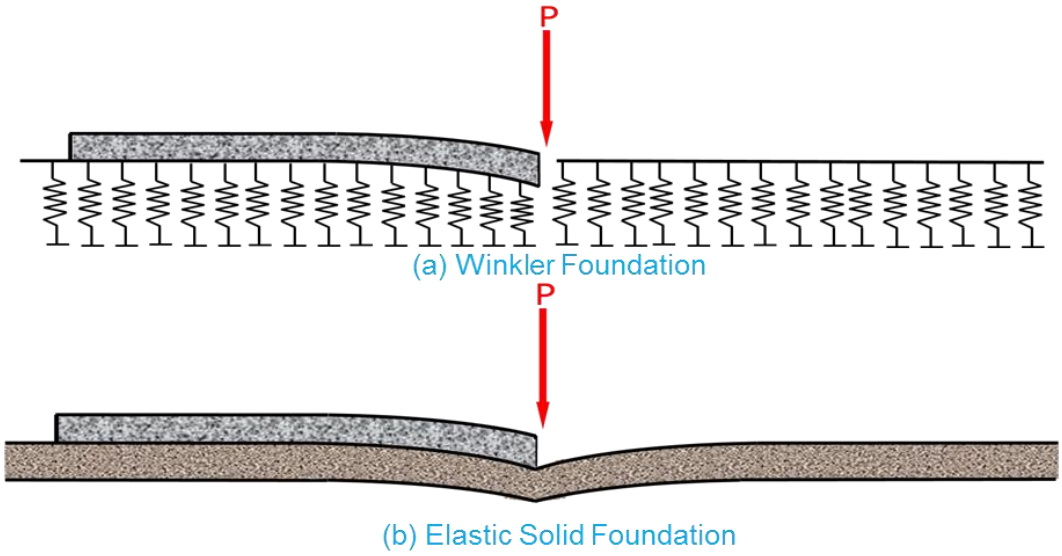

Figure 4-2. Foundation displacement under an applied load

4.2.3 Transverse and Longitudinal Joints

Many studies have been conducted to model the load transfer mechanism of dowel bars at the joints. In previous models, dowel bars were modeled by linear elastic spring elements, torsional spring elements, or a combination of these (Huang and Wang 1973; Tia et al. 1987). This is illustrated in Figure 4-3.

In a study conducted by Channakeshava et al. (1993), dowel bars were modeled as beam elements and connected to the concrete elements with springs to represent the interaction between the concrete and the dowel bars. In a similar approach (Dere et al. 2006), the dowel bars were modeled as beam elements and connected to the concrete elements nodes by two linear spring elements in horizontal and vertical directions. A new approach was presented by William and Shoukry (2001) by modeling dowel bars as eight-node solid brick elements with frictional surface between the dowel bar and the surrounding concrete. However, this model requires very

fine mesh for the dowel bar and the surrounding concrete in order to properly simulate the mechanism of interaction between the dowel bars and the concrete.

In this study, two approaches were selected to simulate the load transfer mechanism: (a) aggregate interlocking modeled by linear elastic spring with 3 degree of freedom, and (b) 3-D solid element with actual bar dimensions and properties for dowelled joint. In the actual dowel bar model, the dowel bars were modeled using a fine mesh in order to account for the mechanism of dowel contact and the associated states of stresses. The sliding interface between each dowel and the surrounding concrete was also modeled using a frictional contact surface. Figure 4-4 shows the modeling of dowel bars at a joint in the 3-D model developed.

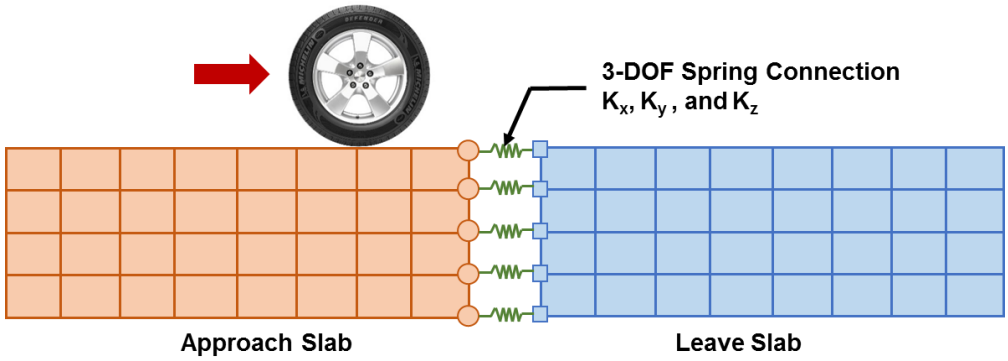

Figure 4-3. Modeling of joint by linear springs

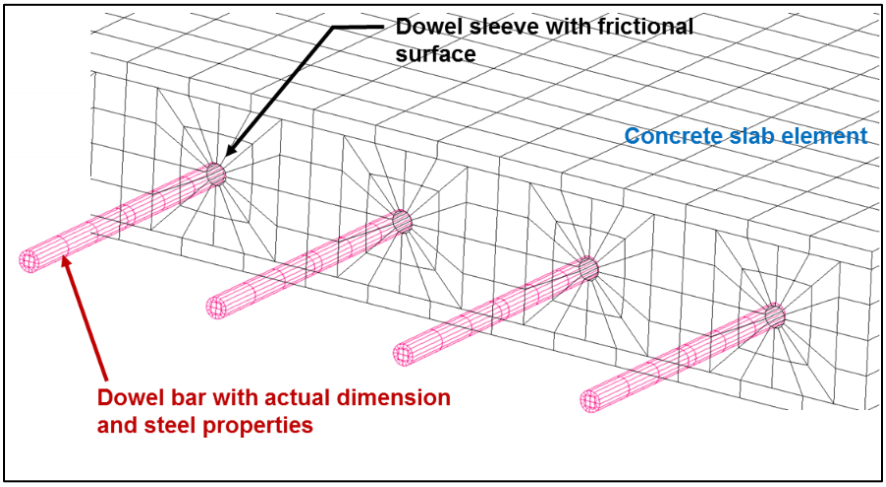

Figure 4-4. Modeling of dowel bar with actual dimension and steel properties

4.2.4 Interface between Concrete Slab and Base

The slab-base layer interface can have three different conditions, namely fully bonded, partially bonded, and unbonded. In the case of the fully bonded condition, the concrete slab and base layer are fully bonded and have the same deflection profiles under temperature-load effects. To model this condition, the adjacent nodes between the concrete and base layer are rigidly connected to each other.

In the case of unbonded interface condition, the concrete slab may be separated from the base layer due to curling movement of the concrete slab and acts like a separated layer under the combined effects of load and temperature. Therefore, there cannot be any tensile load transfer across the interface, but there can still be transfer of compressive load across the interface. This unbonded interface is modeled by a special spring which has an infinite stiffness value when the spring is in compression; however, when the spring is in tension, the stiffness value is zero (Tia et al. 1987). Another method for simulation of unbonded layer is the use of contact and target elements (William and Shoukry 2001).

For the partially bonded interface condition, translational spring elements are used to connect the bottom of the concrete layer with the top of the base layer at the nodes, with zero distance between the two layers. Three spring constants which represent stiffness along the three different directions are used to model the partially bonded condition. K_x and K_y represent the stiffness in the interface plane (x- and y-directions), while K_z represents stiffness perpendicular to that plane (z-direction).

In this study, a combined approach using the contact surface element and spring element method is used and is shown in Figure 4-5. Three different interface conditions can be simulated by adjusting the magnitude of coefficient of friction and spring stiffness in the same model. For

instance, the unbonded interface condition can be simulated by using a zero spring stiffness in the z-direction.

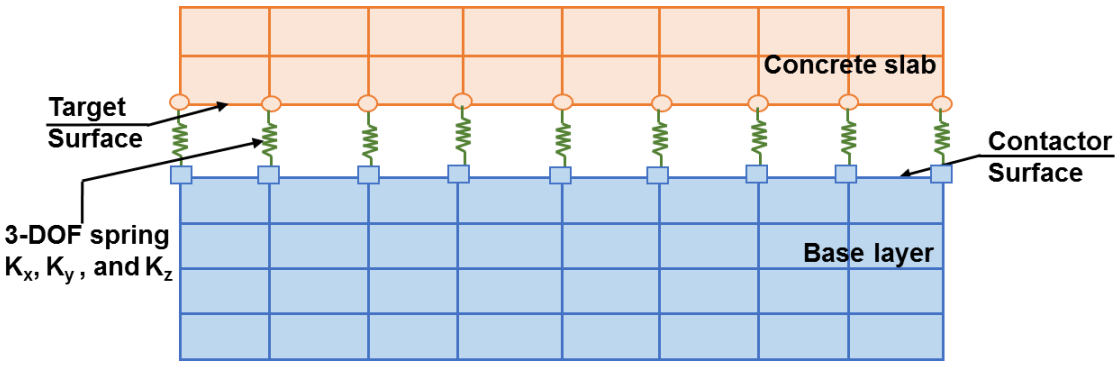

Figure 4-5. Interface model used in this study

4.2.5 Applied Loads

The actual applied traffic loads to pavements are dynamic. Also, the magnitude of the tire contact pressure and contact area are affected by roughness of the pavement surface and vehicle suspension system. However, result of dynamic analyses, conducted in the past, indicate that dynamic responses of the concrete pavements are equal or lower than those of static analysis, and concluded that dynamic analysis is not necessary for design of rigid pavement(Chatti et al. 1994). In addition, the effect of vehicle velocity on maximum tensile stress has no significant effects in JPCP (Kim et al. 2002; Kim et al. 2001).

Thus, in this study, applied traffic loads were modeled as static loads. The required inputs to specify the applied loads include (1) the magnitude of each load, (2) the contact tire pressure, (3) the width of the tire, and (3) the location of each load. To calculate the length of the tire contact area, the following equation was used:

$$L = \frac{F}{p \cdot W} \tag{4.1}$$

Where, L is a length of the tire

F is force exerted by vehicle

p is tire pressure

W is a width of the tire

4.2.6 Temperature and Moisture Effects

Environmental effects considered in concrete pavement analysis are those caused by changes in temperature and changes in moisture content both of which can cause expansion or contraction of the concrete. However, the effect of moisture gradient in concrete slab is similar to that of temperature gradient. A positive moisture differential has the same effect as that of a positive temperature differential on curling of a concrete slab. The effect of a moisture differential in a concrete slab can be modeled as an equivalent temperature differential in the slab. Also, the moisture differential usually works in the opposite direction to the temperature differential. For instance, in the daytime, when the temperature differential is usually positive (hotter at the top of the slab), the moisture differential is usually negative (drier at the top). The effect of moisture differential usually tends to mitigate the effect of temperature differential. Therefore, when the effect of moisture differential is not considered and only the effect of temperature differential is considered, a more conservative (or higher) estimate of the maximum stresses induced would be obtained.

The required inputs to specify the temperature and moisture differential are (1) the temperature differential in the slab and (2) the equivalent temperature differential due to the moisture differential.

4.3 Modeling Pavement Slab Using Concrete Containing RAP

4.3.1 Background

The use of reclaimed or recycled asphalt pavement (RAP) materials in Portland cement concrete (PCC) pavement has become more and more popular in recent years. RAP materials have been used to replace coarse, and fine aggregates in PCC pavement. Previous studies on concrete containing RAP shows that the compressive strength, modulus of elasticity, splitting tensile strength and flexural strength decrease as the percentage of RAP increases in the concrete mix (Berry et al. 2013; Delwar et al. 1997; Hossiney et al. 2010; Hossiney et al. 2008; Huang et al. 2005; Tia et al. 2012; Tia et al. 2009). Also, RAP in concrete mix gives greatly improved toughness and energy absorbing capacity of PCC, since the asphalt film in RAP at the interface of cement mortar and aggregate can dissipate more energy when cracks propagate (Huang et al. 2005).

More recently, concrete pavements containing RAP have been evaluated through a field demonstration project near Lewistown, Montana. The RAP concretes in these slabs were batched, placed, and finished using conventional equipment, and contractors were satisfied with its constructability. The performance of these slabs was monitored via site visual observation and internal vibrating wire gauges over a two-year period. The test slabs containing RAP did not experience visual damage (cracking and spalling) and excessive shrinkage or curling (Berry et al. 2015). In another study, the structural behavior of RAP concrete was evaluated using a Finite Element (FE) model (Hossiney et al. 2010). The FE analysis results indicated that the stress-to-strength ratio under critical temperature-load conditions decreases as the RAP content of the mix increases. For pavement applications, a lower stress-to-strength ratio is desirable, since a lower stress-to-strength ratio indicates that the material can withstand more stress cycles before failure and can perform better.

Although the previous research studies show the benefits of RAP in concrete mix through laboratory study, field demonstration, and FE analysis, it is still needed to study how the non-linear stress-strain characteristics of these ductile concrete may affect the structural behavior and performance characteristic of the RAP concrete pavements. Since, most of the currently used finite element programs, such as WESLIQID, FEACONS, and EverFE, consider the concrete slabs as a linear elastic material, there is a need to develop an appropriate FE model by incorporating actual stress-strain behavior of the RAP concrete to analyze the behavior of the concrete slab to better predict the behavior and performance of this type of pavement.

This subtask presents the results of an analytical study to evaluate the effects of the non-linear stress-strain behavior of the RAP concrete on the response of the concrete pavement under critical temperature-load conditions.

4.3.2 Mechanical Properties of Hardened Concrete Containing RAP

RAP is an asphalt concrete material removed and reprocessed from pavements. The RAP material is a combination of both aged asphalt and aggregate. The properties of RAP dominantly depend on the condition of reclaimed pavement, and can have significant variation due to difference of the type of mix, aggregate quality and size, asphalt mix consistency, and asphalt content. Typically, the fine RAP is much coarser than the virgin fine aggregate, and the coarse RAP is much finer than the virgin coarse aggregate (Huang et al. 2006). Toughness of the concrete could be improved by the addition of RAP due to the asphalt thin film in RAP.

4.3.2.1 Compressive, Flexural, and Splitting Tensile Strength

In concrete incorporating RAP, the compressive strength, flexural strength, and splitting tensile strength of concrete decrease as the percent of RAP increases (Hassan et al. 2000; Hossiney et al. 2010; Huang et al. 2006; Tia et al. 2012; Tia et al. 2009). Also, it was found that the use of fine RAP and coarse RAP cause more reduction in strength than the use of coarse RAP

and sand (Hassan et al. 2000). According to a previous study (Al-Oraimi et al. 2009), RAP can be used as aggregate in non-structural application but the percentage of RAP should be limited to achieve the required performance for the desired application. Figure 4-6 shows the reduction of strength with increase in percentage of RAP from a previous study (Hossiney et al. 2010).

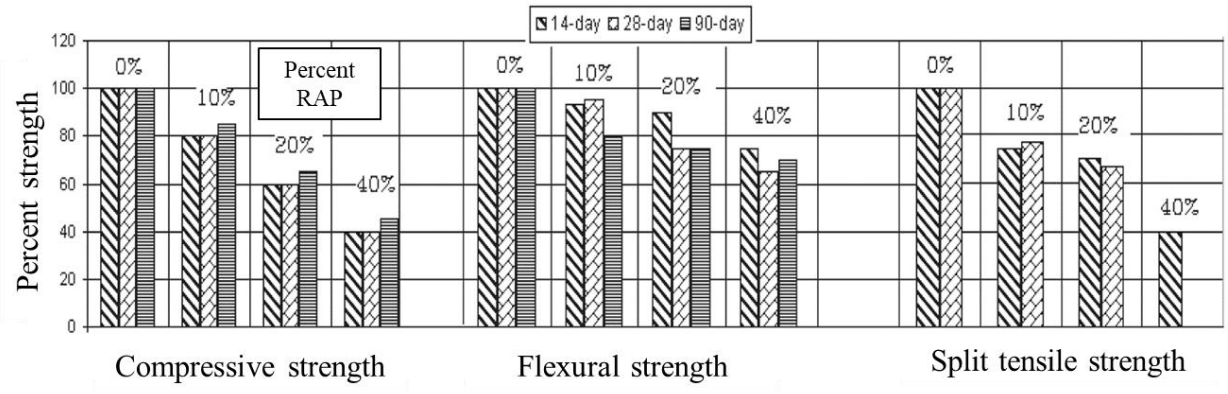

Figure 4-6. Reduction in compressive, flexural, and splitting tensile strength (Hossiney et al. 2010)

4.3.2.2 Modulus of Elasticity

The elastic modulus of concrete containing RAP decreases with increasing percentage of RAP (Delwar et al. 1997; Hossiney et al. 2010; Tia et al. 2012; Tia et al. 2009). It can be explained by the well-known fact that the elastic modulus of concrete is highly affected by the modulus of elasticity of the aggregate and the content of aggregate in the mix. RAP is softer than the natural aggregate, and has lower elasticity, which results in decrease of the elastic modulus of concrete. Thus, an increase in the percentage of RAP in the mix would further reduce the modulus of elasticity of the concrete.

4.3.2.3 Coefficient of Thermal Expansion

The coefficient of thermal expansion increases slightly with increasing percentage of RAP in the concrete mixture (Tia et al. 2012). However, there is no clear trend observed in the

difference between the RAP mix and the conventional concrete mix. This could be due to the variation in the RAP properties, since coefficient of thermal expansion of a concrete mix depends on the properties of the aggregate. Based on the fact that RAP contains asphalt, it can be expected that concrete containing RAP should have a higher coefficient of thermal expansion as compared with the concrete made with the virgin aggregate.

4.3.2.4 Toughness

The modulus of toughness generally increases with increasing percentage of RAP in concrete mixture as shown in Figure 4-7 (Tia et al. 2012). These stress-strain plots were obtained from beam tests, and the toughness was defined as the area under the stress-strain curve. From these results, it can be observed that the failure stress decreases with increasing percentage of RAP, but the strain at failure increases as the percentage of RAP increases due to increased ductile behavior of the material. In the case of concrete without RAP, the failure stress is much higher, but the strain at failure is much lower due to the more brittle behavior of the concrete material.

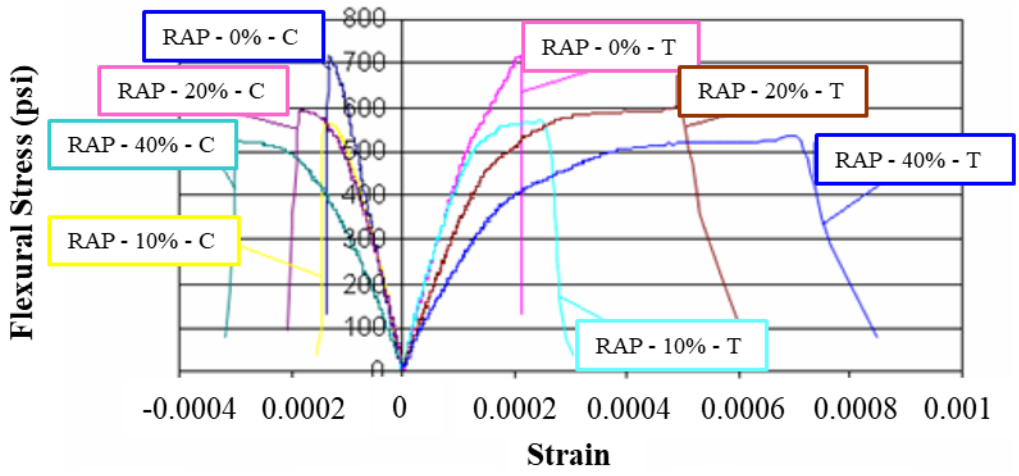

Figure 4-7. Example of stress-strain behavior of RAP concrete

4.3.3 Characterization of the RAP Concrete

The details of the RAP concrete testing results which are presented in this section were presented in a 2012 report by Tia et al. (Tia et al. 2009). The RAP concrete mixtures were produced by replacing a part of both coarse and fine aggregate with a pre-wetted RAP and were mixed in the laboratory using a drum mixer. The mix designs of the concrete are presented in Table 4-1. For the hardened concrete samples at 28 days, compressive strength, flexural strength, splitting tensile, Poisson's ratio, and coefficient of thermal expansion (ASTM C39, C78, C496, C469 and AASHTO TP60) data are presented in Table 4-2.

Table 4-1. Mix designs of the RAP concrete in the study by Tia et al. (2009)

Material	Mixture Design			
	RAP-0%	RAP-10%	RAP-20%	RAP-40%
Cement (lb/yd^3)	508	508	508	508
Water (lb/yd^3)	270	270	270	270
Virgin Coarse Aggregate (lb/yd^3)	1,782	1,604	1,426	1,069
RAP Coarse Aggregate (lb/yd^3)	0	167	335	670
Virgin Fine Aggregate (lb/yd^3)	1,239	1,115	991	743
RAP Fine Aggregate (lb/yd^3)	0	103	205	410
Water-concrete ratio	0.53	0.53	0.53	0.53

Table 4-2. The RAP concrete material properties from the study by Tia et al. (2009)

Property	Mixture Type			
	RAP-0%	RAP-10%	RAP-20%	RAP-40%
Compressive Strength (psi)	5,596	4,936	3,778	2,521
Flexural Strength (psi)	699	566	596	531
Splitting Tensile Strength (psi)	470	488	374	351
Coefficient of Thermal Expansion ($\times 10^{-6}$/°F)	6.05	6.07	6.43	6.20
Poisson's ratio	0.24	0.24	0.25	0.25

4.3.4 Finite Element Modeling

Most of the existing FE models for analysis of concrete pavements considered the concrete slab as a linear elastic material. According to the previous studies, the RAP concrete had a more non-linear stress-strain behavior and failed at a higher strain level. For more realistic and effective modeling of the RAP concrete behavior, the actual stress-strain characteristics of the concrete was incorporated in the model. The three dimensional finite element model using the ADINA software for analysis of concrete pavement slabs, which was developed in this study, was used to analyze the structural behavior of these RAP concrete pavements under critical temperature-load conditions in Florida.

4.3.4.1 Modeling of RAP Concrete Material

Figure 4-8 shows the difference between an assumed linear elastic behavior and an actual stress-strain behavior of the concrete. The elastic modulus is obtained by the standard method (slope of stress versus strain at stress range from 0 to 40% of ultimate concrete strength). As shown in Figure 4-8, the concrete exhibits almost linear behavior up to the proportional limit at point $\sigma_{y,}$ and the actual stress-strain values start to deviate from the assumed linear elastic behavior. Therefore, it is expected that the actual behavior of concrete pavement containing RAP will exhibit some difference as compared with the assumed linear elastic behavior at a higher stress level.

There are several material options to be considered for modeling of the RAP concrete in ADINA software. These material options for concrete range from simple elastic material to a nonlinear-plastic material. In this study, the actual stress-strain characteristics of the RAP concretes, which were determined in a previous project (Tia et al. 2009), were used to model the behavior of the RAP concrete. These stress-strain characteristics were determined from the

Flexural Strength Test (ASTM C78) on the RAP concretes. For comparison purpose, a linear elastic model was also used in the analysis.

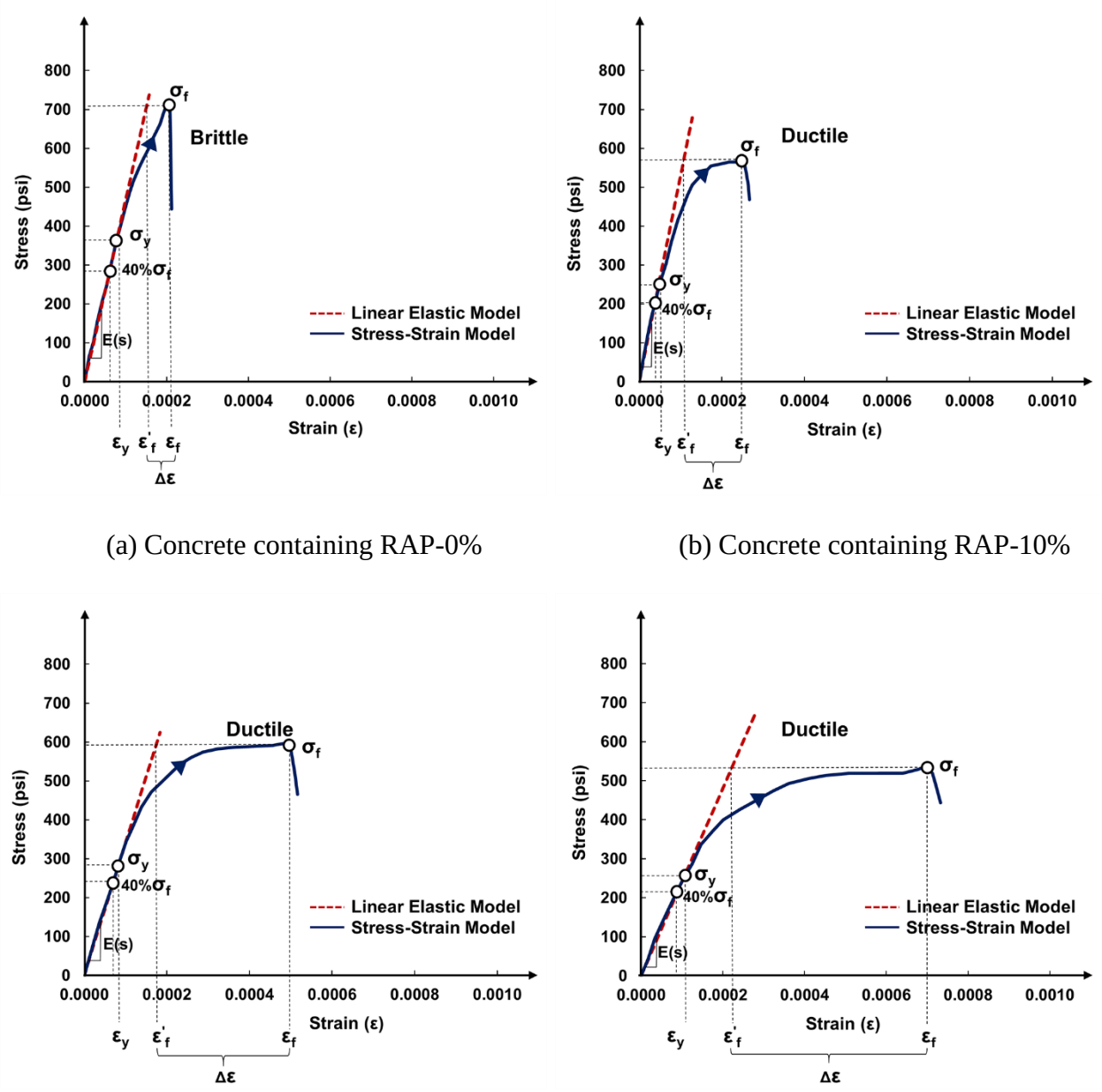

(a) Concrete containing RAP-0%

(b) Concrete containing RAP-10%

(c) Concrete containing RAP-20%

(d) Concrete containing RAP-40%

Figure 4-8. Stress-strain curve for concrete containing RAP

Table 4-3 presents the actual stress-stain values obtained from the flexural strength test on the concrete specimens containing different levels of RAP, and Table 4-4 shows the elastic material properties obtained by the standard method and used in the linear elastic FE model.

Table 4-3. Stress-strain values used in the non-linear models

RAP-0%		RAP-10%		RAP-20%		RAP-40%	
Strain (ε)	Stress (psi)	Strain (ε)	Stress (psi)	Strain (ε)	Stress (psi)	Strain (ε)	Stress (psi)
0.00	0	0.00	0	0.00	0	0.00	0
3.99×10^{-5}	198	4.57×10^{-5}	218	3.37×10^{-5}	120	4.65×10^{-5}	122
6.31×10^{-5}	301	6.59×10^{-5}	310	8.80×10^{-5}	307	7.97×10^{-5}	206
8.47×10^{-5}	394	7.93×10^{-5}	366	1.30×10^{-4}	413	1.20×10^{-4}	286
1.06×10^{-4}	474	1.03×10^{-4}	441	1.89×10^{-4}	501	1.50×10^{-4}	349
1.20×10^{-4}	518	1.26×10^{-4}	499	2.24×10^{-4}	539	1.81×10^{-4}	379
1.40×10^{-4}	562	1.43×10^{-4}	523	2.71×10^{-4}	566	2.28×10^{-4}	421
1.59×10^{-4}	606	1.67×10^{-4}	547	3.37×10^{-4}	585	2.97×10^{-4}	459
1.83×10^{-4}	653	1.95×10^{-4}	558	4.57×10^{-4}	591	4.22×10^{-4}	509
1.98×10^{-4}	699	2.28×10^{-4}	566	4.98×10^{-4}	596	7.03×10^{-4}	531

Table 4-4. Elastic modulus values used in the linear models

Layer	Modulus (ksi)	Poisson's ratio
RAP-0%	4,964	0.24
RAP-10%	4,778	0.24
RAP-20%	3,560	0.25
RAP-40%	2,625	0.25

4.3.4.2 Modeling of Pavement Structure

The FE model consisted of two layers; which include (1) 144 in (3.65 m) wide, 9 in. (22.86 cm) thick concrete slab, and (2) 144 in (3.65 m) wide and 100 in. (254 cm) thick subgrade

layer. They were modeled by an assemblage of hexahedrons elements defined by eight nodes with three degrees of freedom (i.e. translations in the x-, y-, and z-directions). Mechanical and thermal parameters defined for the concrete slab were (1) modulus of elasticity (E), (2) Poisson's ratio, (3) coefficient of thermal expansion (CTE), and (4) mass density, which were obtained from a previous study (Tia et al. 2009). For the subgrade layer to simulate the real boundary condition with sufficient accuracy but without excessive processing time, the subgrade was modeled as having a thickness of 100 in. (254 cm) and fixed in the z-direction. To reduce computer processing time, the double symmetry about x and y axes was used. Figure 4-9 shows the 3-D FE model developed for the analysis of the RAP concrete pavements.

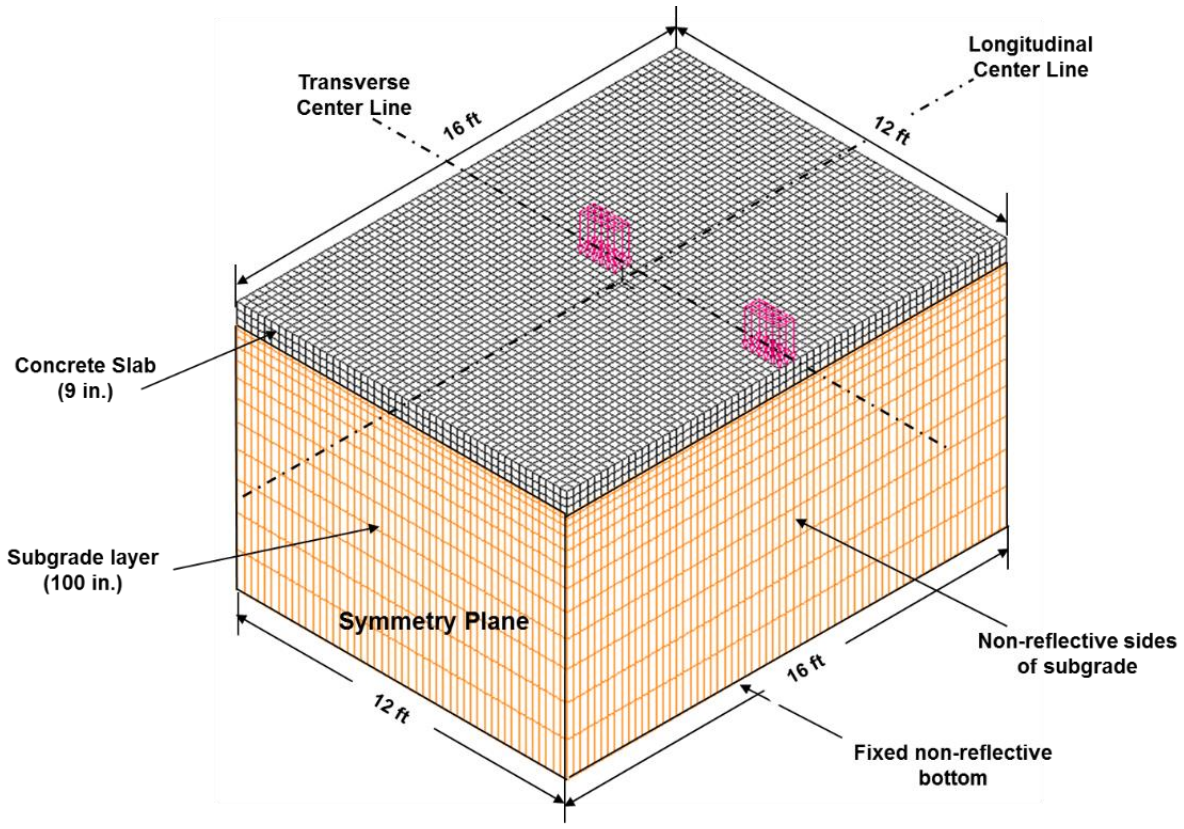

Figure 4-9. 3-D finite element model developed for analysis of a concrete slab

4.3.4.3 Loading Configuration and Temperature Effects

Stress analysis was performed to determine the maximum stresses in the concrete slabs under a critical combined load-temperature conditions. According to a previous study on concrete pavements in Florida (Wu et al. 1993), the maximum tensile stresses in the concrete slab were induced if it were loaded by a 22-kip (98 kN) axle load which is the maximum legal single axle load in Florida at the middle edge with no load transfer across the joints as shown in Figure 4-10. Various temperature differentials in the concrete slab were also considered. The possible temperature differential in the concrete slab was varied from 0°F to 30°F (0°C to 16.7°C).

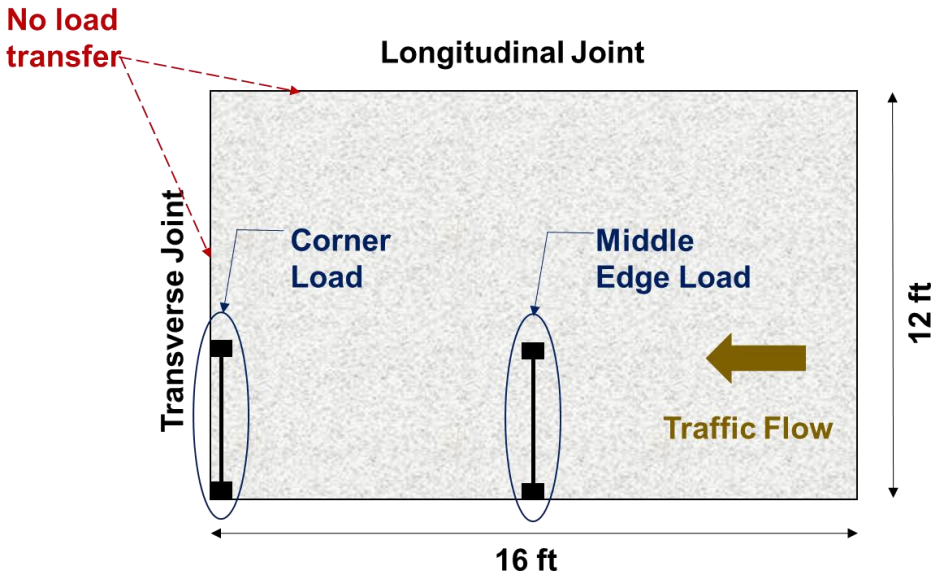

Figure 4-10. Critical loading conditions

4.3.5 FE Results Considering Actual Stress-Strain Characteristics

Using the developed 3-D FE models (i.e., linear elastic and stress-strain model), stress analysis was performed to determine the maximum tensile stresses in the concrete under the combined effect of a critical 22-kp axial load at mid-edge and various temperature differentials

in the slab. The stress-to-strength ratio for each condition was calculated using the flexural strength of the concrete determined from laboratory test.

Figure 4-11 shows the plot of calculated stress-to-strength ratio as a function of temperature differential in the concrete slab using the two different FE model. From these analyses results, the difference between the linear elastic and actual stress-strain model increases as the temperature differential increases. It can also be observed that both models are able to predict similar behavior up to stress-to-strength ratio of approximately 0.6, and thereafter the actual stress-strain model predicts consistently lower stresses in the concrete under the same temperature-load conditions. Since the maximum tensile stresses in the concrete are an important factor influencing the prediction of potential pavement performance, the effect of non-linear behavior of the RAP concrete must be considered when calculating the critical stresses in the concrete pavement. Therefore, it can be concluded that the modeling using actual stress-strain behavior of the RAP concrete, instead of assumption of linear elastic material, can be used to more accurately analyze the concrete pavement containing the RAP under critical temperature-load condition. Tables 4-5 through 4-8 present the maximum stresses and stress-to-strength ratios predicted by the two different FE models.

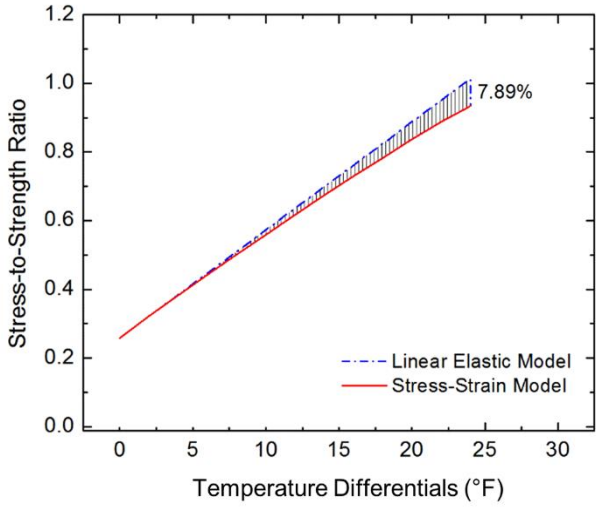

(a) Concrete containing RAP-0%

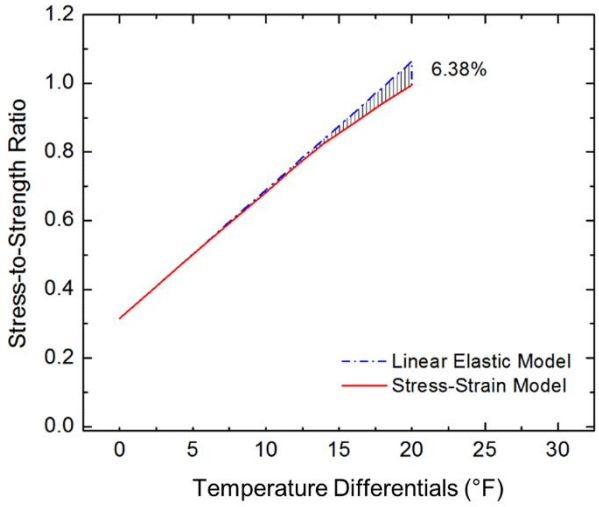

(b) Concrete containing RAP-10%

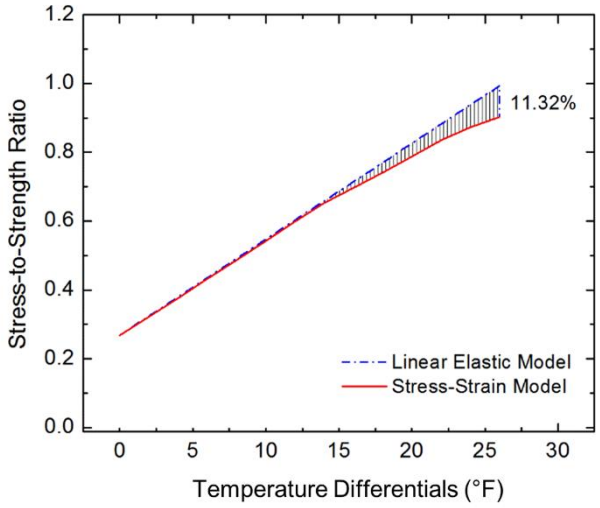

(c) Concrete containing RAP-20%

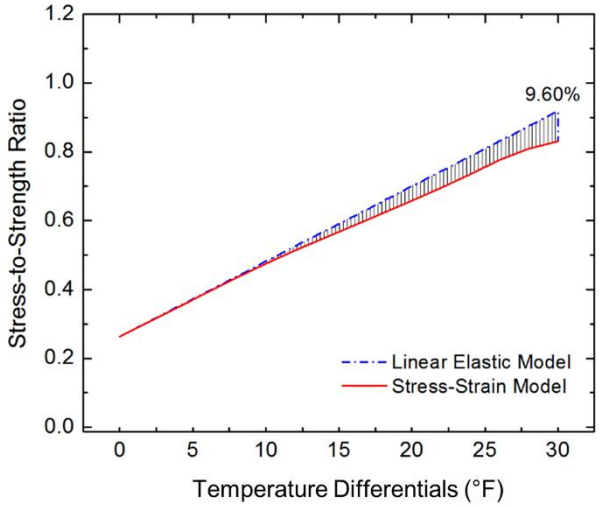

(d) Concrete containing RAP-40%

Figure 4-11. Computed stress-strength ratios for concrete slabs containing RAP

Table 4-5. Comparison of maximum stresses computed by the linear elastic and actual stress-strain models for the concrete mix with 0% RAP

Temperature Differential (°F)	Linear Elastic Model		Stress-Strain Model		Difference (%)
	Stress (psi)	Stress Ratio	Stress (psi)	Stress Ratio	
0	180.7	0.26	180.7	0.26	0.00
2	224.7	0.32	225.2	0.32	-0.20
4	268.7	0.38	267.5	0.38	0.43
6	312.7	0.45	308.9	0.44	1.19
8	356.6	0.51	350.4	0.50	1.76
10	400.6	0.57	391.2	0.56	2.34
12	444.6	0.64	431.1	0.62	3.03
14	488.6	0.70	471.5	0.67	3.49
16	532.5	0.76	510.2	0.73	4.19
18	576.5	0.82	547.6	0.78	5.02
20	620.5	0.89	585.4	0.84	5.66
22	664.5	0.95	620.8	0.89	6.57
24	708.4	1.01	652.6	0.93	7.89

Table 4-6. Comparison of maximum stresses computed by the linear elastic and actual stress-strain models for the concrete mix with 10% RAP

Temperature Differential (°F)	Linear Elastic Model		Stress-Strain Model		Difference (%)
	Stress (psi)	Stress Ratio	Stress (psi)	Stress Ratio	
0	178.2	0.31	178.2	0.31	0.00
2	220.6	0.39	220.6	0.39	0.00
4	262.9	0.46	263.4	0.47	-0.16
6	305.3	0.54	304.4	0.54	0.30
8	347.7	0.61	345.4	0.61	0.66
10	390.0	0.69	386.6	0.68	0.87
12	432.4	0.76	427.7	0.76	1.10
14	474.8	0.84	467.2	0.83	1.59
16	517.1	0.91	499.6	0.88	3.38
18	559.5	0.99	532.9	0.94	4.74
20	601.8	1.06	563.4	1.00	6.38

Table 4-7. Comparison of maximum stresses computed by the linear elastic and actual stress-strain models for the concrete mix with 20% RAP

Temperature Differential (°F)	Linear Elastic Model		Stress-Strain Model		Difference (%)
	Stress (psi)	Stress Ratio	Stress (psi)	Stress Ratio	
0	159.9	0.27	159.5	0.27	0.26
2	193.2	0.32	192.2	0.32	0.51
4	226.4	0.38	224.8	0.38	0.71
6	259.7	0.44	257.5	0.43	0.84
8	292.9	0.49	290.2	0.49	0.95
10	326.2	0.55	322.9	0.54	1.00
12	359.4	0.60	356.9	0.60	0.70
14	392.7	0.66	389.0	0.65	0.95
16	426.0	0.71	415.7	0.70	2.42
18	459.2	0.77	442.3	0.74	3.68
20	492.5	0.83	468.9	0.79	4.79
22	525.7	0.88	497.4	0.83	5.40
24	559.0	0.94	520.4	0.87	6.90
26	592.2	0.99	538.0	0.90	9.15
28	625.5	1.05	554.7	0.93	11.32

Table 4-8. Comparison of maximum stresses computed by the linear elastic and actual stress-strain models for the concrete mix with 40% RAP

Temperature Differential (°F)	Linear Elastic Model		Stress-Strain Model		Difference (%)
	Stress (psi)	Stress Ratio	Stress (psi)	Stress Ratio	
0	139.9	0.26	139.8	0.26	0.08
2	163.1	0.31	162.5	0.31	0.40
4	186.3	0.35	185.1	0.35	0.65
6	209.5	0.39	207.6	0.39	0.88
8	232.6	0.44	231.0	0.44	0.68
10	255.8	0.48	252.7	0.48	1.21
12	279.0	0.53	272.3	0.51	2.41
14	302.2	0.57	291.9	0.55	3.39
16	325.4	0.61	311.4	0.59	4.30
18	348.5	0.66	330.5	0.62	5.17
20	371.7	0.70	349.7	0.66	5.92
22	394.9	0.74	369.6	0.70	6.40
24	418.1	0.79	390.7	0.74	6.54
26	441.2	0.83	412.6	0.78	6.49
28	464.4	0.87	429.8	0.81	7.45
30	487.6	0.92	440.8	0.83	9.60

4.3.6 Summary of Findings

In this subtask, a non-linear FE model by incorporating the actual stress-strain behavior of the RAP concrete obtained from the flexural strength test was developed to evaluate the effects of the non-linear stress-strain behavior of the RAP concrete in a critical stress analysis. The analytical results from the FE model incorporating the actual stress-strain behavior of the RAP concrete were compared with the corresponding results from the linear elastic FE model. From the results, it was observed that the maximum computed tensile stresses in the concrete using the linear elastic model tend to overestimate the induced stresses at high stress level. Therefore, it can be concluded that in the design of the concrete pavement containing RAP concrete, an appropriate analytical model using the actual stress-strain characteristics, instead of the assumption of the concrete as linear elastic material, should be employed to accurately predict the maximum stresses in the concrete. The model incorporating the actual stress-strain behavior of the RAP concrete can simulate the structural responses more accurately and can better predict the potential performance of the pavement.

4.4 Application of Actual Dowel Bar System

In this subtask, a three-dimensional finite element model was developed to evaluate the applicability of modeling the dowel bars by their actual dimensions, instead of the use of beam element, in a jointed plain concrete pavement (JPCP). A typical three-slab configuration was selected. Each slab is 15 ft long, 12 ft wide, and 8 in. thick. The subgrade is modeled as an elastic foundation with a modulus of elasticity corresponding to that of a limerock base.

4.4.1 Overview of Dowel Bar

The primary load transfer of dowel bar is shear mechanism especially for joint opening less than 0.25 in. while the moment mechanism is considered negligible (Guo et al. 1995). The total shear load transferred by dowel bars is generally less than 50 percent of the applied wheel

load. The magnitude of transferred shear load is a function of the dowel bar diameter, dowel bar length, dowel bar spacing, stiffness of base layer, and slab dimension including thickness, length, and width. A previous study found that the maximum load transferred by the critical dowel is generally between 41 and 43 percent of applied load (Heinrichs et al. 1987). Therefore, the dowel diameter and cross-section area mainly affect the behavior and performance of the dowel-pavement system. The peak bearing stresses and deflections at a joint can be reduced by increase in the dowel stiffness. Dowel diameter may be increased or decreased due to the dowel spacing, dowel bar properties including modulus of elasticity, material (e.g., mild steel, fiber-reinforced polymer etc.), and dowel bar shapes (e.g., round, or non-round dowel). Table 4-9 presents the recommended dowel bar diameter as a function of pavement thickness in US state highway agencies.

Table 4-9. Recommended dowel bar diameter (in.) by pavement thickness

Slab Thickness	8.0	8.5	9.0	9.5	10.0	10.5	11.0	11.5	12.0	12.5
Florida	—	1.00	1.25	1.25	1.25	1.25	1.50	1.50	1.50	1.50
California	1.25	1.50	1.50	1.50	1.50	1.50	1.50	1.50	1.50	1.50
Iowa	1.25	1.25	1.25	1.25	1.50	1.50	1.50	1.50	1.50	1.50
Illinois	1.50	1.50	1.50	1.50	1.50	1.50	1.50	1.50	1.50	1.50
Indiana	1.00	1.00	1.25	1.25	1.25	1.25	1.25	1.25	1.25	1.50
Michigan	1.25	1.25	1.25	1.25	1.25	1.25	1.25	1.50	1.50	1.50
Minnesota	1.25	1.25	1.25	1.25	1.25	1.50	1.50	1.50	1.50	1.50
Missouri	1.25	1.25	1.25	1.25	1.25	1.50	1.50	1.50	1.50	1.50
North Dakota	1.25	1.25	1.25	1.25	1.25	1.50	1.50	1.50	1.50	1.50
Ohio	1.00	1.25	1.25	1.25	1.25	1.50	1.50	1.50	1.50	1.50
Texas	1.00	—	1.125	—	1.25	—	1.375	—	1.50	—
Wisconsin	1.25	1.25	1.25	1.25	1.50	1.50	1.50	1.50	1.50	1.50

Note: Slab thickness and dowel bar diameter are in inches.

Teller and Cashell (1959) conducted repeated load tests to determine the requirement of the length of dowel embedment for maximum load transfer. The results indicated that dowels could be embedded about 8 times of dowel diameter for ¾ in. diameter, while 1 in. and 1.25 in dowels require only 6 times of diameter (i.e., 6 in. and 7.5 in. respectively). Figures 4-12 and 4-13 show the effects of the length of dowel embedment on the load transfer efficiency and looseness conducted by Teller and Cashell (1959). The recent recommended length of dowel bar is 18 in. to achieve good pavement joint performance.

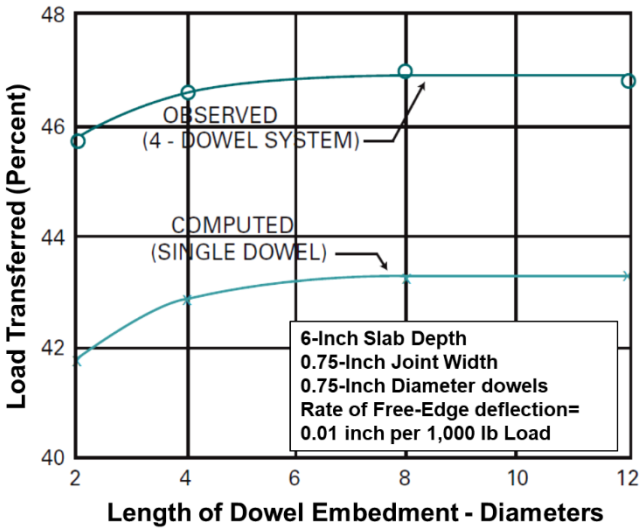

Figure 4-12. Load transfer versus dowel embedment (Teller and Cashell 1959)

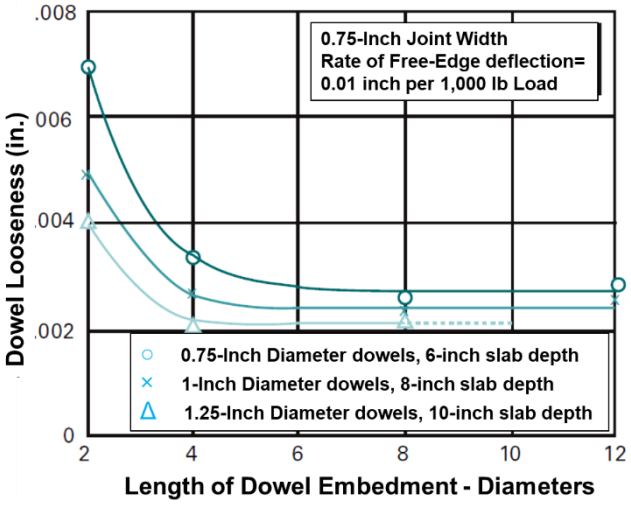

Figure 4-13. Effect of dowel embedment and diameter on dowel looseness after 600,000 repetitions (Teller and Cashell 1959)

Dowel bar misalignment does not necessarily result in the slab distresses, however, if the number of consecutive joints lock up, the potential of development of slab distress increases due to the failure of stress relief at the joints. Most highway agencies have adopted the Federal Highway Administration (FHWA) recommendation limits on horizontal and vertical rotation of ¼ in. per ft of dowel bar length or 2% (FHWA 1990). It must be noted that there is no clear evidence that what level of tolerance is required to achieve good performance of joint. Table 4-10 presents the tolerance of dowel bar misalignment for several states.

Table 4-10. Specification of dowel bar misalignment tolerance

States	Maximum rotation (in.)	Vertical translation (in.)	Longitudinal translation (in.)
Florida	1/2	1	2
Illinois	3/16	-	-
Indiana	3/8	-	-
Iowa	1/4	-	-
Kansas	3/8	1/10 of slab thickness	-
Minnesota	1/4	-	-
Nebraska	1/4	-	-
Georgia	9/16	-	-
North Carolina	3/8	-	-
South Carolina	9/16	3/4	3

When the concrete slabs are subjected to loads, bearing stresses and deflection are mainly affected by the spacing of dowel bars. Decreased dowel bar spacing results in the decrease in bearing stresses and deflection. However, if dowel spacing decreases to less than 8 in., a horizontal plane of weakness in the concrete at the joint face will occur. Conversely, increased dowel spacing results in excessive bearing stresses and deflection at the joint. Now, most

highway agencies have adopted a 12-inch spacing, which can vary depending on the thickness of slab and subgrade condition.

4.4.2 Finite Element Modeling using Actual Dowel Bar System

A three-dimensional finite element model of the rigid pavement was developed to model the load transfer mechanism of dowel bars. The modeled section consisted of three slabs with a transverse joint width of ¼ in, supported by 100-in.-thick subgrade layer as shown in Figure 4-14. The transverse joint width was selected in order to allow expansion and contraction of the PCC slab. For the subgrade layer boundary conditions (BCs), a fixed BC was applied in the z-direction, and symmetric BCs were inserted along the x- and y- directions. The interface between the concrete slab and the subgrade was modelled using contact and target elements. The slab contact with the subgrade layer was only maintained by the self-weight of the slab. There was no restraint imposed on the concrete slab, and thus the loss of contact due to the temperature gradients through the depth of slab was allowed. The interface model was also capable of capturing the effect of friction, and a value of 1.5 for the coefficient of friction was assumed. Figure 4-15 shows the interface modeling and contact elements between the slab and subgrade layer.

The concrete slab, subgrade layer, and dowel bars were modeled by an assemblage of 8-node hexahedron elements with using various mesh sizes. To accurately capture the dowel behavior, a finer mesh was implemented around the dowel bar and sleeves in the concrete. The length of the smallest element used was 0.375 in. of the dowel bar.

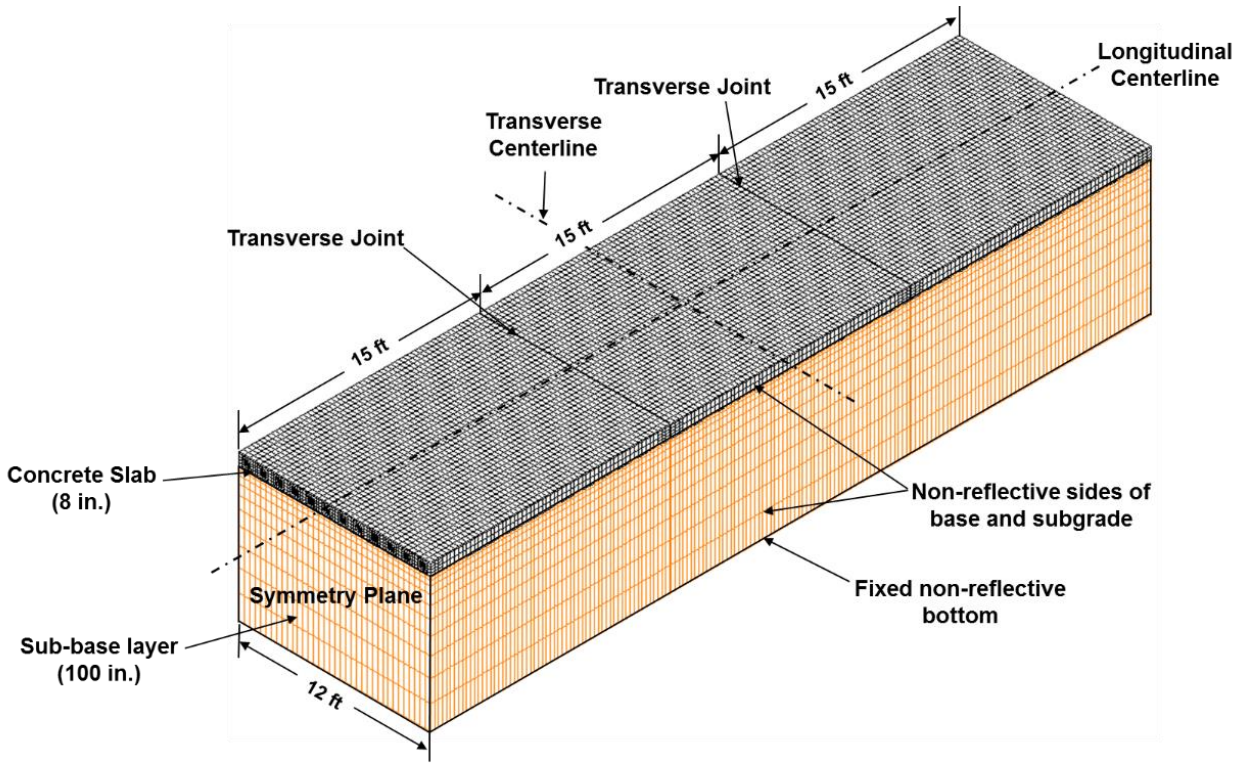

Figure 4-14. Finite element model of JPCP with actual dowel bar dimension

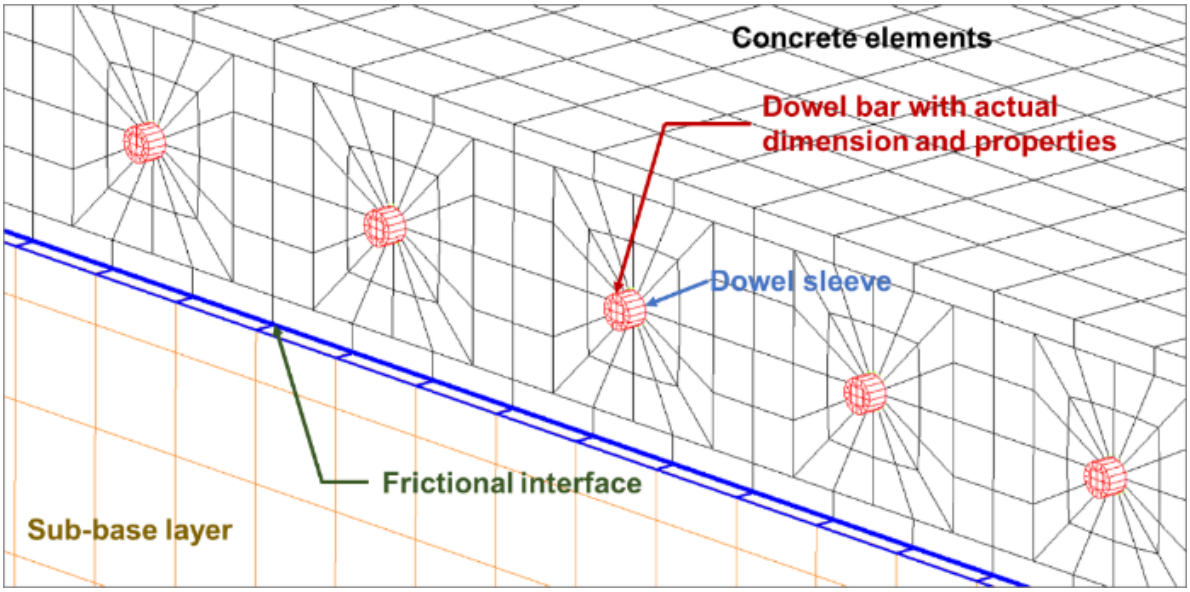

Figure 4-15. Modeling the interface condition

The mechanical and thermal behavior of the concrete slab are characterized by its (1) modulus of elasticity, (2) Poisson's ratio, (3) coefficient of thermal expansion, and (4) density, while the subgrade layer and dowel bars were considered as linear elastic materials characterized by their modulus of elasticity and Poisson' ratio.

Sliding interface between the concrete and the dowel bars were modeled in order to simulate the dowel movements under temperature effects. The typical size of dowel dimension and spacing were considered with 1 in. diameter, 9 in. embedment in both sides, and 12 in. dowel spacing as shown in Figure 4-16. Table 4-11 presents the material properties used in the FE model.

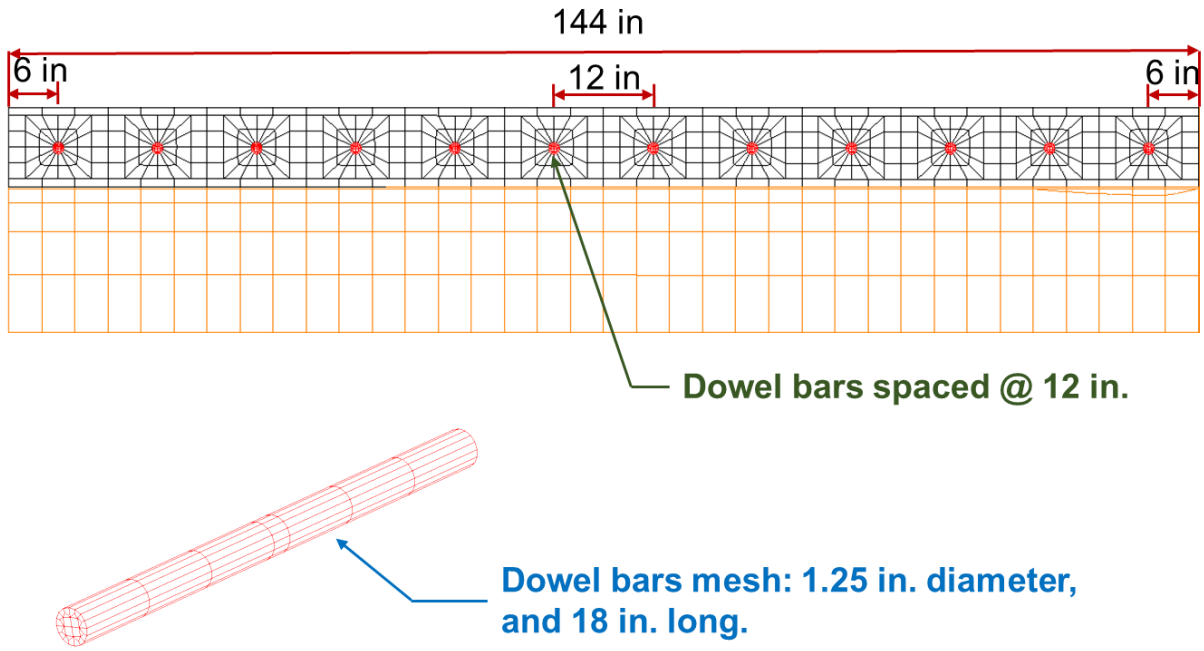

Figure 4-16. Slab and dowel bar mesh

Table 4-11. Material properties used in the FE model for JPCP with dowel bars

Layer	Property	Value
Concrete	Modulus of Elasticity (ksi)	4,310
	Poisson's ratio	0.2
	Coefficient of thermal expansion (/°F)	6.53×10^{-6}
	Density (pcf)	145
Dowel bar	Modulus of Elasticity (ksi)	29,000
	Poisson's ratio	0.3
	Diameter of dowel bar (in.)	1.0
	Length of dowel bar (in.)	18
Subgrade	Modulus of Elasticity (ksi)	100
	Poisson's ratio	0.35

4.4.3 Calibration and Validation of FE model using FWD data

The 3-D FE model developed was validated with FWD deflection basins performed on the JPCP section constructed in US-1 Edgewater City (constructed in 1988), Florida. The FWD deflection basins caused by a 12-kip load were used to estimate the load transfer characteristics of doweled joints. To eliminate the effect of dowel looseness, the FWD data, conducted in 1988, was selected from the FDOT archive. For analysis of the deflection basin, a twelve inches by twelve inches square loading was used to model the FWD load. This set of FWD tests was performed in the daytime when the slab tends to have a positive temperature differential and to have full contact with the subgrade at the slab joint.

Figure 4-17 shows a comparison of the analytical FWD deflection basin with measured deflection basins. As presented in Figure 4-17, a very good match between the measured and the calculated deflection basin was achieved using the contact sliding surface between the concrete and the dowel bars, and actual size of 3-D dowel bar model.

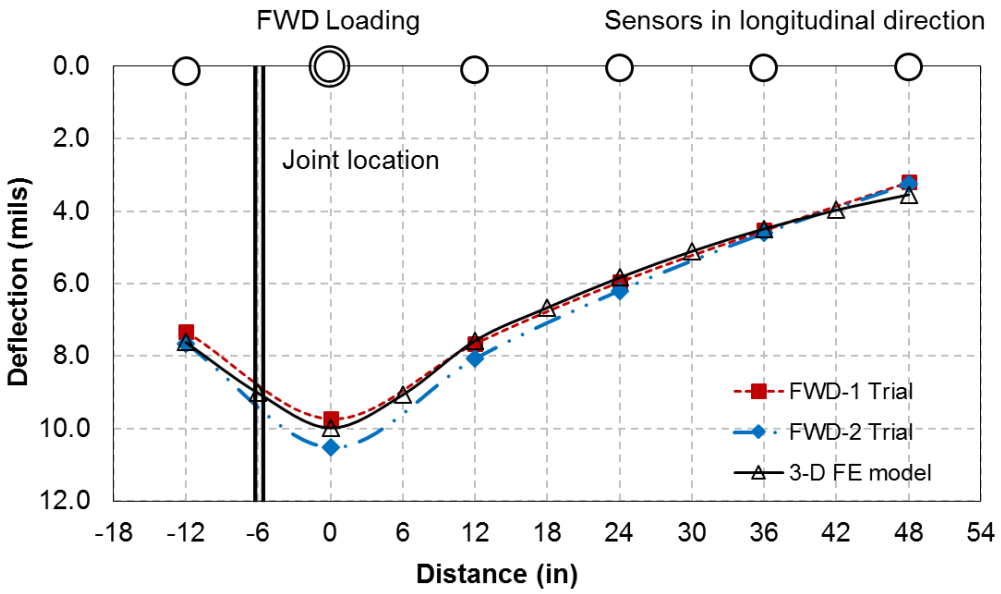

Figure 4-17. Matching of deflection basin across the doweled joint

4.4.4 Summary of Findings

In this subtask, a 3-D FE model was developed to evaluate the applicability of modeling the dowel bars by their actual dimensions and material properties in JPCP. The FE model was validated by matching the measured FWD deflection basins with analytical deflection basins. The main findings are summarized as follow:

- The load transfer mechanism across the doweled joint can be modeled well by using the contact sliding surface between the concrete and dowel bars.
- For modeling the dowel sleeve and dowel bar, very fine mesh size less than 2/5 in. was required to accurately capture the bearing stresses in the concrete.
- The 3-D FE model presented in this section can be used to study the behavior of dowel bars under combined temperature-load conditions, and the effects of various special dowel bar configurations including the maximum dowel deflection, the bearing stress on dowel-concrete interface, and shear force transfer.

CHAPTER 5
DEVELOPMENT OF A FINITE ELEMENT MODEL FOR ANALYSIS OF CONTINUOUSLY REINFORCED CONCRETE PAVEMENT (CRCP)

5.1 Introduction

5.1.1 Background

A continuously reinforced concrete pavement (CRCP) is constructed without transverse joints except for construction joints. CRCP has embedded steel reinforcement in the transverse and longitudinal direction. CRCP allows the concrete to crack as a result of drying shrinkage. The subsequent transverse cracks are held tightly together by the longitudinal steel and thus provides good serviceability or ride quality. Previous research has indicated that CRCP outperforms other types of concrete pavement due to its durable nature (Smith et al. 1998). CRCP has been used primarily in urban areas where delay associated with repairs and rehabilitation can cause higher user cost. Because of its durable character, the Florida Department of Transportation has movement to consider CRCP for heavy-load and heavy-traffic facilities (FDOT 2011).

Field evaluation of distresses indicated that punch-out distress is the most severe performance problem in CRCP (Darter et al. 1979; McCullough et al. 1980; Zollinger 1989). However, in-depth evaluations of punch-outs during their repair revealed that this type of distress was associated with horizontal cracking at the depth of the longitudinal steel. Furthermore, full-depth punch-outs are quite rare in Texas (Won 2011). The horizontal cracking has not been well recognized until recently due to the difficulty of detection before full-depth rehabilitation. The horizontal crack prevents the transverse crack propagation into the full-depth of concrete slab. These transverse and horizontal cracks may ultimately cause a half-depth punch-out as shown in Figure 5-1 (Choi et al. 2011). In addition, even though the top half of the concrete had deteriorated, the bottom of half of the concrete was still healthy (Won 2011).

Previous research has been conducted to identify the mechanism of horizontal cracking in CRCP due to environmental effects and found that the longitudinal steel plays a significant role in the development of horizontal cracking. Significant tensile stress occurred in concrete near the longitudinal steel due to environmental effects and steel restraint (Choi et al. 2011; Kim and Won 2004). In addition, horizontal cracking could be affected by concrete material properties, environmental conditions, and longitudinal steel layout (Choi et al. 2011; Won et al. 2002). However, only three research papers have been identified to address horizontal cracking and they focused on effects of environmental loading only, due to the limitation of two-dimensional (2-D) finite-element (FE) model. Even though axle loading may also affect the development of horizontal cracking of CRCP, it has not been well considered in previous studies. Therefore, the current lack of understanding of the horizontal cracking compared to other distress type under environmental and critical loading conditions is probably the great deficiency in the evaluation of the CRCP system. The effects of combination of environmental and wheel loading need to be evaluated and understood in order to mitigate this type of cracking. A better understanding about the mechanism of horizontal cracking under combined action of wheel loads and environmental loads may help in the understanding of some of the existing problems and provide better guidelines for the design and construction of the CRCP system.

In this study, a three-dimensional (3-D) FE model was developed for analyzing a CRCP system. The 3-D model was used to evaluate the effects of various design parameters on the vertical tensile stress in concrete near the longitudinal steel, where the horizontal crack generally occurs.

5.1.2 Objectives

The analysis conducted herein was focused on the evaluation of factors influencing horizontal cracking in CRCP under combined environmental and traffic loads. The design parameters evaluated include:

- Location of combined environmental and traffic loads
- Concrete properties (coefficient of thermal expansion, and modulus of elasticity).
- Structural design parameters (base modulus, base friction coefficient, slab thickness, and crack spacing).
- Longitudinal steel design (spacing of steel reinforcement and steel-concrete ratio).

5.1.3 Scope

In this study, a 3-D finite element model was developed for computing the vertical tensile stresses in the concrete in CRCP under critical temperature-load conditions. The developed 3-D model was used to perform a parametric analysis to determine the effects of loading location, concrete material properties, pavement design parameters, and longitudinal steel design on the vertical tensile stress near the longitudinal steel causing horizontal cracking.

Figure 5-1. Horizontal cracking in CRCP (Choi et al. 2011)

5.2 Mechanism of Horizontal Cracking in CRCP

Temperature and moisture gradients in a concrete pavement slab can cause the slab to curl. However, this distortion can be restrained by the longitudinal steel across the transverse crack, resulting in a significant vertical tensile stress at the depth of the longitudinal steel. Because the longitudinal steel resists curling, this force is applied to the upper and lower halves of the slab. As a result, a substantial stress in the vertical direction occurs at the depth of the longitudinal steel, which may result in horizontal cracking in CRCP (Choi et al. 2011). It is expected that a greater tensile stress zone would be developed under an extreme temperature or moisture condition, especially when wheel loads are applied. Figure 5-2 illustrates how vertical tensile stresses are developed at the depth of steel when the concrete slab is subjected to environmental loadings of a temperature differential of ±20°F (±11.1°C) in the concrete slab. When the vertical tensile stress near the steel is excessive, the concrete would crack horizontally along the plane of the slab, splitting the slab into two separate slabs of much lower thickness. The upper thin slab would easily crack under combined temperature and load effects. Therefore, it is important to evaluate this vertical tensile stress in order to prevent this type of cracking which will eventually lead to punch-out failure in CRCP.

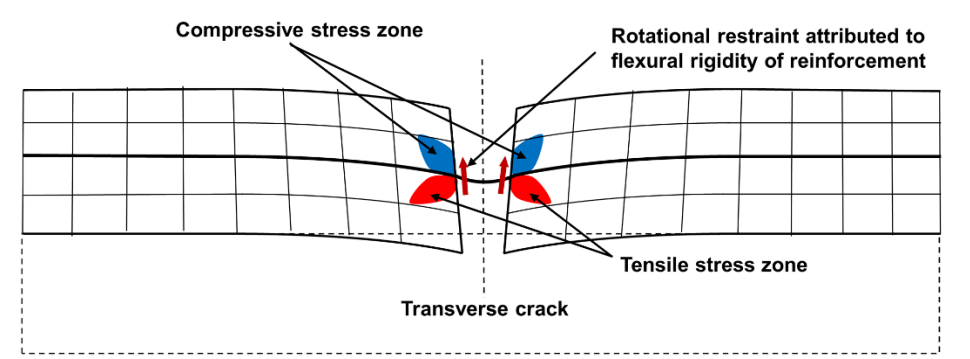

(a) Area of compressive and tensile stress zones at a transverse crack in CRCP due to a positive temperature differential in the slab

Figure 5-2. Vertical stress of concrete in CRCP

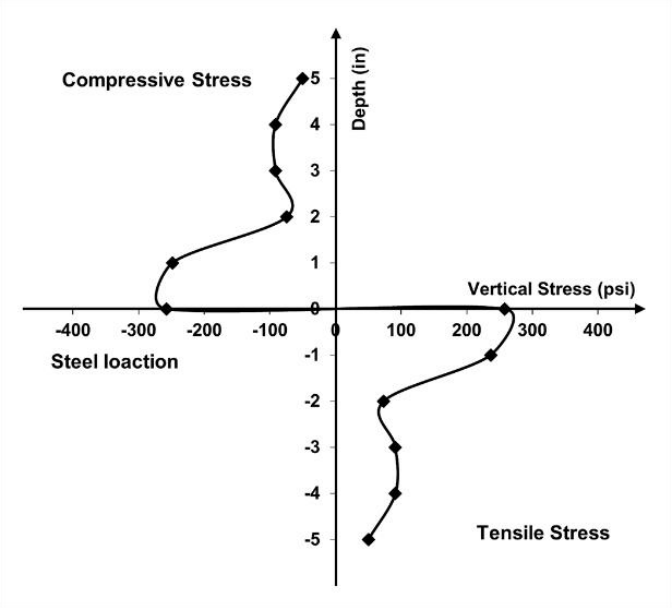

(b) Vertical stress in concrete near steel due to temperature differential of +20 °F

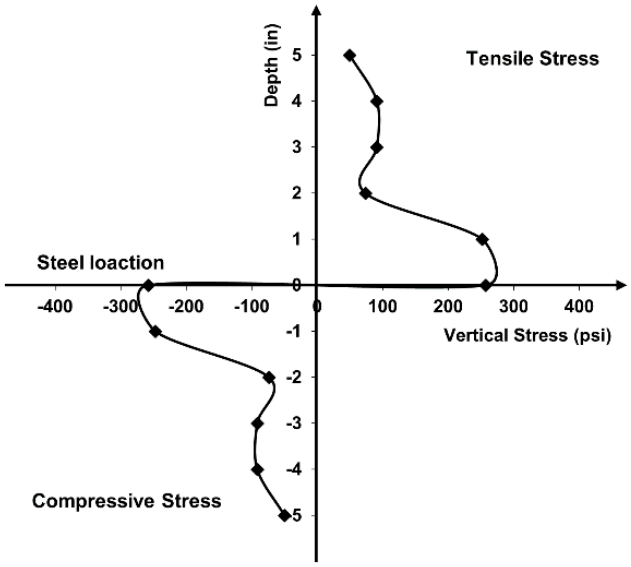

(c) Vertical stress in concrete near steel due to temperature differential of -20 °F

Figure 5-2. Continued

5.3 Finite Element Modeling of CRCP

The 3-D finite element model developed in this study consists of two concrete slabs with one transverse crack supported by base and subgrade as shown in Figure 5-3. The spacing of the transvers crack was initially assumed to be 10 ft (3 m). To eliminate the boundary condition effects, the concrete slabs were modeled at their full width and the base and subgrade layers were extended 24 inch (61 cm) on each side. The concrete slabs' contact with the base layer was maintained by applying the concrete self-weight and there was no external constraint. The concrete slab-base layer interface friction factor (μ) was assumed to be 1.5, since the AASHTO 93 Guide recommends a range of concrete-base friction of 0.9 to 2.2. The concrete slab was modeled by an assemblage of eight-node isoparametric solid brick elements and the reinforce steels were modeled by beam elements. The bond-slip between the concrete and the steel bars was modeled using spring elements. Figure 5-4 shows the frictional bond-slip relation between the concrete and the steel bars which has been used by other researchers and which was used in this study (Kim et al. 1998; Kim et al. 2000). The thickness of the base layer was 6 in. (15 cm) over a 100-in (254 cm) subgrade. It was found that increasing the thickness of the subgrade layer to more than 100 in. (254 cm) had no significant effect on the computed stresses in the concrete slabs. The base and subgrade materials were modeled as isotropic and linearly elastic characterized by their modulus of elasticity and Poisson's ratio. The contraction and expansion of the concrete due to temperature effects are also considered, and characterized by its coefficient of thermal expansion. The double symmetry of the geometry about x- and y- axes was selected in order to reduce computation time. The subgrade layer was fixed in the z-direction. The geometry and material properties used in this study are presented in Table 5-1.

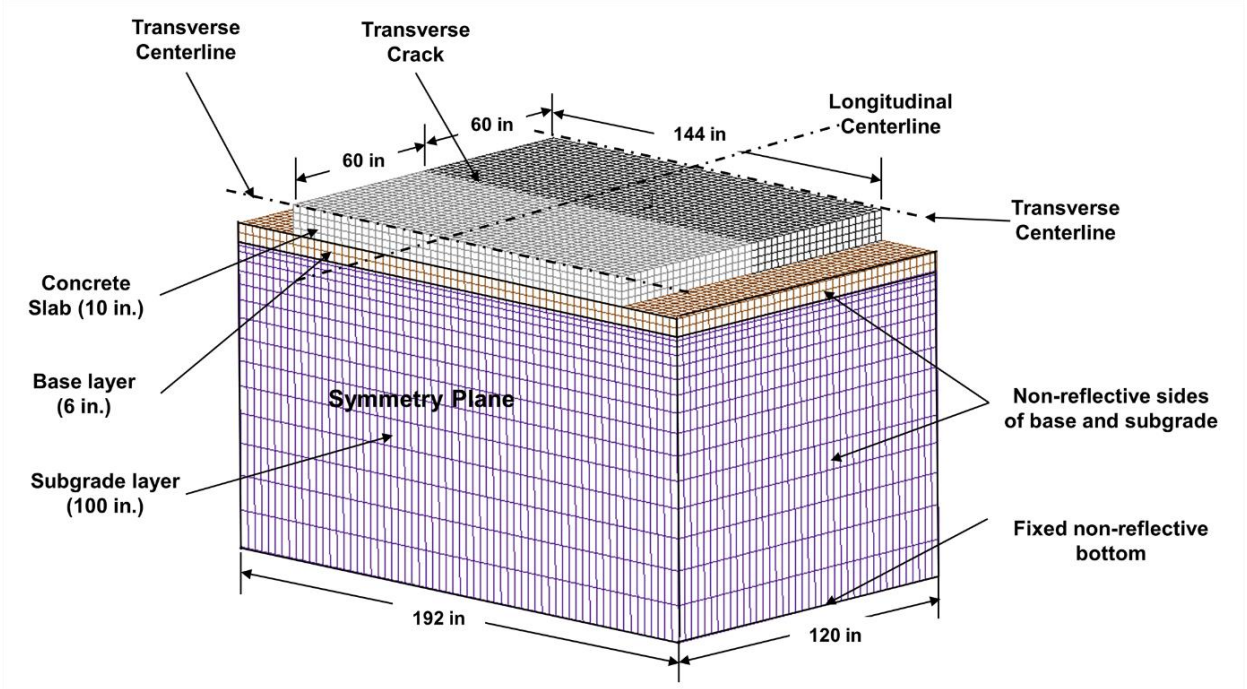

Figure 5-3. Finite element model of CRCP

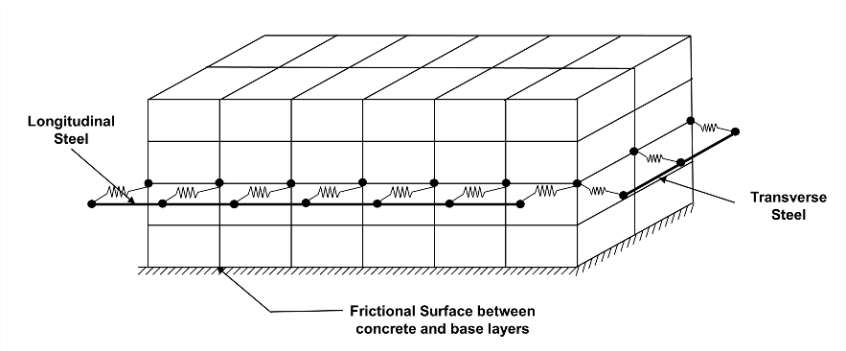

(a) Spring for bond-slip between concrete and reinforce bar

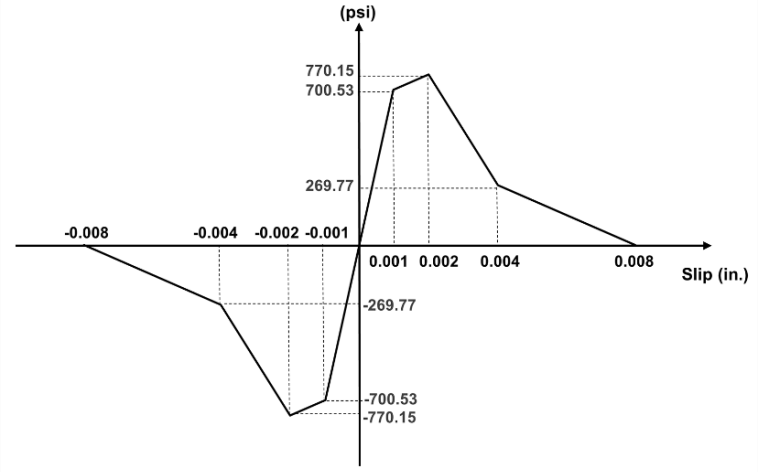

(b) Bond stress-slip relationship used

Figure 5-4. Finite element model for concrete-steel interface

Table 5-1. Geometry and material properties used in the CRCP model

Transverse crack spacing	10 ft (3 m)
Pavement width	12 ft (3.6 m)
Pavement thickness	10 in. (25.4 cm)
Coefficient of thermal expansion (concrete)	5.8×10^{-6}/°F (10.4×10^{-6}/°C)
Coefficient of thermal expansion (steel)	5.0×10^{-6}/°F (9.0×10^{-6}/°C)
Elastic modulus of Concrete slab	4,800,000 psi (33.1 GPa)
Elastic modulus of steel	29,000,000 psi (200 GPa)
Depth of steel	5 in. (12.7 cm)
Diameter of longitudinal steel	0.75 in. (19 mm)
Diameter of transverse steel	0.625 in. (16 mm)
Longitudinal steel spacing	6 in. (15.2 cm)
Transverse steel spacing	18 in. (45.7 cm)

5.4 Effect of Critical Loading Condition on Horizontal Cracking

The effects of combined temperature and load on the vertical tensile stress near the longitudinal steels in CRCP has not been studied previously. Critical vertical stress analysis at the depth of steel was performed to determine the maximum tensile stresses in the concrete slabs if they were subject to some critical load and temperature conditions which would produce the highest thermal-load-induced stresses in the concrete. The two temperature differentials considered in the analysis were +20°F (+11.1°C) and -20°F (-11.1°C), which represent typical severe temperature differential in concrete pavement slabs in Florida. A 22-kip (98 kN) axle load, which represents the maximum legal load limit for single axle loads in Florida, was used as the applied load in the analysis. The four load positions were (1) slab corner at transverse crack, (2) slab center at transverse crack, (3) slab edge between transverse cracks, and (4) slab center between transverse cracks. Vertical tensile stresses at the depth of steel in concrete caused by the

axle load for the various combination of temperature differentials and load positions were computed using the 3-D FE model developed.

Figure 5-5 shows the computed vertical tensile stress in concrete at the depth of steel caused by the different combinations of temperature differential and axle load. The results of the analysis indicate that when the temperature differential in the slab is positive, the critical load position is at the slab corner. Therefore, the corner load positon at transverse crack was used in the computation of the maximum thermal-load-induced vertical tensile stresses for most of the cases in this study.

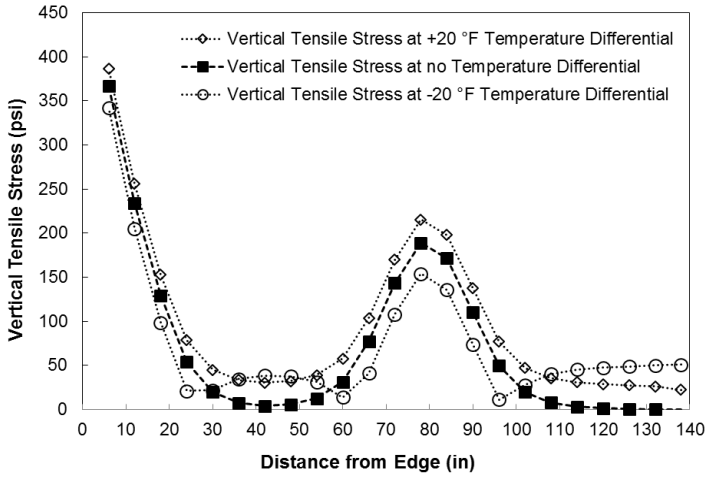

(a) Slab corner loading at transverse crack

Figure 5-5. Continued

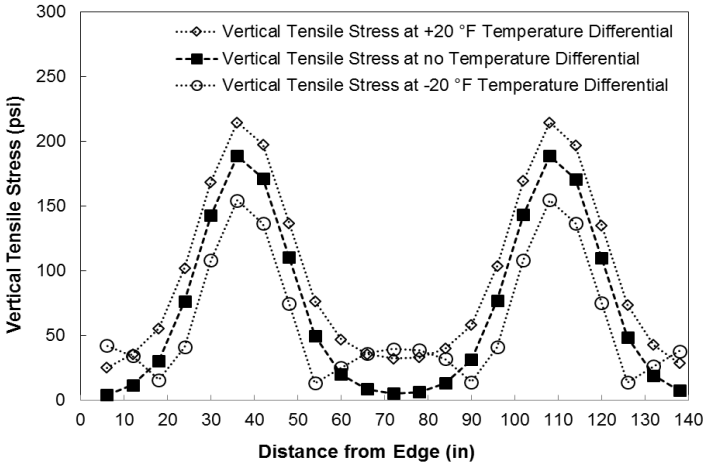

(b) Slab center loading at transverse crack

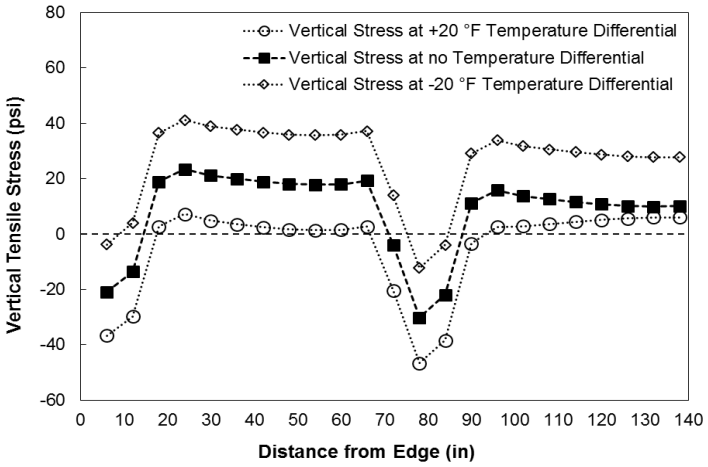

(c) Slab edge loading between transverse cracks

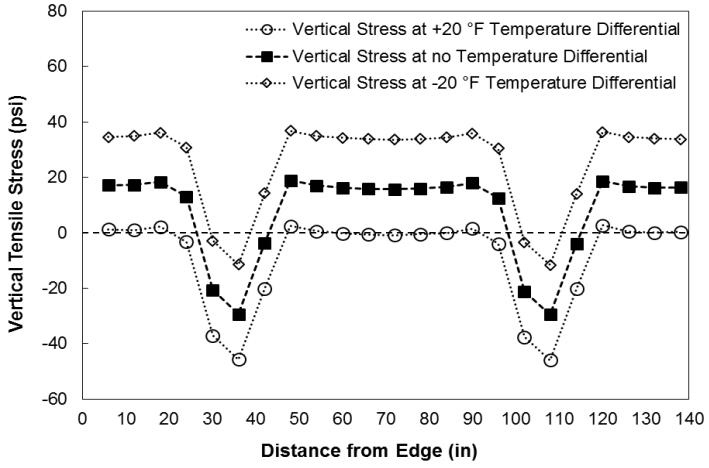

(d) Slab center loading between transverse cracks

Figure 5-5. Computed vertical tensile stresses at the depth of steels

5.5 Effects of Concrete Properties

5.5.1 Effects of Coefficient of Thermal Expansion

The 3-D finite element model was also used to evaluate the effects of coefficient of thermal expansion on the maximum tensile stresses in CRCP under the critical loading condition, when the load is applied to the corner of the slab as formed by the transverse cracks with a temperature differential of +20°F (+11.1°C). The effects of the coefficient of thermal expansion of the pavement concrete ranging from 5.0×10^{-6} to 7.0×10^{-6}°F (9×10^{-6} to 12.6×10^{-6}°C) on the maximum induced vertical stresses were analyzed. For comparison purpose, the vertical tensile stresses due to environment loading only were also calculated. Using the different values of the coefficient of thermal expansion, the maximum vertical stresses at the depth of steel were calculated and presented in Figure 5-6. As expected, the maximum vertical tensile stresses increase as the coefficient of thermal expansion increases. However, the effects of coefficient of thermal expansion on the environmental tensile stresses are much higher than those on the tensile stress caused by the critical combined temperature-load effects, even though the magnitude of environmental stress is much lower than that caused by the combined temperature-load effects.

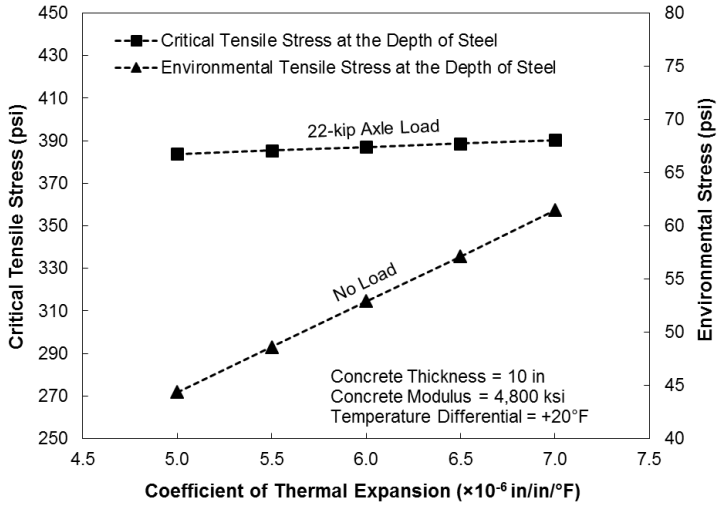

Figure 5-6. Effects of coefficient of thermal expansion on maximum vertical stresses at the depth of steel

5.5.2 Effects of Concrete Modulus

The effects of elastic modulus of concrete on the maximum vertical stresses were analyzed. The maximum vertical tensile stress in the slab caused by a 22-kip (98 kN) single axle load at the edge of the transverse crack at a temperature differential of +20°F (+11.1°C) were computed. Figure 5-7 shows the maximum vertical tensile stresses as a function of elastic modulus of concrete. It can be seen that the calculated maximum stress increases by around 4.7% when the elastic modulus increases from 4,000 to 6,000 ksi (27.6 to 41.4 GPa).

However, an increase in elastic modulus of the concrete is usually accompanied by an increase in its flexural strength when the same aggregate is used. In order to evaluate the possibility for the concrete to crack at the various conditions, the maximum computed tensile stresses were divided by the flexural strength of concrete to obtain the stress-to-strength ratio. In this study, the flexural strength of the concrete was related to its elastic modulus and unit weight by the following equation for a Florida concrete made with a Florida limestone (Tia et al. 1990):

$$MR = \frac{E}{4.2 \times w^{1.5}} \tag{5.1}$$

Where, E = elastic modulus, in psi

MR = flexural strength, in psi

w = unit weight, in pcf

Using this equation and a unit weight of 145 pcf (2,323 kg/m3), the concrete flexural strengths at various values of elastic modulus were calculated, and the stress-to-strength ratios were also plotted against the concrete elastic modulus in Figure 5-7. It can be noted that the maximum stress-to-strength ratio decreases as the concrete modulus increases. Decrease in stress-to-strength ratio with increase in modulus can be explained by the increase in flexural

strength which can be obtained by using a lower water-cement ratio in concrete mixture. However, it must also be noted that if a different type of aggregate is used to produce a concrete of lower elastic modulus without a decrease in strength, the use of a low- modulus concrete can give a lower stress-strength ratio and a lower horizontal cracking potential.

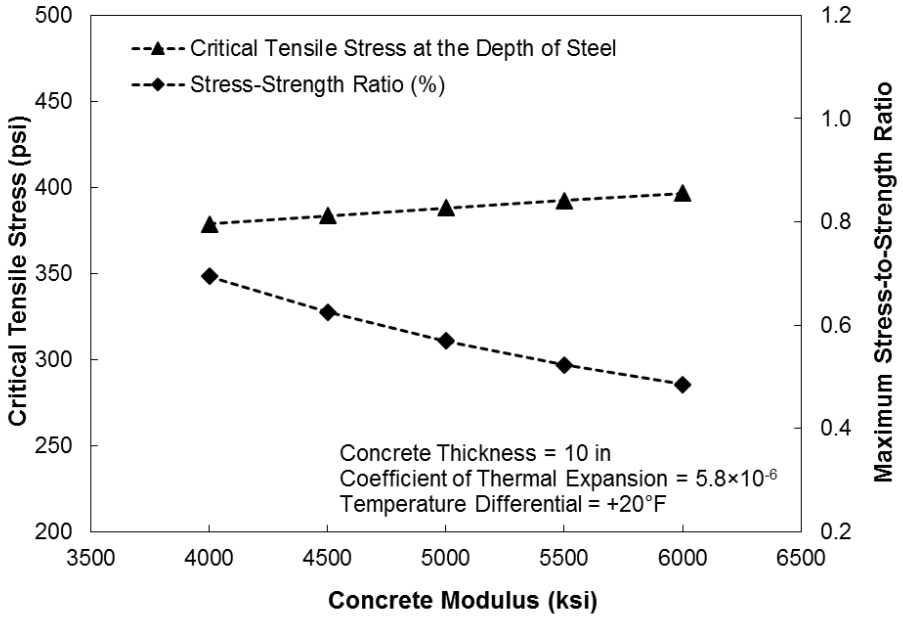

Figure 5-7. Effects of concrete modulus on maximum vertical tensile stresses in CRCP under critical temperature-load condition

5.6 Effects of Structural Design Parameters

5.6.1 Effects of Base Layer Modulus

The effects of base layer modulus on maximum vertical tensile stresses in CRCP were analyzed. The maximum vertical tensile stresses in the concrete slabs were computed using the same critical loading condition and environmental condition. The base modulus was varied from 50 ksi to 400 ksi (0.35 GPa to 2.76 GPa). Figure 5-8 shows the plots of vertical tensile stresses in concrete as a function of base modulus. It can be noted that the maximum vertical tensile stress decreases as the base modulus increases under critical loading condition. Conversely, the environmental stresses increase slightly as the base modulus increases.

In the case of critical temperature-load condition, the slab edge deflects down into the base layer due to traffic load and curling movement, which causes the base reaction near the transverse crack. The magnitude of base reaction at the transverse crack varies depending on the stiffness of the base layer. The higher reaction force near the transverse crack causes less bending deflection which results in less vertical tensile stresses in concrete near the longitudinal steel.

In case of the environmental loading condition, the maximum tensile stress increases slightly as the base layer stiffness increases. Since a higher stiffness of base layer may result in smaller supporting area and higher force exerted by the weight of unsupported slab region, which causes the higher vertical tensile stress near the steel. Thus, a softer base may offer more uniform slab support resulting in lower tensile stresses in the concrete slab due to self-weight force.

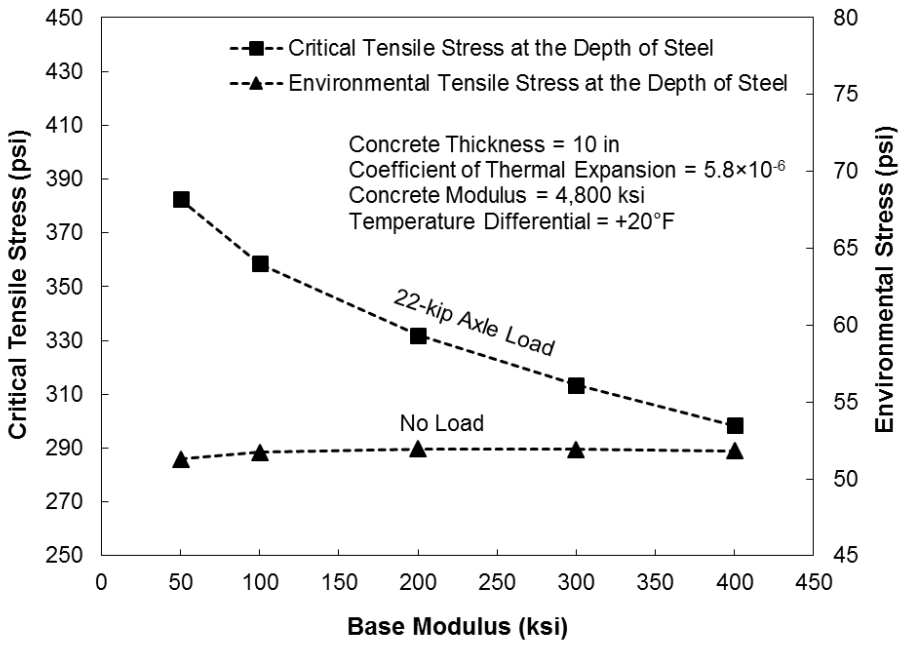

Figure 5-8. Effects of subgrade stiffness on maximum vertical stresses in CRCP under critical temperature-load condition

5.6.2 Effects of Base Friction

The frictional force between the concrete slabs and the base layer is an important factor in the early development of CRCP cracks. In the case of transverse cracks, numerous investigations have looked into the effects of slab-base friction on CRCP, but little research has been found regarding base friction on horizontal cracking in CRCP. The base friction coefficient was varied from 0.9 to 2.2. Figure 5-9 shows the plots of maximum vertical tensile stresses in concrete slab at the depth of steel as a function of the coefficient of slab-base friction. The sensitivity study indicated that changes in base friction had very little effect on the environmental tensile stresses, while the maximum tensile stresses caused by critical temperature-load effects decrease as the base friction increases. This can be explained by the fact that the frictional force increases as the coefficient of base friction increases, which results in decrease of slab movements near the transverse crack under the critical temperature-load condition. As a result, the vertical tensile stresses also decrease. Based on the above observation, it appears that the horizontal cracking potential deceases with an increase in base friction.

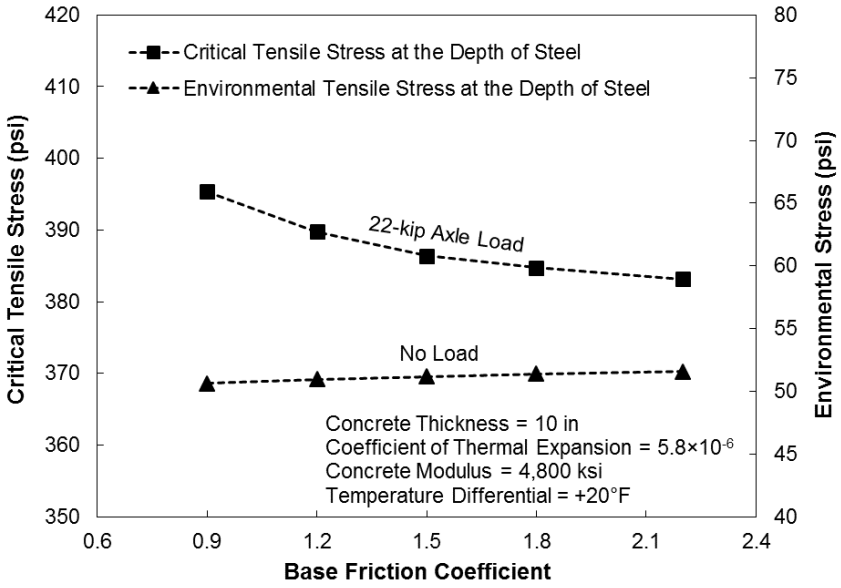

Figure 5-9. Effects of base friction on maximum vertical stresses in CRCP under critical temperature-load condition

5.6.3 Effects of Concrete Slab Thickness

The effects of slab thickness on maximum vertical stress in CRCP were analyzed and presented in Figure 5-10. Obviously, increasing thickness reduces the vertical tensile stress at the depth of steel. The calculated vertical tensile stresses decrease by approximately 23% when the concrete slab thickness increases from 10 in. to 13 in. (254 mm to 330 mm).

In addition to the vertical tensile stress, the principal tensile stress was also evaluated since the cracks occur in perpendicular direction to the principal stress vectors. The maximum principal stress vectors were perpendicular to the direction of longitudinal steel, which indicates that horizontal cracking was likely to occur at the half depth of slab in the longitudinal direction. As expected, the maximum principal stress also decreases as the thickness of concrete slab increases.

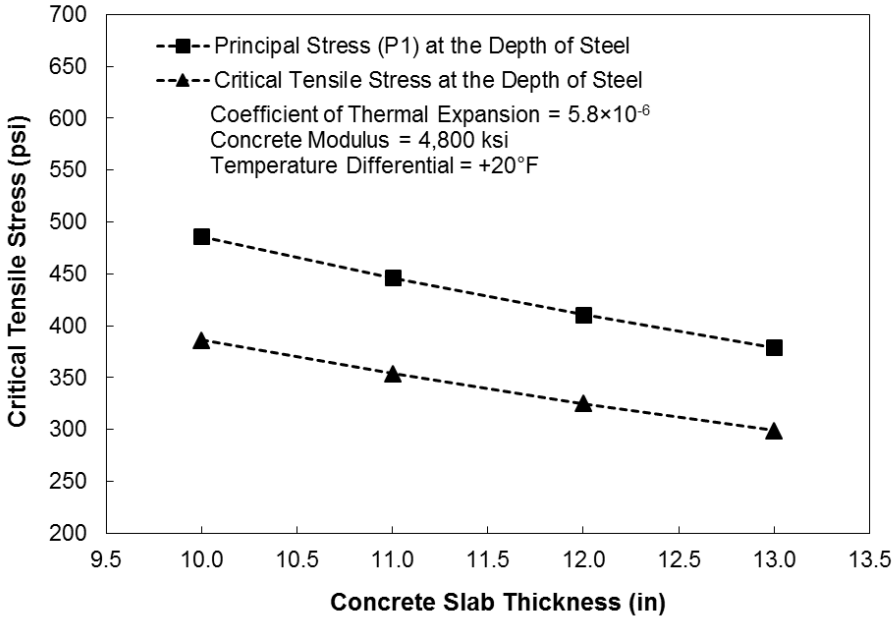

Figure 5-10. Effects of concrete slab thickness on maximum vertical stresses in CRCP under critical temperature-load condition

5.6.4 Effects of Transverse Crack Spacing

As shown in the previous results, the maximum vertical stresses develop at the location of transverse cracks. The LTPP data for CRCP sections show a spectrum of transverse cracking varying from 0.25 ft to 10 ft (0.08 m to 3 m) and mean crack spacing values vary between 1 ft and 7.5 ft (0.3 m and 2.3 m) (Selezneva et al. 2003). The effects of the transverse crack spacing ranging from 3 ft to 10 ft (0.9 m to 3 m) on horizontal cracking were analyzed. Using the different values of crack spacing, the maximum vertical tensile stress and principal stress were calculated and presented in Figure 5-11. The critical stresses were reduced slightly when the transverse crack spacing increased. Variations in the transverse crack spacing can be noted to have relatively minimal effect on the horizontal cracking.

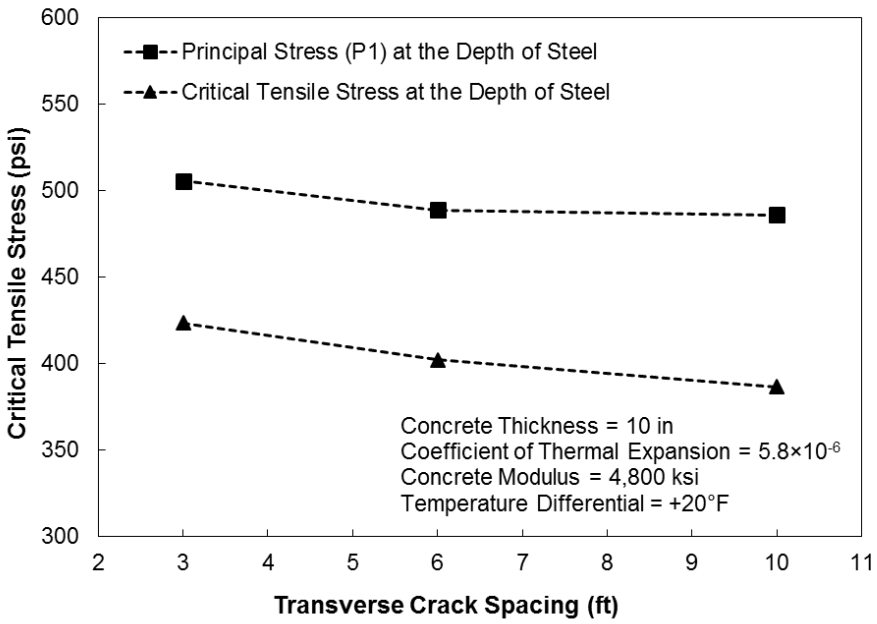

Figure 5-11. Effects of transverse crack spacing on maximum vertical stresses in CRCP under critical temperature-load condition

5.7 Effects of Longitudinal Steel Design

The effects of longitudinal steel design on the horizontal cracking potential were analyzed. Previous study (Choi et al. 2011; Won et al. 2002) found that a two-mat steel bar has the advantages in preventing horizontal cracking. However, the two-mat placement requires more materials or labor in implementation. In this study, the effects of the longitudinal steel spacing ranging from 3 in. to 12 in. (7.62 cm to 30.48 cm) on horizontal cracking potential were analyzed. Using the different longitudinal steel spacing, the maximum vertical tensile stresses were calculated and presented in Figure 5-12. The vertical tensile stresses were significantly reduced when the steel spacing was reduced. In addition, the analysis results indicated that the vertical tensile stress in the region far away from the tire load was affected little by longitudinal crack spacing. From this result, it can be concluded that the use of varying longitudinal steel spacing can be one of the effective ways to reduce the horizontal cracking potential. For instance, the use of narrow steel spacing under wheel path and wide steel spacing for other region could be a possible solution without changing the steel ratio of the slab.

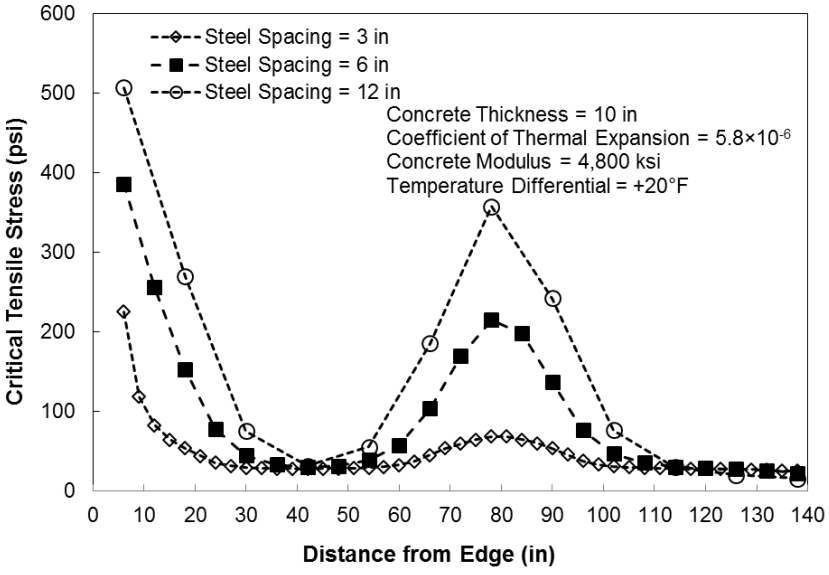

Figure 5-12. Effects of longitudinal steel spacing on maximum vertical stresses in CRCP under critical temperature-load condition

5.8 Conclusion and Recommendations

A 3-D finite elements model was developed to study the structural response of CRCP under typical Florida conditions. The model developed was used to perform a parametric analysis to determine the effects of important pavement parameters on the maximum induced vertical tensile stresses for estimating the horizontal cracking potential. The main findings are summarized as follows:

- The results of the analysis indicate that the critical load position is at the corner of slab formed by transverse cracks when the concrete slab has a positive temperature differential.
- The maximum vertical tensile stresses under the critical temperature-load condition is affected little by the coefficient of thermal expansion of the concrete.
- The maximum stress-to-strength ratio decreases as the concrete's flexural strength increases.
- The maximum vertical tensile stresses decrease as the base modulus increases under the critical temperature-load condition.
- The maximum tensile stresses decrease as the base friction increases under the critical temperature-load condition.
- Increasing slab thickness reduces the vertical tensile stress at the depth of steel.
- The critical vertical stresses decrease slightly when the transverse crack spacing increases.
- The vertical tensile stresses are significantly reduced when the steel spacing is reduced. In addition, the vertical tensile stress in the region far away from the tire load is affected little by the longitudinal steel spacing. From this result, the use of varying longitudinal steel spacing (i.e., small steel spacing under wheel path and wide steel spacing for other region) may be one of the ways to reduce the horizontal cracking potential in CRCP.

The following procedures are recommended for analysis of CRCP to minimize horizontal cracking:

(1) Analyze the maximum vertical tensile stress at the depth of the longitudinal steel under critical temperature-load condition.

(2) Compare the maximum vertical tensile stress to flexural strength of the concrete used.

(3) If maximum tensile stress is greater than 50% of the flexural strength of the concrete, try to reduce it to 50% or less by the following options (Tia et al. 2012):

   (a) Reduce longitudinal steel spacing

   (b) Increase flexural strength of concrete

   (c) Increase base modulus

   (d) Increase slab thickness

CHAPTER 6
DEVELOPMENT OF A USER-FRIENDLY INTERFACE PROGRAM

6.1 Overview

In this chapter, improved analysis models have been developed for concrete pavements using the ADINA Software. The capabilities of the developed models include analysis of (1) jointed plain concrete pavement (JPCP) using RAP concrete, (2) precast prestressed concrete pavement (PPCP), (3) continuously reinforced concrete pavement (CRCP), and (4) JPCP with dowel joints where the dowel bars are modeled by their actual physical dimensions and properties. While the developed models have shown to be very effective tools, the application of these models requires the users to have a good knowledge of finite-element method, and the commands and procedures of the ADINA Software. There was a need to develop user-friendly interface software and guides, so that someone without extensive training in finite-element method or the ADINA Software can also perform the analysis using these developed models. To meet this need, a user-friendly interface software, named AIFG (ADINA Input File Generator) was developed for use in the analysis of JPCP. User-friendly guides were also developed for ADINA input files for analysis of PPCP, JPCP, CRCP, and JPCP with dowel joints as presented in APPENDIX A.

6.2 ADINA Input File Generator for JPCP

6.2.1 Overview of AIFG

A user-friendly software named "ADINA Input File Generator" (AIFG) was developed using the MATLAB programming language to prompt the user for the required information for analysis of a jointed plain concrete pavement (JPCP). AIFG will then generate the input file for ADINA to perform the analysis of the JPCP. AIFG's interface screen is shown in Figure 6-1.

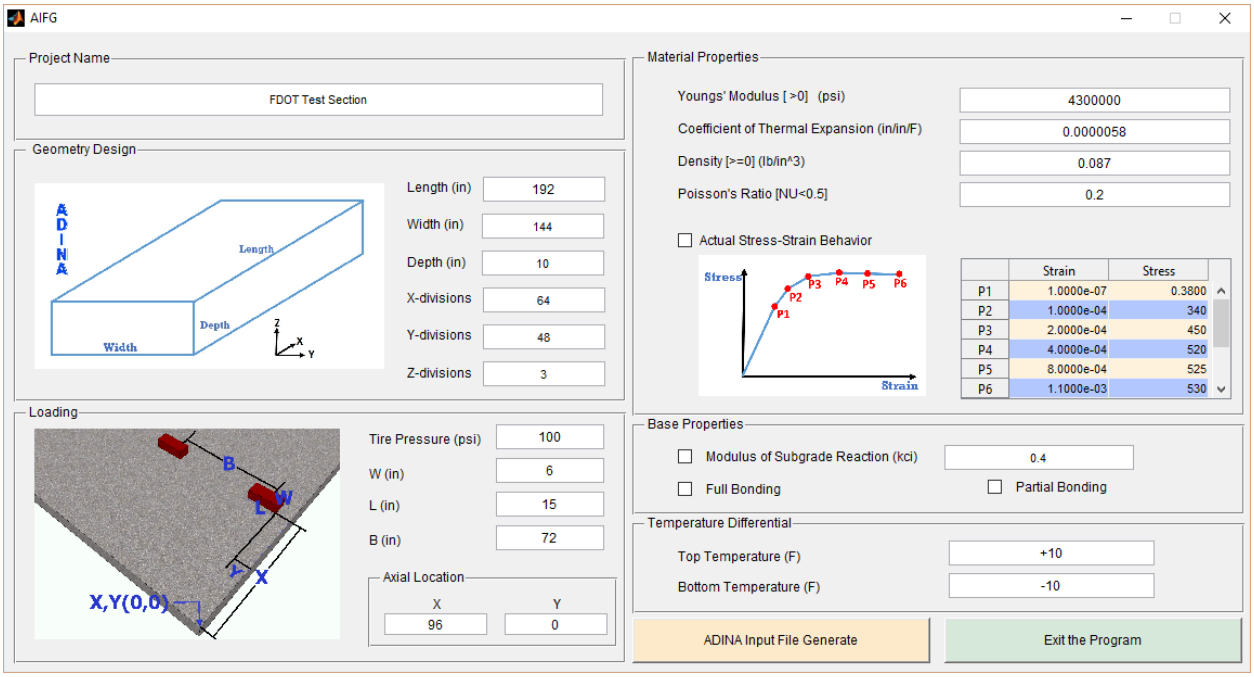

Figure 6-1. AIFG interface screen

Through the interface screen, the user inputs the following information:

(1) In the box "Geometry Design": the Length (x), Width (y), and Depth (z) of the concrete slab, and the numbers of divisions in the x, y, and z directions in the finite element mesh to be used.

(2) In the box "Loading": the Tire pressure, the Width (W) and Length (L) of the tire contact area, the distance between the two tires (B), and the location of the tire placement (X, Y).

(3) In the box "Material Properties": Young's modulus (E), coefficient of thermal expansion (CTE), density (ρ), and Poisson's ratio of concrete (ν); stress-strain relationship of concrete containing RAP.

(4) In the box "Base Properties": Modulus of Subgrade Reaction (ksi/ft), Full Bonding or Partial Bonding

(5) In the box "Temperature Differential"; Top and Bottom temperatures.

Finally, when all the parameters are determined and entered, the user may click the "Generate" button to start the generating of an ADINA input file. The user can specify the input file name of concrete pavement being modeled for ADINA in the "Project Names" box. The file

name must have the extension of ".in". After the save location has been set up, AIFG will set up the ADINA 9.0. environment and automatically create an ADINA input file. If the generating process is successfully completed, the input file will be shown in the folder which the user has created.

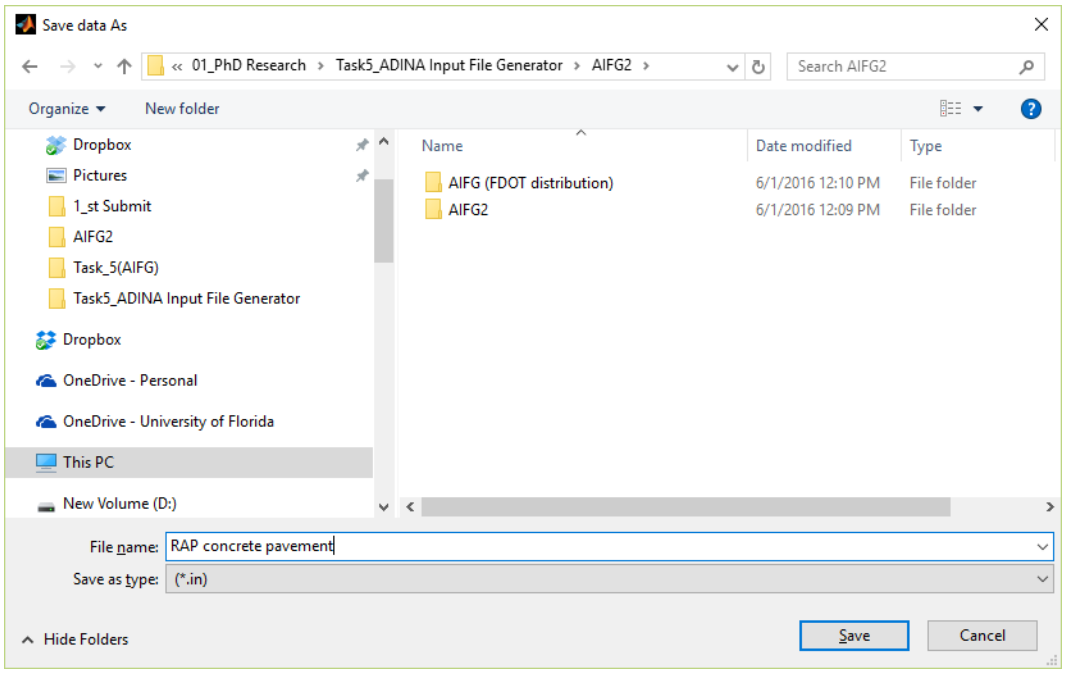

Figure 6-2. Browsing an ADINA input file

6.2.2 An Example of Inputting Data for Analysis of JPCP using AIFG

A concrete slab containing RAP is to be modeled and analyzed to illustrate the use of AIFG and ADINA. The slab has the dimension of 12ft by 16 ft with 10 in. thickness. The steps to create the finite element model using AIFG are as follows:

- Step 1: Enter a length of 192 in. (in x-direction), a width of 144 in. (in y-direction), and a depth of 10 in. (in z-direction) in Box A (see Figure 6-3).
- Step 2: Enter 64, 48, and 3 for divisions in x, y, and z-directions in Box B. This will create 64 × 48 × 3 = 9,216 elements for the concrete with size of 3 in. × 3 in. × 3.3 in.
- Step 3: In Box C, enter 100 psi for the Tire Pressure with contact area of 6 in (W) × 15 in (L) and distance of 72 in (B) between tires.

- Step 4: Enter the location of Axle Load Location in Box D. To apply the tire loads at the mid-edge of the slab, enter the “96” and “0” in X and Y coordinates, respectively.

- Step 5: Enter the concrete properties including Young’s modulus, coefficient of thermal expansion, density (lb/in^3), and Poisson’s ratio in Box E.

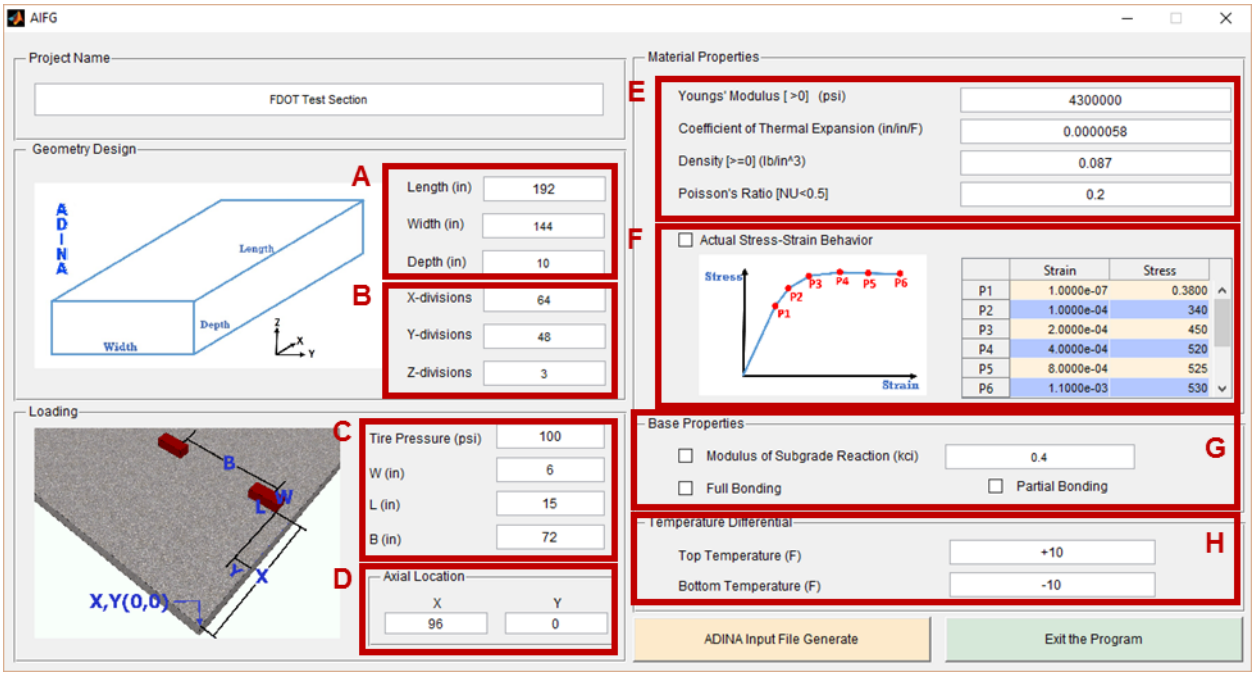

Figure 6-3. Input parameters for AIFG

- Step 6: If the concrete slab is made with RAP, check the “Actual Stress-Strain Behavior” check box and fill out the stress-strain values obtained by the flexural strength test in Box F. If it is normal concrete, please ignore this step.

> Note: When analyzing a concrete slab containing RAP, the Modulus of Elasticity must be obtained from the slope of point 0 and 1 in the stress-strain curve.

- Step 7: Enter Modulus of Subgrade Reaction (ksi) in Box G and select the bonding condition. The force-displacement relationship of the springs will be calculated and applied automatically in Winkler foundation. For instance, the compressive stiffness of each spring would be 3,600 lbf/in, which was calculated form the modulus of subgrade reaction (4.8 ksi/ft) and the effective area (element size of 3× 3 in.) supported by each

spring as given by the following equation: $K = 0.4\ kci \times 1000 \times 3\ in \times 3\ in = 3{,}600\ lbf/in$.

- Step 8: Enter the top and bottom temperatures of the slab in Box H.
- Step 9: Click the "ADINA Input File Generate" button. Enter or brows a file name of the FE model. AIFG will generate an ADINA input file with a file name extension of "*.in". After that, run ADINA by follow the steps described in Section 3.

6.3 User's Guide for Running ADINA and Post-processing

6.3.1 Running ADINA

Once the ADINA input file is generated, it is ready to be used in ADINA. The user should run the ADINA Software using the following steps:

- Choose programs → ADINA System → ADINA User Interface (AUI)
- From the drop down menu, select "ADINA Structures" to prepare for preprocessing (see Figure 6-4)
- Click "Open" icon and select the ADINA input file that has been generated, then click "Open"

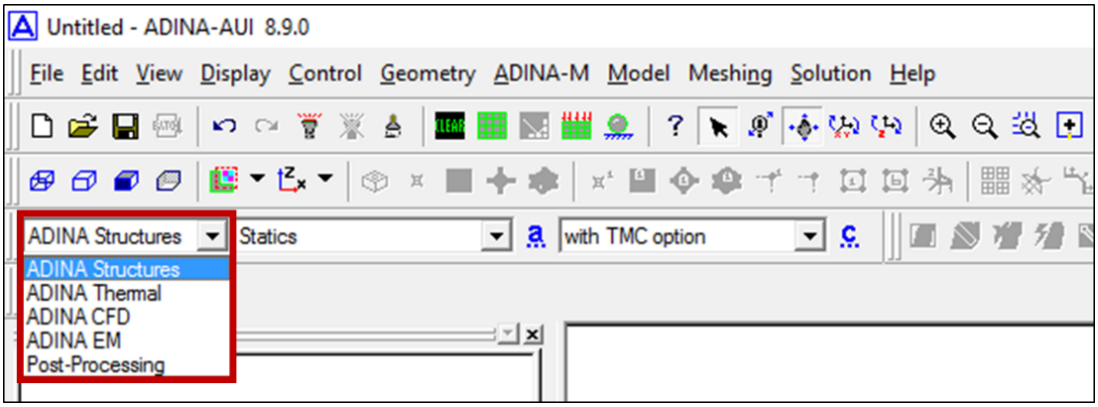

Figure 6-4. Selection of ADINA structures to start preprocessing

After reading input is completed, ADINA will then show a pavement model to be analyzed as shown in Figure 6-5.

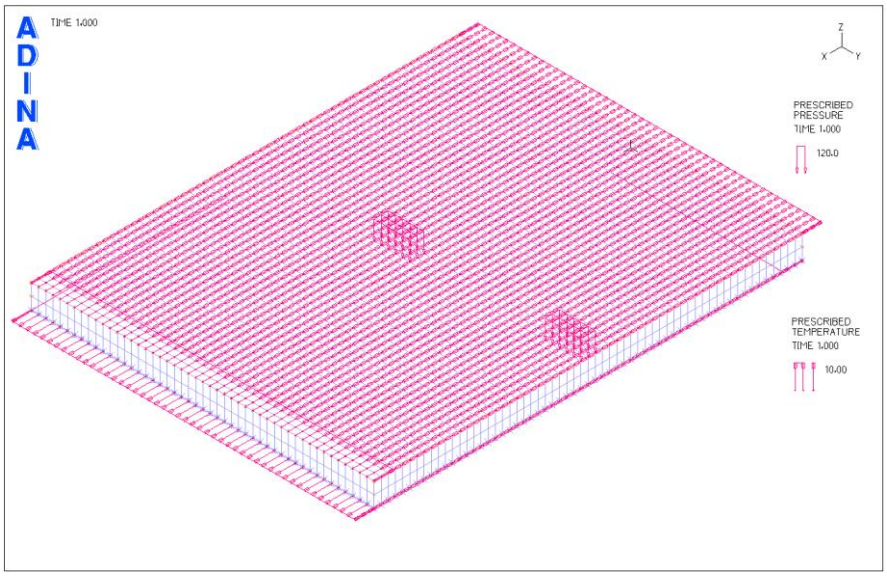

Figure 6-5. Pavement model shown after input file is opened

To check the boundary condition applied in the model, click the Boundary Plot icon . If the mesh is not visible, rotate the mesh out-of-plane with the mouse to check if the boundary conditions are applied or not. The graphics window should look like Figure 6-6.

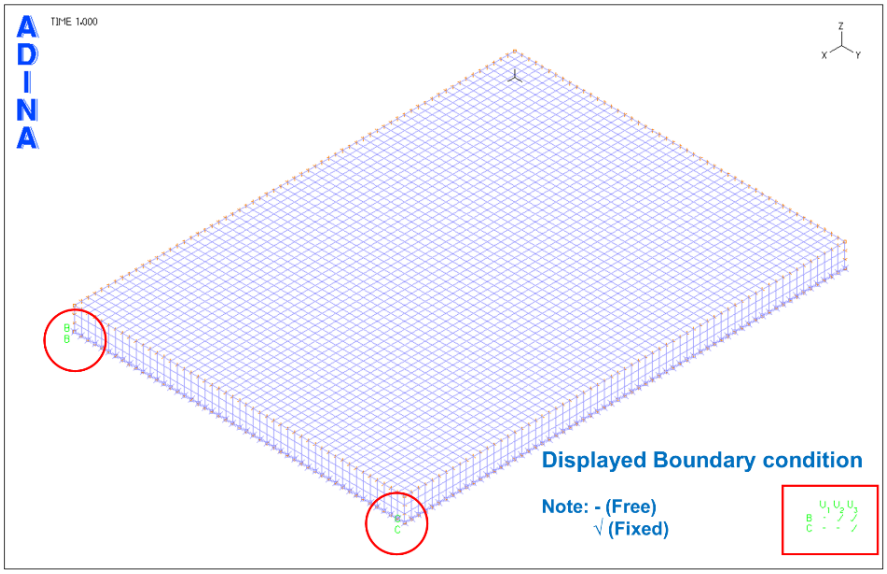

Figure 6-6. Boundary conditions applied in the FE model

- Click the Load Plot icon  to check the load type, location of tire footprint, and temperature differential.

- If changes have been made, click the Save icon  and to save the database to file (the "File type" should be "ADINA-IN Database Files (*.idb)").

- Click the DATA File/Solution icon  to run ADINA.

- If the generating process is successfully completed, a message will be shown by the software as shown in Figure 6-7.

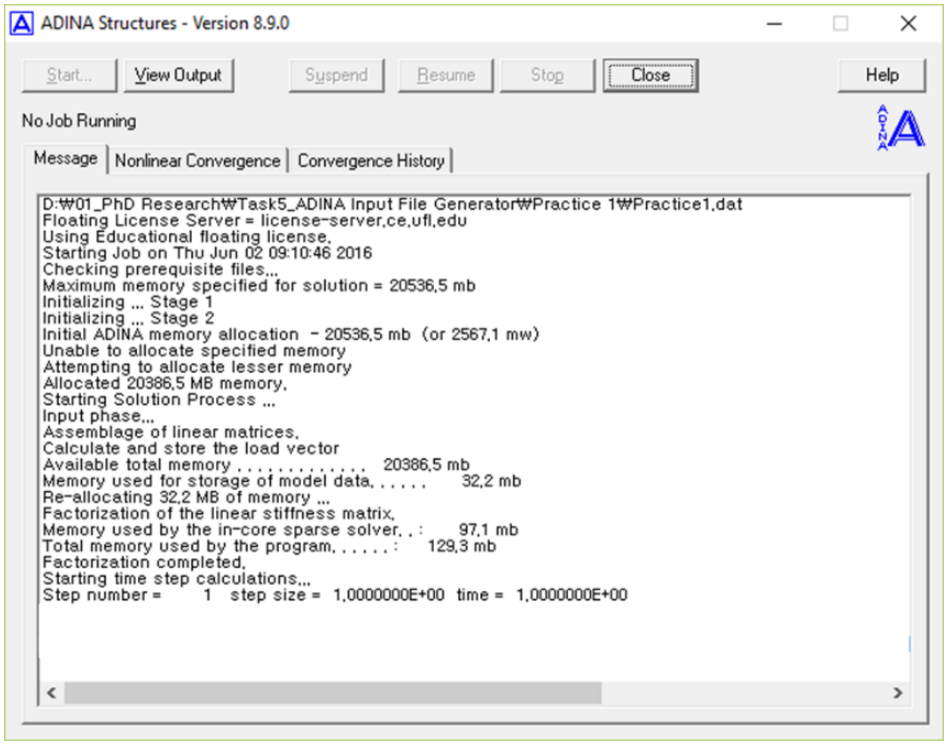

Figure 6-7. Message during generating process

When ADINA is finished with the solution process, it displays the message "Solution successful, please check the results" and a message will pop up as shown in Figure 6-8. It takes several minutes, depending on the size of the FE model.

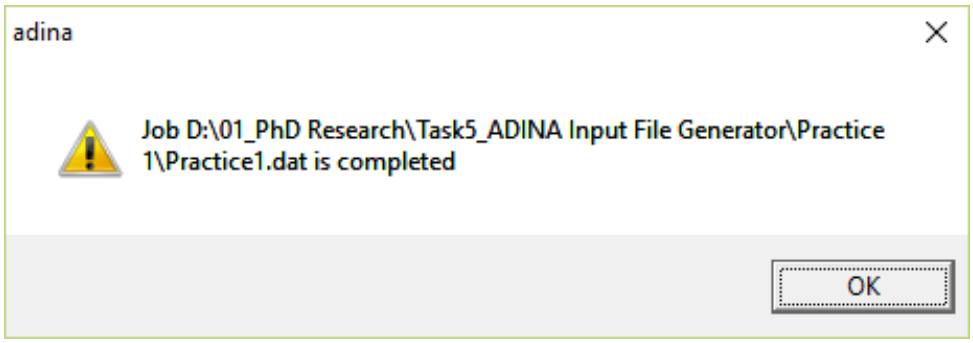

Figure 6-8. Message indicating the solution is completed

6.3.2 Results and Post-processing in ADINA

After ADINA is finished with the solution process, choose "Post-processing" from the program module drop-down list as shown in Figure 6-9, and then click "Yes".

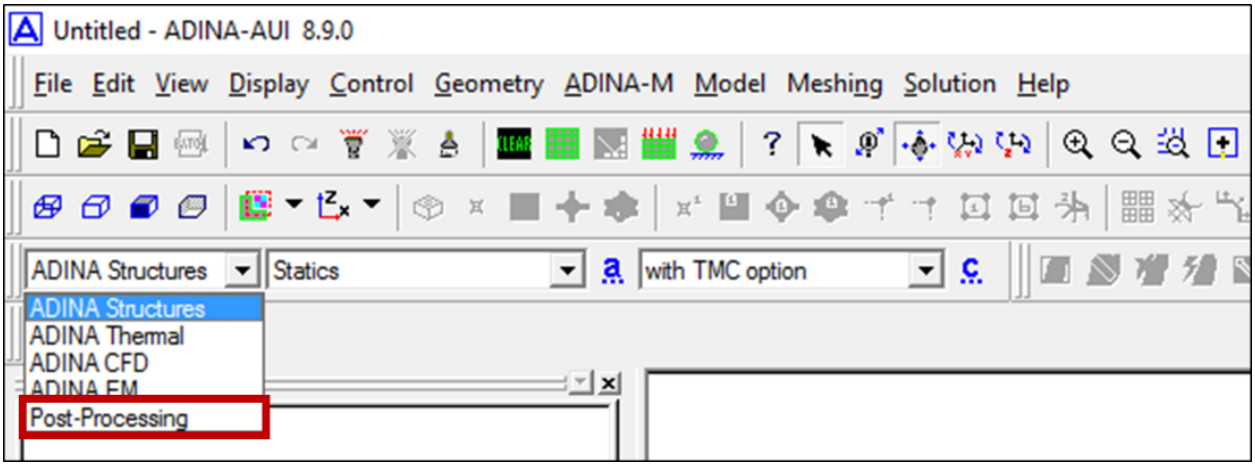

Figure 6-9. Selection of post-processing module

To view the analytical results, click the Open icon  and open porthole file with file extension of "*.por". The visualized model will appear as shown in Figure 6-10.

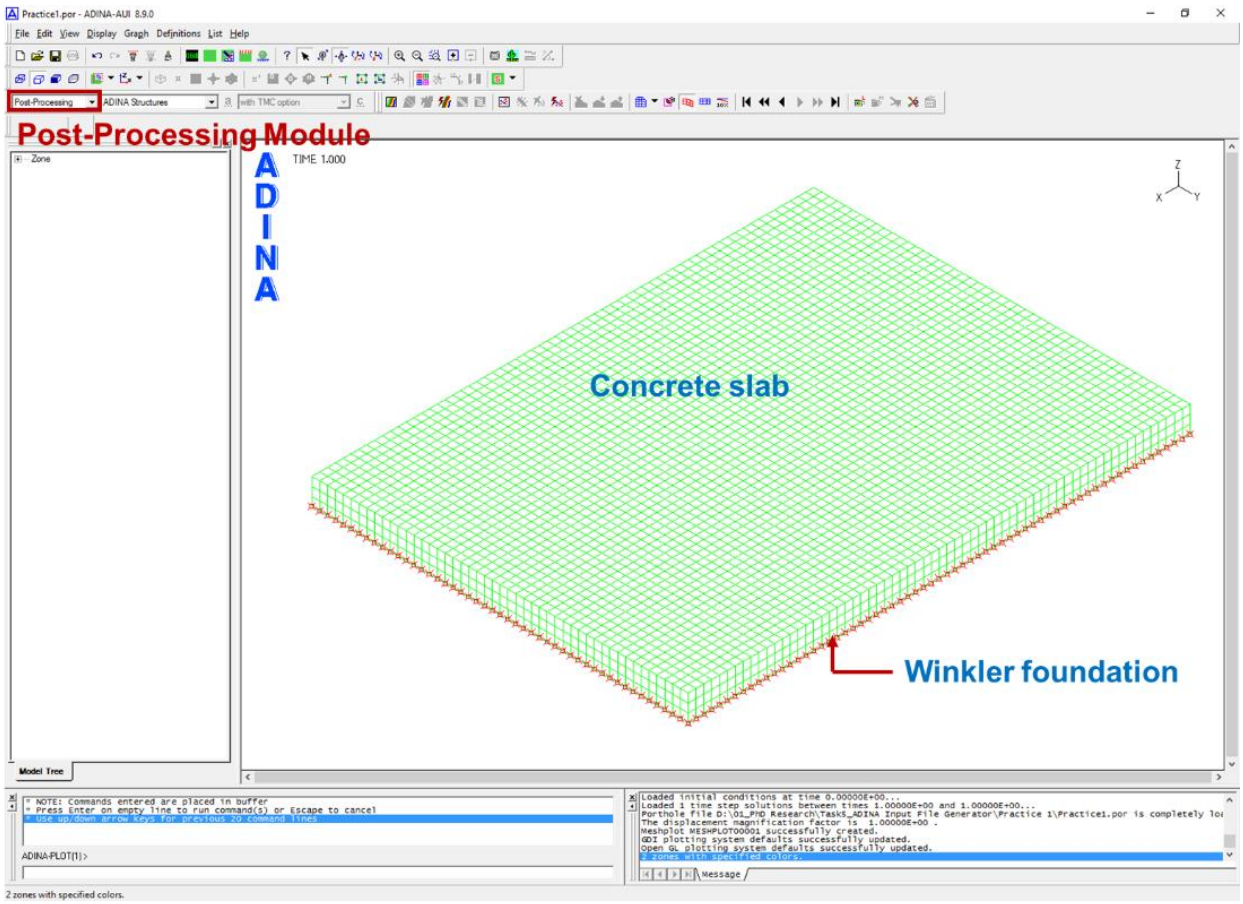

Figure 6-10. FE model solved by ADINA

6.3.2.1 Plotting the Stress Diagram

Click the Create Band Plot icon  to see the longitudinal stress distribution, and then set the Band plot Variable to (Stress: Stress-XX). The graphics window shows the stress distribution due to combined temperature and tire loads (see Figure 6-11).

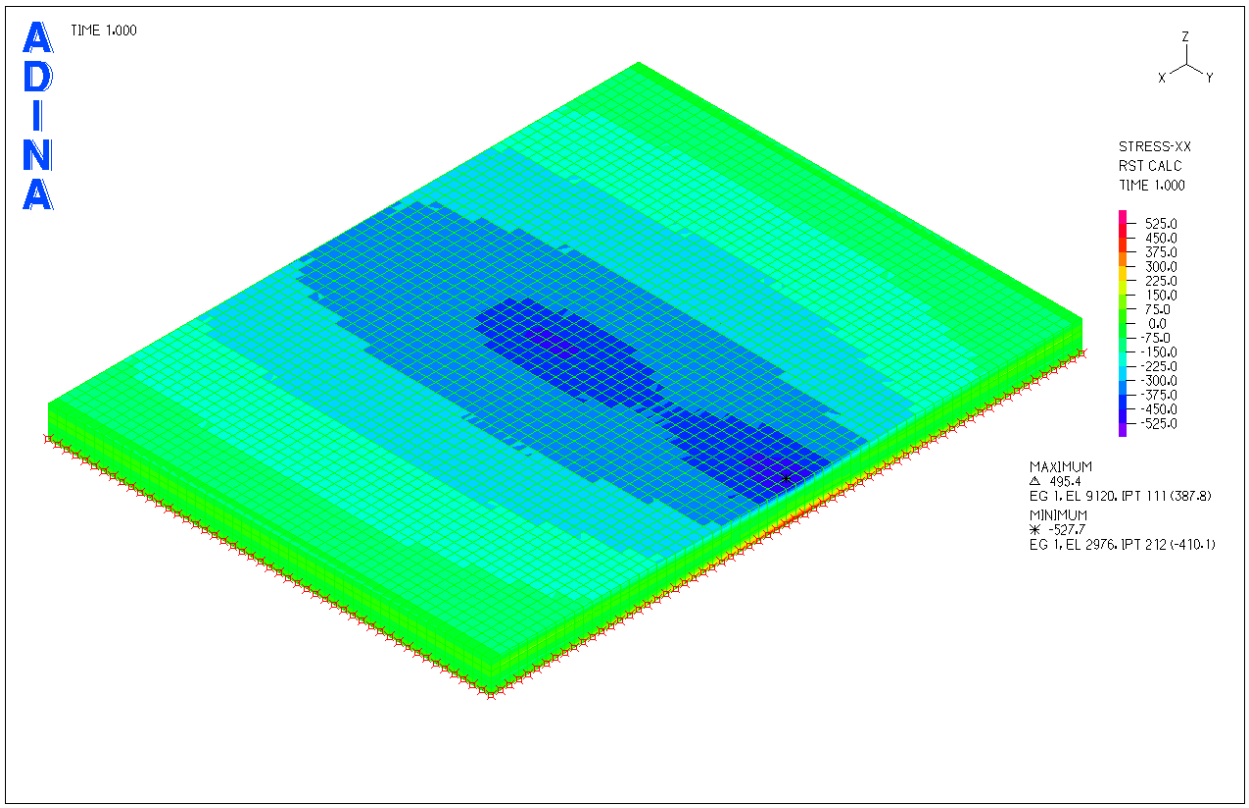

Figure 6-11. Longitudinal tensile stress distribution

The user will notice that the maximum and minimum stress along with the corresponding element numbers are also provided in the graphics window.

6.3.2.2 Results Along a Transverse Center Line

The user would like to examine the results along a transverse centerline to examine the stress distribution due to the tire load. Choose Definitions → Model line → Stress Classification Line; add line TRANSCENTER, and set model line coordinates as shown in Figure 6-12. Then choose Display → Result Line Plot → Create, and click OK. The model line will be shown in the graphics window as illustrated in Figure 6-13.

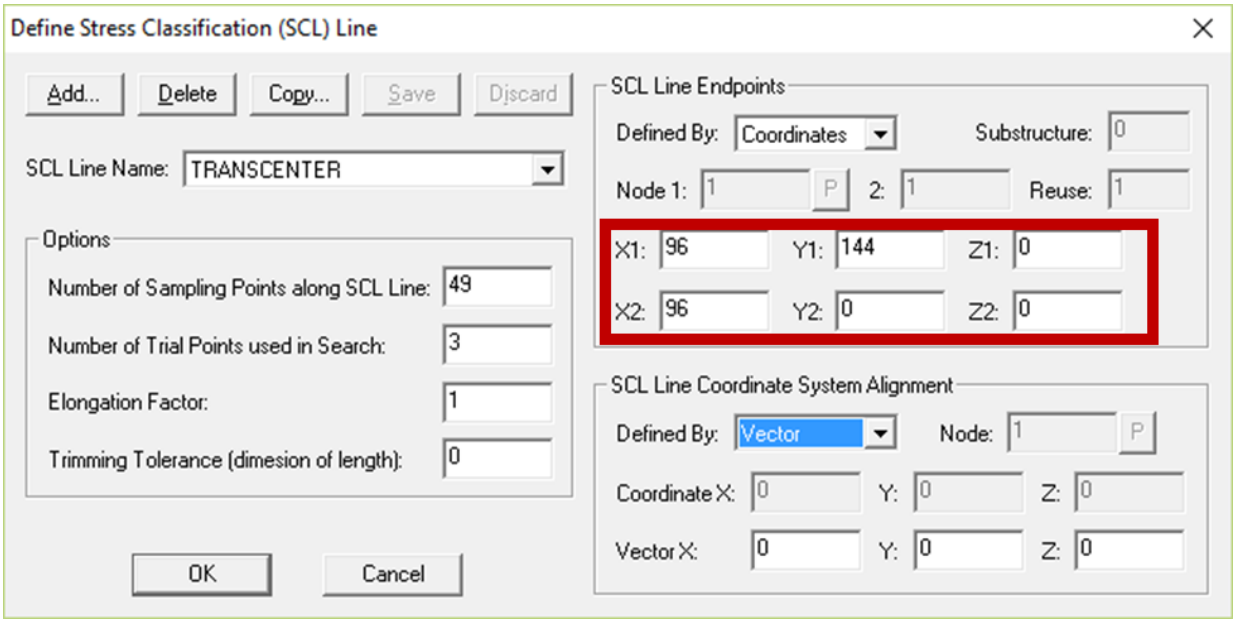

Figure 6-12. Model line coordinate setup

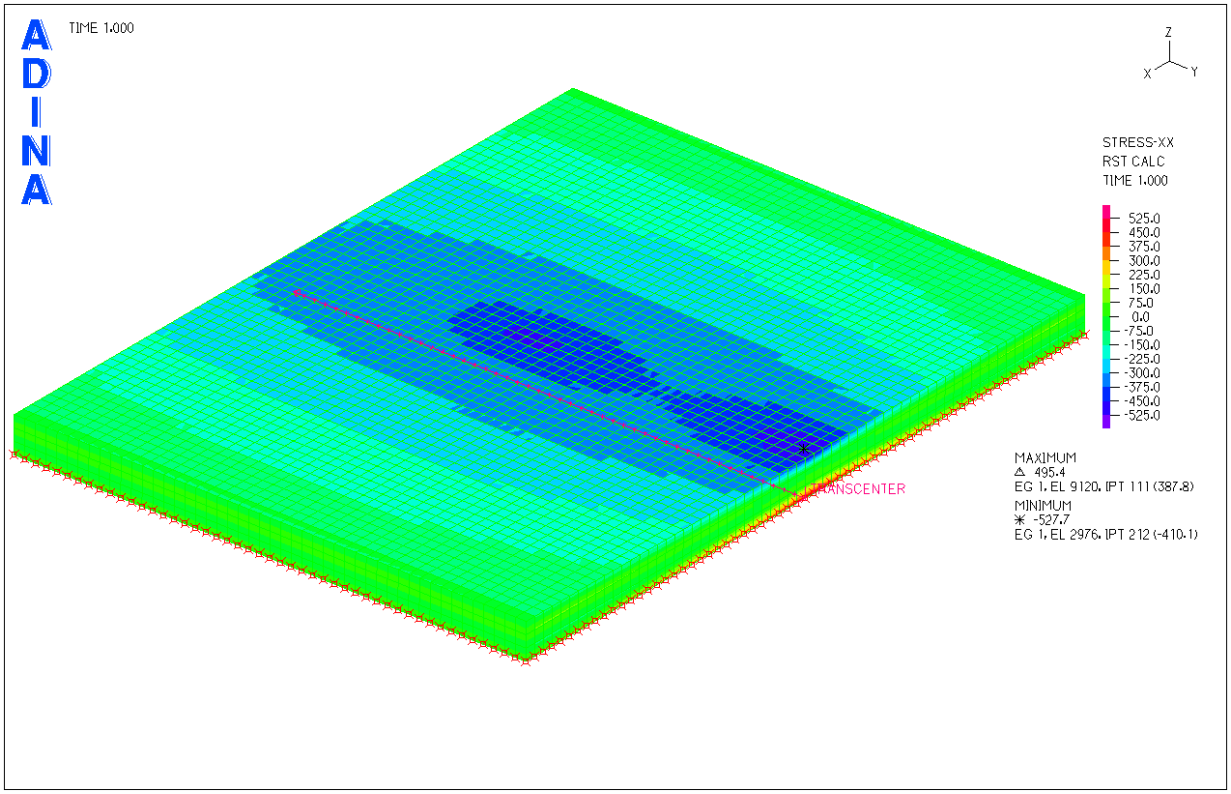

Figure 6-13. Model line generated in ADINA

Now, click the Clear icon CLEAR, choose Graph → Response Curve (Model Line); set the X Coordinate Variable to (Coordinate: DISTANCE), and set the Y Coordinate Variable to (Stress: STRESS-XX). The longitudinal stress along the transverse center line will be shown in the graphics window as shown in Figure 6-14.

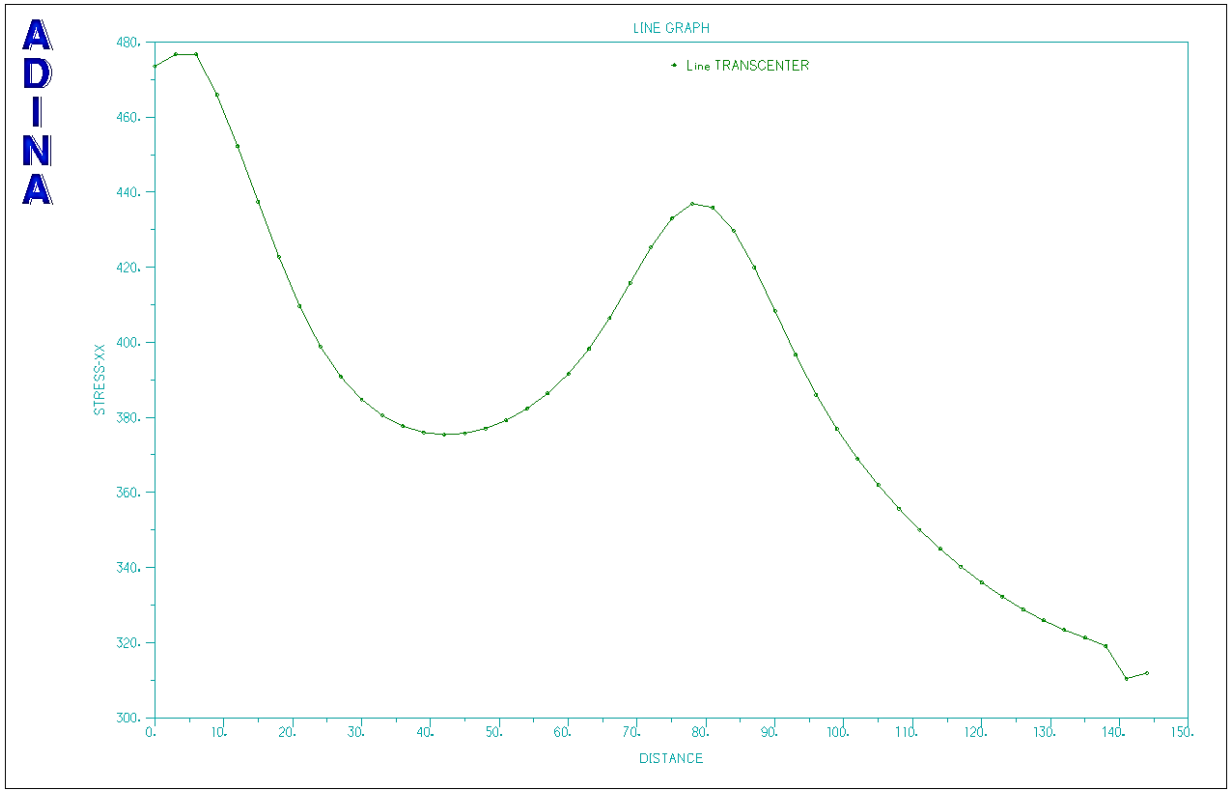

Figure 6-14. Plot of longitudinal tensile stresses along the transverse centerline

The user would like to get these stress values for further examination or presentation purpose. To get these stress values, choose List → Value List → Model Line; set the Variables to List (Stress: STRESS-XX). ADINA will show the actual stress values, as shown in Figure 6-15, and the user can copy these numbers to paste into EXCEL or other programs for further analysis.

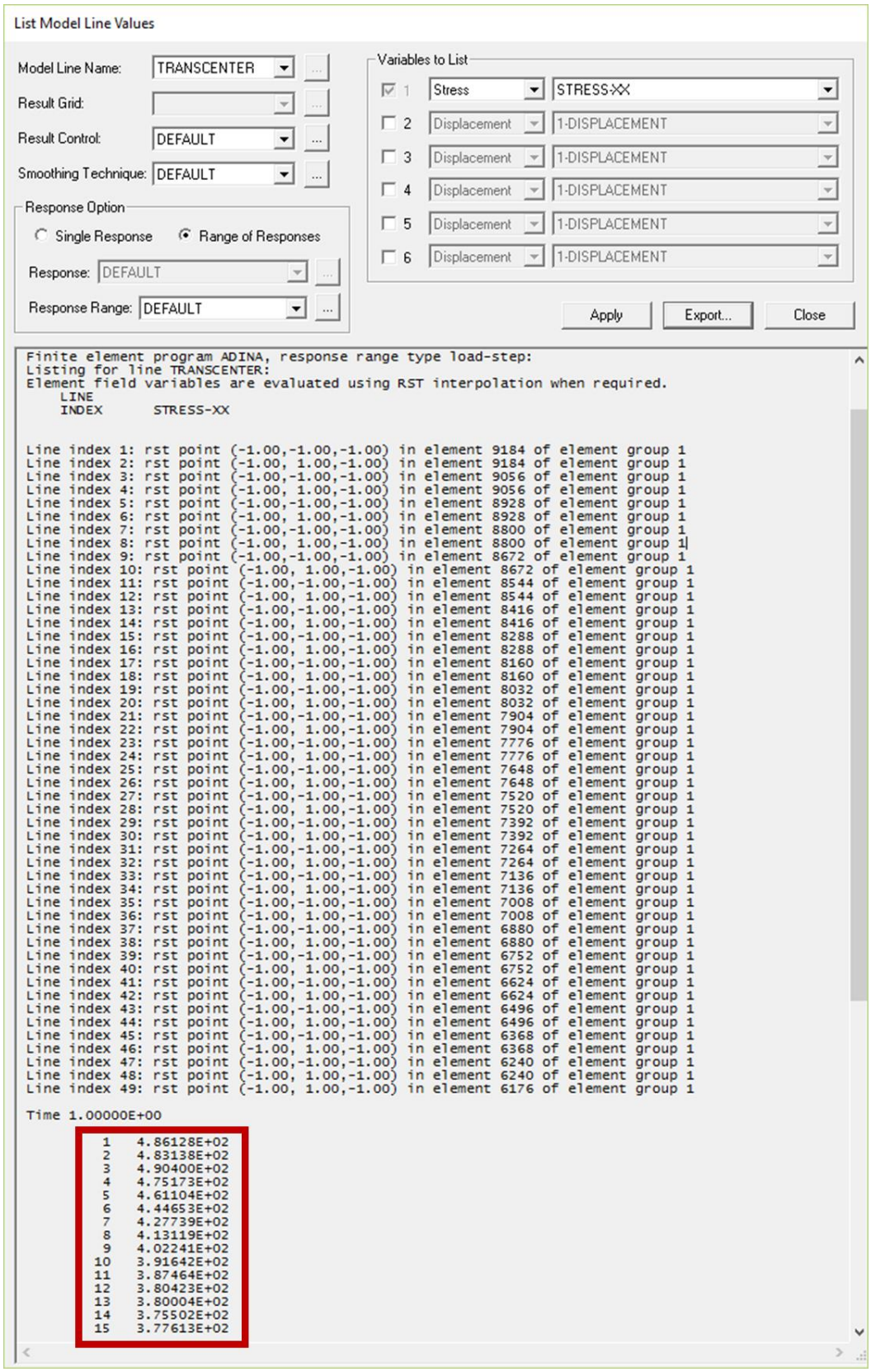

Figure 6-15. Longitudinal tensile stress values along the transverse centerline

6.3.2.3 Displaying the Deformed Model

The user would like to examine the model deformation or displacement due to the applied loads. To examine the visualized results, click the Load Plot icon  to display the finite element mesh and loads, and then click the Scale Displacement icon  to magnify the displacements, or deformation of FE model as shown in Figure 6-16.

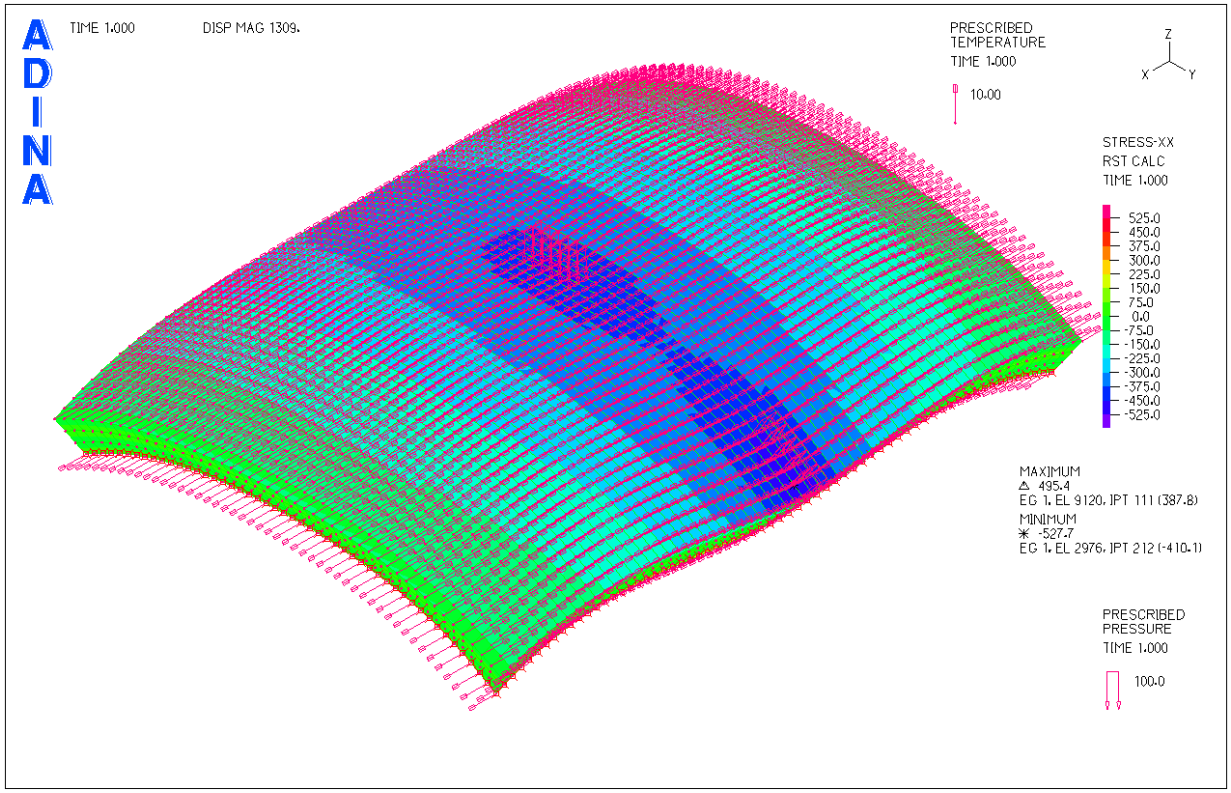

Figure 6-16. Magnified FE model deformation due to temperature-load condition

CHAPTER 7
LABORATORY STUDY TO EVALUATE THE PERFORMANCE AND SUITABILITY OF SENSORS

7.1 Background

Monitoring of strains at critical locations in concrete pavements can provide useful information regarding its structural behavior and performance. These strains can be caused by temperature variation, shrinkage, creep, and traffic loads. Data collected from the sensors installed in the test road can be used to develop new pavement designs, rehabilitation methods, and decision making for maintenance as well as to validate and verify analytical models by comparing the measured and calculated responses in terms of strain, stress, and deflections.

The most common type of sensor used in pavement instrumentation is the electrical resistance strain gauge, which has been successfully used for strain measurement due to their simplicity, low cost, and ease of installation. However, for real-time monitoring of pavement structures, it is required that these sensors employ long cables without compromising data quality, provide reliable data over a long time period (up to 10 years), and have limited susceptibility to damage from lightning strike for the geographic region and configuration of the road. One possible way to overcome this shortcoming in conventional resistance gauges is to use fiber optic sensors. The fiber optic sensors, have been introduced as an alternative to electrical resistance strain gauges and possess potential advantages including durability, reliability, high sensitivity, and electromagnetic immunity (Casas and Cruz 2003; Grattan and Sun 2000; Yehia et al. 2008).

Although several researchers have used and documented the response from fiber optic sensors, literature on the precision of these sensors in concrete pavement application is very limited (Rice and Lloyd 2014; Wang and Tang 2005). Though the fiber optic technology is advanced for accurately measuring an object's strain, the assessment of fiber optic sensor for use

in concrete has not been thoroughly done in comparison with electrical resistance strain gauges. Therefore, a laboratory study was conducted to evaluate these sensors' performance and behavior when embedded in concrete in terms of their accuracy, repeatability, and reproducibility. The different strain sensors to be evaluated were embedded in concrete specimens which were then subjected to the same and known static and dynamic loads, and their responses were compared to each other on the same basis. In addition to evaluating the response due to load, the measurements due to concrete drying shrinkage were also evaluated.

7.2 Overview of Instrumentation

At present, the most commonly used sensors for measuring strains in concrete pavements are vibrating wire gauges for long-term static strains, and electrical resistance strain gauges for dynamic strains. Fiber optic strain gauges have also been experimented. Each one of these types of strain gauges are discussed in this section.

7.2.1 Vibrating Wire Gauge

The vibrating wire strain gauges used for this study were purchased from Geokon Inc. The Geokon Model 4200 as shown in Figure 7-1 is primarily designed for long-term strain measurements as embedment type.

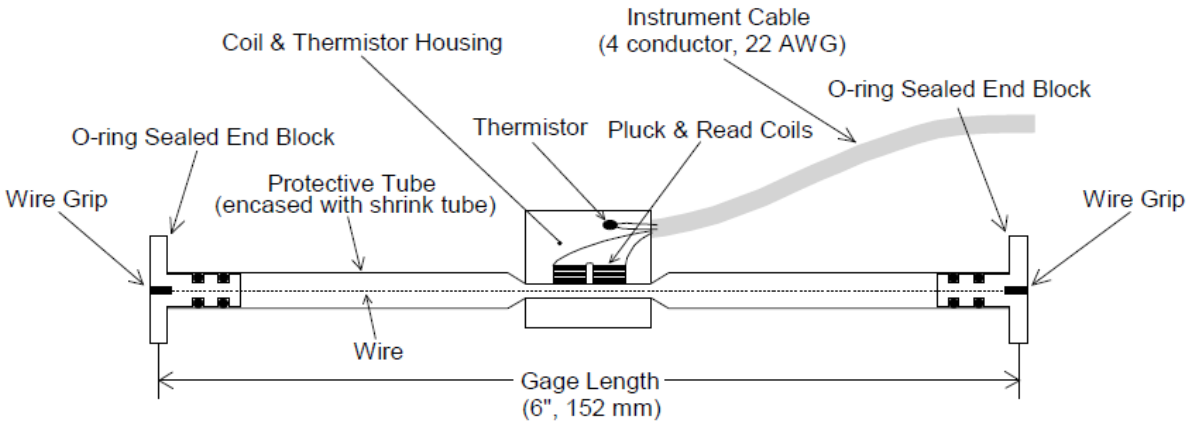

Figure 7-1. Model 4200 vibrating wire strain gauge (Geokon 2016)

The vibrating wire strain gauge consists of a tensioning cable, two end block, and an encasing tube. Strains are measured using the resonance frequency of the wire. Deformations in the concrete will cause an altering of the tension in the steel wire as well as changing the resonant frequency of vibration of the wire. Electromagnetic coils accomplish excitation and readout of the gauge resonance frequency. As the length of the wire inside the gauge also changes with temperature change, the readings are affected by changes in temperatures. Each vibrating strain gauge is also equipped with a thermistor which measures thermal changes. The strain reading can be corrected using the exact local temperature thermistor reading.

The main advantage of the vibrating wire strain gauge is that it can be used to measure long-term strain events, since it is based on the natural frequency of the wire which will not change with time. If the vibrating wire output is properly corrected, the reference reading can be used to correct the long-term strain variations. On the other hand, the resistance base gauges (conventional strain gauges) require an excitation voltage which may change over time. The output from an electrical resistance-based strain gauge system may contain an offset relative to the change in excitation voltage.

7.2.2 Electrical Resistance Strain Gauges

The principle of electrical resistance strain gauges is based on the fact that the change in resistance of a strain gauge corresponds to the change in length of the strain gauge. These tiny changes of resistance are measured by means of a Wheatstone bridge connection and in terms of an output voltage. In this study, three types of electrical resistance strain gauges were evaluated, namely the EPG-5-120, the EPG-5-350, and the KM-120-120-H2-11. The EPG-series strain gauges are manufactured by Miro-Measurement (Vishay Precision Group) and specially designed for measuring strains inside concrete. The KM gauge is manufactured by Kyowa and

designed for measuring interior strain in concrete or mortar. The body of the all gauges are sealed and specially treated to ensure adequate bonding between the gauge and the concrete.

One of the problems of the electrical resistance strain gauge is the lead-wire thermal effect because the lead-wires between the gauge and the strain-gauge bridge also change in electrical resistance strain gauge with changes in temperature. To eliminate the thermal effect from the gauge output, the three wire system was used. As shown in Figure 7-2, the 3-wire system has lead-wires connecting to the gauge side of the bridge and also to the adjacent side of the bridge. These lead-wires have the same change in electrical resistance strain gauge due to temperature change, and thus would balance each other out in the Wheatstone bridge circuit. Three lead-wire connections were used in this study.

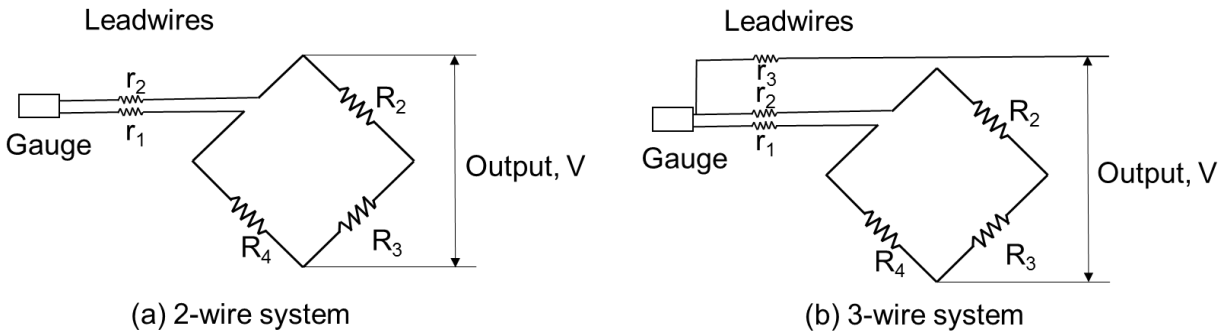

Figure 7-2. Comparison of 2-wire and 3-wire connections for electrical resistance strain gauge

7.2.3 Fiber Optic Sensor

In this study, the os3600 FBG fiber optic sensor manufactured by Micron Optics was evaluated. The os3600 is designed to be embedded in concrete and adhere to the concrete during curing process. This sensor is made of stainless steel and a Teflon encasing with strain sensitivity of 1.2 pm/με and temperature sensitivity of 23.8 pm/°C. According to the os3600 specification, the fatigue life is 100 million cycles at 2,000 με and operating temperature range is -40°C to +80°C with strain limit of 2,500 με. For data acquisition, the Micro Optics sm130 interrogator

was used. It has four optical channels with wavelength range of 1510-1590 nm and a typical FBG sensor capacity of 40. It is also designed for harsh environments with operating temperature of 0°C to 50°C, and the operating humidity of 0 to 80%. Figure 7-3 shows the os3600 FBG fiber optic sensor and sm130 interrogator used.

(a)

(b)

Figure 7-3. Fiber optic sensor system: (a) os3600 FBG fiber optic embeddable strain sensor (MicronOptics 2012); (b) sm130 dynamic optical sensing interrogator (MicronOptics 2009)

A FBG sensor has Bragg gratings that reflect particular wavelengths of light called the Bragg wavelength. The basic principle of operation of an FBG sensor is based on detecting the shift of wavelength of the reflected "Bragg" signals as the reflected Bragg wavelength is a function of the spacing between the gratings as shown in Figure 7-4. A change in the peak Bragg wavelength is related to a change in mechanical properties including strain, temperature, and displacements (Grattan and Sun 2000).

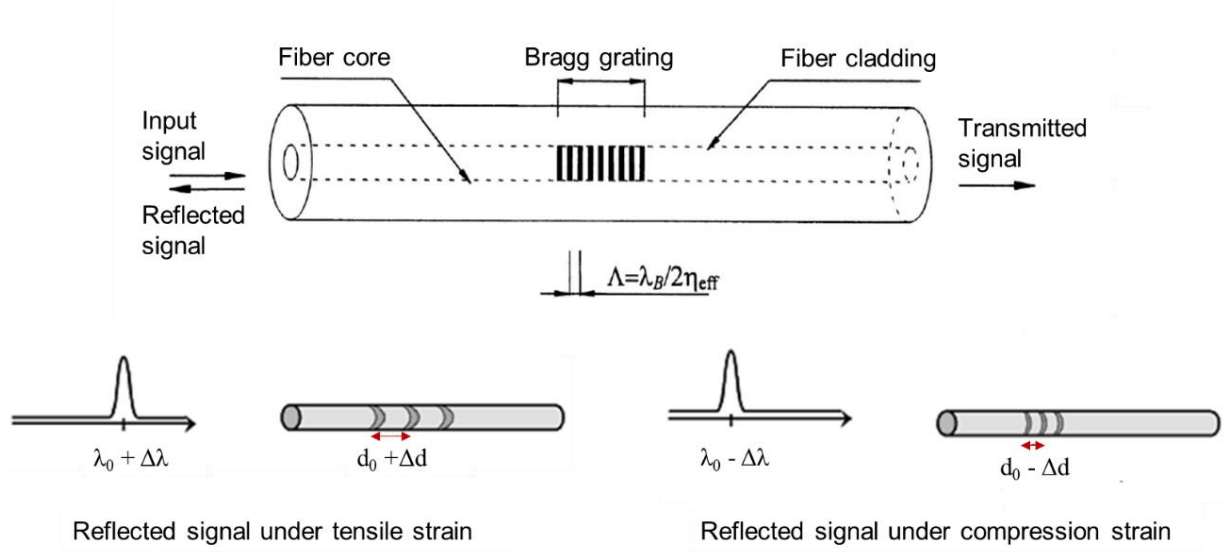

Figure 7-4. Principle of operation of a FBG sensor

To measure the reflection spectrum, the fiber optic sensor requires a light source with a particular wavelength range and detector of reflected signal which is called an interrogator. This interrogator is needed due to the inherent characteristics of fiber optic sensor including the use of light instead of electricity and glass fiber instead of copper wire. The interrogator measures the full optical spectrum and the peak wavelength of the optical sensor signals which is related to a

change in physical length of the sensor. The sm130 dynamic optical sensing interrogator used in this study served this purpose.

7.3 Laboratory Testing Program

A laboratory study was conducted to evaluate the performance of different concrete embedment strain sensors. The different strain sensors were embedded in concrete cylinders, and the concrete cylinders were subjected to various known static and dynamic strains. The measured strains obtained from the various strain sensors were then compared with the known strains to evaluate their performance with regards to accuracy, repeatability, and reproducibility. In addition to the evaluation of the performance of strain sensors in measuring load-induced strains, the vibrating wire gauge and fiber optic gauge were also tested to evaluate their performance in measuring concrete shrinkage strains. The strain readings at the early age (up to 14 days) of the concrete specimen were compared with the strain reading as measured by the calibrated LVDTs in the standard drying shrinkage test. In this study, a total of 5 different strain gauge types were used, including three types of electrical resistance strain gauges, a vibrating wire gauge, and a fiber optic gauge.

7.3.1 Concrete Specimens

Two different sizes of concrete specimens were used to evaluate sensor performance under different loading conditions. The concrete cylinders used were 6 inches (152.4 mm) in diameter and 16 inches (406.4 mm) in height for fiber optic sensors. This longer cylinder size was needed in order to allow for the os3600 fiber optic sensor to be fully embedded in it. The other sensors were embedded in 6 by 12 inches (152.4mm by 304.8mm) cylinders. The sensors to be evaluated were placed in the center of the cylinder and in the vertical direction to minimize the effects of eccentricity and offset errors in sensor location that could cause variation in the measurements. All sensors were placed along the same axis, equidistance from the edge of the

cylinder. The sensors were suspended by steel wires, and the concrete was placed in three layers to ensure that the gauges were vertically in line with cylinder axis. Four vibrating gauges, six electrical resistance strain gauges, and four fiber optic sensors were used for this evaluation.

7.3.2 Concrete Mixtures

A concrete mixture with high workability and small nominal maximum aggregate size (#89 stone with a nominal maximum size of 3/8 inches) was used for testing. Table 7-1 shows the mix proportions for the concrete mix. It can be seen that the slump of the concrete mix was high to allow the mixture flow into the space between the mold and the sensor easily. Figure 7-5 shows how the sensors were placed in the concrete test specimens.

Table 7-1. Mix proportions for concrete mixture used

Material	Amount	Remarks
Cement (lb/yd^3)	685	Argos
Fine Aggregate (lb/yd^3)	1,240	GA-397 Silica sand
Coarse Aggregate (lb/yd^3)	1,378	#89 stone
Water (lb/yd^3)	365	
Air Content (%)	1.0	
Slump Range (in)	6	
Air Entrainer (oz/yd^3)	3.3	Vinsol Resin
Admixture (oz/yd^3)	39.5	ADVA CAST 600
Water-concrete ratio	0.555	

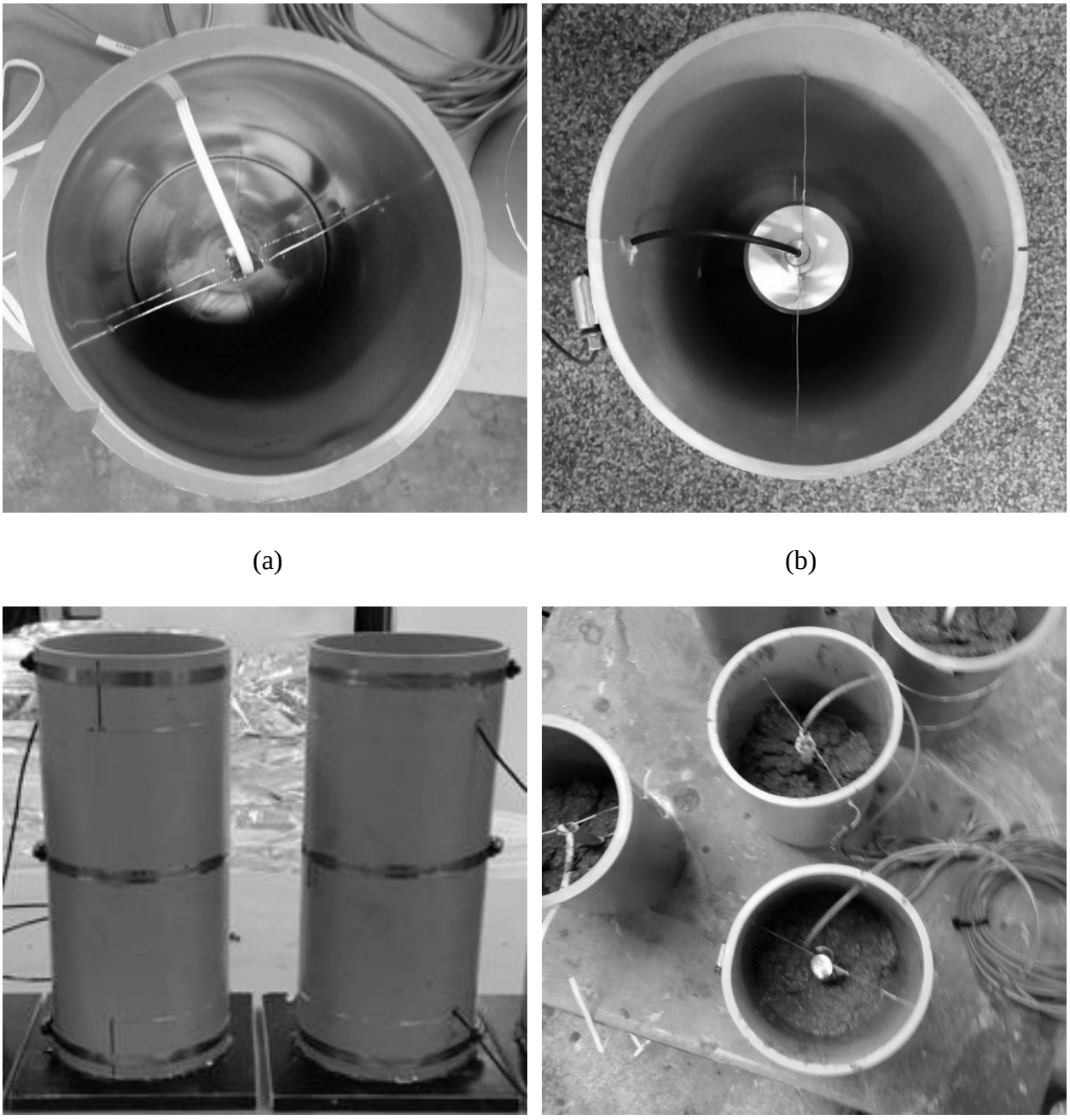

(a) (b)

(c) (d)

Figure 7-5. Locations of sensors in concrete specimens: (a) Strain gauge inside 6 "× 12" cylinder; (b) FOS sensor embedded in 6" × 16" cylinder; (c) 6" × 12" cylinders made of PVC pipe; (d) cylinders during casting

7.3.3 Compression Test

To evaluate the performance of the different embeddable sensors, a concrete cylinder was instrumented and tested under various known strains. The cylindrical specimens were ground at the two ends to ensure that they were smooth and perpendicular with respect to the vertical side of the cylinder. The cylinders were loaded in compression in the vertical direction at a curing age of 36 days. An extensometer, manufactured by Epsilon, was attached on the outside of the concrete cylinder and used to measure the vertical deformation and strain of the test cylinder. The measured compressive strains from the embedded sensors were compared with strains from the extensometer mounted on the concrete cylinder. A universal testing machine (UTM), manufactured by Instron, was used for the compression test, and seven different loading cases (as presented in Table 7-2) were used on the concrete specimens.

The first six loading cases were static loads from 5 to 50 kips, which were applied and held for 30 seconds each. The seventh loading case was a dynamic load cycling between 20 and 25 kips in compression as presented in Table 7-2. For all of the loading cases, the strain gauges were zeroed at the beginning of each test.

Table 7-2. Compression loading cases used

Load Case	Load Type	Load (kip)
Seating load	Static	2
1	Static	5
2	Static	10
3	Static	15
4	Static	20
5	Static	35
6	Static	50
7	Dynamic	20-25

A sampling rate of 100 Hz was used for the electrical resistance strain gauges and fiber optic gauge. For the VWSG, a sampling rate of 1 Hz was chosen because the pluck-read operation on a VWSG required the read time to be not less than 1 sec. Figure 7-6 shows the specimen and extensometer in the UTM before testing.

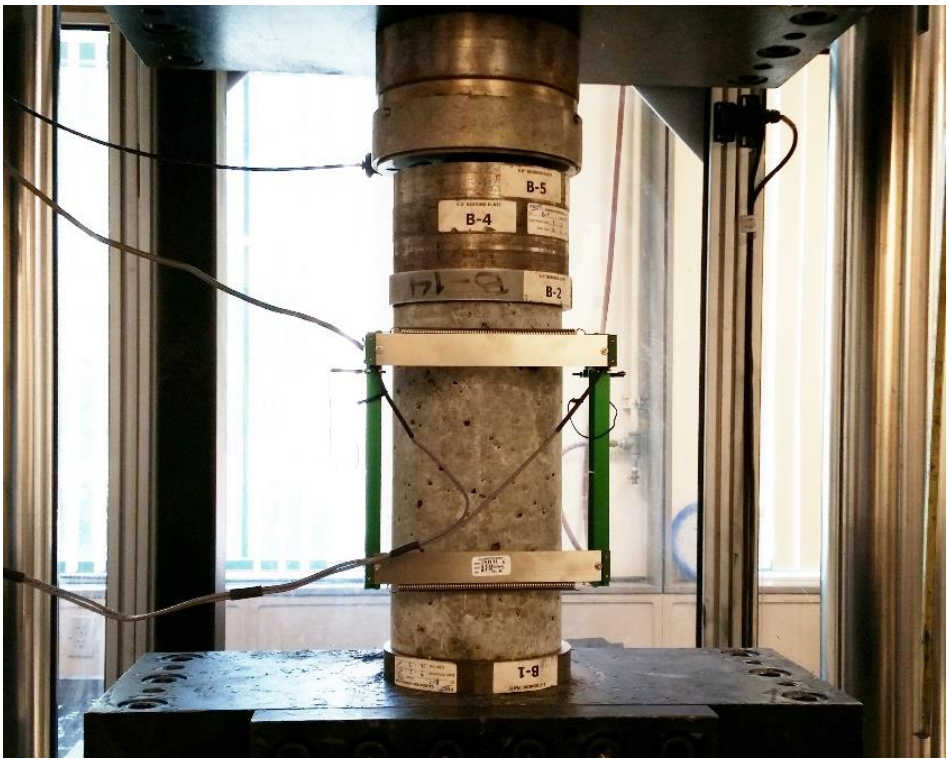

Figure 7-6. Concrete specimen tested in compression

7.3.4 Shrinkage Test

Shrinkage strain measurements were taken on concrete specimens with embedded VWSGs and FOSs. Displacement measurements were also taken by a LVDT attached to surface of concrete cylinder. The setup for free shrinkage test consisted of a DC-powered LVDT connected to a shrinkage test frame. The outputs from the LVDTs and strain gauges were connected to a data acquisition system (DAQ). The LVDTs have a sleeve bearing structure on one end that supports a spring-loaded shaft attached to the core to facilitate mounting. All

LVDTs are hermetically sealed to operate in harsh environments such as a moist room, and have an operating temperature range of 0°F to 160°F (-17.8°C to 71.1°C). The test setup for measuring the free shrinkage using a LVDT is shown in Figure 7-7.

Figure 7-7. Setup for free shrinkage measurement using a LVDT

The following steps were used in conducting the free shrinkage test:

(1) After concrete casting is done, cover the concrete samples with plastic sheets for one day.

(2) After one day, remove the concrete samples from the molds and place them into the shrinkage test frames as shown in Figure 7-7.

(3) Adjust the LVDT readings to zero. It is somewhat difficult to set the LVDT reading to zero due to its high sensitivity. Thus, just adjust it to as close to zero as possible.

(4) After the LVDT readings are set to zero, set the DAQ to record readings every 15 minutes continuously.

(5) Download the readings from the DAQ to a computer after 7 to 14 days.

7.4 Results of Sensor Evaluation

The objective of this analysis was to assess the performance in terms of accuracy, repeatability, and reproducibility for load-induced and shrinkage strain measurements.

7.4.1 Evaluation of Gauge Accuracy

Sensor accuracy can be defined as the degree of agreement of the measured quantity to its true value. To evaluate the accuracy of sensors, ten cylinders were tested and summarized in Table 7-3. The measured strains were compared with the strains as measured by the calibrated extensometer. Figure 7-8 presents the results of the accuracy test. The results show that the strains measured by the Kyowa, FOS, and VWSG gauges matched well with the strains as measured by the extensometer. However, the strains measured by the Vishay strain gauges show larger deviations from those by the extensometer. It can be seen that the FOS had the lowest average difference among all the gauges evaluated. Paired two-sample t tests were run to determine if the difference in accuracy for the other four types of sensors were statistically different from that for the FOS. For the cases when the variance and number of data points from each group were different from each other, the Welch equations were used for calculating the pooled variance and degree of freedom. It can be seen that the differences in accuracy of the Kyowa and VWSG gauges with the accuracy of the FOS are statistically insignificant with a confidence level of 95%. However, the two Vishay gauges were significantly different as compared with the FOS in accuracy as presented in Table 7-4.

Table 7-3. Summary of sensor accuracy test results

Sensor types	Average difference as compared to the extensometer readings (με)	Average difference for the same sensor type (με)
FOS-1	1.025	2.697
FOS-2	4.370	
Kyowa-1	3.758	5.698
Kyowa-2	7.637	
Vishay-120Ω-1	28.819	31.828
Vishay-120Ω-2	34.838	
Vishay-350Ω-1	15.521	17.729
Vishay-350Ω-2	19.938	
VWSG-1	4.218	5.625
VWSG-2	7.032	

Table 7-4. Results of t-tests on the accuracy test at 95% confidence level

Test set	Sensor type	t-test (p-value)	Significantly different at 95% confidence?
1	FOS Kyowa	0.362	No
2	FOS Vishay-120Ω	0.014	Yes
3	FOS Vishay-350Ω	0.032	Yes
4	FOS VWSG	0.312	No

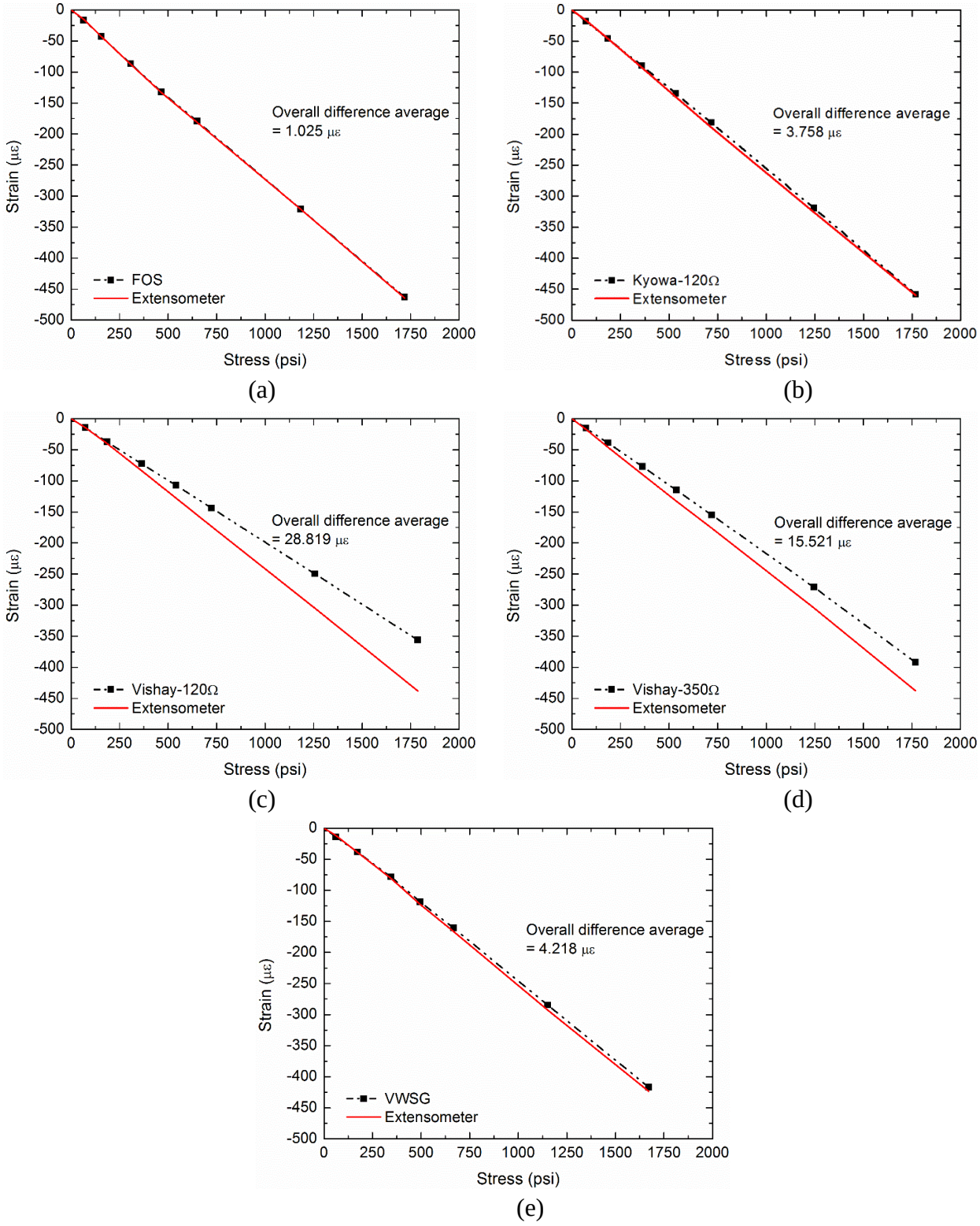

Figure 7-8. Accuracy test results: (a) Fiber optic sensor results; (b) Kyowa sensor results; (c) Vishay-120Ω sensor results; (d) Vishay-350Ω sensor results; (e) VWSG sensor results

7.4.2 Evaluation of Gauge Repeatability and Reproducibility

Sensor repeatability can be defined as the measure of agreement between the results of successive measurements of the same sensor under the same condition. Sensor reproducibility can be defined as the closeness of the agreement between the results of measurements of the two or more sensors under similar condition.

To evaluate the repeatability and reproducibility of strain sensors, the magnitude of strain, defined as the absolute difference between the minimum and maximum strain value of the strain pulse, was calculated as the response variable and then a statistical analysis described in ASTM C802, Standard Principles for Conducting an Inter-laboratory Test Program to Determine the Precision of Test Methods for Construction Material (ASTM(C802-09a) 2010), was applied to process the data. The pooled standard deviation and coefficient of variations were calculated, including variance within and between similar sensors measuring the same strain. The results of the analysis include within and between coefficient of variations (COV) which indicate the degree of variability in measured strains with the same gauge (within) and the variability in measured strains with similar gauges (between). Table 7-5 presents the measured strains from the two Kyowa gauges in ten repeated load tests and the calculated statistics from these data.

Table 7-5. Measured dynamic strains from two Kyowa gauges and calculated statistics

Gauge	1	2	3	4	5	6	7	8	9	10	Average	Variance
Kyowa-1	42.63	40.00	44.11	44.38	44.27	44.03	43.68	43.96	43.82	44.82	43.57	1.90
Kyowa-2	46.72	47.70	43.78	41.71	47.56	47.03	46.74	46.73	47.30	41.41	45.67	5.88
Average											44.62	3.89

Note: Values are in units of με.

$p = Number\ of\ gauges = 2$

$n = Number\ of\ readings = 10$

$\overline{x_1} = \ Average\ of\ Kyowa\ 1\ reading\ = \sum \frac{x_i}{n} = 43.57$

$\overline{x_2} = \ Average\ of\ Kyowa\ 2\ reading\ = \sum \frac{x_i}{n} = 45.67$

$\overline{x_A} = Mean\ of\ gauge\ averages = \frac{x_1 + x_2}{p} = 44.62$

$S_1^2(pooled) = variance\ of\ measurements\ from\ Kyowa\ 1 = \frac{\sum(x_i - \overline{x_1})^2}{n-1} = 1.90$

$S_2^2(pooled) = variance\ of\ measurements\ from\ Kyowa\ 2 = \frac{\sum(x_i - \overline{x_2})^2}{n-1} = 5.88$

$S_A^2(pooled) = Average\ of\ within\_gauge\ variance = \frac{S_1^2 + S_2^2}{p} = 3.89$

$S\overline{x}_A^2 = \frac{\sum \overline{x}_i^2 - p(\overline{x}_A)^2}{p-1} = 2.198$

$SL_A^2 = \left(S\overline{x}_A^2\right) - \frac{S_A^2(pooled)}{n} = 1.81$

Variance within gauge $= S_A^2(pooled) = 3.89$

Variance between gauges $= S_A^2(pooled) + SL_A^2 = \ 5.70$

Coefficient of variation (COV) $within\ gauges = \frac{\sqrt{Variance\ within\ gauge}}{Mean\ of\ gauge\ average} \times 100 = 4.42\%$

Coefficient of variation (COV) $between\ gauges = \frac{\sqrt{Variance\ between\ gauges}}{Mean\ of\ gauge\ average} \times 100$

$= 5.35\%$

Table 7-6 presents the results of statistical analysis on the measured strains from the four different gauges in the repeated load tests.

Table 7-6. Summary of statistical analysis results

Sensor	Average (με)	Variance		Standard Deviation (με)		Coefficient of variation (%)	
		within gauge	between gauge	within gauge	between gauge	within gauge	between gauge
Kyowa	44.62	3.89	5.70	1.97	2.39	4.42	5.35
Vishay-120Ω	35.79	11.74	12.93	3.43	3.60	9.58	10.05
Vishay-350Ω	39.36	4.84	5.05	2.20	2.25	5.59	5.71
FOS	48.14	12.96	22.23	3.60	4.72	7.48	9.79

7.4.2.1 Repeatability

It can be seen that the Kyowa gauges show the best repeatability (with the lowest within gauge coefficient of variation), to be followed by Vishay-350Ω, FOS, and Vishay-120Ω gauges. The previous study conducted by FDOT (FDOT 2008) stated that a strain gauge repeatability with COV of ≤ 10 percent was deemed acceptable and a COV between 10 percent and 20 percent was considered as marginal. The overall COV was found to be less than 10 percent (within gauge) for all sensors.

7.4.2.2 Reproducibility

It can be seen that the Kyowa gauges show the best reproducibility (with the lowest COV between gauges) to be followed by Vishay-350Ω, FOS, and Vishay-120Ω gauges.

7.4.3 Results of Concrete Shrinkage Measurements

The measured shrinkage strains from the sensors were compared with the strains calculated from the LVDTs readings as shown in Figure 7-9. It can be noted that there were two data gaps from 27 h to 50 h and from 268 h to 288 h due to power failure. During the monitoring period, the average difference in strain output between the fiber optic sensor and LVDT was 14.28 με with a standard deviation of 8.07 με, while the average difference between vibrating

wire gauge and LVDT was 12.84 με with a standard deviation of 7.78 με. In this experiment, the measurements obtained through both embedded sensors show good agreement with the LVDTs readings. The overall strain during the 14 days of monitoring period due to shrinkage and the statistical analysis results are summarized in Table 7-7. It can be seen that the difference in accuracy of the FOS and the VWSG were statistically insignificant at 95% confidence level.

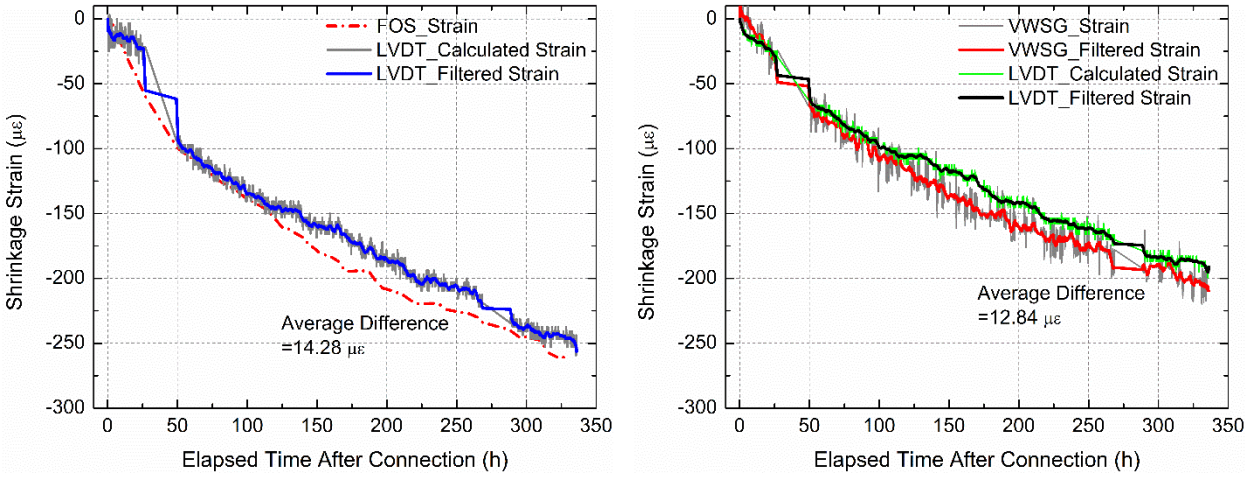

(a) (b)

Figure 7-9. Comparison of free shrinkage strain measurements: (a) Free shrinkage strain from FOS; (b) Free shrinkage strain from VWSG

Table 7-7. Summary of shrinkage test and t-test results at 95% confidence level

Test set	Sensor type	Maximum measured shrinkage strain (με)	Average difference between sensor and LVDT	Average difference for same sensor type (με)	t-test p-value	Significantly Different at 95% confidence?
1	FOS-1	-267.45	14.28	30.37	0.903	No
	LVDT	-256.27				
2	FOS-2	-246.43	46.45			
	LVDT	-209.09				
3	VWSG-1	-209.49	12.84	34.04		
	LVDT	-191.07				
4	VWSG-2	-232.81	55.24			
	LVDT	-182.76				

7.5 Conclusion and Recommendations

An experimental study was conducted to evaluate the performance characteristics of fiber optic, vibrating wire, and electrical resistance strain gauges in measuring strains in concrete due to load and drying shrinkage. The different sensors were evaluated in terms of accuracy, repeatability, and reproducibility. The main findings are summarized as follows:

- When compared with the strains measured by a calibrated extensometer in a compression test where the strains varied from 0 to around 450 με, the fiber optic strain sensor (FOS) showed an average error of 2.7 με, as compared with average errors of 5.7 με and 5.6 με for an electrical resistance strain gauge and a vibrating wire strain gauge (VWSG), respectively. However, their differences in error were found to be statistically insignificant at 95% confidence level.

- The repeatability of the strain measurements by the FOS in terms of coefficient of variation (COV) was 7.5 % as compared with COVs of 4.4, 5.6, and 9.6% for the three different electrical resistance strain gauges.

- The reproducibility of the strain measurements by the FOS in terms of COV was 9.8% as compared with COVs of 5.4, 5.7, and 10.1 % for the three different electrical resistance strain gauges.

- When compared with the strains measured by a calibrated LVDT in a concrete drying shrinkage test where the strains varied from 0 to around 250 με, the FOS showed an average difference of 30.37 με, while the VWSG showed an average difference of 34.04 με. The difference in strain measurements by the different gauges was statistically insignificant at 95% confidence level.

Based on the results of this laboratory evaluation, the FOS is found to have similar accuracy, repeatability, and reproducibility as compared to electrical resistance strain gauge and VWSG, and can be used for measuring dynamic and long-term strains in concrete pavement.

CHAPTER 8
FIELD TESTING PROGRAM TO DETERMINE EFFECTIVE INSTRUMENTATION PLAN AND ANALYSIS METHODOLOGY

8.1 Introduction

8.1.1 Background and Objectives of the Study

In Task 7 of this study, various embeddable strain gauges were tested in the laboratory to evaluate their performance characteristics with respect to accuracy, repeatability, and reproducibility in measuring load-induced strains and shrinkage strains in concrete samples. However, when these strain sensors are used in actual concrete pavement slabs, there may be other factors which are not present in the controlled laboratory environment and which can influence their performance. In this Task 8, evaluation of the various strain sensors was evaluated in full-size concrete pavement slabs subjected to the actual outside environment and realistic wheel loads by a Heavy Vehicle Simulator (HVS). This field testing program was also conducted to assess the validity of the analysis results from the Finite Element (FE) model for jointed plain concrete pavement which has been developed for this study.

The main objectives of Task 8 are (1) to evaluate the performance of various strain sensors in full-size concrete pavement slabs, (2) to develop effective configurations for strain and temperature sensors in concrete test slabs, (3) to assess the validity of predicted results (deflections, strains, and stresses) from the developed FE model for jointed plain concrete pavement (JPCP), and (4) to recommend effective testing and analysis methodology for concrete pavements.

8.1.2 Overview of the Field Testing Program

The field testing program consisted of testing two sets of concrete test slabs at the FDOT Accelerated Pavement Testing (APT) facility in Gainesville, Florida. The first set of test slabs consisted of three concrete test slabs, which were constructed and evaluated in the period from

December 2014 through March 2015. The main objectives for the first set of test slabs were (1) to assess the feasibility of the instrumentation system for monitoring temperature and strain in concrete pavement slabs, (2) to validate the predicted results from the FE model for JPCP, and (3) to evaluate the effectiveness of the critical stress analysis methodology in determining the potential performance of JPCP.

The second set of test slabs consisted of four test slabs, which were constructed and evaluated in the period from October 2016 through April 2017. The main objectives for the second set of test slabs were (1) to evaluate the performance of various strain sensors in actual concrete pavement slabs, (2) to validate the predicted results from the FE model for JPCP, (3) to evaluate the effectiveness of the critical stress analysis methodology in determining the potential performance of JPCP, and (4) to assess the feasibility of using a series of evenly-spaced strain sensors to determine the location of the applied wheel load on the test slabs.

8.2 First Set of Test Slabs

8.2.1 Description of Test Slabs and Instrumentation

Three test slabs were constructed at the Accelerated Pavement Testing (APT) facility in the FDOT Materials Research Park in Gainesville, Florida, in December 2014. To construct the three test slabs, three different concrete mixes were selected for use, and were referred to as (1) Test-1 (Standard Mix), (2) Test-2 (ICC-1), and (3) Test-3 (ICC-2), respectively. Each of the three concrete test slabs was 12 ft by 16 ft in size and 9 in. in thickness, and was constructed over an existing two-inch thick asphalt layer, which was placed over a 10.5 in. limerock base. There was no dowel bar used at the slab joints. Figure 8-1 shows the instrumentation layout for the test slabs. The locations for the dynamic strain gauges were selected based on the anticipated maximum strain responses in the test slabs from the anticipated HVS loading. At each indicated gauge location, two embedded strain gauges were placed at a depth of 1 in. from the concrete

surface, and 1 in. from the bottom of the concrete layer. This was achieved by securing the strain gauges between two nylon rods which were securely driven into the asphalt layer before the pouring of the concrete to form the test slab.

Each test slab was loaded by a Heavy Vehicle Simulator (HVS). During the HVS testing, dynamic strain data from the tested slab were recorded at every 15-minute interval, for 30 seconds each time, at a rate of 100 values per second for each strain gauge. Temperature data were recorded at five-minute intervals.

8.2.2 FE Modeling of Test Slab Section

A 3-D finite element model for concrete slabs was developed using the ADINA (version 9) finite element software. Figure 8-2 shows the 3-D finite element model which was developed for the analysis of the three test slabs. A concrete slab is modeled by an assemblage of elastic hexahedron elements. A hexahedron element is defined by eight nodes with each node having three degrees of freedom, i.e., translations in the x-, y-, and z-directions. The effects of temperature changes in the concrete slab can also be considered in the analysis. The concrete is characterized by its elastic modulus, Poisson's ratio, and coefficient of thermal expansion (CTE).

The test slabs are modeled as not bonded to the underlying foundation. The pavement foundation is modeled as an isotropic and linearly elastic subgrade material characterized by its elastic modulus and Poisson's ratio. A depth of 100 inches was used to model the subgrade material. The bottom of subgrade layer was modeled as fixed in z- direction.

The properties of the three concretes used in the model were initially obtained from the measured properties of the sampled concrete. The elastic modulus of the subgrade was obtained through back-calculation method by matching the analytical to the measured FWD deflections of the test slabs, as presented in the next section. Load transfer across the joint between two adjacent slabs is modeled by translational springs connecting the nodes of the finite elements

along the joint. Spring elements also have three degrees of freedom. Three values of spring constants are used to represent the stiffnesses along x-, y-, and z-directions.

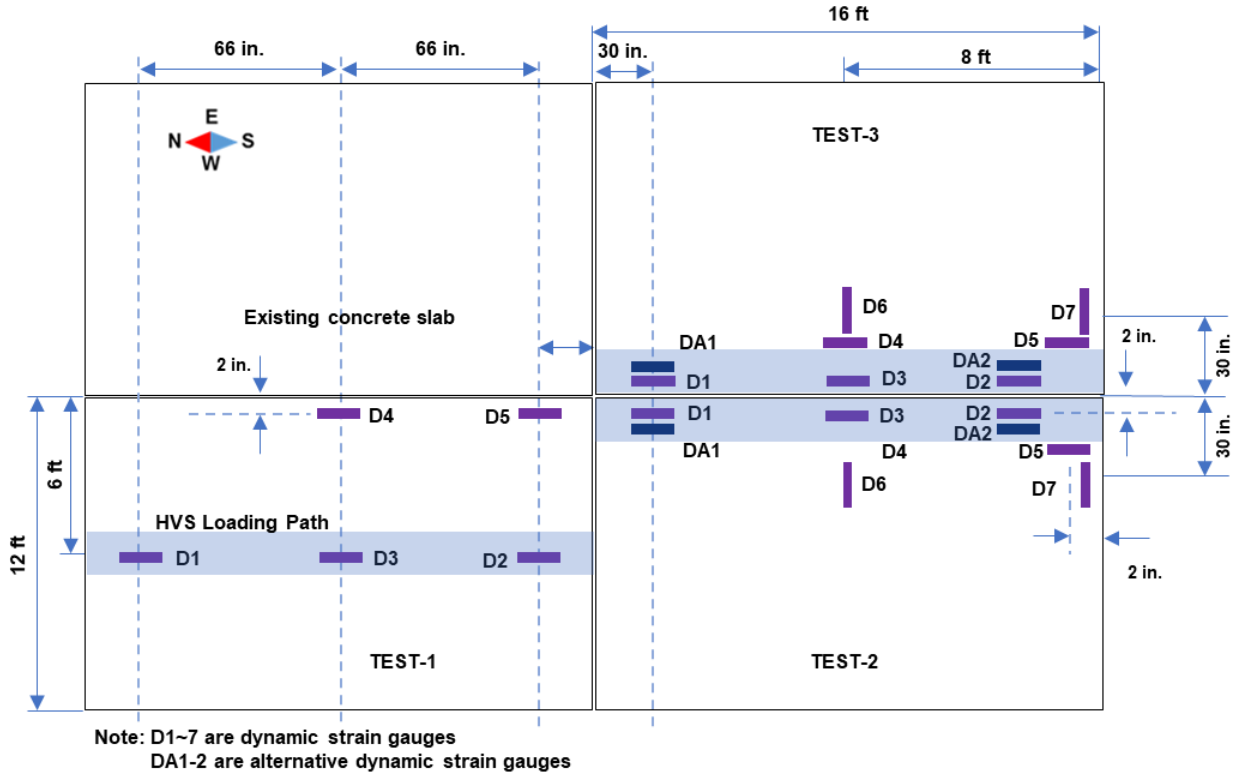

Figure 8-1. Instrumentation layout

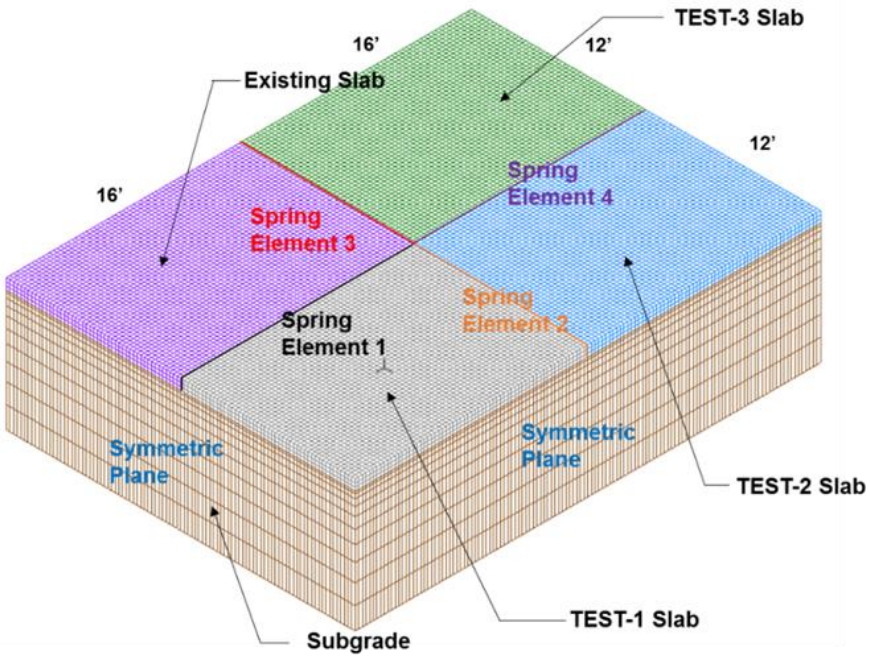

Figure 8-2. 3-D finite element model for test slabs

8.2.3 Calibration and Validation of the FE Model

In order for the 3-D analytical model to accurately analyze the performance of the test slabs under the HVS loading and critical loading conditions, it needs to have accurate properties of the test slab materials and the correct values of spring stiffness for modeling the behavior of joints and edges. The elastic modulus of the concrete material was initially estimated from the results of laboratory tests on the sampled concrete. The elastic modulus of subgrade and the spring stiffnesses of joint and edges were estimated by back-calculation of the FWD deflection data using the FE model. The elastic moduli of the concrete were also adjusted by back-calculation method. The results of the FWD tests at the slab center were used to estimate the elastic modulus of the subgrade. The results of the FWD test at the joints and edges were used to calibrate values of spring stiffness at the joints and edges by matching the analytically computed deflections with the measured FWD deflections. This process is referred to as "calibration of model parameters" of the model in this study. The estimation of the test slab materials properties and parameters was further verified by matching the analytically computed strains with the measured strains in the test slabs caused by HVS wheel loads. This process is referred to as "verification of model parameters" in this study.

Pavement surface deflection basins caused by a 9-kip FWD applied load were used to estimate the values of the elastic modulus of the subgrade and the stiffness of the springs used to model the load transfer at the joints. Figure 8-3 shows an example of measured and computed deflection basin caused by a 9-kip FWD load at the center of slab. This set of FWD tests was done in the early morning when the slab would tend to have a negative temperature differential and to have full contact with the subgrade at the slab center. The measured deflection basins in

the transverse direction were very similar to those in the longitudinal direction. The analytical deflection basin was calculated by using an elastic modulus of the subgrade of 115 ksi.

Deflection basins caused by FWD load applied at the joint were used to estimate the joint spring stiffnesses, which were used to model the load transfer at the joints. All the joints between two adjacent slabs were tested. This set of FWD tests was performed at midday when the slab would tend to have a positive temperature differential and to have full contact with the subgrade at the joints. The estimated elastic moduli of the slab and subgrade were used in the FE model to compute the deflection basin across the joint. Figure 8-4 shows the matched deflection basins from the back-calculation process for estimating the joint spring stiffnesses. Using the previously estimated parameters and material properties, a fairly good match between the measured and the calculated deflection basins was achieved with a vertical stiffness of 100,000 lb/in. and with stiffness of 10,000 lb/in. in the x- and y-directions.

In order to verify the parameters for the FE models for the test slabs, the measured strains from strain gauges embedded in the test slab were compared with the computed strains. The strain at each gauge location was computed by using the FE model for the case of static load shifted according to the locations of the HVS wheel at different times. The strains at different times were obtained by placing the HVS load at the different locations at the corresponding times. A total of 64 shifted applied wheel loads were used to simulate one pass of the HVS loading with a speed of 7.5 miles per hour. Figure 8-5 shows the comparison between the analytical strains predicted using the FE model and the measured strains from the full-scale test slabs.

Table 8-1 presents a summary of model parameters calibrated for the test slabs in this study. The 3-D FE models with the calibrated parameters were used to perform the analysis of

stresses under critical loading condition in Florida. As shown in Figures 8-3 through 8-5, the analytical responses matched well with measured responses.

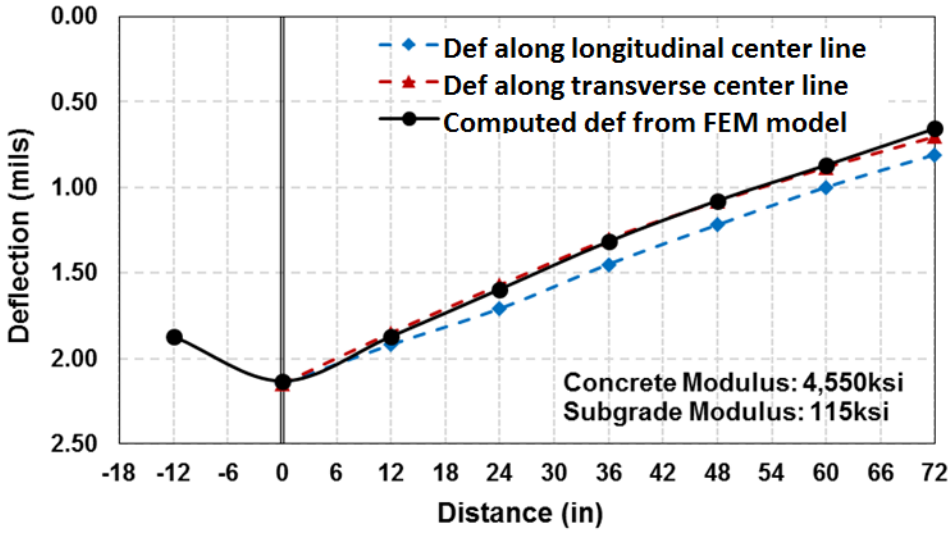

Figure 8-3. Example of determination of elastic modulus using FWD deflection basin caused by a 9-kip FWD load at slab center for test-1 slab

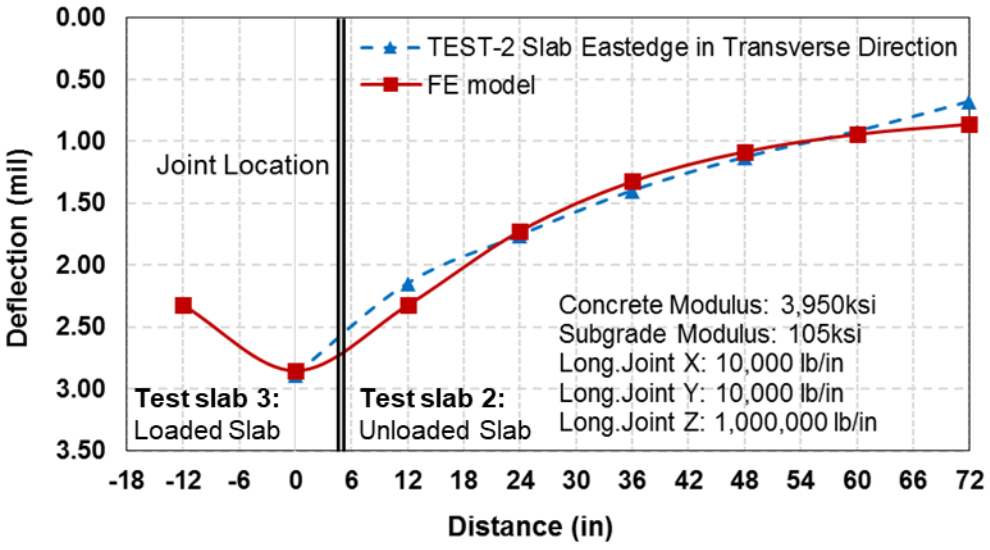

Figure 8-4. Example of determination of spring stiffness across the joint using FWD basin caused by a 9-kip FWD load at the joint for standard mix slab

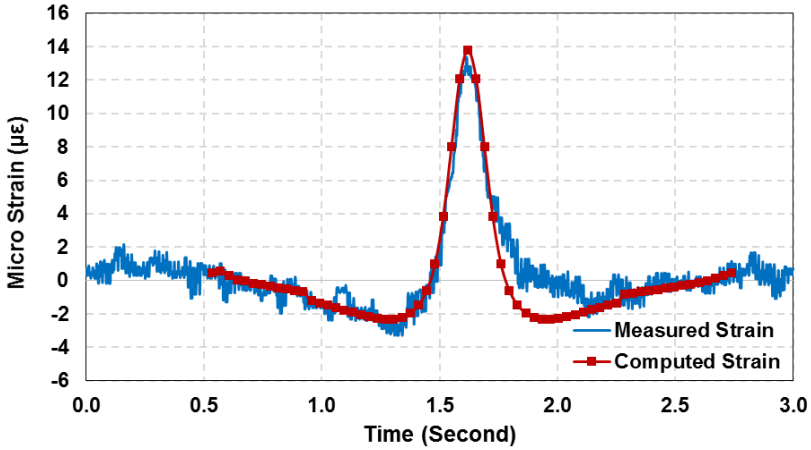

(a)

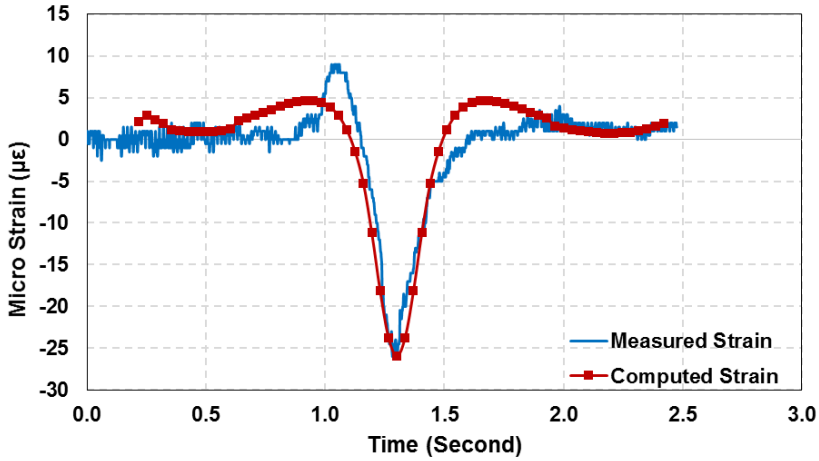

(b)

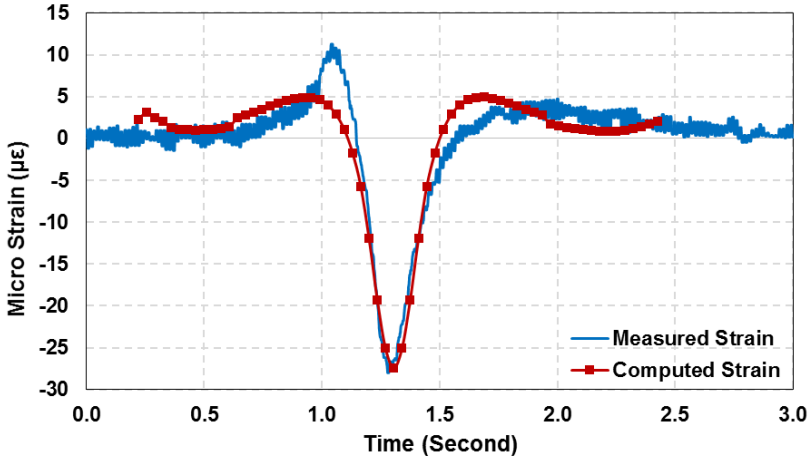

(c)

Figure 8-5. Measured and computed strains at selected gauge locations: (a) Test-1 slab from sensor D1-Bottom, (b) Test-2 slab from sensor DA1-Top, (c) Test-3 slab from sensor D1-Top

Table 8-1. Summary of model parameters calibrated for the test slabs

Parameters used in FE model	Test-1 slab	Test-2 slab	Test-3 slab
Elastic Modulus of Concrete (ksi)	4,550	3,950	3,800
Density of Concrete (pcf)	138.3	129.9	130.4
Coefficient of Thermal Expansion (in/in/°F)	4.425E-6	4.239E-6	4.239E-6
Poisson's ratio	0.2	0.2	0.2
Elastic Modulus of Subgrade (ksi)	115	115	115
Spring Constant for Load Transfer (lb/in)			
Transverse Joint X	10,000	10,000	-
Transverse Joint Y	10,000	10,000	-
Transverse Joint Z	100,000	1,000,000	-
Longitudinal Joint X	10,000	-	10,000
Longitudinal Joint Y	10,000	-	10,000
Longitudinal Joint Z	1,000,000	-	100,000

8.2.4 Assessment by Critical Stress Analysis

Previous research studies on concrete pavements in Florida have shown that concrete pavement slabs tend to have a positive temperature differential (where the temperature at the top of the slab is higher than the temperature at the bottom) at midday and the slabs tend to curl upward at the slab center. A typical severe temperature differential in the concrete slab at midday has been found to be +20°F. At this temperature condition, the most critical loading position is when the axle load is placed at the mid-edge of the slab.

Conversely, concrete pavement slabs tend to have a negative temperature differential at night, and the slabs tend to curl up at the slab edges and corners. A typical severe temperature differential in the concrete slab at night has been found to be -10°F. At this temperature

condition, the most critical loading position is when the axle load is placed at the corner of the slab.

Using the developed 3-D finite element models for the three test slabs, which were calibrated with the measured deflection basins from FWD tests and validated with the measured strains from HVS tests, analysis was performed to determine the maximum stresses in the slabs if they were subject to some critical load and temperature conditions. A 22-kip axle load, which represents the maximum legal load limit for single axle load in Florida, was used as the applied load in the analysis. Analysis for the following two critical load-temperature conditions was performed:

(1) A 22-kip axle load was applied to the mid-edge of the pavement slab with a temperature differential of +20°F.

(2) A 22-kip axle load was applied to the corner of the pavement slab with a temperature differential of -10°F.

These two critical loading conditions are shown in Figure 8-6. For comparison purpose, analysis was also performed for the following load-temperature conditions:

(1) A 22-kip axle load was applied to the mid-edge of the pavement slab with no temperature differential.

(2) A 22-kip axle load was applied to the mid-edge of the pavement slab with a temperature differential of -10°F.

(3) A 22-kip axle load was applied to the corner of the pavement slab with no temperature differential.

(4) A 22-kip axle load was applied to the corner of the pavement slab with a temperature differential of +20°F.

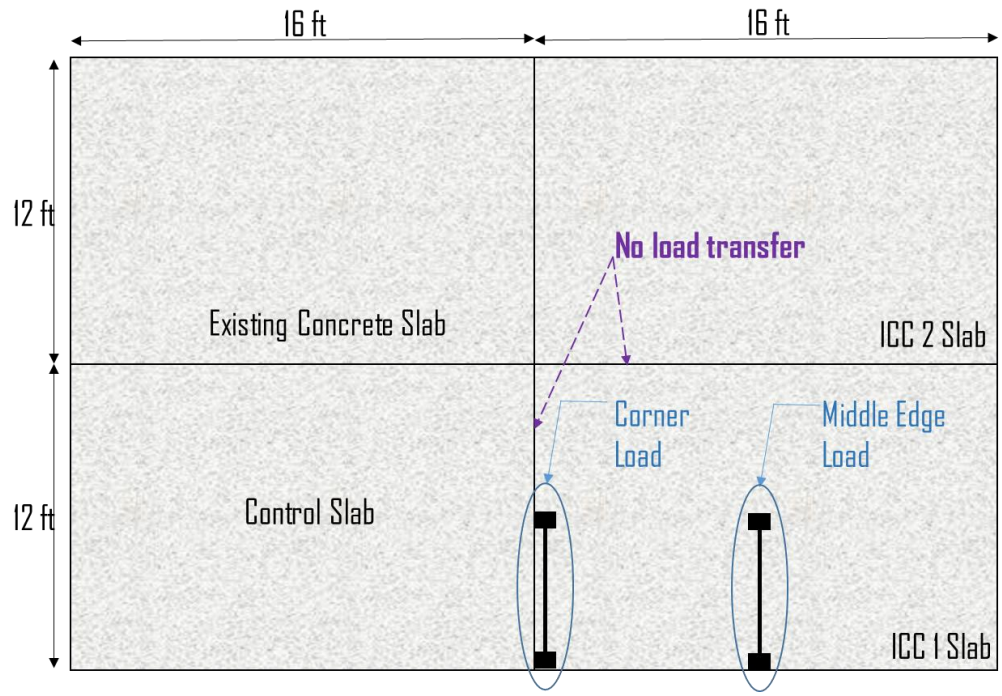

Figure 8-6. Critical loading conditions.

Table 8-2 shows the maximum computed stresses in the three test slabs from the critical stress analysis. In order to assess the potential performance of these test slabs in service, the maximum computed stresses were divided by the flexural strength of the concrete of the test slab to obtain the stress-to-strength ratios. According to fatigue theory, the number of load repetitions to failure of concrete increases as the stress-to-strength ratio decreases. Thus, a lower computed stress-to-strength ratio would indicate a higher allowable number of load repetitions to failure and a better-expected performance in service. The measured 28-day flexural strengths of the concrete sampled from the test slabs were used to compute the stress-to-strength ratios, which are also shown in Table 8-2. Since the measured flexural strength of ICC-1 with water-concrete ratio of 0.32 (662 psi) was substantially lower than the flexural strength of the corresponding ICC mixture with the same Water-concrete ratio from the laboratory study (820 psi), the flexural

strength value of 820 psi was also used in the calculation of the stress-to-strength ratios for the ICC-1 test slab.

Table 8-2. Computed maximum stresses and stress-to-strength ratios for the test slabs

Mix	Water-concrete ratio	CTE (in/in/°F)	Modulus of Elasticity (ksi)	Flexural Strength (psi)	Computed Stress (psi)		Stress-to-Strength Ratio	
					Corner	Mid-edge	Corner	Mid-edge
Temperature Differential of +20°F Between Top and Bottom								
SM	0.40	4.425	4,550	725	217.8	451.0	0.30	0.62
ICC-1	0.32	4.239	3,950	662 (820*)	194.3	397.4	0.29 (0.24#)	0.60 (0.48#)
ICC-2	0.40	4.239	3,800	705	190.6	389.7	0.27	0.55
Temperature Differential of -10°F Between Top and Bottom								
SM	0.40	4.425	4,550	725	217.4	154.7	0.30	0.21
ICC-1	0.32	4.239	3,950	662 (820*)	205.2	138.1	0.31 (0.25#)	0.21 (0.17#)
ICC-2	0.40	4.239	3,800	705	204.1	135.8	0.29	0.19
Temperature Differential of 0°F Between Top and Bottom								
SM	0.40	4.425	4,550	725	173.3	235.3	0.24	0.32
ICC-1	0.32	4.239	3,950	662 (820*)	164.9	227.2	0.25 (0.20#)	0.34 (0.28#)
ICC-2	0.40	4.239	3,800	705	163.3	225.7	0.23	0.32

Note: * Flexural strength of similar ICC mix from a laboratory study.
 # Stress-to-strength ratio computed using flexural strength from a laboratory study.

From the results presented in Table 8-2, it can be seen that the maximum stresses and the maximum stress-to-strength ratios were obtained at the condition when a 22-kip axle load was applied to the mid-edge of the pavement slab with a temperature differential of +20°F. At this critical loading condition, the computed stress-to-strength ratios for the ICC-2 and ICC-1 slabs (0.55 & 0.60, respectively) were all lower than that for the standard-mix slab (0.62). When the more appropriate flexural strength value of 820 psi was used for the ICC-1 slab, the stress-to-strength ratio was reduced to 0.48, which is substantially lower than that for the standard-mix

slab. Thus, based on the results of the critical stress analysis, the two internally cured concrete slabs will likely have better potential performance than the standard-mix slab in service.

8.2.5 Assessment by Visual Observation

Figure 8-7 shows a picture of the surface of the standard-mix slab after it has been loaded by the HVS. Though the standard-mix slab remained in good condition, some hairline cracks could be seen next to the wheel path of the HVS wheel load. These hairline cracks could be caused by micro shrinkage cracks which developed into hairline cracks after the slab was loaded repetitively by the HVS wheel load. Figures 8-8 and 8-9 show the pictures of the surface of the ICC-2 and ICC-1 slabs after they were loaded by the HVS. No visible crack was observed from these two test slabs. From the visual observation of these three test slabs, the ICC slabs appeared to have better performance than the standard-mix slab.

Figure 8-7. Surface of standard-mix slab after HVS loading

Figure 8-8. Surface of ICC-2 slab after HVS loading

Figure 8-9. Surface of ICC-1 slab after HVS loading

8.3 Second Set of Test Slabs

8.3.1 Description of the Test Slabs and Instrumentation

Four test slabs were constructed at the accelerated pavement testing (APT) facility located in the FDOT State Materials Research Park. Each test slab was 12 ft by 15 ft in size and 9 in. in thickness with no dowel bar at the joints. To evaluate the strain sensor's performance and data analysis methodologies under real temperature-load conditions, the concrete slabs were made with four different concrete mixtures with a variation of low to high strength and modulus of elasticity. These test slabs were constructed over the existing two-inch thick asphalt layer, which acted as a leveling course and provided firm and consistent foundation for the concrete slabs, supported by 10.5 in. limerock base layer. A vibrating leveling bar was used to level off the concrete surface of the test slab and then a broom was passed over the concrete surface to produce a rough surface texture before it hardened. A curing compound was applied over the top and sides of the slabs to prevent excessive water evaporation. The ICC-1 slab (Slab 1) and standard mix slab (Slab 4) were constructed on October 24, 2016, and HVS loading was applied after 129 days and 134 days, respectively. The ICC-2 slab (Slab 2) and ICC-3 slab (Slab 3) were both constructed on October 31, 2016, and tested after 137 days and 116 days, respectively.

The test slabs were instrumented with seven different types of strain gauges and with thermocouple wires to monitor temperature variation in the concrete slabs. The strain gauges used in this study were the Micron Optics OS3600, OS3500, Geokon 4200, Vishay, Kyowa, Tokyo Sokki, and CTL models. Table 8-3 summarizes the information on the sensors used in the test slabs. The strain gauge array was placed at the mid-edge of the slab on the HVS wheel path to evaluate the sensor's performance by comparing the responses obtained from each sensor type. For each gauge location, two strain gauges of the same type were placed at a depth of two inches from the concrete surface, and two inches from the bottom of the concrete layer. Both

gauges were placed in the longitudinal direction. In addition, five Kyowa strain gauges oriented in the longitudinal direction were placed along the transverse center line to capture the spatially distributed strain responses.

Thermocouple trees, each of which consisted of eight wires which were located at depths of 1, 2, 3, 4.5, 6, 7, and 8 in. from the surface of the concrete slab, were placed at the slab center and at the corner of the slab. One thermocouple wire was placed in the asphalt layer at a depth of 1 in. from the top of the asphalt layer, or at a depth of 10 in. from the concrete surface to monitor the temperature in the asphalt layer.

Nylon rods were used to secure the installation of sensors as well as to minimize the thermal effect on the gauge readings. PVC buckets without bottom plate were used to protect the gauges during concrete placement. The concrete was poured manually around the strain sensors inside the PVC buckets, which were pulled out vertically to remove them. Figure 8-10 presents the instrumentation layout for the four test slabs.

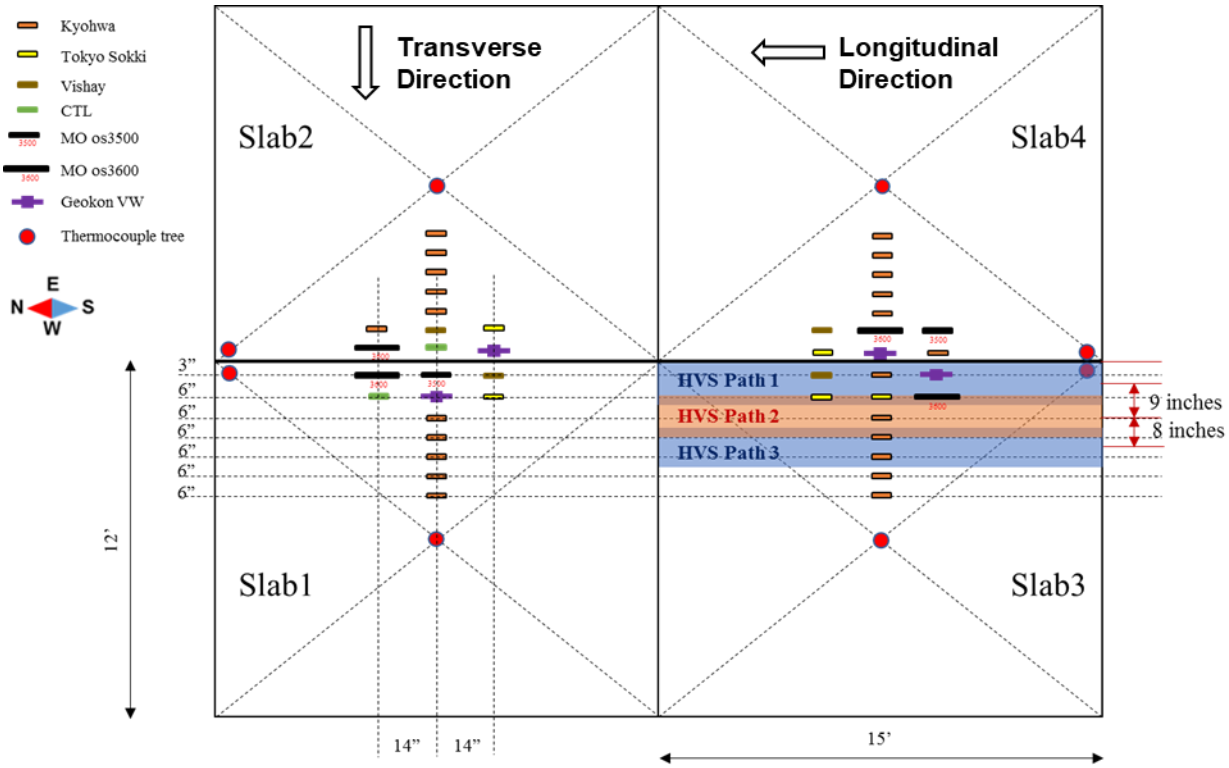

Figure 8-10. Instrumentation layout

Table 8-3. List of strain sensors installed in the test slabs

Type	Manufacturer	Model	Gauge length (in.)	Operating range (°F)
Fiber optic	Micron Optics	os3600	9.8	-40 to +176
Fiber optic	Micron Optics	os3500	4.3	-40 to +176
Vibrating Wire	Geokon	4200A-2	6.0	-4 to +176
Resistance	Vishay	EPG-5-120	4.3	23 to +122
Resistance	Kyowa	KM-120-120-H2-11	4.7	14 to +158
Resistance	Tokyo Sokki	PML-60-sL	2.4	-4 to +140
Resistance	CTL	-	8.0	-29 to +399

8.3.2 HVS Loading Configuration

The HVS loading was applied using a super single tire with a contact pressure of 110 psi and a load of 12 kips, traveling at about 7.5 mph in a unidirectional mode with no wander. The HVS loading was applied at three different locations in each slab, namely at 6 inches, 15 inches, and 23 inches from the edge of the slab. For each loading path as shown in Figure 8-10, the slab was loaded for a minimum duration of 24 hours.

8.3.3 Data Acquisition System

During HVS testing, dynamic strain data from the tested slab were recorded at every 1-hour interval, for 200 seconds each time. This recording scheme allowed recording of data for at least 20 passes of HVS load for each interval. Temperature data were recorded at fifteen-minute intervals. The AC unit and regulator were equipped on the DAQ system cabinet for maintaining a stable condition in terms of temperature, humidity, and electric power.

8.3.4 Finite Element Modeling of Test Slabs

A 3-D finite element model for concrete slabs was developed using the ADINA (version 9) finite element software. Figure 8-11 shows the 3-D finite element model which was developed for the analysis of the four test slabs. A concrete slab is modeled by an assemblage of elastic hexahedron elements. A hexahedron element is defined by eight nodes with each node having three degrees of freedom, i.e., translations in the x-, y-, and z-directions. The effects of temperature changes in the concrete slab can also be considered in the analysis. The concrete is characterized by its elastic modulus, Poisson's ratio, and coefficient of thermal expansion (CTE).

The test slabs are modeled as not bonded to the underlying foundation. The pavement foundation is modeled as an isotropic and linearly elastic subgrade material characterized by its elastic modulus and Poisson's ratio. A depth of 150 inches was used to model the subgrade material. The bottom of subgrade layer was modeled as fixed in z- direction.

The properties of the four concretes used in the model were initially obtained from the measured properties of the sampled concrete. The elastic modulus of the subgrade was obtained through the back-calculation method by matching the analytical to the measured FWD deflections of the test slabs, as presented in the next section. Load transfer across the joint between two adjacent slabs is modeled by translational springs connecting the nodes of the finite elements along the joint, as illustrated in Figure 8-12. Spring elements also have three degrees of freedom. Three values of spring constants are used to represent the springs stiffness along x-, y-, and z-directions.

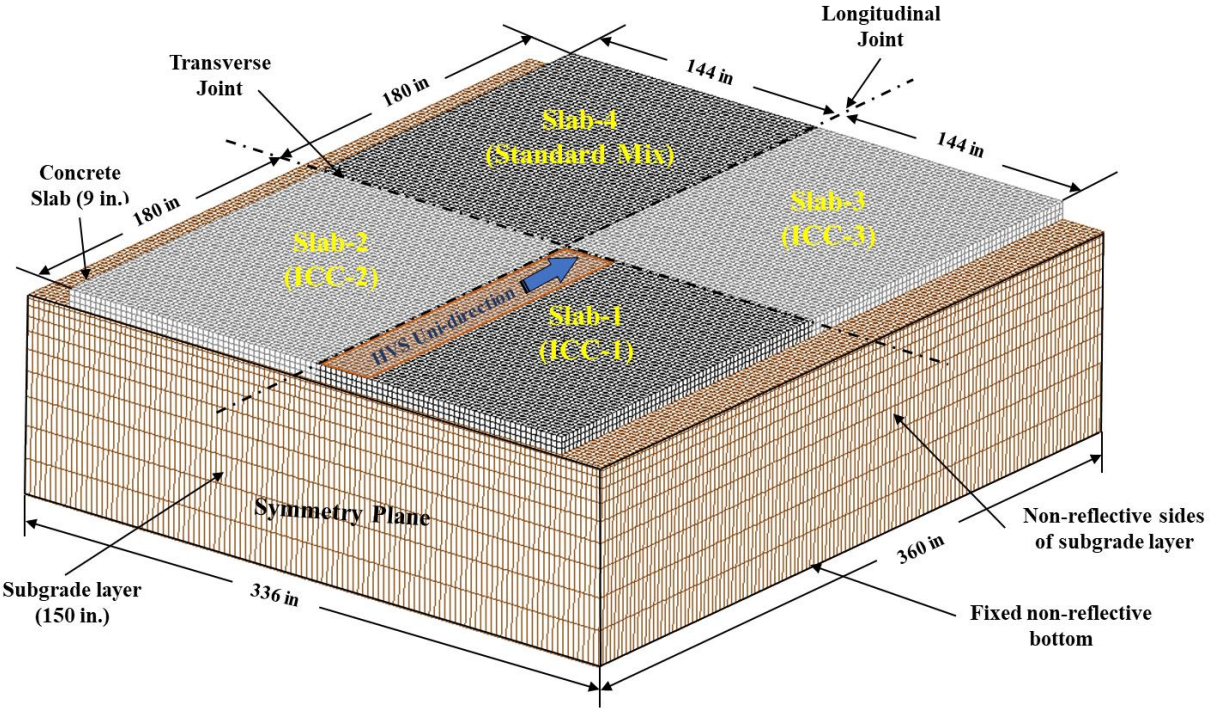

Figure 8-11. 3-D finite element model for the four test slabs

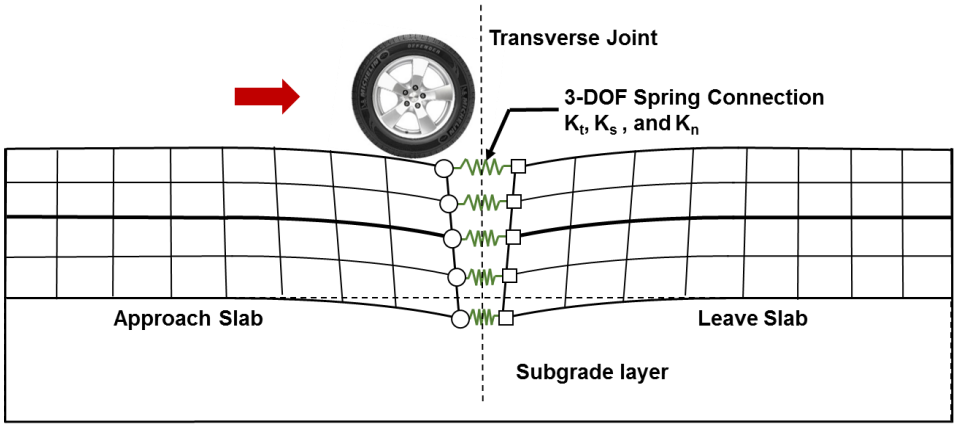

Figure 8-12. Modeling of transverse joint using spring elements

8.3.5 Calibration of the FE Model

The elastic modulus of the concrete material was initially estimated from the results of laboratory tests on the sampled concrete. The elastic modulus of subgrade and the stiffness of the joint and edge springs were estimated by back-calculation of the FWD deflection data. The results of the FWD tests at the slab center were used to estimate the elastic modulus of the subgrade. The results of the FWD test at the joints were used to calibrate values of spring stiffness at the joints by matching the analytically computed deflections with the measured FWD deflections.

Surface deflections in the concrete pavement caused by a 12-kip FWD were used to estimate the values of the elastic modulus of the subgrade and the stiffness of the springs for the load transfer at the joints in the FE model. Figure 8-13 shows an example of measured and computed deflection basin caused by a 12-kip FWD load at the center of the slab. This set of FWD tests was done in the midday when the slab would tend to have a positive temperature differential resulting in full contact with the subgrade at the slab edge. The measured deflection basins in the transverse direction were very similar to those in the longitudinal direction. The

analytical deflection basin was calculated by using an elastic modulus of the subgrade of between 70,000 and 80,000 psi.

Deflection basin caused by FWD load applied at the joint were used to estimate the springs joint stiffness, which was used to model the load transfer at the joints. The estimated elastic moduli of the slab and subgrade were used in the FE model to compute the deflection basin across the joint. Figure 8-13 shows the matched deflection basins from the back-calculation process for estimating the joint springs stiffness. Using the previously estimated parameters and material properties, fairly well-matched results between the measured and the calculated deflection basins were achieved with a vertical stiffness of 100,000 lb/in. and with the stiffness of 10,000 lb/in. in the x- and y- directions. Table 8-4 presents a summary of model parameters for the four test slabs.

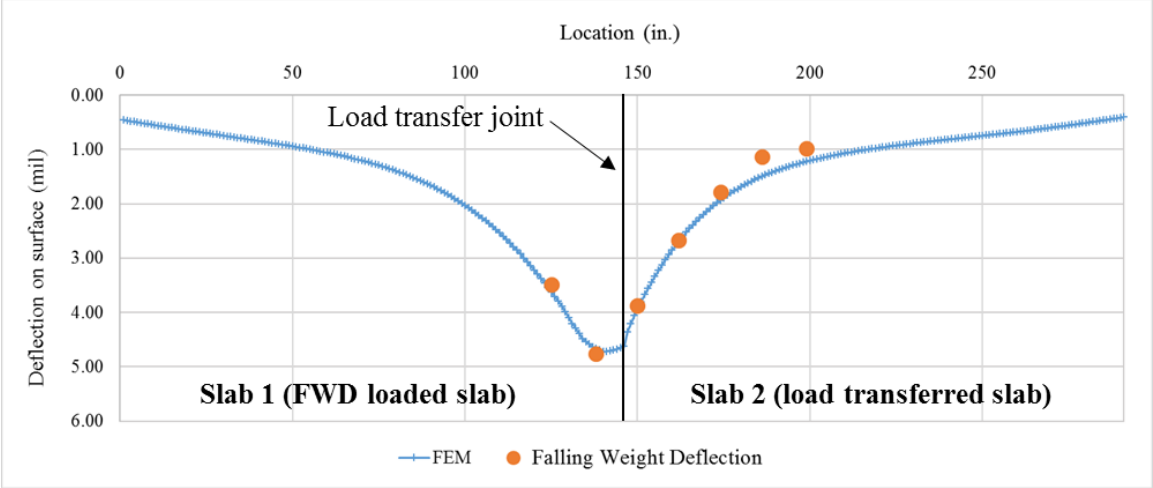

(a)

Figure 8-13. Continued

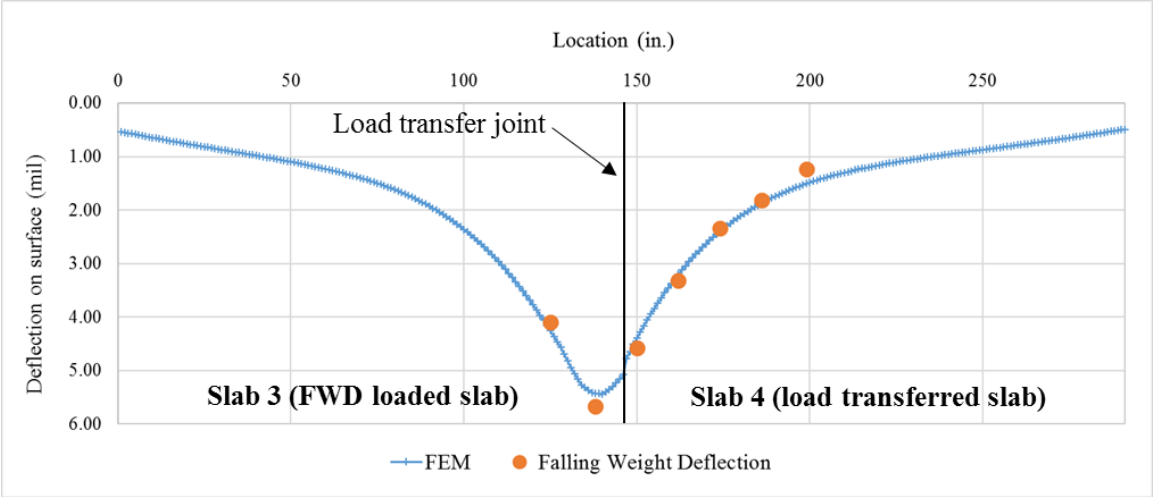

(b)

Figure 8-13. Determination of spring stiffness across the joint using FWD basin caused by a 12-kip FWD load at the joint for (a) Slab 1 and Slab 2 and (b) Slab 3 and Slab 4

Table 8-4. Summary of model parameters calibrated for the four test slabs

Parameters used in FE model	SM Slab 4	ICC-1 Slab 1	ICC-2 Slab 2	ICC-3 Slab 3
Elastic Modulus of Concrete (ksi)	4,300	3,750	2,100	2,650
Density of Concrete (pcf)	150	150	150	150
Coefficient of Thermal Expansion (/°F x 10^{-6})	6.07	5.56	5.80	5.94
Poisson's ratio	0.2	0.21	0.21	0.21
Elastic Modulus of Subgrade (ksi)	80	70	70	80
Spring Constant for Load Transfer (lb/in)				
Transverse Joint X	10,000	10,000	-	-
Transverse Joint Y	10,000	10,000	-	-
Transverse Joint Z	1,000,000	1,000,000	-	-
Longitudinal Joint X	10,000	-	10,000	-
Longitudinal Joint Y	10,000	-	10,000	-
Longitudinal Joint Z	1,000,000	-	1,000,000	-

8.3.6 Assessment of Critical Stress Analysis

Using the developed 3-D finite element models for the four test slabs, which were calibrated with the measured deflection basins from FWD tests, analysis was performed to determine the maximum stresses in the slabs if they were subject to some critical load and temperature conditions. A 22-kip axle load, which represents the maximum legal load limit for single axle load in Florida, was used as the applied load in the analysis. Analysis for the following two critical load-temperature conditions was performed:

(1) A 22-kip axle load was applied to the mid-edge of the pavement slab with a temperature differential of +20°F.

(2) A 22-kip axle load was applied to the corner of the pavement slab with a temperature differential of -10°F.

These two critical loading conditions are shown in Figure 8-14. For comparison purpose, analysis was also performed for the following load-temperature conditions:

(1) A 22-kip axle load was applied to the mid-edge of the pavement slab with no temperature differential.

(2) A 22-kip axle load was applied to the mid-edge of the pavement slab with a temperature differential of -10°F.

(3) A 22-kip axle load was applied to the corner of the pavement slab with no temperature differential.

(4) A 22-kip axle load was applied to the corner of the pavement slab with a temperature differential of +20°F.

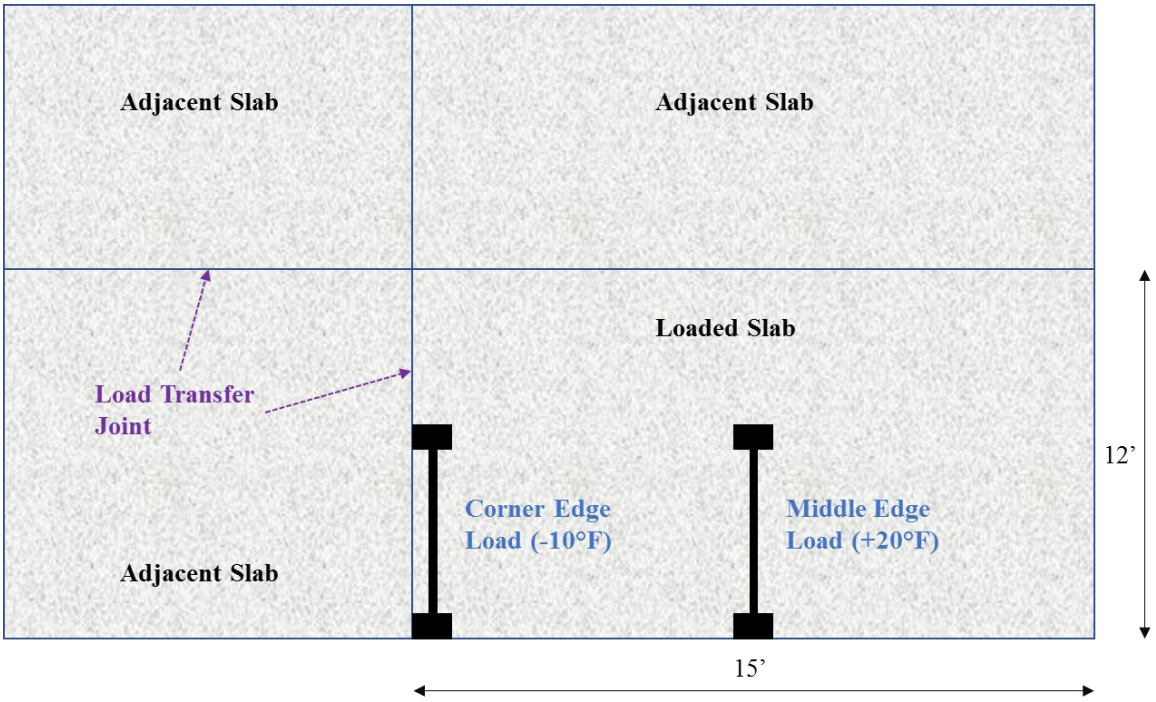

Figure 8-14. Critical load-temperature conditions for the test slabs

Table 8-5 shows the maximum computed stresses in the four test slabs from the critical stress analysis. In order to assess the potential performance of these test slabs in service, the maximum computed stresses were divided by the flexural strength of the concrete of the test slab to obtain the stress-to-strength ratios. According to fatigue theory, the number of load repetitions to failure of concrete increases as the stress-to-strength ratio decreases. Thus, a lower computed stress-to-strength ratio would indicate a higher allowable number of load repetitions to failure and a better-expected performance in service. The measured 28-day flexural strengths of the concrete sampled from the test slabs were used to compute the stress-to-strength ratios, which are also shown in Table 8-5.

Table 8-5. Computed maximum stresses and stress-to-strength ratios for the test slabs

	Mix	CTE (x 10^{-6}°F)	Modulus of Elasticity (ksi)	Flexural Strength (psi)	Computed Stress (psi)		Stress-to-Strength Ratio	
					Corner	Mid-edge	Corner	Mid-edge
Temperature Differences of +20°F	SM	6.07	4,300	805	407.0	460.3	0.51	0.57
	ICC-1	5.56	3,750	715	340.9	369.4	0.48	0.52
	ICC-2	5.80	2,100	300	264.7	294.2	0.88	0.98
	ICC-3	5.94	2,650	305	317.8	339.5	1.04	1.11
Temperature Differences of -10°F	SM	6.07	4,300	805	190.1	173.5	0.24	0.22
	ICC-1	5.56	3,750	715	168.3	149.5	0.24	0.21
	ICC-2	5.80	2,100	300	132.1	125.1	0.44	0.42
	ICC-3	5.94	2,650	305	142.9	126.9	0.47	0.42
Temperature Differences of ±0°F	SM	6.07	4,300	805	179.7	181.2	0.22	0.23
	ICC-1	5.56	3,750	715	157.7	174.7	0.22	0.24
	ICC-2	5.80	2,100	300	132.5	172.3	0.44	0.58
	ICC-3	5.94	2,650	305	145.1	174.3	0.48	0.56

From the results presented in Table 8-5, it can be seen that the maximum stresses and the maximum stress-to-strength ratios were obtained at the condition when a 22-kip axle load was applied to the mid-edge of the pavement slab with a temperature differential of +20°F. At this critical loading condition, the computed stress-to-strength ratios for SM (Slab 4), ICC-1 (Slab 1), ICC-2 (Slab 2), and ICC-3 (Slab 3) are 0.57, 0.52, 0.98, and 1.11, respectively. Based on the maximum stress-to-strength ratios, the ranking of the test slabs from best to worst should be ICC-1 (Slab 1), SM (Slab 4), ICC-2 (Slab 2), and ICC-3 (Slab 3). It is to be noted that the high stress-to-strength ratios for the ICC-2 and ICC-3 slabs were due to the very low flexural strengths (300 and 305 psi) of these two concrete mixes caused by exceptional high air voids (18.9%).

8.3.7 Assessment by Visual Observation

HVS loading was applied on ICC-1 slab (Slab 1) and standard mix slab (Slab 4) 129 days and 134 days after their construction, respectively. HVS loading was applied on ICC-2 slab (Slab 2) and ICC-3 slab (Slab 3) 137 days and 116 days after their construction, respectively. No visible cracks were observed on all four test slabs before the HVS loading. After HVS loading, visible corner cracks were observed on Slab 2 and Slab 3, which had high computed maximum stress-to-strength ratios (0.98 and 1.11) from the critical stress analysis. Figures 8-15 and 8-16 show pictures of the surface of Slabs 2 and 3, respectively, after HVS loading.

Figure 8-15. Slab 2 after HVS loading

Figure 8-16. Slab 3 after HVS loading

Slab 1 and Slab 4, which had low computed stress-to-strength ratios (0.52 and 0.57) did not show any visible cracks after HVS loading. Figures 8-17 and 8-18 show pictures of the surface of Slabs 1 and 4, respectively, after HVS loading.

Figure 8-17. Slab 1 after HVS loading

Figure 8-18. Slab 4 after HVS loading

8.3.8 Evaluation of Sensors for Dynamic Strains

8.3.8.1 Overview

HVS loading was applied to the four test slabs using a super single tire with a contact pressure of 110 psi and a load of 12 kips, traveling at about 7.5 mph in a unidirectional mode with no wander. The HVS loading was applied at three different locations in each slab, namely at 6 inches, 15 inches, and 23 inches from the edge of the slab. For each loading path, the slab was loaded for a minimum duration of 24 hours. During HVS testing, dynamic strain data from the tested slab were recorded at every 1-hour interval, for 200 seconds each time. This recording scheme allowed recording of data for at least 20 passes of HVS load for each interval. Six different strain gauges were used to measure the dynamic strains along the first wheel path which was six inches from the edge of the slab. This section presents the analysis of the dynamic strain data and the evaluation of these six different strain gauges when the HVS load was applied along the first wheel path which was six inches from the edge of the slab.

8.3.8.2 Preprocessing of Dynamic Strain Data

The recorded dynamic strain data from the various strain gauges were found to contain a substantial amount of noises from various sources including electric power, equipment, and environmental vibration. Thus, it is necessary to filter the measured signals to get rid of the unwanted noises before the measured signal could be properly analyzed.

The unfiltered measured signals were first evaluated using a Fast Fourier Transform (FFT) tool from the MATLAB toolbox (Krauss et al. 2001). The FFT tool transforms the evaluated signals into a frequency spectrum. Figures 8-19a and 8-19b show the typical frequency spectrums of the measured signals from the electrical resistance strain gauges during HVS loading and without HVS loading, respectively. From these two figures, it can be seen that when there was no HVS loading, noises were present at frequencies around 60 Hz, and around

180 Hz. From these two figures, it can also be seen that the measured dynamic strains due to the HVS load had frequencies lower than 20 Hz. Moreover, Sun (1998) has also reported that the main frequency distributions of the measured strains due to dynamic vehicle loads ranged from 1 to 15Hz. This finding is similar our observation of the dynamic strains due to HVS loading. Thus, it was decided to apply a low-pass filter to the measured signals using the Butterworth method from the MATLAB Toolbox, to filter out signals with frequencies higher than 20 Hz. Figure 8-19c shows the frequency spectrum of the filtered signal after the low-pass filter had been applied.

The measured signals from the fiber optic strain sensors also contained noises. Figure 8-20a shows a typical frequency spectrum of the measured signals from the fiber optic strain sensors during HVS loading. Similarly, noises can be observed at frequencies around 180 Hz. However, unlike the measured signals from the electrical resistance strain gauges, there was no noise at frequencies around 60 Hz, which was due to electric power supply. A low-pass filter using the Butterworth method was also applied to the fiber optic strain sensor signals to filter out signals with frequencies higher than 20 Hz. Figure 8-20b shows the frequency spectrum of the filtered signal after the low-pass filter had been applied. Figures 8-21 through 8-24 shows the comparison of unfiltered versus filtered strain signals obtained from Slabs 1 through 4, respectively.

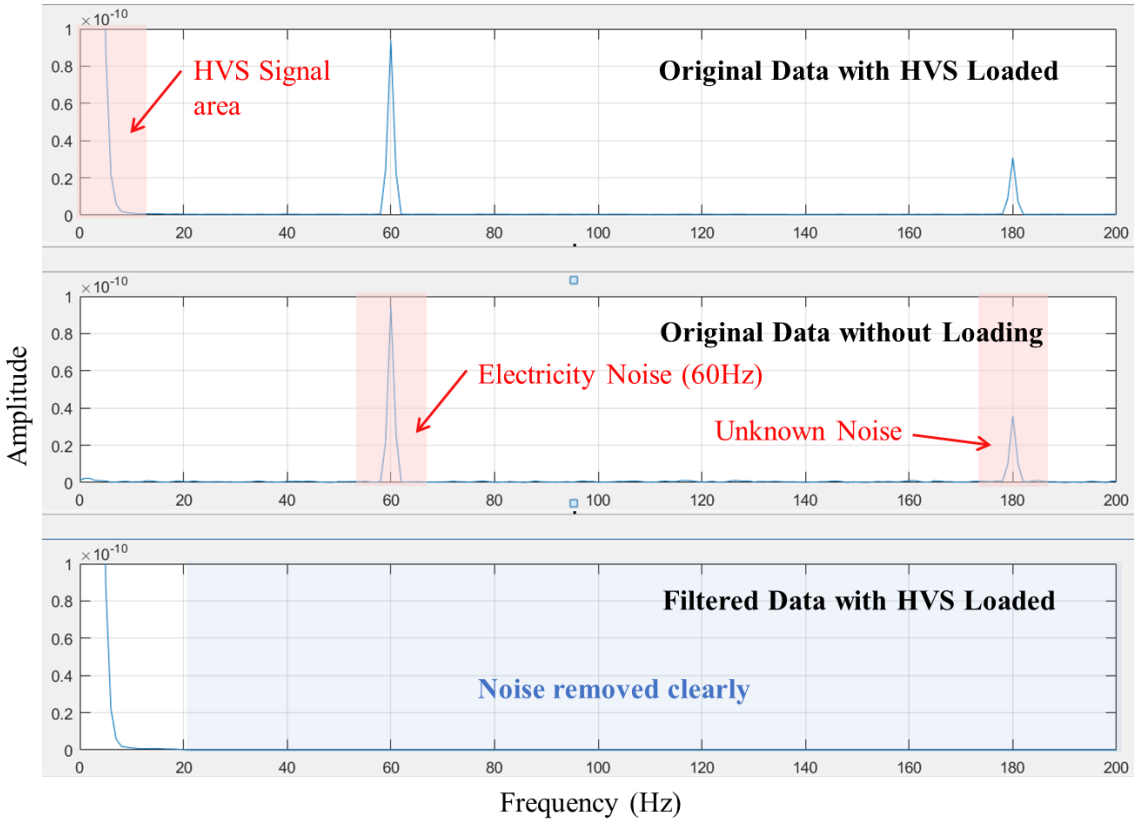

Figure 8-19. Frequency spectrum of measured strain signals from electrical resistance strain gauges (a) with HVS loading, (b) without HVS loading, and (c) with HVS loading after low-pass filtering

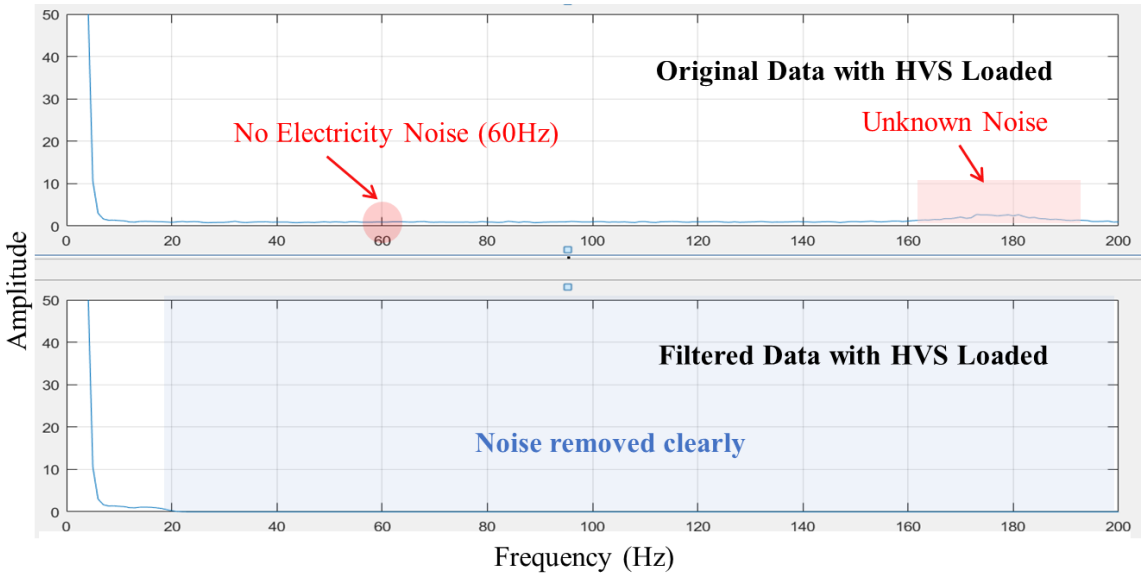

Figure 8-20. Frequency spectrum of measured strain signals from fiber optic strain sensors (a) with HVS loading, (b) with HVS loading after low-pass filtering

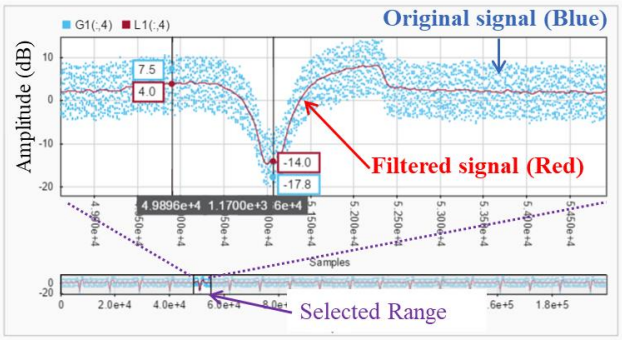

(a) Vishay - Top Sensor

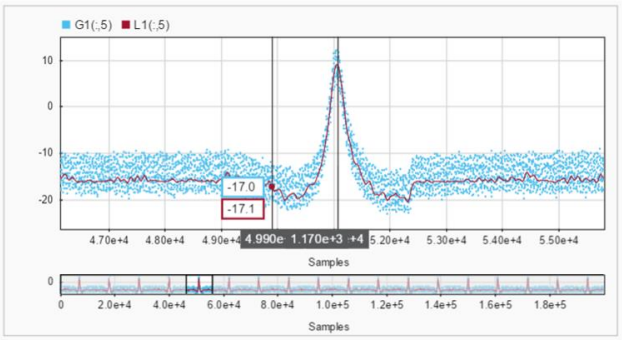

(b) Vishay - Bottom Sensor

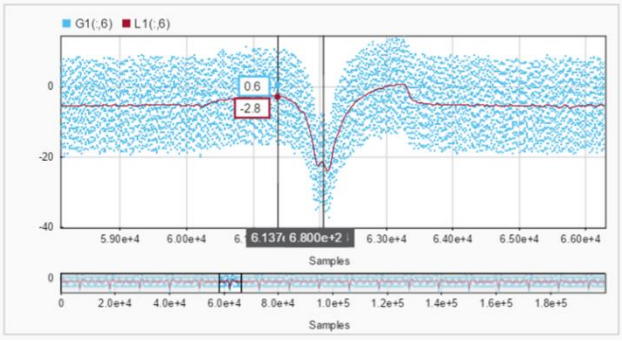

(c) CTL - Top Sensor

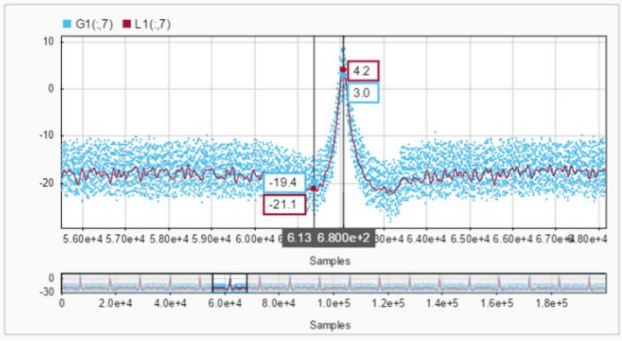

(d) CTL - Bottom Sensor

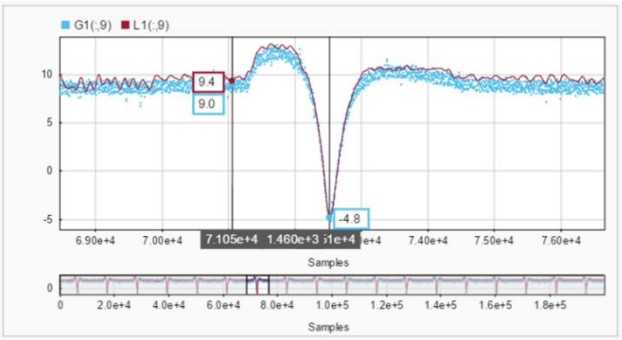

(e) Tokyo Sokki - Top Sensor

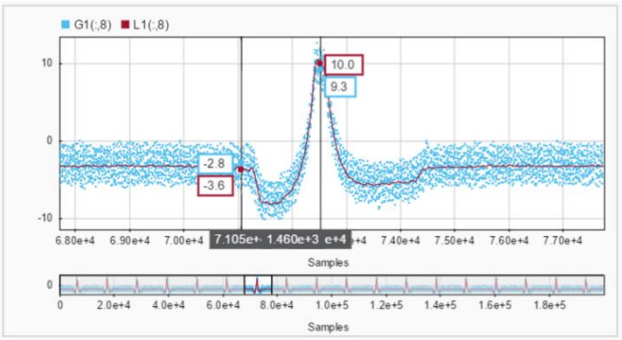

(f) Tokyo Sokki - Bottom Sensor

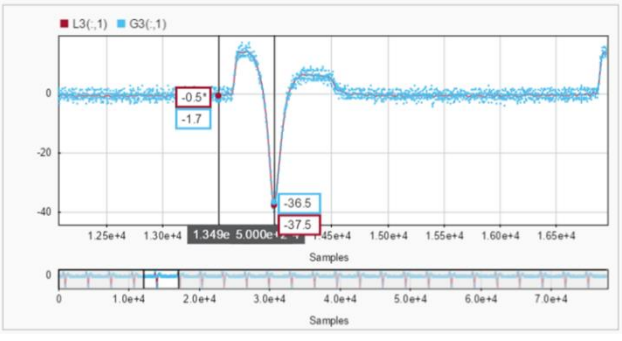

(g) OS3600 - Top Sensor

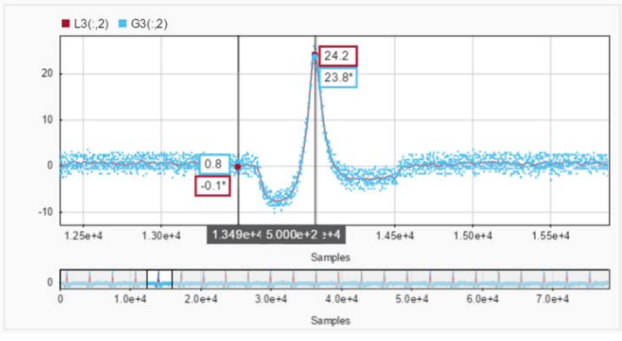

(h) OS3600 - Bottom Sensor

Figure 8-21. Continued

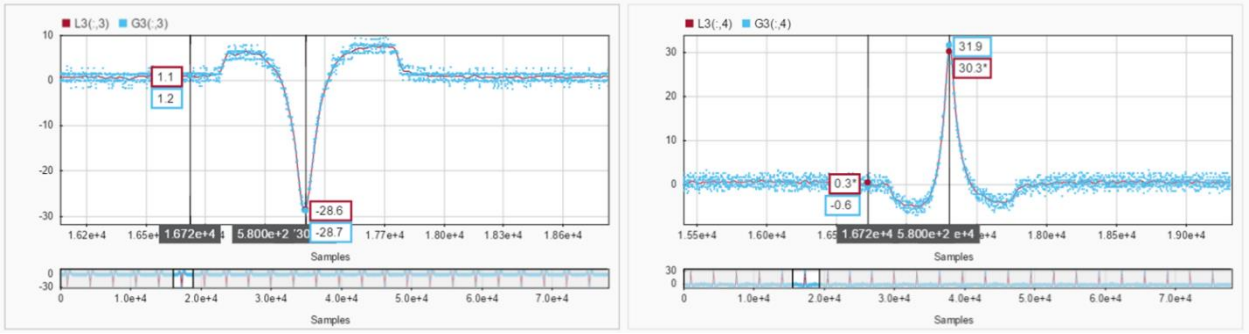

(i) OS3500 - Top Sensor (j) OS3500 - Bottom Sensor

Figure 8-21. Comparison of original versus filtered strain signals obtained from Slab 1

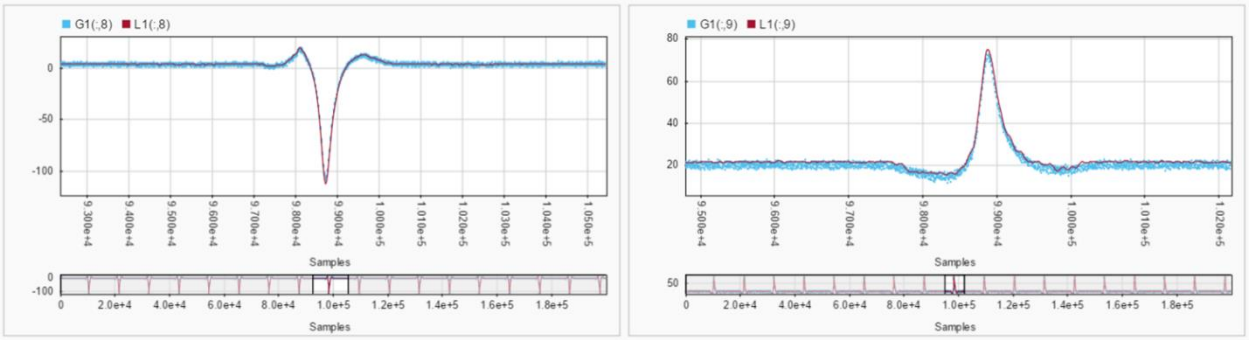

(a) Vishay - Top Sensor (b) Vishay - Bottom Sensor

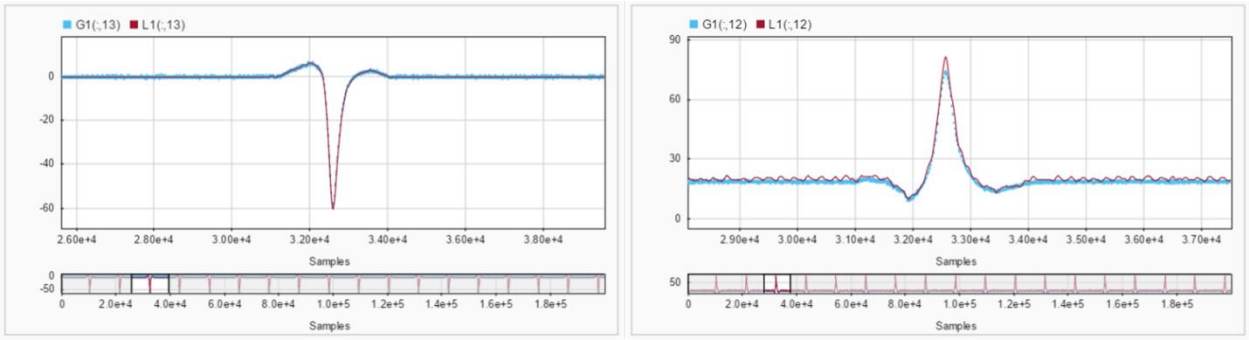

(c) CTL - Top Sensor (d) CTL - Bottom Sensor

Figure 8-22. Continued

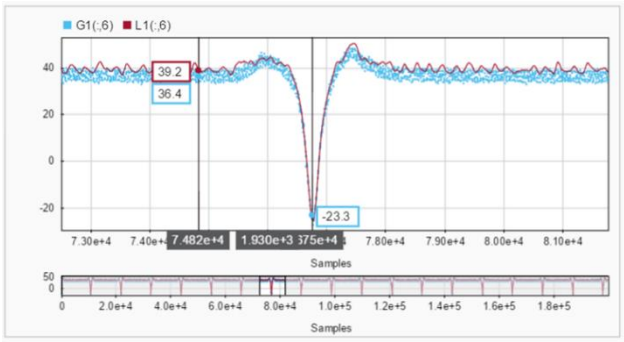

(e) Tokyo Sokki - Top Sensor

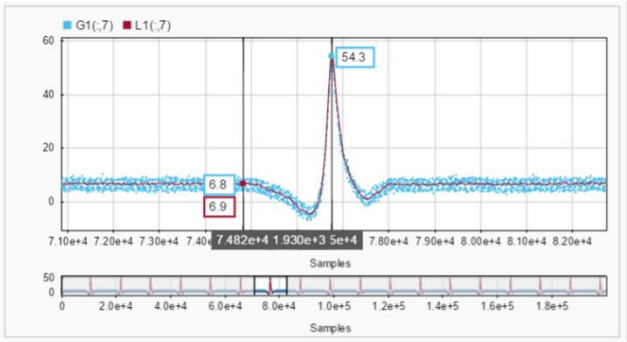

(f) Tokyo Sokki - Bottom Sensor

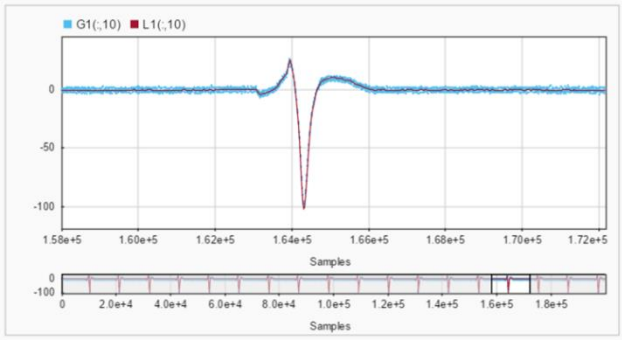

(g) Kyowa - Top Sensor

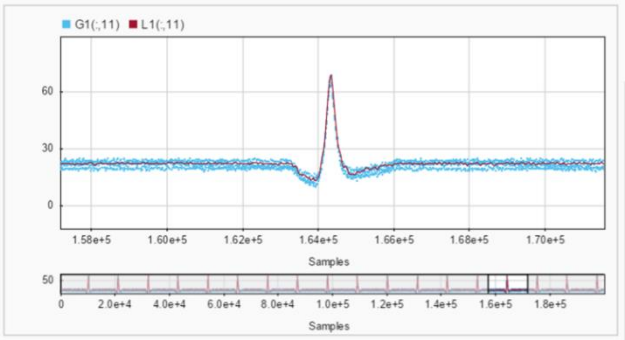

(h) Kyowa - Bottom Sensor

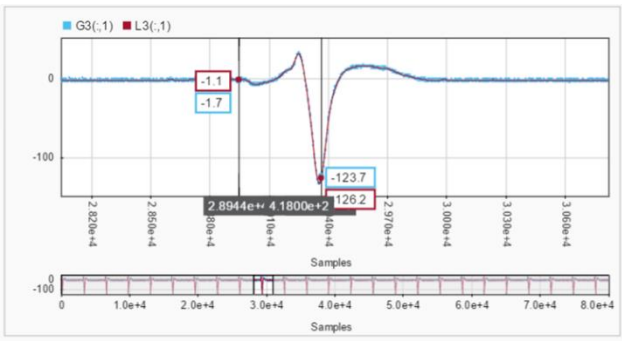

(i) OS3600 - Top Sensor

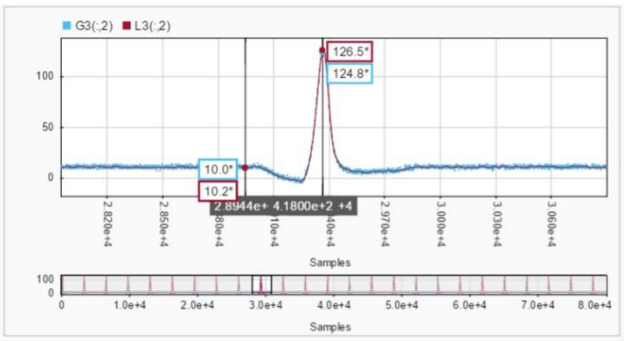

(j) OS3600 - Bottom Sensor

Figure 8-22. Comparison of original versus filtered strain signals obtained from Slab 2

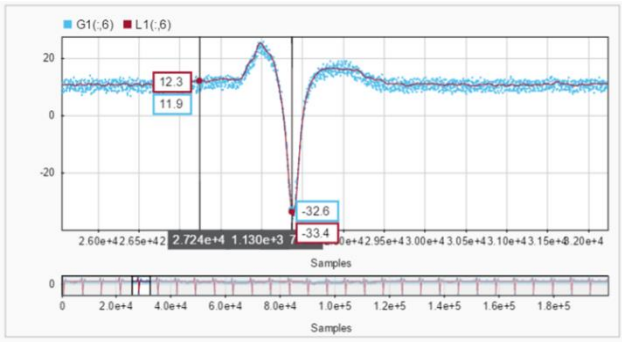

(a) Vishay - Top Sensor

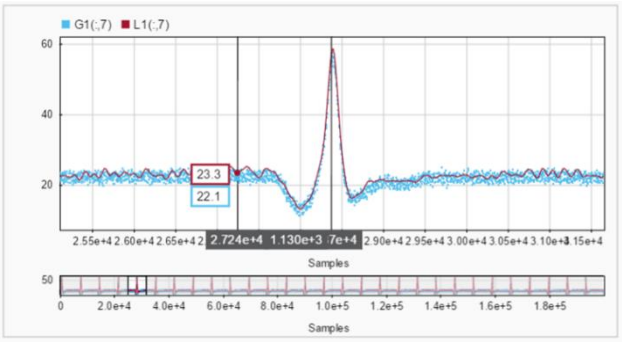

(b) Vishay - Bottom Sensor

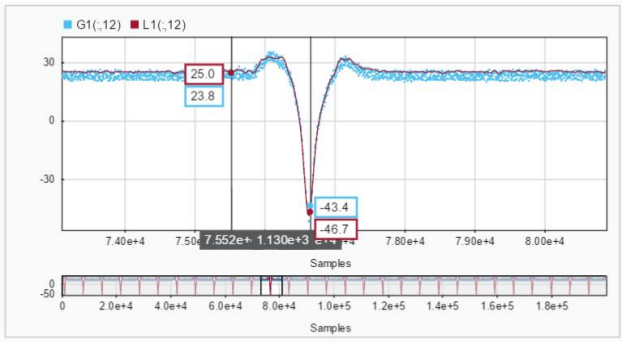

(c) Tokyo Sokki - Top Sensor

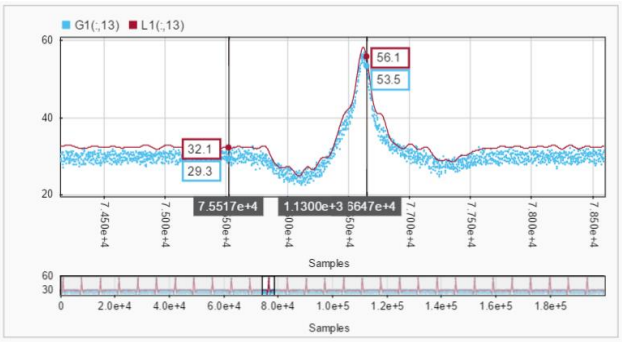

(d) Tokyo Sokki - Bottom Sensor

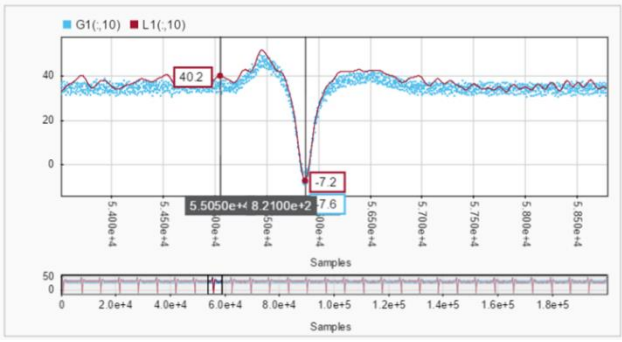

(e) Tokyo Sokki - Top Sensor

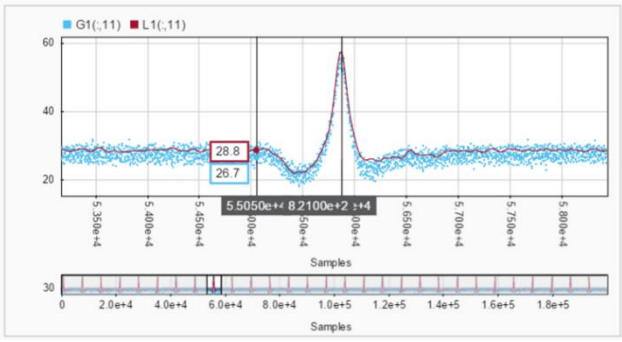

(f) Tokyo Sokki - Bottom Sensor

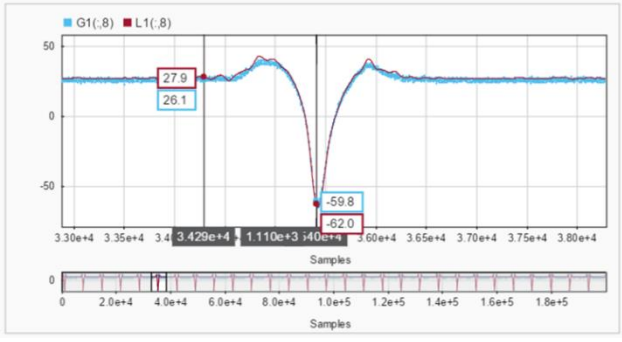

(g) Kyowa - Top Sensor

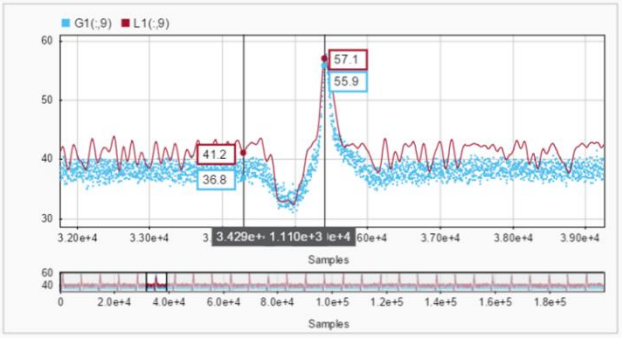

(h) Kyowa - Bottom Sensor

Figure 8-23. Continued

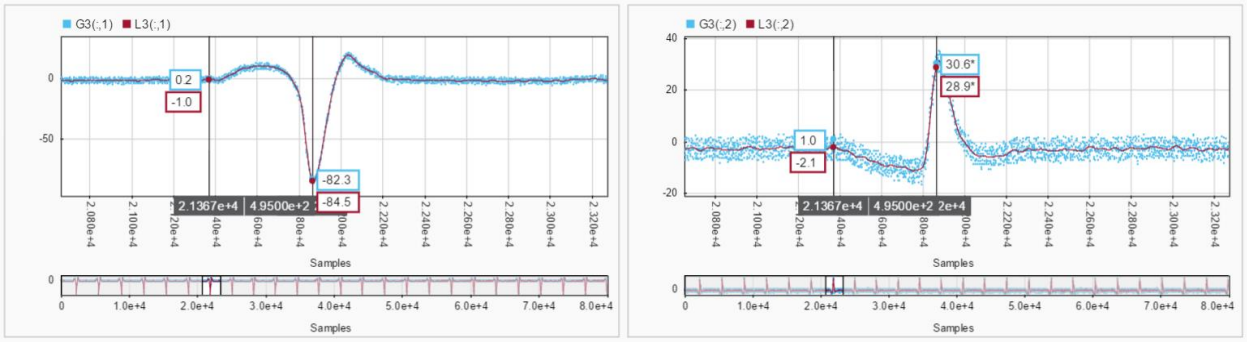

(i) OS3600 - Top Sensor (j) OS3600 - Bottom Sensor

Figure 8-23. Comparison of original versus filtered strain signals obtained from Slab 3

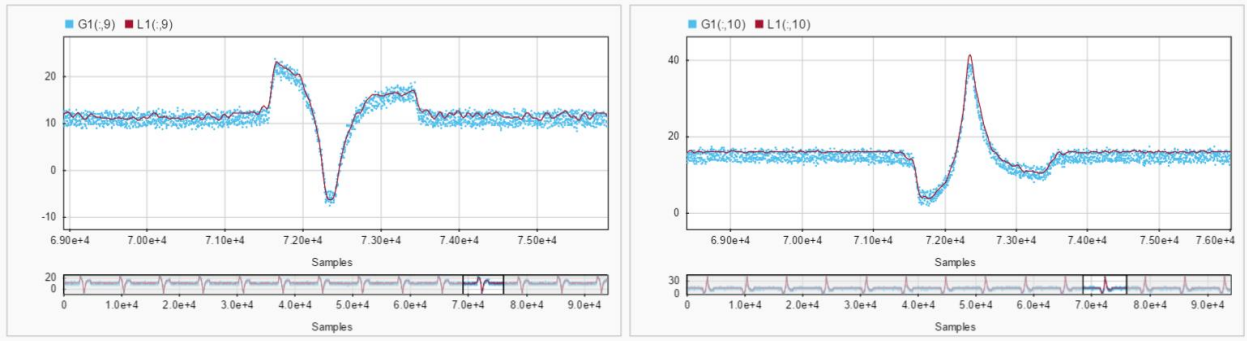

(a) Vishay - Top Sensor (b) Vishay - Bottom Sensor

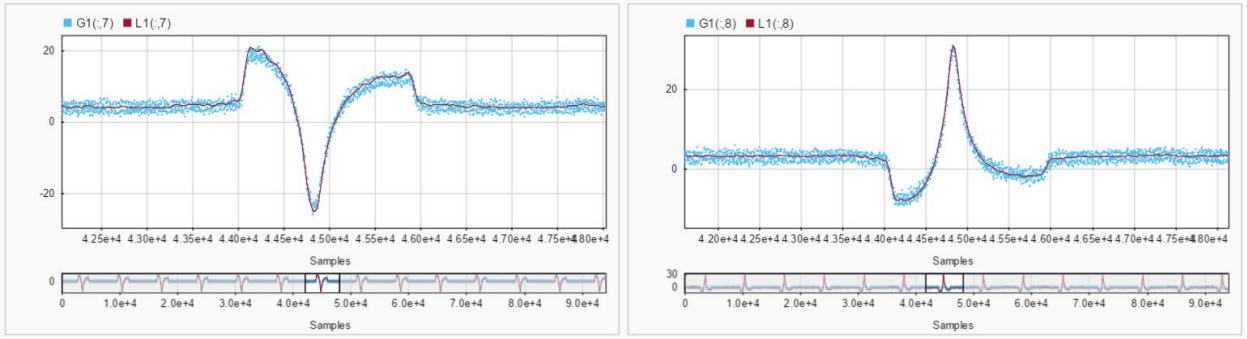

(c) Tokyo Sokki - Top Sensor (d) Tokyo Sokki - Bottom Sensor

Figure 8-24. Continued

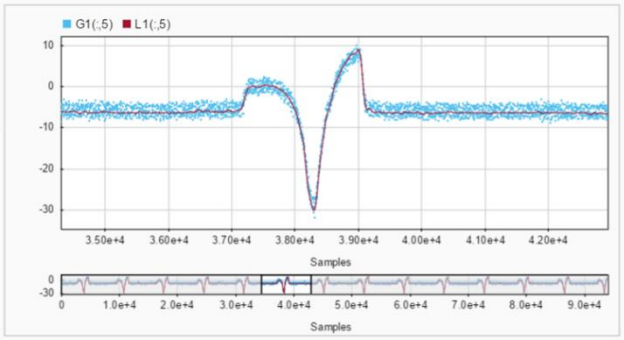

(e) Kyowa - Top Sensor

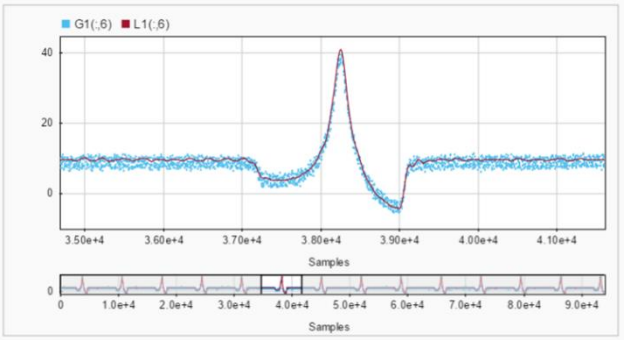

(f) Kyowa - Bottom Sensor

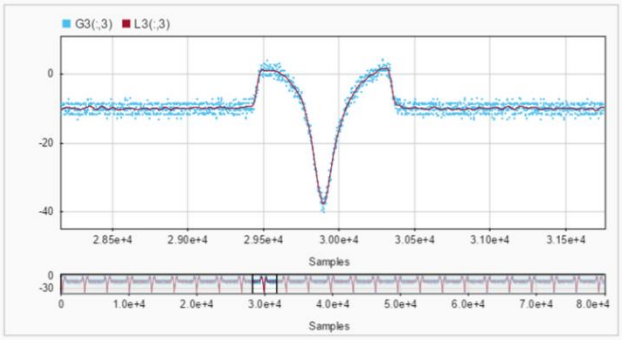

(g) OS3500 - Top Sensor

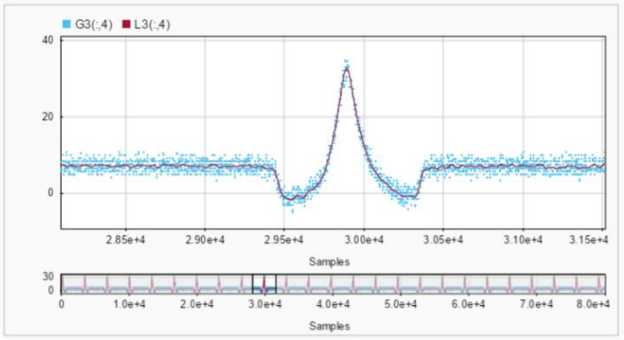

(h) OS3500 - Bottom Sensor

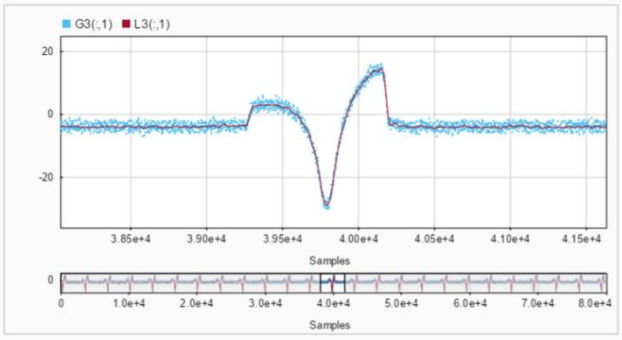

(i) OS3600 - Top Sensor

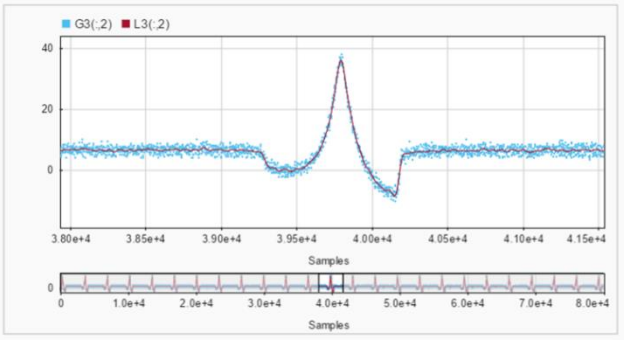

(j) OS3600 - Bottom Sensor

Figure 8-24. Comparison of original versus filtered strain signals obtained from Slab 4

8.3.8.3 Determination of Maximum Load-Induced Strains

Figure 8-25a shows a typical plot of the measured strain versus time as measured by a strain gauge at the top of the slab as a HVS load passed over it. It can be seen that there were measured compressive strains when the HVS load was directly over the strain gauge, and there were measured tensile strains right before and right after the HVS load passed over the strain gauge. The maximum load-induced compressive strain was taken to be the difference between the maximum compressive strain and the strain at the baseline as shown in the figure.

Figure 8-25b shows a typical plot of the measured strain versus time as measured by a strain gauge at the bottom of the slab as a HVS load passed over it. It can be seen that there were measured tensile strains when the HVS load was directly over the strain gauge, and there were measured compressive strains right before and right after the HVS load passed over the strain gauge. The maximum load-induced tensile strain was taken to be the difference between the maximum tensile strain and the strain at the baseline as shown in the figure.

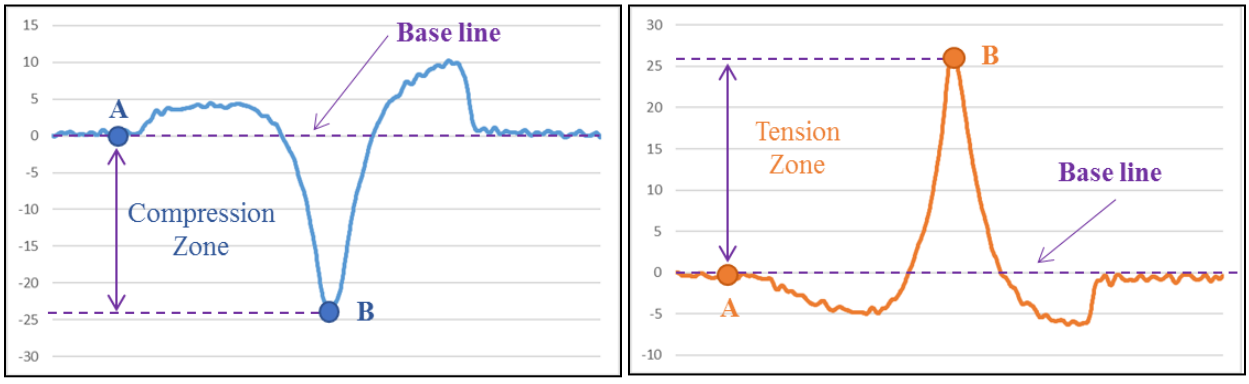

(a) (b)

Figure 8-25. Determination of maximum strains due to HVS load from OS3500 sensor at (a) top of slab and (b) bottom of slab

8.3.8.4 Evaluation of Accuracy of Strain Gauges for Dynamic Strain Measurement

Using the filtered strain data and the methodology as described in Section 3.8.3, the maximum compressive and tensile strains (caused by the 12-kip HVS load) as measured by the various strain gauges on the first HVS wheel path were determined. These determined maximum compressive and tensile strains from the six different strain gauges in the four test slabs at various testing times are presented in Appendix G.

In order to evaluate the accuracy of the various strain gauges in this field testing program, the measured maximum strain values were compared to each other and to the computed values from the FE models. Table 8-6 presents the computed maximum strains (caused by the 12-kip HVS load) at the locations of the strain gauges (2 inches from the top, and 2 inches from the bottom of the slab) for the four test slabs, and for temperature differentials of 0 and +20 ºF.

Table 8-6. Maximum computed strains at locations of gauges caused by a 12-kip HVS load

	Slab1		Slab2		Slab3		Slab4	
	Top	Bottom	Top	Bottom	Top	Bottom	Top	Bottom
Temp differential (+ 20 ºF)	-24.8	31.4	-29.2	37.1	-27.5	35.8	-24.5	29.4
Temp differential (± 0 ºF)	-25.5	29.7	-30.3	35.1	-28.0	33.6	-24.7	27.4

Note: values are in units of micro strain (με).

As can be seen from Table 8-6, the temperature differential in the concrete slab has some effects on the maximum strains in the slab. A positive temperature differential causes a slight decrease in the compressive strain at the top of the slab, but a slight increase in the tensile strain at the bottom of the slab. In order to compare the measured strains with the computed strains, a similar condition of temperature differential in the concrete slab must be used. The maximum measured strains obtained under the condition of close to zero temperature differential in the concrete slabs were used for this purpose. The selected measured strain data were obtained from

the following testing times when the temperature differential was close to zero: (1) Test 21 at 8:48 am for Slab 1, (2) Test 22 at 8:46 am for Slab 2, (3) Test 4 at 6:46 pm for Slab 3, and (4) Test 16 at 12:30 pm for Slab 4. The measured maximum strains the various strain gauges in the four test slabs are presented in Table 8-7. When these measured strain values are compared to the computed values in Table 8-6, it can be seen that only three sets of strain gauges have recorded reasonable strain values which are comparable to the computed values. The strain values which compare well with the computed strain values are highlighted in the table. These three sets of strain gauges are (1) OS3500 fiber optic sensor in Slab 1, (2) Kyowa KM-120 resistance strain gauge in Slab 4, and (3) OS3500 fiber optic sensor in Slab 4. The shorter OS3500 fiber optic sensor appeared to record more accurate strains than the longer OS3600 fiber optic sensor.

Table 8-7. Maximum measured strains from various strain gauges in the test slabs at zero temperature differential

Slab 1 (ICC1)	Sensor	OS3600	OS3500	Vishay	CTL	Tokyo
	TOP	-43.9	**-28.3**	-14.2	-14.2	-17.8
	Bottom	25.6	**31.6**	25.3	13.2	23.0
Slab 2 (ICC2)	Sensor	CTL	OS3600	Tokyo	Vishay	Kyowa
	TOP	-73.5	-128.3	-36.4	-105.6	-88.8
	Bottom	51.6	123.5	48.9	55.9	38.4
Slab 3 (ICC3)	Sensor	Vishay	Kyowa	Tokyo	Tokyo	OS3600
	TOP	-48.4	-89.4	-44.5	-72.2	-83.6
	Bottom	34.7	20.1	27.0	26.2	35.3
Slab 4 (Standard Mix)	Sensor	Kyowa	Tokyo	OS3500	OS3600	Vishay
	TOP	**-23.9**	-31.5	**-25.0**	-27.7	-16.6
	Bottom	**29.5**	26.5	**29.5**	25.4	22.3

Note: Values are in units of micro strain (με).
The highlighted values are the ones which compare well with the computed strain values.

Investigation was made to determine the possible causes of why most of the strain gauges appeared to be not working properly. FWD loads were applied to locations on the wheel path and close to the strain gauges and the FWD-load-induced strains were recorded to determine whether or not some of the strain gauges might be incorrectly identified. The results of this set of tests indicated that all the strain gauges were properly identified. However, the results also indicated that, with the exception of the same three sets of strain gauges, all the other strain gauges appeared to be not working properly. The results of this set of tests are presented in Appendix H.

8.3.9 Evaluation of Configuration of Strain Gauges for Test Slab

Since the measured strains from embedded strain gauges due to applied wheel loads are affected by the location of the wheel load, the variation of wheel load location would cause variation in the measured data and subsequently uncertainty in the analysis of the data. It is recommended that a series of five to seven uniformly-spaced strain gauges be placed at and around the wheel path to record the load-induced strains in the test slabs in the Concrete Test Road. This configuration of strain gauges would allow for the capture of the maximum load-induced strains in spite of possible variation of wheel load positions. It would also allow for the recording of the profile of load-induced strains at the wheel load position. This recommended configuration of strain gauges was evaluated in this field test.

Figure 8-26 shows the layout of seven strain sensors, which were uniformly spaced at a distance of 6 inches across the HVS wheel paths for each of the four test slabs. It also shows the location of the three HVS wheel paths used in the experiment. The 12-kip HVS wheel loading was applied at three different paths in each slab, namely at 6 inches, 15 inches, and 23 inches from the edge of the slab.

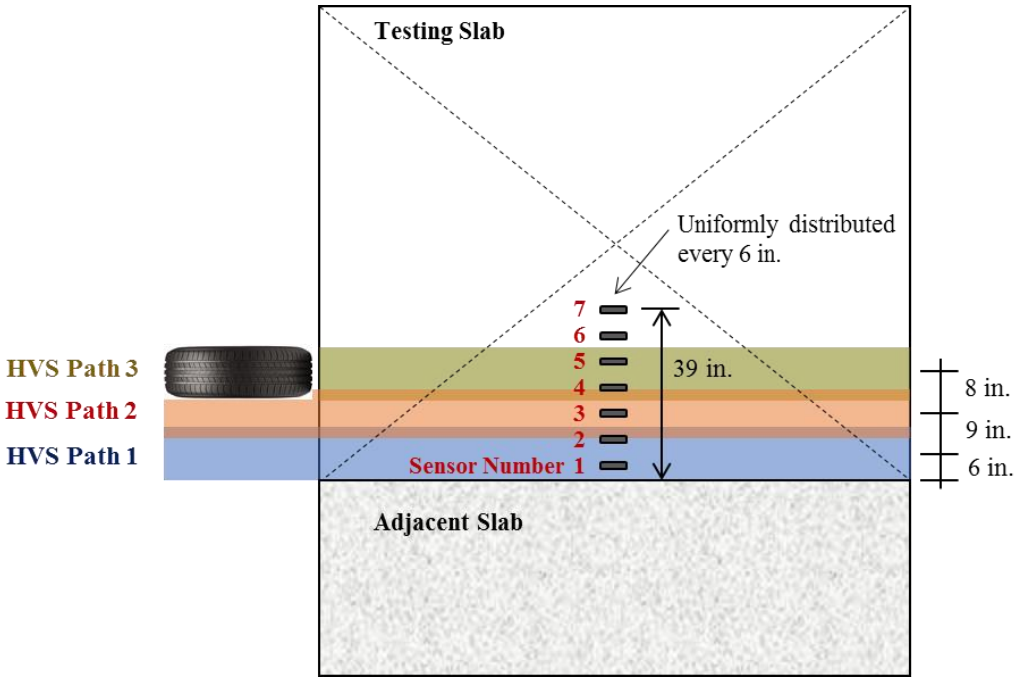

Figure 8-26. Layout of the sensors and HVS paths on each test slab

The load-induced strains from the seven strain sensors were recorded during the HVS loading to observe how the different wheel load positions affected the recorded data. Maximum load-induced strains recorded by the seven sensors when the temperature differential in the slab was close to zero were used in this analysis, and are presented in Appendix I. Maximum load-induced strains recorded by the seven sensors due to HVS loading at the three different wheel paths on Test Slab 4 are shown in Figure 8-27. It can be seen, from the profiles of the recorded strains, that the peak strain was recorded by the strain gauges at the location of the wheel load. As the location of the wheel load shifted, the profile of the recorded strains also changed to reflect the location of the applied load. The maximum load-induced strains in the concrete slab were also captured through the use of this strain gauge configuration.

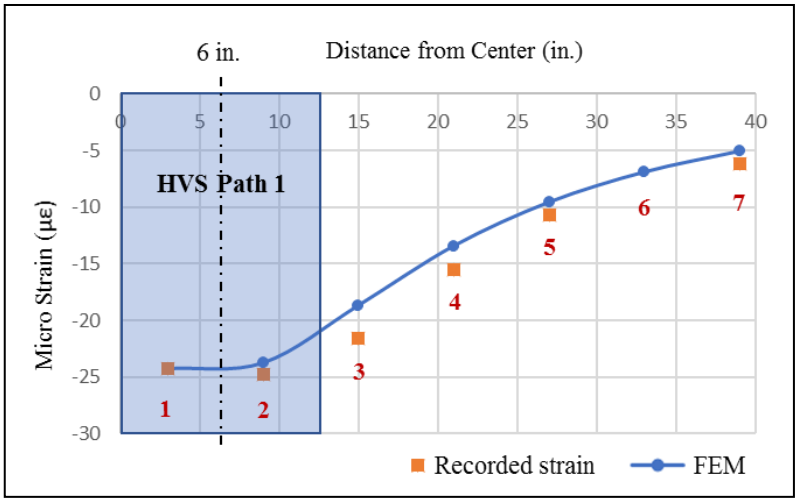

(a)

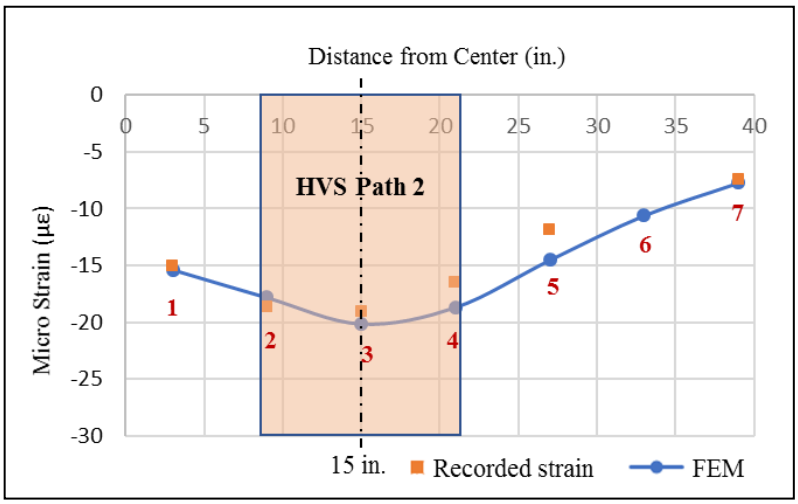

(b)

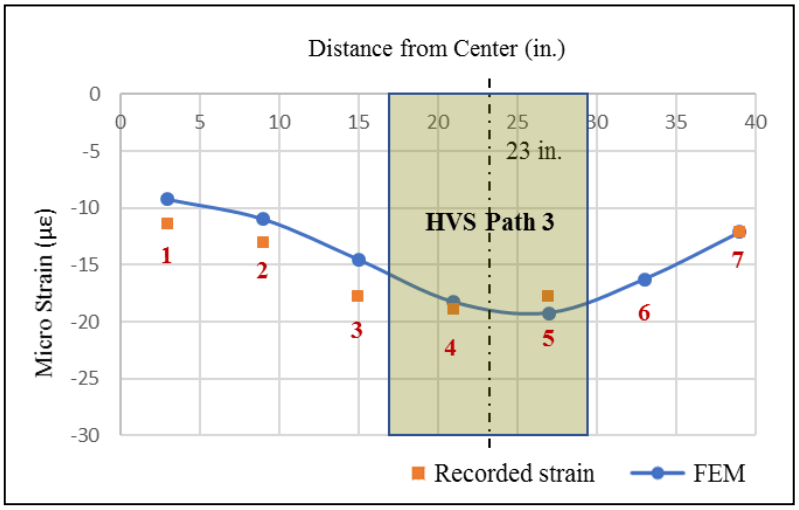

(c)

Figure 8-27. Maximum strains recorded by the seven sensors due to HVS loading at (a) Path 1, (b) Path 2, and (c) Path 3 on Test Slab 4

8.3.10 Evaluation of Sensors for Environmental Strains

8.3.10.1 Overview

Vibrating wire strain gauges (VWSG) were used to measure the environmental strains in the test slabs. Fiber optic strain sensors (FOS), which were used to measure dynamic strains in the test slabs, were also used to measure the environmental strains in this study. This section presents the evaluation of the VWSG and the FOS for measurement of environmental strains in the test slabs.

8.3.10.2 Calculation of Strains from VWSG and FOS

The VWSG measures the strains through measurement of changes of resonant frequency of the vibrating wire as the wire lengthens or shortens. The calculation of strains can be done by the following equation:

$$\varepsilon_{Actual} = (R_1 - R_0)B + (T_1 - T_0)(C_1) \tag{8.1}$$

Where, R_1 is the current reading of the resonant frequency

R_0 is the initial reading of the resonant frequency

B is the batch gauge factor

T_1 is the current temperature

T_0 is the initial temperature

C_1 is the coefficient expansion of steel

The FOS measures the strains through measurement of shifts in wavelength of the fiber optic as the sensor lengthens or shortens. The calculation of strains can be done by the following equation:

$$\varepsilon_{Actual} = 10^6 \left[\frac{(\Delta\lambda / \lambda_o)_S - (\Delta\lambda / \lambda_o)_T}{F_G} \right] + \frac{(\Delta\lambda / \lambda_o)_T}{S_T} CTE_T \tag{8.2}$$

Where, $\Delta\lambda$ is the wavelength shift (either due to strain and temperature),

λ_o is the nominal wavelength (either due to strain and temperature),

F_G is the gauge factor for the optical strain gauge,

S_T is the temperature compensator thermal response,

CTE_T is the coefficient of thermal expansion for FBG mount, and

CTE_C is the coefficient of thermal expansion for concrete pavement.

Note: calculated values are in units of micro strain (με).

The strain in the concrete due to temperature effects alone can be computed by the following equation:

$$\varepsilon_{thermal} = \frac{(\Delta\lambda / \lambda_o)_T}{S_T} CTE_C \tag{8.3}$$

Note: calculated values are in units of micro strain (με).

8.3.10.3 Comparison of Environmental Strains Measured by VWSG and FOS

The environmental strain data as recorded by the VWSG and FOS in Slab 1 during the 18-day period from March 30 through April 17, 2017, were used in this evaluation. During this period of time, the HVS testing on the test slabs had been finished and the HVS had been moved away from the test slab. Thus, it can be stated that the behavior of the test slabs during this period of time was not affected by the HVS.

Figure 8-28 presents the recorded temperature at the top (two-inch depth) and bottom (seven-inch depth) of Test Slab 1 during this period of time. Table 8-8 presents the recorded temperature differentials in the four test slabs during this period of time. It can be seen that both the temperatures at the top and the bottom went through daily cycles of high and low

temperatures. The temperature differential in the slab can also be seen to change from a positive to a negative value on a daily basis.

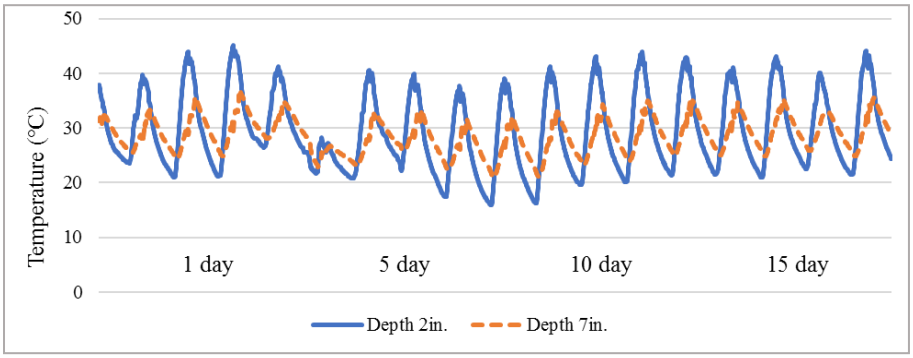

Figure 8-28. Recorded temperature at the top and bottom of concrete slab 1

Table 8-8. Maximum positive and negative temperature differentials in the four test slabs

	Slab 1		Slab 2		Slab 3		Slab 4	
	Positive Temp. Difference	Negative Temp. Difference	Positive Temp. Difference	Negative Temp. Difference	Positive Temp. Difference	Negative Temp. Difference	Positive Temp. Difference	Negative Temp. Difference
3/30/17	18.2	-	21.1	-	16.1	-	12.2	-
3/31/17	24.1	-3.6	30.8	-4.1	22.8	-3.2	16.6	-3.5
4/1/17	29.8	-7.6	37.2	-10.8	28.2	-10.3	22.1	-7.7
4/2/17	30.1	-8.7	37.9	-12.1	29.8	-11.4	21.0	-8.6
4/3/17	17.1	-2.8	22.4	-3.4	19.9	-3.4	15.2	-3.3
4/4/17	3.2	-6.2	2.5	-7.6	2.5	-7.1	1.9	-6.3
4/5/17	24.8	-6.2	28.7	-8.5	22.1	-7.9	17.9	-6.0
4/6/17	22.1	-6.0	23.8	-9.4	17.7	-9.8	16.3	-7.8
4/7/17	24.0	-11.9	27.0	-17.0	17.6	-15.6	13.2	-11.5
4/8/17	27.1	-11.5	31.8	-15.9	22.0	-14.5	16.3	-10.6
4/9/17	28.6	-11.6	34.4	-15.9	25.4	-14.6	18.4	-10.7
4/10/17	28.6	-8.3	34.8	-11.1	25.8	-10.4	18.6	-7.7
4/11/17	30.7	-9.3	33.3	-13.3	28.4	-12.7	20.1	-9.1
4/12/17	23.1	-8.2	28.7	-11.3	25.3	-10.6	18.8	-7.9
4/13/17	24.7	-8.8	26.3	-12.3	21.3	-11.5	14.6	-8.6
4/14/17	22.5	-9.0	26.0	-12.8	21.9	-11.8	16.3	-8.6
4/15/17	17.0	-7.4	21.2	-10.2	19.4	-9.4	14.7	-7.1
4/16/17	24.7	-8.1	28.6	-10.9	24.7	-10.0	18.8	-7.5
4/17/17	-	-7.7	-	-10.7	-	-10.0	-	-7.5

Note: values are in units of temperature (°F).

The VWSG and the FOS on Slab 1 were both located at the mid-edge of the slab and should have similar environmental strains. However, a comparison between these two sets of measured strains from the top of the slab, as shown in Figure 8-29, show that they were substantially different. The variation of measured strains from the VWDG was substantially greater than that from the FOS.

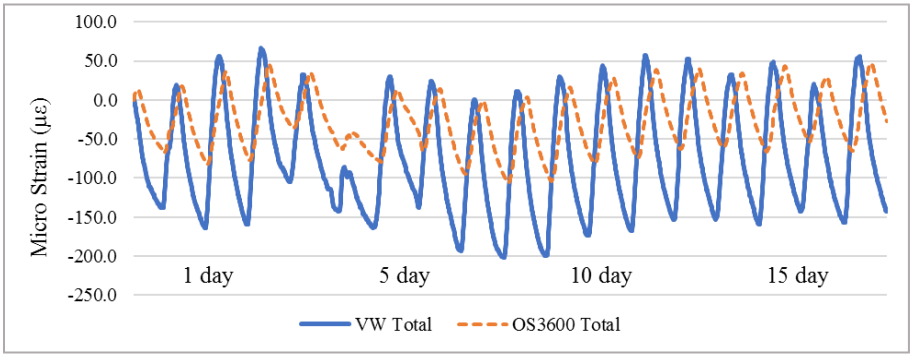

Figure 8-29. Comparison of the recorded strains by VWSG and FOS at top of Slab 1

Upon closer examination of the measured strains from the VWSG, it was found that they were essentially equal to thermal strains in the concrete. The FOS has an internal dummy gauge which measures the temperature of the material it is embedded in. The data from this dummy gauge of the FOS were used to compute the thermal strains in the concrete using Equation 8-3. When the computed thermal strains from the FOS were compared with the corresponding measured environmental strains from the VWSG, the two sets of strains were found to match very well with one another. Figures 8-30 through 8-33 show the good matching between the measured environmental strains from the VWSG with the computed thermal strains from the corresponding FOS on Slabs 1 through 4, respectively. It appears that the VWSGs were measuring the environmental strains correctly, and the environmental strains were essentially equal to the thermal strains in the concrete.

(a)

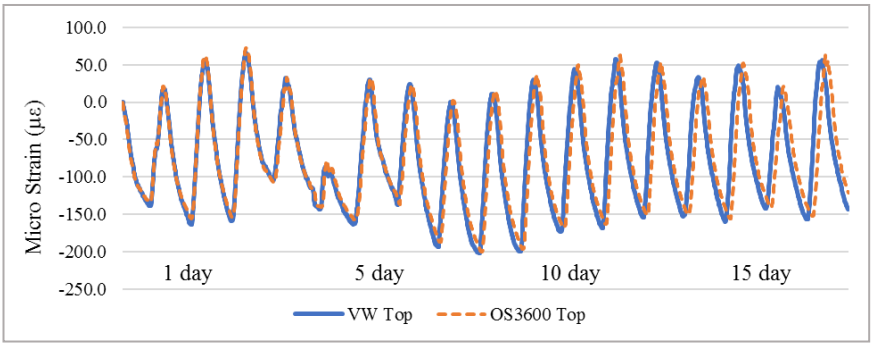

(b)

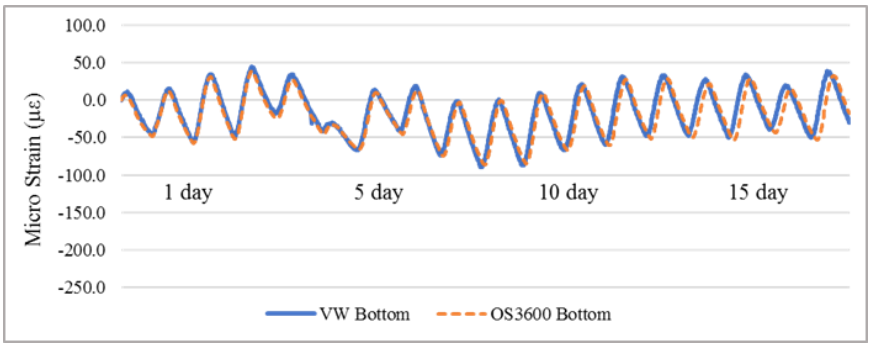

(c)

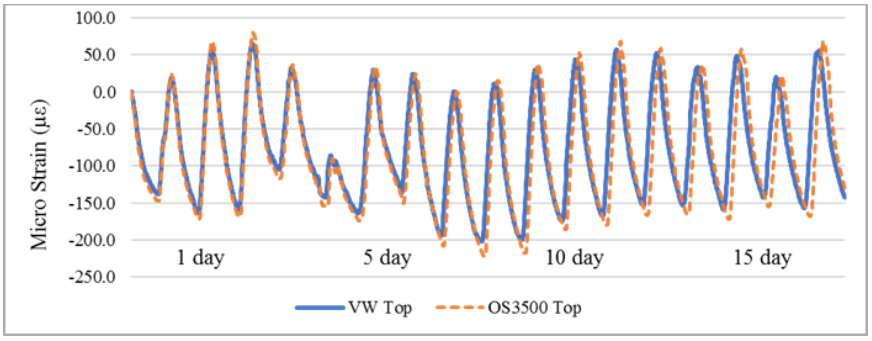

(d)

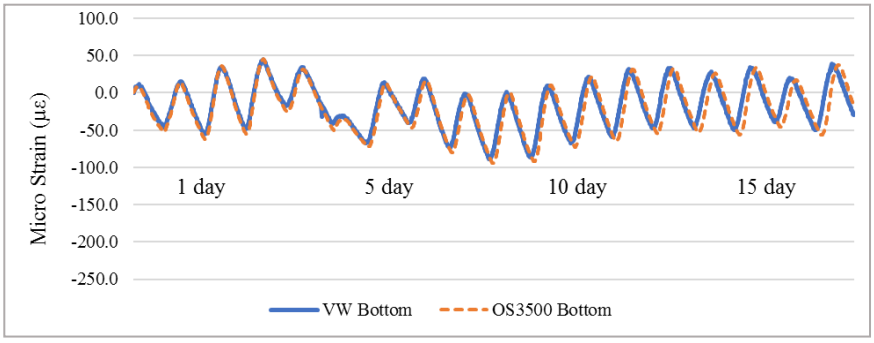

Figure 8-30. Comparison of the measured environmental strains from VWSG with the calculated thermal strains from (a) OS3600 at the top, (b) OS3600 at the bottom, (c) OS3500 at the top, and (d) OS3500 at bottom of Slab 1

(a)

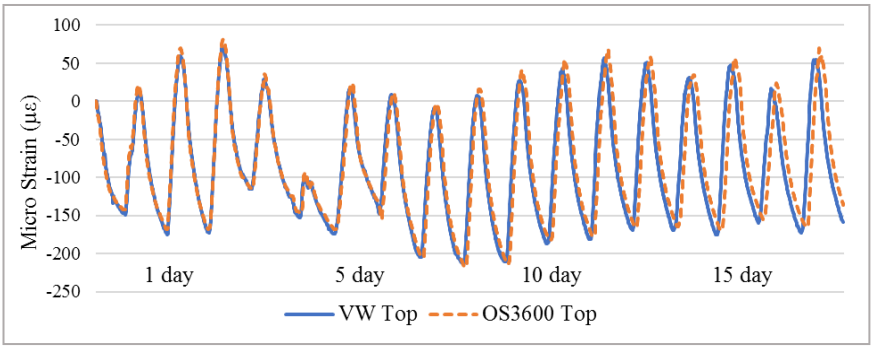

(b)

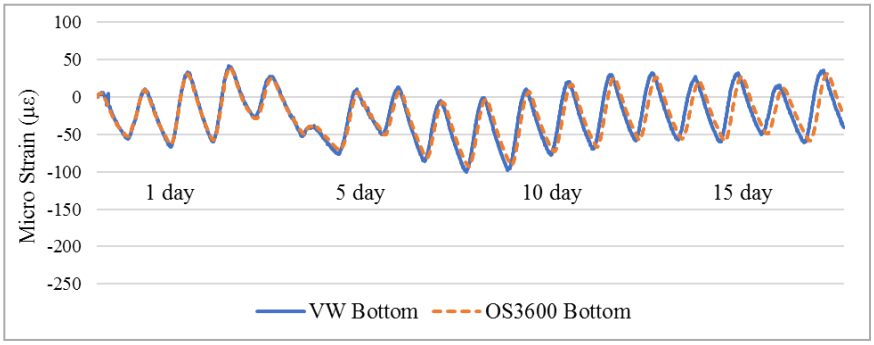

Figure 8-31. Comparison of the measured environmental strains from VWSG with the calculated thermal strains from OS3600 (a) at the top and (b) bottom of Slab 2

(a)

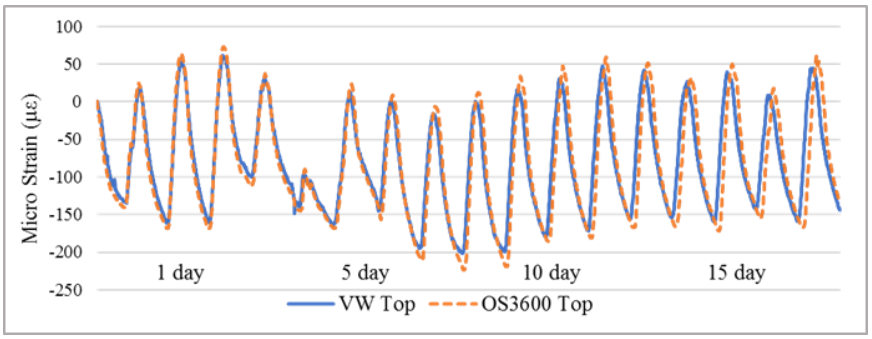

(b)

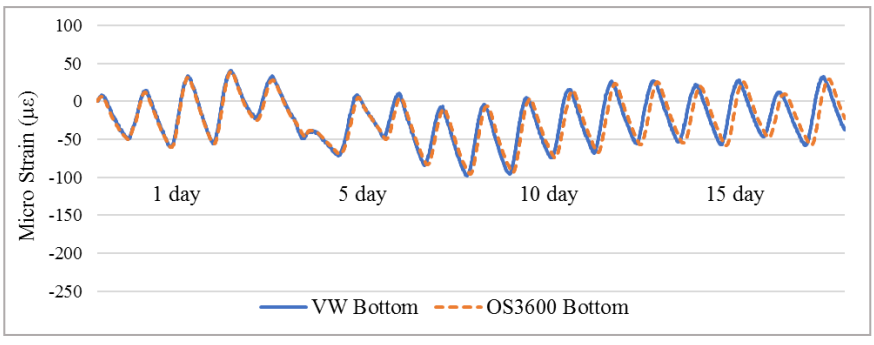

Figure 8-32. Comparison of the measured environmental strains from VWSG with the calculated thermal strains from OS3600 (a) at the top and (b) bottom of Slab 3

(a)

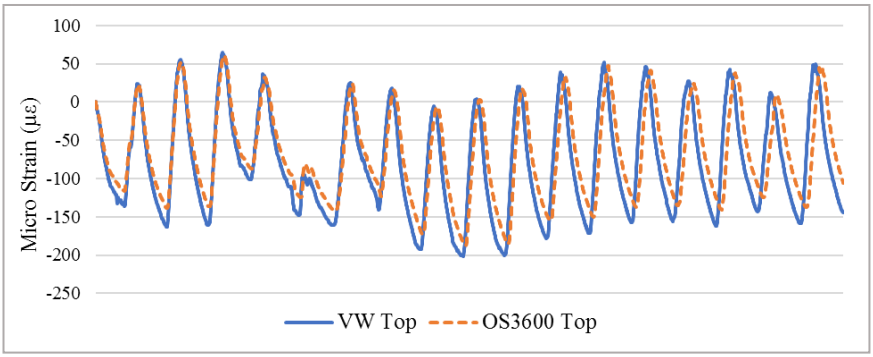

(b)

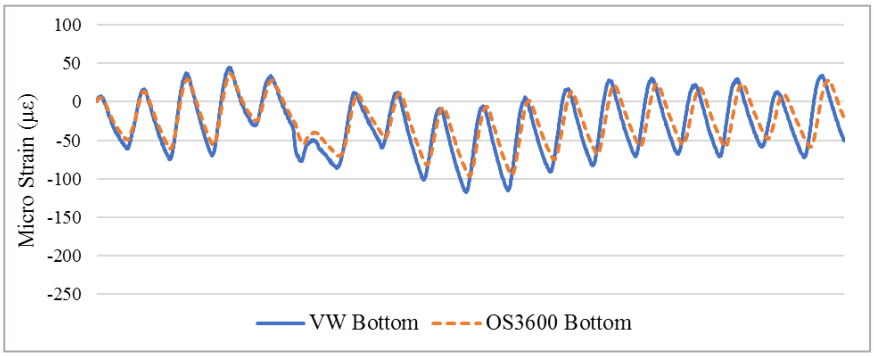

(c)

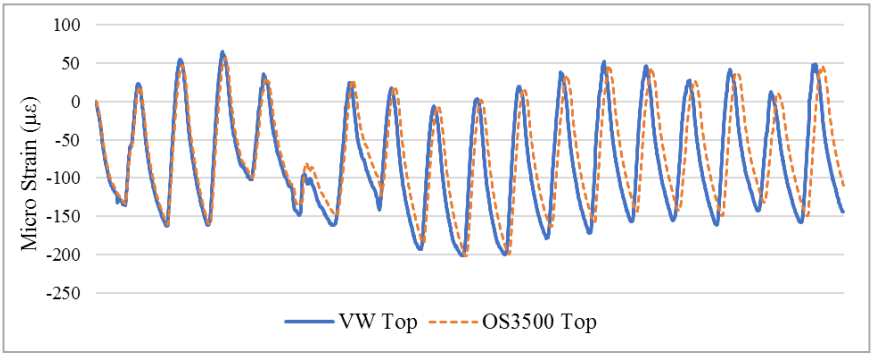

(d)

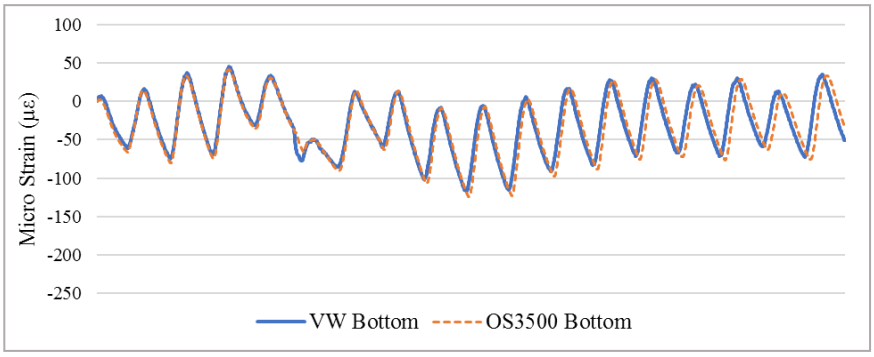

Figure 8-33. Comparison of the measured environmental strains from VWSG with the calculated thermal strains from (a) OS3600 at the top, (b) OS3600 at the bottom, (c) OS3500 at the top, and (d) OS3500 at bottom of Slab 4

8.4 Summary of Findings

The main findings of the field testing program are as follows:

(1) The developed FE model for JPCP can predict load-induced deflections and strains on the concrete pavement slabs fairly accurately. The results of Falling Weight Deflectometer tests on the concrete slabs can be used to calibrate the FE model parameters for the concrete slabs.

(2) The use of critical stress-analysis and the computed maximum stress-to-strength ratio have been shown to be effective in assessing the potential performance of concrete pavement slabs.

(3) The arrangement of a series of uniformly spaced strain gauges placed at and around the wheel path can be used to determine the location of the applied load and to record the maximum strain caused by the applied load.

(4) The fiber optic sensor and the Kyowa electrical resistance strain gauge were observed to record dynamic load-induced strains fairly accurately. The shorter fiber optic sensor (with gauge length of 4.3 inches) was observed to record more accurate strains in the concrete test slabs than the longer fiber optic sensor (with gauge length of 9.8 inches).

(5) The total environmental strains measured by the VWSG were observed to be equal to the thermal strain as measured by the fiber optic sensor.

CHAPTER 9
FINDINGS AND RECOMMENDATIONS

9.1 Scope of Work

The main objectives of this research project are (1) to develop improved analysis tools for concrete pavements using 3-D finite element (FE) modeling, and (2) to develop an effective instrumentation plan for the US-301 Concrete Test Road.

The developed analysis tools include (1) a FE model to properly consider the effects of longitudinal and transverse prestress forces in precast prestressed concrete pavement (PPCP), (2) a FE model for analysis of jointed plain concrete pavement (JPCP) containing RAP by incorporating the actual stress-strain characteristics of the concrete instead of assuming a linear elastic behavior, (3) a FE model for JPCP which models dowel bars with actual bar dimensions and properties, and (4) an improved analysis model for continuously reinforced concrete pavement (CRCP) to analyze the horizontal cracking potential under environmental and traffic loading conditions. Using the developed models, parametric analyses on the effects of various design parameters on the potential performance of the concrete pavements were also conducted.

A user-friendly interface software and guides were also developed, so that engineers and researchers without extensive training in finite-element method can also perform the analysis using these developed models. A user-friendly interface software, named AIFG (ADINA Input File Generator) which prompts for user inputs and generate input file for the developed software was developed for use in the analysis of JPCP. User-friendly guides were also developed for ADINA input files for analysis of PPCP, JPCP, CRCP, and JPCP with dowel joints.

Various selected strain sensors were evaluated in the laboratory to assess their behavior and performance in concrete cylinders under known static and dynamic strain conditions. Various selected strain sensors were also evaluated in full-size concrete test slabs subjected to

HVS loading. The responses of the strain sensors in the concrete test slabs under different loading configurations were studied in order to develop an effective instrumentation and analysis methodology for evaluation of concrete test pavements.

9.2 Summary of Findings

9.2.1 Modeling of PPCP

A 3-D finite elements model was developed to analyze the structural response of PPCP under typical Florida conditions. The model was calibrated using the measured FWD deflection data from a PPCP test section in Florida. The model was then used to perform a parametric analysis to determine the effects of a few important pavement parameters on the maximum induced stresses in PPCP. The main findings are summarized as follows:

(1) With respect to the longitudinal tensile stress, the most critical loading condition for PPCP is the combination of a positive temperature differential and a maximum wheel load applied at the mid-edge of the slab. However, with respect to the transverse tensile stress, the most critical loading condition is the combination of a positive temperature differential and a maximum wheel load at the inner corner of the slab.

(2) Results from the parametric analysis indicated that the maximum stress in the concrete slab increases significantly as the concrete modulus increases. However, the stress-to-strength ratio decreases due to increase of flexural strength as the concrete modulus increases.

(3) The maximum stress in the concrete slab increases as the coefficient of thermal expansion increases.

(4) Based on the fact that a lower stress-to-strength ratio was related to better observed pavement performance, the PPCP system evaluated appeared to have a good predicted performance with computed stress-to-strength ratio of less than 0.5 up to a loss of 20 % of prestress force in the longitudinal and transverse directions.

(5) The maximum stress decreases with an increase of subgrade stiffness. However, the effects of the subgrade stiffness are relatively small as compared with the effects of other parameters.

9.2.2 Modeling of JPCP Containing RAP

A non-linear FE model which incorporated the actual stress-strain behavior of the RAP concrete obtained from the flexural strength test was developed to evaluate the effects of the non-linear stress-strain behavior of the RAP concrete in a JPCP. The analytical results from the FE model incorporating the actual stress-strain behavior of the RAP concrete were compared with the corresponding results from the linear elastic FE model. It was observed that the maximum computed tensile stresses in the concrete using the linear elastic model tend to overestimate the induced stresses at high stress level. Thus, the non-linear model using the actual stress-strain characteristics of the RAP concrete should be used in order to obtain more accurate estimation of stresses in the concrete slabs.

9.2.3 Modeling of Dowel Bars by Their Actual Dimensions

A 3-D FE model was developed to model the behavior of dowel bars in JPCP by using the actual dimensions and properties of the dowel bars. The developed FE model was validated by matching the measured FWD deflection basins with analytical deflection basins. The main findings are summarized as follow:

(1) The load transfer mechanism across the doweled joint can be modeled well by using the contact sliding surface between the concrete and dowel bars.

(2) For modeling the dowel sleeve and dowel bar, very fine mesh size less than 2/5 in. was required to accurately capture the bearing stresses in the concrete.

(3) The developed 3-D FE model can be used to study the behavior of dowel bars under combined temperature-load conditions, and the effects of various special dowel bar configurations including the maximum dowel deflection, the bearing stress on dowel-concrete interface, and shear force transfer.

9.2.4 Modeling of CRCP

A 3-D finite elements model was developed to analyze the structural response of CRCP under typical Florida conditions. This model can be used to calculate the maximum vertical

tensile stress in a CRCP. When the vertical tensile stress is excessive, it can cause the formation of horizontal cracking at mid-depth of the CRCP slab. Once this horizontal cracking occurs, the upper thin slab would easily crack under combined temperature and load effects. The developed model was used to perform a parametric analysis to determine the effects of important pavement parameters on the maximum induced vertical tensile stresses for estimating the horizontal cracking potential. The main findings are summarized as follows:

(1) The critical load position is at the corner of slab formed by transverse cracks when the concrete slab has a positive temperature differential.

(2) The maximum vertical tensile stresses under the critical temperature-load condition is affected little by the coefficient of thermal expansion of the concrete.

(3) The maximum stress-to-strength ratio decreases as the concrete's flexural strength increases.

(4) The maximum vertical tensile stresses decrease as the base modulus increases under the critical temperature-load condition.

(5) The maximum tensile stresses decrease as the base friction increases under the critical temperature-load condition.

(6) Increasing slab thickness reduces the vertical tensile stress at the depth of steel.

(7) The critical vertical stresses decrease slightly when the transverse crack spacing increases.

(8) The vertical tensile stresses are significantly reduced when the steel spacing is reduced. In addition, the vertical tensile stress in the region far away from the tire load is affected little by the longitudinal steel spacing. From this result, the use of varying longitudinal steel spacing (i.e., small steel spacing under wheel path and wide steel spacing for other region) may be one of the ways to reduce the horizontal cracking potential in CRCP.

9.2.5 Laboratory Evaluation of Strain Sensors

An experimental testing program was conducted to evaluate the performance characteristics of fiber optic, vibrating wire, and electrical resistance strain gauges in measuring strains in concrete due to load and drying shrinkage. The different sensors were evaluated in

terms of accuracy, repeatability, and reproducibility. The main findings are summarized as follows:

(1) When compared with the strains measured by a calibrated extensometer in a compression test where the strains varied from 0 to around 450 με, the fiber optic strain sensor (FOS) showed an average error of 2.7 με, as compared with average errors of 5.7 με and 5.6 με for an electrical resistance strain gauge and a vibrating wire strain gauge (VWSG), respectively. However, their differences in error were found to be statistically insignificant at 95% confidence level.

(2) The repeatability of the strain measurements by the FOS in terms of coefficient of variation (COV) was 7.5 % as compared with COVs of 4.4, 5.6, and 9.6% for the three different electrical resistance strain gauges.

(3) The reproducibility of the strain measurements by the FOS in terms of COV was 9.8% as compared with COVs of 5.4, 5.7, and 10.1 % for the three different electrical resistance strain gauges.

(4) When compared with the strains measured by a calibrated LVDT in a concrete drying shrinkage test where the strains varied from 0 to around 250 με, the FOS showed an average difference of 30.37 με, while the VWSG showed an average difference of 34.04 με. The difference in strain measurements by the different gauges was statistically insignificant at 95% confidence level.

Based on the results of this laboratory evaluation, the FOS is found to have similar accuracy, repeatability, and reproducibility as compared to electrical resistance strain gauge and VWSG, and can be used for measuring dynamic and long-term strains in concrete pavement.

9.2.6 Field Evaluation of Strain Sensors and Analysis Methodology

Various strain sensors were evaluated in full-size concrete pavement slabs subjected to actual outside environment and realistic wheel loads by a Heavy Vehicle Simulator (HVS). This field testing program was also conducted to assess the validity of the analysis results from the Finite Element (FE) model for jointed plain concrete pavement which has been developed for this study.

The main findings of the field testing program are as follows:

(1) The developed FE model for JPCP can predict load-induced deflections and strains on the concrete pavement slabs fairly accurately. The results of Falling Weight

Deflectometer tests on the concrete slabs can be used to calibrate the FE model parameters for the concrete slabs.

(2) The use of critical stress-analysis and the computed maximum stress-to-strength ratio have been shown to be effective in assessing the potential performance of concrete pavement slabs.

(3) The arrangement of a series of uniformly spaced strain gauges placed at and around the wheel path can be used to capture the location of the applied load and the maximum strains caused by the applied load.

(4) The fiber optic sensor and the Kyowa electrical resistance strain gauge were observed to record dynamic load-induced strains fairly accurately. The shorter fiber optic sensor (with gauge length of 4.3 in.) was observed to record more accurate strains in the concrete test slabs than the longer fiber optic sensor (with gauge length of 9.8 in.).

(5) The total environmental strains measured by the Vibrating Wire Strain Gauges were observed to be equal to the thermal strain as measured by the fiber optic sensors.

9.3 Recommendations

Based on the findings from this study, the following recommendations are made:

(1) The developed 3-D FE model for PPCP is recommended for use in evaluation of structural behavior and performance of PPCP systems under Florida conditions. In the design of PPCP, correct values of concrete properties and design parameters should be employed in an appropriate analytical model rather than the use of the stress equivalency concept or the strength equivalency concept to evaluate the response of the PPCP.

(2) The developed non-linear 3-D FE model incorporating the actual stress-strain characteristics of the concrete is recommended for use for analysis of JPCP using RAP concrete. In the analysis of the concrete pavement containing RAP, an analytical model using the actual stress-strain characteristics, instead of the assumption of the concrete as a linear elastic material, should be employed to calculate the maximum stresses in the concrete.

(3) The developed 3-D FE model which models dowel bars using its actual dimensions is recommended for use. It can be used to study the behavior of dowel bars under combined temperature-load conditions, and the effects of various special dowel bar configurations including the maximum dowel deflection, the bearing stress on dowel-concrete interface, and shear force transfer.

(4) The developed 3-D FE model for CRCP is recommended for use in determining the maximum vertical tensile stresses in CRCP. When the vertical tensile stresses are excessive, horizontal cracking at mid-depth of the slab will occur. The following procedures are recommended for analysis of CRCP to minimize horizontal cracking:

4. Analyze the maximum vertical tensile stress at the depth of the longitudinal steel under critical temperature-load condition.
5. Compare the maximum vertical tensile stress to flexural strength of the concrete used.
6. If maximum tensile stress is greater than 50% of the flexural strength of the concrete, try to reduce it to 50% or less by the following options (Tia et al. 2012):

    i) Reduce longitudinal steel spacing
    ii) Increase flexural strength of concrete
    iii) Increase base modulus
    iv) Increase slab thickness

(5) Fiber optic sensor and electrical resistance strain gauge can be used to measure dynamic strains in concrete slabs. Fiber optic sensor and vibrating wire strain gauge can be used to measure static and long-term strains in concrete slabs. The use of shorter fiber optic sensor (with gauge length of less than 5 in.) is recommended over the longer ones. A hybrid system with combination of fiber optic sensors, electrical resistance strain gauges, and vibrating wire strain gauges can be used. Fiber optic sensors are to be chosen for consideration of long-term durability, while electrical resistance strain gauges and VWSGs are to be chosen for cost consideration.

(6) It is recommended that a series of 5 to 7 uniformly spaced strain gauges be placed at and around the wheel path on the test slab in order to be able to capture the location of the applied load and the maximum strain caused by the applied load. At each location, one strain gauge is to be placed at 1 inch below the top of the concrete slab and one strain gauge is to be placed at 1 inch above the bottom of the slab.

(7) It is recommended that the critical stress-analysis and the computed maximum stress-to-strength ratio be used to assess the potential performance of concrete pavement slabs. A lower computed stress-to-strength ratio under critical loading condition would mean a better potential pavement performance.

LIST OF REFERENCES

ACI, 2002. *Building code requirements for structural concrete and commentary.* American Concrete Institute. Farmington Hills, MI.

ADINA, 2015. *ADINA Primer 9.0.* Watertown, MA.

Al-Oraimi, S., Hassan, H. F., and Hago, A., 2009. "Recycling of Reclaimed Asphalt Pavement in Portland Cement Concrete." *The Journal of Engineering Research,* 6(1), pp. 37-45.

ASTM(C802-09a), 2010. "Standard Practice for Conducting an Interlaboratory Test Program to Determine the Precision of Test Methods for Construction Materials." in *Annual Book of ASTM Standards,* American Society of Testing Materials (ASTM), West Conshohocken, PA, pp. 408-425.

Berry, M., Dalton, K., and Murray, F., 2015. *Feasibility of Reclaimed Asphalt Pavement as Aggregate in Portland Cement Concrete Pavements Phase II: Field Demonstration.* Final report, Montana Department of Transportation, Lansing, MI.

Berry, M., Stephens, J., Bermel, B., Hagel, A., and Schroeder, D., 2013. *Feasibility of Reclaimed Asphalt Pavement as Aggregate in Portland Cement Concrete.* Final report, Montana Department of Transportation, Lansing, MI.

Casas, J. R., and Cruz, P. J., 2003. "Fiber optic sensors for bridge monitoring." *Journal of Bridge Engineering,* 8(6), pp. 362-373.

Channakeshava, C., Barzegar, F., and Voyiadjis, G. Z., 1993. "Nonlinear FE analysis of plain concrete pavements with doweled joints." *Journal of Transportation Engineering,* 119(5), pp. 763-781.

Chatti, K., Lysmer, J., and Monismith, C. L., 1994. *Dynamic finite-element analysis of jointed concrete pavements.* University of California Transportation Center, Berkeley, CA.

Choi, S., Ha, S., and Won, M. C., 2011. "Horizontal cracking of continuously reinforced concrete pavement under environmental loadings." *Construction and Building Materials,* 25(11), pp. 4250-4262.

Chou, Y. T., 1981. *Structural Analysis Computer Programs for Rigid Multicomponent Pavement Structures with Discontinuities--WESLIQID and WESLAYER. Report 1. Program Development and Numerical Presentations*. DTIC Document, Ft.Belvoir, VA.

Darter, M. I., LaCoursiere, S. A., and Smiley, S. A., 1979. "Structural Distress Mechanisms in Continuously Reinforced Concrete Pavement." *Transportation Research Record: Journal of the Transportation Research Board,* (715), pp. 1-7.

Davids, W. G., Turkiyyah, G. M., and Mahoney, J. P., 1998. *Modeling of rigid pavements: joint shear transfer mechanisms and finite element solution strategies,* Final Report, Washington State Department of Transportation, Olympia, WA.

Delwar, M., Fahmy, M., and Taha, R., 1997. "Use of reclaimed asphalt pavement as an aggregate in Portland cement concrete." *ACI Materials Journal*, 94(3), pp. 251-256.

Dere, Y., Asgari, A., Sotelino, E. D., and Archer, G. C., 2006. "Failure prediction of skewed jointed plain concrete pavements using 3D FE analysis." *Engineering Failure Analysis*, 13(6), pp. 898-913.

FDOT, 2008. *Evaluation of Pavement Strain Gauge Repeatability Under Accelerated Pavement Testing.* Research Report, Florida Department of Transportation, Tallahassee, FL.

FDOT, 2011. *Portland Cement Concrete Pavement Specifications: State of the Practice.* Research Report, Florida Department of Transportation, Tallahassee, FL.

FHWA, 1990. *Technical Advisory T 5040.30 Concrete Pavement Joints.* Federal Highway Administration, Washington, D.C.

Geokon, 2016. *Instruction Manual Model 4200 Series Vibrating Wire Strain Gauges.* Geokon, Lebanon, NH.

Grattan, K., and Sun, T., 2000. "Fiber optic sensor technology: an overview." *Sensors and Actuators A: Physical*, 82(1), pp. 40-61.

Guo, H., Sherwood, J. A., and Snyder, M. B., 1995. "Component dowel-bar model for load-transfer systems in PCC pavements." *Journal of Transportation Engineering*, 121(3), pp. 289-298.

Hassan, K., Brooks, J., and Erdman, M., 2000. "The use of reclaimed asphalt pavement (RAP) aggregates in concrete." *Waste Management Series*, 1, pp. 121-128.

Heinrichs, K., Liu, M., Darter, M., Carpenter, S., and Ioannides, A., 1987. *Rigid Pavement Analysis and Design.* Federal Highway Administration, Washington, D.C.

Hossiney, N., Tia, M., and Bergin, M. J., 2010. "Concrete containing RAP for use in concrete pavement." *International Journal of Pavement Research and Technology*, 3(5), pp. 251-258.

Hossiney, N., Wang, G., Tia, M., and Bergin, M., 2008. "Evaluation of Concrete Containing Recycled Asphalt Pavement for Use in Concrete Pavement." *Proc., Transportation Research Board 87th Annual Meeting*, (No.08-2711).

Huang, B., Shu, X., and Burdette, E., 2006. "Mechanical properties of concrete containing recycled asphalt pavements." *Magazine of Concrete Research*, 58(5), pp. 313-320.

Huang, B., Shu, X., and Li, G., 2005. "Laboratory investigation of portland cement concrete containing recycled asphalt pavements." *Cement and Concrete Research*, 35(10), pp. 2008-2013.

Huang, Y., and Wang, S., 1973. "Finite-element analysis of concrete slabs and its implications for rigid pavement design." *Highway Research Record* (466), pp. 55-69.

Huang, Y. H., 1974. "Finite element analysis of slabs on elastic solids." *Journal of the Transportation Engineering Division*, 100(2), pp. 403-416.

Huang, Y. H., and Deng, X.-J., 1983. "Finite element analysis of jointed concrete pavements." *Journal of Transportation Engineering*, 109(5), pp. 689-705.

Ioannides, A., and Donnelly, J., 1988. *Three-dimensional analysis of slab on stress-dependent foundation, Transportation Research Record: Journal of the Transportation Research Board,* (1196), pp. 72-84.

Kim, S.-M., Won, M., and Frank McCullough, B., 2002. "Dynamic stress response of concrete pavements to moving tandem-axle loads." *Transportation research record: journal of the transportation research board,* (1809), pp. 32-41.

Kim, S.-M., Won, M., and McCullough, B., 1998. "Numerical modeling of continuously reinforced concrete pavement subjected to environmental loads." *Transportation research record: journal of the transportation research board,* (1629), pp. 76-89.

Kim, S.-M., Won, M., and McCullough, B., 2000. "Three-dimensional analysis of continuously reinforced concrete pavements." *Transportation research record: journal of the transportation research board,* (1730), pp. 43-52.

Kim, S.-M., Won, M., and McCullough, B. F., 2001. *Transformed field domain analysis of pavements subjected to moving dynamic tandem-axle loads and integrating their effects into the CRCP-10 program.* Center for Transportation Research, Bureau of Engineering Research, University of Texas at Austin, Austin, TX.

Kim, S.-M., and Won, M. C., 2004. "Horizontal cracking in continuously reinforced concrete pavements." *ACI Structural Journal*, 101(6), pp. 784-791.

Krauss, Thomas P., Loren Shure, and John N. Little, 2001. *Signal Processing Toolbox for use with MATLAB*. Natick, MA

Kuo, C.-M., Hall, K. T., and Darter, M. I., 1995. "Three-dimensional finite element model for analysis of concrete pavement support." *Transportation research record: journal of the transportation research board,* (1505), pp. 119-127.

Mallela, J., Abbas, A., Harman, T., Rao, C., Liu, R., and Darter, M., 2005. "Measurement and significance of the coefficient of thermal expansion of concrete in rigid pavement design." *Transportation research record: Journal of the transportation research board,* (1919), pp. 38-46.

Masad, E., Taha, R., and Muhunthan, B., 1996. "Finite-element analysis of temperature effects on plain-jointed concrete pavements." *Journal of Transportation Engineering*, 122(5), pp.388-398.

McCullough, B. F., Ma, J., and Noble, C., 1980. "Limiting Criteria for the Design Of Continuously Reinforced Concrete Pavements." Center for Transportation Research, Bureau of Engineering Research, University of Texas at Austin, Austin, TX.

Merritt, D., McCullough, B., and Burns, N., 2001. "Feasibility of using precast concrete panels to expedite construction of portland cement concrete pavements." *Transportation research record: journal of the transportation research board,* (1761), pp.3-9.

Merritt, D., Rogers, R., and Rasmussen, R., 2008. *Construction of a Precast Prestressed Concrete Pavement Demonstration Project on Interstate 57 near Sikeston, Missouri.* FHWA-HIF-08-009. Washington, DC: Federal Highway Administration.

Merritt, D. K., McCullough, B. F., and Burns, N. H., 2002. *Construction and Preliminary Monitoring of the Georgetown, Texas Precast Prestressed Concrete Pavement.* Citeseer.

Merritt, D. K., and Tayabji, S., 2009. *Precast Prestressed Concrete Pavement for Reconstruction and Rehabilitation of Existing Pavements.* No. FHWA-HIF-09-008.

MicronOptics, 2009. *Optical sensing Interrogator (sm130).* MicronOptics, ed.Atlanta, GA.

MicronOptics, 2012. *Embeddable Strain Sensor (os3600).* MicronOptics, ed.Atlanta, GA.

PCA, 1984. *Thickness design for concrete highway and street pavements*, Portland Cement Association, Skokie, IL.

Pickett, G., and Ray, G. K., 1951. "Influence charts for rigid pavements." *American Society of Civil Engineers Transactions*, pp. 105-121.

Rice, J. A., and Lloyd, J., 2014. *Optimization of a Pavement Instrumentation Plan for a Full-Scale Test Road: Evaluation.* Final Report, Florida Department of Transportation, Tallahassee, FL.

Selezneva, O., Darter, M., Zollinger, D., and Shoukry, S., 2003. "Characterization of transverse cracking spatial variability: Use of long-term pavement performance data for continuously reinforced concrete pavement design." *Transportation research record: journal of the transportation research board,* (1849), pp. 147-155.

Smith, K., Wade, M., Peshkin, D., Khazanovich, L., Yu, H., and Darter, M., 1998. *Performance of Concrete Pavements. Volume II: Evaluation of Inservice Concrete Pavements.* No. FHWA-RD-95-110

Sun, L., and Deng, X., 1998. "Predicting vertical dynamic loads caused by vehicle-pavement interaction." *Journal of transportation engineering,* 124(5), pp. 470-478.

Tabatabaie, A. M., and Barenberg, E. J., 1978. "Finite-element analysis of jointed or cracked concrete pavements." *Transportation research record: journal of the transportation research board,* (671), pp. 11-19.

Tayabji, S., Ye, D., and Buch, N., 2013. *Precast concrete pavement technology*. Transportation Research Board, Washington, DC.

Tayabji, S. D., and Colley, B. E., 1986. *Analysis of jointed concrete pavements.* FHWA/RD-86-041.

Teller, L. W., and Cashell, H. D., 1959. "Performance of doweled joints under repetitive loading." *Highway Research Board Bulletin*, (217).

Tia, M., Armaghani, J. M., Wu, C.-L., Lei, S., and Toye, K. L., 1987. "FEACONS III computer program for analysis of jointed concrete pavements." *Transportation research record: journal of the transportation research board*, (1136), pp. 12-22.

Tia, M., Bloomquist, D., Alungbe, G., and Richardson, D., 1991. *Coefficient of Thermal Expansion of Concrete Used in Florida.* Final Report, Florida Department of Transportation, Tallahassee, FL.

Tia, M., Bloomquist, D., Yang, M., Soongswang, P., Meletiou, C., Amornsrivilai, P., Dobson, E., and Richardson, D., 1990. *Field and Laboratory Study of Modulus of Rupture and Permeability of Structural Concrete in Florida.* Final Report, Florida Department of Transportation, Tallahassee, FL.

Tia, M., Hossiney, N., Su, Y.-M., Chen, Y., and Do, T. A., 2012. *Use of Reclaimed Asphalt Pavement in Concrete Pavement Slabs.* Final Report, Florida Department of Transportation, Tallahassee, FL.

Tia, M., Verdugo, D. and Kwon, O., 2012. *Evaluation of Long-Life Concrete Pavement Practices for Use in Florida*. Final Report, Florida Department of Transportation, Tallahassee, FL.

Tia, M., Liu, Y., Haranki, B., and Su, Y.-M., 2009. *Modulus of Elasticity, Creep and Shrinkage of Concrete–PHASE II: Part 1–Creep Study*. Final Report, Florida Department of Transportation, Tallahassee, FL.

Uddin, W., Hackett, R. M., Joseph, A., Pan, Z., and Crawley, A. B., 1995. "Three-dimensional finite-element analysis of jointed concrete pavement with discontinuities." *Transportation research record: journal of the transportation research board*, (1482), pp. 26-32.

Wang, J.-N., and Tang, J.-L., 2005. "Using Fiber Bragg Grating Sensors to Monitor Pavement Structures." *Transportation research record: journal of the transportation research board*, (1913), pp. 165-176.

Westergaard, H., 1927. "Analysis of stresses in concrete pavements due to variations of temperature." *Proc., Highway Research Board Proceedings*, (6), pp. 201-215.

William, G. W., and Shoukry, S. N., 2001. "3D finite element analysis of temperature-induced stresses in dowel jointed concrete pavements." *International Journal of Geomechanics*, 1(3), pp. 291-307.

Won, M., 2011. "Continuously reinforced concrete pavement: identification of distress mechanisms and improvement of mechanistic-empirical design procedures." *Transportation research record: journal of the transportation research board*, (2226), pp. 51-59.

Won, M. C., Kim, S.-M., Merritt, D., and McCullough, B. F., 2002. "Horizontal cracking and pavement distress in Portland cement concrete pavement." *Proc., Designing, constructing, maintaining and financing today's airport projects, 27th international air transport conference*, Orlando, FL.

Wu, C., Tia, M., and Larsen, T., 1993. "Analysis of structural response of concrete pavements under critical thermal-loading conditions." *Proc., Fifth International Conference on Concrete Pavement Design and Rehabilitation*, (1).

Ye, D., and Tayabji, S., 2012. "Evaluation of Behavior and Performance of Precast Concrete Pavements." *Proc., Transportation Research Board 91st Annual Meeting*.

Yehia, S., Abudayyeh, O., Abdel-Qader, I., Zalt, A., and Meganathan, V., 2008. "Evaluation of sensor performance for concrete applications." *Transportation research record: journal of the transportation research board*, (2050), pp. 101-110.

Zaghloul, S. M., White, T. D., and Kuczek, T., 1994. "Evaluation of heavy load damage effect on concrete pavements using three-dimensional, nonlinear dynamic analysis." *Transportation research record: journal of the transportation research board*, (1449), pp. 123-133.

Zollinger, D. G., 1989. *Investigation of punchout distress of continuously reinforced concrete pavement.* Dissertation, University of Illinois at Urbana-Champaign, Champaign, IL.

APPENDIX A
USER-FRIENDLY GUIDES FOR ADINA INPUT FILES

A.1 User's Guide of Input File for Analysis of PPCP

A.1.1 Overview

This section provides instructions on creating an input file for analysis of precast prestressed concrete pavement (PPCP) using ADINA. Instead of creating an input file from scratch, a sample input file is provided, and the user only needs to insert the necessary information into the sample input file according to the dimension and conditions of the PPCP to be analyzed. The sample input file which is named "PPCP-Sample.in." is provided in Appendix B. A Notepad software is recommended for use to make the necessary modification to the input file. The geometry design of the FE model developed in this task is shown in Figure A-1.

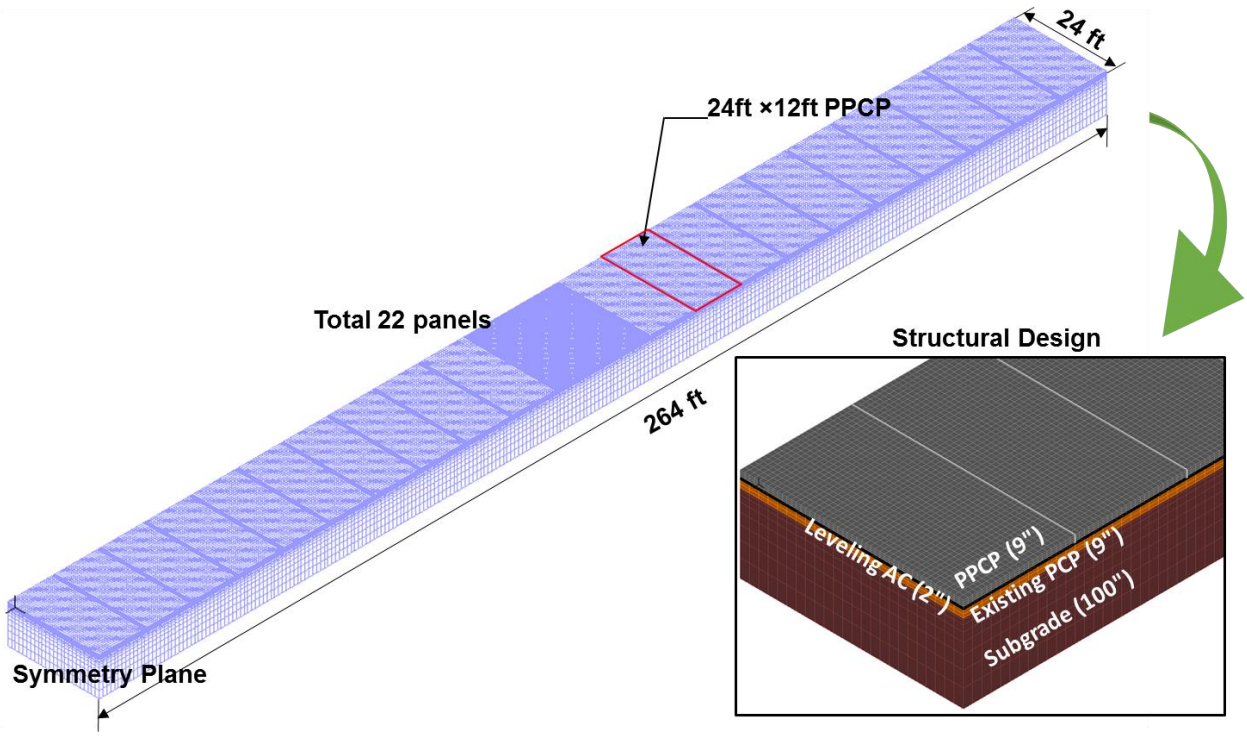

Figure A-1. FE model developed for PPCP

A.1.2 Inputs for PPCP Structural Design

Start with the sample input file for PPCP named "PPCP-Sample.in". Navigate to Comment 1 (Slab dimension) code line and change the DX1 (x-dimension), DX2 (y-dimension), and DX3 (z-dimension) in inches. Figure A-2 shows the ADINA code for model dimension in the PPCP model.

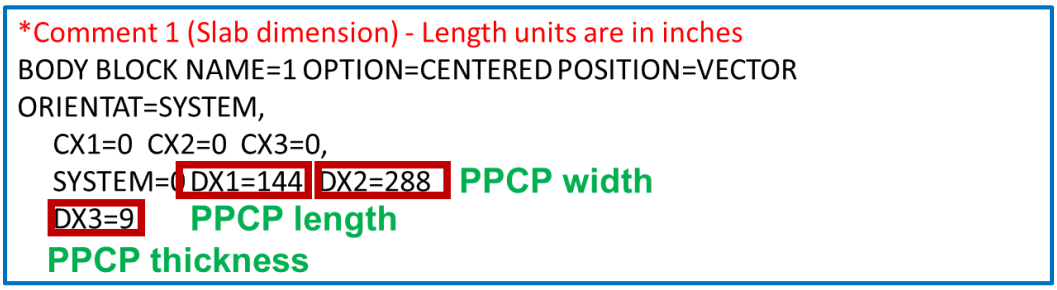

Figure A-2. ADINA code for PPCP slab dimension

The user can also change the model dimensions of AC leveling layer, existing concrete layer, and subgrade layer. Go to comment 2, 3, and 4 respectively and change the model dimensions as illustrated in Figures A-3 through A-5.

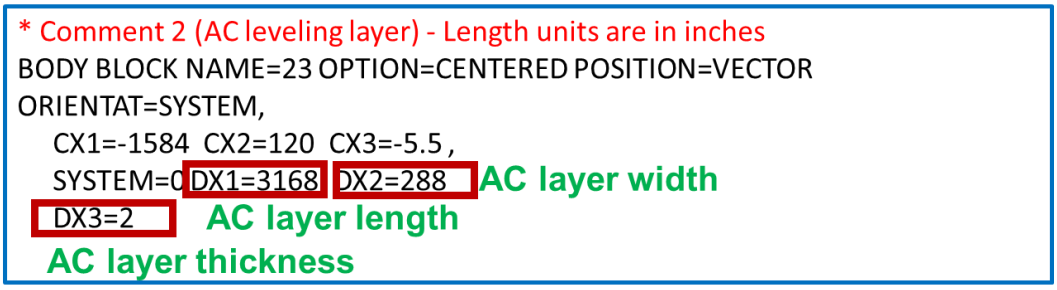

Figure A-3. ADINA code for AC leveling course dimension

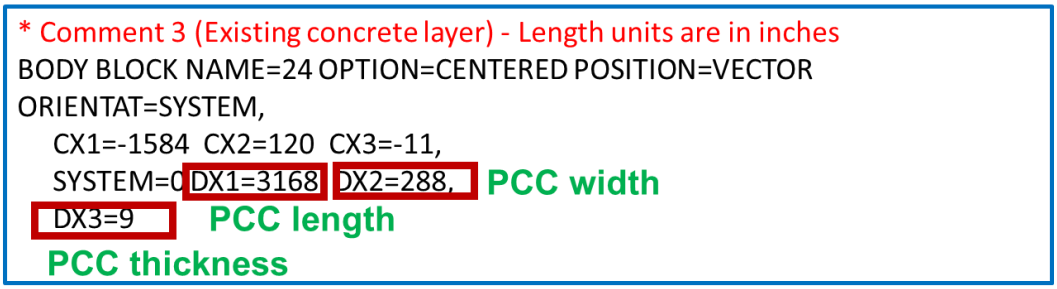

Figure A-4. ADINA code for existing PCC slab dimension

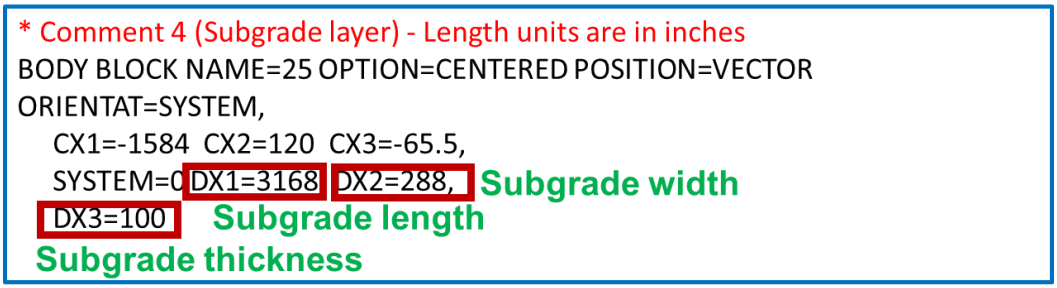

Figure A-5. ADINA code for subgrade layer dimension

A.1.3 Inputs for Material Properties

When the actual material properties obtained from field are available, the user can modify the material properties in the input file. Navigate to comment 5 (PPCP concrete properties) code line and change the values of Young's modulus (E), Poisson's ratio (ν), density (ρ), and coefficient of thermal expansion (CTE) as illustrated in Figure A-6. For other structural layers, the material properties can also be modified. Navigate to comment 6, 7, and 8 for AC leveling course, existing concrete pavement, and subgrade layer, respectively as shown in Figures A-7 through A-9. Notice that all values are in U.S. Customary units.

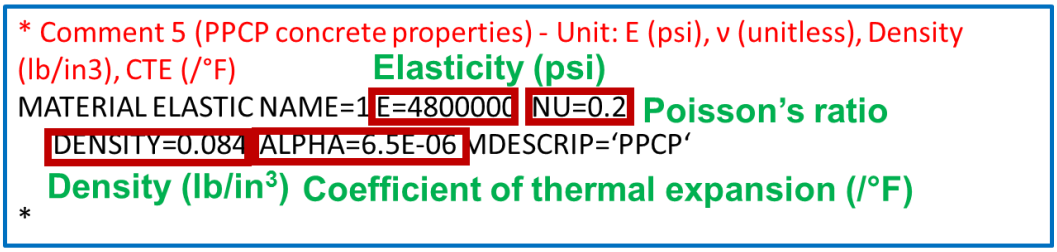

Figure A-6. ADINA code for material properties of PPCP concrete slabs

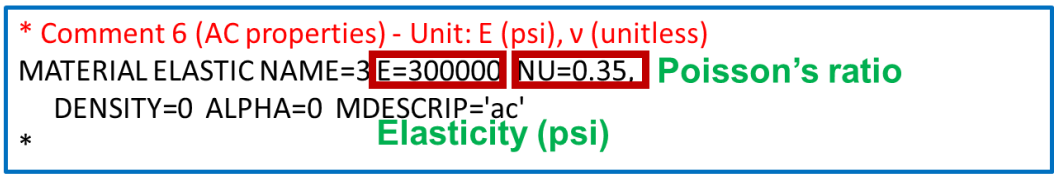

Figure A-7. ADINA code for material properties of AC leveling course

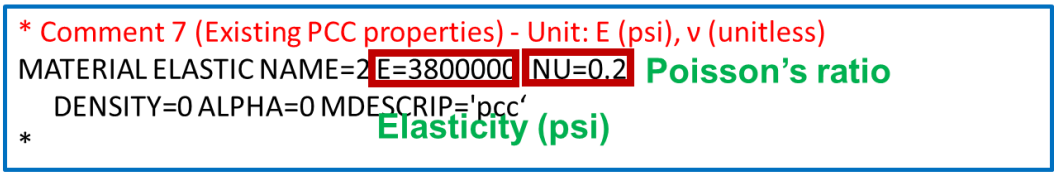

Figure A-8. ADINA code for material properties of existing concrete layer

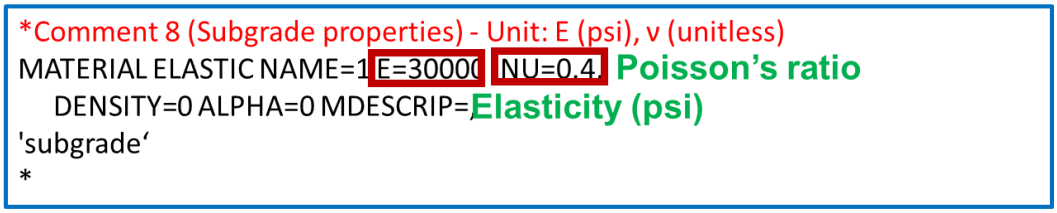

Figure A-9. ADINA code for material properties of subgrade

Another unique feature developed in this study is modeling of prestress forces in the concrete slab. The slab dimension and material properties can be modified as described above. In

addition, the user can also modify the prestress force and tendon diameter in the input file. To change the properties of tendons, navigate to comment 9 (Longitudinal tendons properties) and comment 10 (Transverse tendons properties) code line and change the values as shown in Figures A-10 and A-11, respectively. Also, the post-tension and pre-tension forces in the concrete in the longitudinal and transverse directions were modeled by the initial strains in the tendon which were induced by these forces. These initial strains are stored in Box A and calculated using the following equation.

$$\varepsilon = \frac{\sigma}{E} = \frac{F}{AE} \tag{A-1}$$

Where, σ = prestress in the tendon

E = elastic modulus of the tendon

F = prestress forces applied to the tendon

A= cross section area of the tendon

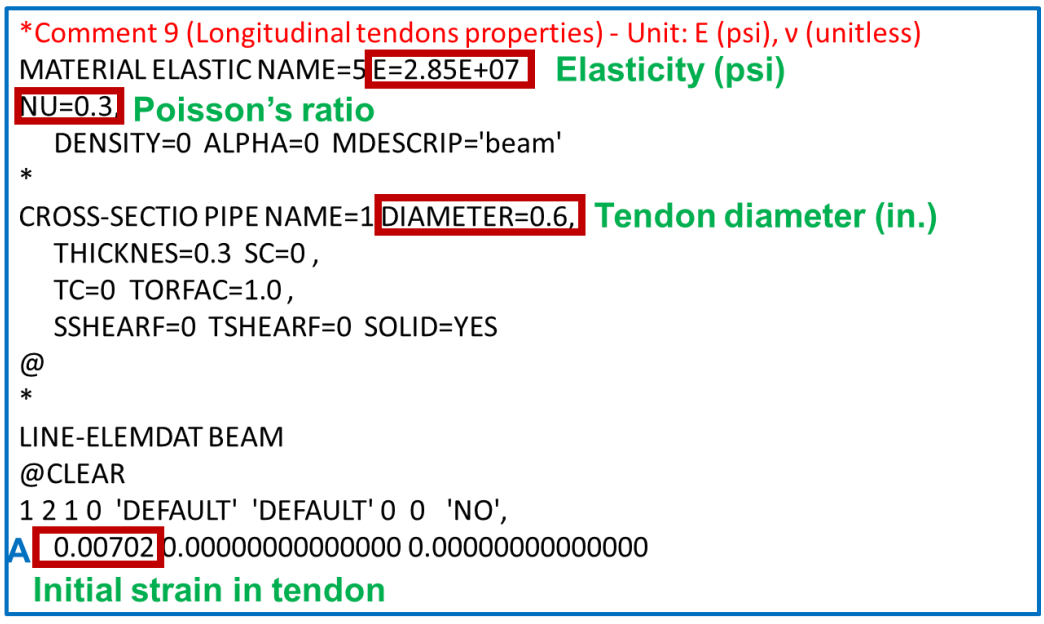

Figure A-10. ADINA code for longitudinal prestress force

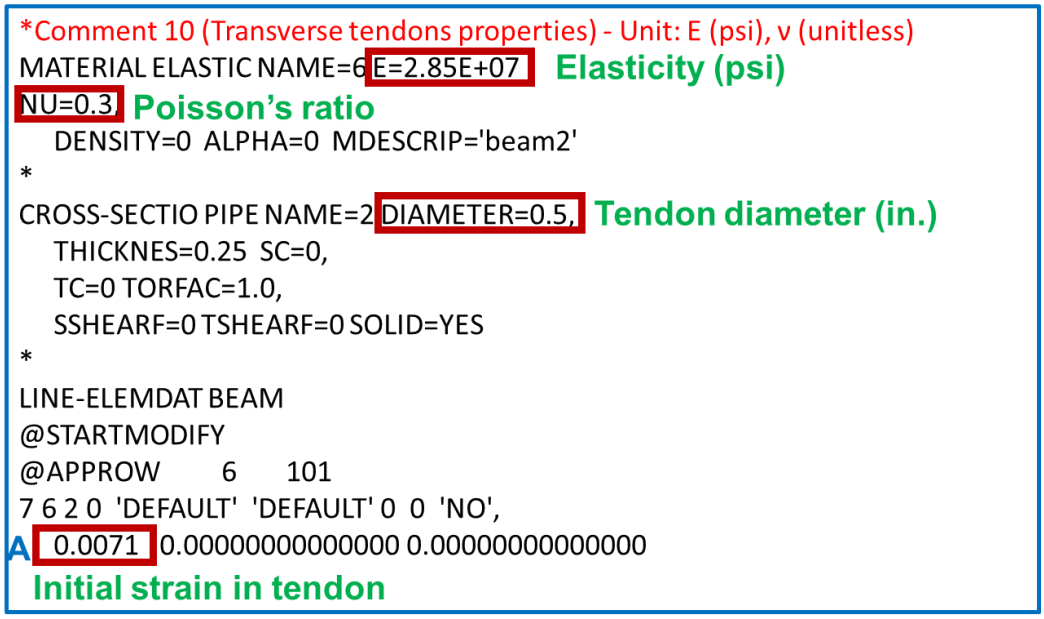

Figure A-11. ADINA code for transverse prestress force

A.1.4 Inputs for Load Transfer Across Joints

In this model, the load transfer across the joints was modeled through a contact surface with a certain coefficient of friction. The user of the software can simply change the coefficient of friction to adjust the load transfer across the joints as needed. Navigate to comment 11 (Load transfer contact surface) in the ADINA input file and change the value of coefficient of friction as shown in Figure A-12.

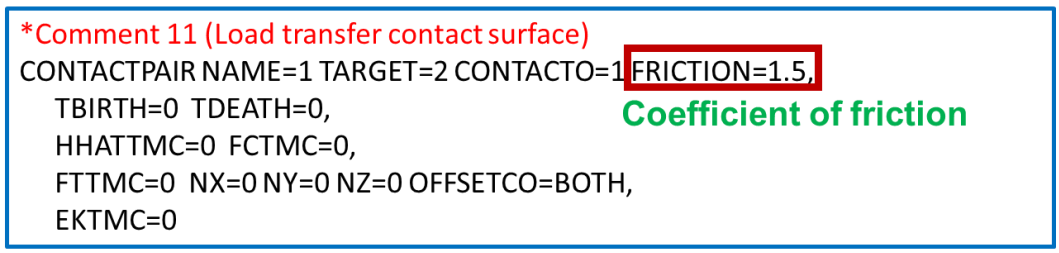

Figure A-12. ADINA code for load transfer across the joints

A.1.5 Inputs for Applied Tire Load

The required inputs to specify the applied tire load include (1) the tire contact pressure, and (2) location of load. Before changing the Input file, open the FE model in ADINA as described above and determine the element number of concrete slab where the tire load is applied to. Click the Element Labels icon  to determine the element number. The graphics window should look something like Figure A-13.

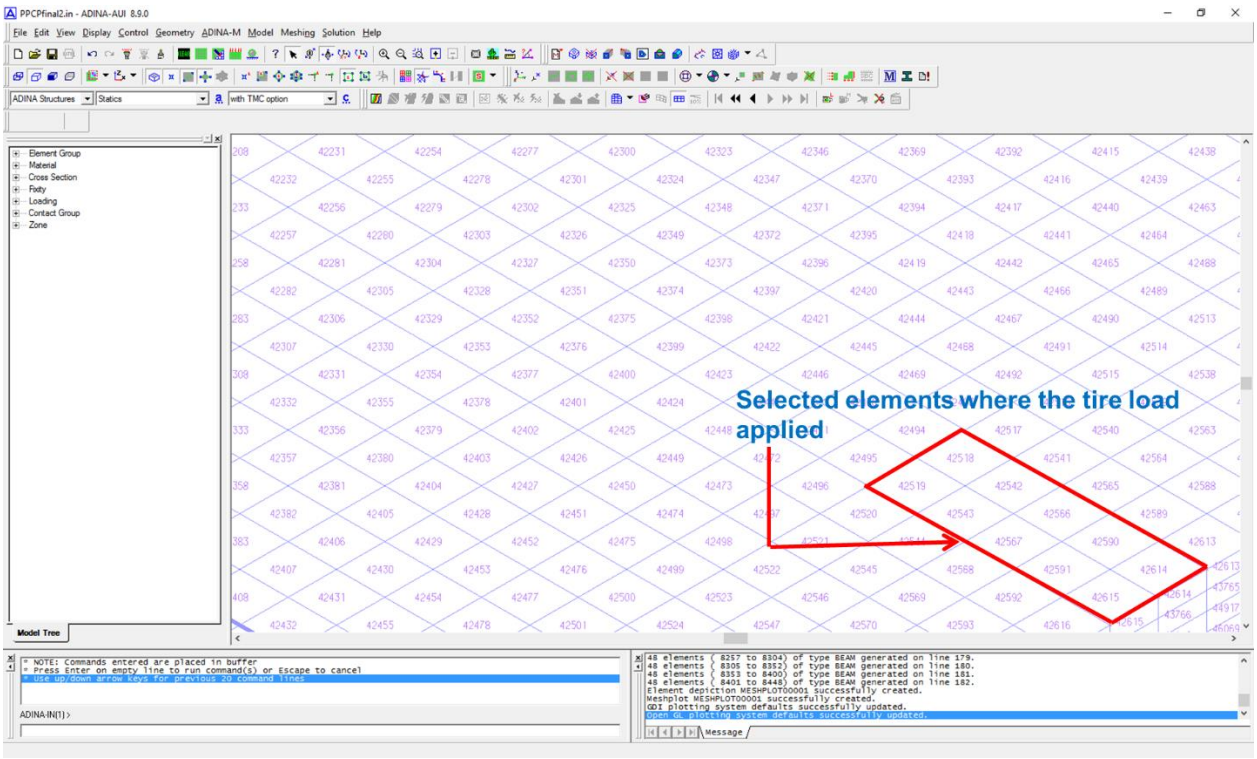

Figure A-13. Element number of PPCP panel in ADINA AUI

Then, navigate to Comment 12 (Tire load) code line in ADINA input file, and change the element number in Box A (concrete element number) in Figure A-14. The tire pressure is also changed by adjusting the value in Box B. Notice that the tire pressure is in psi.

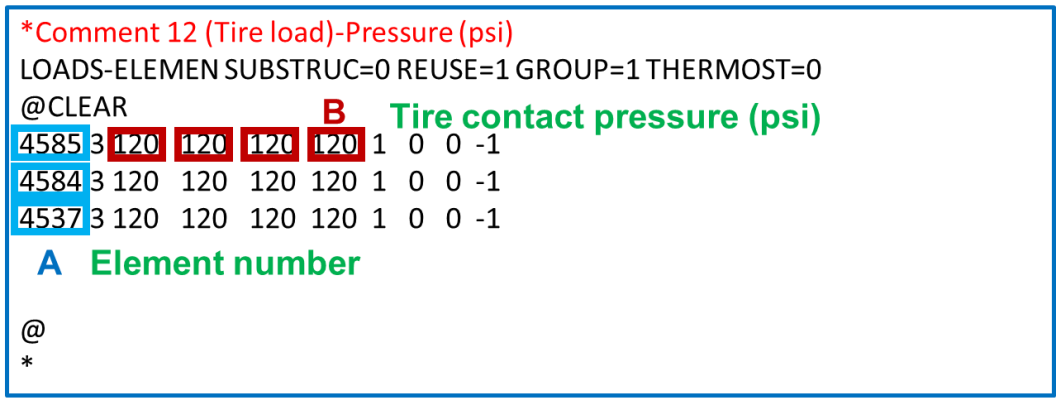

Figure A-14. ADINA code for tire load on concrete element

A.1.6 Inputs for Temperature Effect

In this model, the effect of temperature differentials in the concrete slab can be considered. To specify the temperature differential in the slab, go to Comment 13 (Temperature differential) code line and then specify the temperature differentials in Box A as shown in Figure A-15. After defining the temperature differential, go to the FACE number. FACE '1' indicates the top surface of the slab while FACE '5' represents the bottom surface of the slab. Figure A-15 shows the example of +20°F temperature differential. In this example, the top temperature is +10°F and the bottom temperature is -10°F, and so the temperature differential is +20°F.

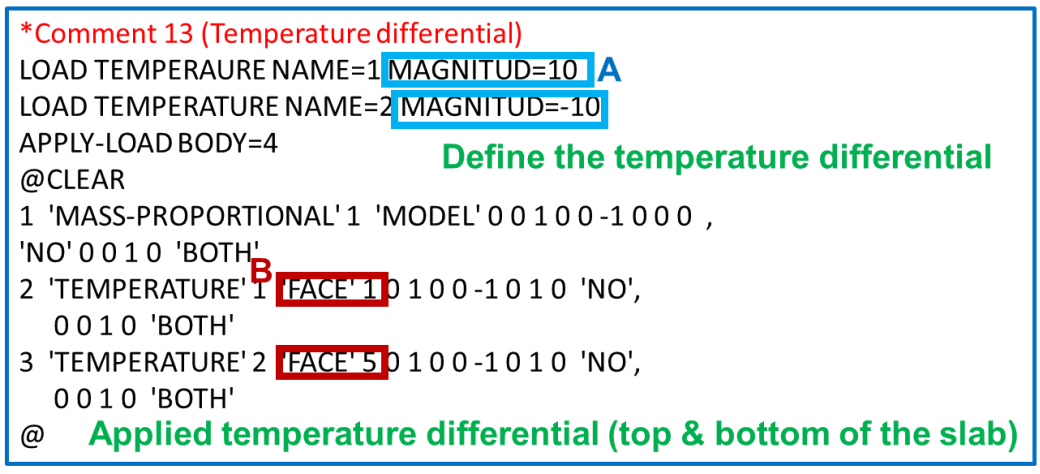

Figure A-15. Example of ADINA code for temperature effect

A.1.7 Running ADINA

After the ADINA input file is created, open the ADINA input file and click the DATA File/Solution icon . When the ADINA run is finished, close all open dialog boxes and choose Post-processing from the Program Module drop-down list. Open the porthole file with extension of "*.por" to view the analysis results of ADINA analysis.

A.1.8 Post-Processing of Results

A.1.8.1 Displaying curling movement due to temperature differential

To examine the solution, click the Create Band Plot icon , and then set the Band plot Variable to (Displacement: Z-DISPLACEMENT). The graphics window shows the curling movement due to positive temperature differential of + 20°F as shown in Figure A-16.

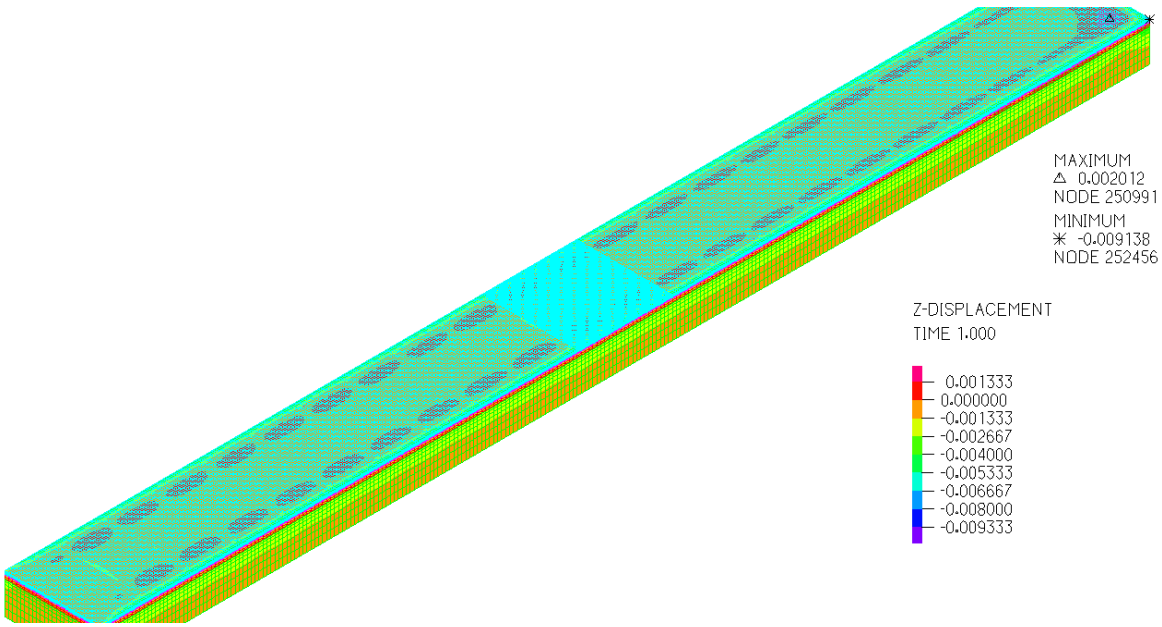

Figure A-16. Plot of PPCP curling movements due to temperature differential of + 20°F

A.1.8.2 Reading the tensile stress at the bottom of the slab

In order to examine the longitudinal stress at the bottom of the slab due to the positive temperature differential of +20 °F, define the model point using the following data:

Model Point Name	BOTTOM
Element Group	4
Element Number	82873
Node #	194783

Then choose → Value list → Model Point…; set the Model Point Name to (BOTTOM); set the Smoothing Technique to (AVERAGED); set the Variable to List to (Stress: STRESS-XX); verify that the model point name is BOTTOM; then click Apply.

The graphics window should look something like Figure A-17. The pop-up window shows the longitudinal tensile stress at the bottom of the slab.

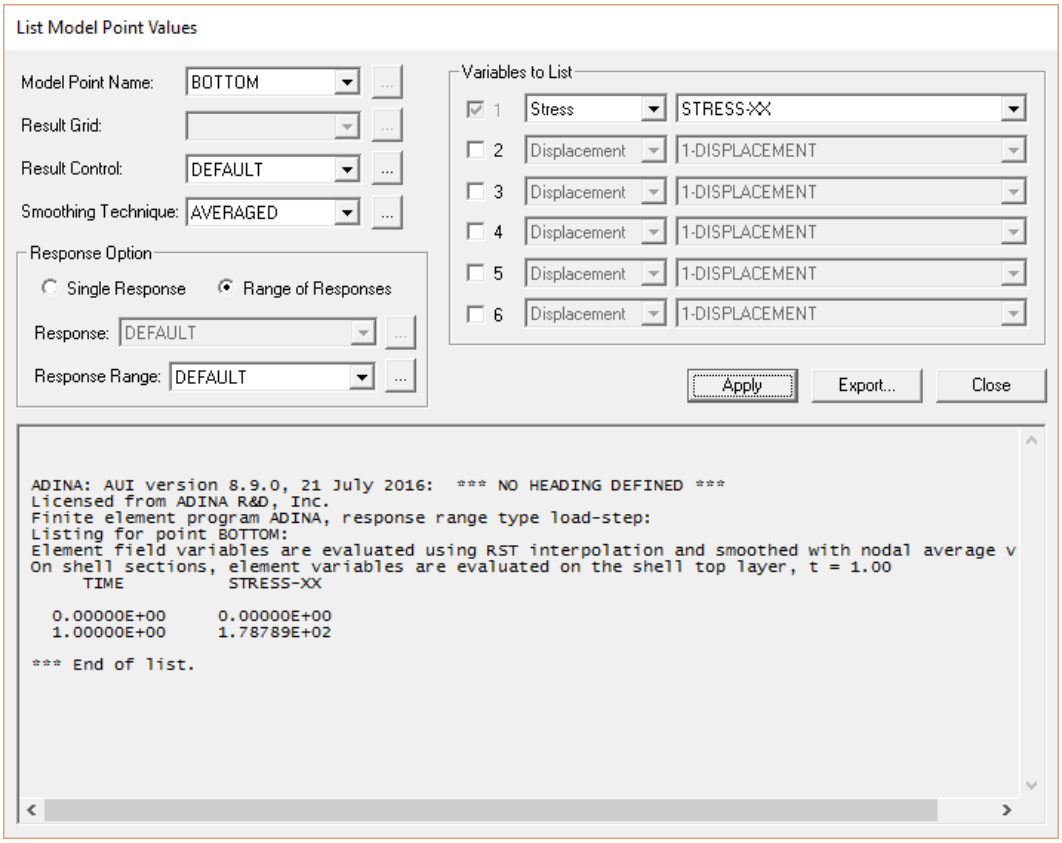

Figure A-17. Longitudinal tensile stress at the bottom of the slab

A.1.8.3 Reading the deflection at the corner of the slab

The user would like to examine the maximum curling movement due to the slab temperature differential. In this case, since the slab has a positive temperature differential, the maximum vertical movement occurs at the corner of the slab. To define the model point to get the actual value rather than graphical results, choose Definitions → Model Point → Element, then set the model point using the following data:

Model Point Name	CORNER
Element Group	4
Element Number	82944
Node #	194905

Then choose → Value list → Model Point…, set the Model Point Name to (CORNER), set the Smoothing Technique to (DEFAULT), set the Variable to List to (Displacement: Z-DISPLACEMENT), verify that the model point name is CORNER, then click Apply.

The graphics window should look something like Figure A-18. The pop-up window shows the vertical movement at the corner of the slab.

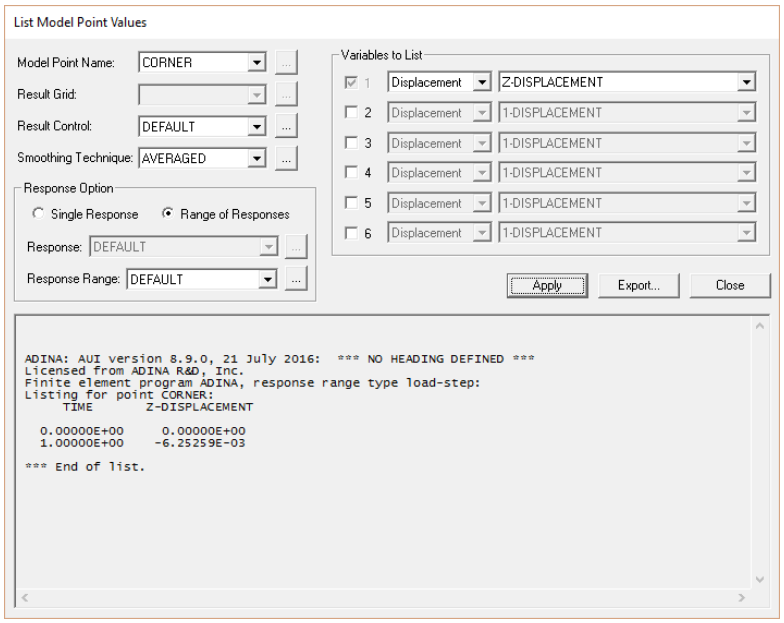

Figure A-18. Vertical deflection at the corner of the slab

A.2 User's Guide of Input File for Analysis of JPCP

A.2.1 Overview

This section provides instructions on creating an input file for analysis of jointed plain concrete pavement (JPCP) using ADINA. A sample input file, named "JPCP-Sample.in" is provided in Appendix C. The user only needs to insert the necessary information into the sample input file according to the dimensions and condition of the JPCP to be analyzed. The geometry design of the FE model developed in this task is shown in Figure A-19.

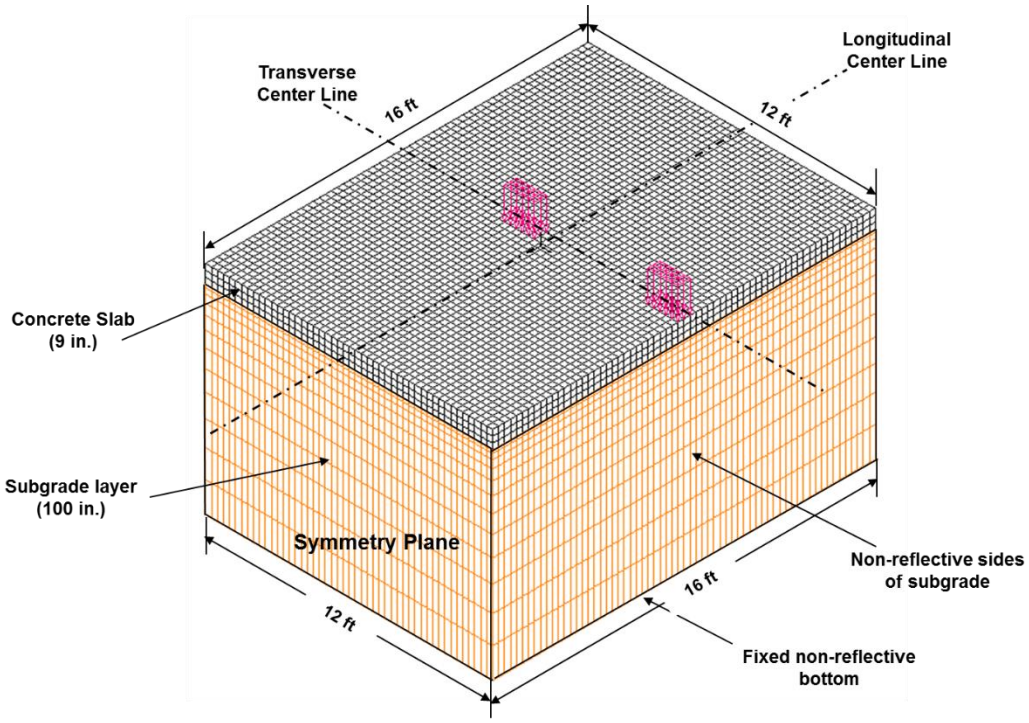

Figure A-19. FE model developed for JPCP

A.2.2 Inputs for Pavement Structural Design

Start with the sample input file named "JPCP-Sample.in". Navigate to Comment 1 (Slab dimension) and Comment 2 (Subgrade dimension) code line and change the DX1 (x-dimension), DX2 (y-dimension), and DX3 (z-dimension) in inches. Figures A-20 through A-21 show the ADINA codes for model dimension in the JPCP model.

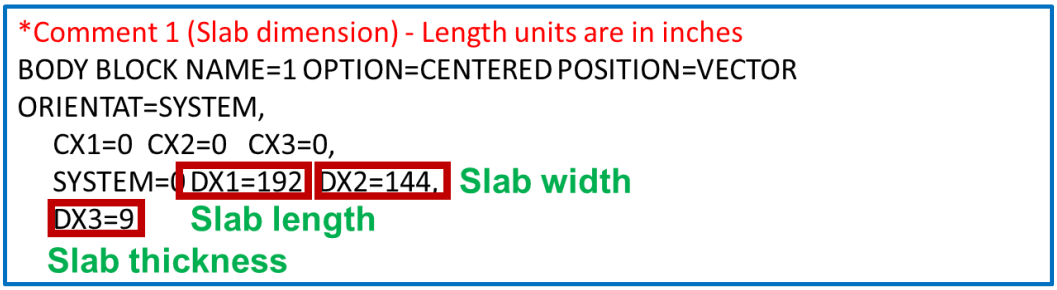

Figure A-20. ADINA code for concrete slab dimension

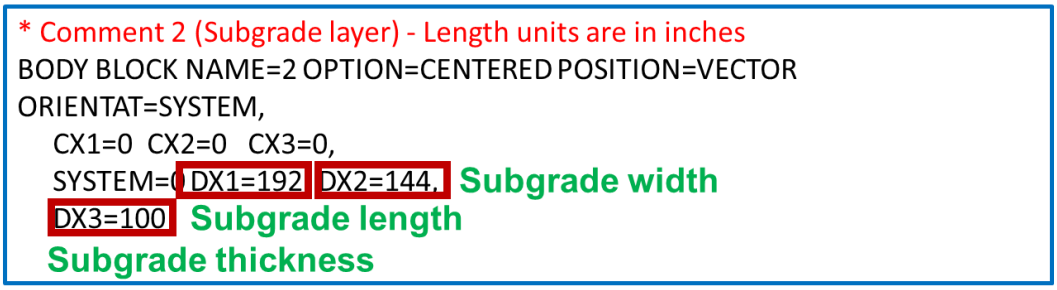

Figure A-21. ADINA code for subgrade layer dimension

A.2.3 Inputs for Material Properties

When the user wants to analyze the concrete containing RAP, the concrete properties code line shown in Figure A2-4 must be specified by the actual stress-strain behavior of RAP concrete. For concrete containing different percentage of RAP, the "stress-strain behavior of RAP concrete" must be obtained from laboratory test.

If the user wants to analyze this model with normal concrete (i.e., elastic material) pavement, the concrete material properties as shown in Figure A-22 must be deleted and re-written by following code as presented in Figure A-23. These elastic material properties will be applied in the concrete slab elements.

In addition, for modifying the subgrade layer properties, go to Comment 4 (subgrade properties) code line and change the values as shown in Figure A-24.

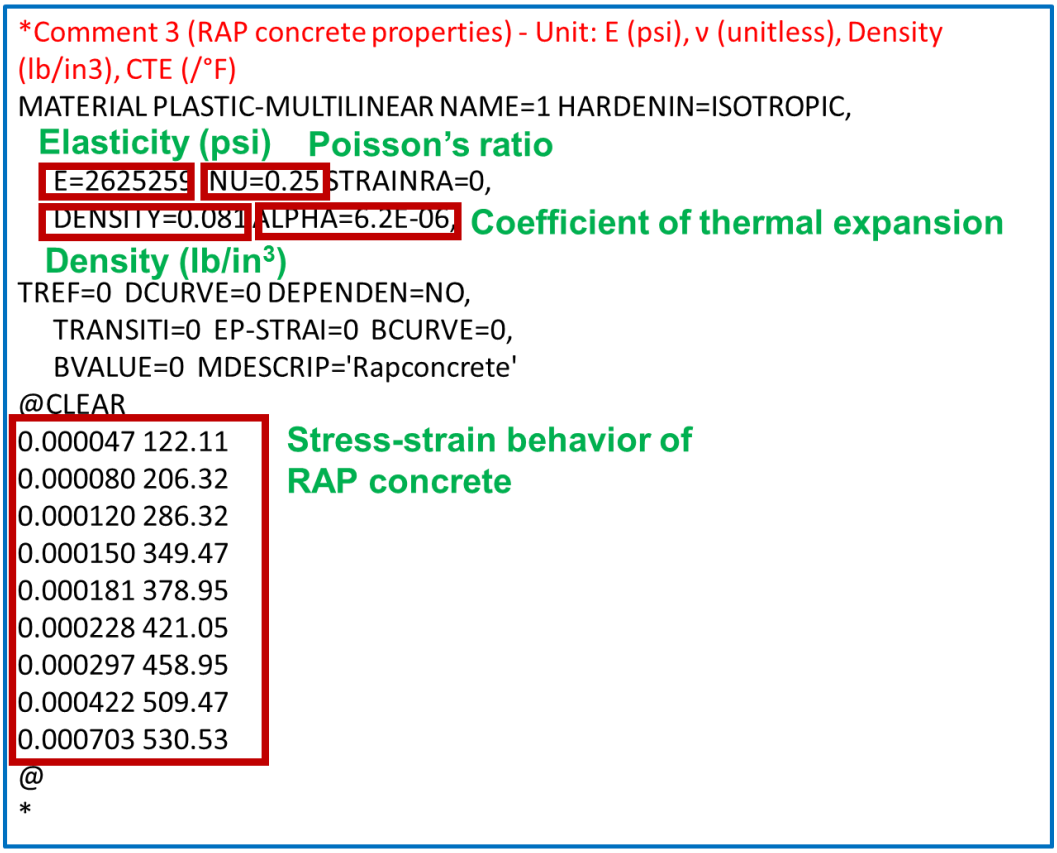

Figure A-22. ADINA code for RAP concrete properties

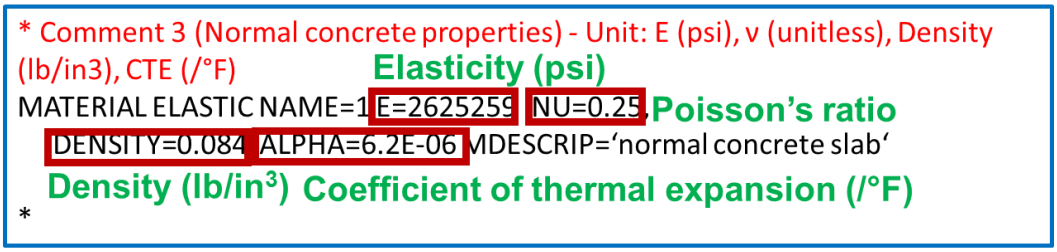

Figure A-23. ADINA code for normal concrete

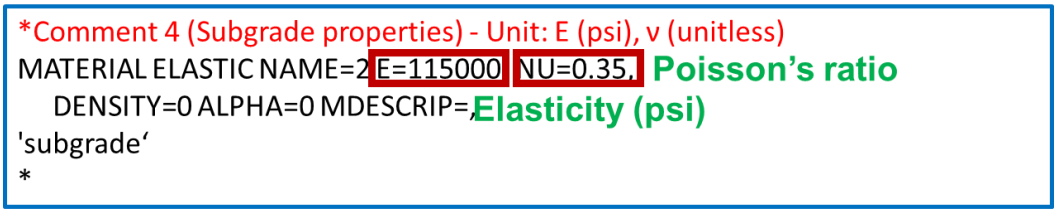

Figure A-24. ADINA code for material properties of subgrade

A.2.4 Inputs for Applied Tire Load

To change the location and tire load, navigate to the Comment 5 (Tire load) code line in the ADINA input file, and change the element number in Box A (concrete element number) which is related to tire contact area. The tire pressure is also changed by adjusting the value in Box B in Figure A-25.

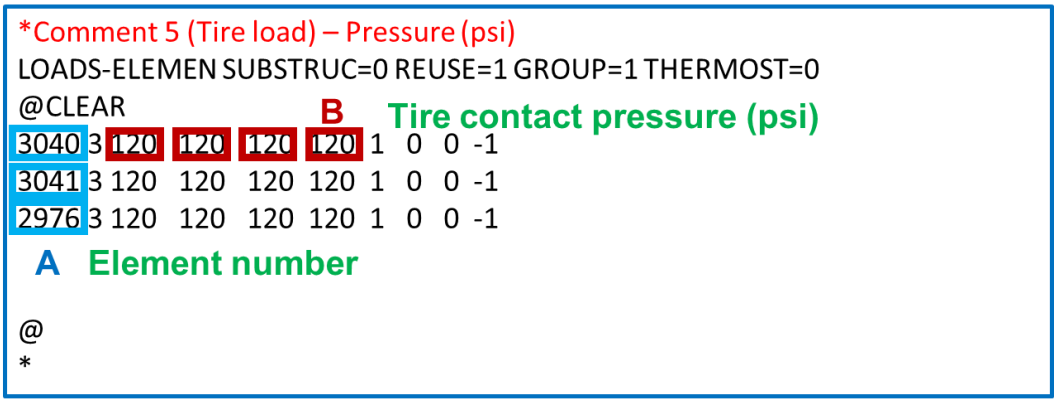

Figure A-25. ADINA code for tire load on concrete element

A.2.5 Inputs for Temperature Effect

For specifying the temperature differentials in the concrete slab, go to Comment 6 (Temperature differential) code line and change the magnitude in Box A as shown in Figure A-26. Box B indicates the FACE number applying specified temperature load. FACE '1' means the top surface of the slab while FACE '5' means the bottom surface of the slab.

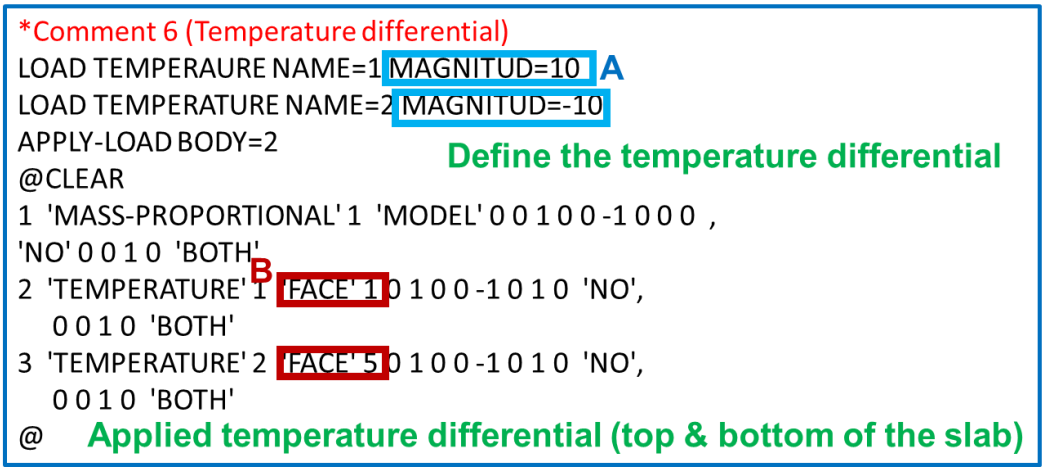

Figure A-26. ADINA code for temperature effect

A.2.6 Running ADINA

After ADINA input file is created, open the ADINA input file and click the DATA File/Solution icon  . When the ADINA run is finished, close all open dialog boxes and choose Post-processing from the Program Module drop-down list. Open the porthole file named as "*.por" to view the results of ADINA analysis.

A.2.7 Post-Processing of Results

A.2.7.1 Displaying tensile stresses at the bottom of slab

To examine the solution, click the Create Band Plot icon  , and then set the Band plot Variable to (Stress: STRESS-XX). The graphics window shows the tensile stress at the bottom of slab due to combined temperature-load condition as shown in Figure A-27. In this figure, red color means tensile stress while blue color means compressive stress in the concrete slab.

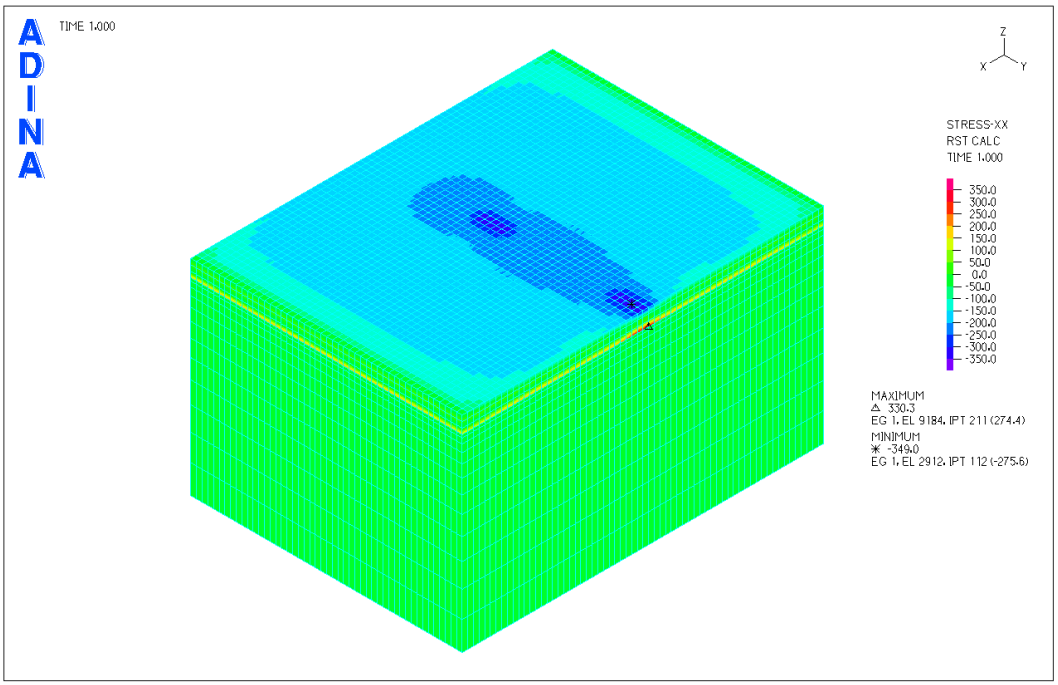

Figure A-27. Plot of tensile stress at the bottom of slab

A.2.7.2 Reading the tensile stress at the bottom of the slab

In order to examine the longitudinal stress at the bottom of the slab due to combined temperature-load conditions, define the model point. Choose Definitions → Model Point → Element, then set the model point using the following data:

Model Point Name	BOTTOM
Element Group	1
Element Number	9185
Node #	12644

Then choose → Value list → Model Point…; set the Model Point Name to (BOTTOM); set the Variable to List to (Stress: STRESS-XX), verify that the model point name is BOTTOM, then click Apply.

The graphics window should look something like Figure A-28. The pop-up window shows the longitudinal tensile stress at the bottom of the slab.

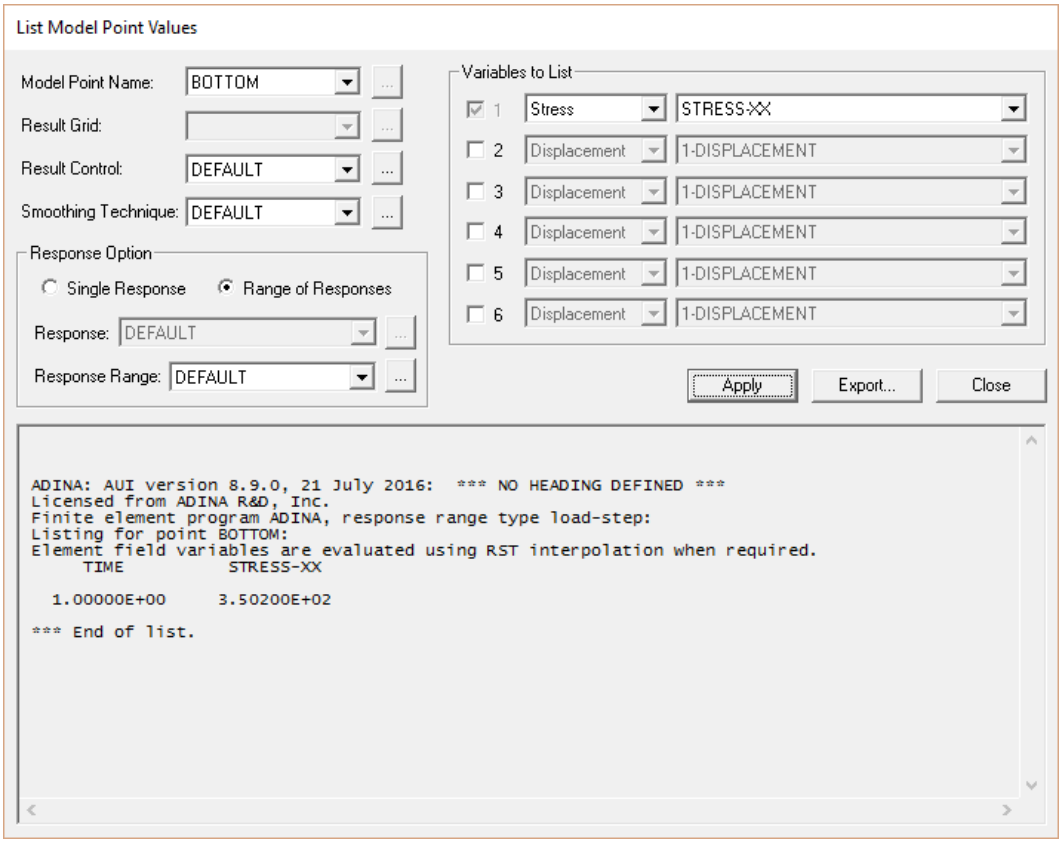

Figure A-28. Longitudinal tensile stress at the bottom of the slab

A.2.7.3 Reading the tensile strain at the bottom of the slab

To get the actual strain value rather than graphical results, choose → Value list → Model Point…; set the Model Point Name to (BOTTOM); set the Variable to List to (Strain: STRAIN-XX); verify that the model point name is BOTTOM; then click Apply.

The graphics window should look something like Figure A-29. The pop-up window shows the longitudinal tensile strain at the bottom of the slab.

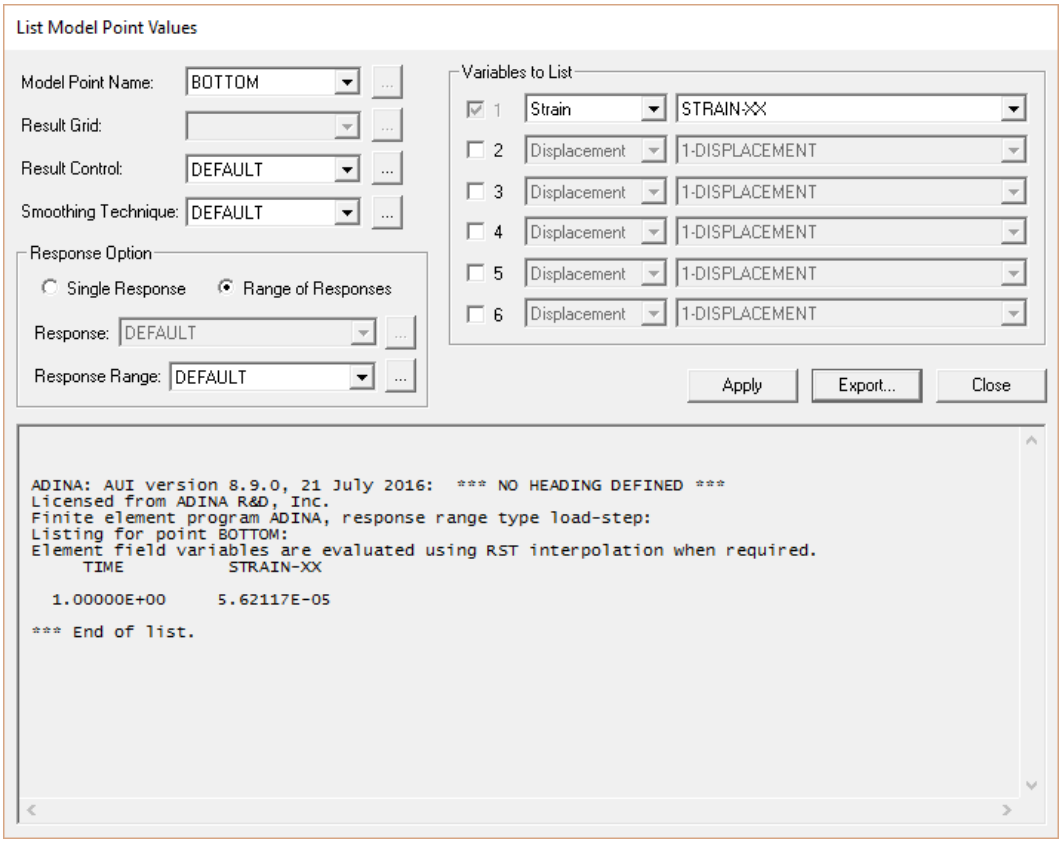

Figure A-29. Longitudinal tensile strain at the bottom of the slab

A.2.7.4 Reading the deflection at the corner of the slab.

The user would like to examine the vertical movements at the corner of the slab. Choose Definitions → Model Point → Element, then set the model point using the following data:

Model Point Name	CORNER
Element Group	1
Element Number	9216
Node #	12740

Then choose → Value list → Model Point…; set the Model Point Name to (CORNER); set the Smoothing Technique to (DEFAULT); set the Variable to List to (Displacement: Z-DISPLACEMENT); verify that the model point name is CORNER; then click Apply.

The graphics window should look something like Figure A-30. The pop-up window shows the vertical movement at the corner of the slab.

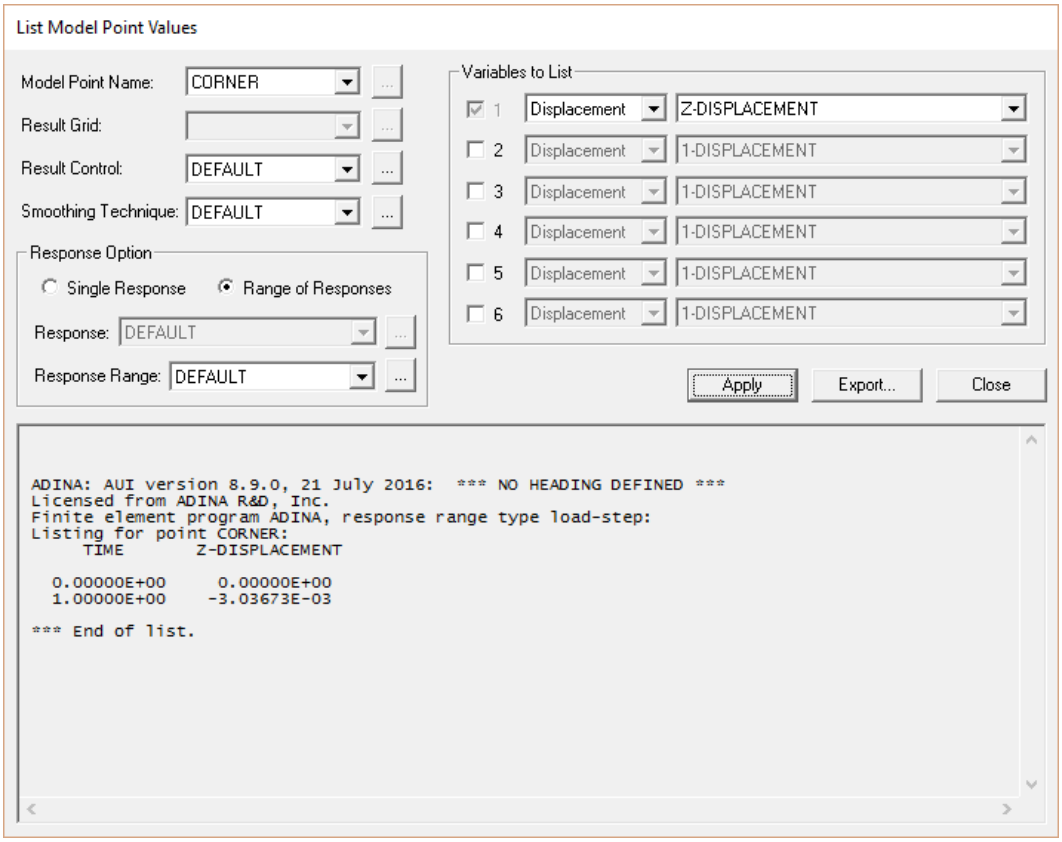

Figure A-30. Vertical deflection at the corner of the slab

A.3 User's Guide of Input File for Analysis of Concrete Slab with Dowel Bars

A.3.1 Overview

This section provides instructions on creating an ADINA input files for analysis of concrete slabs where the dowel joints are modeled with the actual dimensions and physical properties of the dowel bars. A sample input file, named "Dowel-Sample.in" is provided in Appendix D. The user only needs to insert the necessary information into the sample input file according to the dimension and condition of the concrete slab and dowel bars. The geometry design of the FE model developed in this task is shown in Figure A-31.

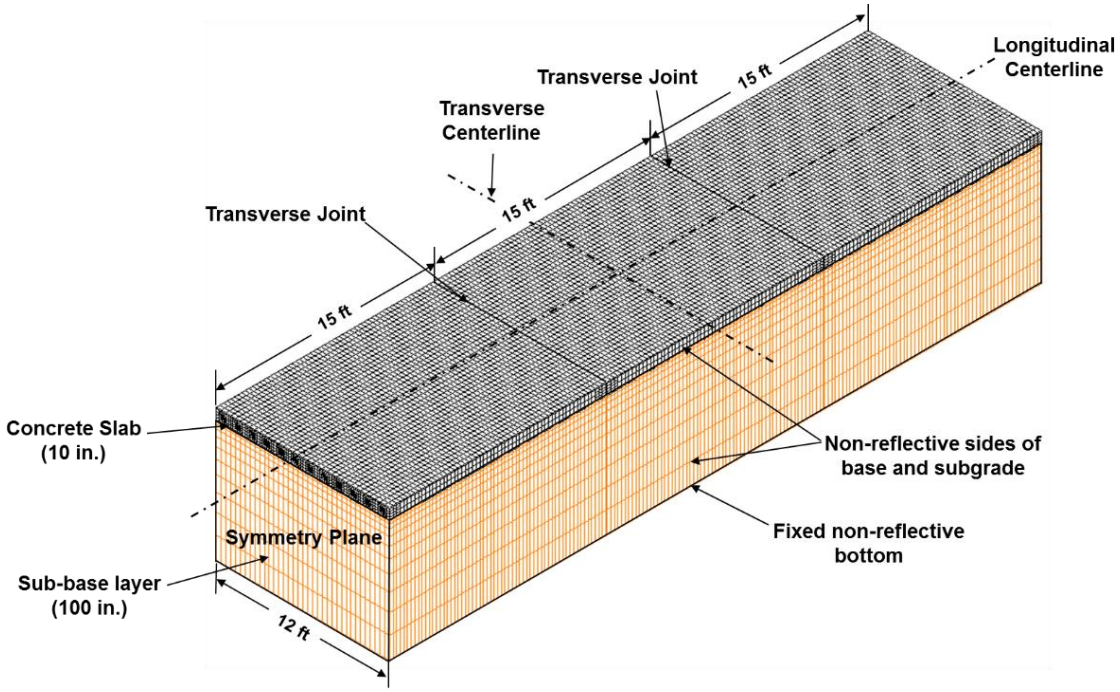

Figure A-31. FE model developed for JPCP with actual dowel bar

A.3.2 Inputs for Dowel Bar Design

In this model, the unique features are the use of actual size of dowel bar and modeling of dowel sleeves which allows the dowel bars to move with certain frictional resistance. Figures A-

32 through A-34 illustrate how to change the dowel size, dowel bar spacing, number of dowel bars per joint, and frictional force in dowel sleeve.

```
*Comment 1 (Dowel bar size) – Length units are in inches
BODY BLOCK NAME=1 OPTION=CENTERED POSITION=VECTOR
ORIENTAT=SYSTEM,
   CX1=-4.5  CX2=0  CX3=0 ,
   SYSTEM=0 DX1=9  DX2=8
   DX3=8        Dowel bar length (in)
*
BODY CYLINDER NAME=2 OPTION=CENTERED POSITION=VECTOR
ORIENTAT=SYSTEM,
   CX1=-4.5  CX2=0  CX3=0 ,
   SYSTEM=0 AXIS=XL RADIUS=0.625.   Dowel bar radius (in)
   LENGTH=9  SHEET=NO
*  Dowel bar length (in)
```

Figure A-32. ADINA code for dowel bar dimension

```
*Comment 2 (Dowel bar spacing and number of dowel bar per joints)
TRANSFORMATI TRANSLATION NAME=2 MODE=SYSTEM SYSTEM=0,
   DX=0  DY=12  DZ=0
*          Dowel bar spacing (in)
BODY TRANSFORMED NAME=7 OPTION=COPY PARENT=1 TRANSFOR=2
NCOPY=11,    Number of dowel bar per joint
   MESH=YES EGROUP=0 NCOINCID=YES NTOLERAN=1.00000000000000E-05
@CLEAR
2
3
4
5
6
@
*
```

Figure A-33. ADINA code for dowel bar spacing and number of dowel bar per joint

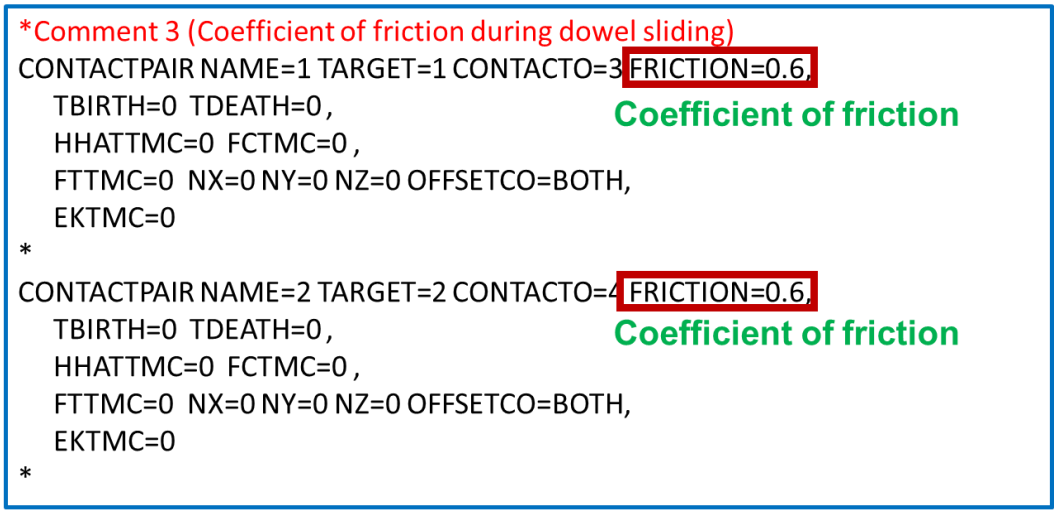

Figure A-34. ADINA code for frictional force in dowel sleeve

A.3.3 Inputs for Structural Design

After finishing the dowel bar design, the user can modify the model dimensions of the concrete slab and subgrade layer. Go to Comments 4 and 5. Change the model dimensions as illustrated in Figures A-35 through A-36.

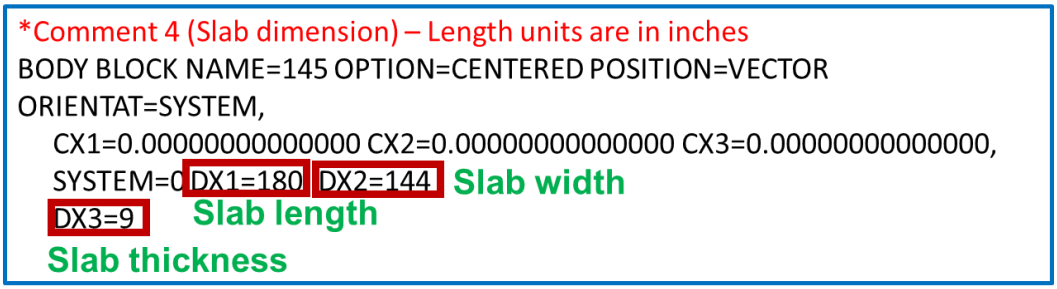

Figure A-35. ADINA code for slab dimension

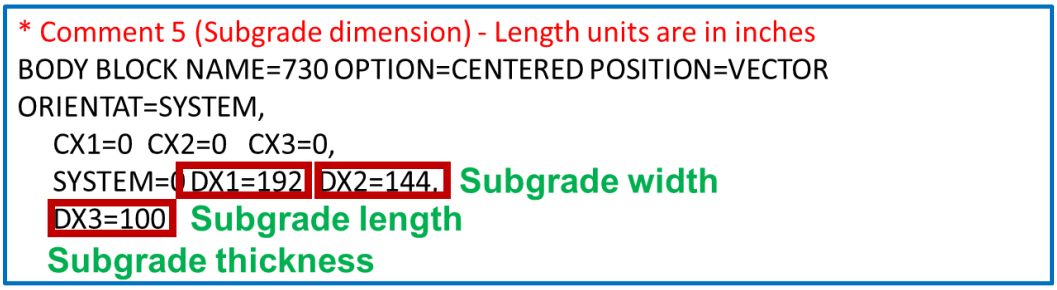

Figure A-36. ADINA code for subgrade layer dimension

A.3.4 Inputs for Material Properties

When the actual material properties obtained from field are available, the user can input the material properties. Navigate to corresponding comment lines and change the values of Young's modulus (E), Poisson's ratio (ν), density (ρ), and coefficient of thermal expansion (CTE) as illustrated in Figures A-37 through A-40.

If the user wants to analyze this model with RAP concrete (i.e., actual stress-strain behavior model) pavement, the concrete material properties as shown in Figure A-38 must be deleted and re-written by following the codes as presented in Figure A-39. These actual stress-strain properties will be applied in the concrete slab elements.

```
* Comment 6 (Dowel bar properties) - Unit: E (psi), v (unitless)
MATERIAL ELASTIC NAME=2 E=2.9E+07 NU=0.3,
   DENSITY=0 ALPHA=0,
 MDESCRIP='dowel'
*
```

Figure A-37. ADINA code for material properties of dowel bar

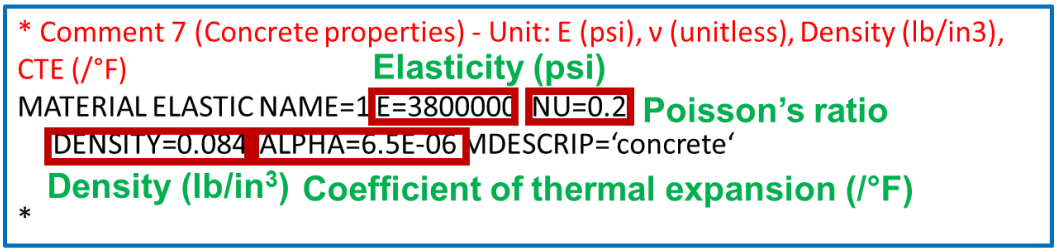

Figure A-38. ADINA code for material properties of concrete

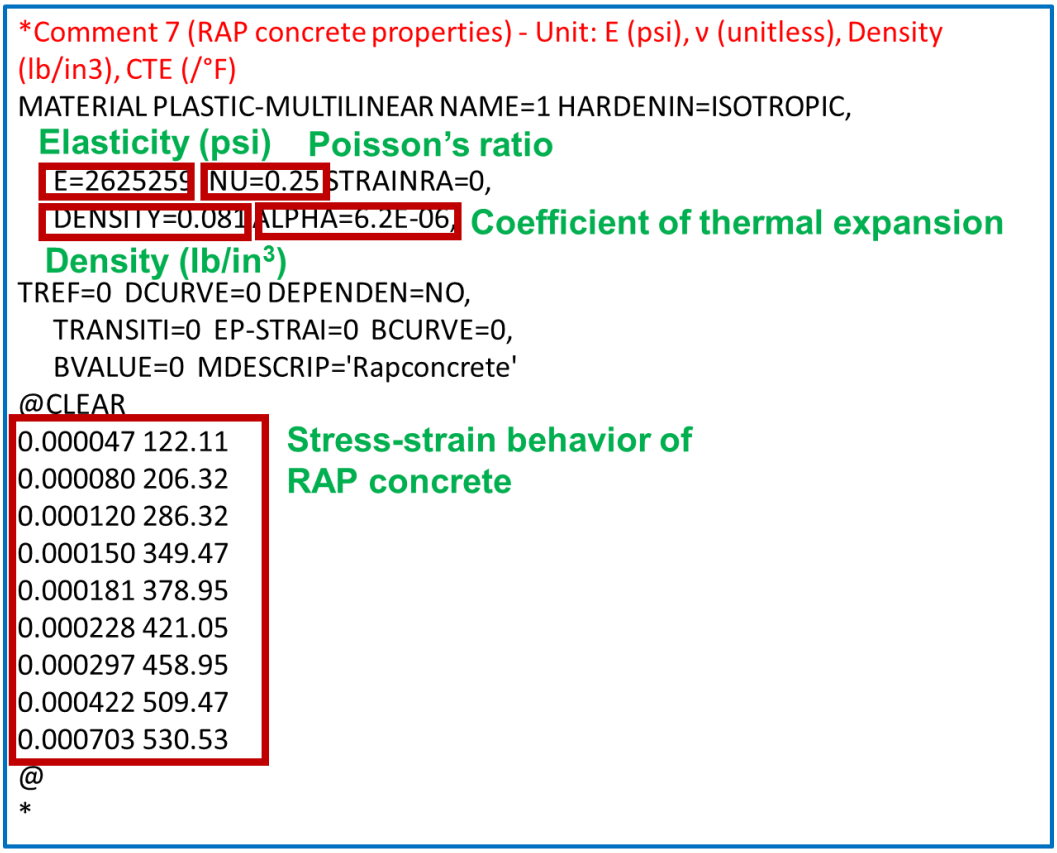

Figure A-39. ADINA code for material properties of existing concrete layer

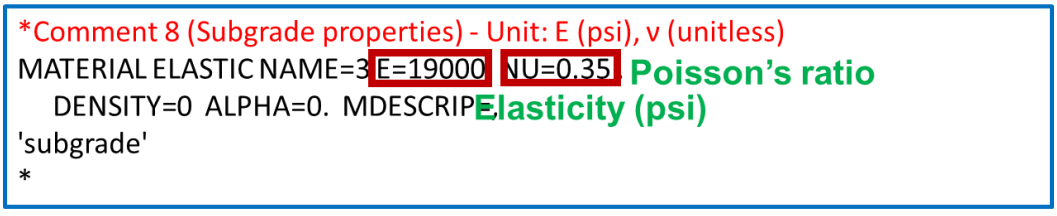

Figure A-40. ADINA code for material properties of subgrade

A.3.5 Inputs for Interface Condition

In this model, three different types of interface bond conditions, namely fully bonded, partially bonded, and unbonded can be modeled using spring elements and frictional contact surface. Since in a fully bonded interface condition, the slab is firmly bonded to the base and cannot be separated from the base, the stiffness of spring elements must be set to infinite for this condition in comment 9 (interface condition) code line as shown in Figure A-41. In a partially bonded condition, the slab can separate from the base by overcoming some restrains, which are controlled by stiffness of spring element. Finally, since an unbonded condition, the slab can separate from the base without any restraint from the base, the spring stiffness in tension should be equal to zero. Also, contact area between the slab and the base has some frictional force which can be simulated using contact surface as shown in Figure A-42.

For selecting the interface bond condition, navigate to Comments 9 (interface condition) and 10 (frictional interface condition) code lines and adjust the values.

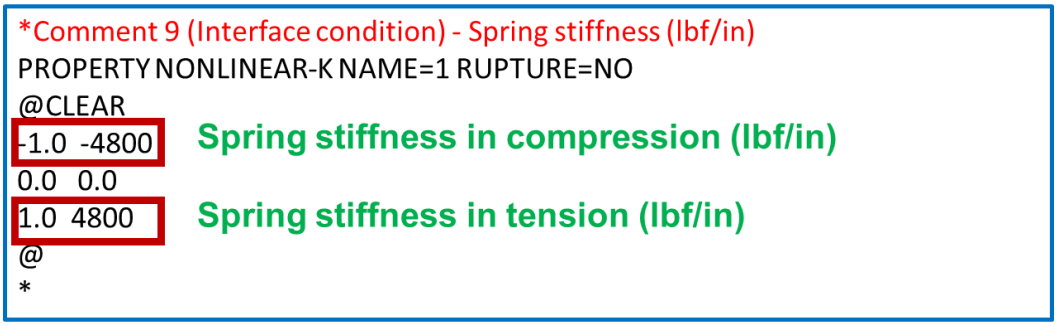

Figure A-41. ADINA code for interface condition

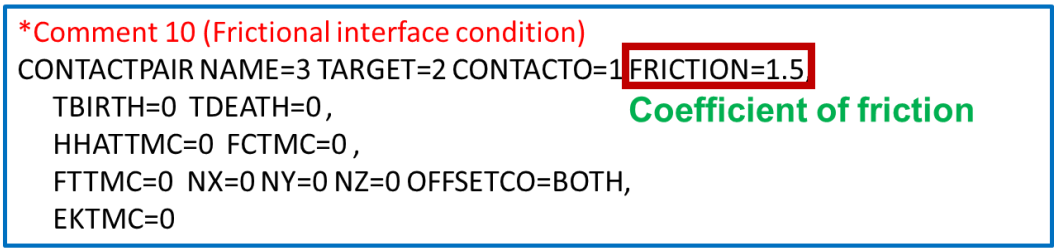

Figure A-42. ADINA code for frictional interface condition

A.3.6 Inputs for Applied Tire Load and Temperature Effect

These codes are basically same as described above. To modify these effects, go to Comments 11 (Tire load) and 12 (Temperature differentials) code lines and adjust the values as shown in Figures A-43 through A-44.

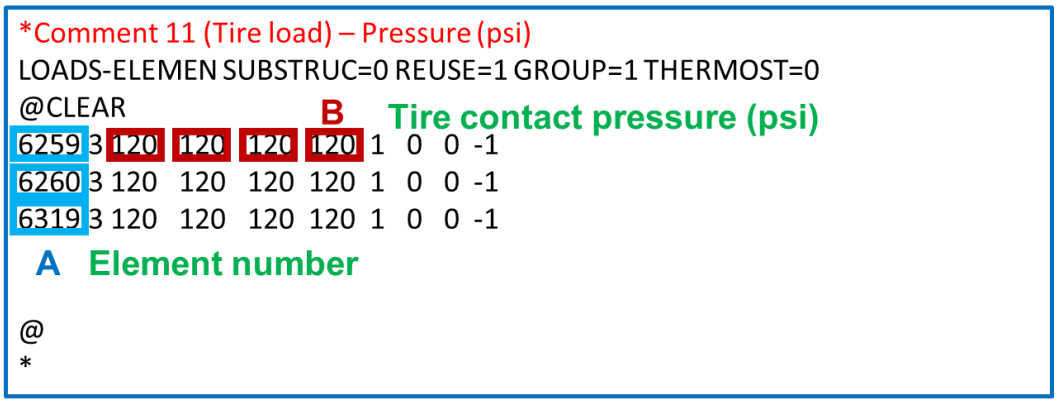

Figure A-43. ADINA code for tire load on concrete element

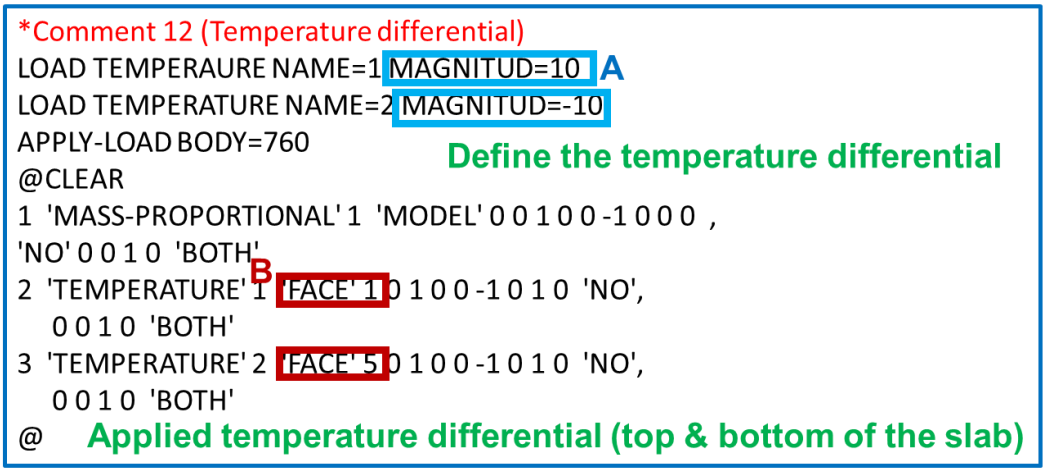

Figure A-44. ADINA code for temperature differentials

A.3.7 Running ADINA

After ADINA input file is created, open the ADINA input file and click the DATA File/Solution icon. When the ADINA run is finished, close all open dialog boxes and choose Post-processing from the Program Module drop-down list. Open the porthole file named as "*.por" to view the results of ADINA analysis.

A.3.8 Post-Processing of Results

A.3.8.1 Displaying bearing stress in the dowel sleeve

To examine the solution, click the Create Band Plot icon, and then set the Band plot Variable to (Stress: STRESS-ZZ). The graphics window shows the bearing stresses in the dowel sleeve under critical temperature-load condition as shown in Figure A-45.

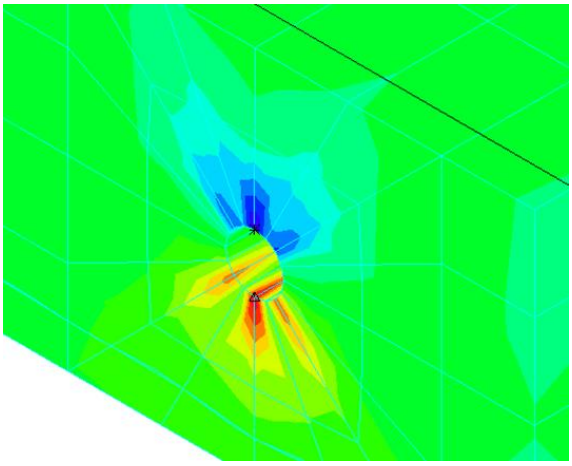

Figure A-45. Plot of bearing stresses in the dowel sleeve due to critical loading condition

In this model, the primary purpose is to examine the dowel bar load transfer characteristics which could be determined by the bearing stress in the surrounding concrete, peak edge stresses in the slab, and deflections under the critical loading condition. Therefore, this tutorial will demonstrate how to get these values using ADINA AUI.

A.3.8.2 Reading the bearing stress in the surrounding concrete

In order to examine the maximum bearing stress in the surrounding concrete, zoom into the critical dowel sleeve. Then choose Definitions → Model Point → Element, and set the model point using the following data:

Model Point Name	BEARING
Element Group	2
Element Number	785
Node #	-

Then choose → Value list → Model Point…; set the Model Point Name to (BEARING); set the Variable to List to (Stress: STRESS-ZZ); verify that the model point name is BEARING; then click Apply.

The graphics window should look something like Figure A-46. The pop-up window shows the maximum bearing stress in the concrete slab.

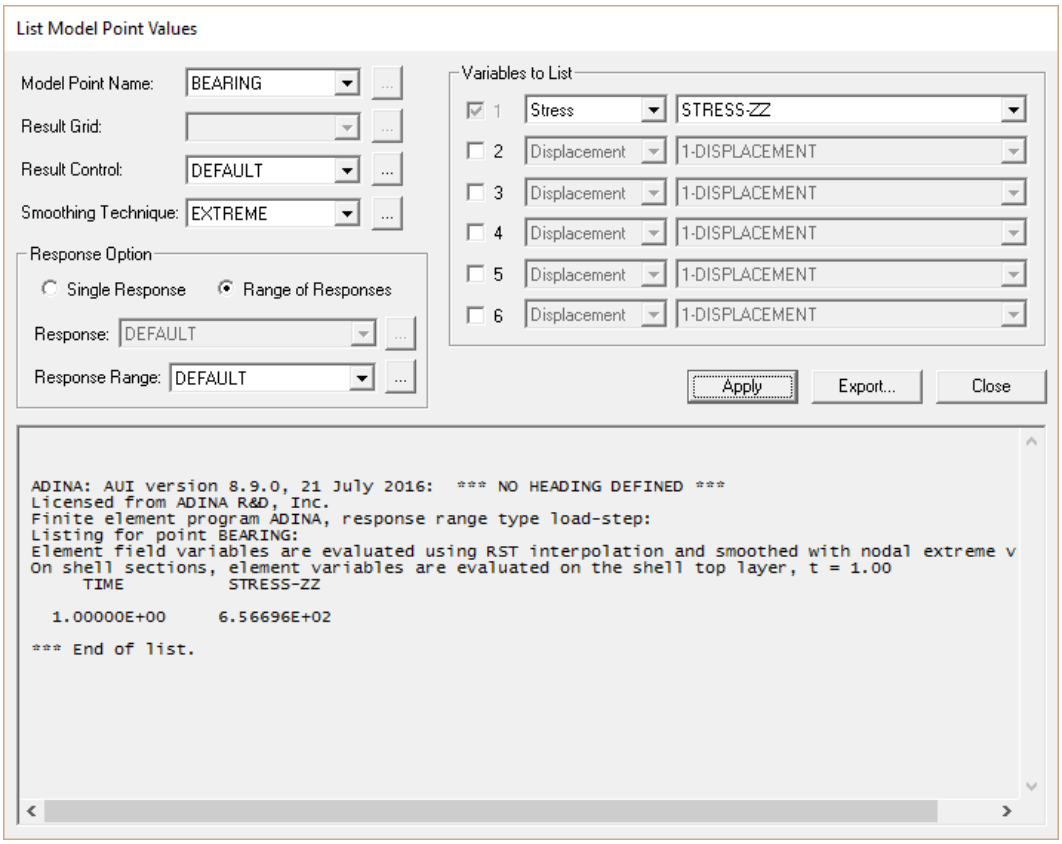

Figure A-46. Bearing stress in the surrounding concrete

A.3.8.3 Reading the peak edge stress

In order to examine the maximum edge stress in the slab, choose Definitions → Model Point → Element, and set the model point using the following data:

Model Point Name	EDGE
Element Group	1
Element Number	9768
Node #	-

Then choose → Value list → Model Point…; set the Model Point Name to (EDGE); set the Variable to List to (Stress: STRESS-XX); then click Apply. The graphics window should look something like Figure A-47. The pop-up window shows the peak edge stress in the concrete slab.

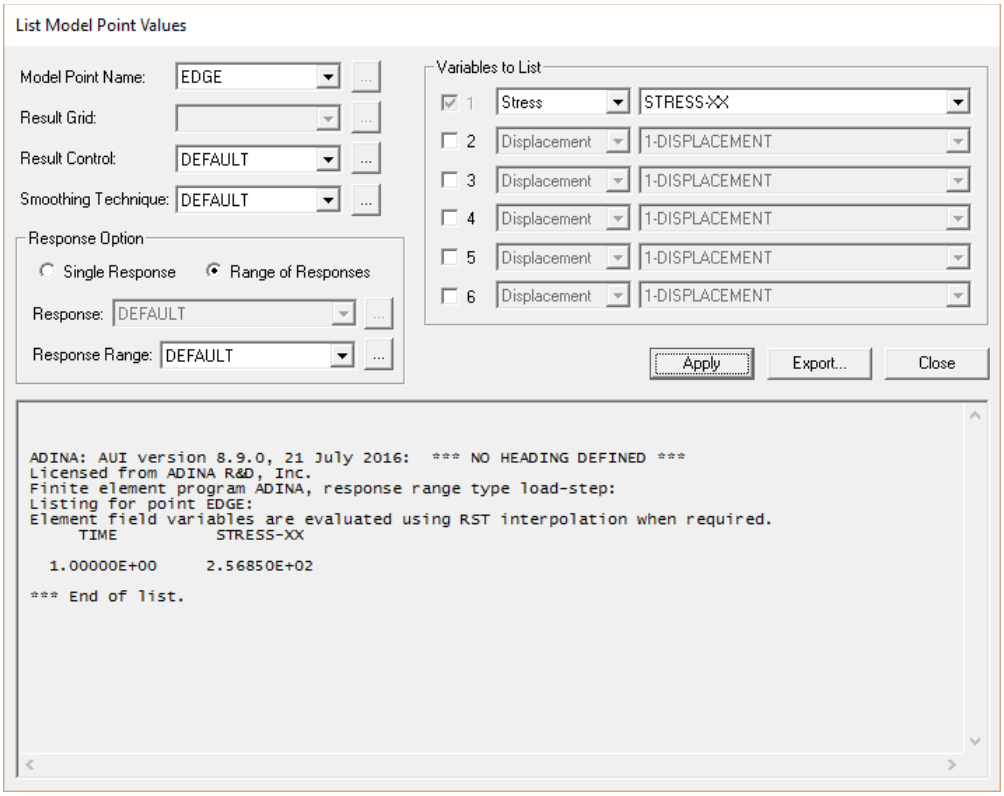

Figure A-47. Peak edge stress in the concrete slab

A.3.8.4 Reading the deflection at the corner of the slab

The user would like to examine the vertical deflection movements at the corner of the slab. Choose Definitions → Model Point → Element, then set the model point using the following data:

Model Point Name	CORNER
Element Group	1

Element Number	9768
Node #	15573

Then choose → Value list → Model Point…; set the Model Point Name to (CORNER); set the Variable to List to (Displacement: Z-DISPLACEMENT); verify that the model point name is CORNER; then click Apply.

The graphics window should look something like Figure A-48. The pop-up window shows the vertical movement at the corner of the slab.

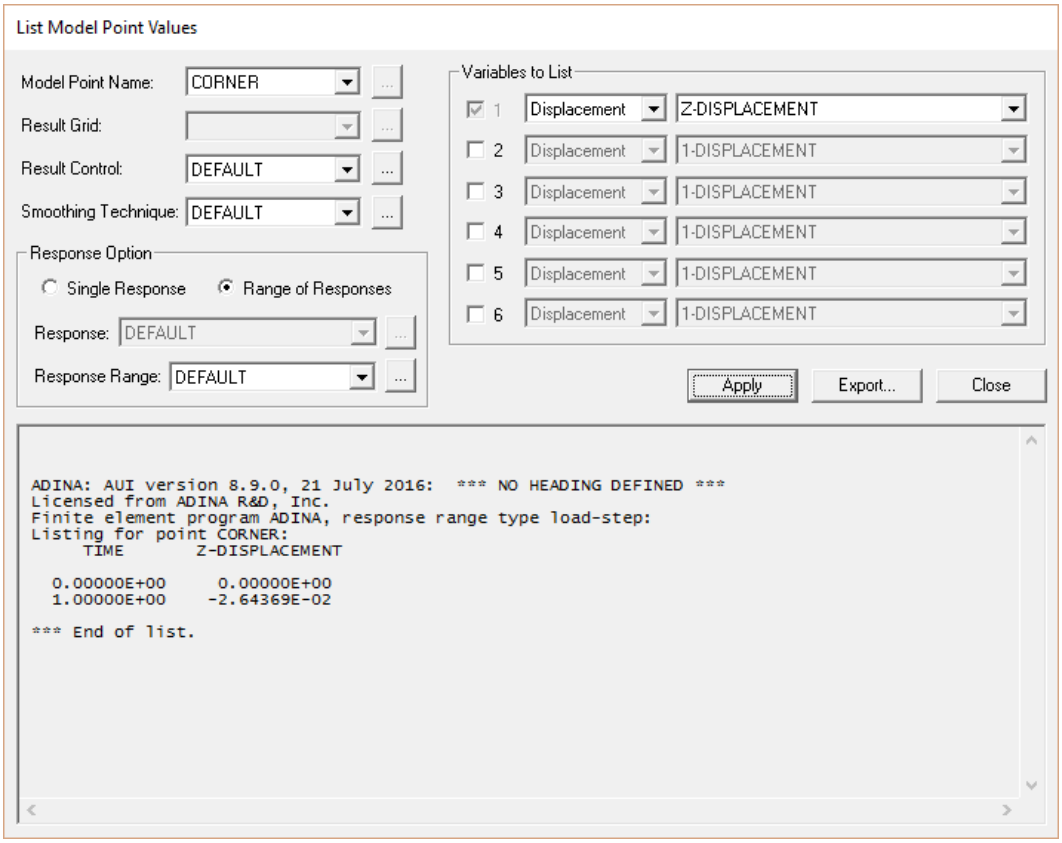

Figure A-48. Corner deflection in the concrete slab

A.4 User's Guide of Input File for Analysis of CRCP

A.4.1 Overview

This section provides instructions on creating an ADINA input file for analysis of continuously reinforced concrete pavement (CRCP). A sample input file, named "CRCP-Sample.in" is provided in Appendix E. The user only needs to insert the necessary information into the sample input file according to the dimension and condition of the concrete slab and steel reinforcement. The geometry design of the FE model developed in this task is shown in Figure A-49.

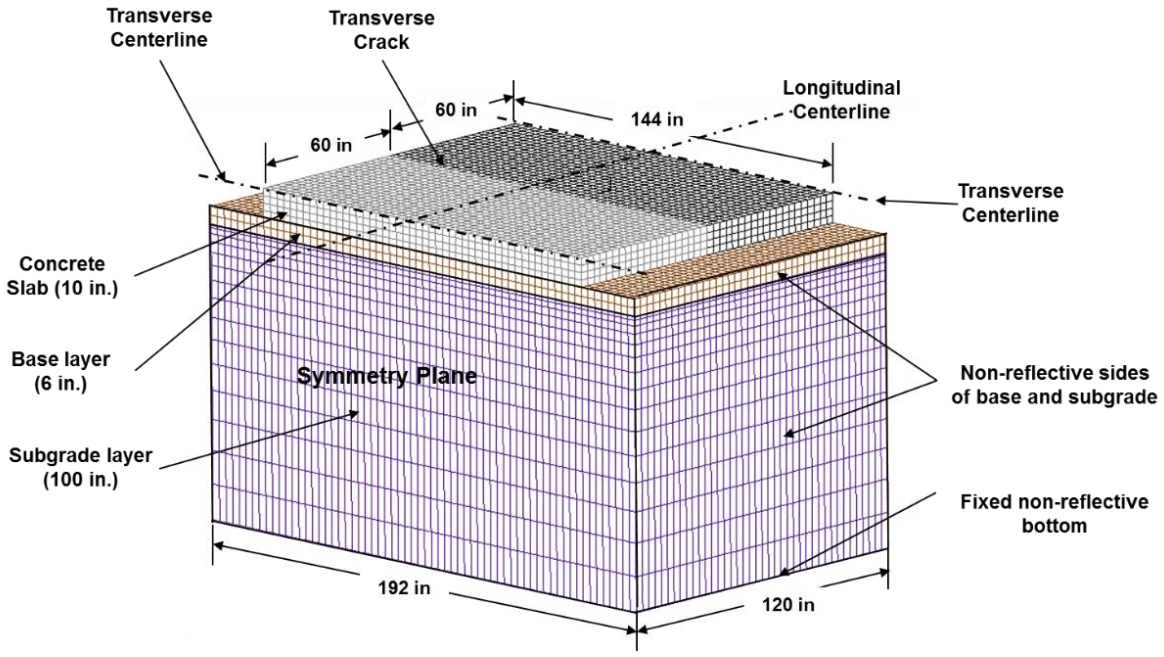

Figure A-49. FE model developed for CRCP

A.4.2 Inputs for CRCP Structural Design

To enter the structural design of CRCP evaluated, navigate to Comment 1 (Slab dimension) code line and change the DX1 (x-dimension), DX2 (y-dimension), and DX3 (z-dimension) in inches. Figures A-50 through A-52 show the ADINA code for model dimension in

CRCP model. In this model, CRCP slabs are formed as a result of transverse shrinkage cracks and held together by longitudinal reinforcing steel. Therefore, the user must enter the slab dimensions two times and the longitudinal length of the slab must be same as the transverse crack spacing. To enter the dimensions for the base and subgrade layers, go to Comments 2 and 3 code lines, respectively.

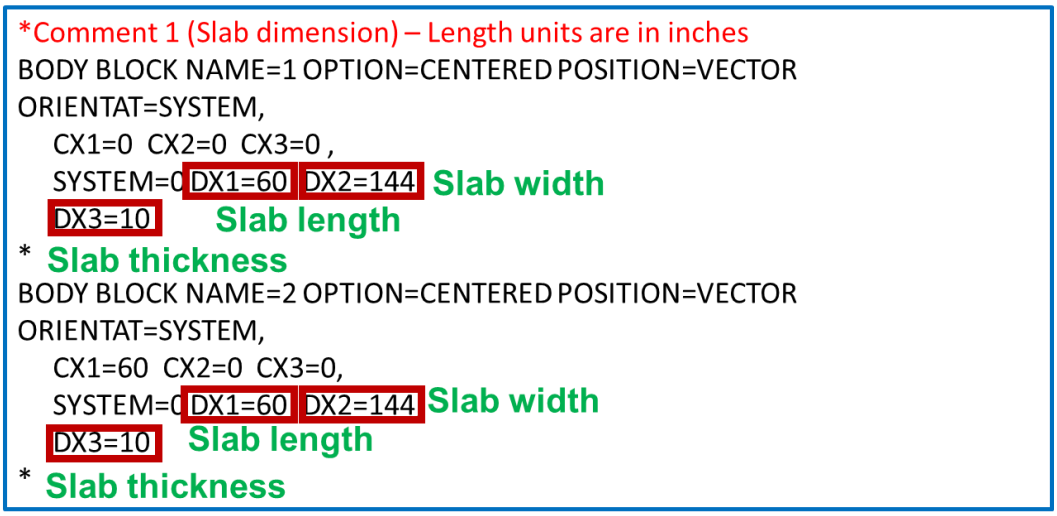

Figure A-50. ADINA code for slab dimension

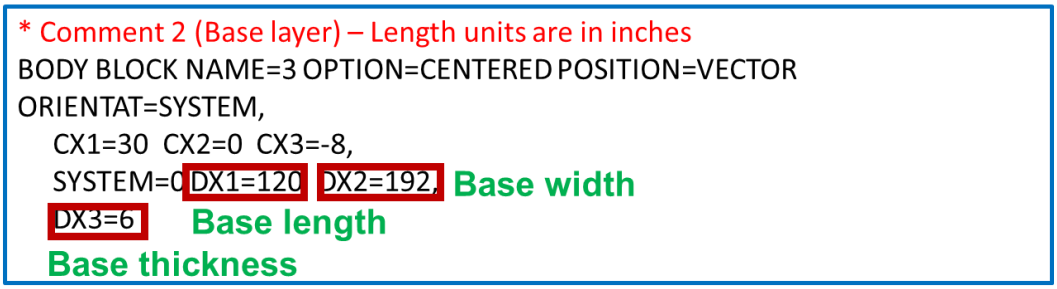

Figure A-51. ADINA code for base layer dimension

```
* Comment 3 (Subgrade layer) – Length units are in inches
BODY BLOCK NAME=4 OPTION=CENTERED POSITION=VECTOR
ORIENTAT=SYSTEM,
   CX1=30  CX2=0  CX3=-61,
   SYSTEM=0 DX1=120 DX2=192,   Subgrade width
   DX3=100   Subgrade length
   Subgrade thickness
```

Figure A-52. ADINA code for subgrade layer dimension

A.4.3 Inputs for Reinforced Steel Design

The longitudinal and transverse reinforce steels are evenly distributed in the slab and the user can enter the number of steels and steel spacing as shown in Figures A-53 through A-54. In the case of the longitudinal steel, the initial steel is generated in the center of the slab and then copied to left and right side of the slab. So, the number of copies must be half of the steels placed in the slab. In the case of transverse steel, the initial steel is also generated in the location of transverse crack and then copied to both sides. When the slab length is shorter than crack spacing, put zero in the number of steel box.

```
* Comment 4 (Longitudinal reinforced steel design) - Length units are in inches
TRANSFORMATI TRANSLATION NAME=1 MODE=SYSTEM SYSTEM=0,
    DX=0 DY=-6 DZ=0
*          Longitudinal steel spacing (in)
LINE TRANSFORMED NAME=4 PARENT=1 TRANSFOR=1 PCOINCID=YES,
    PTOLERAN=1.0E-05 COUPLED=YES NCOPY=11 MESH=YES,
    EGROUP=0 NCOINCID=NO NTOLERAN=1.0E-05  Number of steel
@CLEAR
2
3
@
*
TRANSFORMATI TRANSLATION NAME=2 MODE=SYSTEM SYSTEM=0,
    DX=0 DY=6 DZ=0
*          Longitudinal steel spacing (in)
LINE TRANSFORMED NAME=37 PARENT=1 TRANSFOR=2 PCOINCID=YES,
    PTOLERAN=1.0E-05 COUPLED=YES NCOPY=11 MESH=YES,
    EGROUP=0 NCOINCID=YES NTOLERAN=1.0E-05  Number of steel
@CLEAR
2
3
@
```

Figure A-53. ADINA code for longitudinal steel design

```
*Comment 5 (Transverse reinforced steel design) - Length units are in inches
TRANSFORMATI TRANSLATION NAME=3 MODE=SYSTEM SYSTEM=0,
   DX=-36 DY=0  DZ=0
* Transverse steel spacing (in)
LINE TRANSFORMED NAME=71 PARENT=70 TRANSFOR=3 PCOINCID=YES,
    PTOLERAN=1.0E-05  COUPLED=YES NCOPY=1 MESH=YES,
    EGROUP=0 NCOINCID=YES NTOLERAN=1.0E-05 Number of steel
*
TRANSFORMATI TRANSLATION NAME=4 MODE=SYSTEM SYSTEM=0,
   DX=36 DY=0  DZ=0
* Transverse steel spacing (in)
LINE TRANSFORMED NAME=72 PARENT=70 TRANSFOR=4 PCOINCID=YES,
    PTOLERAN=1.0E-05  COUPLED=YES NCOPY=1 MESH=YES,
    EGROUP=0 NCOINCID=YES NTOLERAN=1.0E-05 Number of steel
```

Figure A-54. ADINA code for transverse steel design

A.4.4 Inputs for Material Properties

The way to input the material properties used in this model is same as in the previous description. Figure A-55 through A-58 illustrate how to change the material properties including concrete, steel, base, and subgrade. To find the correct code line, use the comment number shown in the figures. Note that all values are in US Customary units.

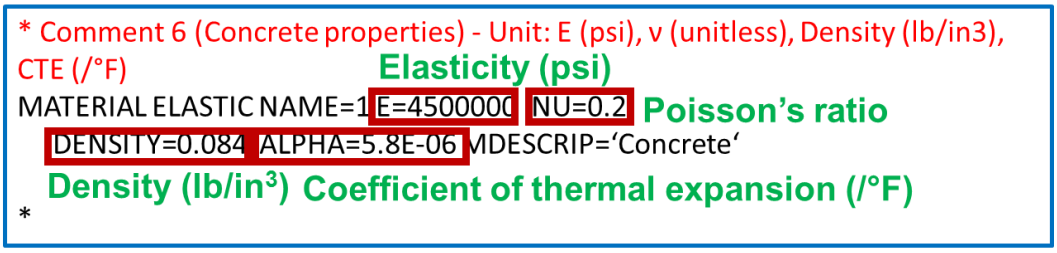

Figure A-55. ADINA code for concrete slab properties

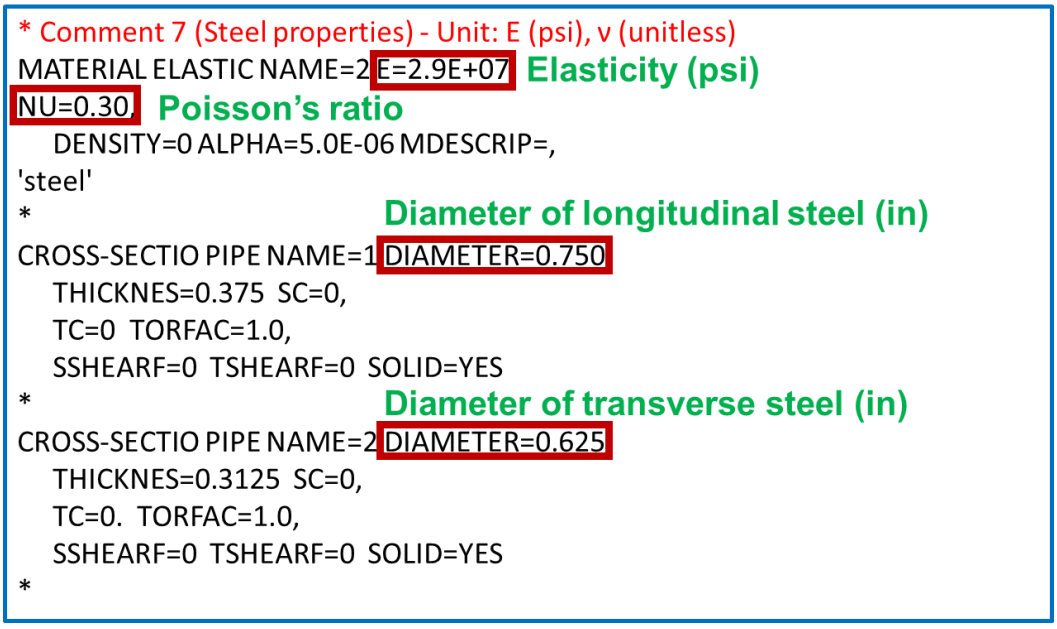

Figure A-56. ADINA code for reinforce steel properties

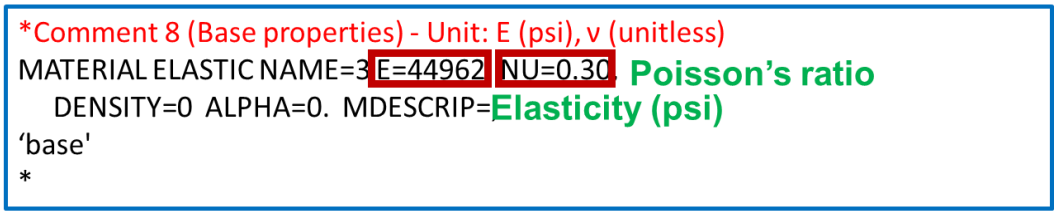

Figure A-57. ADINA code for base layer properties

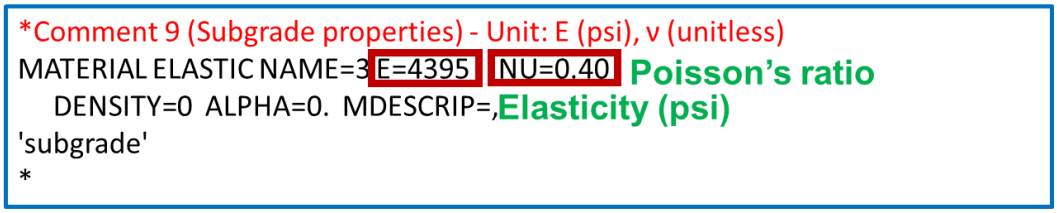

Figure A-58. ADINA code for subgrade layer properties

A.4.5 Inputs for Interface between Concrete Slab and Base

In this model, the interface between the slab and base layer is modeled as unbonded condition. To adjust the interface frictional force, the user can input the coefficient of friction in the input file as shown in Figure A-59. Go to Comment 10 (Frictional interface condition) code line and input the value of coefficient of friction. The interface friction factor may range from 0.9 to 2.2.

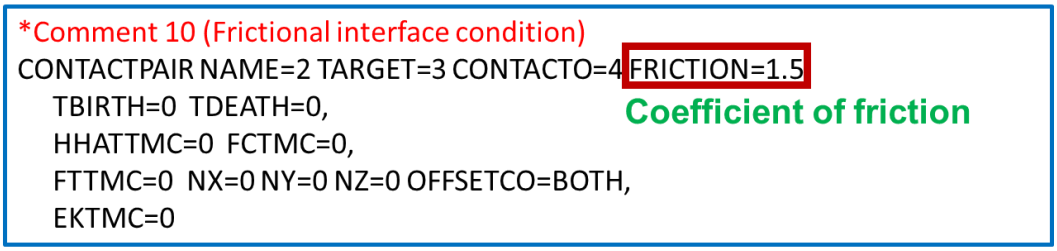

Figure A-59. ADINA code for prestress force

A.4.6 Inputs for Applied Tire Load and Temperature Effect

Finally, the temperature-load condition can be entered in the ADINA input file provided. To enter these values, go to Comments 11 (Tire load) and 12 (Temperature differentials) code lines and adjust the values as shown in Figures A-60 through A-61.

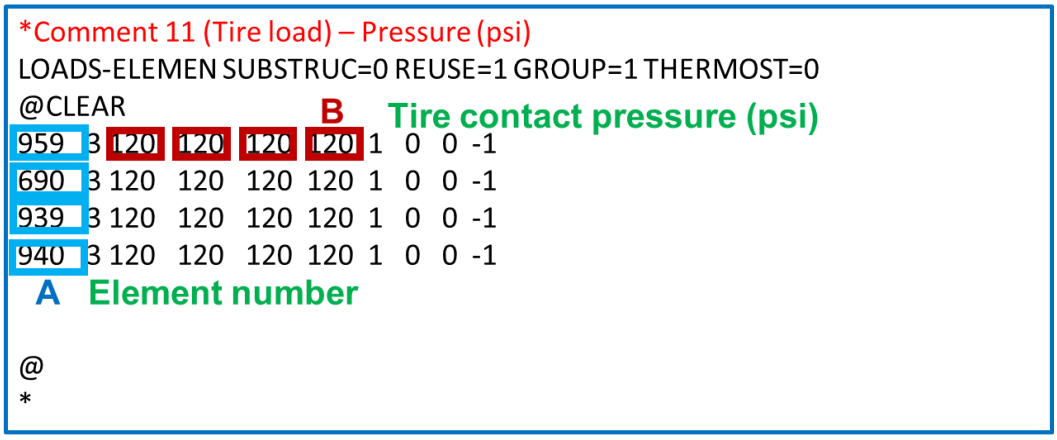

Figure A-60. ADINA code for tire load on concrete element

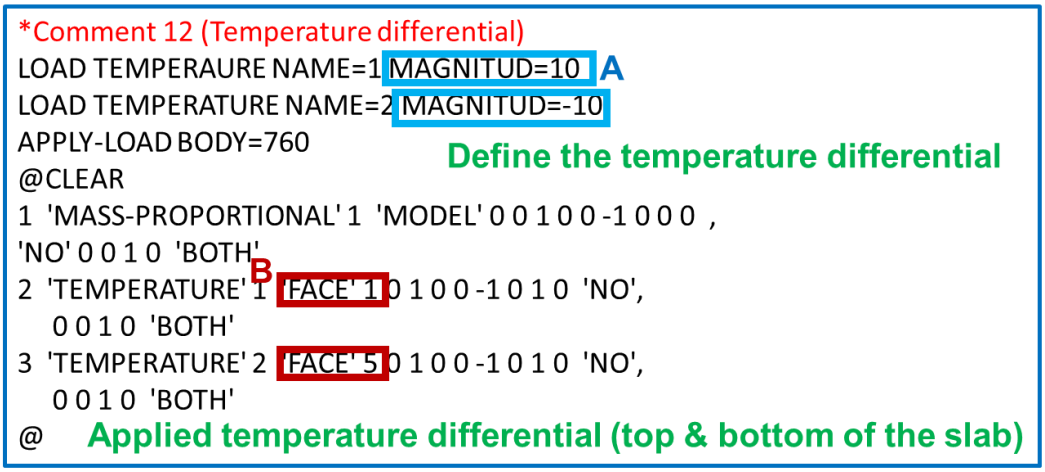

Figure A-61. ADINA code for temperature differentials

A.4.7 Running ADINA

After the ADINA input file is created, open the ADINA input file and click the DATA File/Solution icon . When the ADINA run is finished, close all open dialog boxes and choose Post-processing from the Program Module drop-down list. Open the porthole file named as "*.por" to view the results of ADINA analysis.

A.4.8 Post-Processing of Results

A.4.8.1 Displaying plots of vertical tensile stresses

To examine the solution, click the Create Band Plot icon , and then set the Band plot Variable to (Stress: STRESS-ZZ). The graphics window shows the vertical tensile stresses at the joint due to positive temperature differential of + 20°F as shown in Figure A-62.

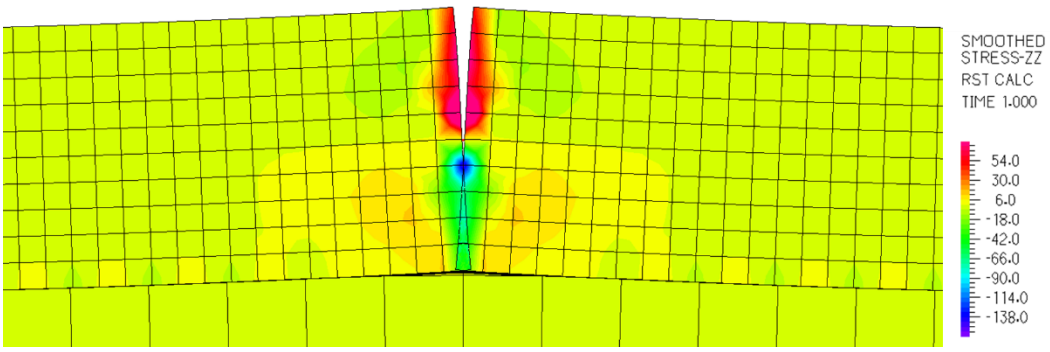

Figure A-62. Plot of vertical tensile stresses due to temperature differential of +20°F

A.4.8.2 Reading the vertical tensile stress at the depth of steel

In this study, the primary purpose is to evaluate the factors influencing horizontal cracking in CRCP which is caused by the vertical tensile stresses near the longitudinal steel. In order to examine the vertical tensile stresses at the depth of steels, define the model line. Choose Definitions → Model Line → Node…; then set the model line using the following data:

#	Node
1	2121
2	2163
3	2205
4	2247
5	2289
6	2331
7	2373
8	2415
9	2457
10	2499
11	2541
12	2583
13	2625
14	2667
15	2709
16	2751
17	2793
18	2835
19	2877
20	2919
21	2961
22	3003
23	3045

Then choose → Value list → Model Line…; set the Model Line Name to (STEEL_LOCATION); set the Variable to List to (Stress: STRESS-ZZ); then click Apply.

The graphics window should look something like Figure A-63. The pop-up window shows the vertical tensile stresses at the depth of steel.

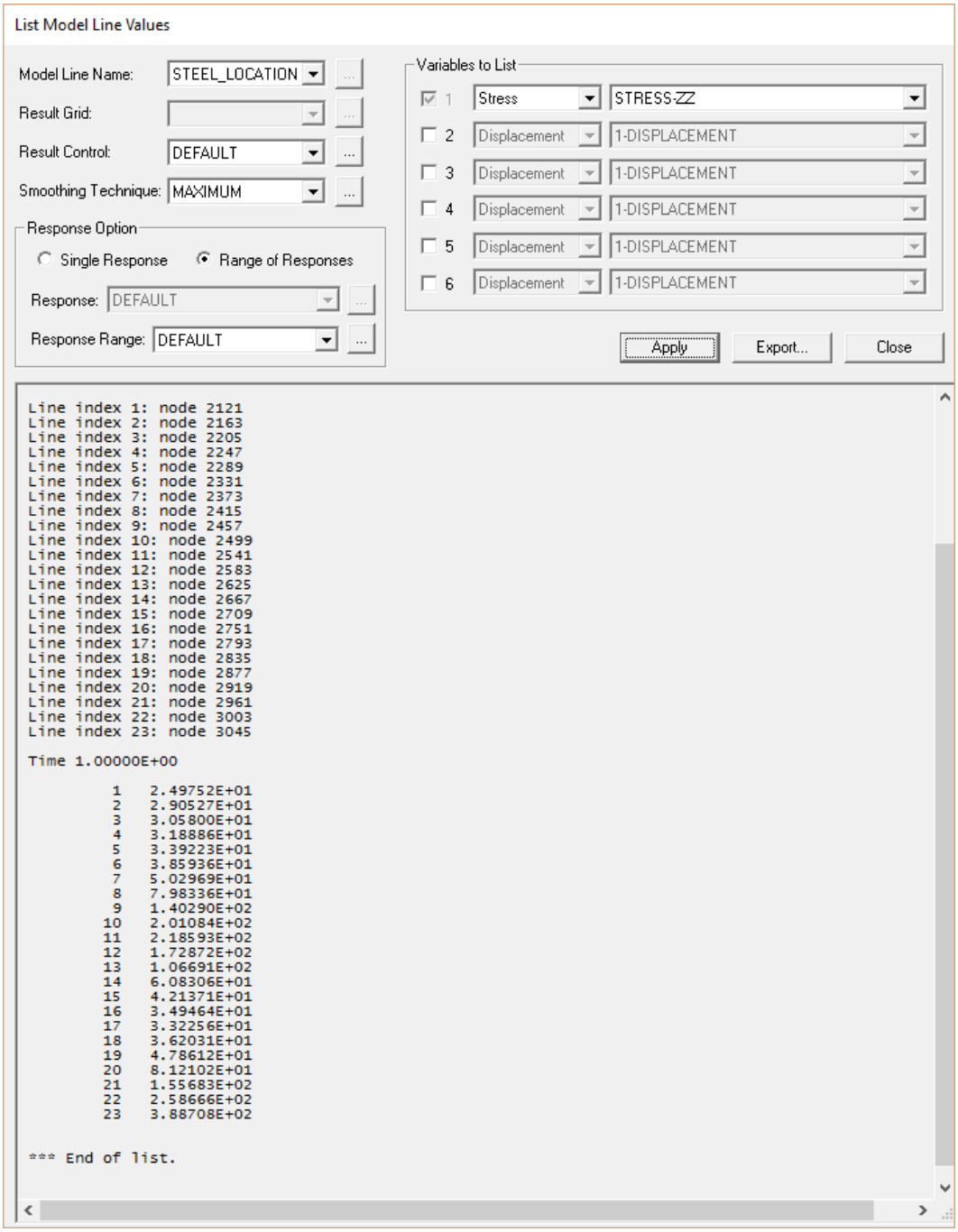

Figure A-63. Vertical tensile stresses in CRCP at the depth of steel

APPENDIX B
PPCP: SAMPLE INPUT FILE

```
*
* Command file created from session file information stored within AUI database
*
DATABASE NEW SAVE=NO PROMPT=NO
FEPROGRAM ADINA
CONTROL FILEVERSION=V89
*
FEPROGRAM PROGRAM=ADINA
*
CONTROL PLOTUNIT=PERCENT VERBOSE=YES ERRORLIM=0 LOGLIMIT=0 UNDO=5,
   PROMPTDE=UNKNOWN AUTOREPA=YES DRAWMATT=YES DRAWTEXT=EXACT,
   DRAWLINE=EXACT DRAWFILL=EXACT AUTOMREB=YES ZONECOPY=NO,
   SWEEPCOI=YES SESSIONS=YES DYNAMICT=YES UPDATETH=YES AUTOREGE=NO,
   ERRORACT=CONTINUE FILEVERS=V89 INITFCHE=NO SIGDIGIT=6,
   AUTOZONE=YES PSFILEVE=V0
*
*Comment 1 (Slab dimension) ? Length units are in inches
*
BODY BLOCK NAME=1 OPTION=CENTERED POSITION=VECTOR ORIENTAT=SYSTEM,
   CX1=-72.0000000000000 CX2=120.000000000000 CX3=0.00000000000000,
   SYSTEM=0 DX1=144.000000000000 DX2=288.000000000000,
   DX3=9.00000000000000
*
SUBDIVIDE BODY NAME=1 MODE=LENGTH SIZE=3.00000000000000,
   MAX-SIZE=0.00000000000000
@CLEAR
1
@
*
SUBDIVIDE EDGE NAME=1 BODY=1 MODE=DIVISIONS NDIV=96,
   RATIO=1.00000000000000 PROGRESS=ARITHMETIC BLTABLE=0
*
SUBDIVIDE EDGE NAME=5 BODY=1 MODE=DIVISIONS NDIV=4,
   RATIO=1.00000000000000 PROGRESS=ARITHMETIC BLTABLE=0
@CLEAR
6
7
8
@
*
TRANSFORMATI TRANSLATION NAME=1 MODE=SYSTEM SYSTEM=0,
   DX=-144.000000000000 DY=0.00000000000000 DZ=0.00000000000000
*
BODY TRANSFORMED NAME=2 OPTION=COPY PARENT=1 TRANSFOR=1 NCOPY=21,
   MESH=YES EGROUP=0 NCOINCID=NO NTOLERAN=1.00000000000000E-05
*
BODY BLOCK NAME=23 OPTION=CENTERED POSITION=VECTOR ORIENTAT=SYSTEM,
   CX1=-3096.00000000000 CX2=120.000000000000 CX3=-5.50000000000000,
   SYSTEM=0 DX1=3168.00000000000 DX2=288.000000000000,
   DX3=2.00000000000000
*
BODY BLOCK NAME=23 OPTION=CENTERED POSITION=VECTOR ORIENTAT=SYSTEM,
```

```
    CX1=0.00000000000000 CX2=120.000000000000 CX3=-5.50000000000000,
    SYSTEM=0 DX1=3168.00000000000 DX2=288.000000000000,
    DX3=2.00000000000000
*
BODY BLOCK NAME=23 OPTION=CENTERED POSITION=VECTOR ORIENTAT=SYSTEM,
    CX1=-1512.00000000000 CX2=120.000000000000 CX3=-5.50000000000000,
    SYSTEM=0 DX1=3168.00000000000 DX2=288.000000000000,
    DX3=2.00000000000000
*
BODY BLOCK NAME=23 OPTION=CENTERED POSITION=VECTOR ORIENTAT=SYSTEM,
    CX1=-1659.00000000000 CX2=120.000000000000 CX3=-5.50000000000000,
    SYSTEM=0 DX1=3168.00000000000 DX2=288.000000000000,
    DX3=2.00000000000000
*
* Comment 2 (AC leveling layer) ? Length units are in inches
*
BODY BLOCK NAME=23 OPTION=CENTERED POSITION=VECTOR ORIENTAT=SYSTEM,
    CX1=-1584.00000000000 CX2=120.000000000000 CX3=-5.50000000000000,
    SYSTEM=0 DX1=3168.00000000000 DX2=288.000000000000,
    DX3=2.00000000000000
*
SUBDIVIDE BODY NAME=23 MODE=LENGTH SIZE=3.00000000000000,
    MAX-SIZE=0.00000000000000
*
SUBDIVIDE EDGE NAME=5 BODY=23 MODE=DIVISIONS NDIV=2,
    RATIO=1.00000000000000 PROGRESS=ARITHMETIC BLTABLE=0
@CLEAR
6
7
8
@
*
* Comment 3 (Existing concrete layer) ? Length units are in inches
*
BODY BLOCK NAME=24 OPTION=CENTERED POSITION=VECTOR ORIENTAT=SYSTEM,
    CX1=-1584.00000000000 CX2=120.000000000000 CX3=-11.0000000000000,
    SYSTEM=0 DX1=3168.00000000000 DX2=288.000000000000,
    DX3=9.00000000000000
*
SUBDIVIDE BODY NAME=24 MODE=LENGTH SIZE=3.00000000000000,
    MAX-SIZE=0.00000000000000
*
SUBDIVIDE EDGE NAME=5 BODY=24 MODE=DIVISIONS NDIV=2,
    RATIO=1.00000000000000 PROGRESS=ARITHMETIC BLTABLE=0
@CLEAR
6
7
8
@
*
* Comment 4 (Subgrade layer) ? Length units are in inches
*
BODY BLOCK NAME=25 OPTION=CENTERED POSITION=VECTOR ORIENTAT=SYSTEM,
    CX1=-1584.00000000000 CX2=120.000000000000 CX3=-65.5000000000000,
    SYSTEM=0 DX1=3168.00000000000 DX2=288.000000000000,
    DX3=100.000000000000
```

```
*
SUBDIVIDE BODY NAME=25 MODE=LENGTH SIZE=3.00000000000000,
   MAX-SIZE=0.00000000000000
*
SUBDIVIDE EDGE NAME=5 BODY=25 MODE=DIVISIONS NDIV=3,
   RATIO=10.0000000000000 PROGRESS=ARITHMETIC BLTABLE=0
@CLEAR
6
7
8
@
*
SUBDIVIDE EDGE NAME=5 BODY=25 MODE=DIVISIONS NDIV=5,
   RATIO=0.100000000000000 PROGRESS=ARITHMETIC BLTABLE=0
@CLEAR
6
7
8
@
*
SUBDIVIDE EDGE NAME=5 BODY=25 MODE=DIVISIONS NDIV=10,
   RATIO=0.100000000000000 PROGRESS=ARITHMETIC BLTABLE=0
@CLEAR
6
7
8
@
*
FIXITY NAME=XFIX
@CLEAR
 'X-TRANSLATION'
 'OVALIZATION'
@
*
FIXITY NAME=YFIX
@CLEAR
 'Y-TRANSLATION'
 'OVALIZATION'
@
*
MASTER ANALYSIS=STATIC MODEX=EXECUTE TSTART=0.00000000000000 IDOF=111,
   OVALIZAT=NONE FLUIDPOT=AUTOMATIC CYCLICPA=1 IPOSIT=STOP,
   REACTION=YES INITIALS=NO FSINTERA=NO IRINT=DEFAULT CMASS=NO,
   SHELLNDO=AUTOMATIC AUTOMATI=OFF SOLVER=SPARSE,
   CONTACT-=CONSTRAINT-FUNCTION TRELEASE=0.00000000000000,
   RESTART-=NO FRACTURE=NO LOAD-CAS=NO LOAD-PEN=NO SINGULAR=YES,
   STIFFNES=0.000100000000000000 MAP-OUTP=NONE MAP-FORM=NO,
   NODAL-DE=" POROUS-C=NO ADAPTIVE=0 ZOOM-LAB=1 AXIS-CYC=0,
   PERIODIC=NO VECTOR-S=GEOMETRY EPSI-FIR=NO STABILIZ=NO,
   STABFACT=1.00000000000000E-10 RESULTS=PORTHOLE FEFCORR=NO,
   BOLTSTEP=1 EXTEND-S=YES CONVERT-=NO DEGEN=YES TMC-MODE=NO,
   ENSIGHT-=NO IRSTEPS=1 INITIALT=NO TEMP-INT=NO ESINTERA=NO,
   OP2GEOM=NO INSITU-D=NO
*
FIXBOUNDARY FACES FIXITY=ALL BODY=25
@CLEAR
```

```
6  'XFIX'
3  'XFIX'
4  'YFIX'
2  'YFIX'
5  'ALL'
@
*
FIXBOUNDARY FACES FIXITY=ALL BODY=24
@CLEAR
6  'XFIX'
3  'XFIX'
2  'YFIX'
4  'YFIX'
@
*
FIXBOUNDARY FACES FIXITY=ALL BODY=23
@CLEAR
6  'XFIX'
3  'XFIX'
4  'YFIX'
2  'YFIX'
@
*
LOAD TEMPERATURE NAME=1 MAGNITUD=10.0000000000000
*
LOAD TEMPERATURE NAME=2 MAGNITUD=-10.0000000000000
*
APPLY-LOAD BODY=25
@CLEAR
1  'TEMPERATURE' 1  'FACE' 1 0 1 0.00000000000000 0 -1 0 1 0  'NO',
    0.00000000000000 0.00000000000000 1 0  'BOTH'
2  'TEMPERATURE' 2  'FACE' 5 0 1 0.00000000000000 0 -1 0 1 0  'NO',
    0.00000000000000 0.00000000000000 1 0  'BOTH'
3  'TEMPERATURE' 1  'FACE' 1 0 1 0.00000000000000 0 -1 0 2 0  'NO',
    0.00000000000000 0.00000000000000 1 0  'BOTH'
4  'TEMPERATURE' 2  'FACE' 5 0 1 0.00000000000000 0 -1 0 2 0  'NO',
    0.00000000000000 0.00000000000000 1 0  'BOTH'
5  'TEMPERATURE' 1  'FACE' 1 0 1 0.00000000000000 0 -1 0 3 0  'NO',
    0.00000000000000 0.00000000000000 1 0  'BOTH'
6  'TEMPERATURE' 2  'FACE' 5 0 1 0.00000000000000 0 -1 0 3 0  'NO',
    0.00000000000000 0.00000000000000 1 0  'BOTH'
7  'TEMPERATURE' 1  'FACE' 1 0 1 0.00000000000000 0 -1 0 4 0  'NO',
    0.00000000000000 0.00000000000000 1 0  'BOTH'
8  'TEMPERATURE' 2  'FACE' 5 0 1 0.00000000000000 0 -1 0 4 0  'NO',
    0.00000000000000 0.00000000000000 1 0  'BOTH'
9  'TEMPERATURE' 1  'FACE' 1 0 1 0.00000000000000 0 -1 0 5 0  'NO',
    0.00000000000000 0.00000000000000 1 0  'BOTH'
10  'TEMPERATURE' 2  'FACE' 5 0 1 0.00000000000000 0 -1 0 5 0  'NO',
    0.00000000000000 0.00000000000000 1 0  'BOTH'
11  'TEMPERATURE' 1  'FACE' 1 0 1 0.00000000000000 0 -1 0 6 0  'NO',
    0.00000000000000 0.00000000000000 1 0  'BOTH'
12  'TEMPERATURE' 2  'FACE' 5 0 1 0.00000000000000 0 -1 0 6 0  'NO',
    0.00000000000000 0.00000000000000 1 0  'BOTH'
13  'TEMPERATURE' 1  'FACE' 1 0 1 0.00000000000000 0 -1 0 7 0  'NO',
    0.00000000000000 0.00000000000000 1 0  'BOTH'
14  'TEMPERATURE' 2  'FACE' 5 0 1 0.00000000000000 0 -1 0 7 0  'NO',
```

```
    0.00000000000000 0.00000000000000 1 0  'BOTH'
15  'TEMPERATURE' 1  'FACE' 1 0 1 0.00000000000000 0 -1 0 8 0  'NO',
    0.00000000000000 0.00000000000000 1 0  'BOTH'
16  'TEMPERATURE' 2  'FACE' 5 0 1 0.00000000000000 0 -1 0 8 0  'NO',
    0.00000000000000 0.00000000000000 1 0  'BOTH'
17  'TEMPERATURE' 1  'FACE' 1 0 1 0.00000000000000 0 -1 0 9 0  'NO',
    0.00000000000000 0.00000000000000 1 0  'BOTH'
18  'TEMPERATURE' 2  'FACE' 5 0 1 0.00000000000000 0 -1 0 9 0  'NO',
    0.00000000000000 0.00000000000000 1 0  'BOTH'
19  'TEMPERATURE' 1  'FACE' 1 0 1 0.00000000000000 0 -1 0 10 0  'NO',
    0.00000000000000 0.00000000000000 1 0  'BOTH'
20  'TEMPERATURE' 2  'FACE' 5 0 1 0.00000000000000 0 -1 0 10 0  'NO',
    0.00000000000000 0.00000000000000 1 0  'BOTH'
21  'TEMPERATURE' 1  'FACE' 1 0 1 0.00000000000000 0 -1 0 11 0  'NO',
    0.00000000000000 0.00000000000000 1 0  'BOTH'
22  'TEMPERATURE' 2  'FACE' 5 0 1 0.00000000000000 0 -1 0 11 0  'NO',
    0.00000000000000 0.00000000000000 1 0  'BOTH'
23  'TEMPERATURE' 1  'FACE' 1 0 1 0.00000000000000 0 -1 0 12 0  'NO',
    0.00000000000000 0.00000000000000 1 0  'BOTH'
24  'TEMPERATURE' 2  'FACE' 5 0 1 0.00000000000000 0 -1 0 12 0  'NO',
    0.00000000000000 0.00000000000000 1 0  'BOTH'
25  'TEMPERATURE' 1  'FACE' 1 0 1 0.00000000000000 0 -1 0 13 0  'NO',
    0.00000000000000 0.00000000000000 1 0  'BOTH'
26  'TEMPERATURE' 2  'FACE' 5 0 1 0.00000000000000 0 -1 0 13 0  'NO',
    0.00000000000000 0.00000000000000 1 0  'BOTH'
27  'TEMPERATURE' 1  'FACE' 1 0 1 0.00000000000000 0 -1 0 14 0  'NO',
    0.00000000000000 0.00000000000000 1 0  'BOTH'
28  'TEMPERATURE' 2  'FACE' 5 0 1 0.00000000000000 0 -1 0 14 0  'NO',
    0.00000000000000 0.00000000000000 1 0  'BOTH'
29  'TEMPERATURE' 1  'FACE' 1 0 1 0.00000000000000 0 -1 0 15 0  'NO',
    0.00000000000000 0.00000000000000 1 0  'BOTH'
30  'TEMPERATURE' 2  'FACE' 5 0 1 0.00000000000000 0 -1 0 15 0  'NO',
    0.00000000000000 0.00000000000000 1 0  'BOTH'
31  'TEMPERATURE' 1  'FACE' 1 0 1 0.00000000000000 0 -1 0 16 0  'NO',
    0.00000000000000 0.00000000000000 1 0  'BOTH'
32  'TEMPERATURE' 2  'FACE' 5 0 1 0.00000000000000 0 -1 0 16 0  'NO',
    0.00000000000000 0.00000000000000 1 0  'BOTH'
33  'TEMPERATURE' 1  'FACE' 1 0 1 0.00000000000000 0 -1 0 17 0  'NO',
    0.00000000000000 0.00000000000000 1 0  'BOTH'
34  'TEMPERATURE' 2  'FACE' 5 0 1 0.00000000000000 0 -1 0 17 0  'NO',
    0.00000000000000 0.00000000000000 1 0  'BOTH'
35  'TEMPERATURE' 1  'FACE' 1 0 1 0.00000000000000 0 -1 0 18 0  'NO',
    0.00000000000000 0.00000000000000 1 0  'BOTH'
36  'TEMPERATURE' 2  'FACE' 5 0 1 0.00000000000000 0 -1 0 18 0  'NO',
    0.00000000000000 0.00000000000000 1 0  'BOTH'
37  'TEMPERATURE' 1  'FACE' 1 0 1 0.00000000000000 0 -1 0 19 0  'NO',
    0.00000000000000 0.00000000000000 1 0  'BOTH'
38  'TEMPERATURE' 2  'FACE' 5 0 1 0.00000000000000 0 -1 0 19 0  'NO',
    0.00000000000000 0.00000000000000 1 0  'BOTH'
39  'TEMPERATURE' 1  'FACE' 1 0 1 0.00000000000000 0 -1 0 20 0  'NO',
    0.00000000000000 0.00000000000000 1 0  'BOTH'
40  'TEMPERATURE' 2  'FACE' 5 0 1 0.00000000000000 0 -1 0 20 0  'NO',
    0.00000000000000 0.00000000000000 1 0  'BOTH'
41  'TEMPERATURE' 1  'FACE' 1 0 1 0.00000000000000 0 -1 0 21 0  'NO',
    0.00000000000000 0.00000000000000 1 0  'BOTH'
42  'TEMPERATURE' 2  'FACE' 5 0 1 0.00000000000000 0 -1 0 21 0  'NO',
```

```
    0.00000000000000 0.00000000000000 1 0  'BOTH'
43  'TEMPERATURE' 1  'FACE' 1 0 1 0.00000000000000 0 -1 0 22 0  'NO',
    0.00000000000000 0.00000000000000 1 0  'BOTH'
44  'TEMPERATURE' 2  'FACE' 5 0 1 0.00000000000000 0 -1 0 22 0  'NO',
    0.00000000000000 0.00000000000000 1 0  'BOTH'
@
*
MASTER ANALYSIS=STATIC MODEX=EXECUTE TSTART=0.00000000000000 IDOF=111,
    OVALIZAT=NONE FLUIDPOT=AUTOMATIC CYCLICPA=1 IPOSIT=STOP,
    REACTION=YES INITIALS=NO FSINTERA=NO IRINT=DEFAULT CMASS=NO,
    SHELLNDO=AUTOMATIC AUTOMATI=OFF SOLVER=SPARSE,
    CONTACT-=CONSTRAINT-FUNCTION TRELEASE=0.00000000000000,
    RESTART-=NO FRACTURE=NO LOAD-CAS=NO LOAD-PEN=NO SINGULAR=YES,
    STIFFNES=0.00010000000000000 MAP-OUTP=NONE MAP-FORM=NO,
    NODAL-DE='' POROUS-C=NO ADAPTIVE=0 ZOOM-LAB=1 AXIS-CYC=0,
    PERIODIC=NO VECTOR-S=GEOMETRY EPSI-FIR=NO STABILIZ=NO,
    STABFACT=1.00000000000000E-10 RESULTS=PORTHOLE FEFCORR=NO,
    BOLTSTEP=1 EXTEND-S=YES CONVERT-=NO DEGEN=YES TMC-MODE=NO,
    ENSIGHT-=NO IRSTEPS=1 INITIALT=NO TEMP-INT=NO ESINTERA=NO,
    OP2GEOM=NO INSITU-D=NO
*
CGROUP CONTACT3 NAME=1 FORCES=YES TRACTION=YES NODETONO=NO,
    FRICTION=0.600000000000000 EPSN=1.00000000000000E-12,
    EPST=0.00000000000000 DIRECTIO=NORMAL CONTINUO=YES,
    INITIAL-=ALLOWED PENETRAT=ONE DEPTH=0.00000000000000,
    OFFSET=0.00000000000000 OFFSET-T=CONSTANT CORNER-C=NO,
    TBIRTH=0.00000000000000 TDEATH=0.00000000000000 TIED=NO,
    TIED-OFF=0.00000000000000 HHATTMC=0.00000000000000,
    FCTMC=0.500000000000000 FTTMC=0.500000000000000 RIGID-TA=NO,
    NORMAL-S=1.00000000000000E+11 TANGENTI=0.00000000000000,
    PTOLERAN=1.00000000000000E-08 RESIDUAL=0.00100000000000000,
    LIMIT-FO=1.00000000000000 ITERATIO=2 TIME-PEN=0.00000000000000,
    CONSISTE=DEFAULT USER-FRI=NO DESCRIPT='NONE',
    CFACTOR1=0.00000000000000 CS-EXTEN=0.00100000000000000,
    ALGORITH=DEFAULT RTP-CHEC=NO RTP-MAX=0.00100000000000000,
    XDAMP=NO XNDAMP=0.100000000000000 SLIDING-=1.00000000000000E-10,
    TENSILE-=0.00100000000000000 OSCILLAT=5,
    GAP-BIAS=0.00000000000000 OFFSET-D=AUTOMATIC DISPLACE=DEFAULT,
    FRIC-DEL=NO GAP-VALU=0.00000000000000 TENS-CON=YES FREE-OVE=NO,
    GAP-PUSH=0.00000000000000 EKTMC=0.00000000000000
*
CONTACTSURFA NAME=1 PRINT=DEFAULT SAVE=DEFAULT SOLID=YES BODY=23,
    ORIENTAT=AUTOMATIC MARQUEEB=0 DESCRIPT='NONE'
@CLEAR
1 1 0
@
*
CONTACTSURFA NAME=2 PRINT=DEFAULT SAVE=DEFAULT SOLID=MULT BODY=25,
    ORIENTAT=AUTOMATIC MARQUEEB=0 DESCRIPT='NONE'
@CLEAR
5 1 1
5 1 2
5 1 3
5 1 4
5 1 5
5 1 6
```

```
5 1 7
5 1 8
5 1 9
5 1 10
5 1 11
5 1 12
5 1 13
5 1 14
5 1 15
5 1 16
5 1 17
5 1 18
5 1 19
5 1 20
5 1 21
5 1 22
@
*
SET CGROUP NAME=1
*
SET CGROUP NAME=1
*
SET CGROUP NAME=1
*
SET CGROUP NAME=1
*
COPY ZONE NAME1=WHOLE_MODEL NAME2=MESHPLOT00001 POSITION=1
*
ZONE NAME=MESHPLOT00001 NODEATTA=YES GEOMATTA=YES
@CLEAR
 'whole model'
 'CONTACT GROUP 1 OF REUSE 1 OF SUBSTRUCTURE 0 OF PROGRAM ADINA'
@
*
ZONE NAME=MESHPLOT00001 NODEATTA=YES GEOMATTA=YES
@CLEAR
 'whole model'
 'contact group 1'
 'CONTACT GROUP 1 OF REUSE 1 OF SUBSTRUCTURE 0 OF PROGRAM ADINA'
@
*
DELETE CONTACTBODY FIRST=2 LAST=2
*
DELETE CONTACTBODY FIRST=2 LAST=2
*
*Comment 11 (Load transfer contact surface)
*
CONTACTPAIR NAME=1 TARGET=2 CONTACTO=1 FRICTION=0.600000000000000,
    TBIRTH=0.00000000000000 TDEATH=0.00000000000000,
    HHATTMC=0.00000000000000 FCTMC=0.00000000000000,
    FTTMC=0.00000000000000 NX=0 NY=0 NZ=0 OFFSETCO=BOTH,
    EKTMC=0.00000000000000
*
ZONE NAME=MESHPLOT00001 NODEATTA=YES GEOMATTA=YES
@CLEAR
 'whole model'
```

```
 'contact group 1'
 'contact group 1'
 'CONTACT GROUP 1 OF REUSE 1 OF SUBSTRUCTURE 0 OF PROGRAM ADINA'
@
*
ZONE NAME=MESHPLOT00001 NODEATTA=YES GEOMATTA=YES
@CLEAR
 'whole model'
 'contact group 1'
 'contact group 1'
 'contact group 1'
 'CONTACT GROUP 1 OF REUSE 1 OF SUBSTRUCTURE 0 OF PROGRAM ADINA'
@
*
ZONE NAME=MESHPLOT00001 NODEATTA=YES GEOMATTA=YES
@CLEAR
 'whole model'
 'contact group 1'
 'contact group 1'
 'contact group 1'
 'contact group 1'
 'CONTACT GROUP 1 OF REUSE 1 OF SUBSTRUCTURE 0 OF PROGRAM ADINA'
@
*
SET CGROUP NAME=1
*
SET CGROUP NAME=1
*
ZONE NAME=MESHPLOT00001 NODEATTA=YES GEOMATTA=YES
@CLEAR
 'whole model'
 'contact group 1'
 'contact group 1'
 'contact group 1'
 'contact group 1'
 'contact group 1'
 'CONTACT GROUP 1 OF REUSE 1 OF SUBSTRUCTURE 0 OF PROGRAM ADINA'
@
*
ZONE NAME=MESHPLOT00001 NODEATTA=YES GEOMATTA=YES
@CLEAR
 'whole model'
 'contact group 1'
 'contact group 1'
 'contact group 1'
 'contact group 1'
 'contact group 1'
 'contact group 1'
 'CONTACT GROUP 1 OF REUSE 1 OF SUBSTRUCTURE 0 OF PROGRAM ADINA'
@
*
ZONE NAME=MESHPLOT00001 NODEATTA=YES GEOMATTA=YES
@CLEAR
 'whole model'
 'contact group 1'
 'contact group 1'
```

```
 'contact group 1'
 'contact group 1'
 'contact group 1'
 'contact group 1'
 'contact group 1'
 'CONTACT GROUP 1 OF REUSE 1 OF SUBSTRUCTURE 0 OF PROGRAM ADINA'
@
*
SET CGROUP NAME=1
*
SET CGROUP NAME=1
*
CONTACTBODY NAME=2 PRINT=DEFAULT SAVE=DEFAULT SOLID=NO BODY=25,
    DESCRIPT='NONE'
*
LOAD MASS-PROPORTIONAL NAME=1 MAGNITUD=1.00000000000000,
    AX=0.00000000000000 AY=0.00000000000000 AZ=-1.00000000000000,
    INTERPRE=BODY-FORCE
*
*Comment 13 (Temperature differential)
*
APPLY-LOAD BODY=25
@CLEAR
1  'TEMPERATURE' 1  'FACE' 1 0 1 0.00000000000000 0 -1 0 1 0  'NO',
    0.00000000000000 0.00000000000000 1 0  'BOTH'
2  'TEMPERATURE' 2  'FACE' 5 0 1 0.00000000000000 0 -1 0 1 0  'NO',
    0.00000000000000 0.00000000000000 1 0  'BOTH'
3  'TEMPERATURE' 1  'FACE' 1 0 1 0.00000000000000 0 -1 0 2 0  'NO',
    0.00000000000000 0.00000000000000 1 0  'BOTH'
4  'TEMPERATURE' 2  'FACE' 5 0 1 0.00000000000000 0 -1 0 2 0  'NO',
    0.00000000000000 0.00000000000000 1 0  'BOTH'
5  'TEMPERATURE' 1  'FACE' 1 0 1 0.00000000000000 0 -1 0 3 0  'NO',
    0.00000000000000 0.00000000000000 1 0  'BOTH'
6  'TEMPERATURE' 2  'FACE' 5 0 1 0.00000000000000 0 -1 0 3 0  'NO',
    0.00000000000000 0.00000000000000 1 0  'BOTH'
7  'TEMPERATURE' 1  'FACE' 1 0 1 0.00000000000000 0 -1 0 4 0  'NO',
    0.00000000000000 0.00000000000000 1 0  'BOTH'
8  'TEMPERATURE' 2  'FACE' 5 0 1 0.00000000000000 0 -1 0 4 0  'NO',
    0.00000000000000 0.00000000000000 1 0  'BOTH'
9  'TEMPERATURE' 1  'FACE' 1 0 1 0.00000000000000 0 -1 0 5 0  'NO',
    0.00000000000000 0.00000000000000 1 0  'BOTH'
10  'TEMPERATURE' 2  'FACE' 5 0 1 0.00000000000000 0 -1 0 5 0  'NO',
    0.00000000000000 0.00000000000000 1 0  'BOTH'
11  'TEMPERATURE' 1  'FACE' 1 0 1 0.00000000000000 0 -1 0 6 0  'NO',
    0.00000000000000 0.00000000000000 1 0  'BOTH'
12  'TEMPERATURE' 2  'FACE' 5 0 1 0.00000000000000 0 -1 0 6 0  'NO',
    0.00000000000000 0.00000000000000 1 0  'BOTH'
13  'TEMPERATURE' 1  'FACE' 1 0 1 0.00000000000000 0 -1 0 7 0  'NO',
    0.00000000000000 0.00000000000000 1 0  'BOTH'
14  'TEMPERATURE' 2  'FACE' 5 0 1 0.00000000000000 0 -1 0 7 0  'NO',
    0.00000000000000 0.00000000000000 1 0  'BOTH'
15  'TEMPERATURE' 1  'FACE' 1 0 1 0.00000000000000 0 -1 0 8 0  'NO',
    0.00000000000000 0.00000000000000 1 0  'BOTH'
16  'TEMPERATURE' 2  'FACE' 5 0 1 0.00000000000000 0 -1 0 8 0  'NO',
    0.00000000000000 0.00000000000000 1 0  'BOTH'
17  'TEMPERATURE' 1  'FACE' 1 0 1 0.00000000000000 0 -1 0 9 0  'NO',
```

```
    0.00000000000000 0.00000000000000 1 0  'BOTH'
18  'TEMPERATURE' 2  'FACE' 5 0 1 0.00000000000000 0 -1 0 9 0  'NO',
    0.00000000000000 0.00000000000000 1 0  'BOTH'
19  'TEMPERATURE' 1  'FACE' 1 0 1 0.00000000000000 0 -1 0 10 0  'NO',
    0.00000000000000 0.00000000000000 1 0  'BOTH'
20  'TEMPERATURE' 2  'FACE' 5 0 1 0.00000000000000 0 -1 0 10 0  'NO',
    0.00000000000000 0.00000000000000 1 0  'BOTH'
21  'TEMPERATURE' 1  'FACE' 1 0 1 0.00000000000000 0 -1 0 11 0  'NO',
    0.00000000000000 0.00000000000000 1 0  'BOTH'
22  'TEMPERATURE' 2  'FACE' 5 0 1 0.00000000000000 0 -1 0 11 0  'NO',
    0.00000000000000 0.00000000000000 1 0  'BOTH'
23  'TEMPERATURE' 1  'FACE' 1 0 1 0.00000000000000 0 -1 0 12 0  'NO',
    0.00000000000000 0.00000000000000 1 0  'BOTH'
24  'TEMPERATURE' 2  'FACE' 5 0 1 0.00000000000000 0 -1 0 12 0  'NO',
    0.00000000000000 0.00000000000000 1 0  'BOTH'
25  'TEMPERATURE' 1  'FACE' 1 0 1 0.00000000000000 0 -1 0 13 0  'NO',
    0.00000000000000 0.00000000000000 1 0  'BOTH'
26  'TEMPERATURE' 2  'FACE' 5 0 1 0.00000000000000 0 -1 0 13 0  'NO',
    0.00000000000000 0.00000000000000 1 0  'BOTH'
27  'TEMPERATURE' 1  'FACE' 1 0 1 0.00000000000000 0 -1 0 14 0  'NO',
    0.00000000000000 0.00000000000000 1 0  'BOTH'
28  'TEMPERATURE' 2  'FACE' 5 0 1 0.00000000000000 0 -1 0 14 0  'NO',
    0.00000000000000 0.00000000000000 1 0  'BOTH'
29  'TEMPERATURE' 1  'FACE' 1 0 1 0.00000000000000 0 -1 0 15 0  'NO',
    0.00000000000000 0.00000000000000 1 0  'BOTH'
30  'TEMPERATURE' 2  'FACE' 5 0 1 0.00000000000000 0 -1 0 15 0  'NO',
    0.00000000000000 0.00000000000000 1 0  'BOTH'
31  'TEMPERATURE' 1  'FACE' 1 0 1 0.00000000000000 0 -1 0 16 0  'NO',
    0.00000000000000 0.00000000000000 1 0  'BOTH'
32  'TEMPERATURE' 2  'FACE' 5 0 1 0.00000000000000 0 -1 0 16 0  'NO',
    0.00000000000000 0.00000000000000 1 0  'BOTH'
33  'TEMPERATURE' 1  'FACE' 1 0 1 0.00000000000000 0 -1 0 17 0  'NO',
    0.00000000000000 0.00000000000000 1 0  'BOTH'
34  'TEMPERATURE' 2  'FACE' 5 0 1 0.00000000000000 0 -1 0 17 0  'NO',
    0.00000000000000 0.00000000000000 1 0  'BOTH'
35  'TEMPERATURE' 1  'FACE' 1 0 1 0.00000000000000 0 -1 0 18 0  'NO',
    0.00000000000000 0.00000000000000 1 0  'BOTH'
36  'TEMPERATURE' 2  'FACE' 5 0 1 0.00000000000000 0 -1 0 18 0  'NO',
    0.00000000000000 0.00000000000000 1 0  'BOTH'
37  'TEMPERATURE' 1  'FACE' 1 0 1 0.00000000000000 0 -1 0 19 0  'NO',
    0.00000000000000 0.00000000000000 1 0  'BOTH'
38  'TEMPERATURE' 2  'FACE' 5 0 1 0.00000000000000 0 -1 0 19 0  'NO',
    0.00000000000000 0.00000000000000 1 0  'BOTH'
39  'TEMPERATURE' 1  'FACE' 1 0 1 0.00000000000000 0 -1 0 20 0  'NO',
    0.00000000000000 0.00000000000000 1 0  'BOTH'
40  'TEMPERATURE' 2  'FACE' 5 0 1 0.00000000000000 0 -1 0 20 0  'NO',
    0.00000000000000 0.00000000000000 1 0  'BOTH'
41  'TEMPERATURE' 1  'FACE' 1 0 1 0.00000000000000 0 -1 0 21 0  'NO',
    0.00000000000000 0.00000000000000 1 0  'BOTH'
42  'TEMPERATURE' 2  'FACE' 5 0 1 0.00000000000000 0 -1 0 21 0  'NO',
    0.00000000000000 0.00000000000000 1 0  'BOTH'
43  'TEMPERATURE' 1  'FACE' 1 0 1 0.00000000000000 0 -1 0 22 0  'NO',
    0.00000000000000 0.00000000000000 1 0  'BOTH'
44  'TEMPERATURE' 2  'FACE' 5 0 1 0.00000000000000 0 -1 0 22 0  'NO',
    0.00000000000000 0.00000000000000 1 0  'BOTH'
45  'MASS-PROPORTIONAL' 1  'MODEL' 0 0 1 0.00000000000000 0 -1 0 0 0,
```

```
    'NO' 0.00000000000000 0.00000000000000 1 0  'MID'
@
*
ZONE NAME=MESHPLOT00001 NODEATTA=YES GEOMATTA=YES
@CLEAR
 'whole model'
 'contact group 1'
 'contact group 1'
 'contact group 1'
 'contact group 1'
 'contact group 1'
 'contact group 1'
 'contact group 1'
 'contact group 1'
 'CONTACT GROUP 1 OF REUSE 1 OF SUBSTRUCTURE 0 OF PROGRAM ADINA'
@
*
ZONE NAME=MESHPLOT00001 NODEATTA=YES GEOMATTA=YES
@CLEAR
 'whole model'
 'contact group 1'
 'contact group 1'
 'contact group 1'
 'contact group 1'
 'contact group 1'
 'contact group 1'
 'contact group 1'
 'contact group 1'
 'contact group 1'
 'CONTACT GROUP 1 OF REUSE 1 OF SUBSTRUCTURE 0 OF PROGRAM ADINA'
@
*
COORDINATES POINT SYSTEM=0
@STARTMODIFY
@APPROW      104        2
135 0.00000000000000 0.00000000000000 0.00000000000000 0
136 3168.00000000000 0.00000000000000 0.00000000000000 0
@ENDMODIFY
*
LINE STRAIGHT NAME=1 P1=135 P2=136
*
DELETE LINE ALL FIRST=1 LAST=1
*
COORDINATES POINT SYSTEM=0
@STARTMODIFY
@CHAROW      106      106        1
136 -3168.00000000000 0.00000000000000 0.00000000000000 0
@ENDMODIFY
*
LINE STRAIGHT NAME=1 P1=135 P2=136
*
SUBDIVIDE LINE NAME=1 MODE=LENGTH SIZE=3.00000000000000
*
TRANSFORMATI TRANSLATION NAME=2 MODE=SYSTEM SYSTEM=0,
   DX=0.00000000000000 DY=48.0000000000000 DZ=0.00000000000000
*
```

```
LINE TRANSFORMED NAME=2 PARENT=1 TRANSFOR=2 PCOINCID=NO,
   PTOLERAN=1.00000000000000E-05 COUPLED=YES NCOPY=5 MESH=YES,
   EGROUP=0 NCOINCID=NO NTOLERAN=1.00000000000000E-05
*
COORDINATES POINT SYSTEM=0
@STARTMODIFY
@APPROW      116        4
147 -18.0000000000000 -24.0000000000000 2.25000000000000 0
148 -18.0000000000000 264.000000000000 2.25000000000000 0
149 -18.0000000000000 -24.0000000000000 -2.25000000000000 0
150 -18.0000000000000 264.000000000000 -2.25000000000000 0
@ENDMODIFY
*
LINE STRAIGHT NAME=7 P1=147 P2=148
*
LINE STRAIGHT NAME=8 P1=149 P2=150
*
SUBDIVIDE LINE NAME=7 MODE=LENGTH SIZE=3.00000000000000
@CLEAR
8
@
*
TRANSFORMATI TRANSLATION NAME=3 MODE=SYSTEM SYSTEM=0,
   DX=-36.0000000000000 DY=0.00000000000000 DZ=0.00000000000000
*
LINE TRANSFORMED NAME=9 PARENT=7 TRANSFOR=3 PCOINCID=NO,
   PTOLERAN=1.00000000000000E-05 COUPLED=YES NCOPY=3 MESH=YES,
   EGROUP=0 NCOINCID=NO NTOLERAN=1.00000000000000E-05
@CLEAR
8
@
*
TRANSFORMATI TRANSLATION NAME=4 MODE=SYSTEM SYSTEM=0,
   DX=-144.000000000000 DY=0.00000000000000 DZ=0.00000000000000
*
LINE TRANSFORMED NAME=15 PARENT=7 TRANSFOR=4 PCOINCID=NO,
   PTOLERAN=1.00000000000000E-05 COUPLED=YES NCOPY=1 MESH=YES,
   EGROUP=0 NCOINCID=NO NTOLERAN=1.00000000000000E-05
@CLEAR
8
9
10
11
12
13
14
@
*
LINE TRANSFORMED NAME=23 PARENT=15 TRANSFOR=4 PCOINCID=NO,
   PTOLERAN=1.00000000000000E-05 COUPLED=YES NCOPY=20 MESH=YES,
   EGROUP=0 NCOINCID=NO NTOLERAN=1.00000000000000E-05
@CLEAR
16
17
18
19
```

```
20
21
22
@
*
CGROUP CONTACT3 NAME=2 FORCES=YES TRACTION=YES NODETONO=NO,
   FRICTION=0.00000000000000 EPSN=1.00000000000000E-12,
   EPST=0.00000000000000 DIRECTIO=NORMAL CONTINUO=YES,
   INITIAL-=ALLOWED PENETRAT=ONE DEPTH=0.00000000000000,
   OFFSET=0.00000000000000 OFFSET-T=CONSTANT CORNER-C=NO,
   TBIRTH=0.00000000000000 TDEATH=0.00000000000000 TIED=NO,
   TIED-OFF=0.00000000000000 HHATTMC=0.00000000000000,
   FCTMC=0.500000000000000 FTTMC=0.500000000000000 RIGID-TA=NO,
   NORMAL-S=1.00000000000000E+11 TANGENTI=0.00000000000000,
   PTOLERAN=1.00000000000000E-08 RESIDUAL=0.00100000000000000,
   LIMIT-FO=1.00000000000000 ITERATIO=2 TIME-PEN=0.00000000000000,
   CONSISTE=DEFAULT USER-FRI=NO DESCRIPT='NONE',
   CFACTOR1=0.00000000000000 CS-EXTEN=0.00100000000000000,
   ALGORITH=DEFAULT RTP-CHEC=NO RTP-MAX=0.00100000000000000,
   XDAMP=NO XNDAMP=0.100000000000000 SLIDING-=1.00000000000000E-10,
   TENSILE-=0.00100000000000000 OSCILLAT=5,
   GAP-BIAS=0.00000000000000 OFFSET-D=AUTOMATIC DISPLACE=DEFAULT,
   FRIC-DEL=NO GAP-VALU=0.00000000000000 TENS-CON=YES FREE-OVE=NO,
   GAP-PUSH=0.00000000000000 EKTMC=0.00000000000000
*
CONTACTSURFA NAME=1 PRINT=DEFAULT SAVE=DEFAULT SOLID=MULT BODY=25,
   ORIENTAT=AUTOMATIC MARQUEEB=0 DESCRIPT='NONE'
@CLEAR
3 1 1
3 1 2
3 1 3
3 1 4
3 1 5
3 1 6
3 1 7
3 1 8
3 1 9
3 1 10
3 1 11
3 1 12
3 1 13
3 1 14
3 1 15
3 1 16
3 1 17
3 1 18
3 1 19
3 1 20
3 1 21
@
*
CONTACTSURFA NAME=2 PRINT=DEFAULT SAVE=DEFAULT SOLID=MULT BODY=25,
   ORIENTAT=AUTOMATIC MARQUEEB=0 DESCRIPT='NONE'
@CLEAR
6 1 2
6 1 3
```

```
6 1 4
6 1 5
6 1 6
6 1 7
6 1 8
6 1 9
6 1 10
6 1 11
6 1 12
6 1 13
6 1 14
6 1 15
6 1 16
6 1 17
6 1 18
6 1 19
6 1 20
6 1 21
6 1 22
@
*
CONTACTPAIR NAME=1 TARGET=2 CONTACTO=1 FRICTION=0.00000000000000,
    TBIRTH=0.00000000000000 TDEATH=0.00000000000000,
    HHATTMC=0.00000000000000 FCTMC=0.00000000000000,
    FTTMC=0.00000000000000 NX=0 NY=0 NZ=0 OFFSETCO=BOTH,
    EKTMC=0.00000000000000
*
FIXITY NAME=XYFIX
@CLEAR
 'X-TRANSLATION'
 'Y-TRANSLATION'
 'X-ROTATION'
 'Y-ROTATION'
 'Z-ROTATION'
 'OVALIZATION'
@
*
FIXBOUNDARY FACES FIXITY=ALL BODY=1
@CLEAR
6  'XYFIX'
@
*
*Comment 8 (Subgrade properties) - Unit: E (psi), ν (unitless)
*
MATERIAL ELASTIC NAME=1 E=30000.0000000000 NU=0.400000000000000,
    DENSITY=0.00000000000000 ALPHA=0.00000000000000 MDESCRIP=,
'subgrade'
*
* Comment 7 (Existing PCC properties) - Unit: E (psi), ν (unitless)
*
MATERIAL ELASTIC NAME=2 E=3800000.00000000 NU=0.200000000000000,
    DENSITY=0.00000000000000 ALPHA=0.00000000000000 MDESCRIP='pcc'
*
* Comment 6 (AC properties) - Unit: E (psi), ν (unitless)
*
MATERIAL ELASTIC NAME=3 E=300000.000000000 NU=0.350000000000000,
```

```
    DENSITY=0.00000000000000 ALPHA=0.00000000000000 MDESCRIP='ac'
*
* Comment 5 (PPCP concrete properties) ? Unit: E (psi), ν (unitless), Density (lb/in3), CTE (/°F)
*
MATERIAL ELASTIC NAME=4 E=3800000.00000000 NU=0.200000000000000,
    DENSITY=0.0868000000000000 ALPHA=5.50000000000000E-06 MDESCRIP=,
'ppcp'
*
*Comment 9 (Longitudinal tendons properties) - Unit: E (psi), ν (unitless)
*
MATERIAL ELASTIC NAME=5 E=2.85000000000000E+07 NU=0.300000000000000,
    DENSITY=0.00000000000000 ALPHA=0.00000000000000 MDESCRIP='beam'
*
CROSS-SECTIO PIPE NAME=1 DIAMETER=0.600000000000000,
    THICKNES=0.300000000000000 SC=0.00000000000000,
    TC=0.00000000000000 TORFAC=1.00000000000000,
    SSHEARF=0.00000000000000 TSHEARF=0.00000000000000 SOLID=YES
*
LINE-ELEMDAT BEAM
@CLEAR
1 5 1 0  'DEFAULT'  'DEFAULT' 0.00000000000000 0.00000000000000  'NO',
    0.00702000000000000 0.00000000000000 0.00000000000000
2 5 1 0  'DEFAULT'  'DEFAULT' 0.00000000000000 0.00000000000000  'NO',
    0.00702000000000000 0.00000000000000 0.00000000000000
3 5 1 0  'DEFAULT'  'DEFAULT' 0.00000000000000 0.00000000000000  'NO',
    0.00702000000000000 0.00000000000000 0.00000000000000
4 5 1 0  'DEFAULT'  'DEFAULT' 0.00000000000000 0.00000000000000  'NO',
    0.00702000000000000 0.00000000000000 0.00000000000000
5 5 1 0  'DEFAULT'  'DEFAULT' 0.00000000000000 0.00000000000000  'NO',
    0.00702000000000000 0.00000000000000 0.00000000000000
6 5 1 0  'DEFAULT'  'DEFAULT' 0.00000000000000 0.00000000000000  'NO',
    0.00702000000000000 0.00000000000000 0.00000000000000
@
*
*Comment 10 (Transverse tendons properties) - Unit: E (psi), ν (unitless)
*
MATERIAL ELASTIC NAME=6 E=2.85000000000000E+07 NU=0.300000000000000,
    DENSITY=0.00000000000000 ALPHA=0.00000000000000 MDESCRIP='beam2'
*
CROSS-SECTIO PIPE NAME=2 DIAMETER=0.500000000000000,
    THICKNES=0.250000000000000 SC=0.00000000000000,
    TC=0.00000000000000 TORFAC=1.00000000000000,
    SSHEARF=0.00000000000000 TSHEARF=0.00000000000000 SOLID=YES
*
LINE-ELEMDAT BEAM
@STARTMODIFY
@APPROW        6      101
7 6 2 0  'DEFAULT'  'DEFAULT' 0.00000000000000 0.00000000000000  'NO',
    0.00710000000000000 0.00000000000000 0.00000000000000
8 6 2 0  'DEFAULT'  'DEFAULT' 0.00000000000000 0.00000000000000  'NO',
    0.00710000000000000 0.00000000000000 0.00000000000000
9 6 2 0  'DEFAULT'  'DEFAULT' 0.00000000000000 0.00000000000000  'NO',
    0.00710000000000000 0.00000000000000 0.00000000000000
10 6 2 0  'DEFAULT'  'DEFAULT' 0.00000000000000 0.00000000000000  'NO',
    0.00710000000000000 0.00000000000000 0.00000000000000
11 6 2 0  'DEFAULT'  'DEFAULT' 0.00000000000000 0.00000000000000  'NO',
```

0.00710000000000000 0.00000000000000 0.00000000000000
12 6 2 0 'DEFAULT' 'DEFAULT' 0.00000000000000 0.00000000000000 'NO',
0.00710000000000000 0.00000000000000 0.00000000000000
13 6 2 0 'DEFAULT' 'DEFAULT' 0.00000000000000 0.00000000000000 'NO',
0.00710000000000000 0.00000000000000 0.00000000000000
14 6 2 0 'DEFAULT' 'DEFAULT' 0.00000000000000 0.00000000000000 'NO',
0.00710000000000000 0.00000000000000 0.00000000000000
15 6 2 0 'DEFAULT' 'DEFAULT' 0.00000000000000 0.00000000000000 'NO',
0.00710000000000000 0.00000000000000 0.00000000000000
16 6 2 0 'DEFAULT' 'DEFAULT' 0.00000000000000 0.00000000000000 'NO',
0.00710000000000000 0.00000000000000 0.00000000000000
17 6 2 0 'DEFAULT' 'DEFAULT' 0.00000000000000 0.00000000000000 'NO',
0.00710000000000000 0.00000000000000 0.00000000000000
18 6 2 0 'DEFAULT' 'DEFAULT' 0.00000000000000 0.00000000000000 'NO',
0.00710000000000000 0.00000000000000 0.00000000000000
19 6 2 0 'DEFAULT' 'DEFAULT' 0.00000000000000 0.00000000000000 'NO',
0.00710000000000000 0.00000000000000 0.00000000000000
20 6 2 0 'DEFAULT' 'DEFAULT' 0.00000000000000 0.00000000000000 'NO',
0.00710000000000000 0.00000000000000 0.00000000000000
21 6 2 0 'DEFAULT' 'DEFAULT' 0.00000000000000 0.00000000000000 'NO',
0.00710000000000000 0.00000000000000 0.00000000000000
22 6 2 0 'DEFAULT' 'DEFAULT' 0.00000000000000 0.00000000000000 'NO',
0.00710000000000000 0.00000000000000 0.00000000000000
23 6 2 0 'DEFAULT' 'DEFAULT' 0.00000000000000 0.00000000000000 'NO',
0.00710000000000000 0.00000000000000 0.00000000000000
24 6 2 0 'DEFAULT' 'DEFAULT' 0.00000000000000 0.00000000000000 'NO',
0.00710000000000000 0.00000000000000 0.00000000000000
25 6 2 0 'DEFAULT' 'DEFAULT' 0.00000000000000 0.00000000000000 'NO',
0.00710000000000000 0.00000000000000 0.00000000000000
26 6 2 0 'DEFAULT' 'DEFAULT' 0.00000000000000 0.00000000000000 'NO',
0.00710000000000000 0.00000000000000 0.00000000000000
27 6 2 0 'DEFAULT' 'DEFAULT' 0.00000000000000 0.00000000000000 'NO',
0.00710000000000000 0.00000000000000 0.00000000000000
28 6 2 0 'DEFAULT' 'DEFAULT' 0.00000000000000 0.00000000000000 'NO',
0.00710000000000000 0.00000000000000 0.00000000000000
29 6 2 0 'DEFAULT' 'DEFAULT' 0.00000000000000 0.00000000000000 'NO',
0.00710000000000000 0.00000000000000 0.00000000000000
30 6 2 0 'DEFAULT' 'DEFAULT' 0.00000000000000 0.00000000000000 'NO',
0.00710000000000000 0.00000000000000 0.00000000000000
31 6 2 0 'DEFAULT' 'DEFAULT' 0.00000000000000 0.00000000000000 'NO',
0.00710000000000000 0.00000000000000 0.00000000000000
32 6 2 0 'DEFAULT' 'DEFAULT' 0.00000000000000 0.00000000000000 'NO',
0.00710000000000000 0.00000000000000 0.00000000000000
33 6 2 0 'DEFAULT' 'DEFAULT' 0.00000000000000 0.00000000000000 'NO',
0.00710000000000000 0.00000000000000 0.00000000000000
34 6 2 0 'DEFAULT' 'DEFAULT' 0.00000000000000 0.00000000000000 'NO',
0.00710000000000000 0.00000000000000 0.00000000000000
35 6 2 0 'DEFAULT' 'DEFAULT' 0.00000000000000 0.00000000000000 'NO',
0.00710000000000000 0.00000000000000 0.00000000000000
36 6 2 0 'DEFAULT' 'DEFAULT' 0.00000000000000 0.00000000000000 'NO',
0.00710000000000000 0.00000000000000 0.00000000000000
37 6 2 0 'DEFAULT' 'DEFAULT' 0.00000000000000 0.00000000000000 'NO',
0.00710000000000000 0.00000000000000 0.00000000000000
38 6 2 0 'DEFAULT' 'DEFAULT' 0.00000000000000 0.00000000000000 'NO',
0.00710000000000000 0.00000000000000 0.00000000000000
39 6 2 0 'DEFAULT' 'DEFAULT' 0.00000000000000 0.00000000000000 'NO',

0.00710000000000000 0.00000000000000 0.00000000000000
40 6 2 0 'DEFAULT' 'DEFAULT' 0.00000000000000 0.00000000000000 'NO',
0.00710000000000000 0.00000000000000 0.00000000000000
41 6 2 0 'DEFAULT' 'DEFAULT' 0.00000000000000 0.00000000000000 'NO',
0.00710000000000000 0.00000000000000 0.00000000000000
42 6 2 0 'DEFAULT' 'DEFAULT' 0.00000000000000 0.00000000000000 'NO',
0.00710000000000000 0.00000000000000 0.00000000000000
43 6 2 0 'DEFAULT' 'DEFAULT' 0.00000000000000 0.00000000000000 'NO',
0.00710000000000000 0.00000000000000 0.00000000000000
44 6 2 0 'DEFAULT' 'DEFAULT' 0.00000000000000 0.00000000000000 'NO',
0.00710000000000000 0.00000000000000 0.00000000000000
45 6 2 0 'DEFAULT' 'DEFAULT' 0.00000000000000 0.00000000000000 'NO',
0.00710000000000000 0.00000000000000 0.00000000000000
46 6 2 0 'DEFAULT' 'DEFAULT' 0.00000000000000 0.00000000000000 'NO',
0.00710000000000000 0.00000000000000 0.00000000000000
47 6 2 0 'DEFAULT' 'DEFAULT' 0.00000000000000 0.00000000000000 'NO',
0.00710000000000000 0.00000000000000 0.00000000000000
48 6 2 0 'DEFAULT' 'DEFAULT' 0.00000000000000 0.00000000000000 'NO',
0.00710000000000000 0.00000000000000 0.00000000000000
49 6 2 0 'DEFAULT' 'DEFAULT' 0.00000000000000 0.00000000000000 'NO',
0.00710000000000000 0.00000000000000 0.00000000000000
50 6 2 0 'DEFAULT' 'DEFAULT' 0.00000000000000 0.00000000000000 'NO',
0.00710000000000000 0.00000000000000 0.00000000000000
51 6 2 0 'DEFAULT' 'DEFAULT' 0.00000000000000 0.00000000000000 'NO',
0.00710000000000000 0.00000000000000 0.00000000000000
52 6 2 0 'DEFAULT' 'DEFAULT' 0.00000000000000 0.00000000000000 'NO',
0.00710000000000000 0.00000000000000 0.00000000000000
53 6 2 0 'DEFAULT' 'DEFAULT' 0.00000000000000 0.00000000000000 'NO',
0.00710000000000000 0.00000000000000 0.00000000000000
54 6 2 0 'DEFAULT' 'DEFAULT' 0.00000000000000 0.00000000000000 'NO',
0.00710000000000000 0.00000000000000 0.00000000000000
55 6 2 0 'DEFAULT' 'DEFAULT' 0.00000000000000 0.00000000000000 'NO',
0.00710000000000000 0.00000000000000 0.00000000000000
56 6 2 0 'DEFAULT' 'DEFAULT' 0.00000000000000 0.00000000000000 'NO',
0.00710000000000000 0.00000000000000 0.00000000000000
57 6 2 0 'DEFAULT' 'DEFAULT' 0.00000000000000 0.00000000000000 'NO',
0.00710000000000000 0.00000000000000 0.00000000000000
58 6 2 0 'DEFAULT' 'DEFAULT' 0.00000000000000 0.00000000000000 'NO',
0.00710000000000000 0.00000000000000 0.00000000000000
59 6 2 0 'DEFAULT' 'DEFAULT' 0.00000000000000 0.00000000000000 'NO',
0.00710000000000000 0.00000000000000 0.00000000000000
60 6 2 0 'DEFAULT' 'DEFAULT' 0.00000000000000 0.00000000000000 'NO',
0.00710000000000000 0.00000000000000 0.00000000000000
61 6 2 0 'DEFAULT' 'DEFAULT' 0.00000000000000 0.00000000000000 'NO',
0.00710000000000000 0.00000000000000 0.00000000000000
62 6 2 0 'DEFAULT' 'DEFAULT' 0.00000000000000 0.00000000000000 'NO',
0.00710000000000000 0.00000000000000 0.00000000000000
63 6 2 0 'DEFAULT' 'DEFAULT' 0.00000000000000 0.00000000000000 'NO',
0.00710000000000000 0.00000000000000 0.00000000000000
64 6 2 0 'DEFAULT' 'DEFAULT' 0.00000000000000 0.00000000000000 'NO',
0.00710000000000000 0.00000000000000 0.00000000000000
65 6 2 0 'DEFAULT' 'DEFAULT' 0.00000000000000 0.00000000000000 'NO',
0.00710000000000000 0.00000000000000 0.00000000000000
66 6 2 0 'DEFAULT' 'DEFAULT' 0.00000000000000 0.00000000000000 'NO',
0.00710000000000000 0.00000000000000 0.00000000000000
67 6 2 0 'DEFAULT' 'DEFAULT' 0.00000000000000 0.00000000000000 'NO',

0.00710000000000000 0.00000000000000 0.00000000000000
68 6 2 0 'DEFAULT' 'DEFAULT' 0.00000000000000 0.00000000000000 'NO',
0.00710000000000000 0.00000000000000 0.00000000000000
69 6 2 0 'DEFAULT' 'DEFAULT' 0.00000000000000 0.00000000000000 'NO',
0.00710000000000000 0.00000000000000 0.00000000000000
70 6 2 0 'DEFAULT' 'DEFAULT' 0.00000000000000 0.00000000000000 'NO',
0.00710000000000000 0.00000000000000 0.00000000000000
71 6 2 0 'DEFAULT' 'DEFAULT' 0.00000000000000 0.00000000000000 'NO',
0.00710000000000000 0.00000000000000 0.00000000000000
72 6 2 0 'DEFAULT' 'DEFAULT' 0.00000000000000 0.00000000000000 'NO',
0.00710000000000000 0.00000000000000 0.00000000000000
73 6 2 0 'DEFAULT' 'DEFAULT' 0.00000000000000 0.00000000000000 'NO',
0.00710000000000000 0.00000000000000 0.00000000000000
74 6 2 0 'DEFAULT' 'DEFAULT' 0.00000000000000 0.00000000000000 'NO',
0.00710000000000000 0.00000000000000 0.00000000000000
75 6 2 0 'DEFAULT' 'DEFAULT' 0.00000000000000 0.00000000000000 'NO',
0.00710000000000000 0.00000000000000 0.00000000000000
76 6 2 0 'DEFAULT' 'DEFAULT' 0.00000000000000 0.00000000000000 'NO',
0.00710000000000000 0.00000000000000 0.00000000000000
77 6 2 0 'DEFAULT' 'DEFAULT' 0.00000000000000 0.00000000000000 'NO',
0.00710000000000000 0.00000000000000 0.00000000000000
78 6 2 0 'DEFAULT' 'DEFAULT' 0.00000000000000 0.00000000000000 'NO',
0.00710000000000000 0.00000000000000 0.00000000000000
79 6 2 0 'DEFAULT' 'DEFAULT' 0.00000000000000 0.00000000000000 'NO',
0.00710000000000000 0.00000000000000 0.00000000000000
80 6 2 0 'DEFAULT' 'DEFAULT' 0.00000000000000 0.00000000000000 'NO',
0.00710000000000000 0.00000000000000 0.00000000000000
81 6 2 0 'DEFAULT' 'DEFAULT' 0.00000000000000 0.00000000000000 'NO',
0.00710000000000000 0.00000000000000 0.00000000000000
82 6 2 0 'DEFAULT' 'DEFAULT' 0.00000000000000 0.00000000000000 'NO',
0.00710000000000000 0.00000000000000 0.00000000000000
83 6 2 0 'DEFAULT' 'DEFAULT' 0.00000000000000 0.00000000000000 'NO',
0.00710000000000000 0.00000000000000 0.00000000000000
84 6 2 0 'DEFAULT' 'DEFAULT' 0.00000000000000 0.00000000000000 'NO',
0.00710000000000000 0.00000000000000 0.00000000000000
85 6 2 0 'DEFAULT' 'DEFAULT' 0.00000000000000 0.00000000000000 'NO',
0.00710000000000000 0.00000000000000 0.00000000000000
86 6 2 0 'DEFAULT' 'DEFAULT' 0.00000000000000 0.00000000000000 'NO',
0.00710000000000000 0.00000000000000 0.00000000000000
87 6 2 0 'DEFAULT' 'DEFAULT' 0.00000000000000 0.00000000000000 'NO',
0.00710000000000000 0.00000000000000 0.00000000000000
88 6 2 0 'DEFAULT' 'DEFAULT' 0.00000000000000 0.00000000000000 'NO',
0.00710000000000000 0.00000000000000 0.00000000000000
89 6 2 0 'DEFAULT' 'DEFAULT' 0.00000000000000 0.00000000000000 'NO',
0.00710000000000000 0.00000000000000 0.00000000000000
90 6 2 0 'DEFAULT' 'DEFAULT' 0.00000000000000 0.00000000000000 'NO',
0.00710000000000000 0.00000000000000 0.00000000000000
91 6 2 0 'DEFAULT' 'DEFAULT' 0.00000000000000 0.00000000000000 'NO',
0.00710000000000000 0.00000000000000 0.00000000000000
92 6 2 0 'DEFAULT' 'DEFAULT' 0.00000000000000 0.00000000000000 'NO',
0.00710000000000000 0.00000000000000 0.00000000000000
93 6 2 0 'DEFAULT' 'DEFAULT' 0.00000000000000 0.00000000000000 'NO',
0.00710000000000000 0.00000000000000 0.00000000000000
94 6 2 0 'DEFAULT' 'DEFAULT' 0.00000000000000 0.00000000000000 'NO',
0.00710000000000000 0.00000000000000 0.00000000000000
95 6 2 0 'DEFAULT' 'DEFAULT' 0.00000000000000 0.00000000000000 'NO',

0.00710000000000000 0.00000000000000 0.00000000000000
96 6 2 0 'DEFAULT' 'DEFAULT' 0.00000000000000 0.00000000000000 'NO',
0.00710000000000000 0.00000000000000 0.00000000000000
97 6 2 0 'DEFAULT' 'DEFAULT' 0.00000000000000 0.00000000000000 'NO',
0.00710000000000000 0.00000000000000 0.00000000000000
98 6 2 0 'DEFAULT' 'DEFAULT' 0.00000000000000 0.00000000000000 'NO',
0.00710000000000000 0.00000000000000 0.00000000000000
99 6 2 0 'DEFAULT' 'DEFAULT' 0.00000000000000 0.00000000000000 'NO',
0.00710000000000000 0.00000000000000 0.00000000000000
100 6 2 0 'DEFAULT' 'DEFAULT' 0.00000000000000 0.00000000000000 ,
'NO' 0.00710000000000000 0.00000000000000 0.00000000000000
101 6 2 0 'DEFAULT' 'DEFAULT' 0.00000000000000 0.00000000000000 ,
'NO' 0.00710000000000000 0.00000000000000 0.00000000000000
102 6 2 0 'DEFAULT' 'DEFAULT' 0.00000000000000 0.00000000000000 ,
'NO' 0.00710000000000000 0.00000000000000 0.00000000000000
103 6 2 0 'DEFAULT' 'DEFAULT' 0.00000000000000 0.00000000000000 ,
'NO' 0.00710000000000000 0.00000000000000 0.00000000000000
104 6 2 0 'DEFAULT' 'DEFAULT' 0.00000000000000 0.00000000000000 ,
'NO' 0.00710000000000000 0.00000000000000 0.00000000000000
105 6 2 0 'DEFAULT' 'DEFAULT' 0.00000000000000 0.00000000000000 ,
'NO' 0.00710000000000000 0.00000000000000 0.00000000000000
106 6 2 0 'DEFAULT' 'DEFAULT' 0.00000000000000 0.00000000000000 ,
'NO' 0.00710000000000000 0.00000000000000 0.00000000000000
107 6 2 0 'DEFAULT' 'DEFAULT' 0.00000000000000 0.00000000000000 ,
'NO' 0.00710000000000000 0.00000000000000 0.00000000000000
@APPROW 107 75
108 6 2 0 'DEFAULT' 'DEFAULT' 0.00000000000000 0.00000000000000 ,
'NO' 0.00710000000000000 0.00000000000000 0.00000000000000
109 6 2 0 'DEFAULT' 'DEFAULT' 0.00000000000000 0.00000000000000 ,
'NO' 0.00710000000000000 0.00000000000000 0.00000000000000
110 6 2 0 'DEFAULT' 'DEFAULT' 0.00000000000000 0.00000000000000 ,
'NO' 0.00710000000000000 0.00000000000000 0.00000000000000
111 6 2 0 'DEFAULT' 'DEFAULT' 0.00000000000000 0.00000000000000 ,
'NO' 0.00710000000000000 0.00000000000000 0.00000000000000
112 6 2 0 'DEFAULT' 'DEFAULT' 0.00000000000000 0.00000000000000 ,
'NO' 0.00710000000000000 0.00000000000000 0.00000000000000
113 6 2 0 'DEFAULT' 'DEFAULT' 0.00000000000000 0.00000000000000 ,
'NO' 0.00710000000000000 0.00000000000000 0.00000000000000
114 6 2 0 'DEFAULT' 'DEFAULT' 0.00000000000000 0.00000000000000 ,
'NO' 0.00710000000000000 0.00000000000000 0.00000000000000
115 6 2 0 'DEFAULT' 'DEFAULT' 0.00000000000000 0.00000000000000 ,
'NO' 0.00710000000000000 0.00000000000000 0.00000000000000
116 6 2 0 'DEFAULT' 'DEFAULT' 0.00000000000000 0.00000000000000 ,
'NO' 0.00710000000000000 0.00000000000000 0.00000000000000
117 6 2 0 'DEFAULT' 'DEFAULT' 0.00000000000000 0.00000000000000 ,
'NO' 0.00710000000000000 0.00000000000000 0.00000000000000
118 6 2 0 'DEFAULT' 'DEFAULT' 0.00000000000000 0.00000000000000 ,
'NO' 0.00710000000000000 0.00000000000000 0.00000000000000
119 6 2 0 'DEFAULT' 'DEFAULT' 0.00000000000000 0.00000000000000 ,
'NO' 0.00710000000000000 0.00000000000000 0.00000000000000
120 6 2 0 'DEFAULT' 'DEFAULT' 0.00000000000000 0.00000000000000 ,
'NO' 0.00710000000000000 0.00000000000000 0.00000000000000
121 6 2 0 'DEFAULT' 'DEFAULT' 0.00000000000000 0.00000000000000 ,
'NO' 0.00710000000000000 0.00000000000000 0.00000000000000
122 6 2 0 'DEFAULT' 'DEFAULT' 0.00000000000000 0.00000000000000 ,
'NO' 0.00710000000000000 0.00000000000000 0.00000000000000

123 6 2 0 'DEFAULT' 'DEFAULT' 0.00000000000000 0.00000000000000 ,
'NO' 0.00710000000000000 0.00000000000000 0.00000000000000
124 6 2 0 'DEFAULT' 'DEFAULT' 0.00000000000000 0.00000000000000 ,
'NO' 0.00710000000000000 0.00000000000000 0.00000000000000
125 6 2 0 'DEFAULT' 'DEFAULT' 0.00000000000000 0.00000000000000 ,
'NO' 0.00710000000000000 0.00000000000000 0.00000000000000
126 6 2 0 'DEFAULT' 'DEFAULT' 0.00000000000000 0.00000000000000 ,
'NO' 0.00710000000000000 0.00000000000000 0.00000000000000
127 6 2 0 'DEFAULT' 'DEFAULT' 0.00000000000000 0.00000000000000 ,
'NO' 0.00710000000000000 0.00000000000000 0.00000000000000
128 6 2 0 'DEFAULT' 'DEFAULT' 0.00000000000000 0.00000000000000 ,
'NO' 0.00710000000000000 0.00000000000000 0.00000000000000
129 6 2 0 'DEFAULT' 'DEFAULT' 0.00000000000000 0.00000000000000 ,
'NO' 0.00710000000000000 0.00000000000000 0.00000000000000
130 6 2 0 'DEFAULT' 'DEFAULT' 0.00000000000000 0.00000000000000 ,
'NO' 0.00710000000000000 0.00000000000000 0.00000000000000
131 6 2 0 'DEFAULT' 'DEFAULT' 0.00000000000000 0.00000000000000 ,
'NO' 0.00710000000000000 0.00000000000000 0.00000000000000
132 6 2 0 'DEFAULT' 'DEFAULT' 0.00000000000000 0.00000000000000 ,
'NO' 0.00710000000000000 0.00000000000000 0.00000000000000
133 6 2 0 'DEFAULT' 'DEFAULT' 0.00000000000000 0.00000000000000 ,
'NO' 0.00710000000000000 0.00000000000000 0.00000000000000
134 6 2 0 'DEFAULT' 'DEFAULT' 0.00000000000000 0.00000000000000 ,
'NO' 0.00710000000000000 0.00000000000000 0.00000000000000
135 6 2 0 'DEFAULT' 'DEFAULT' 0.00000000000000 0.00000000000000 ,
'NO' 0.00710000000000000 0.00000000000000 0.00000000000000
136 6 2 0 'DEFAULT' 'DEFAULT' 0.00000000000000 0.00000000000000 ,
'NO' 0.00710000000000000 0.00000000000000 0.00000000000000
137 6 2 0 'DEFAULT' 'DEFAULT' 0.00000000000000 0.00000000000000 ,
'NO' 0.00710000000000000 0.00000000000000 0.00000000000000
138 6 2 0 'DEFAULT' 'DEFAULT' 0.00000000000000 0.00000000000000 ,
'NO' 0.00710000000000000 0.00000000000000 0.00000000000000
139 6 2 0 'DEFAULT' 'DEFAULT' 0.00000000000000 0.00000000000000 ,
'NO' 0.00710000000000000 0.00000000000000 0.00000000000000
140 6 2 0 'DEFAULT' 'DEFAULT' 0.00000000000000 0.00000000000000 ,
'NO' 0.00710000000000000 0.00000000000000 0.00000000000000
141 6 2 0 'DEFAULT' 'DEFAULT' 0.00000000000000 0.00000000000000 ,
'NO' 0.00710000000000000 0.00000000000000 0.00000000000000
142 6 2 0 'DEFAULT' 'DEFAULT' 0.00000000000000 0.00000000000000 ,
'NO' 0.00710000000000000 0.00000000000000 0.00000000000000
143 6 2 0 'DEFAULT' 'DEFAULT' 0.00000000000000 0.00000000000000 ,
'NO' 0.00710000000000000 0.00000000000000 0.00000000000000
144 6 2 0 'DEFAULT' 'DEFAULT' 0.00000000000000 0.00000000000000 ,
'NO' 0.00710000000000000 0.00000000000000 0.00000000000000
145 6 2 0 'DEFAULT' 'DEFAULT' 0.00000000000000 0.00000000000000 ,
'NO' 0.00710000000000000 0.00000000000000 0.00000000000000
146 6 2 0 'DEFAULT' 'DEFAULT' 0.00000000000000 0.00000000000000 ,
'NO' 0.00710000000000000 0.00000000000000 0.00000000000000
147 6 2 0 'DEFAULT' 'DEFAULT' 0.00000000000000 0.00000000000000 ,
'NO' 0.00710000000000000 0.00000000000000 0.00000000000000
148 6 2 0 'DEFAULT' 'DEFAULT' 0.00000000000000 0.00000000000000 ,
'NO' 0.00710000000000000 0.00000000000000 0.00000000000000
149 6 2 0 'DEFAULT' 'DEFAULT' 0.00000000000000 0.00000000000000 ,
'NO' 0.00710000000000000 0.00000000000000 0.00000000000000
150 6 2 0 'DEFAULT' 'DEFAULT' 0.00000000000000 0.00000000000000 ,
'NO' 0.00710000000000000 0.00000000000000 0.00000000000000

151 6 2 0 'DEFAULT' 'DEFAULT' 0.00000000000000 0.00000000000000 ,
'NO' 0.00710000000000000 0.00000000000000 0.00000000000000
152 6 2 0 'DEFAULT' 'DEFAULT' 0.00000000000000 0.00000000000000 ,
'NO' 0.00710000000000000 0.00000000000000 0.00000000000000
153 6 2 0 'DEFAULT' 'DEFAULT' 0.00000000000000 0.00000000000000 ,
'NO' 0.00710000000000000 0.00000000000000 0.00000000000000
154 6 2 0 'DEFAULT' 'DEFAULT' 0.00000000000000 0.00000000000000 ,
'NO' 0.00710000000000000 0.00000000000000 0.00000000000000
155 6 2 0 'DEFAULT' 'DEFAULT' 0.00000000000000 0.00000000000000 ,
'NO' 0.00710000000000000 0.00000000000000 0.00000000000000
156 6 2 0 'DEFAULT' 'DEFAULT' 0.00000000000000 0.00000000000000 ,
'NO' 0.00710000000000000 0.00000000000000 0.00000000000000
157 6 2 0 'DEFAULT' 'DEFAULT' 0.00000000000000 0.00000000000000 ,
'NO' 0.00710000000000000 0.00000000000000 0.00000000000000
158 6 2 0 'DEFAULT' 'DEFAULT' 0.00000000000000 0.00000000000000 ,
'NO' 0.00710000000000000 0.00000000000000 0.00000000000000
159 6 2 0 'DEFAULT' 'DEFAULT' 0.00000000000000 0.00000000000000 ,
'NO' 0.00710000000000000 0.00000000000000 0.00000000000000
160 6 2 0 'DEFAULT' 'DEFAULT' 0.00000000000000 0.00000000000000 ,
'NO' 0.00710000000000000 0.00000000000000 0.00000000000000
161 6 2 0 'DEFAULT' 'DEFAULT' 0.00000000000000 0.00000000000000 ,
'NO' 0.00710000000000000 0.00000000000000 0.00000000000000
162 6 2 0 'DEFAULT' 'DEFAULT' 0.00000000000000 0.00000000000000 ,
'NO' 0.00710000000000000 0.00000000000000 0.00000000000000
163 6 2 0 'DEFAULT' 'DEFAULT' 0.00000000000000 0.00000000000000 ,
'NO' 0.00710000000000000 0.00000000000000 0.00000000000000
164 6 2 0 'DEFAULT' 'DEFAULT' 0.00000000000000 0.00000000000000 ,
'NO' 0.00710000000000000 0.00000000000000 0.00000000000000
165 6 2 0 'DEFAULT' 'DEFAULT' 0.00000000000000 0.00000000000000 ,
'NO' 0.00710000000000000 0.00000000000000 0.00000000000000
166 6 2 0 'DEFAULT' 'DEFAULT' 0.00000000000000 0.00000000000000 ,
'NO' 0.00710000000000000 0.00000000000000 0.00000000000000
167 6 2 0 'DEFAULT' 'DEFAULT' 0.00000000000000 0.00000000000000 ,
'NO' 0.00710000000000000 0.00000000000000 0.00000000000000
168 6 2 0 'DEFAULT' 'DEFAULT' 0.00000000000000 0.00000000000000 ,
'NO' 0.00710000000000000 0.00000000000000 0.00000000000000
169 6 2 0 'DEFAULT' 'DEFAULT' 0.00000000000000 0.00000000000000 ,
'NO' 0.00710000000000000 0.00000000000000 0.00000000000000
170 6 2 0 'DEFAULT' 'DEFAULT' 0.00000000000000 0.00000000000000 ,
'NO' 0.00710000000000000 0.00000000000000 0.00000000000000
171 6 2 0 'DEFAULT' 'DEFAULT' 0.00000000000000 0.00000000000000 ,
'NO' 0.00710000000000000 0.00000000000000 0.00000000000000
172 6 2 0 'DEFAULT' 'DEFAULT' 0.00000000000000 0.00000000000000 ,
'NO' 0.00710000000000000 0.00000000000000 0.00000000000000
173 6 2 0 'DEFAULT' 'DEFAULT' 0.00000000000000 0.00000000000000 ,
'NO' 0.00710000000000000 0.00000000000000 0.00000000000000
174 6 2 0 'DEFAULT' 'DEFAULT' 0.00000000000000 0.00000000000000 ,
'NO' 0.00710000000000000 0.00000000000000 0.00000000000000
175 6 2 0 'DEFAULT' 'DEFAULT' 0.00000000000000 0.00000000000000 ,
'NO' 0.00710000000000000 0.00000000000000 0.00000000000000
176 6 2 0 'DEFAULT' 'DEFAULT' 0.00000000000000 0.00000000000000 ,
'NO' 0.00710000000000000 0.00000000000000 0.00000000000000
177 6 2 0 'DEFAULT' 'DEFAULT' 0.00000000000000 0.00000000000000 ,
'NO' 0.00710000000000000 0.00000000000000 0.00000000000000
178 6 2 0 'DEFAULT' 'DEFAULT' 0.00000000000000 0.00000000000000 ,
'NO' 0.00710000000000000 0.00000000000000 0.00000000000000

```
179 6 2 0  'DEFAULT'  'DEFAULT' 0.00000000000000 0.00000000000000  ,
'NO' 0.00710000000000000 0.00000000000000 0.00000000000000
180 6 2 0  'DEFAULT'  'DEFAULT' 0.00000000000000 0.00000000000000  ,
'NO' 0.00710000000000000 0.00000000000000 0.00000000000000
181 6 2 0  'DEFAULT'  'DEFAULT' 0.00000000000000 0.00000000000000  ,
'NO' 0.00710000000000000 0.00000000000000 0.00000000000000
182 6 2 0  'DEFAULT'  'DEFAULT' 0.00000000000000 0.00000000000000  ,
'NO' 0.00710000000000000 0.00000000000000 0.00000000000000
@ENDMODIFY
*
SUBDIVIDE BODY NAME=25 MODE=LENGTH SIZE=12.0000000000000,
    MAX-SIZE=0.00000000000000
*
SUBDIVIDE EDGE NAME=5 BODY=25 MODE=DIVISIONS NDIV=8,
    RATIO=0.100000000000000 PROGRESS=ARITHMETIC BLTABLE=0
@CLEAR
6
7
8
@
*
SUBDIVIDE BODY NAME=24 MODE=LENGTH SIZE=12.0000000000000,
    MAX-SIZE=0.00000000000000
@CLEAR
23
@
*
SUBDIVIDE EDGE NAME=5 BODY=24 MODE=DIVISIONS NDIV=2,
    RATIO=1.00000000000000 PROGRESS=ARITHMETIC BLTABLE=0
@CLEAR
6
7
8
@
*
SUBDIVIDE BODY NAME=23 MODE=LENGTH SIZE=6.00000000000000,
    MAX-SIZE=0.00000000000000
*
SUBDIVIDE BODY NAME=23 MODE=LENGTH SIZE=12.0000000000000,
    MAX-SIZE=0.00000000000000
*
SUBDIVIDE EDGE NAME=5 BODY=23 MODE=DIVISIONS NDIV=2,
    RATIO=1.00000000000000 PROGRESS=ARITHMETIC BLTABLE=0
@CLEAR
6
7
8
@
*
SUBDIVIDE BODY NAME=1 MODE=LENGTH SIZE=6.0000000000000,
    MAX-SIZE=0.00000000000000
@CLEAR
2
3
4
5
```

```
6
7
8
9
14
15
16
17
18
19
20
21
22
@
*
SUBDIVIDE EDGE NAME=5 BODY=1 MODE=DIVISIONS NDIV=4,
   RATIO=1.00000000000000 PROGRESS=ARITHMETIC BLTABLE=0
@CLEAR
6
7
8
@
*
SUBDIVIDE EDGE NAME=5 BODY=2 MODE=DIVISIONS NDIV=4,
   RATIO=1.00000000000000 PROGRESS=ARITHMETIC BLTABLE=0
@CLEAR
6
7
8
@
*
SUBDIVIDE EDGE NAME=5 BODY=3 MODE=DIVISIONS NDIV=4,
   RATIO=1.00000000000000 PROGRESS=ARITHMETIC BLTABLE=0
@CLEAR
6
7
8
@
*
SUBDIVIDE EDGE NAME=5 BODY=4 MODE=DIVISIONS NDIV=4,
   RATIO=1.00000000000000 PROGRESS=ARITHMETIC BLTABLE=0
@CLEAR
6
7
8
@
*
SUBDIVIDE EDGE NAME=5 BODY=5 MODE=DIVISIONS NDIV=4,
   RATIO=1.00000000000000 PROGRESS=ARITHMETIC BLTABLE=0
@CLEAR
6
7
8
@
*
SUBDIVIDE EDGE NAME=5 BODY=6 MODE=DIVISIONS NDIV=4,
```

```
   RATIO=1.00000000000000 PROGRESS=ARITHMETIC BLTABLE=0
@CLEAR
6
7
8
@
*
SUBDIVIDE EDGE NAME=5 BODY=7 MODE=DIVISIONS NDIV=4,
   RATIO=1.00000000000000 PROGRESS=ARITHMETIC BLTABLE=0
@CLEAR
6
7
8
@
*
SUBDIVIDE EDGE NAME=5 BODY=8 MODE=DIVISIONS NDIV=4,
   RATIO=1.00000000000000 PROGRESS=ARITHMETIC BLTABLE=0
@CLEAR
6
7
8
@
*
SUBDIVIDE EDGE NAME=5 BODY=9 MODE=DIVISIONS NDIV=4,
   RATIO=1.00000000000000 PROGRESS=ARITHMETIC BLTABLE=0
@CLEAR
6
7
8
@
*
SUBDIVIDE EDGE NAME=5 BODY=14 MODE=DIVISIONS NDIV=4,
   RATIO=1.00000000000000 PROGRESS=ARITHMETIC BLTABLE=0
@CLEAR
6
7
8
@
*
SUBDIVIDE EDGE NAME=5 BODY=15 MODE=DIVISIONS NDIV=4,
   RATIO=1.00000000000000 PROGRESS=ARITHMETIC BLTABLE=0
@CLEAR
6
7
8
@
*
SUBDIVIDE EDGE NAME=5 BODY=16 MODE=DIVISIONS NDIV=4,
   RATIO=1.00000000000000 PROGRESS=ARITHMETIC BLTABLE=0
@CLEAR
6
7
8
@
*
SUBDIVIDE EDGE NAME=5 BODY=17 MODE=DIVISIONS NDIV=4,
```

```
   RATIO=1.00000000000000 PROGRESS=ARITHMETIC BLTABLE=0
@CLEAR
6
7
8
@
*
SUBDIVIDE EDGE NAME=5 BODY=18 MODE=DIVISIONS NDIV=4,
   RATIO=1.00000000000000 PROGRESS=ARITHMETIC BLTABLE=0
@CLEAR
6
7
8
@
*
SUBDIVIDE EDGE NAME=5 BODY=19 MODE=DIVISIONS NDIV=4,
   RATIO=1.00000000000000 PROGRESS=ARITHMETIC BLTABLE=0
@CLEAR
6
7
8
@
*
SUBDIVIDE EDGE NAME=5 BODY=20 MODE=DIVISIONS NDIV=4,
   RATIO=1.00000000000000 PROGRESS=ARITHMETIC BLTABLE=0
@CLEAR
6
7
8
@
*
SUBDIVIDE EDGE NAME=5 BODY=21 MODE=DIVISIONS NDIV=4,
   RATIO=1.00000000000000 PROGRESS=ARITHMETIC BLTABLE=0
@CLEAR
6
7
8
@
*
SUBDIVIDE EDGE NAME=5 BODY=22 MODE=DIVISIONS NDIV=4,
   RATIO=1.00000000000000 PROGRESS=ARITHMETIC BLTABLE=0
@CLEAR
6
7
8
@
*
SUBDIVIDE BODY NAME=10 MODE=LENGTH SIZE=6.00000000000000,
   MAX-SIZE=0.00000000000000
@CLEAR
13
@
*
SUBDIVIDE EDGE NAME=5 BODY=10 MODE=DIVISIONS NDIV=4,
   RATIO=1.00000000000000 PROGRESS=ARITHMETIC BLTABLE=0
@CLEAR
```

6
7
8
@
*
SUBDIVIDE EDGE NAME=5 BODY=13 MODE=DIVISIONS NDIV=4,
RATIO=1.00000000000000 PROGRESS=ARITHMETIC BLTABLE=0
@CLEAR
6
7
8
@
*
SUBDIVIDE LINE NAME=1 MODE=LENGTH SIZE=6.0000000000000
2
3
4
5
6
7
8
9
10
11
12
13
14
15
16
17
18
19
20
21
22
23
24
25
26
27
28
29
30
31
32
33
34
35
36
37
38
39
40
41
42
43

156
157
158
159
160
161
162
163
164
165
166
167
168
169
170
171
172
173
174
175
176
177
178
179
180
181
182
@
*
EGROUP THREEDSOLID NAME=1 DISPLACE=DEFAULT STRAINS=DEFAULT MATERIAL=1,
    RSINT=DEFAULT TINT=DEFAULT RESULTS=STRESSES DEGEN=DEFAUL,
    FORMULAT=0 STRESSRE=GLOBAL INITIALS=NONE FRACTUR=NO,
    CMASS=DEFAULT STRAIN-F=0 UL-FORMU=DEFAULT LVUS1=0 LVUS2=0 SED=NO,
    RUPTURE=ADINA INCOMPAT=DEFAULT TIME-OFF=0.00000000000000,
    POROUS=NO WTMC=1.00000000000000 OPTION=NONE DESCRIPT='NONE',
    PRINT=DEFAULT SAVE=DEFAULT TBIRTH=0.00000000000000,
    TDEATH=0.00000000000000 TMC-MATE=1 RUPTURE-=0 EM=NO JOULE=NO,
    BOLT-NUM=0 BOLT-PLA=0 BOLT-LOA=0.00000000000000,
    BOLT-TOL=0.00000000000000
*
GBODY NODES=8 NCOINCID=BOUNDARIES NCTOLERA=1.00000000000000E-05,
    SUBSTRUC=0 GROUP=1 PREFSHAP=AUTOMATIC COLLAPSE=NO SIZE-FUN=0,
    DELETE-S=NO ANGLE-MI=5.00000000000000 MIDNODES=CURVED,
    METHOD=DELAUNAY PATTERN=0 MESHING=MAPPED DEGENERA=NO,
    BOUNDARY=ADVFRONT DEG-EDGE=0 GEO-ERRO=0.00000000000000,
    SAMPLING=20 MIN-SIZE=0.00000000000000 NLAYER=1 NLTABL=0,
    AUTO-GRA=NO SIMULATE=NO PYRAMIDS=NO DANGMAXB=80.0000000000000,
    DANGMAXC=60.0000000000000 DANGMAXD=80.0000000000000 HEXALAYE=NO,
    AUTO-REF=YES EVEN=SUM DENSITY=1.20000000000000 MIDFACEN=QUAD,
    REFINE=ALONG-EDGE GRID=NO BREFINE=ALONG-EDGE BLTABL=0,
    PREFSHA2=QUADRILATERAL NOPTI=1
@CLEAR
25 0
@
*
EGROUP THREEDSOLID NAME=2 DISPLACE=DEFAULT STRAINS=DEFAULT MATERIAL=2,

```
    RSINT=DEFAULT TINT=DEFAULT RESULTS=STRESSES DEGEN=DEFAUL,
    FORMULAT=0 STRESSRE=GLOBAL INITIALS=NONE FRACTUR=NO,
    CMASS=DEFAULT STRAIN-F=0 UL-FORMU=DEFAULT LVUS1=0 LVUS2=0 SED=NO,
    RUPTURE=ADINA INCOMPAT=DEFAULT TIME-OFF=0.00000000000000,
    POROUS=NO WTMC=1.00000000000000 OPTION=NONE DESCRIPT='NONE',
    PRINT=DEFAULT SAVE=DEFAULT TBIRTH=0.00000000000000,
    TDEATH=0.00000000000000 TMC-MATE=1 RUPTURE-=0 EM=NO JOULE=NO,
    BOLT-NUM=0 BOLT-PLA=0 BOLT-LOA=0.00000000000000,
    BOLT-TOL=0.00000000000000
*
GBODY NODES=8 NCOINCID=BOUNDARIES NCTOLERA=1.00000000000000E-05,
    SUBSTRUC=0 GROUP=2 PREFSHAP=AUTOMATIC COLLAPSE=NO SIZE-FUN=0,
    DELETE-S=NO ANGLE-MI=5.00000000000000 MIDNODES=CURVED,
    METHOD=DELAUNAY PATTERN=0 MESHING=MAPPED DEGENERA=NO,
    BOUNDARY=ADVFRONT DEG-EDGE=0 GEO-ERRO=0.00000000000000,
    SAMPLING=20 MIN-SIZE=0.00000000000000 NLAYER=1 NLTABL=0,
    AUTO-GRA=NO SIMULATE=NO PYRAMIDS=NO DANGMAXB=80.0000000000000,
    DANGMAXC=60.0000000000000 DANGMAXD=80.0000000000000 HEXALAYE=NO,
    AUTO-REF=YES EVEN=SUM DENSITY=1.20000000000000 MIDFACEN=QUAD,
    REFINE=ALONG-EDGE GRID=NO BREFINE=ALONG-EDGE BLTABL=0,
    PREFSHA2=QUADRILATERAL NOPTI=1
@CLEAR
24 0
@
*
EGROUP THREEDSOLID NAME=3 DISPLACE=DEFAULT STRAINS=DEFAULT MATERIAL=3,
    RSINT=DEFAULT TINT=DEFAULT RESULTS=STRESSES DEGEN=DEFAUL,
    FORMULAT=0 STRESSRE=GLOBAL INITIALS=NONE FRACTUR=NO,
    CMASS=DEFAULT STRAIN-F=0 UL-FORMU=DEFAULT LVUS1=0 LVUS2=0 SED=NO,
    RUPTURE=ADINA INCOMPAT=DEFAULT TIME-OFF=0.00000000000000,
    POROUS=NO WTMC=1.00000000000000 OPTION=NONE DESCRIPT='NONE',
    PRINT=DEFAULT SAVE=DEFAULT TBIRTH=0.00000000000000,
    TDEATH=0.00000000000000 TMC-MATE=1 RUPTURE-=0 EM=NO JOULE=NO,
    BOLT-NUM=0 BOLT-PLA=0 BOLT-LOA=0.00000000000000,
    BOLT-TOL=0.00000000000000
*
GBODY NODES=8 NCOINCID=BOUNDARIES NCTOLERA=1.00000000000000E-05,
    SUBSTRUC=0 GROUP=3 PREFSHAP=AUTOMATIC COLLAPSE=NO SIZE-FUN=0,
    DELETE-S=NO ANGLE-MI=5.00000000000000 MIDNODES=CURVED,
    METHOD=DELAUNAY PATTERN=0 MESHING=MAPPED DEGENERA=NO,
    BOUNDARY=ADVFRONT DEG-EDGE=0 GEO-ERRO=0.00000000000000,
    SAMPLING=20 MIN-SIZE=0.00000000000000 NLAYER=1 NLTABL=0,
    AUTO-GRA=NO SIMULATE=NO PYRAMIDS=NO DANGMAXB=80.0000000000000,
    DANGMAXC=60.0000000000000 DANGMAXD=80.0000000000000 HEXALAYE=NO,
    AUTO-REF=YES EVEN=SUM DENSITY=1.20000000000000 MIDFACEN=QUAD,
    REFINE=ALONG-EDGE GRID=NO BREFINE=ALONG-EDGE BLTABL=0,
    PREFSHA2=QUADRILATERAL NOPTI=1
@CLEAR
23 0
@
*
EGROUP THREEDSOLID NAME=4 DISPLACE=DEFAULT STRAINS=DEFAULT MATERIAL=4,
    RSINT=DEFAULT TINT=DEFAULT RESULTS=STRESSES DEGEN=DEFAUL,
    FORMULAT=0 STRESSRE=GLOBAL INITIALS=NONE FRACTUR=NO,
    CMASS=DEFAULT STRAIN-F=0 UL-FORMU=DEFAULT LVUS1=0 LVUS2=0 SED=NO,
    RUPTURE=ADINA INCOMPAT=DEFAULT TIME-OFF=0.00000000000000,
```

```
    POROUS=NO WTMC=1.00000000000000 OPTION=NONE DESCRIPT='NONE',
    PRINT=DEFAULT SAVE=DEFAULT TBIRTH=0.00000000000000,
    TDEATH=0.00000000000000 TMC-MATE=1 RUPTURE-=0 EM=NO JOULE=NO,
    BOLT-NUM=0 BOLT-PLA=0 BOLT-LOA=0.00000000000000,
    BOLT-TOL=0.00000000000000
*
GBODY NODES=8 NCOINCID=NO SUBSTRUC=0 GROUP=4 PREFSHAP=AUTOMATIC,
    COLLAPSE=NO SIZE-FUN=0 DELETE-S=NO ANGLE-MI=5.00000000000000,
    MIDNODES=CURVED METHOD=DELAUNAY PATTERN=0 MESHING=MAPPED,
    DEGENERA=NO BOUNDARY=ADVFRONT DEG-EDGE=0,
    GEO-ERRO=0.00000000000000 SAMPLING=20 MIN-SIZE=0.00000000000000,
    NLAYER=1 NLTABL=0 AUTO-GRA=NO SIMULATE=NO PYRAMIDS=NO,
    DANGMAXB=80.0000000000000 DANGMAXC=60.0000000000000,
    DANGMAXD=80.0000000000000 HEXALAYE=NO AUTO-REF=YES EVEN=SUM,
    DENSITY=1.20000000000000 MIDFACEN=QUAD REFINE=ALONG-EDGE GRID=NO,
    BREFINE=ALONG-EDGE BLTABL=0 PREFSHA2=QUADRILATERAL NOPTI=1
@CLEAR
1 0
2 0
3 0
4 0
5 0
6 0
7 0
8 0
9 0
10 0
11 0
12 0
13 0
14 0
15 0
16 0
17 0
18 0
19 0
20 0
21 0
22 0
@
*
EGROUP BEAM NAME=5 SUBTYPE=THREE-D DISPLACE=DEFAULT MATERIAL=5 RINT=5,
    SINT=DEFAULT TINT=DEFAULT RESULTS=STRESSES INITIALS=BOTH,
    CMASS=DEFAULT RIGIDEND=NONE MOMENT-C=NO RIGIDITY=1,
    MULTIPLY=1000000.00000000 RUPTURE=ADINA OPTION=NONE,
    BOLT-TOL=0.00000000000000 DESCRIPT='NONE' SECTION=1,
    PRINT=DEFAULT SAVE=DEFAULT TBIRTH=0.00000000000000,
    TDEATH=0.00000000000000 SPOINT=4 BOLTFORC=0.00000000000000,
    BOLTNCUR=0 TMC-MATE=1 BOLT-NUM=0 BOLT-LOA=0.00000000000000,
    WARP=NO ENDRELEA=ACCURATE
*
GLINE NODES=2 AUXPOINT=0 NCOINCID=ALL NCTOLERA=1.00000000000000E-05,
    SUBSTRUC=0 GROUP=5 MIDNODES=CURVED XO=0.00000000000000,
    YO=1.00000000000000 ZO=0.00000000000000 XYZOSYST=SKEW
@CLEAR
1
```

```
2
3
4
5
6
@
*
COPY ZONE NAME1=WHOLE_MODEL NAME2=MESHPLOT00001 POSITION=1
*
ZONE NAME=MESHPLOT00001 NODEATTA=YES GEOMATTA=YES
@CLEAR
 'whole model'
 ,
'SUBTRACT CONTACT GROUP 1 OF REUSE 1 OF SUBSTRUCTURE 0 OF PROG
RAM ADINA'
 ,
'SUBTRACT CONTACT GROUP 2 OF REUSE 1 OF SUBSTRUCTURE 0 OF PROG
RAM ADINA'
@
*
EGROUP BEAM NAME=6 SUBTYPE=THREE-D DISPLACE=DEFAULT MATERIAL=6 RINT=5,
    SINT=DEFAULT TINT=DEFAULT RESULTS=STRESSES INITIALS=BOTH,
    CMASS=DEFAULT RIGIDEND=NONE MOMENT-C=NO RIGIDITY=1,
    MULTIPLY=1000000.00000000 RUPTURE=ADINA OPTION=NONE,
    BOLT-TOL=0.00000000000000 DESCRIPT='NONE' SECTION=2,
    PRINT=DEFAULT SAVE=DEFAULT TBIRTH=0.00000000000000,
    TDEATH=0.00000000000000 SPOINT=4 BOLTFORC=0.00000000000000,
    BOLTNCUR=0 TMC-MATE=1 BOLT-NUM=0 BOLT-LOA=0.00000000000000,
    WARP=NO ENDRELEA=ACCURATE
*
GLINE NODES=2 AUXPOINT=0 NCOINCID=ALL NCTOLERA=1.00000000000000E-05,
    SUBSTRUC=0 GROUP=6 MIDNODES=CURVED XO=1.00000000000000,
    YO=0.00000000000000 ZO=0.00000000000000 XYZOSYST=SKEW
7
8
9
10
11
12
13
14
15
16
17
18
19
20
21
22
23
24
25
26
27
28
29
```

142
143
144
145
146
147
148
149
150
151
152
153
154
155
156
157
158
159
160
161
162
163
164
165
166
167
168
169
170
171
172
173
174
175
176
177
178
179
180
181
182
@

APPENDIX C
JPCP: SAMPLE INPUT FILE

```
*
* Command file created from session file information stored within AUI database
*
DATABASE NEW SAVE=NO PROMPT=NO
FEPROGRAM ADINA
CONTROL FILEVERSION=V89
*
FEPROGRAM PROGRAM=ADINA
*
CONTROL PLOTUNIT=PERCENT VERBOSE=YES ERRORLIM=0 LOGLIMIT=0 UNDO=5,
    PROMPTDE=UNKNOWN AUTOREPA=YES DRAWMATT=YES DRAWTEXT=EXACT,
    DRAWLINE=EXACT DRAWFILL=EXACT AUTOMREB=YES ZONECOPY=NO,
    SWEEPCOI=YES SESSIONS=YES DYNAMICT=YES UPDATETH=YES AUTOREGE=NO,
    ERRORACT=CONTINUE FILEVERS=V89 INITFCHE=NO SIGDIGIT=6,
    AUTOZONE=YES PSFILEVE=V0
*
*Comment 1 (Slab dimension) - Length units are in inches
*
BODY BLOCK NAME=1 OPTION=CENTERED POSITION=VECTOR ORIENTAT=SYSTEM,
    CX1=0.00000000000000 CX2=0.00000000000000 CX3=0.00000000000000,
    SYSTEM=0 DX1=192.000000000000 DX2=144.000000000000,
    DX3=9.00000000000000
*
*Comment 2 (Subgrade dimension) - Length units are in inches
*
BODY BLOCK NAME=2 OPTION=CENTERED POSITION=VECTOR ORIENTAT=SYSTEM,
    CX1=0.00000000000000 CX2=0.00000000000000 CX3=-54.5000000000000,
    SYSTEM=0 DX1=192.000000000000 DX2=144.000000000000,
    DX3=100.000000000000
*
SUBDIVIDE BODY NAME=1 MODE=LENGTH SIZE=3.00000000000000,
    MAX-SIZE=0.00000000000000
@CLEAR
2
@
*
SUBDIVIDE EDGE NAME=5 BODY=2 MODE=DIVISIONS NDIV=12,
    RATIO=0.100000000000000 PROGRESS=ARITHMETIC BLTABLE=0
@CLEAR
6
7
8
@
*
FIXITY NAME=X_FIX
@CLEAR
 'X-TRANSLATION'
 'OVALIZATION'
@
*
FIXITY NAME=Y_FIX
@CLEAR
```

```
 'Y-TRANSLATION'
 'OVALIZATION'
@
*
FIXBOUNDARY FACES FIXITY=ALL BODY=2
@CLEAR
5  'ALL'
6  'X_FIX'
3  'X_FIX'
2  'Y_FIX'
4  'Y_FIX'
@
*
MASTER ANALYSIS=STATIC MODEX=EXECUTE TSTART=0.00000000000000 IDOF=111,
    OVALIZAT=NONE FLUIDPOT=AUTOMATIC CYCLICPA=1 IPOSIT=STOP,
    REACTION=YES INITIALS=NO FSINTERA=NO IRINT=DEFAULT CMASS=NO,
    SHELLNDO=AUTOMATIC AUTOMATI=OFF SOLVER=SPARSE,
    CONTACT-=CONSTRAINT-FUNCTION TRELEASE=0.00000000000000,
    RESTART-=NO FRACTURE=NO LOAD-CAS=NO LOAD-PEN=NO SINGULAR=YES,
    STIFFNES=0.000100000000000000 MAP-OUTP=NONE MAP-FORM=NO,
    NODAL-DE='' POROUS-C=NO ADAPTIVE=0 ZOOM-LAB=1 AXIS-CYC=0,
    PERIODIC=NO VECTOR-S=GEOMETRY EPSI-FIR=NO STABILIZ=NO,
    STABFACT=1.00000000000000E-10 RESULTS=PORTHOLE FEFCORR=NO,
    BOLTSTEP=1 EXTEND-S=YES CONVERT-=NO DEGEN=YES TMC-MODE=NO,
    ENSIGHT-=NO IRSTEPS=1 INITIALT=NO TEMP-INT=NO ESINTERA=NO,
    OP2GEOM=NO INSITU-D=NO
*
*Comment 3 (RAP concrete properties) - Unit: E (psi), ν (unitless), Density (lb/in3), CTE (/°F)
*
MATERIAL PLASTIC-MULTILINEAR NAME=1 HARDENIN=ISOTROPIC,
    E=2625259.00000000 NU=0.250000000000000 STRAINRA=0,
    DENSITY=0.081000000000000 ALPHA=6.20000000000000E-06,
    TREF=0.00000000000000 DCURVE=0 DEPENDEN=NO,
    TRANSITI=0.000100000000000000 EP-STRAI=0.00000000000000 BCURVE=0,
    BVALUE=0.00000000000000 MDESCRIP='NONE'
@CLEAR
0.000047 122.11
0.000080 206.32
0.000120 286.32
0.000150 349.47
0.000181 378.95
0.000228 421.05
0.000297 458.95
0.000422 509.47
0.000703 530.53
@
*
*Comment 4 (Subgrade properties) - Unit: E (psi), ν (unitless)
*
MATERIAL ELASTIC NAME=2 E=115000.000000000 NU=0.350000000000000,
    DENSITY=0.00000000000000 ALPHA=0.00000000000000 MDESCRIP=,
'subgrade'
*
EGROUP TRUSS NAME=1 SUBTYPE=GENERAL DISPLACE=DEFAULT MATERIAL=1,
    INT=DEFAULT GAPS=NO INITIALS=NONE CMASS=DEFAULT,
    TIME-OFF=0.00000000000000 OPTION=NONE RB-LINE=1 DESCRIPT='slab',
```

```
    AREA=1.00000000000000 PRINT=DEFAULT SAVE=DEFAULT,
    TBIRTH=0.00000000000000 TDEATH=0.00000000000000 TMC-MATE=1,
    RUPTURE=ADINA GAPWIDTH=0.00000000000000
*
DELETE EGROUP ALL FIRST=1 LAST=1 ELEMENTS=YES NODES=YES
*
EGROUP THREEDSOLID NAME=1 DISPLACE=DEFAULT STRAINS=DEFAULT MATERIAL=1,
    RSINT=DEFAULT TINT=DEFAULT RESULTS=STRESSES DEGEN=DEFAUL,
    FORMULAT=0 STRESSRE=GLOBAL INITIALS=NONE FRACTUR=NO,
    CMASS=DEFAULT STRAIN-F=0 UL-FORMU=DEFAULT LVUS1=0 LVUS2=0 SED=NO,
    RUPTURE=ADINA INCOMPAT=DEFAULT TIME-OFF=0.00000000000000,
    POROUS=NO WTMC=1.00000000000000 OPTION=NONE DESCRIPT='NONE',
    PRINT=DEFAULT SAVE=DEFAULT TBIRTH=0.00000000000000,
    TDEATH=0.00000000000000 TMC-MATE=1 RUPTURE-=0 EM=NO JOULE=NO,
    BOLT-NUM=0 BOLT-PLA=0 BOLT-LOA=0.00000000000000,
    BOLT-TOL=0.00000000000000
*
EGROUP THREEDSOLID NAME=2 DISPLACE=DEFAULT STRAINS=DEFAULT MATERIAL=2,
    RSINT=DEFAULT TINT=DEFAULT RESULTS=STRESSES DEGEN=DEFAUL,
    FORMULAT=0 STRESSRE=GLOBAL INITIALS=NONE FRACTUR=NO,
    CMASS=DEFAULT STRAIN-F=0 UL-FORMU=DEFAULT LVUS1=0 LVUS2=0 SED=NO,
    RUPTURE=ADINA INCOMPAT=DEFAULT TIME-OFF=0.00000000000000,
    POROUS=NO WTMC=1.00000000000000 OPTION=NONE DESCRIPT='NONE',
    PRINT=DEFAULT SAVE=DEFAULT TBIRTH=0.00000000000000,
    TDEATH=0.00000000000000 TMC-MATE=1 RUPTURE-=0 EM=NO JOULE=NO,
    BOLT-NUM=0 BOLT-PLA=0 BOLT-LOA=0.00000000000000,
    BOLT-TOL=0.00000000000000
*
GBODY NODES=8 NCOINCID=BOUNDARIES NCTOLERA=1.00000000000000E-05,
    SUBSTRUC=0 GROUP=1 PREFSHAP=AUTOMATIC COLLAPSE=NO SIZE-FUN=0,
    DELETE-S=NO ANGLE-MI=5.00000000000000 MIDNODES=CURVED,
    METHOD=DELAUNAY PATTERN=0 MESHING=MAPPED DEGENERA=NO,
    BOUNDARY=ADVFRONT DEG-EDGE=0 GEO-ERRO=0.00000000000000,
    SAMPLING=20 MIN-SIZE=0.00000000000000 NLAYER=1 NLTABL=0,
    AUTO-GRA=NO SIMULATE=NO PYRAMIDS=NO DANGMAXB=80.0000000000000,
    DANGMAXC=60.0000000000000 DANGMAXD=80.0000000000000 HEXALAYE=NO,
    AUTO-REF=YES EVEN=SUM DENSITY=1.20000000000000 MIDFACEN=QUAD,
    REFINE=ALONG-EDGE GRID=NO BREFINE=ALONG-EDGE BLTABL=0,
    PREFSHA2=QUADRILATERAL NOPTI=1
@CLEAR
1 0
@
*
GBODY NODES=8 NCOINCID=BOUNDARIES NCTOLERA=1.00000000000000E-05,
    SUBSTRUC=0 GROUP=2 PREFSHAP=AUTOMATIC COLLAPSE=NO SIZE-FUN=0,
    DELETE-S=NO ANGLE-MI=5.00000000000000 MIDNODES=CURVED,
    METHOD=DELAUNAY PATTERN=0 MESHING=MAPPED DEGENERA=NO,
    BOUNDARY=ADVFRONT DEG-EDGE=0 GEO-ERRO=0.00000000000000,
    SAMPLING=20 MIN-SIZE=0.00000000000000 NLAYER=1 NLTABL=0,
    AUTO-GRA=NO SIMULATE=NO PYRAMIDS=NO DANGMAXB=80.0000000000000,
    DANGMAXC=60.0000000000000 DANGMAXD=80.0000000000000 HEXALAYE=NO,
    AUTO-REF=YES EVEN=SUM DENSITY=1.20000000000000 MIDFACEN=QUAD,
    REFINE=ALONG-EDGE GRID=NO BREFINE=ALONG-EDGE BLTABL=0,
    PREFSHA2=QUADRILATERAL NOPTI=1
@CLEAR
2 0
```

```
@
*
LOAD MASS-PROPORTIONAL NAME=1 MAGNITUD=1.00000000000000,
    AX=0.00000000000000 AY=0.00000000000000 AZ=-1.00000000000000,
    INTERPRE=BODY-FORCE
*
APPLY-LOAD BODY=2
@CLEAR
1  'MASS-PROPORTIONAL' 1  'MODEL' 0 0 1 0.00000000000000 0 -1 0 0 0  ,
'NO' 0.00000000000000 0.00000000000000 1 0  'MID'
@
*
*Comment 6 (Temperature differential)
*
LOAD TEMPERATURE NAME=1 MAGNITUD=10.0000000000000
*
LOAD TEMPERATURE NAME=2 MAGNITUD=-10.0000000000000
*
APPLY-LOAD BODY=2
@CLEAR
1  'MASS-PROPORTIONAL' 1  'MODEL' 0 0 1 0.00000000000000 0 -1 0 0 0  ,
'NO' 0.00000000000000 0.00000000000000 1 0  'BOTH'
@
*
APPLY-LOAD BODY=2
@CLEAR
1  'MASS-PROPORTIONAL' 1  'MODEL' 0 0 1 0.00000000000000 0 -1 0 0 0  ,
'NO' 0.00000000000000 0.00000000000000 1 0  'BOTH'
2  'TEMPERATURE' 1  'FACE' 1 0 1 0.00000000000000 0 -1 0 1 0  'NO',
    0.00000000000000 0.00000000000000 1 0  'MID'
@
*
APPLY-LOAD BODY=2
@CLEAR
1  'MASS-PROPORTIONAL' 1  'MODEL' 0 0 1 0.00000000000000 0 -1 0 0 0  ,
'NO' 0.00000000000000 0.00000000000000 1 0  'BOTH'
2  'TEMPERATURE' 1  'FACE' 1 0 1 0.00000000000000 0 -1 0 1 0  'NO',
    0.00000000000000 0.00000000000000 1 0  'BOTH'
@
*
APPLY-LOAD BODY=2
@CLEAR
1  'MASS-PROPORTIONAL' 1  'MODEL' 0 0 1 0.00000000000000 0 -1 0 0 0  ,
'NO' 0.00000000000000 0.00000000000000 1 0  'BOTH'
2  'TEMPERATURE' 1  'FACE' 1 0 1 0.00000000000000 0 -1 0 1 0  'NO',
    0.00000000000000 0.00000000000000 1 0  'BOTH'
@
*
APPLY-LOAD BODY=2
@CLEAR
1  'MASS-PROPORTIONAL' 1  'MODEL' 0 0 1 0.00000000000000 0 -1 0 0 0  ,
'NO' 0.00000000000000 0.00000000000000 1 0  'BOTH'
2  'TEMPERATURE' 1  'FACE' 1 0 1 0.00000000000000 0 -1 0 1 0  'NO',
    0.00000000000000 0.00000000000000 1 0  'BOTH'
3  'TEMPERATURE' 2  'FACE' 5 0 1 0.00000000000000 0 -1 0 1 0  'NO',
    0.00000000000000 0.00000000000000 1 0  'MID'
```

```
@
*
*Comment 5 (Tire load) - Pressure (psi)
*
LOADS-ELEMEN SUBSTRUC=0 REUSE=1 GROUP=1 THERMOST=0
@CLEAR
3040 3 120.000000000000 120.000000000000 120.000000000000,
    120.000000000000 1 0.00000000000000 0 -1
3041 3 120.000000000000 120.000000000000 120.000000000000,
    120.000000000000 1 0.00000000000000 0 -1
2976 3 120.000000000000 120.000000000000 120.000000000000,
    120.000000000000 1 0.00000000000000 0 -1
2977 3 120.000000000000 120.000000000000 120.000000000000,
    120.000000000000 1 0.00000000000000 0 -1
2912 3 120.000000000000 120.000000000000 120.000000000000,
    120.000000000000 1 0.00000000000000 0 -1
2913 3 120.000000000000 120.000000000000 120.000000000000,
    120.000000000000 1 0.00000000000000 0 -1
2848 3 120.000000000000 120.000000000000 120.000000000000,
    120.000000000000 1 0.00000000000000 0 -1
2849 3 120.000000000000 120.000000000000 120.000000000000,
    120.000000000000 1 0.00000000000000 0 -1
2784 3 120.000000000000 120.000000000000 120.000000000000,
    120.000000000000 1 0.00000000000000 0 -1
2785 3 120.000000000000 120.000000000000 120.000000000000,
    120.000000000000 1 0.00000000000000 0 -1
1504 3 120.000000000000 120.000000000000 120.000000000000,
    120.000000000000 1 0.00000000000000 0 -1
1505 3 120.000000000000 120.000000000000 120.000000000000,
    120.000000000000 1 0.00000000000000 0 -1
1440 3 120.000000000000 120.000000000000 120.000000000000,
    120.000000000000 1 0.00000000000000 0 -1
1441 3 120.000000000000 120.000000000000 120.000000000000,
    120.000000000000 1 0.00000000000000 0 -1
1376 3 120.000000000000 120.000000000000 120.000000000000,
    120.000000000000 1 0.00000000000000 0 -1
1377 3 120.000000000000 120.000000000000 120.000000000000,
    120.000000000000 1 0.00000000000000 0 -1
1312 3 120.000000000000 120.000000000000 120.000000000000,
    120.000000000000 1 0.00000000000000 0 -1
1313 3 120.000000000000 120.000000000000 120.000000000000,
    120.000000000000 1 0.00000000000000 0 -1
1248 3 120.000000000000 120.000000000000 120.000000000000,
    120.000000000000 1 0.00000000000000 0 -1
1249 3 120.000000000000 120.000000000000 120.000000000000,
    120.000000000000 1 0.00000000000000 0 -1
@
*
```

APPENDIX D
DOWEL: SAMPLE INPUT FILE

```
*
* Command file created from session file information stored within AUI database
*
DATABASE NEW SAVE=NO PROMPT=NO
FEPROGRAM ADINA
CONTROL FILEVERSION=V89
*
FEPROGRAM PROGRAM=ADINA
*
CONTROL PLOTUNIT=PERCENT VERBOSE=YES ERRORLIM=0 LOGLIMIT=0 UNDO=5,
   PROMPTDE=UNKNOWN AUTOREPA=YES DRAWMATT=YES DRAWTEXT=EXACT,
   DRAWLINE=EXACT DRAWFILL=EXACT AUTOMREB=YES ZONECOPY=NO,
   SWEEPCOI=YES SESSIONS=YES DYNAMICT=YES UPDATETH=YES AUTOREGE=NO,
   ERRORACT=CONTINUE FILEVERS=V89 INITFCHE=NO SIGDIGIT=6,
   AUTOZONE=YES PSFILEVE=V0
*
FEPROGRAM PROGRAM=ADINA
*
CONTROL PLOTUNIT=PERCENT VERBOSE=YES ERRORLIM=0 LOGLIMIT=0 UNDO=5,
   PROMPTDE=UNKNOWN AUTOREPA=YES DRAWMATT=YES DRAWTEXT=EXACT,
   DRAWLINE=EXACT DRAWFILL=EXACT AUTOMREB=YES ZONECOPY=NO,
   SWEEPCOI=YES SESSIONS=YES DYNAMICT=YES UPDATETH=YES AUTOREGE=NO,
   ERRORACT=CONTINUE FILEVERS=V89 INITFCHE=NO SIGDIGIT=6,
   AUTOZONE=YES PSFILEVE=V0
*
MASTER ANALYSIS=STATIC MODEX=EXECUTE TSTART=0.00000000000000 IDOF=111,
   OVALIZAT=NONE FLUIDPOT=AUTOMATIC CYCLICPA=1 IPOSIT=STOP,
   REACTION=YES INITIALS=NO FSINTERA=NO IRINT=DEFAULT CMASS=NO,
   SHELLNDO=AUTOMATIC AUTOMATI=OFF SOLVER=SPARSE,
   CONTACT-=CONSTRAINT-FUNCTION TRELEASE=0.00000000000000,
   RESTART-=NO FRACTURE=NO LOAD-CAS=NO LOAD-PEN=NO SINGULAR=YES,
   STIFFNES=0.000100000000000000 MAP-OUTP=NONE MAP-FORM=NO,
   NODAL-DE='' POROUS-C=NO ADAPTIVE=0 ZOOM-LAB=1 AXIS-CYC=0,
   PERIODIC=NO VECTOR-S=GEOMETRY EPSI-FIR=NO STABILIZ=NO,
   STABFACT=1.00000000000000E-10 RESULTS=PORTHOLE FEFCORR=NO,
   BOLTSTEP=1 EXTEND-S=YES CONVERT-=NO DEGEN=YES TMC-MODE=NO,
   ENSIGHT-=NO IRSTEPS=1 INITIALT=NO TEMP-INT=NO ESINTERA=NO,
   OP2GEOM=NO INSITU-D=NO
*
*Comment 1 (Dowel bar size) - Length units are in inches
*
BODY BLOCK NAME=1 OPTION=CENTERED POSITION=VECTOR ORIENTAT=SYSTEM,
   CX1=-4.50000000000000 CX2=0.00000000000000 CX3=0.00000000000000,
   SYSTEM=0 DX1=9.00000000000000 DX2=8.00000000000000,
   DX3=8.00000000000000
*
BODY CYLINDER NAME=2 OPTION=CENTERED POSITION=VECTOR ORIENTAT=SYSTEM,
   CX1=-4.50000000000000 CX2=0.00000000000000 CX3=0.00000000000000,
   SYSTEM=0 AXIS=XL RADIUS=0.625000000000000,
   LENGTH=9.00000000000000 SHEET=NO
*
BODY SUBTRACT NAME=1 KEEP-TOO=NO KEEP-IMP=NO
```

```
@CLEAR
2
@
*
BODY SHEET NAME=2 DELETE-L=YES OPTION=POLYGON SYSTEM=0
@CLEAR
8
5
2
4
@
*
BODY SHEET NAME=3 DELETE-L=YES OPTION=POLYGON SYSTEM=0
@CLEAR
7
3
1
6
@
*
BODY SUBTRACT NAME=1 KEEP-TOO=NO KEEP-IMP=NO
@CLEAR
3
@
*
BODY SUBTRACT NAME=1 KEEP-TOO=YES KEEP-IMP=NO
@CLEAR
2
@
*
BODY SUBTRACT NAME=4 KEEP-TOO=NO KEEP-IMP=NO
@CLEAR
2
@
*
DELETE BODY FIRST=6 LAST=6
*
DELETE BODY FIRST=5 LAST=5
*
DELETE BODY FIRST=4 LAST=4
*
SUBDIVIDE EDGE NAME=1 BODY=1 MODE=DIVISIONS NDIV=4,
   RATIO=1.00000000000000 PROGRESS=ARITHMETIC BLTABLE=0
@CLEAR
2
3
8
@
*
SUBDIVIDE EDGE NAME=12 BODY=1 MODE=DIVISIONS NDIV=3,
   RATIO=1.00000000000000 PROGRESS=ARITHMETIC BLTABLE=0
@CLEAR
7
4
9
@
```

```
*
SUBDIVIDE EDGE NAME=5 BODY=1 MODE=DIVISIONS NDIV=2,
   RATIO=1.00000000000000 PROGRESS=ARITHMETIC BLTABLE=0
@CLEAR
6
10
11
@
*
TRANSFORMATI ROTATION NAME=1 MODE=AXIS SYSTEM=0 AXIS=XL,
   ANGLE=90.0000000000000
*
BODY TRANSFORMED NAME=2 OPTION=COPY PARENT=1 TRANSFOR=1 NCOPY=3,
   MESH=NO EGROUP=0 NCOINCID=NO NTOLERAN=1.00000000000000E-05
*
BODY BLOCK NAME=5 OPTION=CENTERED POSITION=VECTOR ORIENTAT=SYSTEM,
   CX1=-4.50000000000000 CX2=5.00000000000000 CX3=0.00000000000000,
   SYSTEM=0 DX1=9.00000000000000 DX2=2.00000000000000,
   DX3=8.00000000000000
*
BODY BLOCK NAME=6 OPTION=CENTERED POSITION=VECTOR ORIENTAT=SYSTEM,
   CX1=-4.50000000000000 CX2=-5.00000000000000 CX3=0.00000000000000,
   SYSTEM=0 DX1=9.00000000000000 DX2=2.00000000000000,
   DX3=8.00000000000000
*
SUBDIVIDE EDGE NAME=5 BODY=5 MODE=DIVISIONS NDIV=4,
   RATIO=1.00000000000000 PROGRESS=ARITHMETIC BLTABLE=0
@CLEAR
6
7
8
@
*
SUBDIVIDE EDGE NAME=10 BODY=5 MODE=DIVISIONS NDIV=3,
   RATIO=1.00000000000000 PROGRESS=ARITHMETIC BLTABLE=0
@CLEAR
12
4
2
@
*
SUBDIVIDE EDGE NAME=10 BODY=6 MODE=DIVISIONS NDIV=3,
   RATIO=1.00000000000000 PROGRESS=ARITHMETIC BLTABLE=0
@CLEAR
12
4
2
@
*
SUBDIVIDE EDGE NAME=5 BODY=6 MODE=DIVISIONS NDIV=4,
   RATIO=1.00000000000000 PROGRESS=ARITHMETIC BLTABLE=0
@CLEAR
6
7
8
@
```

```
*
*Comment 7 (Concrete properties) - Unit: E (psi), ν (unitless), Density (lb/in3), CTE (/°F)
*
MATERIAL ELASTIC NAME=1 E=3000000.00000000 NU=0.180000000000000,
   DENSITY=0.0810000000000000 ALPHA=6.53000000000000E-06 MDESCRIP=,
'concrete'
*
EGROUP THREEDSOLID NAME=1 DISPLACE=DEFAULT STRAINS=DEFAULT MATERIAL=1,
   RSINT=DEFAULT TINT=DEFAULT RESULTS=STRESSES DEGEN=DEFAUL,
   FORMULAT=0 STRESSRE=GLOBAL INITIALS=NONE FRACTUR=NO,
   CMASS=DEFAULT STRAIN-F=0 UL-FORMU=DEFAULT LVUS1=0 LVUS2=0 SED=NO,
   RUPTURE=ADINA INCOMPAT=DEFAULT TIME-OFF=0.00000000000000,
   POROUS=NO WTMC=1.00000000000000 OPTION=NONE DESCRIPT='concrete',
   PRINT=DEFAULT SAVE=DEFAULT TBIRTH=0.00000000000000,
   TDEATH=0.00000000000000 TMC-MATE=1 RUPTURE-=0 EM=NO JOULE=NO,
   BOLT-NUM=0 BOLT-PLA=0 BOLT-LOA=0.00000000000000,
   BOLT-TOL=0.00000000000000
*
GBODY NODES=8 NCOINCID=BOUNDARIES NCTOLERA=1.00000000000000E-05,
   SUBSTRUC=0 GROUP=1 PREFSHAP=AUTOMATIC COLLAPSE=NO SIZE-FUN=0,
   DELETE-S=NO ANGLE-MI=5.00000000000000 MIDNODES=CURVED,
   METHOD=DELAUNAY PATTERN=0 MESHING=MAPPED DEGENERA=NO,
   BOUNDARY=ADVFRONT DEG-EDGE=0 GEO-ERRO=0.00000000000000,
   SAMPLING=20 MIN-SIZE=0.00000000000000 NLAYER=1 NLTABL=0,
   AUTO-GRA=NO SIMULATE=NO PYRAMIDS=NO DANGMAXB=80.0000000000000,
   DANGMAXC=60.0000000000000 DANGMAXD=80.0000000000000 HEXALAYE=NO,
   AUTO-REF=YES EVEN=SUM DENSITY=1.20000000000000 MIDFACEN=QUAD,
   REFINE=ALONG-EDGE GRID=NO BREFINE=ALONG-EDGE BLTABL=0,
   PREFSHA2=QUADRILATERAL NOPTI=1
@CLEAR
1 0
2 0
3 0
4 0
5 0
6 0
@
*
*Comment 2 (Dowel bar spacing and number of dowel bar per joints)
*
TRANSFORMATI TRANSLATION NAME=2 MODE=SYSTEM SYSTEM=0,
   DX=0.00000000000000 DY=12.0000000000000 DZ=0.00000000000000
*
BODY TRANSFORMED NAME=7 OPTION=COPY PARENT=1 TRANSFOR=2 NCOPY=11,
   MESH=YES EGROUP=0 NCOINCID=YES NTOLERAN=1.00000000000000E-05
@CLEAR
2
3
4
5
6
@
*
TRANSFORMATI TRANSLATION NAME=3 MODE=SYSTEM SYSTEM=0,
   DX=-171.000000000000 DY=0.00000000000000 DZ=0.00000000000000
*
```

```
BODY TRANSFORMED NAME=73 OPTION=COPY PARENT=1 TRANSFOR=3 NCOPY=1,
   MESH=YES EGROUP=1 NCOINCID=YES NTOLERAN=1.00000000000000E-05
@CLEAR
2
3
4
5
6
7
8
9
10
11
12
13
14
15
16
17
18
19
20
21
22
23
24
25
26
27
28
29
30
31
32
33
34
35
36
37
38
39
40
41
42
43
44
45
46
47
48
49
50
51
52
53
54
```

```
55
56
57
58
59
60
61
62
63
64
65
66
67
68
69
70
71
72
@
*
*Comment 4 (Slab dimension) - Length units are in inches
*
BODY BLOCK NAME=145 OPTION=CENTERED POSITION=VECTOR ORIENTAT=SYSTEM,
   CX1=-90.0000000000000 CX2=66.0000000000000 CX3=0.00000000000000,
   SYSTEM=0 DX1=162.000000000000 DX2=144.000000000000,
   DX3=8.00000000000000
*
SUBDIVIDE EDGE NAME=12 BODY=145 MODE=DIVISIONS NDIV=54,
   RATIO=1.00000000000000 PROGRESS=ARITHMETIC BLTABLE=0
@CLEAR
10
4
2
@
*
SUBDIVIDE EDGE NAME=5 BODY=145 MODE=DIVISIONS NDIV=2,
   RATIO=1.00000000000000 PROGRESS=ARITHMETIC BLTABLE=0
@CLEAR
6
7
8
@
*
SUBDIVIDE EDGE NAME=1 BODY=145 MODE=DIVISIONS NDIV=36,
   RATIO=1.00000000000000 PROGRESS=ARITHMETIC BLTABLE=0
@CLEAR
3
9
11
@
*
GBODY NODES=8 NCOINCID=BOUNDARIES NCTOLERA=1.00000000000000E-05,
   SUBSTRUC=0 GROUP=1 PREFSHAP=AUTOMATIC COLLAPSE=NO SIZE-FUN=0,
   DELETE-S=NO ANGLE-MI=5.00000000000000 MIDNODES=CURVED,
   METHOD=DELAUNAY PATTERN=0 MESHING=MAPPED DEGENERA=NO,
   BOUNDARY=ADVFRONT DEG-EDGE=0 GEO-ERRO=0.00000000000000,
```

```
    SAMPLING=20 MIN-SIZE=0.00000000000000 NLAYER=1 NLTABL=0,
    AUTO-GRA=NO SIMULATE=NO PYRAMIDS=NO DANGMAXB=80.0000000000000,
    DANGMAXC=60.0000000000000 DANGMAXD=80.0000000000000 HEXALAYE=NO,
    AUTO-REF=YES EVEN=SUM DENSITY=1.20000000000000 MIDFACEN=QUAD,
    REFINE=ALONG-EDGE GRID=NO BREFINE=ALONG-EDGE BLTABL=0,
    PREFSHA2=QUADRILATERAL NOPTI=1
@CLEAR
145 0
@
*
BODY BLOCK NAME=146 OPTION=CENTERED POSITION=VECTOR ORIENTAT=SYSTEM,
    CX1=-90.0000000000000 CX2=66.0000000000000 CX3=4.50000000000000,
    SYSTEM=0 DX1=180.000000000000 DX2=144.000000000000,
    DX3=1.00000000000000
*
BODY BLOCK NAME=147 OPTION=CENTERED POSITION=VECTOR ORIENTAT=SYSTEM,
    CX1=-90.0000000000000 CX2=66.0000000000000 CX3=-4.50000000000000,
    SYSTEM=0 DX1=180.000000000000 DX2=144.000000000000,
    DX3=1.00000000000000
*
SUBDIVIDE EDGE NAME=12 BODY=146 MODE=DIVISIONS NDIV=60,
    RATIO=1.00000000000000 PROGRESS=ARITHMETIC BLTABLE=0
@CLEAR
10
4
2
@
*
SUBDIVIDE EDGE NAME=1 BODY=146 MODE=DIVISIONS NDIV=36,
    RATIO=1.00000000000000 PROGRESS=ARITHMETIC BLTABLE=0
@CLEAR
3
9
11
@
*
SUBDIVIDE EDGE NAME=1 BODY=147 MODE=DIVISIONS NDIV=36,
    RATIO=1.00000000000000 PROGRESS=ARITHMETIC BLTABLE=0
@CLEAR
3
9
11
@
*
SUBDIVIDE EDGE NAME=12 BODY=147 MODE=DIVISIONS NDIV=60,
    RATIO=1.00000000000000 PROGRESS=ARITHMETIC BLTABLE=0
@CLEAR
10
4
2
@
*
GBODY NODES=8 NCOINCID=BOUNDARIES NCTOLERA=1.00000000000000E-05,
    SUBSTRUC=0 GROUP=1 PREFSHAP=AUTOMATIC COLLAPSE=NO SIZE-FUN=0,
    DELETE-S=NO ANGLE-MI=5.00000000000000 MIDNODES=CURVED,
    METHOD=DELAUNAY PATTERN=0 MESHING=MAPPED DEGENERA=NO,
```

```
    BOUNDARY=ADVFRONT DEG-EDGE=0 GEO-ERRO=0.00000000000000,
    SAMPLING=20 MIN-SIZE=0.00000000000000 NLAYER=1 NLTABL=0,
    AUTO-GRA=NO SIMULATE=NO PYRAMIDS=NO DANGMAXB=80.0000000000000,
    DANGMAXC=60.0000000000000 DANGMAXD=80.0000000000000 HEXALAYE=NO,
    AUTO-REF=YES EVEN=SUM DENSITY=1.20000000000000 MIDFACEN=QUAD,
    REFINE=ALONG-EDGE GRID=NO BREFINE=ALONG-EDGE BLTABL=0,
    PREFSHA2=QUADRILATERAL NOPTI=1
@CLEAR
146 0
147 0
@
*
ZONE NAME=RIGHTSLAB NODEATTA=YES GEOMATTA=YES
*
ACTIVEZONE
@CLEAR
 'RIGHTSLAB'
@
*
TRANSFORMATI TRANSLATION NAME=4 MODE=SYSTEM SYSTEM=0,
    DX=-180.750000000000 DY=0.00000000000000 DZ=0.00000000000000
*
BODY TRANSFORMED NAME=148 OPTION=COPY PARENT=1 TRANSFOR=4 NCOPY=1,
    MESH=YES EGROUP=0 NCOINCID=YES NTOLERAN=1.00000000000000E-05
2
3
4
5
6
7
8
9
10
11
12
13
14
15
16
17
18
19
20
21
22
23
24
25
26
27
28
29
30
31
32
33
```

```
146
147
@
*
ZONE NAME=LEFTSLAB NODEATTA=YES GEOMATTA=YES
*
ACTIVEZONE
@CLEAR
 'LEFTSLAB'
@
*
TRANSFORMATI TRANSLATION NAME=5 MODE=SYSTEM SYSTEM=0,
    DX=180.750000000000 DY=0.00000000000000 DZ=0.00000000000000
*
BODY TRANSFORMED NAME=295 OPTION=COPY PARENT=1 TRANSFOR=5 NCOPY=1,
    MESH=YES EGROUP=0 NCOINCID=YES NTOLERAN=1.00000000000000E-05
2
3
4
5
6
7
8
9
10
11
12
13
14
15
16
17
18
19
20
21
22
23
24
25
26
27
28
29
30
31
32
33
34
35
36
37
38
39
40
41
```

98
99
100
101
102
103
104
105
106
107
108
109
110
111
112
113
114
115
116
117
118
119
120
121
122
123
124
125
126
127
128
129
130
131
132
133
134
135
136
137
138
139
140
141
142
143
144
145
146
147
@
*
ZONE NAME=DOWEL NODEATTA=YES GEOMATTA=YES
*
ACTIVEZONE
@CLEAR

```
 'DOWEL'
@
*
ACTIVEZONE
@CLEAR
 'DOWEL'
@
*
BODY CYLINDER NAME=442 OPTION=CENTERED POSITION=VECTOR,
    ORIENTAT=SYSTEM CX1=-4.50000000000000 CX2=0.00000000000000,
    CX3=0.00000000000000 SYSTEM=0 AXIS=XL RADIUS=0.625000000000000,
    LENGTH=9.00000000000000 SHEET=NO
*
BODY CYLINDER NAME=443 OPTION=CENTERED POSITION=VECTOR,
    ORIENTAT=SYSTEM CX1=0.375000000000000 CX2=0.00000000000000,
    CX3=0.00000000000000 SYSTEM=0 AXIS=XL RADIUS=0.625000000000000,
    LENGTH=0.750000000000000 SHEET=NO
*
BODY CYLINDER NAME=444 OPTION=CENTERED POSITION=VECTOR,
    ORIENTAT=SYSTEM CX1=5.25000000000000 CX2=0.00000000000000,
    CX3=0.00000000000000 SYSTEM=0 AXIS=XL RADIUS=0.625000000000000,
    LENGTH=9.00000000000000 SHEET=NO
*
BODY SHEET NAME=445 DELETE-L=YES OPTION=POLYGON SYSTEM=0
@CLEAR
1499
1500
1506
1505
@
*
BODY SUBTRACT NAME=442 KEEP-TOO=YES KEEP-IMP=NO
@CLEAR
445
@
*
BODY SUBTRACT NAME=443 KEEP-TOO=YES KEEP-IMP=NO
@CLEAR
445
@
*
BODY SUBTRACT NAME=444 KEEP-TOO=NO KEEP-IMP=NO
@CLEAR
445
@
*
DELETE BODY FIRST=448 LAST=448
*
DELETE BODY FIRST=447 LAST=447
*
DELETE BODY FIRST=446 LAST=446
*
BODY SHEET NAME=445 DELETE-L=YES OPTION=YPLANE,
    OFFSET=0.00000000000000 SYSTEM=0
*
BODY SUBTRACT NAME=442 KEEP-TOO=YES KEEP-IMP=NO
```

```
@CLEAR
445
@
*
BODY SUBTRACT NAME=443 KEEP-TOO=YES KEEP-IMP=NO
@CLEAR
445
@
*
BODY SUBTRACT NAME=444 KEEP-TOO=NO KEEP-IMP=NO
@CLEAR
445
@
*
DELETE BODY FIRST=448 LAST=448
*
DELETE BODY FIRST=447 LAST=447
*
DELETE BODY FIRST=446 LAST=446
*
SUBDIVIDE EDGE NAME=4 BODY=442 MODE=DIVISIONS NDIV=2,
   RATIO=1.00000000000000 PROGRESS=ARITHMETIC BLTABLE=0
@CLEAR
7
3
5
@
*
SUBDIVIDE EDGE NAME=8 BODY=442 MODE=DIVISIONS NDIV=3,
   RATIO=1.00000000000000 PROGRESS=ARITHMETIC BLTABLE=0
@CLEAR
2
9
@
*
SUBDIVIDE EDGE NAME=1 BODY=442 MODE=DIVISIONS NDIV=4,
   RATIO=1.00000000000000 PROGRESS=ARITHMETIC BLTABLE=0
@CLEAR
6
@
*
SUBDIVIDE EDGE NAME=4 BODY=443 MODE=DIVISIONS NDIV=2,
   RATIO=1.00000000000000 PROGRESS=ARITHMETIC BLTABLE=0
@CLEAR
7
3
5
@
*
SUBDIVIDE EDGE NAME=1 BODY=443 MODE=DIVISIONS NDIV=4,
   RATIO=1.00000000000000 PROGRESS=ARITHMETIC BLTABLE=0
@CLEAR
6
@
*
SUBDIVIDE EDGE NAME=4 BODY=444 MODE=DIVISIONS NDIV=2,
```

```
   RATIO=1.00000000000000 PROGRESS=ARITHMETIC BLTABLE=0
@CLEAR
7
3
5
@
*
SUBDIVIDE EDGE NAME=8 BODY=444 MODE=DIVISIONS NDIV=3,
   RATIO=1.00000000000000 PROGRESS=ARITHMETIC BLTABLE=0
@CLEAR
2
9
@
*
SUBDIVIDE EDGE NAME=1 BODY=444 MODE=DIVISIONS NDIV=4,
   RATIO=1.00000000000000 PROGRESS=ARITHMETIC BLTABLE=0
@CLEAR
6
@
*
BODY TRANSFORMED NAME=445 OPTION=COPY PARENT=442 TRANSFOR=1 NCOPY=3,
   MESH=NO EGROUP=0 NCOINCID=NO NTOLERAN=1.00000000000000E-05
@CLEAR
443
444
@
*
BODY TRANSFORMED NAME=454 OPTION=COPY PARENT=442 TRANSFOR=2 NCOPY=11,
   MESH=NO EGROUP=0 NCOINCID=NO NTOLERAN=1.00000000000000E-05
@CLEAR
443
444
445
446
447
448
449
450
451
452
453
@
*
BODY TRANSFORMED NAME=586 OPTION=COPY PARENT=442 TRANSFOR=4 NCOPY=1,
   MESH=NO EGROUP=0 NCOINCID=NO NTOLERAN=1.00000000000000E-05
@CLEAR
444
445
446
447
448
449
450
451
452
453
```

```
443
@
*
BODY TRANSFORMED NAME=598 OPTION=COPY PARENT=586 TRANSFOR=2 NCOPY=11,
   MESH=NO EGROUP=0 NCOINCID=NO NTOLERAN=1.00000000000000E-05
@CLEAR
588
589
590
591
592
593
594
595
596
597
587
@
*
ACTIVEZONE
@CLEAR
@
*
CGROUP CONTACT3 NAME=1 FORCES=YES TRACTION=YES NODETONO=NO,
   FRICTION=0.00000000000000 EPSN=1.00000000000000E-12,
   EPST=0.00000000000000 DIRECTIO=NORMAL CONTINUO=YES,
   INITIAL-=ALLOWED PENETRAT=ONE DEPTH=0.00000000000000,
   OFFSET=0.00000000000000 OFFSET-T=CONSTANT CORNER-C=NO,
   TBIRTH=0.00000000000000 TDEATH=0.00000000000000 TIED=NO,
   TIED-OFF=0.00000000000000 HHATTMC=0.00000000000000,
   FCTMC=0.500000000000000 FTTMC=0.500000000000000 RIGID-TA=NO,
   NORMAL-S=1.00000000000000E+11 TANGENTI=0.00000000000000,
   PTOLERAN=1.00000000000000E-08 RESIDUAL=0.00100000000000000,
   LIMIT-FO=1.00000000000000 ITERATIO=2 TIME-PEN=0.00000000000000,
   CONSISTE=DEFAULT USER-FRI=NO DESCRIPT='NONE',
   CFACTOR1=0.00000000000000 CS-EXTEN=0.00100000000000000,
   ALGORITH=DEFAULT RTP-CHEC=NO RTP-MAX=0.00100000000000000,
   XDAMP=NO XNDAMP=0.100000000000000 SLIDING-=1.00000000000000E-10,
   TENSILE-=0.00100000000000000 OSCILLAT=5,
   GAP-BIAS=0.00000000000000 OFFSET-D=AUTOMATIC DISPLACE=DEFAULT,
   FRIC-DEL=NO GAP-VALU=0.00000000000000 TENS-CON=YES FREE-OVE=NO,
   GAP-PUSH=0.00000000000000 EKTMC=0.00000000000000
*
CONTACTSURFA NAME=1 PRINT=DEFAULT SAVE=DEFAULT SOLID=MULT BODY=1,
   ORIENTAT=AUTOMATIC MARQUEEB=0 DESCRIPT='NONE'
@CLEAR
2 1 1
2 1 2
2 1 3
2 1 4
2 1 7
2 1 40
2 1 29
2 1 18
2 1 8
2 1 41
```

```
2 1 30
2 1 19
2 1 9
2 1 42
2 1 31
2 1 20
2 1 10
2 1 43
2 1 32
2 1 21
2 1 11
2 1 44
2 1 33
2 1 22
2 1 12
2 1 45
2 1 34
2 1 23
2 1 13
2 1 46
2 1 35
2 1 24
2 1 14
2 1 47
2 1 36
2 1 25
2 1 15
2 1 48
2 1 37
2 1 26
2 1 16
2 1 49
2 1 38
2 1 27
2 1 17
2 1 50
2 1 39
2 1 28
6 1 145
@
*
CONTACTSURFA NAME=2 PRINT=DEFAULT SAVE=DEFAULT SOLID=MULT BODY=1,
   ORIENTAT=AUTOMATIC MARQUEEB=0 DESCRIPT='NONE'
@CLEAR
2 1 148
2 1 149
2 1 150
2 1 151
2 1 154
2 1 165
2 1 176
2 1 187
2 1 155
2 1 166
2 1 177
2 1 188
```

```
2 1 156
2 1 167
2 1 178
2 1 189
2 1 157
2 1 168
2 1 179
2 1 190
2 1 158
2 1 169
2 1 180
2 1 191
2 1 159
2 1 170
2 1 181
2 1 192
2 1 160
2 1 171
2 1 182
2 1 193
2 1 161
2 1 172
2 1 183
2 1 194
2 1 162
2 1 173
2 1 184
2 1 195
2 1 163
2 1 174
2 1 185
2 1 196
2 1 164
2 1 175
2 1 186
2 1 197
6 1 292
@
*
CONTACTSURFA NAME=3 PRINT=DEFAULT SAVE=DEFAULT SOLID=MULT BODY=1,
   ORIENTAT=AUTOMATIC MARQUEEB=0 DESCRIPT='NONE'
@CLEAR
1 1 445
1 1 446
1 1 447
1 1 442
1 1 498
1 1 509
1 1 454
1 1 487
1 1 499
1 1 510
1 1 455
1 1 488
1 1 500
1 1 511
```

1 1 456
1 1 489
1 1 501
1 1 512
1 1 457
1 1 490
1 1 502
1 1 513
1 1 458
1 1 491
1 1 503
1 1 514
1 1 459
1 1 492
1 1 504
1 1 515
1 1 460
1 1 493
1 1 505
1 1 516
1 1 461
1 1 494
1 1 506
1 1 517
1 1 462
1 1 495
1 1 507
1 1 518
1 1 463
1 1 496
1 1 508
1 1 519
1 1 464
1 1 497
2 1 445
2 1 446
2 1 447
2 1 442
2 1 498
2 1 509
2 1 454
2 1 487
2 1 499
2 1 510
2 1 455
2 1 488
2 1 500
2 1 511
2 1 456
2 1 489
2 1 501
2 1 512
2 1 457
2 1 490
2 1 502
2 1 513

```
2 1 458
2 1 491
2 1 503
2 1 514
2 1 459
2 1 492
2 1 504
2 1 515
2 1 460
2 1 493
2 1 505
2 1 516
2 1 461
2 1 494
2 1 506
2 1 517
2 1 462
2 1 495
2 1 507
2 1 518
2 1 463
2 1 496
2 1 508
2 1 519
2 1 464
2 1 497
@
*
CONTACTSURFA NAME=4 PRINT=DEFAULT SAVE=DEFAULT SOLID=MULT BODY=1,
   ORIENTAT=AUTOMATIC MARQUEEB=0 DESCRIPT='NONE'
@CLEAR
1 1 586
1 1 588
1 1 589
1 1 590
1 1 598
1 1 609
1 1 620
1 1 631
1 1 599
1 1 610
1 1 621
1 1 632
1 1 600
1 1 611
1 1 622
1 1 633
1 1 601
1 1 612
1 1 623
1 1 634
1 1 602
1 1 613
1 1 624
1 1 635
1 1 603
```

1 1 614
1 1 625
1 1 636
1 1 604
1 1 615
1 1 626
1 1 637
1 1 605
1 1 616
1 1 627
1 1 638
1 1 606
1 1 617
1 1 628
1 1 639
1 1 607
1 1 618
1 1 629
1 1 640
1 1 608
1 1 619
1 1 630
1 1 641
2 1 586
2 1 588
2 1 589
2 1 590
2 1 598
2 1 609
2 1 620
2 1 631
2 1 599
2 1 610
2 1 621
2 1 632
2 1 600
2 1 611
2 1 622
2 1 633
2 1 601
2 1 612
2 1 623
2 1 634
2 1 602
2 1 613
2 1 624
2 1 635
2 1 603
2 1 614
2 1 625
2 1 636
2 1 604
2 1 615
2 1 626
2 1 637
2 1 605

```
2 1 616
2 1 627
2 1 638
2 1 606
2 1 617
2 1 628
2 1 639
2 1 607
2 1 618
2 1 629
2 1 640
2 1 608
2 1 619
2 1 630
2 1 641
@
*
*Comment 3 (Coefficient of friction during dowel sliding)
*
CONTACTPAIR NAME=1 TARGET=1 CONTACTO=3 FRICTION=0.00000000000000,
    TBIRTH=0.00000000000000 TDEATH=0.00000000000000,
    HHATTMC=0.00000000000000 FCTMC=0.00000000000000,
    FTTMC=0.00000000000000 NX=0 NY=0 NZ=0 OFFSETCO=BOTH,
    EKTMC=0.00000000000000
*
CONTACTPAIR NAME=2 TARGET=2 CONTACTO=4 FRICTION=0.00000000000000,
    TBIRTH=0.00000000000000 TDEATH=0.00000000000000,
    HHATTMC=0.00000000000000 FCTMC=0.00000000000000,
    FTTMC=0.00000000000000 NX=0 NY=0 NZ=0 OFFSETCO=BOTH,
    EKTMC=0.00000000000000
*
*Comment 6 (Dowel bar properties) - Length units are in inches
*
MATERIAL ELASTIC NAME=2 E=2.90000000000000E+07 NU=0.300000000000000,
    DENSITY=0.00000000000000 ALPHA=0.00000000000000 MDESCRIP='dowel'
*
EGROUP THREEDSOLID NAME=6 DISPLACE=DEFAULT STRAINS=DEFAULT MATERIAL=2,
    RSINT=DEFAULT TINT=DEFAULT RESULTS=STRESSES DEGEN=DEFAUL,
    FORMULAT=0 STRESSRE=GLOBAL INITIALS=NONE FRACTUR=NO,
    CMASS=DEFAULT STRAIN-F=0 UL-FORMU=DEFAULT LVUS1=0 LVUS2=0 SED=NO,
    RUPTURE=ADINA INCOMPAT=DEFAULT TIME-OFF=0.00000000000000,
    POROUS=NO WTMC=1.00000000000000 OPTION=NONE DESCRIPT='NONE',
    PRINT=DEFAULT SAVE=DEFAULT TBIRTH=0.00000000000000,
    TDEATH=0.00000000000000 TMC-MATE=1 RUPTURE-=0 EM=NO JOULE=NO,
    BOLT-NUM=0 BOLT-PLA=0 BOLT-LOA=0.00000000000000,
    BOLT-TOL=0.00000000000000
*
GBODY NODES=8 NCOINCID=BOUNDARIES NCTOLERA=1.00000000000000E-05,
    SUBSTRUC=0 GROUP=6 PREFSHAP=AUTOMATIC COLLAPSE=NO SIZE-FUN=0,
    DELETE-S=NO ANGLE-MI=5.00000000000000 MIDNODES=CURVED,
    METHOD=DELAUNAY PATTERN=0 MESHING=MAPPED DEGENERA=NO,
    BOUNDARY=ADVFRONT DEG-EDGE=0 GEO-ERRO=0.00000000000000,
    SAMPLING=20 MIN-SIZE=0.00000000000000 NLAYER=1 NLTABL=0,
    AUTO-GRA=NO SIMULATE=NO PYRAMIDS=NO DANGMAXB=80.0000000000000,
    DANGMAXC=60.0000000000000 DANGMAXD=80.0000000000000 HEXALAYE=NO,
    AUTO-REF=YES EVEN=SUM DENSITY=1.20000000000000 MIDFACEN=QUAD,
```

REFINE=ALONG-EDGE GRID=NO BREFINE=ALONG-EDGE BLTABL=0,
PREFSHA2=QUADRILATERAL NOPTI=1
@CLEAR
449 0
450 0
443 0
448 0
452 0
453 0
451 0
444 0
531 0
542 0
465 0
520 0
564 0
575 0
476 0
553 0
532 0
543 0
466 0
521 0
565 0
576 0
477 0
554 0
533 0
544 0
467 0
522 0
566 0
577 0
478 0
555 0
534 0
545 0
468 0
523 0
567 0
578 0
479 0
556 0
535 0
546 0
469 0
524 0
568 0
579 0
480 0
557 0
536 0
547 0
470 0
525 0
569 0

580 0
481 0
558 0
537 0
548 0
471 0
526 0
570 0
581 0
482 0
559 0
538 0
549 0
472 0
527 0
571 0
582 0
483 0
560 0
539 0
550 0
473 0
528 0
572 0
583 0
484 0
561 0
540 0
551 0
474 0
529 0
573 0
584 0
485 0
562 0
541 0
552 0
475 0
530 0
574 0
585 0
486 0
563 0
@
*
GBODY NODES=8 NCOINCID=BOUNDARIES NCTOLERA=1.00000000000000E-05,
SUBSTRUC=0 GROUP=6 PREFSHAP=AUTOMATIC COLLAPSE=NO SIZE-FUN=0,
DELETE-S=NO ANGLE-MI=5.00000000000000 MIDNODES=CURVED,
METHOD=DELAUNAY PATTERN=0 MESHING=MAPPED DEGENERA=NO,
BOUNDARY=ADVFRONT DEG-EDGE=0 GEO-ERRO=0.00000000000000,
SAMPLING=20 MIN-SIZE=0.00000000000000 NLAYER=1 NLTABL=0,
AUTO-GRA=NO SIMULATE=NO PYRAMIDS=NO DANGMAXB=80.0000000000000,
DANGMAXC=60.0000000000000 DANGMAXD=80.0000000000000 HEXALAYE=NO,
AUTO-REF=YES EVEN=SUM DENSITY=1.20000000000000 MIDFACEN=QUAD,
REFINE=ALONG-EDGE GRID=NO BREFINE=ALONG-EDGE BLTABL=0,
PREFSHA2=QUADRILATERAL NOPTI=1

@CLEAR
591 0
592 0
593 0
597 0
587 0
594 0
595 0
596 0
642 0
653 0
664 0
708 0
675 0
686 0
697 0
719 0
643 0
654 0
665 0
709 0
676 0
687 0
698 0
720 0
644 0
655 0
666 0
710 0
677 0
688 0
699 0
721 0
645 0
656 0
667 0
711 0
678 0
689 0
700 0
722 0
646 0
657 0
668 0
712 0
679 0
690 0
701 0
723 0
647 0
658 0
669 0
713 0
680 0
691 0
702 0

724 0
648 0
659 0
670 0
714 0
681 0
692 0
703 0
725 0
649 0
660 0
671 0
715 0
682 0
693 0
704 0
726 0
650 0
661 0
672 0
716 0
683 0
694 0
705 0
727 0
651 0
662 0
673 0
717 0
684 0
695 0
706 0
728 0
652 0
663 0
674 0
718 0
685 0
696 0
707 0
729 0
@
*
GBODY NODES=8 NCOINCID=GROUP NCTOLERA=1.00000000000000E-05 SUBSTRUC=0,
GROUP=6 PREFSHAP=AUTOMATIC COLLAPSE=NO SIZE-FUN=0 DELETE-S=NO,
ANGLE-MI=5.00000000000000 MIDNODES=CURVED METHOD=DELAUNAY,
PATTERN=0 MESHING=MAPPED DEGENERA=NO BOUNDARY=ADVFRONT,
DEG-EDGE=0 GEO-ERRO=0.00000000000000 SAMPLING=20,
MIN-SIZE=0.00000000000000 NLAYER=1 NLTABL=0 AUTO-GRA=NO,
SIMULATE=NO PYRAMIDS=NO DANGMAXB=80.0000000000000,
DANGMAXC=60.0000000000000 DANGMAXD=80.0000000000000 HEXALAYE=NO,
AUTO-REF=YES EVEN=SUM DENSITY=1.20000000000000 MIDFACEN=QUAD,
REFINE=ALONG-EDGE GRID=NO BREFINE=ALONG-EDGE BLTABL=0,
PREFSHA2=QUADRILATERAL NOPTI=1
@CLEAR
445 0

446 0
447 0
442 0
498 0
509 0
454 0
487 0
499 0
510 0
455 0
488 0
500 0
511 0
456 0
489 0
501 0
512 0
457 0
490 0
502 0
513 0
458 0
491 0
503 0
514 0
459 0
492 0
504 0
515 0
460 0
493 0
505 0
516 0
461 0
494 0
506 0
517 0
462 0
495 0
507 0
518 0
463 0
496 0
508 0
519 0
464 0
497 0
@
*
GBODY NODES=8 NCOINCID=GROUP NCTOLERA=1.00000000000000E-05 SUBSTRUC=0,
GROUP=6 PREFSHAP=AUTOMATIC COLLAPSE=NO SIZE-FUN=0 DELETE-S=NO,
ANGLE-MI=5.00000000000000 MIDNODES=CURVED METHOD=DELAUNAY,
PATTERN=0 MESHING=MAPPED DEGENERA=NO BOUNDARY=ADVFRONT,
DEG-EDGE=0 GEO-ERRO=0.00000000000000 SAMPLING=20,
MIN-SIZE=0.00000000000000 NLAYER=1 NLTABL=0 AUTO-GRA=NO,
SIMULATE=NO PYRAMIDS=NO DANGMAXB=80.0000000000000,

```
    DANGMAXC=60.0000000000000 DANGMAXD=80.0000000000000 HEXALAYE=NO,
    AUTO-REF=YES EVEN=SUM DENSITY=1.20000000000000 MIDFACEN=QUAD,
    REFINE=ALONG-EDGE GRID=NO BREFINE=ALONG-EDGE BLTABL=0,
    PREFSHA2=QUADRILATERAL NOPTI=1
@CLEAR
586 0
588 0
589 0
590 0
598 0
609 0
620 0
631 0
599 0
610 0
621 0
632 0
600 0
611 0
622 0
633 0
601 0
612 0
623 0
634 0
602 0
613 0
624 0
635 0
603 0
614 0
625 0
636 0
604 0
615 0
626 0
637 0
605 0
616 0
627 0
638 0
606 0
617 0
628 0
639 0
607 0
618 0
629 0
640 0
608 0
619 0
630 0
641 0
@
*
*Comment 5 (Subgrade dimension) - Length units are in inches
```

```
*
BODY BLOCK NAME=730 OPTION=CENTERED POSITION=VECTOR ORIENTAT=SYSTEM,
   CX1=-90.0000000000000 CX2=66.0000000000000 CX3=-55.0000000000000,
   SYSTEM=0 DX1=180.000000000000 DX2=144.000000000000,
   DX3=100.000000000000
*
SUBDIVIDE EDGE NAME=5 BODY=730 MODE=DIVISIONS NDIV=10,
   RATIO=0.100000000000000 PROGRESS=ARITHMETIC BLTABLE=0
@CLEAR
6
7
8
@
*
SUBDIVIDE EDGE NAME=1 BODY=730 MODE=DIVISIONS NDIV=36,
   RATIO=1.00000000000000 PROGRESS=ARITHMETIC BLTABLE=0
@CLEAR
3
9
11
@
*
SUBDIVIDE EDGE NAME=12 BODY=730 MODE=DIVISIONS NDIV=60,
   RATIO=1.00000000000000 PROGRESS=ARITHMETIC BLTABLE=0
@CLEAR
10
4
2
@
*
BODY BLOCK NAME=731 OPTION=CENTERED POSITION=VECTOR ORIENTAT=SYSTEM,
   CX1=90.7500000000000 CX2=66.0000000000000 CX3=-55.0000000000000,
   SYSTEM=0 DX1=180.000000000000 DX2=144.000000000000,
   DX3=100.000000000000
*
SUBDIVIDE EDGE NAME=5 BODY=731 MODE=DIVISIONS NDIV=10,
   RATIO=0.100000000000000 PROGRESS=ARITHMETIC BLTABLE=0
@CLEAR
6
7
8
@
*
SUBDIVIDE EDGE NAME=1 BODY=731 MODE=DIVISIONS NDIV=36,
   RATIO=1.00000000000000 PROGRESS=ARITHMETIC BLTABLE=0
@CLEAR
3
9
11
@
*
SUBDIVIDE EDGE NAME=12 BODY=731 MODE=DIVISIONS NDIV=60,
   RATIO=1.00000000000000 PROGRESS=ARITHMETIC BLTABLE=0
@CLEAR
10
4
```

```
2
@
*
BODY BLOCK NAME=732 OPTION=CENTERED POSITION=VECTOR ORIENTAT=SYSTEM,
   CX1=-270.750000000000 CX2=66.0000000000000 CX3=-55.0000000000000,
   SYSTEM=0 DX1=180.000000000000 DX2=144.000000000000,
   DX3=100.000000000000
*
SUBDIVIDE EDGE NAME=5 BODY=732 MODE=DIVISIONS NDIV=10,
   RATIO=0.100000000000000 PROGRESS=ARITHMETIC BLTABLE=0
@CLEAR
6
7
8
@
*
SUBDIVIDE EDGE NAME=1 BODY=732 MODE=DIVISIONS NDIV=36,
   RATIO=1.00000000000000 PROGRESS=ARITHMETIC BLTABLE=0
@CLEAR
3
9
11
@
*
SUBDIVIDE EDGE NAME=12 BODY=732 MODE=DIVISIONS NDIV=60,
   RATIO=1.00000000000000 PROGRESS=ARITHMETIC BLTABLE=0
@CLEAR
10
4
2
@
*
BODY BLOCK NAME=733 OPTION=CENTERED POSITION=VECTOR ORIENTAT=SYSTEM,
   CX1=-180.375000000000 CX2=66.0000000000000 CX3=-55.0000000000000,
   SYSTEM=0 DX1=0.750000000000000 DX2=144.000000000000,
   DX3=100.000000000000
*
SUBDIVIDE EDGE NAME=5 BODY=733 MODE=DIVISIONS NDIV=10,
   RATIO=0.100000000000000 PROGRESS=ARITHMETIC BLTABLE=0
@CLEAR
6
7
8
@
*
SUBDIVIDE EDGE NAME=1 BODY=733 MODE=DIVISIONS NDIV=36,
   RATIO=1.00000000000000 PROGRESS=ARITHMETIC BLTABLE=0
@CLEAR
3
9
11
@
*
BODY BLOCK NAME=734 OPTION=CENTERED POSITION=VECTOR ORIENTAT=SYSTEM,
   CX1=0.375000000000000 CX2=66.0000000000000 CX3=-55.0000000000000,
   SYSTEM=0 DX1=0.750000000000000 DX2=144.000000000000,
```

```
   DX3=100.000000000000
*
SUBDIVIDE EDGE NAME=5 BODY=734 MODE=DIVISIONS NDIV=10,
   RATIO=0.100000000000000 PROGRESS=ARITHMETIC BLTABLE=0
@CLEAR
6
7
8
@
*
SUBDIVIDE EDGE NAME=1 BODY=734 MODE=DIVISIONS NDIV=36,
   RATIO=1.00000000000000 PROGRESS=ARITHMETIC BLTABLE=0
@CLEAR
3
9
11
@
*
CGROUP CONTACT3 NAME=2 FORCES=YES TRACTION=YES NODETONO=NO,
   FRICTION=0.00000000000000 EPSN=1.00000000000000E-12,
   EPST=0.00000000000000 DIRECTIO=NORMAL CONTINUO=YES,
   INITIAL-=ALLOWED PENETRAT=ONE DEPTH=0.00000000000000,
   OFFSET=0.00000000000000 OFFSET-T=CONSTANT CORNER-C=NO,
   TBIRTH=0.00000000000000 TDEATH=0.00000000000000 TIED=NO,
   TIED-OFF=0.00000000000000 HHATTMC=0.00000000000000,
   FCTMC=0.500000000000000 FTTMC=0.500000000000000 RIGID-TA=NO,
   NORMAL-S=1.00000000000000E+11 TANGENTI=0.00000000000000,
   PTOLERAN=1.00000000000000E-08 RESIDUAL=0.00100000000000000,
   LIMIT-FO=1.00000000000000 ITERATIO=2 TIME-PEN=0.00000000000000,
   CONSISTE=DEFAULT USER-FRI=NO DESCRIPT='NONE',
   CFACTOR1=0.00000000000000 CS-EXTEN=0.00100000000000000,
   ALGORITH=DEFAULT RTP-CHEC=NO RTP-MAX=0.00100000000000000,
   XDAMP=NO XNDAMP=0.100000000000000 SLIDING-=1.00000000000000E-10,
   TENSILE-=0.00100000000000000 OSCILLAT=5,
   GAP-BIAS=0.00000000000000 OFFSET-D=AUTOMATIC DISPLACE=DEFAULT,
   FRIC-DEL=NO GAP-VALU=0.00000000000000 TENS-CON=YES FREE-OVE=NO,
   GAP-PUSH=0.00000000000000 EKTMC=0.00000000000000
*
CONTACTSURFA NAME=5 PRINT=DEFAULT SAVE=DEFAULT SOLID=MULT BODY=0,
   ORIENTAT=AUTOMATIC MARQUEEB=0 DESCRIPT='NONE'
@CLEAR
5 1 147
5 1 294
5 1 441
@
*
CONTACTSURFA NAME=6 PRINT=DEFAULT SAVE=DEFAULT SOLID=MULT BODY=0,
   ORIENTAT=AUTOMATIC MARQUEEB=0 DESCRIPT='NONE'
@CLEAR
1 1 730
1 1 731
1 1 732
1 1 733
1 1 734
@
*
```

```
*Comment 10 (Interface condition)
*
CONTACTPAIR NAME=2 TARGET=5 CONTACTO=6 FRICTION=0.00000000000000,
    TBIRTH=0.00000000000000 TDEATH=0.00000000000000,
    HHATTMC=0.00000000000000 FCTMC=0.00000000000000,
    FTTMC=0.00000000000000 NX=0 NY=0 NZ=0 OFFSETCO=BOTH,
    EKTMC=0.00000000000000
*
*Comment 8 (Subgrade properties) - Unit: E (psi), ν (unitless)
*
MATERIAL ELASTIC NAME=3 E=19000.0000000000 NU=0.350000000000000,
    DENSITY=0.00000000000000 ALPHA=0.00000000000000 MDESCRIP=,
'subbase'
*
EGROUP THREEDSOLID NAME=7 DISPLACE=DEFAULT STRAINS=DEFAULT MATERIAL=3,
    RSINT=DEFAULT TINT=DEFAULT RESULTS=STRESSES DEGEN=DEFAUL,
    FORMULAT=0 STRESSRE=GLOBAL INITIALS=NONE FRACTUR=NO,
    CMASS=DEFAULT STRAIN-F=0 UL-FORMU=DEFAULT LVUS1=0 LVUS2=0 SED=NO,
    RUPTURE=ADINA INCOMPAT=DEFAULT TIME-OFF=0.00000000000000,
    POROUS=NO WTMC=1.00000000000000 OPTION=NONE DESCRIPT='NONE',
    PRINT=DEFAULT SAVE=DEFAULT TBIRTH=0.00000000000000,
    TDEATH=0.00000000000000 TMC-MATE=1 RUPTURE-=0 EM=NO JOULE=NO,
    BOLT-NUM=0 BOLT-PLA=0 BOLT-LOA=0.00000000000000,
    BOLT-TOL=0.00000000000000
*
GBODY NODES=8 NCOINCID=GROUP NCTOLERA=1.00000000000000E-05 SUBSTRUC=0,
    GROUP=7 PREFSHAP=AUTOMATIC COLLAPSE=NO SIZE-FUN=0 DELETE-S=NO,
    ANGLE-MI=5.00000000000000 MIDNODES=CURVED METHOD=DELAUNAY,
    PATTERN=0 MESHING=MAPPED DEGENERA=NO BOUNDARY=ADVFRONT,
    DEG-EDGE=0 GEO-ERRO=0.00000000000000 SAMPLING=20,
    MIN-SIZE=0.00000000000000 NLAYER=1 NLTABL=0 AUTO-GRA=NO,
    SIMULATE=NO PYRAMIDS=NO DANGMAXB=80.0000000000000,
    DANGMAXC=60.0000000000000 DANGMAXD=80.0000000000000 HEXALAYE=NO,
    AUTO-REF=YES EVEN=SUM DENSITY=1.20000000000000 MIDFACEN=QUAD,
    REFINE=ALONG-EDGE GRID=NO BREFINE=ALONG-EDGE BLTABL=0,
    PREFSHA2=QUADRILATERAL NOPTI=1
@CLEAR
730 0
731 0
732 0
733 0
734 0
@
*
*Comment 9 (Interface condition) - Spring stiffness (lbf/in)
*
PROPERTY NONLINEAR-K NAME=1 RUPTURE=NO
@CLEAR
-1.00000000000000 -4800.00000000000
0.00000000000000 0.00000000000000
1.00000000000000 0.0100000000000000
@
*
PROPERTYSET NAME=1 K=0.00000000000000 M=0.00000000000000,
    C=0.00000000000000 NONLINEA=YES NK=1 NM=0 NC=0
*
```

```
EGROUP SPRING NAME=5 PROPERTY=1 RESULTS=FORCES NONLINEA=NO,
    SKEWSYST=NO OPTION=NONE DESCRIPT='NONE' PRINT=DEFAULT,
    SAVE=DEFAULT TBIRTH=0.00000000000000 TDEATH=0.00000000000000,
    6DOF-SPR=NO
*
ENODES SUBSTRUC=0 GROUP=5 NNODES=32
1 13317 3 51136 3
2 13318 3 51137 3
3 13319 3 51138 3
4 13320 3 51139 3
5 13321 3 51140 3
6 13322 3 51141 3
7 13323 3 51142 3
8 13324 3 51143 3
9 13325 3 51144 3
10 13326 3 51145 3
11 13327 3 51146 3
12 13328 3 51147 3
13 13329 3 51148 3
14 13330 3 51149 3
15 13331 3 51150 3
16 13332 3 51151 3
17 13333 3 51152 3
18 13334 3 51153 3
19 13335 3 51154 3
20 13336 3 51155 3
21 13337 3 51156 3
22 13338 3 51157 3
23 13339 3 51158 3
24 13340 3 51159 3
25 13341 3 51160 3
26 13342 3 51161 3
27 13343 3 51162 3
28 13344 3 51163 3
29 13345 3 51164 3
30 13346 3 51165 3
31 13347 3 51166 3
32 13348 3 51167 3
33 13349 3 51168 3
34 13350 3 51169 3
35 13351 3 51170 3
36 13352 3 51171 3
37 13353 3 51172 3
38 13354 3 51173 3
39 13355 3 51174 3
40 13356 3 51175 3
41 13357 3 51176 3
42 13358 3 51177 3
43 13359 3 51178 3
44 13360 3 51179 3
45 13361 3 51180 3
46 13362 3 51181 3
47 13363 3 51182 3
48 13364 3 51183 3
49 13365 3 51184 3
50 13366 3 51185 3
```

51 13367 3 51186 3
52 13368 3 51187 3
53 13369 3 51188 3
54 13370 3 51189 3
55 13371 3 51190 3
56 13372 3 51191 3
57 13373 3 51192 3
58 13374 3 51193 3
59 13375 3 51194 3
60 13376 3 51195 3
61 13377 3 51196 3
62 13378 3 51197 3
63 13379 3 51198 3
64 13380 3 51199 3
65 13381 3 51200 3
66 13382 3 51201 3
67 13383 3 51202 3
68 13384 3 51203 3
69 13385 3 51204 3
70 13386 3 51205 3
71 13387 3 51206 3
72 13388 3 51207 3
73 13389 3 51208 3
74 13390 3 51209 3
75 13391 3 51210 3
76 13392 3 51211 3
77 13393 3 51212 3
78 13394 3 51213 3
79 13395 3 51214 3
80 13396 3 51215 3
81 13397 3 51216 3
82 13398 3 51217 3
83 13399 3 51218 3
84 13400 3 51219 3
85 13401 3 51220 3
86 13402 3 51221 3
87 13403 3 51222 3
88 13404 3 51223 3
89 13405 3 51224 3
90 13406 3 51225 3
91 13407 3 51226 3
92 13408 3 51227 3
93 13409 3 51228 3
94 13410 3 51229 3
95 13411 3 51230 3
96 13412 3 51231 3
97 13413 3 51232 3
98 13414 3 51233 3
99 13415 3 51234 3
100 13416 3 51235 3
101 13417 3 51236 3
102 13418 3 51237 3
103 13419 3 51238 3
104 13420 3 51239 3
105 13421 3 51240 3
106 13422 3 51241 3

107 13423 3 51242 3
108 13424 3 51243 3
109 13425 3 51244 3
110 13426 3 51245 3
111 13427 3 51246 3
112 13428 3 51247 3
113 13429 3 51248 3
114 13430 3 51249 3
115 13431 3 51250 3
116 13432 3 51251 3
117 13433 3 51252 3
118 13434 3 51253 3
119 13435 3 51254 3
120 13436 3 51255 3
121 13437 3 51256 3
122 13438 3 51257 3
123 13439 3 51258 3
124 13440 3 51259 3
125 13441 3 51260 3
126 13442 3 51261 3
127 13443 3 51262 3
128 13444 3 51263 3
129 13445 3 51264 3
130 13446 3 51265 3
131 13447 3 51266 3
132 13448 3 51267 3
133 13449 3 51268 3
134 13450 3 51269 3
135 13451 3 51270 3
136 13452 3 51271 3
137 13453 3 51272 3
138 13454 3 51273 3
139 13455 3 51274 3
140 13456 3 51275 3
141 13457 3 51276 3
142 13458 3 51277 3
143 13459 3 51278 3
144 13460 3 51279 3
145 13461 3 51280 3
146 13462 3 51281 3
147 13463 3 51282 3
148 13464 3 51283 3
149 13465 3 51284 3
150 13466 3 51285 3
151 13467 3 51286 3
152 13468 3 51287 3
153 13469 3 51288 3
154 13470 3 51289 3
155 13471 3 51290 3
156 13472 3 51291 3
157 13473 3 51292 3
158 13474 3 51293 3
159 13475 3 51294 3
160 13476 3 51295 3
161 13477 3 51296 3
162 13478 3 51297 3

163 13479 3 51298 3
164 13480 3 51299 3
165 13481 3 51300 3
166 13482 3 51301 3
167 13483 3 51302 3
168 13484 3 51303 3
169 13485 3 51304 3
170 13486 3 51305 3
171 13487 3 51306 3
172 13488 3 51307 3
173 13489 3 51308 3
174 13490 3 51309 3
175 13491 3 51310 3
176 13492 3 51311 3
177 13493 3 51312 3
178 13494 3 51313 3
179 13495 3 51314 3
180 13496 3 51315 3
181 13497 3 51316 3
182 13498 3 51317 3
183 13499 3 51318 3
184 13500 3 51319 3
185 13501 3 51320 3
186 13502 3 51321 3
187 13503 3 51322 3
188 13504 3 51323 3
189 13505 3 51324 3
190 13506 3 51325 3
191 13507 3 51326 3
192 13508 3 51327 3
193 13509 3 51328 3
194 13510 3 51329 3
195 13511 3 51330 3
196 13512 3 51331 3
197 13513 3 51332 3
198 13514 3 51333 3
199 13515 3 51334 3
200 13516 3 51335 3
201 13517 3 51336 3
202 13518 3 51337 3
203 13519 3 51338 3
204 13520 3 51339 3
205 13521 3 51340 3
206 13522 3 51341 3
207 13523 3 51342 3
208 13524 3 51343 3
209 13525 3 51344 3
210 13526 3 51345 3
211 13527 3 51346 3
212 13528 3 51347 3
213 13529 3 51348 3
214 13530 3 51349 3
215 13531 3 51350 3
216 13532 3 51351 3
217 13533 3 51352 3
218 13534 3 51353 3

219 13535 3 51354 3
220 13536 3 51355 3
221 13537 3 51356 3
222 13538 3 51357 3
223 13539 3 51358 3
224 13540 3 51359 3
225 13541 3 51360 3
226 13542 3 51361 3
227 13543 3 51362 3
228 13544 3 51363 3
229 13545 3 51364 3
230 13546 3 51365 3
231 13547 3 51366 3
232 13548 3 51367 3
233 13549 3 51368 3
234 13550 3 51369 3
235 13551 3 51370 3
236 13552 3 51371 3
237 13553 3 51372 3
238 13554 3 51373 3
239 13555 3 51374 3
240 13556 3 51375 3
241 13557 3 51376 3
242 13558 3 51377 3
243 13559 3 51378 3
244 13560 3 51379 3
245 13561 3 51380 3
246 13562 3 51381 3
247 13563 3 51382 3
248 13564 3 51383 3
249 13565 3 51384 3
250 13566 3 51385 3
251 13567 3 51386 3
252 13568 3 51387 3
253 13569 3 51388 3
254 13570 3 51389 3
255 13571 3 51390 3
256 13572 3 51391 3
257 13573 3 51392 3
258 13574 3 51393 3
259 13575 3 51394 3
260 13576 3 51395 3
261 13577 3 51396 3
262 13578 3 51397 3
263 13579 3 51398 3
264 13580 3 51399 3
265 13581 3 51400 3
266 13582 3 51401 3
267 13583 3 51402 3
268 13584 3 51403 3
269 13585 3 51404 3
270 13586 3 51405 3
271 13587 3 51406 3
272 13588 3 51407 3
273 13589 3 51408 3
274 13590 3 51409 3

275 13591 3 51410 3
276 13592 3 51411 3
277 13593 3 51412 3
278 13594 3 51413 3
279 13595 3 51414 3
280 13596 3 51415 3
281 13597 3 51416 3
282 13598 3 51417 3
283 13599 3 51418 3
284 13600 3 51419 3
285 13601 3 51420 3
286 13602 3 51421 3
287 13603 3 51422 3
288 13604 3 51423 3
289 13605 3 51424 3
290 13606 3 51425 3
291 13607 3 51426 3
292 13608 3 51427 3
293 13609 3 51428 3
294 13610 3 51429 3
295 13611 3 51430 3
296 13612 3 51431 3
297 13613 3 51432 3
298 13614 3 51433 3
299 13615 3 51434 3
300 13616 3 51435 3
301 13617 3 51436 3
302 13618 3 51437 3
303 13619 3 51438 3
304 13620 3 51439 3
305 13621 3 51440 3
306 13622 3 51441 3
307 13623 3 51442 3
308 13624 3 51443 3
309 13625 3 51444 3
310 13626 3 51445 3
311 13627 3 51446 3
312 13628 3 51447 3
313 13629 3 51448 3
314 13630 3 51449 3
315 13631 3 51450 3
316 13632 3 51451 3
317 13633 3 51452 3
318 13634 3 51453 3
319 13635 3 51454 3
320 13636 3 51455 3
321 13637 3 51456 3
322 13638 3 51457 3
323 13639 3 51458 3
324 13640 3 51459 3
325 13641 3 51460 3
326 13642 3 51461 3
327 13643 3 51462 3
328 13644 3 51463 3
329 13645 3 51464 3
330 13646 3 51465 3

331 13647 3 51466 3
332 13648 3 51467 3
333 13649 3 51468 3
334 13650 3 51469 3
335 13651 3 51470 3
336 13652 3 51471 3
337 13653 3 51472 3
338 13654 3 51473 3
339 13655 3 51474 3
340 13656 3 51475 3
341 13657 3 51476 3
342 13658 3 51477 3
343 13659 3 51478 3
344 13660 3 51479 3
345 13661 3 51480 3
346 13662 3 51481 3
347 13663 3 51482 3
348 13664 3 51483 3
349 13665 3 51484 3
350 13666 3 51485 3
351 13667 3 51486 3
352 13668 3 51487 3
353 13669 3 51488 3
354 13670 3 51489 3
355 13671 3 51490 3
356 13672 3 51491 3
357 13673 3 51492 3
358 13674 3 51493 3
359 13675 3 51494 3
360 13676 3 51495 3
361 13677 3 51496 3
362 13678 3 51497 3
363 13679 3 51498 3
364 13680 3 51499 3
365 13681 3 51500 3
366 13682 3 51501 3
367 13683 3 51502 3
368 13684 3 51503 3
369 13685 3 51504 3
370 13686 3 51505 3
371 13687 3 51506 3
372 13688 3 51507 3
373 13689 3 51508 3
374 13690 3 51509 3
375 13691 3 51510 3
376 13692 3 51511 3
377 13693 3 51512 3
378 13694 3 51513 3
379 13695 3 51514 3
380 13696 3 51515 3
381 13697 3 51516 3
382 13698 3 51517 3
383 13699 3 51518 3
384 13700 3 51519 3
385 13701 3 51520 3
386 13702 3 51521 3

387 13703 3 51522 3
388 13704 3 51523 3
389 13705 3 51524 3
390 13706 3 51525 3
391 13707 3 51526 3
392 13708 3 51527 3
393 13709 3 51528 3
394 13710 3 51529 3
395 13711 3 51530 3
396 13712 3 51531 3
397 13713 3 51532 3
398 13714 3 51533 3
399 13715 3 51534 3
400 13716 3 51535 3
401 13717 3 51536 3
402 13718 3 51537 3
403 13719 3 51538 3
404 13720 3 51539 3
405 13721 3 51540 3
406 13722 3 51541 3
407 13723 3 51542 3
408 13724 3 51543 3
409 13725 3 51544 3
410 13726 3 51545 3
411 13727 3 51546 3
412 13728 3 51547 3
413 13729 3 51548 3
414 13730 3 51549 3
415 13731 3 51550 3
416 13732 3 51551 3
417 13733 3 51552 3
418 13734 3 51553 3
419 13735 3 51554 3
420 13736 3 51555 3
421 13737 3 51556 3
422 13738 3 51557 3
423 13739 3 51558 3
424 13740 3 51559 3
425 13741 3 51560 3
426 13742 3 51561 3
427 13743 3 51562 3
428 13744 3 51563 3
429 13745 3 51564 3
430 13746 3 51565 3
431 13747 3 51566 3
432 13748 3 51567 3
433 13749 3 51568 3
434 13750 3 51569 3
435 13751 3 51570 3
436 13752 3 51571 3
437 13753 3 51572 3
438 13754 3 51573 3
439 13755 3 51574 3
440 13756 3 51575 3
441 13757 3 51576 3
442 13758 3 51577 3

443 13759 3 51578 3
444 13760 3 51579 3
445 13761 3 51580 3
446 13762 3 51581 3
447 13763 3 51582 3
448 13764 3 51583 3
449 13765 3 51584 3
450 13766 3 51585 3
451 13767 3 51586 3
452 13768 3 51587 3
453 13769 3 51588 3
454 13770 3 51589 3
455 13771 3 51590 3
456 13772 3 51591 3
457 13773 3 51592 3
458 13774 3 51593 3
459 13775 3 51594 3
460 13776 3 51595 3
461 13777 3 51596 3
462 13778 3 51597 3
463 13779 3 51598 3
464 13780 3 51599 3
465 13781 3 51600 3
466 13782 3 51601 3
467 13783 3 51602 3
468 13784 3 51603 3
469 13785 3 51604 3
470 13786 3 51605 3
471 13787 3 51606 3
472 13788 3 51607 3
473 13789 3 51608 3
474 13790 3 51609 3
475 13791 3 51610 3
476 13792 3 51611 3
477 13793 3 51612 3
478 13794 3 51613 3
479 13795 3 51614 3
480 13796 3 51615 3
481 13797 3 51616 3
482 13798 3 51617 3
483 13799 3 51618 3
484 13800 3 51619 3
485 13801 3 51620 3
486 13802 3 51621 3
487 13803 3 51622 3
488 13804 3 51623 3
489 13805 3 51624 3
490 13806 3 51625 3
491 13807 3 51626 3
492 13808 3 51627 3
493 13809 3 51628 3
494 13810 3 51629 3
495 13811 3 51630 3
496 13812 3 51631 3
497 13813 3 51632 3
498 13814 3 51633 3

499 13815 3 51634 3
500 13816 3 51635 3
501 13817 3 51636 3
502 13818 3 51637 3
503 13819 3 51638 3
504 13820 3 51639 3
505 13821 3 51640 3
506 13822 3 51641 3
507 13823 3 51642 3
508 13824 3 51643 3
509 13825 3 51644 3
510 13826 3 51645 3
511 13827 3 51646 3
512 13828 3 51647 3
513 13829 3 51648 3
514 13830 3 51649 3
515 13831 3 51650 3
516 13832 3 51651 3
517 13833 3 51652 3
518 13834 3 51653 3
519 13835 3 51654 3
520 13836 3 51655 3
521 13837 3 51656 3
522 13838 3 51657 3
523 13839 3 51658 3
524 13840 3 51659 3
525 13841 3 51660 3
526 13842 3 51661 3
527 13843 3 51662 3
528 13844 3 51663 3
529 13845 3 51664 3
530 13846 3 51665 3
531 13847 3 51666 3
532 13848 3 51667 3
533 13849 3 51668 3
534 13850 3 51669 3
535 13851 3 51670 3
536 13852 3 51671 3
537 13853 3 51672 3
538 13854 3 51673 3
539 13855 3 51674 3
540 13856 3 51675 3
541 13857 3 51676 3
542 13858 3 51677 3
543 13859 3 51678 3
544 13860 3 51679 3
545 13861 3 51680 3
546 13862 3 51681 3
547 13863 3 51682 3
548 13864 3 51683 3
549 13865 3 51684 3
550 13866 3 51685 3
551 13867 3 51686 3
552 13868 3 51687 3
553 13869 3 51688 3
554 13870 3 51689 3

555 13871 3 51690 3
556 13872 3 51691 3
557 13873 3 51692 3
558 13874 3 51693 3
559 13875 3 51694 3
560 13876 3 51695 3
561 13877 3 51696 3
562 13878 3 51697 3
563 13879 3 51698 3
564 13880 3 51699 3
565 13881 3 51700 3
566 13882 3 51701 3
567 13883 3 51702 3
568 13884 3 51703 3
569 13885 3 51704 3
570 13886 3 51705 3
571 13887 3 51706 3
572 13888 3 51707 3
573 13889 3 51708 3
574 13890 3 51709 3
575 13891 3 51710 3
576 13892 3 51711 3
577 13893 3 51712 3
578 13894 3 51713 3
579 13895 3 51714 3
580 13896 3 51715 3
581 13897 3 51716 3
582 13898 3 51717 3
583 13899 3 51718 3
584 13900 3 51719 3
585 13901 3 51720 3
586 13902 3 51721 3
587 13903 3 51722 3
588 13904 3 51723 3
589 13905 3 51724 3
590 13906 3 51725 3
591 13907 3 51726 3
592 13908 3 51727 3
593 13909 3 51728 3
594 13910 3 51729 3
595 13911 3 51730 3
596 13912 3 51731 3
597 13913 3 51732 3
598 13914 3 51733 3
599 13915 3 51734 3
600 13916 3 51735 3
601 13917 3 51736 3
602 13918 3 51737 3
603 13919 3 51738 3
604 13920 3 51739 3
605 13921 3 51740 3
606 13922 3 51741 3
607 13923 3 51742 3
608 13924 3 51743 3
609 13925 3 51744 3
610 13926 3 51745 3

611 13927 3 51746 3
612 13928 3 51747 3
613 13929 3 51748 3
614 13930 3 51749 3
615 13931 3 51750 3
616 13932 3 51751 3
617 13933 3 51752 3
618 13934 3 51753 3
619 13935 3 51754 3
620 13936 3 51755 3
621 13937 3 51756 3
622 13938 3 51757 3
623 13939 3 51758 3
624 13940 3 51759 3
625 13941 3 51760 3
626 13942 3 51761 3
627 13943 3 51762 3
628 13944 3 51763 3
629 13945 3 51764 3
630 13946 3 51765 3
631 13947 3 51766 3
632 13948 3 51767 3
633 13949 3 51768 3
634 13950 3 51769 3
635 13951 3 51770 3
636 13952 3 51771 3
637 13953 3 51772 3
638 13954 3 51773 3
639 13955 3 51774 3
640 13956 3 51775 3
641 13957 3 51776 3
642 13958 3 51777 3
643 13959 3 51778 3
644 13960 3 51779 3
645 13961 3 51780 3
646 13962 3 51781 3
647 13963 3 51782 3
648 13964 3 51783 3
649 13965 3 51784 3
650 13966 3 51785 3
651 13967 3 51786 3
652 13968 3 51787 3
653 13969 3 51788 3
654 13970 3 51789 3
655 13971 3 51790 3
656 13972 3 51791 3
657 13973 3 51792 3
658 13974 3 51793 3
659 13975 3 51794 3
660 13976 3 51795 3
661 13977 3 51796 3
662 13978 3 51797 3
663 13979 3 51798 3
664 13980 3 51799 3
665 13981 3 51800 3
666 13982 3 51801 3

667 13983 3 51802 3
668 13984 3 51803 3
669 13985 3 51804 3
670 13986 3 51805 3
671 13987 3 51806 3
672 13988 3 51807 3
673 13989 3 51808 3
674 13990 3 51809 3
675 13991 3 51810 3
676 13992 3 51811 3
677 13993 3 51812 3
678 13994 3 51813 3
679 13995 3 51814 3
680 13996 3 51815 3
681 13997 3 51816 3
682 13998 3 51817 3
683 13999 3 51818 3
684 14000 3 51819 3
685 14001 3 51820 3
686 14002 3 51821 3
687 14003 3 51822 3
688 14004 3 51823 3
689 14005 3 51824 3
690 14006 3 51825 3
691 14007 3 51826 3
692 14008 3 51827 3
693 14009 3 51828 3
694 14010 3 51829 3
695 14011 3 51830 3
696 14012 3 51831 3
697 14013 3 51832 3
698 14014 3 51833 3
699 14015 3 51834 3
700 14016 3 51835 3
701 14017 3 51836 3
702 14018 3 51837 3
703 14019 3 51838 3
704 14020 3 51839 3
705 14021 3 51840 3
706 14022 3 51841 3
707 14023 3 51842 3
708 14024 3 51843 3
709 14025 3 51844 3
710 14026 3 51845 3
711 14027 3 51846 3
712 14028 3 51847 3
713 14029 3 51848 3
714 14030 3 51849 3
715 14031 3 51850 3
716 14032 3 51851 3
717 14033 3 51852 3
718 14034 3 51853 3
719 14035 3 51854 3
720 14036 3 51855 3
721 14037 3 51856 3
722 14038 3 51857 3

723 14039 3 51858 3
724 14040 3 51859 3
725 14041 3 51860 3
726 14042 3 51861 3
727 14043 3 51862 3
728 14044 3 51863 3
729 14045 3 51864 3
730 14046 3 51865 3
731 14047 3 51866 3
732 14048 3 51867 3
733 14049 3 51868 3
734 14050 3 51869 3
735 14051 3 51870 3
736 14052 3 51871 3
737 14053 3 51872 3
738 14054 3 51873 3
739 14055 3 51874 3
740 14056 3 51875 3
741 14057 3 51876 3
742 14058 3 51877 3
743 14059 3 51878 3
744 14060 3 51879 3
745 14061 3 51880 3
746 14062 3 51881 3
747 14063 3 51882 3
748 14064 3 51883 3
749 14065 3 51884 3
750 14066 3 51885 3
751 14067 3 51886 3
752 14068 3 51887 3
753 14069 3 51888 3
754 14070 3 51889 3
755 14071 3 51890 3
756 14072 3 51891 3
757 14073 3 51892 3
758 14074 3 51893 3
759 14075 3 51894 3
760 14076 3 51895 3
761 14077 3 51896 3
762 14078 3 51897 3
763 14079 3 51898 3
764 14080 3 51899 3
765 14081 3 51900 3
766 14082 3 51901 3
767 14083 3 51902 3
768 14084 3 51903 3
769 14085 3 51904 3
770 14086 3 51905 3
771 14087 3 51906 3
772 14088 3 51907 3
773 14089 3 51908 3
774 14090 3 51909 3
775 14091 3 51910 3
776 14092 3 51911 3
777 14093 3 51912 3
778 14094 3 51913 3

779 14095 3 51914 3
780 14096 3 51915 3
781 14097 3 51916 3
782 14098 3 51917 3
783 14099 3 51918 3
784 14100 3 51919 3
785 14101 3 51920 3
786 14102 3 51921 3
787 14103 3 51922 3
788 14104 3 51923 3
789 14105 3 51924 3
790 14106 3 51925 3
791 14107 3 51926 3
792 14108 3 51927 3
793 14109 3 51928 3
794 14110 3 51929 3
795 14111 3 51930 3
796 14112 3 51931 3
797 14113 3 51932 3
798 14114 3 51933 3
799 14115 3 51934 3
800 14116 3 51935 3
801 14117 3 51936 3
802 14118 3 51937 3
803 14119 3 51938 3
804 14120 3 51939 3
805 14121 3 51940 3
806 14122 3 51941 3
807 14123 3 51942 3
808 14124 3 51943 3
809 14125 3 51944 3
810 14126 3 51945 3
811 14127 3 51946 3
812 14128 3 51947 3
813 14129 3 51948 3
814 14130 3 51949 3
815 14131 3 51950 3
816 14132 3 51951 3
817 14133 3 51952 3
818 14134 3 51953 3
819 14135 3 51954 3
820 14136 3 51955 3
821 14137 3 51956 3
822 14138 3 51957 3
823 14139 3 51958 3
824 14140 3 51959 3
825 14141 3 51960 3
826 14142 3 51961 3
827 14143 3 51962 3
828 14144 3 51963 3
829 14145 3 51964 3
830 14146 3 51965 3
831 14147 3 51966 3
832 14148 3 51967 3
833 14149 3 51968 3
834 14150 3 51969 3

835 14151 3 51970 3
836 14152 3 51971 3
837 14153 3 51972 3
838 14154 3 51973 3
839 14155 3 51974 3
840 14156 3 51975 3
841 14157 3 51976 3
842 14158 3 51977 3
843 14159 3 51978 3
844 14160 3 51979 3
845 14161 3 51980 3
846 14162 3 51981 3
847 14163 3 51982 3
848 14164 3 51983 3
849 14165 3 51984 3
850 14166 3 51985 3
851 14167 3 51986 3
852 14168 3 51987 3
853 14169 3 51988 3
854 14170 3 51989 3
855 14171 3 51990 3
856 14172 3 51991 3
857 14173 3 51992 3
858 14174 3 51993 3
859 14175 3 51994 3
860 14176 3 51995 3
861 14177 3 51996 3
862 14178 3 51997 3
863 14179 3 51998 3
864 14180 3 51999 3
865 14181 3 52000 3
866 14182 3 52001 3
867 14183 3 52002 3
868 14184 3 52003 3
869 14185 3 52004 3
870 14186 3 52005 3
871 14187 3 52006 3
872 14188 3 52007 3
873 14189 3 52008 3
874 14190 3 52009 3
875 14191 3 52010 3
876 14192 3 52011 3
877 14193 3 52012 3
878 14194 3 52013 3
879 14195 3 52014 3
880 14196 3 52015 3
881 14197 3 52016 3
882 14198 3 52017 3
883 14199 3 52018 3
884 14200 3 52019 3
885 14201 3 52020 3
886 14202 3 52021 3
887 14203 3 52022 3
888 14204 3 52023 3
889 14205 3 52024 3
890 14206 3 52025 3

891 14207 3 52026 3
892 14208 3 52027 3
893 14209 3 52028 3
894 14210 3 52029 3
895 14211 3 52030 3
896 14212 3 52031 3
897 14213 3 52032 3
898 14214 3 52033 3
899 14215 3 52034 3
900 14216 3 52035 3
901 14217 3 52036 3
902 14218 3 52037 3
903 14219 3 52038 3
904 14220 3 52039 3
905 14221 3 52040 3
906 14222 3 52041 3
907 14223 3 52042 3
908 14224 3 52043 3
909 14225 3 52044 3
910 14226 3 52045 3
911 14227 3 52046 3
912 14228 3 52047 3
913 14229 3 52048 3
914 14230 3 52049 3
915 14231 3 52050 3
916 14232 3 52051 3
917 14233 3 52052 3
918 14234 3 52053 3
919 14235 3 52054 3
920 14236 3 52055 3
921 14237 3 52056 3
922 14238 3 52057 3
923 14239 3 52058 3
924 14240 3 52059 3
925 14241 3 52060 3
926 14242 3 52061 3
927 14243 3 52062 3
928 14244 3 52063 3
929 14245 3 52064 3
930 14246 3 52065 3
931 14247 3 52066 3
932 14248 3 52067 3
933 14249 3 52068 3
934 14250 3 52069 3
935 14251 3 52070 3
936 14252 3 52071 3
937 14253 3 52072 3
938 14254 3 52073 3
939 14255 3 52074 3
940 14256 3 52075 3
941 14257 3 52076 3
942 14258 3 52077 3
943 14259 3 52078 3
944 14260 3 52079 3
945 14261 3 52080 3
946 14262 3 52081 3

947 14263 3 52082 3
948 14264 3 52083 3
949 14265 3 52084 3
950 14266 3 52085 3
951 14267 3 52086 3
952 14268 3 52087 3
953 14269 3 52088 3
954 14270 3 52089 3
955 14271 3 52090 3
956 14272 3 52091 3
957 14273 3 52092 3
958 14274 3 52093 3
959 14275 3 52094 3
960 14276 3 52095 3
961 14277 3 52096 3
962 14278 3 52097 3
963 14279 3 52098 3
964 14280 3 52099 3
965 14281 3 52100 3
966 14282 3 52101 3
967 14283 3 52102 3
968 14284 3 52103 3
969 14285 3 52104 3
970 14286 3 52105 3
971 14287 3 52106 3
972 14288 3 52107 3
973 14289 3 52108 3
974 14290 3 52109 3
975 14291 3 52110 3
976 14292 3 52111 3
977 14293 3 52112 3
978 14294 3 52113 3
979 14295 3 52114 3
980 14296 3 52115 3
981 14297 3 52116 3
982 14298 3 52117 3
983 14299 3 52118 3
984 14300 3 52119 3
985 14301 3 52120 3
986 14302 3 52121 3
987 14303 3 52122 3
988 14304 3 52123 3
989 14305 3 52124 3
990 14306 3 52125 3
991 14307 3 52126 3
992 14308 3 52127 3
993 14309 3 52128 3
994 14310 3 52129 3
995 14311 3 52130 3
996 14312 3 52131 3
997 14313 3 52132 3
998 14314 3 52133 3
999 14315 3 52134 3
1000 14316 3 52135 3
1001 14317 3 52136 3
1002 14318 3 52137 3

1003 14319 3 52138 3
1004 14320 3 52139 3
1005 14321 3 52140 3
1006 14322 3 52141 3
1007 14323 3 52142 3
1008 14324 3 52143 3
1009 14325 3 52144 3
1010 14326 3 52145 3
1011 14327 3 52146 3
1012 14328 3 52147 3
1013 14329 3 52148 3
1014 14330 3 52149 3
1015 14331 3 52150 3
1016 14332 3 52151 3
1017 14333 3 52152 3
1018 14334 3 52153 3
1019 14335 3 52154 3
1020 14336 3 52155 3
1021 14337 3 52156 3
1022 14338 3 52157 3
1023 14339 3 52158 3
1024 14340 3 52159 3
1025 14341 3 52160 3
1026 14342 3 52161 3
1027 14343 3 52162 3
1028 14344 3 52163 3
1029 14345 3 52164 3
1030 14346 3 52165 3
1031 14347 3 52166 3
1032 14348 3 52167 3
1033 14349 3 52168 3
1034 14350 3 52169 3
1035 14351 3 52170 3
1036 14352 3 52171 3
1037 14353 3 52172 3
1038 14354 3 52173 3
1039 14355 3 52174 3
1040 14356 3 52175 3
1041 14357 3 52176 3
1042 14358 3 52177 3
1043 14359 3 52178 3
1044 14360 3 52179 3
1045 14361 3 52180 3
1046 14362 3 52181 3
1047 14363 3 52182 3
1048 14364 3 52183 3
1049 14365 3 52184 3
1050 14366 3 52185 3
1051 14367 3 52186 3
1052 14368 3 52187 3
1053 14369 3 52188 3
1054 14370 3 52189 3
1055 14371 3 52190 3
1056 14372 3 52191 3
1057 14373 3 52192 3
1058 14374 3 52193 3

1059 14375 3 52194 3
1060 14376 3 52195 3
1061 14377 3 52196 3
1062 14378 3 52197 3
1063 14379 3 52198 3
1064 14380 3 52199 3
1065 14381 3 52200 3
1066 14382 3 52201 3
1067 14383 3 52202 3
1068 14384 3 52203 3
1069 14385 3 52204 3
1070 14386 3 52205 3
1071 14387 3 52206 3
1072 14388 3 52207 3
1073 14389 3 52208 3
1074 14390 3 52209 3
1075 14391 3 52210 3
1076 14392 3 52211 3
1077 14393 3 52212 3
1078 14394 3 52213 3
1079 14395 3 52214 3
1080 14396 3 52215 3
1081 14397 3 52216 3
1082 14398 3 52217 3
1083 14399 3 52218 3
1084 14400 3 52219 3
1085 14401 3 52220 3
1086 14402 3 52221 3
1087 14403 3 52222 3
1088 14404 3 52223 3
1089 14405 3 52224 3
1090 14406 3 52225 3
1091 14407 3 52226 3
1092 14408 3 52227 3
1093 14409 3 52228 3
1094 14410 3 52229 3
1095 14411 3 52230 3
1096 14412 3 52231 3
1097 14413 3 52232 3
1098 14414 3 52233 3
1099 14415 3 52234 3
1100 14416 3 52235 3
1101 14417 3 52236 3
1102 14418 3 52237 3
1103 14419 3 52238 3
1104 14420 3 52239 3
1105 14421 3 52240 3
1106 14422 3 52241 3
1107 14423 3 52242 3
1108 14424 3 52243 3
1109 14425 3 52244 3
1110 14426 3 52245 3
1111 14427 3 52246 3
1112 14428 3 52247 3
1113 14429 3 52248 3
1114 14430 3 52249 3

1115 14431 3 52250 3
1116 14432 3 52251 3
1117 14433 3 52252 3
1118 14434 3 52253 3
1119 14435 3 52254 3
1120 14436 3 52255 3
1121 14437 3 52256 3
1122 14438 3 52257 3
1123 14439 3 52258 3
1124 14440 3 52259 3
1125 14441 3 52260 3
1126 14442 3 52261 3
1127 14443 3 52262 3
1128 14444 3 52263 3
1129 14445 3 52264 3
1130 14446 3 52265 3
1131 14447 3 52266 3
1132 14448 3 52267 3
1133 14449 3 52268 3
1134 14450 3 52269 3
1135 14451 3 52270 3
1136 14452 3 52271 3
1137 14453 3 52272 3
1138 14454 3 52273 3
1139 14455 3 52274 3
1140 14456 3 52275 3
1141 14457 3 52276 3
1142 14458 3 52277 3
1143 14459 3 52278 3
1144 14460 3 52279 3
1145 14461 3 52280 3
1146 14462 3 52281 3
1147 14463 3 52282 3
1148 14464 3 52283 3
1149 14465 3 52284 3
1150 14466 3 52285 3
1151 14467 3 52286 3
1152 14468 3 52287 3
1153 14469 3 52288 3
1154 14470 3 52289 3
1155 14471 3 52290 3
1156 14472 3 52291 3
1157 14473 3 52292 3
1158 14474 3 52293 3
1159 14475 3 52294 3
1160 14476 3 52295 3
1161 14477 3 52296 3
1162 14478 3 52297 3
1163 14479 3 52298 3
1164 14480 3 52299 3
1165 14481 3 52300 3
1166 14482 3 52301 3
1167 14483 3 52302 3
1168 14484 3 52303 3
1169 14485 3 52304 3
1170 14486 3 52305 3

1171 14487 3 52306 3
1172 14488 3 52307 3
1173 14489 3 52308 3
1174 14490 3 52309 3
1175 14491 3 52310 3
1176 14492 3 52311 3
1177 14493 3 52312 3
1178 14494 3 52313 3
1179 14495 3 52314 3
1180 14496 3 52315 3
1181 14497 3 52316 3
1182 14498 3 52317 3
1183 14499 3 52318 3
1184 14500 3 52319 3
1185 14501 3 52320 3
1186 14502 3 52321 3
1187 14503 3 52322 3
1188 14504 3 52323 3
1189 14505 3 52324 3
1190 14506 3 52325 3
1191 14507 3 52326 3
1192 14508 3 52327 3
1193 14509 3 52328 3
1194 14510 3 52329 3
1195 14511 3 52330 3
1196 14512 3 52331 3
1197 14513 3 52332 3
1198 14514 3 52333 3
1199 14515 3 52334 3
1200 14516 3 52335 3
1201 14517 3 52336 3
1202 14518 3 52337 3
1203 14519 3 52338 3
1204 14520 3 52339 3
1205 14521 3 52340 3
1206 14522 3 52341 3
1207 14523 3 52342 3
1208 14524 3 52343 3
1209 14525 3 52344 3
1210 14526 3 52345 3
1211 14527 3 52346 3
1212 14528 3 52347 3
1213 14529 3 52348 3
1214 14530 3 52349 3
1215 14531 3 52350 3
1216 14532 3 52351 3
1217 14533 3 52352 3
1218 14534 3 52353 3
1219 14535 3 52354 3
1220 14536 3 52355 3
1221 14537 3 52356 3
1222 14538 3 52357 3
1223 14539 3 52358 3
1224 14540 3 52359 3
1225 14541 3 52360 3
1226 14542 3 52361 3

1227 14543 3 52362 3
1228 14544 3 52363 3
1229 14545 3 52364 3
1230 14546 3 52365 3
1231 14547 3 52366 3
1232 14548 3 52367 3
1233 14549 3 52368 3
1234 14550 3 52369 3
1235 14551 3 52370 3
1236 14552 3 52371 3
1237 14553 3 52372 3
1238 14554 3 52373 3
1239 14555 3 52374 3
1240 14556 3 52375 3
1241 14557 3 52376 3
1242 14558 3 52377 3
1243 14559 3 52378 3
1244 14560 3 52379 3
1245 14561 3 52380 3
1246 14562 3 52381 3
1247 14563 3 52382 3
1248 14564 3 52383 3
1249 14565 3 52384 3
1250 14566 3 52385 3
1251 14567 3 52386 3
1252 14568 3 52387 3
1253 14569 3 52388 3
1254 14570 3 52389 3
1255 14571 3 52390 3
1256 14572 3 52391 3
1257 14573 3 52392 3
1258 14574 3 52393 3
1259 14575 3 52394 3
1260 14576 3 52395 3
1261 14577 3 52396 3
1262 14578 3 52397 3
1263 14579 3 52398 3
1264 14580 3 52399 3
1265 14581 3 52400 3
1266 14582 3 52401 3
1267 14583 3 52402 3
1268 14584 3 52403 3
1269 14585 3 52404 3
1270 14586 3 52405 3
1271 14587 3 52406 3
1272 14588 3 52407 3
1273 14589 3 52408 3
1274 14590 3 52409 3
1275 14591 3 52410 3
1276 14592 3 52411 3
1277 14593 3 52412 3
1278 14594 3 52413 3
1279 14595 3 52414 3
1280 14596 3 52415 3
1281 14597 3 52416 3
1282 14598 3 52417 3

1283 14599 3 52418 3
1284 14600 3 52419 3
1285 14601 3 52420 3
1286 14602 3 52421 3
1287 14603 3 52422 3
1288 14604 3 52423 3
1289 14605 3 52424 3
1290 14606 3 52425 3
1291 14607 3 52426 3
1292 14608 3 52427 3
1293 14609 3 52428 3
1294 14610 3 52429 3
1295 14611 3 52430 3
1296 14612 3 52431 3
1297 14613 3 52432 3
1298 14614 3 52433 3
1299 14615 3 52434 3
1300 14616 3 52435 3
1301 14617 3 52436 3
1302 14618 3 52437 3
1303 14619 3 52438 3
1304 14620 3 52439 3
1305 14621 3 52440 3
1306 14622 3 52441 3
1307 14623 3 52442 3
1308 14624 3 52443 3
1309 14625 3 52444 3
1310 14626 3 52445 3
1311 14627 3 52446 3
1312 14628 3 52447 3
1313 14629 3 52448 3
1314 14630 3 52449 3
1315 14631 3 52450 3
1316 14632 3 52451 3
1317 14633 3 52452 3
1318 14634 3 52453 3
1319 14635 3 52454 3
1320 14636 3 52455 3
1321 14637 3 52456 3
1322 14638 3 52457 3
1323 14639 3 52458 3
1324 14640 3 52459 3
1325 14641 3 52460 3
1326 14642 3 52461 3
1327 14643 3 52462 3
1328 14644 3 52463 3
1329 14645 3 52464 3
1330 14646 3 52465 3
1331 14647 3 52466 3
1332 14648 3 52467 3
1333 14649 3 52468 3
1334 14650 3 52469 3
1335 14651 3 52470 3
1336 14652 3 52471 3
1337 14653 3 52472 3
1338 14654 3 52473 3

1339 14655 3 52474 3
1340 14656 3 52475 3
1341 14657 3 52476 3
1342 14658 3 52477 3
1343 14659 3 52478 3
1344 14660 3 52479 3
1345 14661 3 52480 3
1346 14662 3 52481 3
1347 14663 3 52482 3
1348 14664 3 52483 3
1349 14665 3 52484 3
1350 14666 3 52485 3
1351 14667 3 52486 3
1352 14668 3 52487 3
1353 14669 3 52488 3
1354 14670 3 52489 3
1355 14671 3 52490 3
1356 14672 3 52491 3
1357 14673 3 52492 3
1358 14674 3 52493 3
1359 14675 3 52494 3
1360 14676 3 52495 3
1361 14677 3 52496 3
1362 14678 3 52497 3
1363 14679 3 52498 3
1364 14680 3 52499 3
1365 14681 3 52500 3
1366 14682 3 52501 3
1367 14683 3 52502 3
1368 14684 3 52503 3
1369 14685 3 52504 3
1370 14686 3 52505 3
1371 14687 3 52506 3
1372 14688 3 52507 3
1373 14689 3 52508 3
1374 14690 3 52509 3
1375 14691 3 52510 3
1376 14692 3 52511 3
1377 14693 3 52512 3
1378 14694 3 52513 3
1379 14695 3 52514 3
1380 14696 3 52515 3
1381 14697 3 52516 3
1382 14698 3 52517 3
1383 14699 3 52518 3
1384 14700 3 52519 3
1385 14701 3 52520 3
1386 14702 3 52521 3
1387 14703 3 52522 3
1388 14704 3 52523 3
1389 14705 3 52524 3
1390 14706 3 52525 3
1391 14707 3 52526 3
1392 14708 3 52527 3
1393 14709 3 52528 3
1394 14710 3 52529 3

1395 14711 3 52530 3
1396 14712 3 52531 3
1397 14713 3 52532 3
1398 14714 3 52533 3
1399 14715 3 52534 3
1400 14716 3 52535 3
1401 14717 3 52536 3
1402 14718 3 52537 3
1403 14719 3 52538 3
1404 14720 3 52539 3
1405 14721 3 52540 3
1406 14722 3 52541 3
1407 14723 3 52542 3
1408 14724 3 52543 3
1409 14725 3 52544 3
1410 14726 3 52545 3
1411 14727 3 52546 3
1412 14728 3 52547 3
1413 14729 3 52548 3
1414 14730 3 52549 3
1415 14731 3 52550 3
1416 14732 3 52551 3
1417 14733 3 52552 3
1418 14734 3 52553 3
1419 14735 3 52554 3
1420 14736 3 52555 3
1421 14737 3 52556 3
1422 14738 3 52557 3
1423 14739 3 52558 3
1424 14740 3 52559 3
1425 14741 3 52560 3
1426 14742 3 52561 3
1427 14743 3 52562 3
1428 14744 3 52563 3
1429 14745 3 52564 3
1430 14746 3 52565 3
1431 14747 3 52566 3
1432 14748 3 52567 3
1433 14749 3 52568 3
1434 14750 3 52569 3
1435 14751 3 52570 3
1436 14752 3 52571 3
1437 14753 3 52572 3
1438 14754 3 52573 3
1439 14755 3 52574 3
1440 14756 3 52575 3
1441 14757 3 52576 3
1442 14758 3 52577 3
1443 14759 3 52578 3
1444 14760 3 52579 3
1445 14761 3 52580 3
1446 14762 3 52581 3
1447 14763 3 52582 3
1448 14764 3 52583 3
1449 14765 3 52584 3
1450 14766 3 52585 3

1451 14767 3 52586 3
1452 14768 3 52587 3
1453 14769 3 52588 3
1454 14770 3 52589 3
1455 14771 3 52590 3
1456 14772 3 52591 3
1457 14773 3 52592 3
1458 14774 3 52593 3
1459 14775 3 52594 3
1460 14776 3 52595 3
1461 14777 3 52596 3
1462 14778 3 52597 3
1463 14779 3 52598 3
1464 14780 3 52599 3
1465 14781 3 52600 3
1466 14782 3 52601 3
1467 14783 3 52602 3
1468 14784 3 52603 3
1469 14785 3 52604 3
1470 14786 3 52605 3
1471 14787 3 52606 3
1472 14788 3 52607 3
1473 14789 3 52608 3
1474 14790 3 52609 3
1475 14791 3 52610 3
1476 14792 3 52611 3
1477 14793 3 52612 3
1478 14794 3 52613 3
1479 14795 3 52614 3
1480 14796 3 52615 3
1481 14797 3 52616 3
1482 14798 3 52617 3
1483 14799 3 52618 3
1484 14800 3 52619 3
1485 14801 3 52620 3
1486 14802 3 52621 3
1487 14803 3 52622 3
1488 14804 3 52623 3
1489 14805 3 52624 3
1490 14806 3 52625 3
1491 14807 3 52626 3
1492 14808 3 52627 3
1493 14809 3 52628 3
1494 14810 3 52629 3
1495 14811 3 52630 3
1496 14812 3 52631 3
1497 14813 3 52632 3
1498 14814 3 52633 3
1499 14815 3 52634 3
1500 14816 3 52635 3
1501 14817 3 52636 3
1502 14818 3 52637 3
1503 14819 3 52638 3
1504 14820 3 52639 3
1505 14821 3 52640 3
1506 14822 3 52641 3

1507 14823 3 52642 3
1508 14824 3 52643 3
1509 14825 3 52644 3
1510 14826 3 52645 3
1511 14827 3 52646 3
1512 14828 3 52647 3
1513 14829 3 52648 3
1514 14830 3 52649 3
1515 14831 3 52650 3
1516 14832 3 52651 3
1517 14833 3 52652 3
1518 14834 3 52653 3
1519 14835 3 52654 3
1520 14836 3 52655 3
1521 14837 3 52656 3
1522 14838 3 52657 3
1523 14839 3 52658 3
1524 14840 3 52659 3
1525 14841 3 52660 3
1526 14842 3 52661 3
1527 14843 3 52662 3
1528 14844 3 52663 3
1529 14845 3 52664 3
1530 14846 3 52665 3
1531 14847 3 52666 3
1532 14848 3 52667 3
1533 14849 3 52668 3
1534 14850 3 52669 3
1535 14851 3 52670 3
1536 14852 3 52671 3
1537 14853 3 52672 3
1538 14854 3 52673 3
1539 14855 3 52674 3
1540 14856 3 52675 3
1541 14857 3 52676 3
1542 14858 3 52677 3
1543 14859 3 52678 3
1544 14860 3 52679 3
1545 14861 3 52680 3
1546 14862 3 52681 3
1547 14863 3 52682 3
1548 14864 3 52683 3
1549 14865 3 52684 3
1550 14866 3 52685 3
1551 14867 3 52686 3
1552 14868 3 52687 3
1553 14869 3 52688 3
1554 14870 3 52689 3
1555 14871 3 52690 3
1556 14872 3 52691 3
1557 14873 3 52692 3
1558 14874 3 52693 3
1559 14875 3 52694 3
1560 14876 3 52695 3
1561 14877 3 52696 3
1562 14878 3 52697 3

1563 14879 3 52698 3
1564 14880 3 52699 3
1565 14881 3 52700 3
1566 14882 3 52701 3
1567 14883 3 52702 3
1568 14884 3 52703 3
1569 14885 3 52704 3
1570 14886 3 52705 3
1571 14887 3 52706 3
1572 14888 3 52707 3
1573 14889 3 52708 3
1574 14890 3 52709 3
1575 14891 3 52710 3
1576 14892 3 52711 3
1577 14893 3 52712 3
1578 14894 3 52713 3
1579 14895 3 52714 3
1580 14896 3 52715 3
1581 14897 3 52716 3
1582 14898 3 52717 3
1583 14899 3 52718 3
1584 14900 3 52719 3
1585 14901 3 52720 3
1586 14902 3 52721 3
1587 14903 3 52722 3
1588 14904 3 52723 3
1589 14905 3 52724 3
1590 14906 3 52725 3
1591 14907 3 52726 3
1592 14908 3 52727 3
1593 14909 3 52728 3
1594 14910 3 52729 3
1595 14911 3 52730 3
1596 14912 3 52731 3
1597 14913 3 52732 3
1598 14914 3 52733 3
1599 14915 3 52734 3
1600 14916 3 52735 3
1601 14917 3 52736 3
1602 14918 3 52737 3
1603 14919 3 52738 3
1604 14920 3 52739 3
1605 14921 3 52740 3
1606 14922 3 52741 3
1607 14923 3 52742 3
1608 14924 3 52743 3
1609 14925 3 52744 3
1610 14926 3 52745 3
1611 14927 3 52746 3
1612 14928 3 52747 3
1613 14929 3 52748 3
1614 14930 3 52749 3
1615 14931 3 52750 3
1616 14932 3 52751 3
1617 14933 3 52752 3
1618 14934 3 52753 3

1619 14935 3 52754 3
1620 14936 3 52755 3
1621 14937 3 52756 3
1622 14938 3 52757 3
1623 14939 3 52758 3
1624 14940 3 52759 3
1625 14941 3 52760 3
1626 14942 3 52761 3
1627 14943 3 52762 3
1628 14944 3 52763 3
1629 14945 3 52764 3
1630 14946 3 52765 3
1631 14947 3 52766 3
1632 14948 3 52767 3
1633 14949 3 52768 3
1634 14950 3 52769 3
1635 14951 3 52770 3
1636 14952 3 52771 3
1637 14953 3 52772 3
1638 14954 3 52773 3
1639 14955 3 52774 3
1640 14956 3 52775 3
1641 14957 3 52776 3
1642 14958 3 52777 3
1643 14959 3 52778 3
1644 14960 3 52779 3
1645 14961 3 52780 3
1646 14962 3 52781 3
1647 14963 3 52782 3
1648 14964 3 52783 3
1649 14965 3 52784 3
1650 14966 3 52785 3
1651 14967 3 52786 3
1652 14968 3 52787 3
1653 14969 3 52788 3
1654 14970 3 52789 3
1655 14971 3 52790 3
1656 14972 3 52791 3
1657 14973 3 52792 3
1658 14974 3 52793 3
1659 14975 3 52794 3
1660 14976 3 52795 3
1661 14977 3 52796 3
1662 14978 3 52797 3
1663 14979 3 52798 3
1664 14980 3 52799 3
1665 14981 3 52800 3
1666 14982 3 52801 3
1667 14983 3 52802 3
1668 14984 3 52803 3
1669 14985 3 52804 3
1670 14986 3 52805 3
1671 14987 3 52806 3
1672 14988 3 52807 3
1673 14989 3 52808 3
1674 14990 3 52809 3

1675 14991 3 52810 3
1676 14992 3 52811 3
1677 14993 3 52812 3
1678 14994 3 52813 3
1679 14995 3 52814 3
1680 14996 3 52815 3
1681 14997 3 52816 3
1682 14998 3 52817 3
1683 14999 3 52818 3
1684 15000 3 52819 3
1685 15001 3 52820 3
1686 15002 3 52821 3
1687 15003 3 52822 3
1688 15004 3 52823 3
1689 15005 3 52824 3
1690 15006 3 52825 3
1691 15007 3 52826 3
1692 15008 3 52827 3
1693 15009 3 52828 3
1694 15010 3 52829 3
1695 15011 3 52830 3
1696 15012 3 52831 3
1697 15013 3 52832 3
1698 15014 3 52833 3
1699 15015 3 52834 3
1700 15016 3 52835 3
1701 15017 3 52836 3
1702 15018 3 52837 3
1703 15019 3 52838 3
1704 15020 3 52839 3
1705 15021 3 52840 3
1706 15022 3 52841 3
1707 15023 3 52842 3
1708 15024 3 52843 3
1709 15025 3 52844 3
1710 15026 3 52845 3
1711 15027 3 52846 3
1712 15028 3 52847 3
1713 15029 3 52848 3
1714 15030 3 52849 3
1715 15031 3 52850 3
1716 15032 3 52851 3
1717 15033 3 52852 3
1718 15034 3 52853 3
1719 15035 3 52854 3
1720 15036 3 52855 3
1721 15037 3 52856 3
1722 15038 3 52857 3
1723 15039 3 52858 3
1724 15040 3 52859 3
1725 15041 3 52860 3
1726 15042 3 52861 3
1727 15043 3 52862 3
1728 15044 3 52863 3
1729 15045 3 52864 3
1730 15046 3 52865 3

1731 15047 3 52866 3
1732 15048 3 52867 3
1733 15049 3 52868 3
1734 15050 3 52869 3
1735 15051 3 52870 3
1736 15052 3 52871 3
1737 15053 3 52872 3
1738 15054 3 52873 3
1739 15055 3 52874 3
1740 15056 3 52875 3
1741 15057 3 52876 3
1742 15058 3 52877 3
1743 15059 3 52878 3
1744 15060 3 52879 3
1745 15061 3 52880 3
1746 15062 3 52881 3
1747 15063 3 52882 3
1748 15064 3 52883 3
1749 15065 3 52884 3
1750 15066 3 52885 3
1751 15067 3 52886 3
1752 15068 3 52887 3
1753 15069 3 52888 3
1754 15070 3 52889 3
1755 15071 3 52890 3
1756 15072 3 52891 3
1757 15073 3 52892 3
1758 15074 3 52893 3
1759 15075 3 52894 3
1760 15076 3 52895 3
1761 15077 3 52896 3
1762 15078 3 52897 3
1763 15079 3 52898 3
1764 15080 3 52899 3
1765 15081 3 52900 3
1766 15082 3 52901 3
1767 15083 3 52902 3
1768 15084 3 52903 3
1769 15085 3 52904 3
1770 15086 3 52905 3
1771 15087 3 52906 3
1772 15088 3 52907 3
1773 15089 3 52908 3
1774 15090 3 52909 3
1775 15091 3 52910 3
1776 15092 3 52911 3
1777 15093 3 52912 3
1778 15094 3 52913 3
1779 15095 3 52914 3
1780 15096 3 52915 3
1781 15097 3 52916 3
1782 15098 3 52917 3
1783 15099 3 52918 3
1784 15100 3 52919 3
1785 15101 3 52920 3
1786 15102 3 52921 3

1787 15103 3 52922 3
1788 15104 3 52923 3
1789 15105 3 52924 3
1790 15106 3 52925 3
1791 15107 3 52926 3
1792 15108 3 52927 3
1793 15109 3 52928 3
1794 15110 3 52929 3
1795 15111 3 52930 3
1796 15112 3 52931 3
1797 15113 3 52932 3
1798 15114 3 52933 3
1799 15115 3 52934 3
1800 15116 3 52935 3
1801 15117 3 52936 3
1802 15118 3 52937 3
1803 15119 3 52938 3
1804 15120 3 52939 3
1805 15121 3 52940 3
1806 15122 3 52941 3
1807 15123 3 52942 3
1808 15124 3 52943 3
1809 15125 3 52944 3
1810 15126 3 52945 3
1811 15127 3 52946 3
1812 15128 3 52947 3
1813 15129 3 52948 3
1814 15130 3 52949 3
1815 15131 3 52950 3
1816 15132 3 52951 3
1817 15133 3 52952 3
1818 15134 3 52953 3
1819 15135 3 52954 3
1820 15136 3 52955 3
1821 15137 3 52956 3
1822 15138 3 52957 3
1823 15139 3 52958 3
1824 15140 3 52959 3
1825 15141 3 52960 3
1826 15142 3 52961 3
1827 15143 3 52962 3
1828 15144 3 52963 3
1829 15145 3 52964 3
1830 15146 3 52965 3
1831 15147 3 52966 3
1832 15148 3 52967 3
1833 15149 3 52968 3
1834 15150 3 52969 3
1835 15151 3 52970 3
1836 15152 3 52971 3
1837 15153 3 52972 3
1838 15154 3 52973 3
1839 15155 3 52974 3
1840 15156 3 52975 3
1841 15157 3 52976 3
1842 15158 3 52977 3

1843 15159 3 52978 3
1844 15160 3 52979 3
1845 15161 3 52980 3
1846 15162 3 52981 3
1847 15163 3 52982 3
1848 15164 3 52983 3
1849 15165 3 52984 3
1850 15166 3 52985 3
1851 15167 3 52986 3
1852 15168 3 52987 3
1853 15169 3 52988 3
1854 15170 3 52989 3
1855 15171 3 52990 3
1856 15172 3 52991 3
1857 15173 3 52992 3
1858 15174 3 52993 3
1859 15175 3 52994 3
1860 15176 3 52995 3
1861 15177 3 52996 3
1862 15178 3 52997 3
1863 15179 3 52998 3
1864 15180 3 52999 3
1865 15181 3 53000 3
1866 15182 3 53001 3
1867 15183 3 53002 3
1868 15184 3 53003 3
1869 15185 3 53004 3
1870 15186 3 53005 3
1871 15187 3 53006 3
1872 15188 3 53007 3
1873 15189 3 53008 3
1874 15190 3 53009 3
1875 15191 3 53010 3
1876 15192 3 53011 3
1877 15193 3 53012 3
1878 15194 3 53013 3
1879 15195 3 53014 3
1880 15196 3 53015 3
1881 15197 3 53016 3
1882 15198 3 53017 3
1883 15199 3 53018 3
1884 15200 3 53019 3
1885 15201 3 53020 3
1886 15202 3 53021 3
1887 15203 3 53022 3
1888 15204 3 53023 3
1889 15205 3 53024 3
1890 15206 3 53025 3
1891 15207 3 53026 3
1892 15208 3 53027 3
1893 15209 3 53028 3
1894 15210 3 53029 3
1895 15211 3 53030 3
1896 15212 3 53031 3
1897 15213 3 53032 3
1898 15214 3 53033 3

1899 15215 3 53034 3
1900 15216 3 53035 3
1901 15217 3 53036 3
1902 15218 3 53037 3
1903 15219 3 53038 3
1904 15220 3 53039 3
1905 15221 3 53040 3
1906 15222 3 53041 3
1907 15223 3 53042 3
1908 15224 3 53043 3
1909 15225 3 53044 3
1910 15226 3 53045 3
1911 15227 3 53046 3
1912 15228 3 53047 3
1913 15229 3 53048 3
1914 15230 3 53049 3
1915 15231 3 53050 3
1916 15232 3 53051 3
1917 15233 3 53052 3
1918 15234 3 53053 3
1919 15235 3 53054 3
1920 15236 3 53055 3
1921 15237 3 53056 3
1922 15238 3 53057 3
1923 15239 3 53058 3
1924 15240 3 53059 3
1925 15241 3 53060 3
1926 15242 3 53061 3
1927 15243 3 53062 3
1928 15244 3 53063 3
1929 15245 3 53064 3
1930 15246 3 53065 3
1931 15247 3 53066 3
1932 15248 3 53067 3
1933 15249 3 53068 3
1934 15250 3 53069 3
1935 15251 3 53070 3
1936 15252 3 53071 3
1937 15253 3 53072 3
1938 15254 3 53073 3
1939 15255 3 53074 3
1940 15256 3 53075 3
1941 15257 3 53076 3
1942 15258 3 53077 3
1943 15259 3 53078 3
1944 15260 3 53079 3
1945 15261 3 53080 3
1946 15262 3 53081 3
1947 15263 3 53082 3
1948 15264 3 53083 3
1949 15265 3 53084 3
1950 15266 3 53085 3
1951 15267 3 53086 3
1952 15268 3 53087 3
1953 15269 3 53088 3
1954 15270 3 53089 3

1955 15271 3 53090 3
1956 15272 3 53091 3
1957 15273 3 53092 3
1958 15274 3 53093 3
1959 15275 3 53094 3
1960 15276 3 53095 3
1961 15277 3 53096 3
1962 15278 3 53097 3
1963 15279 3 53098 3
1964 15280 3 53099 3
1965 15281 3 53100 3
1966 15282 3 53101 3
1967 15283 3 53102 3
1968 15284 3 53103 3
1969 15285 3 53104 3
1970 15286 3 53105 3
1971 15287 3 53106 3
1972 15288 3 53107 3
1973 15289 3 53108 3
1974 15290 3 53109 3
1975 15291 3 53110 3
1976 15292 3 53111 3
1977 15293 3 53112 3
1978 15294 3 53113 3
1979 15295 3 53114 3
1980 15296 3 53115 3
1981 15297 3 53116 3
1982 15298 3 53117 3
1983 15299 3 53118 3
1984 15300 3 53119 3
1985 15301 3 53120 3
1986 15302 3 53121 3
1987 15303 3 53122 3
1988 15304 3 53123 3
1989 15305 3 53124 3
1990 15306 3 53125 3
1991 15307 3 53126 3
1992 15308 3 53127 3
1993 15309 3 53128 3
1994 15310 3 53129 3
1995 15311 3 53130 3
1996 15312 3 53131 3
1997 15313 3 53132 3
1998 15314 3 53133 3
1999 15315 3 53134 3
2000 15316 3 53135 3
2001 15317 3 53136 3
2002 15318 3 53137 3
2003 15319 3 53138 3
2004 15320 3 53139 3
2005 15321 3 53140 3
2006 15322 3 53141 3
2007 15323 3 53142 3
2008 15324 3 53143 3
2009 15325 3 53144 3
2010 15326 3 53145 3

2011 15327 3 53146 3
2012 15328 3 53147 3
2013 15329 3 53148 3
2014 15330 3 53149 3
2015 15331 3 53150 3
2016 15332 3 53151 3
2017 15333 3 53152 3
2018 15334 3 53153 3
2019 15335 3 53154 3
2020 15336 3 53155 3
2021 15337 3 53156 3
2022 15338 3 53157 3
2023 15339 3 53158 3
2024 15340 3 53159 3
2025 15341 3 53160 3
2026 15342 3 53161 3
2027 15343 3 53162 3
2028 15344 3 53163 3
2029 15345 3 53164 3
2030 15346 3 53165 3
2031 15347 3 53166 3
2032 15348 3 53167 3
2033 15349 3 53168 3
2034 15350 3 53169 3
2035 15351 3 53170 3
2036 15352 3 53171 3
2037 15353 3 53172 3
2038 15354 3 53173 3
2039 15355 3 53174 3
2040 15356 3 53175 3
2041 15357 3 53176 3
2042 15358 3 53177 3
2043 15359 3 53178 3
2044 15360 3 53179 3
2045 15361 3 53180 3
2046 15362 3 53181 3
2047 15363 3 53182 3
2048 15364 3 53183 3
2049 15365 3 53184 3
2050 15366 3 53185 3
2051 15367 3 53186 3
2052 15368 3 53187 3
2053 15369 3 53188 3
2054 15370 3 53189 3
2055 15371 3 53190 3
2056 15372 3 53191 3
2057 15373 3 53192 3
2058 15374 3 53193 3
2059 15375 3 53194 3
2060 15376 3 53195 3
2061 15377 3 53196 3
2062 15378 3 53197 3
2063 15379 3 53198 3
2064 15380 3 53199 3
2065 15381 3 53200 3
2066 15382 3 53201 3

2067 15383 3 53202 3
2068 15384 3 53203 3
2069 15385 3 53204 3
2070 15386 3 53205 3
2071 15387 3 53206 3
2072 15388 3 53207 3
2073 15389 3 53208 3
2074 15390 3 53209 3
2075 15391 3 53210 3
2076 15392 3 53211 3
2077 15393 3 53212 3
2078 15394 3 53213 3
2079 15395 3 53214 3
2080 15396 3 53215 3
2081 15397 3 53216 3
2082 15398 3 53217 3
2083 15399 3 53218 3
2084 15400 3 53219 3
2085 15401 3 53220 3
2086 15402 3 53221 3
2087 15403 3 53222 3
2088 15404 3 53223 3
2089 15405 3 53224 3
2090 15406 3 53225 3
2091 15407 3 53226 3
2092 15408 3 53227 3
2093 15409 3 53228 3
2094 15410 3 53229 3
2095 15411 3 53230 3
2096 15412 3 53231 3
2097 15413 3 53232 3
2098 15414 3 53233 3
2099 15415 3 53234 3
2100 15416 3 53235 3
2101 15417 3 53236 3
2102 15418 3 53237 3
2103 15419 3 53238 3
2104 15420 3 53239 3
2105 15421 3 53240 3
2106 15422 3 53241 3
2107 15423 3 53242 3
2108 15424 3 53243 3
2109 15425 3 53244 3
2110 15426 3 53245 3
2111 15427 3 53246 3
2112 15428 3 53247 3
2113 15429 3 53248 3
2114 15430 3 53249 3
2115 15431 3 53250 3
2116 15432 3 53251 3
2117 15433 3 53252 3
2118 15434 3 53253 3
2119 15435 3 53254 3
2120 15436 3 53255 3
2121 15437 3 53256 3
2122 15438 3 53257 3

2123 15439 3 53258 3
2124 15440 3 53259 3
2125 15441 3 53260 3
2126 15442 3 53261 3
2127 15443 3 53262 3
2128 15444 3 53263 3
2129 15445 3 53264 3
2130 15446 3 53265 3
2131 15447 3 53266 3
2132 15448 3 53267 3
2133 15449 3 53268 3
2134 15450 3 53269 3
2135 15451 3 53270 3
2136 15452 3 53271 3
2137 15453 3 53272 3
2138 15454 3 53273 3
2139 15455 3 53274 3
2140 15456 3 53275 3
2141 15457 3 53276 3
2142 15458 3 53277 3
2143 15459 3 53278 3
2144 15460 3 53279 3
2145 15461 3 53280 3
2146 15462 3 53281 3
2147 15463 3 53282 3
2148 15464 3 53283 3
2149 15465 3 53284 3
2150 15466 3 53285 3
2151 15467 3 53286 3
2152 15468 3 53287 3
2153 15469 3 53288 3
2154 15470 3 53289 3
2155 15471 3 53290 3
2156 15472 3 53291 3
2157 15473 3 53292 3
2158 15474 3 53293 3
2159 15475 3 53294 3
2160 15476 3 53295 3
2161 15477 3 53296 3
2162 15478 3 53297 3
2163 15479 3 53298 3
2164 15480 3 53299 3
2165 15481 3 53300 3
2166 15482 3 53301 3
2167 15483 3 53302 3
2168 15484 3 53303 3
2169 15485 3 53304 3
2170 15486 3 53305 3
2171 15487 3 53306 3
2172 15488 3 53307 3
2173 15489 3 53308 3
2174 15490 3 53309 3
2175 15491 3 53310 3
2176 15492 3 53311 3
2177 15493 3 53312 3
2178 15494 3 53313 3

2179 15495 3 53314 3
2180 15496 3 53315 3
2181 15497 3 53316 3
2182 15498 3 53317 3
2183 15499 3 53318 3
2184 15500 3 53319 3
2185 15501 3 53320 3
2186 15502 3 53321 3
2187 15503 3 53322 3
2188 15504 3 53323 3
2189 15505 3 53324 3
2190 15506 3 53325 3
2191 15507 3 53326 3
2192 15508 3 53327 3
2193 15509 3 53328 3
2194 15510 3 53329 3
2195 15511 3 53330 3
2196 15512 3 53331 3
2197 15513 3 53332 3
2198 15514 3 53333 3
2199 15515 3 53334 3
2200 15516 3 53335 3
2201 15517 3 53336 3
2202 15518 3 53337 3
2203 15519 3 53338 3
2204 15520 3 53339 3
2205 15521 3 53340 3
2206 15522 3 53341 3
2207 15523 3 53342 3
2208 15524 3 53343 3
2209 15525 3 53344 3
2210 15526 3 53345 3
2211 15527 3 53346 3
2212 15528 3 53347 3
2213 15529 3 53348 3
2214 15530 3 53349 3
2215 15531 3 53350 3
2216 15532 3 53351 3
2217 15533 3 53352 3
2218 15534 3 53353 3
2219 15535 3 53354 3
2220 15536 3 53355 3
2221 15537 3 53356 3
2222 15538 3 53357 3
2223 15539 3 53358 3
2224 15540 3 53359 3
2225 15541 3 53360 3
2226 15542 3 53361 3
2227 15543 3 53362 3
2228 15544 3 53363 3
2229 15545 3 53364 3
2230 15546 3 53365 3
2231 15547 3 53366 3
2232 15548 3 53367 3
2233 15549 3 53368 3
2234 15550 3 53369 3

2235 15551 3 53370 3
2236 15552 3 53371 3
2237 15553 3 53372 3
2238 15554 3 53373 3
2239 15555 3 53374 3
2240 15556 3 53375 3
2241 15557 3 53376 3
2242 15558 3 53377 3
2243 15559 3 53378 3
2244 15560 3 53379 3
2245 15561 3 53380 3
2246 15562 3 53381 3
2247 15563 3 53382 3
2248 15564 3 53383 3
2249 15565 3 53384 3
2250 15566 3 53385 3
2251 15567 3 53386 3
2252 15568 3 53387 3
2253 15569 3 53388 3
2254 15570 3 53389 3
2255 15571 3 53390 3
2256 15572 3 53391 3
2257 15573 3 53392 3
2258 28890 3 100790 3
2259 28891 3 100791 3
2260 28892 3 100792 3
2261 28893 3 100793 3
2262 28894 3 100794 3
2263 28895 3 100795 3
2264 28896 3 100796 3
2265 28897 3 100797 3
2266 28898 3 100798 3
2267 28899 3 100799 3
2268 28900 3 100800 3
2269 28901 3 100801 3
2270 28902 3 100802 3
2271 28903 3 100803 3
2272 28904 3 100804 3
2273 28905 3 100805 3
2274 28906 3 100806 3
2275 28907 3 100807 3
2276 28908 3 100808 3
2277 28909 3 100809 3
2278 28910 3 100810 3
2279 28911 3 100811 3
2280 28912 3 100812 3
2281 28913 3 100813 3
2282 28914 3 100814 3
2283 28915 3 100815 3
2284 28916 3 100816 3
2285 28917 3 100817 3
2286 28918 3 100818 3
2287 28919 3 100819 3
2288 28920 3 100820 3
2289 28921 3 100821 3
2290 28922 3 100822 3

2291 28923 3 100823 3
2292 28924 3 100824 3
2293 28925 3 100825 3
2294 28926 3 100826 3
2295 28927 3 100827 3
2296 28928 3 100828 3
2297 28929 3 100829 3
2298 28930 3 100830 3
2299 28931 3 100831 3
2300 28932 3 100832 3
2301 28933 3 100833 3
2302 28934 3 100834 3
2303 28935 3 100835 3
2304 28936 3 100836 3
2305 28937 3 100837 3
2306 28938 3 100838 3
2307 28939 3 100839 3
2308 28940 3 100840 3
2309 28941 3 100841 3
2310 28942 3 100842 3
2311 28943 3 100843 3
2312 28944 3 100844 3
2313 28945 3 100845 3
2314 28946 3 100846 3
2315 28947 3 100847 3
2316 28948 3 100848 3
2317 28949 3 100849 3
2318 28950 3 100850 3
2319 28951 3 100851 3
2320 28952 3 100852 3
2321 28953 3 100853 3
2322 28954 3 100854 3
2323 28955 3 100855 3
2324 28956 3 100856 3
2325 28957 3 100857 3
2326 28958 3 100858 3
2327 28959 3 100859 3
2328 28960 3 100860 3
2329 28961 3 100861 3
2330 28962 3 100862 3
2331 28963 3 100863 3
2332 28964 3 100864 3
2333 28965 3 100865 3
2334 28966 3 100866 3
2335 28967 3 100867 3
2336 28968 3 100868 3
2337 28969 3 100869 3
2338 28970 3 100870 3
2339 28971 3 100871 3
2340 28972 3 100872 3
2341 28973 3 100873 3
2342 28974 3 100874 3
2343 28975 3 100875 3
2344 28976 3 100876 3
2345 28977 3 100877 3
2346 28978 3 100878 3

2347 28979 3 100879 3
2348 28980 3 100880 3
2349 28981 3 100881 3
2350 28982 3 100882 3
2351 28983 3 100883 3
2352 28984 3 100884 3
2353 28985 3 100885 3
2354 28986 3 100886 3
2355 28987 3 100887 3
2356 28988 3 100888 3
2357 28989 3 100889 3
2358 28990 3 100890 3
2359 28991 3 100891 3
2360 28992 3 100892 3
2361 28993 3 100893 3
2362 28994 3 100894 3
2363 28995 3 100895 3
2364 28996 3 100896 3
2365 28997 3 100897 3
2366 28998 3 100898 3
2367 28999 3 100899 3
2368 29000 3 100900 3
2369 29001 3 100901 3
2370 29002 3 100902 3
2371 29003 3 100903 3
2372 29004 3 100904 3
2373 29005 3 100905 3
2374 29006 3 100906 3
2375 29007 3 100907 3
2376 29008 3 100908 3
2377 29009 3 100909 3
2378 29010 3 100910 3
2379 29011 3 100911 3
2380 29012 3 100912 3
2381 29013 3 100913 3
2382 29014 3 100914 3
2383 29015 3 100915 3
2384 29016 3 100916 3
2385 29017 3 100917 3
2386 29018 3 100918 3
2387 29019 3 100919 3
2388 29020 3 100920 3
2389 29021 3 100921 3
2390 29022 3 100922 3
2391 29023 3 100923 3
2392 29024 3 100924 3
2393 29025 3 100925 3
2394 29026 3 100926 3
2395 29027 3 100927 3
2396 29028 3 100928 3
2397 29029 3 100929 3
2398 29030 3 100930 3
2399 29031 3 100931 3
2400 29032 3 100932 3
2401 29033 3 100933 3
2402 29034 3 100934 3

2403 29035 3 100935 3
2404 29036 3 100936 3
2405 29037 3 100937 3
2406 29038 3 100938 3
2407 29039 3 100939 3
2408 29040 3 100940 3
2409 29041 3 100941 3
2410 29042 3 100942 3
2411 29043 3 100943 3
2412 29044 3 100944 3
2413 29045 3 100945 3
2414 29046 3 100946 3
2415 29047 3 100947 3
2416 29048 3 100948 3
2417 29049 3 100949 3
2418 29050 3 100950 3
2419 29051 3 100951 3
2420 29052 3 100952 3
2421 29053 3 100953 3
2422 29054 3 100954 3
2423 29055 3 100955 3
2424 29056 3 100956 3
2425 29057 3 100957 3
2426 29058 3 100958 3
2427 29059 3 100959 3
2428 29060 3 100960 3
2429 29061 3 100961 3
2430 29062 3 100962 3
2431 29063 3 100963 3
2432 29064 3 100964 3
2433 29065 3 100965 3
2434 29066 3 100966 3
2435 29067 3 100967 3
2436 29068 3 100968 3
2437 29069 3 100969 3
2438 29070 3 100970 3
2439 29071 3 100971 3
2440 29072 3 100972 3
2441 29073 3 100973 3
2442 29074 3 100974 3
2443 29075 3 100975 3
2444 29076 3 100976 3
2445 29077 3 100977 3
2446 29078 3 100978 3
2447 29079 3 100979 3
2448 29080 3 100980 3
2449 29081 3 100981 3
2450 29082 3 100982 3
2451 29083 3 100983 3
2452 29084 3 100984 3
2453 29085 3 100985 3
2454 29086 3 100986 3
2455 29087 3 100987 3
2456 29088 3 100988 3
2457 29089 3 100989 3
2458 29090 3 100990 3

2459 29091 3 100991 3
2460 29092 3 100992 3
2461 29093 3 100993 3
2462 29094 3 100994 3
2463 29095 3 100995 3
2464 29096 3 100996 3
2465 29097 3 100997 3
2466 29098 3 100998 3
2467 29099 3 100999 3
2468 29100 3 101000 3
2469 29101 3 101001 3
2470 29102 3 101002 3
2471 29103 3 101003 3
2472 29104 3 101004 3
2473 29105 3 101005 3
2474 29106 3 101006 3
2475 29107 3 101007 3
2476 29108 3 101008 3
2477 29109 3 101009 3
2478 29110 3 101010 3
2479 29111 3 101011 3
2480 29112 3 101012 3
2481 29113 3 101013 3
2482 29114 3 101014 3
2483 29115 3 101015 3
2484 29116 3 101016 3
2485 29117 3 101017 3
2486 29118 3 101018 3
2487 29119 3 101019 3
2488 29120 3 101020 3
2489 29121 3 101021 3
2490 29122 3 101022 3
2491 29123 3 101023 3
2492 29124 3 101024 3
2493 29125 3 101025 3
2494 29126 3 101026 3
2495 29127 3 101027 3
2496 29128 3 101028 3
2497 29129 3 101029 3
2498 29130 3 101030 3
2499 29131 3 101031 3
2500 29132 3 101032 3
2501 29133 3 101033 3
2502 29134 3 101034 3
2503 29135 3 101035 3
2504 29136 3 101036 3
2505 29137 3 101037 3
2506 29138 3 101038 3
2507 29139 3 101039 3
2508 29140 3 101040 3
2509 29141 3 101041 3
2510 29142 3 101042 3
2511 29143 3 101043 3
2512 29144 3 101044 3
2513 29145 3 101045 3
2514 29146 3 101046 3

2515 29147 3 101047 3
2516 29148 3 101048 3
2517 29149 3 101049 3
2518 29150 3 101050 3
2519 29151 3 101051 3
2520 29152 3 101052 3
2521 29153 3 101053 3
2522 29154 3 101054 3
2523 29155 3 101055 3
2524 29156 3 101056 3
2525 29157 3 101057 3
2526 29158 3 101058 3
2527 29159 3 101059 3
2528 29160 3 101060 3
2529 29161 3 101061 3
2530 29162 3 101062 3
2531 29163 3 101063 3
2532 29164 3 101064 3
2533 29165 3 101065 3
2534 29166 3 101066 3
2535 29167 3 101067 3
2536 29168 3 101068 3
2537 29169 3 101069 3
2538 29170 3 101070 3
2539 29171 3 101071 3
2540 29172 3 101072 3
2541 29173 3 101073 3
2542 29174 3 101074 3
2543 29175 3 101075 3
2544 29176 3 101076 3
2545 29177 3 101077 3
2546 29178 3 101078 3
2547 29179 3 101079 3
2548 29180 3 101080 3
2549 29181 3 101081 3
2550 29182 3 101082 3
2551 29183 3 101083 3
2552 29184 3 101084 3
2553 29185 3 101085 3
2554 29186 3 101086 3
2555 29187 3 101087 3
2556 29188 3 101088 3
2557 29189 3 101089 3
2558 29190 3 101090 3
2559 29191 3 101091 3
2560 29192 3 101092 3
2561 29193 3 101093 3
2562 29194 3 101094 3
2563 29195 3 101095 3
2564 29196 3 101096 3
2565 29197 3 101097 3
2566 29198 3 101098 3
2567 29199 3 101099 3
2568 29200 3 101100 3
2569 29201 3 101101 3
2570 29202 3 101102 3

2571 29203 3 101103 3
2572 29204 3 101104 3
2573 29205 3 101105 3
2574 29206 3 101106 3
2575 29207 3 101107 3
2576 29208 3 101108 3
2577 29209 3 101109 3
2578 29210 3 101110 3
2579 29211 3 101111 3
2580 29212 3 101112 3
2581 29213 3 101113 3
2582 29214 3 101114 3
2583 29215 3 101115 3
2584 29216 3 101116 3
2585 29217 3 101117 3
2586 29218 3 101118 3
2587 29219 3 101119 3
2588 29220 3 101120 3
2589 29221 3 101121 3
2590 29222 3 101122 3
2591 29223 3 101123 3
2592 29224 3 101124 3
2593 29225 3 101125 3
2594 29226 3 101126 3
2595 29227 3 101127 3
2596 29228 3 101128 3
2597 29229 3 101129 3
2598 29230 3 101130 3
2599 29231 3 101131 3
2600 29232 3 101132 3
2601 29233 3 101133 3
2602 29234 3 101134 3
2603 29235 3 101135 3
2604 29236 3 101136 3
2605 29237 3 101137 3
2606 29238 3 101138 3
2607 29239 3 101139 3
2608 29240 3 101140 3
2609 29241 3 101141 3
2610 29242 3 101142 3
2611 29243 3 101143 3
2612 29244 3 101144 3
2613 29245 3 101145 3
2614 29246 3 101146 3
2615 29247 3 101147 3
2616 29248 3 101148 3
2617 29249 3 101149 3
2618 29250 3 101150 3
2619 29251 3 101151 3
2620 29252 3 101152 3
2621 29253 3 101153 3
2622 29254 3 101154 3
2623 29255 3 101155 3
2624 29256 3 101156 3
2625 29257 3 101157 3
2626 29258 3 101158 3

2627 29259 3 101159 3
2628 29260 3 101160 3
2629 29261 3 101161 3
2630 29262 3 101162 3
2631 29263 3 101163 3
2632 29264 3 101164 3
2633 29265 3 101165 3
2634 29266 3 101166 3
2635 29267 3 101167 3
2636 29268 3 101168 3
2637 29269 3 101169 3
2638 29270 3 101170 3
2639 29271 3 101171 3
2640 29272 3 101172 3
2641 29273 3 101173 3
2642 29274 3 101174 3
2643 29275 3 101175 3
2644 29276 3 101176 3
2645 29277 3 101177 3
2646 29278 3 101178 3
2647 29279 3 101179 3
2648 29280 3 101180 3
2649 29281 3 101181 3
2650 29282 3 101182 3
2651 29283 3 101183 3
2652 29284 3 101184 3
2653 29285 3 101185 3
2654 29286 3 101186 3
2655 29287 3 101187 3
2656 29288 3 101188 3
2657 29289 3 101189 3
2658 29290 3 101190 3
2659 29291 3 101191 3
2660 29292 3 101192 3
2661 29293 3 101193 3
2662 29294 3 101194 3
2663 29295 3 101195 3
2664 29296 3 101196 3
2665 29297 3 101197 3
2666 29298 3 101198 3
2667 29299 3 101199 3
2668 29300 3 101200 3
2669 29301 3 101201 3
2670 29302 3 101202 3
2671 29303 3 101203 3
2672 29304 3 101204 3
2673 29305 3 101205 3
2674 29306 3 101206 3
2675 29307 3 101207 3
2676 29308 3 101208 3
2677 29309 3 101209 3
2678 29310 3 101210 3
2679 29311 3 101211 3
2680 29312 3 101212 3
2681 29313 3 101213 3
2682 29314 3 101214 3

2683 29315 3 101215 3
2684 29316 3 101216 3
2685 29317 3 101217 3
2686 29318 3 101218 3
2687 29319 3 101219 3
2688 29320 3 101220 3
2689 29321 3 101221 3
2690 29322 3 101222 3
2691 29323 3 101223 3
2692 29324 3 101224 3
2693 29325 3 101225 3
2694 29326 3 101226 3
2695 29327 3 101227 3
2696 29328 3 101228 3
2697 29329 3 101229 3
2698 29330 3 101230 3
2699 29331 3 101231 3
2700 29332 3 101232 3
2701 29333 3 101233 3
2702 29334 3 101234 3
2703 29335 3 101235 3
2704 29336 3 101236 3
2705 29337 3 101237 3
2706 29338 3 101238 3
2707 29339 3 101239 3
2708 29340 3 101240 3
2709 29341 3 101241 3
2710 29342 3 101242 3
2711 29343 3 101243 3
2712 29344 3 101244 3
2713 29345 3 101245 3
2714 29346 3 101246 3
2715 29347 3 101247 3
2716 29348 3 101248 3
2717 29349 3 101249 3
2718 29350 3 101250 3
2719 29351 3 101251 3
2720 29352 3 101252 3
2721 29353 3 101253 3
2722 29354 3 101254 3
2723 29355 3 101255 3
2724 29356 3 101256 3
2725 29357 3 101257 3
2726 29358 3 101258 3
2727 29359 3 101259 3
2728 29360 3 101260 3
2729 29361 3 101261 3
2730 29362 3 101262 3
2731 29363 3 101263 3
2732 29364 3 101264 3
2733 29365 3 101265 3
2734 29366 3 101266 3
2735 29367 3 101267 3
2736 29368 3 101268 3
2737 29369 3 101269 3
2738 29370 3 101270 3

2739 29371 3 101271 3
2740 29372 3 101272 3
2741 29373 3 101273 3
2742 29374 3 101274 3
2743 29375 3 101275 3
2744 29376 3 101276 3
2745 29377 3 101277 3
2746 29378 3 101278 3
2747 29379 3 101279 3
2748 29380 3 101280 3
2749 29381 3 101281 3
2750 29382 3 101282 3
2751 29383 3 101283 3
2752 29384 3 101284 3
2753 29385 3 101285 3
2754 29386 3 101286 3
2755 29387 3 101287 3
2756 29388 3 101288 3
2757 29389 3 101289 3
2758 29390 3 101290 3
2759 29391 3 101291 3
2760 29392 3 101292 3
2761 29393 3 101293 3
2762 29394 3 101294 3
2763 29395 3 101295 3
2764 29396 3 101296 3
2765 29397 3 101297 3
2766 29398 3 101298 3
2767 29399 3 101299 3
2768 29400 3 101300 3
2769 29401 3 101301 3
2770 29402 3 101302 3
2771 29403 3 101303 3
2772 29404 3 101304 3
2773 29405 3 101305 3
2774 29406 3 101306 3
2775 29407 3 101307 3
2776 29408 3 101308 3
2777 29409 3 101309 3
2778 29410 3 101310 3
2779 29411 3 101311 3
2780 29412 3 101312 3
2781 29413 3 101313 3
2782 29414 3 101314 3
2783 29415 3 101315 3
2784 29416 3 101316 3
2785 29417 3 101317 3
2786 29418 3 101318 3
2787 29419 3 101319 3
2788 29420 3 101320 3
2789 29421 3 101321 3
2790 29422 3 101322 3
2791 29423 3 101323 3
2792 29424 3 101324 3
2793 29425 3 101325 3
2794 29426 3 101326 3

2795 29427 3 101327 3
2796 29428 3 101328 3
2797 29429 3 101329 3
2798 29430 3 101330 3
2799 29431 3 101331 3
2800 29432 3 101332 3
2801 29433 3 101333 3
2802 29434 3 101334 3
2803 29435 3 101335 3
2804 29436 3 101336 3
2805 29437 3 101337 3
2806 29438 3 101338 3
2807 29439 3 101339 3
2808 29440 3 101340 3
2809 29441 3 101341 3
2810 29442 3 101342 3
2811 29443 3 101343 3
2812 29444 3 101344 3
2813 29445 3 101345 3
2814 29446 3 101346 3
2815 29447 3 101347 3
2816 29448 3 101348 3
2817 29449 3 101349 3
2818 29450 3 101350 3
2819 29451 3 101351 3
2820 29452 3 101352 3
2821 29453 3 101353 3
2822 29454 3 101354 3
2823 29455 3 101355 3
2824 29456 3 101356 3
2825 29457 3 101357 3
2826 29458 3 101358 3
2827 29459 3 101359 3
2828 29460 3 101360 3
2829 29461 3 101361 3
2830 29462 3 101362 3
2831 29463 3 101363 3
2832 29464 3 101364 3
2833 29465 3 101365 3
2834 29466 3 101366 3
2835 29467 3 101367 3
2836 29468 3 101368 3
2837 29469 3 101369 3
2838 29470 3 101370 3
2839 29471 3 101371 3
2840 29472 3 101372 3
2841 29473 3 101373 3
2842 29474 3 101374 3
2843 29475 3 101375 3
2844 29476 3 101376 3
2845 29477 3 101377 3
2846 29478 3 101378 3
2847 29479 3 101379 3
2848 29480 3 101380 3
2849 29481 3 101381 3
2850 29482 3 101382 3

2851 29483 3 101383 3
2852 29484 3 101384 3
2853 29485 3 101385 3
2854 29486 3 101386 3
2855 29487 3 101387 3
2856 29488 3 101388 3
2857 29489 3 101389 3
2858 29490 3 101390 3
2859 29491 3 101391 3
2860 29492 3 101392 3
2861 29493 3 101393 3
2862 29494 3 101394 3
2863 29495 3 101395 3
2864 29496 3 101396 3
2865 29497 3 101397 3
2866 29498 3 101398 3
2867 29499 3 101399 3
2868 29500 3 101400 3
2869 29501 3 101401 3
2870 29502 3 101402 3
2871 29503 3 101403 3
2872 29504 3 101404 3
2873 29505 3 101405 3
2874 29506 3 101406 3
2875 29507 3 101407 3
2876 29508 3 101408 3
2877 29509 3 101409 3
2878 29510 3 101410 3
2879 29511 3 101411 3
2880 29512 3 101412 3
2881 29513 3 101413 3
2882 29514 3 101414 3
2883 29515 3 101415 3
2884 29516 3 101416 3
2885 29517 3 101417 3
2886 29518 3 101418 3
2887 29519 3 101419 3
2888 29520 3 101420 3
2889 29521 3 101421 3
2890 29522 3 101422 3
2891 29523 3 101423 3
2892 29524 3 101424 3
2893 29525 3 101425 3
2894 29526 3 101426 3
2895 29527 3 101427 3
2896 29528 3 101428 3
2897 29529 3 101429 3
2898 29530 3 101430 3
2899 29531 3 101431 3
2900 29532 3 101432 3
2901 29533 3 101433 3
2902 29534 3 101434 3
2903 29535 3 101435 3
2904 29536 3 101436 3
2905 29537 3 101437 3
2906 29538 3 101438 3

2907 29539 3 101439 3
2908 29540 3 101440 3
2909 29541 3 101441 3
2910 29542 3 101442 3
2911 29543 3 101443 3
2912 29544 3 101444 3
2913 29545 3 101445 3
2914 29546 3 101446 3
2915 29547 3 101447 3
2916 29548 3 101448 3
2917 29549 3 101449 3
2918 29550 3 101450 3
2919 29551 3 101451 3
2920 29552 3 101452 3
2921 29553 3 101453 3
2922 29554 3 101454 3
2923 29555 3 101455 3
2924 29556 3 101456 3
2925 29557 3 101457 3
2926 29558 3 101458 3
2927 29559 3 101459 3
2928 29560 3 101460 3
2929 29561 3 101461 3
2930 29562 3 101462 3
2931 29563 3 101463 3
2932 29564 3 101464 3
2933 29565 3 101465 3
2934 29566 3 101466 3
2935 29567 3 101467 3
2936 29568 3 101468 3
2937 29569 3 101469 3
2938 29570 3 101470 3
2939 29571 3 101471 3
2940 29572 3 101472 3
2941 29573 3 101473 3
2942 29574 3 101474 3
2943 29575 3 101475 3
2944 29576 3 101476 3
2945 29577 3 101477 3
2946 29578 3 101478 3
2947 29579 3 101479 3
2948 29580 3 101480 3
2949 29581 3 101481 3
2950 29582 3 101482 3
2951 29583 3 101483 3
2952 29584 3 101484 3
2953 29585 3 101485 3
2954 29586 3 101486 3
2955 29587 3 101487 3
2956 29588 3 101488 3
2957 29589 3 101489 3
2958 29590 3 101490 3
2959 29591 3 101491 3
2960 29592 3 101492 3
2961 29593 3 101493 3
2962 29594 3 101494 3

2963 29595 3 101495 3
2964 29596 3 101496 3
2965 29597 3 101497 3
2966 29598 3 101498 3
2967 29599 3 101499 3
2968 29600 3 101500 3
2969 29601 3 101501 3
2970 29602 3 101502 3
2971 29603 3 101503 3
2972 29604 3 101504 3
2973 29605 3 101505 3
2974 29606 3 101506 3
2975 29607 3 101507 3
2976 29608 3 101508 3
2977 29609 3 101509 3
2978 29610 3 101510 3
2979 29611 3 101511 3
2980 29612 3 101512 3
2981 29613 3 101513 3
2982 29614 3 101514 3
2983 29615 3 101515 3
2984 29616 3 101516 3
2985 29617 3 101517 3
2986 29618 3 101518 3
2987 29619 3 101519 3
2988 29620 3 101520 3
2989 29621 3 101521 3
2990 29622 3 101522 3
2991 29623 3 101523 3
2992 29624 3 101524 3
2993 29625 3 101525 3
2994 29626 3 101526 3
2995 29627 3 101527 3
2996 29628 3 101528 3
2997 29629 3 101529 3
2998 29630 3 101530 3
2999 29631 3 101531 3
3000 29632 3 101532 3
3001 29633 3 101533 3
3002 29634 3 101534 3
3003 29635 3 101535 3
3004 29636 3 101536 3
3005 29637 3 101537 3
3006 29638 3 101538 3
3007 29639 3 101539 3
3008 29640 3 101540 3
3009 29641 3 101541 3
3010 29642 3 101542 3
3011 29643 3 101543 3
3012 29644 3 101544 3
3013 29645 3 101545 3
3014 29646 3 101546 3
3015 29647 3 101547 3
3016 29648 3 101548 3
3017 29649 3 101549 3
3018 29650 3 101550 3

3019 29651 3 101551 3
3020 29652 3 101552 3
3021 29653 3 101553 3
3022 29654 3 101554 3
3023 29655 3 101555 3
3024 29656 3 101556 3
3025 29657 3 101557 3
3026 29658 3 101558 3
3027 29659 3 101559 3
3028 29660 3 101560 3
3029 29661 3 101561 3
3030 29662 3 101562 3
3031 29663 3 101563 3
3032 29664 3 101564 3
3033 29665 3 101565 3
3034 29666 3 101566 3
3035 29667 3 101567 3
3036 29668 3 101568 3
3037 29669 3 101569 3
3038 29670 3 101570 3
3039 29671 3 101571 3
3040 29672 3 101572 3
3041 29673 3 101573 3
3042 29674 3 101574 3
3043 29675 3 101575 3
3044 29676 3 101576 3
3045 29677 3 101577 3
3046 29678 3 101578 3
3047 29679 3 101579 3
3048 29680 3 101580 3
3049 29681 3 101581 3
3050 29682 3 101582 3
3051 29683 3 101583 3
3052 29684 3 101584 3
3053 29685 3 101585 3
3054 29686 3 101586 3
3055 29687 3 101587 3
3056 29688 3 101588 3
3057 29689 3 101589 3
3058 29690 3 101590 3
3059 29691 3 101591 3
3060 29692 3 101592 3
3061 29693 3 101593 3
3062 29694 3 101594 3
3063 29695 3 101595 3
3064 29696 3 101596 3
3065 29697 3 101597 3
3066 29698 3 101598 3
3067 29699 3 101599 3
3068 29700 3 101600 3
3069 29701 3 101601 3
3070 29702 3 101602 3
3071 29703 3 101603 3
3072 29704 3 101604 3
3073 29705 3 101605 3
3074 29706 3 101606 3

3075 29707 3 101607 3
3076 29708 3 101608 3
3077 29709 3 101609 3
3078 29710 3 101610 3
3079 29711 3 101611 3
3080 29712 3 101612 3
3081 29713 3 101613 3
3082 29714 3 101614 3
3083 29715 3 101615 3
3084 29716 3 101616 3
3085 29717 3 101617 3
3086 29718 3 101618 3
3087 29719 3 101619 3
3088 29720 3 101620 3
3089 29721 3 101621 3
3090 29722 3 101622 3
3091 29723 3 101623 3
3092 29724 3 101624 3
3093 29725 3 101625 3
3094 29726 3 101626 3
3095 29727 3 101627 3
3096 29728 3 101628 3
3097 29729 3 101629 3
3098 29730 3 101630 3
3099 29731 3 101631 3
3100 29732 3 101632 3
3101 29733 3 101633 3
3102 29734 3 101634 3
3103 29735 3 101635 3
3104 29736 3 101636 3
3105 29737 3 101637 3
3106 29738 3 101638 3
3107 29739 3 101639 3
3108 29740 3 101640 3
3109 29741 3 101641 3
3110 29742 3 101642 3
3111 29743 3 101643 3
3112 29744 3 101644 3
3113 29745 3 101645 3
3114 29746 3 101646 3
3115 29747 3 101647 3
3116 29748 3 101648 3
3117 29749 3 101649 3
3118 29750 3 101650 3
3119 29751 3 101651 3
3120 29752 3 101652 3
3121 29753 3 101653 3
3122 29754 3 101654 3
3123 29755 3 101655 3
3124 29756 3 101656 3
3125 29757 3 101657 3
3126 29758 3 101658 3
3127 29759 3 101659 3
3128 29760 3 101660 3
3129 29761 3 101661 3
3130 29762 3 101662 3

3131 29763 3 101663 3
3132 29764 3 101664 3
3133 29765 3 101665 3
3134 29766 3 101666 3
3135 29767 3 101667 3
3136 29768 3 101668 3
3137 29769 3 101669 3
3138 29770 3 101670 3
3139 29771 3 101671 3
3140 29772 3 101672 3
3141 29773 3 101673 3
3142 29774 3 101674 3
3143 29775 3 101675 3
3144 29776 3 101676 3
3145 29777 3 101677 3
3146 29778 3 101678 3
3147 29779 3 101679 3
3148 29780 3 101680 3
3149 29781 3 101681 3
3150 29782 3 101682 3
3151 29783 3 101683 3
3152 29784 3 101684 3
3153 29785 3 101685 3
3154 29786 3 101686 3
3155 29787 3 101687 3
3156 29788 3 101688 3
3157 29789 3 101689 3
3158 29790 3 101690 3
3159 29791 3 101691 3
3160 29792 3 101692 3
3161 29793 3 101693 3
3162 29794 3 101694 3
3163 29795 3 101695 3
3164 29796 3 101696 3
3165 29797 3 101697 3
3166 29798 3 101698 3
3167 29799 3 101699 3
3168 29800 3 101700 3
3169 29801 3 101701 3
3170 29802 3 101702 3
3171 29803 3 101703 3
3172 29804 3 101704 3
3173 29805 3 101705 3
3174 29806 3 101706 3
3175 29807 3 101707 3
3176 29808 3 101708 3
3177 29809 3 101709 3
3178 29810 3 101710 3
3179 29811 3 101711 3
3180 29812 3 101712 3
3181 29813 3 101713 3
3182 29814 3 101714 3
3183 29815 3 101715 3
3184 29816 3 101716 3
3185 29817 3 101717 3
3186 29818 3 101718 3

3187 29819 3 101719 3
3188 29820 3 101720 3
3189 29821 3 101721 3
3190 29822 3 101722 3
3191 29823 3 101723 3
3192 29824 3 101724 3
3193 29825 3 101725 3
3194 29826 3 101726 3
3195 29827 3 101727 3
3196 29828 3 101728 3
3197 29829 3 101729 3
3198 29830 3 101730 3
3199 29831 3 101731 3
3200 29832 3 101732 3
3201 29833 3 101733 3
3202 29834 3 101734 3
3203 29835 3 101735 3
3204 29836 3 101736 3
3205 29837 3 101737 3
3206 29838 3 101738 3
3207 29839 3 101739 3
3208 29840 3 101740 3
3209 29841 3 101741 3
3210 29842 3 101742 3
3211 29843 3 101743 3
3212 29844 3 101744 3
3213 29845 3 101745 3
3214 29846 3 101746 3
3215 29847 3 101747 3
3216 29848 3 101748 3
3217 29849 3 101749 3
3218 29850 3 101750 3
3219 29851 3 101751 3
3220 29852 3 101752 3
3221 29853 3 101753 3
3222 29854 3 101754 3
3223 29855 3 101755 3
3224 29856 3 101756 3
3225 29857 3 101757 3
3226 29858 3 101758 3
3227 29859 3 101759 3
3228 29860 3 101760 3
3229 29861 3 101761 3
3230 29862 3 101762 3
3231 29863 3 101763 3
3232 29864 3 101764 3
3233 29865 3 101765 3
3234 29866 3 101766 3
3235 29867 3 101767 3
3236 29868 3 101768 3
3237 29869 3 101769 3
3238 29870 3 101770 3
3239 29871 3 101771 3
3240 29872 3 101772 3
3241 29873 3 101773 3
3242 29874 3 101774 3

3243 29875 3 101775 3
3244 29876 3 101776 3
3245 29877 3 101777 3
3246 29878 3 101778 3
3247 29879 3 101779 3
3248 29880 3 101780 3
3249 29881 3 101781 3
3250 29882 3 101782 3
3251 29883 3 101783 3
3252 29884 3 101784 3
3253 29885 3 101785 3
3254 29886 3 101786 3
3255 29887 3 101787 3
3256 29888 3 101788 3
3257 29889 3 101789 3
3258 29890 3 101790 3
3259 29891 3 101791 3
3260 29892 3 101792 3
3261 29893 3 101793 3
3262 29894 3 101794 3
3263 29895 3 101795 3
3264 29896 3 101796 3
3265 29897 3 101797 3
3266 29898 3 101798 3
3267 29899 3 101799 3
3268 29900 3 101800 3
3269 29901 3 101801 3
3270 29902 3 101802 3
3271 29903 3 101803 3
3272 29904 3 101804 3
3273 29905 3 101805 3
3274 29906 3 101806 3
3275 29907 3 101807 3
3276 29908 3 101808 3
3277 29909 3 101809 3
3278 29910 3 101810 3
3279 29911 3 101811 3
3280 29912 3 101812 3
3281 29913 3 101813 3
3282 29914 3 101814 3
3283 29915 3 101815 3
3284 29916 3 101816 3
3285 29917 3 101817 3
3286 29918 3 101818 3
3287 29919 3 101819 3
3288 29920 3 101820 3
3289 29921 3 101821 3
3290 29922 3 101822 3
3291 29923 3 101823 3
3292 29924 3 101824 3
3293 29925 3 101825 3
3294 29926 3 101826 3
3295 29927 3 101827 3
3296 29928 3 101828 3
3297 29929 3 101829 3
3298 29930 3 101830 3

3299 29931 3 101831 3
3300 29932 3 101832 3
3301 29933 3 101833 3
3302 29934 3 101834 3
3303 29935 3 101835 3
3304 29936 3 101836 3
3305 29937 3 101837 3
3306 29938 3 101838 3
3307 29939 3 101839 3
3308 29940 3 101840 3
3309 29941 3 101841 3
3310 29942 3 101842 3
3311 29943 3 101843 3
3312 29944 3 101844 3
3313 29945 3 101845 3
3314 29946 3 101846 3
3315 29947 3 101847 3
3316 29948 3 101848 3
3317 29949 3 101849 3
3318 29950 3 101850 3
3319 29951 3 101851 3
3320 29952 3 101852 3
3321 29953 3 101853 3
3322 29954 3 101854 3
3323 29955 3 101855 3
3324 29956 3 101856 3
3325 29957 3 101857 3
3326 29958 3 101858 3
3327 29959 3 101859 3
3328 29960 3 101860 3
3329 29961 3 101861 3
3330 29962 3 101862 3
3331 29963 3 101863 3
3332 29964 3 101864 3
3333 29965 3 101865 3
3334 29966 3 101866 3
3335 29967 3 101867 3
3336 29968 3 101868 3
3337 29969 3 101869 3
3338 29970 3 101870 3
3339 29971 3 101871 3
3340 29972 3 101872 3
3341 29973 3 101873 3
3342 29974 3 101874 3
3343 29975 3 101875 3
3344 29976 3 101876 3
3345 29977 3 101877 3
3346 29978 3 101878 3
3347 29979 3 101879 3
3348 29980 3 101880 3
3349 29981 3 101881 3
3350 29982 3 101882 3
3351 29983 3 101883 3
3352 29984 3 101884 3
3353 29985 3 101885 3
3354 29986 3 101886 3

3355 29987 3 101887 3
3356 29988 3 101888 3
3357 29989 3 101889 3
3358 29990 3 101890 3
3359 29991 3 101891 3
3360 29992 3 101892 3
3361 29993 3 101893 3
3362 29994 3 101894 3
3363 29995 3 101895 3
3364 29996 3 101896 3
3365 29997 3 101897 3
3366 29998 3 101898 3
3367 29999 3 101899 3
3368 30000 3 101900 3
3369 30001 3 101901 3
3370 30002 3 101902 3
3371 30003 3 101903 3
3372 30004 3 101904 3
3373 30005 3 101905 3
3374 30006 3 101906 3
3375 30007 3 101907 3
3376 30008 3 101908 3
3377 30009 3 101909 3
3378 30010 3 101910 3
3379 30011 3 101911 3
3380 30012 3 101912 3
3381 30013 3 101913 3
3382 30014 3 101914 3
3383 30015 3 101915 3
3384 30016 3 101916 3
3385 30017 3 101917 3
3386 30018 3 101918 3
3387 30019 3 101919 3
3388 30020 3 101920 3
3389 30021 3 101921 3
3390 30022 3 101922 3
3391 30023 3 101923 3
3392 30024 3 101924 3
3393 30025 3 101925 3
3394 30026 3 101926 3
3395 30027 3 101927 3
3396 30028 3 101928 3
3397 30029 3 101929 3
3398 30030 3 101930 3
3399 30031 3 101931 3
3400 30032 3 101932 3
3401 30033 3 101933 3
3402 30034 3 101934 3
3403 30035 3 101935 3
3404 30036 3 101936 3
3405 30037 3 101937 3
3406 30038 3 101938 3
3407 30039 3 101939 3
3408 30040 3 101940 3
3409 30041 3 101941 3
3410 30042 3 101942 3

3411 30043 3 101943 3
3412 30044 3 101944 3
3413 30045 3 101945 3
3414 30046 3 101946 3
3415 30047 3 101947 3
3416 30048 3 101948 3
3417 30049 3 101949 3
3418 30050 3 101950 3
3419 30051 3 101951 3
3420 30052 3 101952 3
3421 30053 3 101953 3
3422 30054 3 101954 3
3423 30055 3 101955 3
3424 30056 3 101956 3
3425 30057 3 101957 3
3426 30058 3 101958 3
3427 30059 3 101959 3
3428 30060 3 101960 3
3429 30061 3 101961 3
3430 30062 3 101962 3
3431 30063 3 101963 3
3432 30064 3 101964 3
3433 30065 3 101965 3
3434 30066 3 101966 3
3435 30067 3 101967 3
3436 30068 3 101968 3
3437 30069 3 101969 3
3438 30070 3 101970 3
3439 30071 3 101971 3
3440 30072 3 101972 3
3441 30073 3 101973 3
3442 30074 3 101974 3
3443 30075 3 101975 3
3444 30076 3 101976 3
3445 30077 3 101977 3
3446 30078 3 101978 3
3447 30079 3 101979 3
3448 30080 3 101980 3
3449 30081 3 101981 3
3450 30082 3 101982 3
3451 30083 3 101983 3
3452 30084 3 101984 3
3453 30085 3 101985 3
3454 30086 3 101986 3
3455 30087 3 101987 3
3456 30088 3 101988 3
3457 30089 3 101989 3
3458 30090 3 101990 3
3459 30091 3 101991 3
3460 30092 3 101992 3
3461 30093 3 101993 3
3462 30094 3 101994 3
3463 30095 3 101995 3
3464 30096 3 101996 3
3465 30097 3 101997 3
3466 30098 3 101998 3

3467 30099 3 101999 3
3468 30100 3 102000 3
3469 30101 3 102001 3
3470 30102 3 102002 3
3471 30103 3 102003 3
3472 30104 3 102004 3
3473 30105 3 102005 3
3474 30106 3 102006 3
3475 30107 3 102007 3
3476 30108 3 102008 3
3477 30109 3 102009 3
3478 30110 3 102010 3
3479 30111 3 102011 3
3480 30112 3 102012 3
3481 30113 3 102013 3
3482 30114 3 102014 3
3483 30115 3 102015 3
3484 30116 3 102016 3
3485 30117 3 102017 3
3486 30118 3 102018 3
3487 30119 3 102019 3
3488 30120 3 102020 3
3489 30121 3 102021 3
3490 30122 3 102022 3
3491 30123 3 102023 3
3492 30124 3 102024 3
3493 30125 3 102025 3
3494 30126 3 102026 3
3495 30127 3 102027 3
3496 30128 3 102028 3
3497 30129 3 102029 3
3498 30130 3 102030 3
3499 30131 3 102031 3
3500 30132 3 102032 3
3501 30133 3 102033 3
3502 30134 3 102034 3
3503 30135 3 102035 3
3504 30136 3 102036 3
3505 30137 3 102037 3
3506 30138 3 102038 3
3507 30139 3 102039 3
3508 30140 3 102040 3
3509 30141 3 102041 3
3510 30142 3 102042 3
3511 30143 3 102043 3
3512 30144 3 102044 3
3513 30145 3 102045 3
3514 30146 3 102046 3
3515 30147 3 102047 3
3516 30148 3 102048 3
3517 30149 3 102049 3
3518 30150 3 102050 3
3519 30151 3 102051 3
3520 30152 3 102052 3
3521 30153 3 102053 3
3522 30154 3 102054 3

3523 30155 3 102055 3
3524 30156 3 102056 3
3525 30157 3 102057 3
3526 30158 3 102058 3
3527 30159 3 102059 3
3528 30160 3 102060 3
3529 30161 3 102061 3
3530 30162 3 102062 3
3531 30163 3 102063 3
3532 30164 3 102064 3
3533 30165 3 102065 3
3534 30166 3 102066 3
3535 30167 3 102067 3
3536 30168 3 102068 3
3537 30169 3 102069 3
3538 30170 3 102070 3
3539 30171 3 102071 3
3540 30172 3 102072 3
3541 30173 3 102073 3
3542 30174 3 102074 3
3543 30175 3 102075 3
3544 30176 3 102076 3
3545 30177 3 102077 3
3546 30178 3 102078 3
3547 30179 3 102079 3
3548 30180 3 102080 3
3549 30181 3 102081 3
3550 30182 3 102082 3
3551 30183 3 102083 3
3552 30184 3 102084 3
3553 30185 3 102085 3
3554 30186 3 102086 3
3555 30187 3 102087 3
3556 30188 3 102088 3
3557 30189 3 102089 3
3558 30190 3 102090 3
3559 30191 3 102091 3
3560 30192 3 102092 3
3561 30193 3 102093 3
3562 30194 3 102094 3
3563 30195 3 102095 3
3564 30196 3 102096 3
3565 30197 3 102097 3
3566 30198 3 102098 3
3567 30199 3 102099 3
3568 30200 3 102100 3
3569 30201 3 102101 3
3570 30202 3 102102 3
3571 30203 3 102103 3
3572 30204 3 102104 3
3573 30205 3 102105 3
3574 30206 3 102106 3
3575 30207 3 102107 3
3576 30208 3 102108 3
3577 30209 3 102109 3
3578 30210 3 102110 3

3579 30211 3 102111 3
3580 30212 3 102112 3
3581 30213 3 102113 3
3582 30214 3 102114 3
3583 30215 3 102115 3
3584 30216 3 102116 3
3585 30217 3 102117 3
3586 30218 3 102118 3
3587 30219 3 102119 3
3588 30220 3 102120 3
3589 30221 3 102121 3
3590 30222 3 102122 3
3591 30223 3 102123 3
3592 30224 3 102124 3
3593 30225 3 102125 3
3594 30226 3 102126 3
3595 30227 3 102127 3
3596 30228 3 102128 3
3597 30229 3 102129 3
3598 30230 3 102130 3
3599 30231 3 102131 3
3600 30232 3 102132 3
3601 30233 3 102133 3
3602 30234 3 102134 3
3603 30235 3 102135 3
3604 30236 3 102136 3
3605 30237 3 102137 3
3606 30238 3 102138 3
3607 30239 3 102139 3
3608 30240 3 102140 3
3609 30241 3 102141 3
3610 30242 3 102142 3
3611 30243 3 102143 3
3612 30244 3 102144 3
3613 30245 3 102145 3
3614 30246 3 102146 3
3615 30247 3 102147 3
3616 30248 3 102148 3
3617 30249 3 102149 3
3618 30250 3 102150 3
3619 30251 3 102151 3
3620 30252 3 102152 3
3621 30253 3 102153 3
3622 30254 3 102154 3
3623 30255 3 102155 3
3624 30256 3 102156 3
3625 30257 3 102157 3
3626 30258 3 102158 3
3627 30259 3 102159 3
3628 30260 3 102160 3
3629 30261 3 102161 3
3630 30262 3 102162 3
3631 30263 3 102163 3
3632 30264 3 102164 3
3633 30265 3 102165 3
3634 30266 3 102166 3

3635 30267 3 102167 3
3636 30268 3 102168 3
3637 30269 3 102169 3
3638 30270 3 102170 3
3639 30271 3 102171 3
3640 30272 3 102172 3
3641 30273 3 102173 3
3642 30274 3 102174 3
3643 30275 3 102175 3
3644 30276 3 102176 3
3645 30277 3 102177 3
3646 30278 3 102178 3
3647 30279 3 102179 3
3648 30280 3 102180 3
3649 30281 3 102181 3
3650 30282 3 102182 3
3651 30283 3 102183 3
3652 30284 3 102184 3
3653 30285 3 102185 3
3654 30286 3 102186 3
3655 30287 3 102187 3
3656 30288 3 102188 3
3657 30289 3 102189 3
3658 30290 3 102190 3
3659 30291 3 102191 3
3660 30292 3 102192 3
3661 30293 3 102193 3
3662 30294 3 102194 3
3663 30295 3 102195 3
3664 30296 3 102196 3
3665 30297 3 102197 3
3666 30298 3 102198 3
3667 30299 3 102199 3
3668 30300 3 102200 3
3669 30301 3 102201 3
3670 30302 3 102202 3
3671 30303 3 102203 3
3672 30304 3 102204 3
3673 30305 3 102205 3
3674 30306 3 102206 3
3675 30307 3 102207 3
3676 30308 3 102208 3
3677 30309 3 102209 3
3678 30310 3 102210 3
3679 30311 3 102211 3
3680 30312 3 102212 3
3681 30313 3 102213 3
3682 30314 3 102214 3
3683 30315 3 102215 3
3684 30316 3 102216 3
3685 30317 3 102217 3
3686 30318 3 102218 3
3687 30319 3 102219 3
3688 30320 3 102220 3
3689 30321 3 102221 3
3690 30322 3 102222 3

3691 30323 3 102223 3
3692 30324 3 102224 3
3693 30325 3 102225 3
3694 30326 3 102226 3
3695 30327 3 102227 3
3696 30328 3 102228 3
3697 30329 3 102229 3
3698 30330 3 102230 3
3699 30331 3 102231 3
3700 30332 3 102232 3
3701 30333 3 102233 3
3702 30334 3 102234 3
3703 30335 3 102235 3
3704 30336 3 102236 3
3705 30337 3 102237 3
3706 30338 3 102238 3
3707 30339 3 102239 3
3708 30340 3 102240 3
3709 30341 3 102241 3
3710 30342 3 102242 3
3711 30343 3 102243 3
3712 30344 3 102244 3
3713 30345 3 102245 3
3714 30346 3 102246 3
3715 30347 3 102247 3
3716 30348 3 102248 3
3717 30349 3 102249 3
3718 30350 3 102250 3
3719 30351 3 102251 3
3720 30352 3 102252 3
3721 30353 3 102253 3
3722 30354 3 102254 3
3723 30355 3 102255 3
3724 30356 3 102256 3
3725 30357 3 102257 3
3726 30358 3 102258 3
3727 30359 3 102259 3
3728 30360 3 102260 3
3729 30361 3 102261 3
3730 30362 3 102262 3
3731 30363 3 102263 3
3732 30364 3 102264 3
3733 30365 3 102265 3
3734 30366 3 102266 3
3735 30367 3 102267 3
3736 30368 3 102268 3
3737 30369 3 102269 3
3738 30370 3 102270 3
3739 30371 3 102271 3
3740 30372 3 102272 3
3741 30373 3 102273 3
3742 30374 3 102274 3
3743 30375 3 102275 3
3744 30376 3 102276 3
3745 30377 3 102277 3
3746 30378 3 102278 3

3747 30379 3 102279 3
3748 30380 3 102280 3
3749 30381 3 102281 3
3750 30382 3 102282 3
3751 30383 3 102283 3
3752 30384 3 102284 3
3753 30385 3 102285 3
3754 30386 3 102286 3
3755 30387 3 102287 3
3756 30388 3 102288 3
3757 30389 3 102289 3
3758 30390 3 102290 3
3759 30391 3 102291 3
3760 30392 3 102292 3
3761 30393 3 102293 3
3762 30394 3 102294 3
3763 30395 3 102295 3
3764 30396 3 102296 3
3765 30397 3 102297 3
3766 30398 3 102298 3
3767 30399 3 102299 3
3768 30400 3 102300 3
3769 30401 3 102301 3
3770 30402 3 102302 3
3771 30403 3 102303 3
3772 30404 3 102304 3
3773 30405 3 102305 3
3774 30406 3 102306 3
3775 30407 3 102307 3
3776 30408 3 102308 3
3777 30409 3 102309 3
3778 30410 3 102310 3
3779 30411 3 102311 3
3780 30412 3 102312 3
3781 30413 3 102313 3
3782 30414 3 102314 3
3783 30415 3 102315 3
3784 30416 3 102316 3
3785 30417 3 102317 3
3786 30418 3 102318 3
3787 30419 3 102319 3
3788 30420 3 102320 3
3789 30421 3 102321 3
3790 30422 3 102322 3
3791 30423 3 102323 3
3792 30424 3 102324 3
3793 30425 3 102325 3
3794 30426 3 102326 3
3795 30427 3 102327 3
3796 30428 3 102328 3
3797 30429 3 102329 3
3798 30430 3 102330 3
3799 30431 3 102331 3
3800 30432 3 102332 3
3801 30433 3 102333 3
3802 30434 3 102334 3

3803 30435 3 102335 3
3804 30436 3 102336 3
3805 30437 3 102337 3
3806 30438 3 102338 3
3807 30439 3 102339 3
3808 30440 3 102340 3
3809 30441 3 102341 3
3810 30442 3 102342 3
3811 30443 3 102343 3
3812 30444 3 102344 3
3813 30445 3 102345 3
3814 30446 3 102346 3
3815 30447 3 102347 3
3816 30448 3 102348 3
3817 30449 3 102349 3
3818 30450 3 102350 3
3819 30451 3 102351 3
3820 30452 3 102352 3
3821 30453 3 102353 3
3822 30454 3 102354 3
3823 30455 3 102355 3
3824 30456 3 102356 3
3825 30457 3 102357 3
3826 30458 3 102358 3
3827 30459 3 102359 3
3828 30460 3 102360 3
3829 30461 3 102361 3
3830 30462 3 102362 3
3831 30463 3 102363 3
3832 30464 3 102364 3
3833 30465 3 102365 3
3834 30466 3 102366 3
3835 30467 3 102367 3
3836 30468 3 102368 3
3837 30469 3 102369 3
3838 30470 3 102370 3
3839 30471 3 102371 3
3840 30472 3 102372 3
3841 30473 3 102373 3
3842 30474 3 102374 3
3843 30475 3 102375 3
3844 30476 3 102376 3
3845 30477 3 102377 3
3846 30478 3 102378 3
3847 30479 3 102379 3
3848 30480 3 102380 3
3849 30481 3 102381 3
3850 30482 3 102382 3
3851 30483 3 102383 3
3852 30484 3 102384 3
3853 30485 3 102385 3
3854 30486 3 102386 3
3855 30487 3 102387 3
3856 30488 3 102388 3
3857 30489 3 102389 3
3858 30490 3 102390 3

3859 30491 3 102391 3
3860 30492 3 102392 3
3861 30493 3 102393 3
3862 30494 3 102394 3
3863 30495 3 102395 3
3864 30496 3 102396 3
3865 30497 3 102397 3
3866 30498 3 102398 3
3867 30499 3 102399 3
3868 30500 3 102400 3
3869 30501 3 102401 3
3870 30502 3 102402 3
3871 30503 3 102403 3
3872 30504 3 102404 3
3873 30505 3 102405 3
3874 30506 3 102406 3
3875 30507 3 102407 3
3876 30508 3 102408 3
3877 30509 3 102409 3
3878 30510 3 102410 3
3879 30511 3 102411 3
3880 30512 3 102412 3
3881 30513 3 102413 3
3882 30514 3 102414 3
3883 30515 3 102415 3
3884 30516 3 102416 3
3885 30517 3 102417 3
3886 30518 3 102418 3
3887 30519 3 102419 3
3888 30520 3 102420 3
3889 30521 3 102421 3
3890 30522 3 102422 3
3891 30523 3 102423 3
3892 30524 3 102424 3
3893 30525 3 102425 3
3894 30526 3 102426 3
3895 30527 3 102427 3
3896 30528 3 102428 3
3897 30529 3 102429 3
3898 30530 3 102430 3
3899 30531 3 102431 3
3900 30532 3 102432 3
3901 30533 3 102433 3
3902 30534 3 102434 3
3903 30535 3 102435 3
3904 30536 3 102436 3
3905 30537 3 102437 3
3906 30538 3 102438 3
3907 30539 3 102439 3
3908 30540 3 102440 3
3909 30541 3 102441 3
3910 30542 3 102442 3
3911 30543 3 102443 3
3912 30544 3 102444 3
3913 30545 3 102445 3
3914 30546 3 102446 3

3915 30547 3 102447 3
3916 30548 3 102448 3
3917 30549 3 102449 3
3918 30550 3 102450 3
3919 30551 3 102451 3
3920 30552 3 102452 3
3921 30553 3 102453 3
3922 30554 3 102454 3
3923 30555 3 102455 3
3924 30556 3 102456 3
3925 30557 3 102457 3
3926 30558 3 102458 3
3927 30559 3 102459 3
3928 30560 3 102460 3
3929 30561 3 102461 3
3930 30562 3 102462 3
3931 30563 3 102463 3
3932 30564 3 102464 3
3933 30565 3 102465 3
3934 30566 3 102466 3
3935 30567 3 102467 3
3936 30568 3 102468 3
3937 30569 3 102469 3
3938 30570 3 102470 3
3939 30571 3 102471 3
3940 30572 3 102472 3
3941 30573 3 102473 3
3942 30574 3 102474 3
3943 30575 3 102475 3
3944 30576 3 102476 3
3945 30577 3 102477 3
3946 30578 3 102478 3
3947 30579 3 102479 3
3948 30580 3 102480 3
3949 30581 3 102481 3
3950 30582 3 102482 3
3951 30583 3 102483 3
3952 30584 3 102484 3
3953 30585 3 102485 3
3954 30586 3 102486 3
3955 30587 3 102487 3
3956 30588 3 102488 3
3957 30589 3 102489 3
3958 30590 3 102490 3
3959 30591 3 102491 3
3960 30592 3 102492 3
3961 30593 3 102493 3
3962 30594 3 102494 3
3963 30595 3 102495 3
3964 30596 3 102496 3
3965 30597 3 102497 3
3966 30598 3 102498 3
3967 30599 3 102499 3
3968 30600 3 102500 3
3969 30601 3 102501 3
3970 30602 3 102502 3

3971 30603 3 102503 3
3972 30604 3 102504 3
3973 30605 3 102505 3
3974 30606 3 102506 3
3975 30607 3 102507 3
3976 30608 3 102508 3
3977 30609 3 102509 3
3978 30610 3 102510 3
3979 30611 3 102511 3
3980 30612 3 102512 3
3981 30613 3 102513 3
3982 30614 3 102514 3
3983 30615 3 102515 3
3984 30616 3 102516 3
3985 30617 3 102517 3
3986 30618 3 102518 3
3987 30619 3 102519 3
3988 30620 3 102520 3
3989 30621 3 102521 3
3990 30622 3 102522 3
3991 30623 3 102523 3
3992 30624 3 102524 3
3993 30625 3 102525 3
3994 30626 3 102526 3
3995 30627 3 102527 3
3996 30628 3 102528 3
3997 30629 3 102529 3
3998 30630 3 102530 3
3999 30631 3 102531 3
4000 30632 3 102532 3
4001 30633 3 102533 3
4002 30634 3 102534 3
4003 30635 3 102535 3
4004 30636 3 102536 3
4005 30637 3 102537 3
4006 30638 3 102538 3
4007 30639 3 102539 3
4008 30640 3 102540 3
4009 30641 3 102541 3
4010 30642 3 102542 3
4011 30643 3 102543 3
4012 30644 3 102544 3
4013 30645 3 102545 3
4014 30646 3 102546 3
4015 30647 3 102547 3
4016 30648 3 102548 3
4017 30649 3 102549 3
4018 30650 3 102550 3
4019 30651 3 102551 3
4020 30652 3 102552 3
4021 30653 3 102553 3
4022 30654 3 102554 3
4023 30655 3 102555 3
4024 30656 3 102556 3
4025 30657 3 102557 3
4026 30658 3 102558 3

4027 30659 3 102559 3
4028 30660 3 102560 3
4029 30661 3 102561 3
4030 30662 3 102562 3
4031 30663 3 102563 3
4032 30664 3 102564 3
4033 30665 3 102565 3
4034 30666 3 102566 3
4035 30667 3 102567 3
4036 30668 3 102568 3
4037 30669 3 102569 3
4038 30670 3 102570 3
4039 30671 3 102571 3
4040 30672 3 102572 3
4041 30673 3 102573 3
4042 30674 3 102574 3
4043 30675 3 102575 3
4044 30676 3 102576 3
4045 30677 3 102577 3
4046 30678 3 102578 3
4047 30679 3 102579 3
4048 30680 3 102580 3
4049 30681 3 102581 3
4050 30682 3 102582 3
4051 30683 3 102583 3
4052 30684 3 102584 3
4053 30685 3 102585 3
4054 30686 3 102586 3
4055 30687 3 102587 3
4056 30688 3 102588 3
4057 30689 3 102589 3
4058 30690 3 102590 3
4059 30691 3 102591 3
4060 30692 3 102592 3
4061 30693 3 102593 3
4062 30694 3 102594 3
4063 30695 3 102595 3
4064 30696 3 102596 3
4065 30697 3 102597 3
4066 30698 3 102598 3
4067 30699 3 102599 3
4068 30700 3 102600 3
4069 30701 3 102601 3
4070 30702 3 102602 3
4071 30703 3 102603 3
4072 30704 3 102604 3
4073 30705 3 102605 3
4074 30706 3 102606 3
4075 30707 3 102607 3
4076 30708 3 102608 3
4077 30709 3 102609 3
4078 30710 3 102610 3
4079 30711 3 102611 3
4080 30712 3 102612 3
4081 30713 3 102613 3
4082 30714 3 102614 3

4083 30715 3 102615 3
4084 30716 3 102616 3
4085 30717 3 102617 3
4086 30718 3 102618 3
4087 30719 3 102619 3
4088 30720 3 102620 3
4089 30721 3 102621 3
4090 30722 3 102622 3
4091 30723 3 102623 3
4092 30724 3 102624 3
4093 30725 3 102625 3
4094 30726 3 102626 3
4095 30727 3 102627 3
4096 30728 3 102628 3
4097 30729 3 102629 3
4098 30730 3 102630 3
4099 30731 3 102631 3
4100 30732 3 102632 3
4101 30733 3 102633 3
4102 30734 3 102634 3
4103 30735 3 102635 3
4104 30736 3 102636 3
4105 30737 3 102637 3
4106 30738 3 102638 3
4107 30739 3 102639 3
4108 30740 3 102640 3
4109 30741 3 102641 3
4110 30742 3 102642 3
4111 30743 3 102643 3
4112 30744 3 102644 3
4113 30745 3 102645 3
4114 30746 3 102646 3
4115 30747 3 102647 3
4116 30748 3 102648 3
4117 30749 3 102649 3
4118 30750 3 102650 3
4119 30751 3 102651 3
4120 30752 3 102652 3
4121 30753 3 102653 3
4122 30754 3 102654 3
4123 30755 3 102655 3
4124 30756 3 102656 3
4125 30757 3 102657 3
4126 30758 3 102658 3
4127 30759 3 102659 3
4128 30760 3 102660 3
4129 30761 3 102661 3
4130 30762 3 102662 3
4131 30763 3 102663 3
4132 30764 3 102664 3
4133 30765 3 102665 3
4134 30766 3 102666 3
4135 30767 3 102667 3
4136 30768 3 102668 3
4137 30769 3 102669 3
4138 30770 3 102670 3

4139 30771 3 102671 3
4140 30772 3 102672 3
4141 30773 3 102673 3
4142 30774 3 102674 3
4143 30775 3 102675 3
4144 30776 3 102676 3
4145 30777 3 102677 3
4146 30778 3 102678 3
4147 30779 3 102679 3
4148 30780 3 102680 3
4149 30781 3 102681 3
4150 30782 3 102682 3
4151 30783 3 102683 3
4152 30784 3 102684 3
4153 30785 3 102685 3
4154 30786 3 102686 3
4155 30787 3 102687 3
4156 30788 3 102688 3
4157 30789 3 102689 3
4158 30790 3 102690 3
4159 30791 3 102691 3
4160 30792 3 102692 3
4161 30793 3 102693 3
4162 30794 3 102694 3
4163 30795 3 102695 3
4164 30796 3 102696 3
4165 30797 3 102697 3
4166 30798 3 102698 3
4167 30799 3 102699 3
4168 30800 3 102700 3
4169 30801 3 102701 3
4170 30802 3 102702 3
4171 30803 3 102703 3
4172 30804 3 102704 3
4173 30805 3 102705 3
4174 30806 3 102706 3
4175 30807 3 102707 3
4176 30808 3 102708 3
4177 30809 3 102709 3
4178 30810 3 102710 3
4179 30811 3 102711 3
4180 30812 3 102712 3
4181 30813 3 102713 3
4182 30814 3 102714 3
4183 30815 3 102715 3
4184 30816 3 102716 3
4185 30817 3 102717 3
4186 30818 3 102718 3
4187 30819 3 102719 3
4188 30820 3 102720 3
4189 30821 3 102721 3
4190 30822 3 102722 3
4191 30823 3 102723 3
4192 30824 3 102724 3
4193 30825 3 102725 3
4194 30826 3 102726 3

4195 30827 3 102727 3
4196 30828 3 102728 3
4197 30829 3 102729 3
4198 30830 3 102730 3
4199 30831 3 102731 3
4200 30832 3 102732 3
4201 30833 3 102733 3
4202 30834 3 102734 3
4203 30835 3 102735 3
4204 30836 3 102736 3
4205 30837 3 102737 3
4206 30838 3 102738 3
4207 30839 3 102739 3
4208 30840 3 102740 3
4209 30841 3 102741 3
4210 30842 3 102742 3
4211 30843 3 102743 3
4212 30844 3 102744 3
4213 30845 3 102745 3
4214 30846 3 102746 3
4215 30847 3 102747 3
4216 30848 3 102748 3
4217 30849 3 102749 3
4218 30850 3 102750 3
4219 30851 3 102751 3
4220 30852 3 102752 3
4221 30853 3 102753 3
4222 30854 3 102754 3
4223 30855 3 102755 3
4224 30856 3 102756 3
4225 30857 3 102757 3
4226 30858 3 102758 3
4227 30859 3 102759 3
4228 30860 3 102760 3
4229 30861 3 102761 3
4230 30862 3 102762 3
4231 30863 3 102763 3
4232 30864 3 102764 3
4233 30865 3 102765 3
4234 30866 3 102766 3
4235 30867 3 102767 3
4236 30868 3 102768 3
4237 30869 3 102769 3
4238 30870 3 102770 3
4239 30871 3 102771 3
4240 30872 3 102772 3
4241 30873 3 102773 3
4242 30874 3 102774 3
4243 30875 3 102775 3
4244 30876 3 102776 3
4245 30877 3 102777 3
4246 30878 3 102778 3
4247 30879 3 102779 3
4248 30880 3 102780 3
4249 30881 3 102781 3
4250 30882 3 102782 3

4251 30883 3 102783 3
4252 30884 3 102784 3
4253 30885 3 102785 3
4254 30886 3 102786 3
4255 30887 3 102787 3
4256 30888 3 102788 3
4257 30889 3 102789 3
4258 30890 3 102790 3
4259 30891 3 102791 3
4260 30892 3 102792 3
4261 30893 3 102793 3
4262 30894 3 102794 3
4263 30895 3 102795 3
4264 30896 3 102796 3
4265 30897 3 102797 3
4266 30898 3 102798 3
4267 30899 3 102799 3
4268 30900 3 102800 3
4269 30901 3 102801 3
4270 30902 3 102802 3
4271 30903 3 102803 3
4272 30904 3 102804 3
4273 30905 3 102805 3
4274 30906 3 102806 3
4275 30907 3 102807 3
4276 30908 3 102808 3
4277 30909 3 102809 3
4278 30910 3 102810 3
4279 30911 3 102811 3
4280 30912 3 102812 3
4281 30913 3 102813 3
4282 30914 3 102814 3
4283 30915 3 102815 3
4284 30916 3 102816 3
4285 30917 3 102817 3
4286 30918 3 102818 3
4287 30919 3 102819 3
4288 30920 3 102820 3
4289 30921 3 102821 3
4290 30922 3 102822 3
4291 30923 3 102823 3
4292 30924 3 102824 3
4293 30925 3 102825 3
4294 30926 3 102826 3
4295 30927 3 102827 3
4296 30928 3 102828 3
4297 30929 3 102829 3
4298 30930 3 102830 3
4299 30931 3 102831 3
4300 30932 3 102832 3
4301 30933 3 102833 3
4302 30934 3 102834 3
4303 30935 3 102835 3
4304 30936 3 102836 3
4305 30937 3 102837 3
4306 30938 3 102838 3

4307 30939 3 102839 3
4308 30940 3 102840 3
4309 30941 3 102841 3
4310 30942 3 102842 3
4311 30943 3 102843 3
4312 30944 3 102844 3
4313 30945 3 102845 3
4314 30946 3 102846 3
4315 30947 3 102847 3
4316 30948 3 102848 3
4317 30949 3 102849 3
4318 30950 3 102850 3
4319 30951 3 102851 3
4320 30952 3 102852 3
4321 30953 3 102853 3
4322 30954 3 102854 3
4323 30955 3 102855 3
4324 30956 3 102856 3
4325 30957 3 102857 3
4326 30958 3 102858 3
4327 30959 3 102859 3
4328 30960 3 102860 3
4329 30961 3 102861 3
4330 30962 3 102862 3
4331 30963 3 102863 3
4332 30964 3 102864 3
4333 30965 3 102865 3
4334 30966 3 102866 3
4335 30967 3 102867 3
4336 30968 3 102868 3
4337 30969 3 102869 3
4338 30970 3 102870 3
4339 30971 3 102871 3
4340 30972 3 102872 3
4341 30973 3 102873 3
4342 30974 3 102874 3
4343 30975 3 102875 3
4344 30976 3 102876 3
4345 30977 3 102877 3
4346 30978 3 102878 3
4347 30979 3 102879 3
4348 30980 3 102880 3
4349 30981 3 102881 3
4350 30982 3 102882 3
4351 30983 3 102883 3
4352 30984 3 102884 3
4353 30985 3 102885 3
4354 30986 3 102886 3
4355 30987 3 102887 3
4356 30988 3 102888 3
4357 30989 3 102889 3
4358 30990 3 102890 3
4359 30991 3 102891 3
4360 30992 3 102892 3
4361 30993 3 102893 3
4362 30994 3 102894 3

4363 30995 3 102895 3
4364 30996 3 102896 3
4365 30997 3 102897 3
4366 30998 3 102898 3
4367 30999 3 102899 3
4368 31000 3 102900 3
4369 31001 3 102901 3
4370 31002 3 102902 3
4371 31003 3 102903 3
4372 31004 3 102904 3
4373 31005 3 102905 3
4374 31006 3 102906 3
4375 31007 3 102907 3
4376 31008 3 102908 3
4377 31009 3 102909 3
4378 31010 3 102910 3
4379 31011 3 102911 3
4380 31012 3 102912 3
4381 31013 3 102913 3
4382 31014 3 102914 3
4383 31015 3 102915 3
4384 31016 3 102916 3
4385 31017 3 102917 3
4386 31018 3 102918 3
4387 31019 3 102919 3
4388 31020 3 102920 3
4389 31021 3 102921 3
4390 31022 3 102922 3
4391 31023 3 102923 3
4392 31024 3 102924 3
4393 31025 3 102925 3
4394 31026 3 102926 3
4395 31027 3 102927 3
4396 31028 3 102928 3
4397 31029 3 102929 3
4398 31030 3 102930 3
4399 31031 3 102931 3
4400 31032 3 102932 3
4401 31033 3 102933 3
4402 31034 3 102934 3
4403 31035 3 102935 3
4404 31036 3 102936 3
4405 31037 3 102937 3
4406 31038 3 102938 3
4407 31039 3 102939 3
4408 31040 3 102940 3
4409 31041 3 102941 3
4410 31042 3 102942 3
4411 31043 3 102943 3
4412 31044 3 102944 3
4413 31045 3 102945 3
4414 31046 3 102946 3
4415 31047 3 102947 3
4416 31048 3 102948 3
4417 31049 3 102949 3
4418 31050 3 102950 3

4419 31051 3 102951 3
4420 31052 3 102952 3
4421 31053 3 102953 3
4422 31054 3 102954 3
4423 31055 3 102955 3
4424 31056 3 102956 3
4425 31057 3 102957 3
4426 31058 3 102958 3
4427 31059 3 102959 3
4428 31060 3 102960 3
4429 31061 3 102961 3
4430 31062 3 102962 3
4431 31063 3 102963 3
4432 31064 3 102964 3
4433 31065 3 102965 3
4434 31066 3 102966 3
4435 31067 3 102967 3
4436 31068 3 102968 3
4437 31069 3 102969 3
4438 31070 3 102970 3
4439 31071 3 102971 3
4440 31072 3 102972 3
4441 31073 3 102973 3
4442 31074 3 102974 3
4443 31075 3 102975 3
4444 31076 3 102976 3
4445 31077 3 102977 3
4446 31078 3 102978 3
4447 31079 3 102979 3
4448 31080 3 102980 3
4449 31081 3 102981 3
4450 31082 3 102982 3
4451 31083 3 102983 3
4452 31084 3 102984 3
4453 31085 3 102985 3
4454 31086 3 102986 3
4455 31087 3 102987 3
4456 31088 3 102988 3
4457 31089 3 102989 3
4458 31090 3 102990 3
4459 31091 3 102991 3
4460 31092 3 102992 3
4461 31093 3 102993 3
4462 31094 3 102994 3
4463 31095 3 102995 3
4464 31096 3 102996 3
4465 31097 3 102997 3
4466 31098 3 102998 3
4467 31099 3 102999 3
4468 31100 3 103000 3
4469 31101 3 103001 3
4470 31102 3 103002 3
4471 31103 3 103003 3
4472 31104 3 103004 3
4473 31105 3 103005 3
4474 31106 3 103006 3

4475 31107 3 103007 3
4476 31108 3 103008 3
4477 31109 3 103009 3
4478 31110 3 103010 3
4479 31111 3 103011 3
4480 31112 3 103012 3
4481 31113 3 103013 3
4482 31114 3 103014 3
4483 31115 3 103015 3
4484 31116 3 103016 3
4485 31117 3 103017 3
4486 31118 3 103018 3
4487 31119 3 103019 3
4488 31120 3 103020 3
4489 31121 3 103021 3
4490 31122 3 103022 3
4491 31123 3 103023 3
4492 31124 3 103024 3
4493 31125 3 103025 3
4494 31126 3 103026 3
4495 31127 3 103027 3
4496 31128 3 103028 3
4497 31129 3 103029 3
4498 31130 3 103030 3
4499 31131 3 103031 3
4500 31132 3 103032 3
4501 31133 3 103033 3
4502 31134 3 103034 3
4503 31135 3 103035 3
4504 31136 3 103036 3
4505 31137 3 103037 3
4506 31138 3 103038 3
4507 31139 3 103039 3
4508 31140 3 103040 3
4509 31141 3 103041 3
4510 31142 3 103042 3
4511 31143 3 103043 3
4512 31144 3 103044 3
4513 31145 3 103045 3
4514 31146 3 103046 3
4515 44463 3 75963 3
4516 44464 3 75964 3
4517 44465 3 75965 3
4518 44466 3 75966 3
4519 44467 3 75967 3
4520 44468 3 75968 3
4521 44469 3 75969 3
4522 44470 3 75970 3
4523 44471 3 75971 3
4524 44472 3 75972 3
4525 44473 3 75973 3
4526 44474 3 75974 3
4527 44475 3 75975 3
4528 44476 3 75976 3
4529 44477 3 75977 3
4530 44478 3 75978 3

4531 44479 3 75979 3
4532 44480 3 75980 3
4533 44481 3 75981 3
4534 44482 3 75982 3
4535 44483 3 75983 3
4536 44484 3 75984 3
4537 44485 3 75985 3
4538 44486 3 75986 3
4539 44487 3 75987 3
4540 44488 3 75988 3
4541 44489 3 75989 3
4542 44490 3 75990 3
4543 44491 3 75991 3
4544 44492 3 75992 3
4545 44493 3 75993 3
4546 44494 3 75994 3
4547 44495 3 75995 3
4548 44496 3 75996 3
4549 44497 3 75997 3
4550 44498 3 75998 3
4551 44499 3 75999 3
4552 44500 3 76000 3
4553 44501 3 76001 3
4554 44502 3 76002 3
4555 44503 3 76003 3
4556 44504 3 76004 3
4557 44505 3 76005 3
4558 44506 3 76006 3
4559 44507 3 76007 3
4560 44508 3 76008 3
4561 44509 3 76009 3
4562 44510 3 76010 3
4563 44511 3 76011 3
4564 44512 3 76012 3
4565 44513 3 76013 3
4566 44514 3 76014 3
4567 44515 3 76015 3
4568 44516 3 76016 3
4569 44517 3 76017 3
4570 44518 3 76018 3
4571 44519 3 76019 3
4572 44520 3 76020 3
4573 44521 3 76021 3
4574 44522 3 76022 3
4575 44523 3 76023 3
4576 44524 3 76024 3
4577 44525 3 76025 3
4578 44526 3 76026 3
4579 44527 3 76027 3
4580 44528 3 76028 3
4581 44529 3 76029 3
4582 44530 3 76030 3
4583 44531 3 76031 3
4584 44532 3 76032 3
4585 44533 3 76033 3
4586 44534 3 76034 3

4587 44535 3 76035 3
4588 44536 3 76036 3
4589 44537 3 76037 3
4590 44538 3 76038 3
4591 44539 3 76039 3
4592 44540 3 76040 3
4593 44541 3 76041 3
4594 44542 3 76042 3
4595 44543 3 76043 3
4596 44544 3 76044 3
4597 44545 3 76045 3
4598 44546 3 76046 3
4599 44547 3 76047 3
4600 44548 3 76048 3
4601 44549 3 76049 3
4602 44550 3 76050 3
4603 44551 3 76051 3
4604 44552 3 76052 3
4605 44553 3 76053 3
4606 44554 3 76054 3
4607 44555 3 76055 3
4608 44556 3 76056 3
4609 44557 3 76057 3
4610 44558 3 76058 3
4611 44559 3 76059 3
4612 44560 3 76060 3
4613 44561 3 76061 3
4614 44562 3 76062 3
4615 44563 3 76063 3
4616 44564 3 76064 3
4617 44565 3 76065 3
4618 44566 3 76066 3
4619 44567 3 76067 3
4620 44568 3 76068 3
4621 44569 3 76069 3
4622 44570 3 76070 3
4623 44571 3 76071 3
4624 44572 3 76072 3
4625 44573 3 76073 3
4626 44574 3 76074 3
4627 44575 3 76075 3
4628 44576 3 76076 3
4629 44577 3 76077 3
4630 44578 3 76078 3
4631 44579 3 76079 3
4632 44580 3 76080 3
4633 44581 3 76081 3
4634 44582 3 76082 3
4635 44583 3 76083 3
4636 44584 3 76084 3
4637 44585 3 76085 3
4638 44586 3 76086 3
4639 44587 3 76087 3
4640 44588 3 76088 3
4641 44589 3 76089 3
4642 44590 3 76090 3

4643 44591 3 76091 3
4644 44592 3 76092 3
4645 44593 3 76093 3
4646 44594 3 76094 3
4647 44595 3 76095 3
4648 44596 3 76096 3
4649 44597 3 76097 3
4650 44598 3 76098 3
4651 44599 3 76099 3
4652 44600 3 76100 3
4653 44601 3 76101 3
4654 44602 3 76102 3
4655 44603 3 76103 3
4656 44604 3 76104 3
4657 44605 3 76105 3
4658 44606 3 76106 3
4659 44607 3 76107 3
4660 44608 3 76108 3
4661 44609 3 76109 3
4662 44610 3 76110 3
4663 44611 3 76111 3
4664 44612 3 76112 3
4665 44613 3 76113 3
4666 44614 3 76114 3
4667 44615 3 76115 3
4668 44616 3 76116 3
4669 44617 3 76117 3
4670 44618 3 76118 3
4671 44619 3 76119 3
4672 44620 3 76120 3
4673 44621 3 76121 3
4674 44622 3 76122 3
4675 44623 3 76123 3
4676 44624 3 76124 3
4677 44625 3 76125 3
4678 44626 3 76126 3
4679 44627 3 76127 3
4680 44628 3 76128 3
4681 44629 3 76129 3
4682 44630 3 76130 3
4683 44631 3 76131 3
4684 44632 3 76132 3
4685 44633 3 76133 3
4686 44634 3 76134 3
4687 44635 3 76135 3
4688 44636 3 76136 3
4689 44637 3 76137 3
4690 44638 3 76138 3
4691 44639 3 76139 3
4692 44640 3 76140 3
4693 44641 3 76141 3
4694 44642 3 76142 3
4695 44643 3 76143 3
4696 44644 3 76144 3
4697 44645 3 76145 3
4698 44646 3 76146 3

4699 44647 3 76147 3
4700 44648 3 76148 3
4701 44649 3 76149 3
4702 44650 3 76150 3
4703 44651 3 76151 3
4704 44652 3 76152 3
4705 44653 3 76153 3
4706 44654 3 76154 3
4707 44655 3 76155 3
4708 44656 3 76156 3
4709 44657 3 76157 3
4710 44658 3 76158 3
4711 44659 3 76159 3
4712 44660 3 76160 3
4713 44661 3 76161 3
4714 44662 3 76162 3
4715 44663 3 76163 3
4716 44664 3 76164 3
4717 44665 3 76165 3
4718 44666 3 76166 3
4719 44667 3 76167 3
4720 44668 3 76168 3
4721 44669 3 76169 3
4722 44670 3 76170 3
4723 44671 3 76171 3
4724 44672 3 76172 3
4725 44673 3 76173 3
4726 44674 3 76174 3
4727 44675 3 76175 3
4728 44676 3 76176 3
4729 44677 3 76177 3
4730 44678 3 76178 3
4731 44679 3 76179 3
4732 44680 3 76180 3
4733 44681 3 76181 3
4734 44682 3 76182 3
4735 44683 3 76183 3
4736 44684 3 76184 3
4737 44685 3 76185 3
4738 44686 3 76186 3
4739 44687 3 76187 3
4740 44688 3 76188 3
4741 44689 3 76189 3
4742 44690 3 76190 3
4743 44691 3 76191 3
4744 44692 3 76192 3
4745 44693 3 76193 3
4746 44694 3 76194 3
4747 44695 3 76195 3
4748 44696 3 76196 3
4749 44697 3 76197 3
4750 44698 3 76198 3
4751 44699 3 76199 3
4752 44700 3 76200 3
4753 44701 3 76201 3
4754 44702 3 76202 3

4755 44703 3 76203 3
4756 44704 3 76204 3
4757 44705 3 76205 3
4758 44706 3 76206 3
4759 44707 3 76207 3
4760 44708 3 76208 3
4761 44709 3 76209 3
4762 44710 3 76210 3
4763 44711 3 76211 3
4764 44712 3 76212 3
4765 44713 3 76213 3
4766 44714 3 76214 3
4767 44715 3 76215 3
4768 44716 3 76216 3
4769 44717 3 76217 3
4770 44718 3 76218 3
4771 44719 3 76219 3
4772 44720 3 76220 3
4773 44721 3 76221 3
4774 44722 3 76222 3
4775 44723 3 76223 3
4776 44724 3 76224 3
4777 44725 3 76225 3
4778 44726 3 76226 3
4779 44727 3 76227 3
4780 44728 3 76228 3
4781 44729 3 76229 3
4782 44730 3 76230 3
4783 44731 3 76231 3
4784 44732 3 76232 3
4785 44733 3 76233 3
4786 44734 3 76234 3
4787 44735 3 76235 3
4788 44736 3 76236 3
4789 44737 3 76237 3
4790 44738 3 76238 3
4791 44739 3 76239 3
4792 44740 3 76240 3
4793 44741 3 76241 3
4794 44742 3 76242 3
4795 44743 3 76243 3
4796 44744 3 76244 3
4797 44745 3 76245 3
4798 44746 3 76246 3
4799 44747 3 76247 3
4800 44748 3 76248 3
4801 44749 3 76249 3
4802 44750 3 76250 3
4803 44751 3 76251 3
4804 44752 3 76252 3
4805 44753 3 76253 3
4806 44754 3 76254 3
4807 44755 3 76255 3
4808 44756 3 76256 3
4809 44757 3 76257 3
4810 44758 3 76258 3

4811 44759 3 76259 3
4812 44760 3 76260 3
4813 44761 3 76261 3
4814 44762 3 76262 3
4815 44763 3 76263 3
4816 44764 3 76264 3
4817 44765 3 76265 3
4818 44766 3 76266 3
4819 44767 3 76267 3
4820 44768 3 76268 3
4821 44769 3 76269 3
4822 44770 3 76270 3
4823 44771 3 76271 3
4824 44772 3 76272 3
4825 44773 3 76273 3
4826 44774 3 76274 3
4827 44775 3 76275 3
4828 44776 3 76276 3
4829 44777 3 76277 3
4830 44778 3 76278 3
4831 44779 3 76279 3
4832 44780 3 76280 3
4833 44781 3 76281 3
4834 44782 3 76282 3
4835 44783 3 76283 3
4836 44784 3 76284 3
4837 44785 3 76285 3
4838 44786 3 76286 3
4839 44787 3 76287 3
4840 44788 3 76288 3
4841 44789 3 76289 3
4842 44790 3 76290 3
4843 44791 3 76291 3
4844 44792 3 76292 3
4845 44793 3 76293 3
4846 44794 3 76294 3
4847 44795 3 76295 3
4848 44796 3 76296 3
4849 44797 3 76297 3
4850 44798 3 76298 3
4851 44799 3 76299 3
4852 44800 3 76300 3
4853 44801 3 76301 3
4854 44802 3 76302 3
4855 44803 3 76303 3
4856 44804 3 76304 3
4857 44805 3 76305 3
4858 44806 3 76306 3
4859 44807 3 76307 3
4860 44808 3 76308 3
4861 44809 3 76309 3
4862 44810 3 76310 3
4863 44811 3 76311 3
4864 44812 3 76312 3
4865 44813 3 76313 3
4866 44814 3 76314 3

4867 44815 3 76315 3
4868 44816 3 76316 3
4869 44817 3 76317 3
4870 44818 3 76318 3
4871 44819 3 76319 3
4872 44820 3 76320 3
4873 44821 3 76321 3
4874 44822 3 76322 3
4875 44823 3 76323 3
4876 44824 3 76324 3
4877 44825 3 76325 3
4878 44826 3 76326 3
4879 44827 3 76327 3
4880 44828 3 76328 3
4881 44829 3 76329 3
4882 44830 3 76330 3
4883 44831 3 76331 3
4884 44832 3 76332 3
4885 44833 3 76333 3
4886 44834 3 76334 3
4887 44835 3 76335 3
4888 44836 3 76336 3
4889 44837 3 76337 3
4890 44838 3 76338 3
4891 44839 3 76339 3
4892 44840 3 76340 3
4893 44841 3 76341 3
4894 44842 3 76342 3
4895 44843 3 76343 3
4896 44844 3 76344 3
4897 44845 3 76345 3
4898 44846 3 76346 3
4899 44847 3 76347 3
4900 44848 3 76348 3
4901 44849 3 76349 3
4902 44850 3 76350 3
4903 44851 3 76351 3
4904 44852 3 76352 3
4905 44853 3 76353 3
4906 44854 3 76354 3
4907 44855 3 76355 3
4908 44856 3 76356 3
4909 44857 3 76357 3
4910 44858 3 76358 3
4911 44859 3 76359 3
4912 44860 3 76360 3
4913 44861 3 76361 3
4914 44862 3 76362 3
4915 44863 3 76363 3
4916 44864 3 76364 3
4917 44865 3 76365 3
4918 44866 3 76366 3
4919 44867 3 76367 3
4920 44868 3 76368 3
4921 44869 3 76369 3
4922 44870 3 76370 3

4923 44871 3 76371 3
4924 44872 3 76372 3
4925 44873 3 76373 3
4926 44874 3 76374 3
4927 44875 3 76375 3
4928 44876 3 76376 3
4929 44877 3 76377 3
4930 44878 3 76378 3
4931 44879 3 76379 3
4932 44880 3 76380 3
4933 44881 3 76381 3
4934 44882 3 76382 3
4935 44883 3 76383 3
4936 44884 3 76384 3
4937 44885 3 76385 3
4938 44886 3 76386 3
4939 44887 3 76387 3
4940 44888 3 76388 3
4941 44889 3 76389 3
4942 44890 3 76390 3
4943 44891 3 76391 3
4944 44892 3 76392 3
4945 44893 3 76393 3
4946 44894 3 76394 3
4947 44895 3 76395 3
4948 44896 3 76396 3
4949 44897 3 76397 3
4950 44898 3 76398 3
4951 44899 3 76399 3
4952 44900 3 76400 3
4953 44901 3 76401 3
4954 44902 3 76402 3
4955 44903 3 76403 3
4956 44904 3 76404 3
4957 44905 3 76405 3
4958 44906 3 76406 3
4959 44907 3 76407 3
4960 44908 3 76408 3
4961 44909 3 76409 3
4962 44910 3 76410 3
4963 44911 3 76411 3
4964 44912 3 76412 3
4965 44913 3 76413 3
4966 44914 3 76414 3
4967 44915 3 76415 3
4968 44916 3 76416 3
4969 44917 3 76417 3
4970 44918 3 76418 3
4971 44919 3 76419 3
4972 44920 3 76420 3
4973 44921 3 76421 3
4974 44922 3 76422 3
4975 44923 3 76423 3
4976 44924 3 76424 3
4977 44925 3 76425 3
4978 44926 3 76426 3

4979 44927 3 76427 3
4980 44928 3 76428 3
4981 44929 3 76429 3
4982 44930 3 76430 3
4983 44931 3 76431 3
4984 44932 3 76432 3
4985 44933 3 76433 3
4986 44934 3 76434 3
4987 44935 3 76435 3
4988 44936 3 76436 3
4989 44937 3 76437 3
4990 44938 3 76438 3
4991 44939 3 76439 3
4992 44940 3 76440 3
4993 44941 3 76441 3
4994 44942 3 76442 3
4995 44943 3 76443 3
4996 44944 3 76444 3
4997 44945 3 76445 3
4998 44946 3 76446 3
4999 44947 3 76447 3
5000 44948 3 76448 3
5001 44949 3 76449 3
5002 44950 3 76450 3
5003 44951 3 76451 3
5004 44952 3 76452 3
5005 44953 3 76453 3
5006 44954 3 76454 3
5007 44955 3 76455 3
5008 44956 3 76456 3
5009 44957 3 76457 3
5010 44958 3 76458 3
5011 44959 3 76459 3
5012 44960 3 76460 3
5013 44961 3 76461 3
5014 44962 3 76462 3
5015 44963 3 76463 3
5016 44964 3 76464 3
5017 44965 3 76465 3
5018 44966 3 76466 3
5019 44967 3 76467 3
5020 44968 3 76468 3
5021 44969 3 76469 3
5022 44970 3 76470 3
5023 44971 3 76471 3
5024 44972 3 76472 3
5025 44973 3 76473 3
5026 44974 3 76474 3
5027 44975 3 76475 3
5028 44976 3 76476 3
5029 44977 3 76477 3
5030 44978 3 76478 3
5031 44979 3 76479 3
5032 44980 3 76480 3
5033 44981 3 76481 3
5034 44982 3 76482 3

5035 44983 3 76483 3
5036 44984 3 76484 3
5037 44985 3 76485 3
5038 44986 3 76486 3
5039 44987 3 76487 3
5040 44988 3 76488 3
5041 44989 3 76489 3
5042 44990 3 76490 3
5043 44991 3 76491 3
5044 44992 3 76492 3
5045 44993 3 76493 3
5046 44994 3 76494 3
5047 44995 3 76495 3
5048 44996 3 76496 3
5049 44997 3 76497 3
5050 44998 3 76498 3
5051 44999 3 76499 3
5052 45000 3 76500 3
5053 45001 3 76501 3
5054 45002 3 76502 3
5055 45003 3 76503 3
5056 45004 3 76504 3
5057 45005 3 76505 3
5058 45006 3 76506 3
5059 45007 3 76507 3
5060 45008 3 76508 3
5061 45009 3 76509 3
5062 45010 3 76510 3
5063 45011 3 76511 3
5064 45012 3 76512 3
5065 45013 3 76513 3
5066 45014 3 76514 3
5067 45015 3 76515 3
5068 45016 3 76516 3
5069 45017 3 76517 3
5070 45018 3 76518 3
5071 45019 3 76519 3
5072 45020 3 76520 3
5073 45021 3 76521 3
5074 45022 3 76522 3
5075 45023 3 76523 3
5076 45024 3 76524 3
5077 45025 3 76525 3
5078 45026 3 76526 3
5079 45027 3 76527 3
5080 45028 3 76528 3
5081 45029 3 76529 3
5082 45030 3 76530 3
5083 45031 3 76531 3
5084 45032 3 76532 3
5085 45033 3 76533 3
5086 45034 3 76534 3
5087 45035 3 76535 3
5088 45036 3 76536 3
5089 45037 3 76537 3
5090 45038 3 76538 3

5091 45039 3 76539 3
5092 45040 3 76540 3
5093 45041 3 76541 3
5094 45042 3 76542 3
5095 45043 3 76543 3
5096 45044 3 76544 3
5097 45045 3 76545 3
5098 45046 3 76546 3
5099 45047 3 76547 3
5100 45048 3 76548 3
5101 45049 3 76549 3
5102 45050 3 76550 3
5103 45051 3 76551 3
5104 45052 3 76552 3
5105 45053 3 76553 3
5106 45054 3 76554 3
5107 45055 3 76555 3
5108 45056 3 76556 3
5109 45057 3 76557 3
5110 45058 3 76558 3
5111 45059 3 76559 3
5112 45060 3 76560 3
5113 45061 3 76561 3
5114 45062 3 76562 3
5115 45063 3 76563 3
5116 45064 3 76564 3
5117 45065 3 76565 3
5118 45066 3 76566 3
5119 45067 3 76567 3
5120 45068 3 76568 3
5121 45069 3 76569 3
5122 45070 3 76570 3
5123 45071 3 76571 3
5124 45072 3 76572 3
5125 45073 3 76573 3
5126 45074 3 76574 3
5127 45075 3 76575 3
5128 45076 3 76576 3
5129 45077 3 76577 3
5130 45078 3 76578 3
5131 45079 3 76579 3
5132 45080 3 76580 3
5133 45081 3 76581 3
5134 45082 3 76582 3
5135 45083 3 76583 3
5136 45084 3 76584 3
5137 45085 3 76585 3
5138 45086 3 76586 3
5139 45087 3 76587 3
5140 45088 3 76588 3
5141 45089 3 76589 3
5142 45090 3 76590 3
5143 45091 3 76591 3
5144 45092 3 76592 3
5145 45093 3 76593 3
5146 45094 3 76594 3

5147 45095 3 76595 3
5148 45096 3 76596 3
5149 45097 3 76597 3
5150 45098 3 76598 3
5151 45099 3 76599 3
5152 45100 3 76600 3
5153 45101 3 76601 3
5154 45102 3 76602 3
5155 45103 3 76603 3
5156 45104 3 76604 3
5157 45105 3 76605 3
5158 45106 3 76606 3
5159 45107 3 76607 3
5160 45108 3 76608 3
5161 45109 3 76609 3
5162 45110 3 76610 3
5163 45111 3 76611 3
5164 45112 3 76612 3
5165 45113 3 76613 3
5166 45114 3 76614 3
5167 45115 3 76615 3
5168 45116 3 76616 3
5169 45117 3 76617 3
5170 45118 3 76618 3
5171 45119 3 76619 3
5172 45120 3 76620 3
5173 45121 3 76621 3
5174 45122 3 76622 3
5175 45123 3 76623 3
5176 45124 3 76624 3
5177 45125 3 76625 3
5178 45126 3 76626 3
5179 45127 3 76627 3
5180 45128 3 76628 3
5181 45129 3 76629 3
5182 45130 3 76630 3
5183 45131 3 76631 3
5184 45132 3 76632 3
5185 45133 3 76633 3
5186 45134 3 76634 3
5187 45135 3 76635 3
5188 45136 3 76636 3
5189 45137 3 76637 3
5190 45138 3 76638 3
5191 45139 3 76639 3
5192 45140 3 76640 3
5193 45141 3 76641 3
5194 45142 3 76642 3
5195 45143 3 76643 3
5196 45144 3 76644 3
5197 45145 3 76645 3
5198 45146 3 76646 3
5199 45147 3 76647 3
5200 45148 3 76648 3
5201 45149 3 76649 3
5202 45150 3 76650 3

5203 45151 3 76651 3
5204 45152 3 76652 3
5205 45153 3 76653 3
5206 45154 3 76654 3
5207 45155 3 76655 3
5208 45156 3 76656 3
5209 45157 3 76657 3
5210 45158 3 76658 3
5211 45159 3 76659 3
5212 45160 3 76660 3
5213 45161 3 76661 3
5214 45162 3 76662 3
5215 45163 3 76663 3
5216 45164 3 76664 3
5217 45165 3 76665 3
5218 45166 3 76666 3
5219 45167 3 76667 3
5220 45168 3 76668 3
5221 45169 3 76669 3
5222 45170 3 76670 3
5223 45171 3 76671 3
5224 45172 3 76672 3
5225 45173 3 76673 3
5226 45174 3 76674 3
5227 45175 3 76675 3
5228 45176 3 76676 3
5229 45177 3 76677 3
5230 45178 3 76678 3
5231 45179 3 76679 3
5232 45180 3 76680 3
5233 45181 3 76681 3
5234 45182 3 76682 3
5235 45183 3 76683 3
5236 45184 3 76684 3
5237 45185 3 76685 3
5238 45186 3 76686 3
5239 45187 3 76687 3
5240 45188 3 76688 3
5241 45189 3 76689 3
5242 45190 3 76690 3
5243 45191 3 76691 3
5244 45192 3 76692 3
5245 45193 3 76693 3
5246 45194 3 76694 3
5247 45195 3 76695 3
5248 45196 3 76696 3
5249 45197 3 76697 3
5250 45198 3 76698 3
5251 45199 3 76699 3
5252 45200 3 76700 3
5253 45201 3 76701 3
5254 45202 3 76702 3
5255 45203 3 76703 3
5256 45204 3 76704 3
5257 45205 3 76705 3
5258 45206 3 76706 3

5259 45207 3 76707 3
5260 45208 3 76708 3
5261 45209 3 76709 3
5262 45210 3 76710 3
5263 45211 3 76711 3
5264 45212 3 76712 3
5265 45213 3 76713 3
5266 45214 3 76714 3
5267 45215 3 76715 3
5268 45216 3 76716 3
5269 45217 3 76717 3
5270 45218 3 76718 3
5271 45219 3 76719 3
5272 45220 3 76720 3
5273 45221 3 76721 3
5274 45222 3 76722 3
5275 45223 3 76723 3
5276 45224 3 76724 3
5277 45225 3 76725 3
5278 45226 3 76726 3
5279 45227 3 76727 3
5280 45228 3 76728 3
5281 45229 3 76729 3
5282 45230 3 76730 3
5283 45231 3 76731 3
5284 45232 3 76732 3
5285 45233 3 76733 3
5286 45234 3 76734 3
5287 45235 3 76735 3
5288 45236 3 76736 3
5289 45237 3 76737 3
5290 45238 3 76738 3
5291 45239 3 76739 3
5292 45240 3 76740 3
5293 45241 3 76741 3
5294 45242 3 76742 3
5295 45243 3 76743 3
5296 45244 3 76744 3
5297 45245 3 76745 3
5298 45246 3 76746 3
5299 45247 3 76747 3
5300 45248 3 76748 3
5301 45249 3 76749 3
5302 45250 3 76750 3
5303 45251 3 76751 3
5304 45252 3 76752 3
5305 45253 3 76753 3
5306 45254 3 76754 3
5307 45255 3 76755 3
5308 45256 3 76756 3
5309 45257 3 76757 3
5310 45258 3 76758 3
5311 45259 3 76759 3
5312 45260 3 76760 3
5313 45261 3 76761 3
5314 45262 3 76762 3

5315 45263 3 76763 3
5316 45264 3 76764 3
5317 45265 3 76765 3
5318 45266 3 76766 3
5319 45267 3 76767 3
5320 45268 3 76768 3
5321 45269 3 76769 3
5322 45270 3 76770 3
5323 45271 3 76771 3
5324 45272 3 76772 3
5325 45273 3 76773 3
5326 45274 3 76774 3
5327 45275 3 76775 3
5328 45276 3 76776 3
5329 45277 3 76777 3
5330 45278 3 76778 3
5331 45279 3 76779 3
5332 45280 3 76780 3
5333 45281 3 76781 3
5334 45282 3 76782 3
5335 45283 3 76783 3
5336 45284 3 76784 3
5337 45285 3 76785 3
5338 45286 3 76786 3
5339 45287 3 76787 3
5340 45288 3 76788 3
5341 45289 3 76789 3
5342 45290 3 76790 3
5343 45291 3 76791 3
5344 45292 3 76792 3
5345 45293 3 76793 3
5346 45294 3 76794 3
5347 45295 3 76795 3
5348 45296 3 76796 3
5349 45297 3 76797 3
5350 45298 3 76798 3
5351 45299 3 76799 3
5352 45300 3 76800 3
5353 45301 3 76801 3
5354 45302 3 76802 3
5355 45303 3 76803 3
5356 45304 3 76804 3
5357 45305 3 76805 3
5358 45306 3 76806 3
5359 45307 3 76807 3
5360 45308 3 76808 3
5361 45309 3 76809 3
5362 45310 3 76810 3
5363 45311 3 76811 3
5364 45312 3 76812 3
5365 45313 3 76813 3
5366 45314 3 76814 3
5367 45315 3 76815 3
5368 45316 3 76816 3
5369 45317 3 76817 3
5370 45318 3 76818 3

5371 45319 3 76819 3
5372 45320 3 76820 3
5373 45321 3 76821 3
5374 45322 3 76822 3
5375 45323 3 76823 3
5376 45324 3 76824 3
5377 45325 3 76825 3
5378 45326 3 76826 3
5379 45327 3 76827 3
5380 45328 3 76828 3
5381 45329 3 76829 3
5382 45330 3 76830 3
5383 45331 3 76831 3
5384 45332 3 76832 3
5385 45333 3 76833 3
5386 45334 3 76834 3
5387 45335 3 76835 3
5388 45336 3 76836 3
5389 45337 3 76837 3
5390 45338 3 76838 3
5391 45339 3 76839 3
5392 45340 3 76840 3
5393 45341 3 76841 3
5394 45342 3 76842 3
5395 45343 3 76843 3
5396 45344 3 76844 3
5397 45345 3 76845 3
5398 45346 3 76846 3
5399 45347 3 76847 3
5400 45348 3 76848 3
5401 45349 3 76849 3
5402 45350 3 76850 3
5403 45351 3 76851 3
5404 45352 3 76852 3
5405 45353 3 76853 3
5406 45354 3 76854 3
5407 45355 3 76855 3
5408 45356 3 76856 3
5409 45357 3 76857 3
5410 45358 3 76858 3
5411 45359 3 76859 3
5412 45360 3 76860 3
5413 45361 3 76861 3
5414 45362 3 76862 3
5415 45363 3 76863 3
5416 45364 3 76864 3
5417 45365 3 76865 3
5418 45366 3 76866 3
5419 45367 3 76867 3
5420 45368 3 76868 3
5421 45369 3 76869 3
5422 45370 3 76870 3
5423 45371 3 76871 3
5424 45372 3 76872 3
5425 45373 3 76873 3
5426 45374 3 76874 3

5427 45375 3 76875 3
5428 45376 3 76876 3
5429 45377 3 76877 3
5430 45378 3 76878 3
5431 45379 3 76879 3
5432 45380 3 76880 3
5433 45381 3 76881 3
5434 45382 3 76882 3
5435 45383 3 76883 3
5436 45384 3 76884 3
5437 45385 3 76885 3
5438 45386 3 76886 3
5439 45387 3 76887 3
5440 45388 3 76888 3
5441 45389 3 76889 3
5442 45390 3 76890 3
5443 45391 3 76891 3
5444 45392 3 76892 3
5445 45393 3 76893 3
5446 45394 3 76894 3
5447 45395 3 76895 3
5448 45396 3 76896 3
5449 45397 3 76897 3
5450 45398 3 76898 3
5451 45399 3 76899 3
5452 45400 3 76900 3
5453 45401 3 76901 3
5454 45402 3 76902 3
5455 45403 3 76903 3
5456 45404 3 76904 3
5457 45405 3 76905 3
5458 45406 3 76906 3
5459 45407 3 76907 3
5460 45408 3 76908 3
5461 45409 3 76909 3
5462 45410 3 76910 3
5463 45411 3 76911 3
5464 45412 3 76912 3
5465 45413 3 76913 3
5466 45414 3 76914 3
5467 45415 3 76915 3
5468 45416 3 76916 3
5469 45417 3 76917 3
5470 45418 3 76918 3
5471 45419 3 76919 3
5472 45420 3 76920 3
5473 45421 3 76921 3
5474 45422 3 76922 3
5475 45423 3 76923 3
5476 45424 3 76924 3
5477 45425 3 76925 3
5478 45426 3 76926 3
5479 45427 3 76927 3
5480 45428 3 76928 3
5481 45429 3 76929 3
5482 45430 3 76930 3

5483 45431 3 76931 3
5484 45432 3 76932 3
5485 45433 3 76933 3
5486 45434 3 76934 3
5487 45435 3 76935 3
5488 45436 3 76936 3
5489 45437 3 76937 3
5490 45438 3 76938 3
5491 45439 3 76939 3
5492 45440 3 76940 3
5493 45441 3 76941 3
5494 45442 3 76942 3
5495 45443 3 76943 3
5496 45444 3 76944 3
5497 45445 3 76945 3
5498 45446 3 76946 3
5499 45447 3 76947 3
5500 45448 3 76948 3
5501 45449 3 76949 3
5502 45450 3 76950 3
5503 45451 3 76951 3
5504 45452 3 76952 3
5505 45453 3 76953 3
5506 45454 3 76954 3
5507 45455 3 76955 3
5508 45456 3 76956 3
5509 45457 3 76957 3
5510 45458 3 76958 3
5511 45459 3 76959 3
5512 45460 3 76960 3
5513 45461 3 76961 3
5514 45462 3 76962 3
5515 45463 3 76963 3
5516 45464 3 76964 3
5517 45465 3 76965 3
5518 45466 3 76966 3
5519 45467 3 76967 3
5520 45468 3 76968 3
5521 45469 3 76969 3
5522 45470 3 76970 3
5523 45471 3 76971 3
5524 45472 3 76972 3
5525 45473 3 76973 3
5526 45474 3 76974 3
5527 45475 3 76975 3
5528 45476 3 76976 3
5529 45477 3 76977 3
5530 45478 3 76978 3
5531 45479 3 76979 3
5532 45480 3 76980 3
5533 45481 3 76981 3
5534 45482 3 76982 3
5535 45483 3 76983 3
5536 45484 3 76984 3
5537 45485 3 76985 3
5538 45486 3 76986 3

5539 45487 3 76987 3
5540 45488 3 76988 3
5541 45489 3 76989 3
5542 45490 3 76990 3
5543 45491 3 76991 3
5544 45492 3 76992 3
5545 45493 3 76993 3
5546 45494 3 76994 3
5547 45495 3 76995 3
5548 45496 3 76996 3
5549 45497 3 76997 3
5550 45498 3 76998 3
5551 45499 3 76999 3
5552 45500 3 77000 3
5553 45501 3 77001 3
5554 45502 3 77002 3
5555 45503 3 77003 3
5556 45504 3 77004 3
5557 45505 3 77005 3
5558 45506 3 77006 3
5559 45507 3 77007 3
5560 45508 3 77008 3
5561 45509 3 77009 3
5562 45510 3 77010 3
5563 45511 3 77011 3
5564 45512 3 77012 3
5565 45513 3 77013 3
5566 45514 3 77014 3
5567 45515 3 77015 3
5568 45516 3 77016 3
5569 45517 3 77017 3
5570 45518 3 77018 3
5571 45519 3 77019 3
5572 45520 3 77020 3
5573 45521 3 77021 3
5574 45522 3 77022 3
5575 45523 3 77023 3
5576 45524 3 77024 3
5577 45525 3 77025 3
5578 45526 3 77026 3
5579 45527 3 77027 3
5580 45528 3 77028 3
5581 45529 3 77029 3
5582 45530 3 77030 3
5583 45531 3 77031 3
5584 45532 3 77032 3
5585 45533 3 77033 3
5586 45534 3 77034 3
5587 45535 3 77035 3
5588 45536 3 77036 3
5589 45537 3 77037 3
5590 45538 3 77038 3
5591 45539 3 77039 3
5592 45540 3 77040 3
5593 45541 3 77041 3
5594 45542 3 77042 3

5595 45543 3 77043 3
5596 45544 3 77044 3
5597 45545 3 77045 3
5598 45546 3 77046 3
5599 45547 3 77047 3
5600 45548 3 77048 3
5601 45549 3 77049 3
5602 45550 3 77050 3
5603 45551 3 77051 3
5604 45552 3 77052 3
5605 45553 3 77053 3
5606 45554 3 77054 3
5607 45555 3 77055 3
5608 45556 3 77056 3
5609 45557 3 77057 3
5610 45558 3 77058 3
5611 45559 3 77059 3
5612 45560 3 77060 3
5613 45561 3 77061 3
5614 45562 3 77062 3
5615 45563 3 77063 3
5616 45564 3 77064 3
5617 45565 3 77065 3
5618 45566 3 77066 3
5619 45567 3 77067 3
5620 45568 3 77068 3
5621 45569 3 77069 3
5622 45570 3 77070 3
5623 45571 3 77071 3
5624 45572 3 77072 3
5625 45573 3 77073 3
5626 45574 3 77074 3
5627 45575 3 77075 3
5628 45576 3 77076 3
5629 45577 3 77077 3
5630 45578 3 77078 3
5631 45579 3 77079 3
5632 45580 3 77080 3
5633 45581 3 77081 3
5634 45582 3 77082 3
5635 45583 3 77083 3
5636 45584 3 77084 3
5637 45585 3 77085 3
5638 45586 3 77086 3
5639 45587 3 77087 3
5640 45588 3 77088 3
5641 45589 3 77089 3
5642 45590 3 77090 3
5643 45591 3 77091 3
5644 45592 3 77092 3
5645 45593 3 77093 3
5646 45594 3 77094 3
5647 45595 3 77095 3
5648 45596 3 77096 3
5649 45597 3 77097 3
5650 45598 3 77098 3

5651 45599 3 77099 3
5652 45600 3 77100 3
5653 45601 3 77101 3
5654 45602 3 77102 3
5655 45603 3 77103 3
5656 45604 3 77104 3
5657 45605 3 77105 3
5658 45606 3 77106 3
5659 45607 3 77107 3
5660 45608 3 77108 3
5661 45609 3 77109 3
5662 45610 3 77110 3
5663 45611 3 77111 3
5664 45612 3 77112 3
5665 45613 3 77113 3
5666 45614 3 77114 3
5667 45615 3 77115 3
5668 45616 3 77116 3
5669 45617 3 77117 3
5670 45618 3 77118 3
5671 45619 3 77119 3
5672 45620 3 77120 3
5673 45621 3 77121 3
5674 45622 3 77122 3
5675 45623 3 77123 3
5676 45624 3 77124 3
5677 45625 3 77125 3
5678 45626 3 77126 3
5679 45627 3 77127 3
5680 45628 3 77128 3
5681 45629 3 77129 3
5682 45630 3 77130 3
5683 45631 3 77131 3
5684 45632 3 77132 3
5685 45633 3 77133 3
5686 45634 3 77134 3
5687 45635 3 77135 3
5688 45636 3 77136 3
5689 45637 3 77137 3
5690 45638 3 77138 3
5691 45639 3 77139 3
5692 45640 3 77140 3
5693 45641 3 77141 3
5694 45642 3 77142 3
5695 45643 3 77143 3
5696 45644 3 77144 3
5697 45645 3 77145 3
5698 45646 3 77146 3
5699 45647 3 77147 3
5700 45648 3 77148 3
5701 45649 3 77149 3
5702 45650 3 77150 3
5703 45651 3 77151 3
5704 45652 3 77152 3
5705 45653 3 77153 3
5706 45654 3 77154 3

5707 45655 3 77155 3
5708 45656 3 77156 3
5709 45657 3 77157 3
5710 45658 3 77158 3
5711 45659 3 77159 3
5712 45660 3 77160 3
5713 45661 3 77161 3
5714 45662 3 77162 3
5715 45663 3 77163 3
5716 45664 3 77164 3
5717 45665 3 77165 3
5718 45666 3 77166 3
5719 45667 3 77167 3
5720 45668 3 77168 3
5721 45669 3 77169 3
5722 45670 3 77170 3
5723 45671 3 77171 3
5724 45672 3 77172 3
5725 45673 3 77173 3
5726 45674 3 77174 3
5727 45675 3 77175 3
5728 45676 3 77176 3
5729 45677 3 77177 3
5730 45678 3 77178 3
5731 45679 3 77179 3
5732 45680 3 77180 3
5733 45681 3 77181 3
5734 45682 3 77182 3
5735 45683 3 77183 3
5736 45684 3 77184 3
5737 45685 3 77185 3
5738 45686 3 77186 3
5739 45687 3 77187 3
5740 45688 3 77188 3
5741 45689 3 77189 3
5742 45690 3 77190 3
5743 45691 3 77191 3
5744 45692 3 77192 3
5745 45693 3 77193 3
5746 45694 3 77194 3
5747 45695 3 77195 3
5748 45696 3 77196 3
5749 45697 3 77197 3
5750 45698 3 77198 3
5751 45699 3 77199 3
5752 45700 3 77200 3
5753 45701 3 77201 3
5754 45702 3 77202 3
5755 45703 3 77203 3
5756 45704 3 77204 3
5757 45705 3 77205 3
5758 45706 3 77206 3
5759 45707 3 77207 3
5760 45708 3 77208 3
5761 45709 3 77209 3
5762 45710 3 77210 3

5763 45711 3 77211 3
5764 45712 3 77212 3
5765 45713 3 77213 3
5766 45714 3 77214 3
5767 45715 3 77215 3
5768 45716 3 77216 3
5769 45717 3 77217 3
5770 45718 3 77218 3
5771 45719 3 77219 3
5772 45720 3 77220 3
5773 45721 3 77221 3
5774 45722 3 77222 3
5775 45723 3 77223 3
5776 45724 3 77224 3
5777 45725 3 77225 3
5778 45726 3 77226 3
5779 45727 3 77227 3
5780 45728 3 77228 3
5781 45729 3 77229 3
5782 45730 3 77230 3
5783 45731 3 77231 3
5784 45732 3 77232 3
5785 45733 3 77233 3
5786 45734 3 77234 3
5787 45735 3 77235 3
5788 45736 3 77236 3
5789 45737 3 77237 3
5790 45738 3 77238 3
5791 45739 3 77239 3
5792 45740 3 77240 3
5793 45741 3 77241 3
5794 45742 3 77242 3
5795 45743 3 77243 3
5796 45744 3 77244 3
5797 45745 3 77245 3
5798 45746 3 77246 3
5799 45747 3 77247 3
5800 45748 3 77248 3
5801 45749 3 77249 3
5802 45750 3 77250 3
5803 45751 3 77251 3
5804 45752 3 77252 3
5805 45753 3 77253 3
5806 45754 3 77254 3
5807 45755 3 77255 3
5808 45756 3 77256 3
5809 45757 3 77257 3
5810 45758 3 77258 3
5811 45759 3 77259 3
5812 45760 3 77260 3
5813 45761 3 77261 3
5814 45762 3 77262 3
5815 45763 3 77263 3
5816 45764 3 77264 3
5817 45765 3 77265 3
5818 45766 3 77266 3

5819 45767 3 77267 3
5820 45768 3 77268 3
5821 45769 3 77269 3
5822 45770 3 77270 3
5823 45771 3 77271 3
5824 45772 3 77272 3
5825 45773 3 77273 3
5826 45774 3 77274 3
5827 45775 3 77275 3
5828 45776 3 77276 3
5829 45777 3 77277 3
5830 45778 3 77278 3
5831 45779 3 77279 3
5832 45780 3 77280 3
5833 45781 3 77281 3
5834 45782 3 77282 3
5835 45783 3 77283 3
5836 45784 3 77284 3
5837 45785 3 77285 3
5838 45786 3 77286 3
5839 45787 3 77287 3
5840 45788 3 77288 3
5841 45789 3 77289 3
5842 45790 3 77290 3
5843 45791 3 77291 3
5844 45792 3 77292 3
5845 45793 3 77293 3
5846 45794 3 77294 3
5847 45795 3 77295 3
5848 45796 3 77296 3
5849 45797 3 77297 3
5850 45798 3 77298 3
5851 45799 3 77299 3
5852 45800 3 77300 3
5853 45801 3 77301 3
5854 45802 3 77302 3
5855 45803 3 77303 3
5856 45804 3 77304 3
5857 45805 3 77305 3
5858 45806 3 77306 3
5859 45807 3 77307 3
5860 45808 3 77308 3
5861 45809 3 77309 3
5862 45810 3 77310 3
5863 45811 3 77311 3
5864 45812 3 77312 3
5865 45813 3 77313 3
5866 45814 3 77314 3
5867 45815 3 77315 3
5868 45816 3 77316 3
5869 45817 3 77317 3
5870 45818 3 77318 3
5871 45819 3 77319 3
5872 45820 3 77320 3
5873 45821 3 77321 3
5874 45822 3 77322 3

5875 45823 3 77323 3
5876 45824 3 77324 3
5877 45825 3 77325 3
5878 45826 3 77326 3
5879 45827 3 77327 3
5880 45828 3 77328 3
5881 45829 3 77329 3
5882 45830 3 77330 3
5883 45831 3 77331 3
5884 45832 3 77332 3
5885 45833 3 77333 3
5886 45834 3 77334 3
5887 45835 3 77335 3
5888 45836 3 77336 3
5889 45837 3 77337 3
5890 45838 3 77338 3
5891 45839 3 77339 3
5892 45840 3 77340 3
5893 45841 3 77341 3
5894 45842 3 77342 3
5895 45843 3 77343 3
5896 45844 3 77344 3
5897 45845 3 77345 3
5898 45846 3 77346 3
5899 45847 3 77347 3
5900 45848 3 77348 3
5901 45849 3 77349 3
5902 45850 3 77350 3
5903 45851 3 77351 3
5904 45852 3 77352 3
5905 45853 3 77353 3
5906 45854 3 77354 3
5907 45855 3 77355 3
5908 45856 3 77356 3
5909 45857 3 77357 3
5910 45858 3 77358 3
5911 45859 3 77359 3
5912 45860 3 77360 3
5913 45861 3 77361 3
5914 45862 3 77362 3
5915 45863 3 77363 3
5916 45864 3 77364 3
5917 45865 3 77365 3
5918 45866 3 77366 3
5919 45867 3 77367 3
5920 45868 3 77368 3
5921 45869 3 77369 3
5922 45870 3 77370 3
5923 45871 3 77371 3
5924 45872 3 77372 3
5925 45873 3 77373 3
5926 45874 3 77374 3
5927 45875 3 77375 3
5928 45876 3 77376 3
5929 45877 3 77377 3
5930 45878 3 77378 3

5931 45879 3 77379 3
5932 45880 3 77380 3
5933 45881 3 77381 3
5934 45882 3 77382 3
5935 45883 3 77383 3
5936 45884 3 77384 3
5937 45885 3 77385 3
5938 45886 3 77386 3
5939 45887 3 77387 3
5940 45888 3 77388 3
5941 45889 3 77389 3
5942 45890 3 77390 3
5943 45891 3 77391 3
5944 45892 3 77392 3
5945 45893 3 77393 3
5946 45894 3 77394 3
5947 45895 3 77395 3
5948 45896 3 77396 3
5949 45897 3 77397 3
5950 45898 3 77398 3
5951 45899 3 77399 3
5952 45900 3 77400 3
5953 45901 3 77401 3
5954 45902 3 77402 3
5955 45903 3 77403 3
5956 45904 3 77404 3
5957 45905 3 77405 3
5958 45906 3 77406 3
5959 45907 3 77407 3
5960 45908 3 77408 3
5961 45909 3 77409 3
5962 45910 3 77410 3
5963 45911 3 77411 3
5964 45912 3 77412 3
5965 45913 3 77413 3
5966 45914 3 77414 3
5967 45915 3 77415 3
5968 45916 3 77416 3
5969 45917 3 77417 3
5970 45918 3 77418 3
5971 45919 3 77419 3
5972 45920 3 77420 3
5973 45921 3 77421 3
5974 45922 3 77422 3
5975 45923 3 77423 3
5976 45924 3 77424 3
5977 45925 3 77425 3
5978 45926 3 77426 3
5979 45927 3 77427 3
5980 45928 3 77428 3
5981 45929 3 77429 3
5982 45930 3 77430 3
5983 45931 3 77431 3
5984 45932 3 77432 3
5985 45933 3 77433 3
5986 45934 3 77434 3

5987 45935 3 77435 3
5988 45936 3 77436 3
5989 45937 3 77437 3
5990 45938 3 77438 3
5991 45939 3 77439 3
5992 45940 3 77440 3
5993 45941 3 77441 3
5994 45942 3 77442 3
5995 45943 3 77443 3
5996 45944 3 77444 3
5997 45945 3 77445 3
5998 45946 3 77446 3
5999 45947 3 77447 3
6000 45948 3 77448 3
6001 45949 3 77449 3
6002 45950 3 77450 3
6003 45951 3 77451 3
6004 45952 3 77452 3
6005 45953 3 77453 3
6006 45954 3 77454 3
6007 45955 3 77455 3
6008 45956 3 77456 3
6009 45957 3 77457 3
6010 45958 3 77458 3
6011 45959 3 77459 3
6012 45960 3 77460 3
6013 45961 3 77461 3
6014 45962 3 77462 3
6015 45963 3 77463 3
6016 45964 3 77464 3
6017 45965 3 77465 3
6018 45966 3 77466 3
6019 45967 3 77467 3
6020 45968 3 77468 3
6021 45969 3 77469 3
6022 45970 3 77470 3
6023 45971 3 77471 3
6024 45972 3 77472 3
6025 45973 3 77473 3
6026 45974 3 77474 3
6027 45975 3 77475 3
6028 45976 3 77476 3
6029 45977 3 77477 3
6030 45978 3 77478 3
6031 45979 3 77479 3
6032 45980 3 77480 3
6033 45981 3 77481 3
6034 45982 3 77482 3
6035 45983 3 77483 3
6036 45984 3 77484 3
6037 45985 3 77485 3
6038 45986 3 77486 3
6039 45987 3 77487 3
6040 45988 3 77488 3
6041 45989 3 77489 3
6042 45990 3 77490 3

6043 45991 3 77491 3
6044 45992 3 77492 3
6045 45993 3 77493 3
6046 45994 3 77494 3
6047 45995 3 77495 3
6048 45996 3 77496 3
6049 45997 3 77497 3
6050 45998 3 77498 3
6051 45999 3 77499 3
6052 46000 3 77500 3
6053 46001 3 77501 3
6054 46002 3 77502 3
6055 46003 3 77503 3
6056 46004 3 77504 3
6057 46005 3 77505 3
6058 46006 3 77506 3
6059 46007 3 77507 3
6060 46008 3 77508 3
6061 46009 3 77509 3
6062 46010 3 77510 3
6063 46011 3 77511 3
6064 46012 3 77512 3
6065 46013 3 77513 3
6066 46014 3 77514 3
6067 46015 3 77515 3
6068 46016 3 77516 3
6069 46017 3 77517 3
6070 46018 3 77518 3
6071 46019 3 77519 3
6072 46020 3 77520 3
6073 46021 3 77521 3
6074 46022 3 77522 3
6075 46023 3 77523 3
6076 46024 3 77524 3
6077 46025 3 77525 3
6078 46026 3 77526 3
6079 46027 3 77527 3
6080 46028 3 77528 3
6081 46029 3 77529 3
6082 46030 3 77530 3
6083 46031 3 77531 3
6084 46032 3 77532 3
6085 46033 3 77533 3
6086 46034 3 77534 3
6087 46035 3 77535 3
6088 46036 3 77536 3
6089 46037 3 77537 3
6090 46038 3 77538 3
6091 46039 3 77539 3
6092 46040 3 77540 3
6093 46041 3 77541 3
6094 46042 3 77542 3
6095 46043 3 77543 3
6096 46044 3 77544 3
6097 46045 3 77545 3
6098 46046 3 77546 3

6099 46047 3 77547 3
6100 46048 3 77548 3
6101 46049 3 77549 3
6102 46050 3 77550 3
6103 46051 3 77551 3
6104 46052 3 77552 3
6105 46053 3 77553 3
6106 46054 3 77554 3
6107 46055 3 77555 3
6108 46056 3 77556 3
6109 46057 3 77557 3
6110 46058 3 77558 3
6111 46059 3 77559 3
6112 46060 3 77560 3
6113 46061 3 77561 3
6114 46062 3 77562 3
6115 46063 3 77563 3
6116 46064 3 77564 3
6117 46065 3 77565 3
6118 46066 3 77566 3
6119 46067 3 77567 3
6120 46068 3 77568 3
6121 46069 3 77569 3
6122 46070 3 77570 3
6123 46071 3 77571 3
6124 46072 3 77572 3
6125 46073 3 77573 3
6126 46074 3 77574 3
6127 46075 3 77575 3
6128 46076 3 77576 3
6129 46077 3 77577 3
6130 46078 3 77578 3
6131 46079 3 77579 3
6132 46080 3 77580 3
6133 46081 3 77581 3
6134 46082 3 77582 3
6135 46083 3 77583 3
6136 46084 3 77584 3
6137 46085 3 77585 3
6138 46086 3 77586 3
6139 46087 3 77587 3
6140 46088 3 77588 3
6141 46089 3 77589 3
6142 46090 3 77590 3
6143 46091 3 77591 3
6144 46092 3 77592 3
6145 46093 3 77593 3
6146 46094 3 77594 3
6147 46095 3 77595 3
6148 46096 3 77596 3
6149 46097 3 77597 3
6150 46098 3 77598 3
6151 46099 3 77599 3
6152 46100 3 77600 3
6153 46101 3 77601 3
6154 46102 3 77602 3

6155 46103 3 77603 3
6156 46104 3 77604 3
6157 46105 3 77605 3
6158 46106 3 77606 3
6159 46107 3 77607 3
6160 46108 3 77608 3
6161 46109 3 77609 3
6162 46110 3 77610 3
6163 46111 3 77611 3
6164 46112 3 77612 3
6165 46113 3 77613 3
6166 46114 3 77614 3
6167 46115 3 77615 3
6168 46116 3 77616 3
6169 46117 3 77617 3
6170 46118 3 77618 3
6171 46119 3 77619 3
6172 46120 3 77620 3
6173 46121 3 77621 3
6174 46122 3 77622 3
6175 46123 3 77623 3
6176 46124 3 77624 3
6177 46125 3 77625 3
6178 46126 3 77626 3
6179 46127 3 77627 3
6180 46128 3 77628 3
6181 46129 3 77629 3
6182 46130 3 77630 3
6183 46131 3 77631 3
6184 46132 3 77632 3
6185 46133 3 77633 3
6186 46134 3 77634 3
6187 46135 3 77635 3
6188 46136 3 77636 3
6189 46137 3 77637 3
6190 46138 3 77638 3
6191 46139 3 77639 3
6192 46140 3 77640 3
6193 46141 3 77641 3
6194 46142 3 77642 3
6195 46143 3 77643 3
6196 46144 3 77644 3
6197 46145 3 77645 3
6198 46146 3 77646 3
6199 46147 3 77647 3
6200 46148 3 77648 3
6201 46149 3 77649 3
6202 46150 3 77650 3
6203 46151 3 77651 3
6204 46152 3 77652 3
6205 46153 3 77653 3
6206 46154 3 77654 3
6207 46155 3 77655 3
6208 46156 3 77656 3
6209 46157 3 77657 3
6210 46158 3 77658 3

6211 46159 3 77659 3
6212 46160 3 77660 3
6213 46161 3 77661 3
6214 46162 3 77662 3
6215 46163 3 77663 3
6216 46164 3 77664 3
6217 46165 3 77665 3
6218 46166 3 77666 3
6219 46167 3 77667 3
6220 46168 3 77668 3
6221 46169 3 77669 3
6222 46170 3 77670 3
6223 46171 3 77671 3
6224 46172 3 77672 3
6225 46173 3 77673 3
6226 46174 3 77674 3
6227 46175 3 77675 3
6228 46176 3 77676 3
6229 46177 3 77677 3
6230 46178 3 77678 3
6231 46179 3 77679 3
6232 46180 3 77680 3
6233 46181 3 77681 3
6234 46182 3 77682 3
6235 46183 3 77683 3
6236 46184 3 77684 3
6237 46185 3 77685 3
6238 46186 3 77686 3
6239 46187 3 77687 3
6240 46188 3 77688 3
6241 46189 3 77689 3
6242 46190 3 77690 3
6243 46191 3 77691 3
6244 46192 3 77692 3
6245 46193 3 77693 3
6246 46194 3 77694 3
6247 46195 3 77695 3
6248 46196 3 77696 3
6249 46197 3 77697 3
6250 46198 3 77698 3
6251 46199 3 77699 3
6252 46200 3 77700 3
6253 46201 3 77701 3
6254 46202 3 77702 3
6255 46203 3 77703 3
6256 46204 3 77704 3
6257 46205 3 77705 3
6258 46206 3 77706 3
6259 46207 3 77707 3
6260 46208 3 77708 3
6261 46209 3 77709 3
6262 46210 3 77710 3
6263 46211 3 77711 3
6264 46212 3 77712 3
6265 46213 3 77713 3
6266 46214 3 77714 3

6267 46215 3 77715 3
6268 46216 3 77716 3
6269 46217 3 77717 3
6270 46218 3 77718 3
6271 46219 3 77719 3
6272 46220 3 77720 3
6273 46221 3 77721 3
6274 46222 3 77722 3
6275 46223 3 77723 3
6276 46224 3 77724 3
6277 46225 3 77725 3
6278 46226 3 77726 3
6279 46227 3 77727 3
6280 46228 3 77728 3
6281 46229 3 77729 3
6282 46230 3 77730 3
6283 46231 3 77731 3
6284 46232 3 77732 3
6285 46233 3 77733 3
6286 46234 3 77734 3
6287 46235 3 77735 3
6288 46236 3 77736 3
6289 46237 3 77737 3
6290 46238 3 77738 3
6291 46239 3 77739 3
6292 46240 3 77740 3
6293 46241 3 77741 3
6294 46242 3 77742 3
6295 46243 3 77743 3
6296 46244 3 77744 3
6297 46245 3 77745 3
6298 46246 3 77746 3
6299 46247 3 77747 3
6300 46248 3 77748 3
6301 46249 3 77749 3
6302 46250 3 77750 3
6303 46251 3 77751 3
6304 46252 3 77752 3
6305 46253 3 77753 3
6306 46254 3 77754 3
6307 46255 3 77755 3
6308 46256 3 77756 3
6309 46257 3 77757 3
6310 46258 3 77758 3
6311 46259 3 77759 3
6312 46260 3 77760 3
6313 46261 3 77761 3
6314 46262 3 77762 3
6315 46263 3 77763 3
6316 46264 3 77764 3
6317 46265 3 77765 3
6318 46266 3 77766 3
6319 46267 3 77767 3
6320 46268 3 77768 3
6321 46269 3 77769 3
6322 46270 3 77770 3

6323 46271 3 77771 3
6324 46272 3 77772 3
6325 46273 3 77773 3
6326 46274 3 77774 3
6327 46275 3 77775 3
6328 46276 3 77776 3
6329 46277 3 77777 3
6330 46278 3 77778 3
6331 46279 3 77779 3
6332 46280 3 77780 3
6333 46281 3 77781 3
6334 46282 3 77782 3
6335 46283 3 77783 3
6336 46284 3 77784 3
6337 46285 3 77785 3
6338 46286 3 77786 3
6339 46287 3 77787 3
6340 46288 3 77788 3
6341 46289 3 77789 3
6342 46290 3 77790 3
6343 46291 3 77791 3
6344 46292 3 77792 3
6345 46293 3 77793 3
6346 46294 3 77794 3
6347 46295 3 77795 3
6348 46296 3 77796 3
6349 46297 3 77797 3
6350 46298 3 77798 3
6351 46299 3 77799 3
6352 46300 3 77800 3
6353 46301 3 77801 3
6354 46302 3 77802 3
6355 46303 3 77803 3
6356 46304 3 77804 3
6357 46305 3 77805 3
6358 46306 3 77806 3
6359 46307 3 77807 3
6360 46308 3 77808 3
6361 46309 3 77809 3
6362 46310 3 77810 3
6363 46311 3 77811 3
6364 46312 3 77812 3
6365 46313 3 77813 3
6366 46314 3 77814 3
6367 46315 3 77815 3
6368 46316 3 77816 3
6369 46317 3 77817 3
6370 46318 3 77818 3
6371 46319 3 77819 3
6372 46320 3 77820 3
6373 46321 3 77821 3
6374 46322 3 77822 3
6375 46323 3 77823 3
6376 46324 3 77824 3
6377 46325 3 77825 3
6378 46326 3 77826 3

6379 46327 3 77827 3
6380 46328 3 77828 3
6381 46329 3 77829 3
6382 46330 3 77830 3
6383 46331 3 77831 3
6384 46332 3 77832 3
6385 46333 3 77833 3
6386 46334 3 77834 3
6387 46335 3 77835 3
6388 46336 3 77836 3
6389 46337 3 77837 3
6390 46338 3 77838 3
6391 46339 3 77839 3
6392 46340 3 77840 3
6393 46341 3 77841 3
6394 46342 3 77842 3
6395 46343 3 77843 3
6396 46344 3 77844 3
6397 46345 3 77845 3
6398 46346 3 77846 3
6399 46347 3 77847 3
6400 46348 3 77848 3
6401 46349 3 77849 3
6402 46350 3 77850 3
6403 46351 3 77851 3
6404 46352 3 77852 3
6405 46353 3 77853 3
6406 46354 3 77854 3
6407 46355 3 77855 3
6408 46356 3 77856 3
6409 46357 3 77857 3
6410 46358 3 77858 3
6411 46359 3 77859 3
6412 46360 3 77860 3
6413 46361 3 77861 3
6414 46362 3 77862 3
6415 46363 3 77863 3
6416 46364 3 77864 3
6417 46365 3 77865 3
6418 46366 3 77866 3
6419 46367 3 77867 3
6420 46368 3 77868 3
6421 46369 3 77869 3
6422 46370 3 77870 3
6423 46371 3 77871 3
6424 46372 3 77872 3
6425 46373 3 77873 3
6426 46374 3 77874 3
6427 46375 3 77875 3
6428 46376 3 77876 3
6429 46377 3 77877 3
6430 46378 3 77878 3
6431 46379 3 77879 3
6432 46380 3 77880 3
6433 46381 3 77881 3
6434 46382 3 77882 3

6435 46383 3 77883 3
6436 46384 3 77884 3
6437 46385 3 77885 3
6438 46386 3 77886 3
6439 46387 3 77887 3
6440 46388 3 77888 3
6441 46389 3 77889 3
6442 46390 3 77890 3
6443 46391 3 77891 3
6444 46392 3 77892 3
6445 46393 3 77893 3
6446 46394 3 77894 3
6447 46395 3 77895 3
6448 46396 3 77896 3
6449 46397 3 77897 3
6450 46398 3 77898 3
6451 46399 3 77899 3
6452 46400 3 77900 3
6453 46401 3 77901 3
6454 46402 3 77902 3
6455 46403 3 77903 3
6456 46404 3 77904 3
6457 46405 3 77905 3
6458 46406 3 77906 3
6459 46407 3 77907 3
6460 46408 3 77908 3
6461 46409 3 77909 3
6462 46410 3 77910 3
6463 46411 3 77911 3
6464 46412 3 77912 3
6465 46413 3 77913 3
6466 46414 3 77914 3
6467 46415 3 77915 3
6468 46416 3 77916 3
6469 46417 3 77917 3
6470 46418 3 77918 3
6471 46419 3 77919 3
6472 46420 3 77920 3
6473 46421 3 77921 3
6474 46422 3 77922 3
6475 46423 3 77923 3
6476 46424 3 77924 3
6477 46425 3 77925 3
6478 46426 3 77926 3
6479 46427 3 77927 3
6480 46428 3 77928 3
6481 46429 3 77929 3
6482 46430 3 77930 3
6483 46431 3 77931 3
6484 46432 3 77932 3
6485 46433 3 77933 3
6486 46434 3 77934 3
6487 46435 3 77935 3
6488 46436 3 77936 3
6489 46437 3 77937 3
6490 46438 3 77938 3

6491 46439 3 77939 3
6492 46440 3 77940 3
6493 46441 3 77941 3
6494 46442 3 77942 3
6495 46443 3 77943 3
6496 46444 3 77944 3
6497 46445 3 77945 3
6498 46446 3 77946 3
6499 46447 3 77947 3
6500 46448 3 77948 3
6501 46449 3 77949 3
6502 46450 3 77950 3
6503 46451 3 77951 3
6504 46452 3 77952 3
6505 46453 3 77953 3
6506 46454 3 77954 3
6507 46455 3 77955 3
6508 46456 3 77956 3
6509 46457 3 77957 3
6510 46458 3 77958 3
6511 46459 3 77959 3
6512 46460 3 77960 3
6513 46461 3 77961 3
6514 46462 3 77962 3
6515 46463 3 77963 3
6516 46464 3 77964 3
6517 46465 3 77965 3
6518 46466 3 77966 3
6519 46467 3 77967 3
6520 46468 3 77968 3
6521 46469 3 77969 3
6522 46470 3 77970 3
6523 46471 3 77971 3
6524 46472 3 77972 3
6525 46473 3 77973 3
6526 46474 3 77974 3
6527 46475 3 77975 3
6528 46476 3 77976 3
6529 46477 3 77977 3
6530 46478 3 77978 3
6531 46479 3 77979 3
6532 46480 3 77980 3
6533 46481 3 77981 3
6534 46482 3 77982 3
6535 46483 3 77983 3
6536 46484 3 77984 3
6537 46485 3 77985 3
6538 46486 3 77986 3
6539 46487 3 77987 3
6540 46488 3 77988 3
6541 46489 3 77989 3
6542 46490 3 77990 3
6543 46491 3 77991 3
6544 46492 3 77992 3
6545 46493 3 77993 3
6546 46494 3 77994 3

6547 46495 3 77995 3
6548 46496 3 77996 3
6549 46497 3 77997 3
6550 46498 3 77998 3
6551 46499 3 77999 3
6552 46500 3 78000 3
6553 46501 3 78001 3
6554 46502 3 78002 3
6555 46503 3 78003 3
6556 46504 3 78004 3
6557 46505 3 78005 3
6558 46506 3 78006 3
6559 46507 3 78007 3
6560 46508 3 78008 3
6561 46509 3 78009 3
6562 46510 3 78010 3
6563 46511 3 78011 3
6564 46512 3 78012 3
6565 46513 3 78013 3
6566 46514 3 78014 3
6567 46515 3 78015 3
6568 46516 3 78016 3
6569 46517 3 78017 3
6570 46518 3 78018 3
6571 46519 3 78019 3
6572 46520 3 78020 3
6573 46521 3 78021 3
6574 46522 3 78022 3
6575 46523 3 78023 3
6576 46524 3 78024 3
6577 46525 3 78025 3
6578 46526 3 78026 3
6579 46527 3 78027 3
6580 46528 3 78028 3
6581 46529 3 78029 3
6582 46530 3 78030 3
6583 46531 3 78031 3
6584 46532 3 78032 3
6585 46533 3 78033 3
6586 46534 3 78034 3
6587 46535 3 78035 3
6588 46536 3 78036 3
6589 46537 3 78037 3
6590 46538 3 78038 3
6591 46539 3 78039 3
6592 46540 3 78040 3
6593 46541 3 78041 3
6594 46542 3 78042 3
6595 46543 3 78043 3
6596 46544 3 78044 3
6597 46545 3 78045 3
6598 46546 3 78046 3
6599 46547 3 78047 3
6600 46548 3 78048 3
6601 46549 3 78049 3
6602 46550 3 78050 3

6603 46551 3 78051 3
6604 46552 3 78052 3
6605 46553 3 78053 3
6606 46554 3 78054 3
6607 46555 3 78055 3
6608 46556 3 78056 3
6609 46557 3 78057 3
6610 46558 3 78058 3
6611 46559 3 78059 3
6612 46560 3 78060 3
6613 46561 3 78061 3
6614 46562 3 78062 3
6615 46563 3 78063 3
6616 46564 3 78064 3
6617 46565 3 78065 3
6618 46566 3 78066 3
6619 46567 3 78067 3
6620 46568 3 78068 3
6621 46569 3 78069 3
6622 46570 3 78070 3
6623 46571 3 78071 3
6624 46572 3 78072 3
6625 46573 3 78073 3
6626 46574 3 78074 3
6627 46575 3 78075 3
6628 46576 3 78076 3
6629 46577 3 78077 3
6630 46578 3 78078 3
6631 46579 3 78079 3
6632 46580 3 78080 3
6633 46581 3 78081 3
6634 46582 3 78082 3
6635 46583 3 78083 3
6636 46584 3 78084 3
6637 46585 3 78085 3
6638 46586 3 78086 3
6639 46587 3 78087 3
6640 46588 3 78088 3
6641 46589 3 78089 3
6642 46590 3 78090 3
6643 46591 3 78091 3
6644 46592 3 78092 3
6645 46593 3 78093 3
6646 46594 3 78094 3
6647 46595 3 78095 3
6648 46596 3 78096 3
6649 46597 3 78097 3
6650 46598 3 78098 3
6651 46599 3 78099 3
6652 46600 3 78100 3
6653 46601 3 78101 3
6654 46602 3 78102 3
6655 46603 3 78103 3
6656 46604 3 78104 3
6657 46605 3 78105 3
6658 46606 3 78106 3

6659 46607 3 78107 3
6660 46608 3 78108 3
6661 46609 3 78109 3
6662 46610 3 78110 3
6663 46611 3 78111 3
6664 46612 3 78112 3
6665 46613 3 78113 3
6666 46614 3 78114 3
6667 46615 3 78115 3
6668 46616 3 78116 3
6669 46617 3 78117 3
6670 46618 3 78118 3
6671 46619 3 78119 3
6672 46620 3 78120 3
6673 46621 3 78121 3
6674 46622 3 78122 3
6675 46623 3 78123 3
6676 46624 3 78124 3
6677 46625 3 78125 3
6678 46626 3 78126 3
6679 46627 3 78127 3
6680 46628 3 78128 3
6681 46629 3 78129 3
6682 46630 3 78130 3
6683 46631 3 78131 3
6684 46632 3 78132 3
6685 46633 3 78133 3
6686 46634 3 78134 3
6687 46635 3 78135 3
6688 46636 3 78136 3
6689 46637 3 78137 3
6690 46638 3 78138 3
6691 46639 3 78139 3
6692 46640 3 78140 3
6693 46641 3 78141 3
6694 46642 3 78142 3
6695 46643 3 78143 3
6696 46644 3 78144 3
6697 46645 3 78145 3
6698 46646 3 78146 3
6699 46647 3 78147 3
6700 46648 3 78148 3
6701 46649 3 78149 3
6702 46650 3 78150 3
6703 46651 3 78151 3
6704 46652 3 78152 3
6705 46653 3 78153 3
6706 46654 3 78154 3
6707 46655 3 78155 3
6708 46656 3 78156 3
6709 46657 3 78157 3
6710 46658 3 78158 3
6711 46659 3 78159 3
6712 46660 3 78160 3
6713 46661 3 78161 3
6714 46662 3 78162 3

6715 46663 3 78163 3
6716 46664 3 78164 3
6717 46665 3 78165 3
6718 46666 3 78166 3
6719 46667 3 78167 3
6720 46668 3 78168 3
6721 46669 3 78169 3
6722 46670 3 78170 3
6723 46671 3 78171 3
6724 46672 3 78172 3
6725 46673 3 78173 3
6726 46674 3 78174 3
6727 46675 3 78175 3
6728 46676 3 78176 3
6729 46677 3 78177 3
6730 46678 3 78178 3
6731 46679 3 78179 3
6732 46680 3 78180 3
6733 46681 3 78181 3
6734 46682 3 78182 3
6735 46683 3 78183 3
6736 46684 3 78184 3
6737 46685 3 78185 3
6738 46686 3 78186 3
6739 46687 3 78187 3
6740 46688 3 78188 3
6741 46689 3 78189 3
6742 46690 3 78190 3
6743 46691 3 78191 3
6744 46692 3 78192 3
6745 46693 3 78193 3
6746 46694 3 78194 3
6747 46695 3 78195 3
6748 46696 3 78196 3
6749 46697 3 78197 3
6750 46698 3 78198 3
6751 46699 3 78199 3
6752 46700 3 78200 3
6753 46701 3 78201 3
6754 46702 3 78202 3
6755 46703 3 78203 3
6756 46704 3 78204 3
6757 46705 3 78205 3
6758 46706 3 78206 3
6759 46707 3 78207 3
6760 46708 3 78208 3
6761 46709 3 78209 3
6762 46710 3 78210 3
6763 46711 3 78211 3
6764 46712 3 78212 3
6765 46713 3 78213 3
6766 46714 3 78214 3
6767 46715 3 78215 3
6768 46716 3 78216 3
6769 46717 3 78217 3
6770 46718 3 78218 3

```
6771 46719 3 78219 3
@
*
FIXITY NAME=ZT
@CLEAR
 'X-TRANSLATION'
 'Y-TRANSLATION'
 'X-ROTATION'
 'Y-ROTATION'
 'Z-ROTATION'
 'OVALIZATION'
@
*
FIXITY NAME=ZYT
@CLEAR
 'X-TRANSLATION'
 'X-ROTATION'
 'Y-ROTATION'
 'Z-ROTATION'
 'OVALIZATION'
@
*
FIXITY NAME=X_FIX
@CLEAR
 'X-TRANSLATION'
 'OVALIZATION'
@
*
FIXITY NAME=Y_FIX
@CLEAR
 'Y-TRANSLATION'
 'OVALIZATION'
@
*
FIXITY NAME=XY_FIX
@CLEAR
 'X-TRANSLATION'
 'Y-TRANSLATION'
 'OVALIZATION'
@
*
FIXBOUNDARY FACES FIXITY=X_FIX BODY=731
@CLEAR
6  'X_FIX'
2  'Y_FIX'
4  'Y_FIX'
5  'ALL'
@
*
FIXBOUNDARY FACES FIXITY=ALL BODY=732
@CLEAR
3  'X_FIX'
2  'Y_FIX'
4  'Y_FIX'
5  'ALL'
@
```

```
*
FIXBOUNDARY FACES FIXITY=ALL BODY=730
@CLEAR
2  'Y_FIX'
4  'Y_FIX'
5  'ALL'
@
*
FIXBOUNDARY FACES FIXITY=ALL BODY=733
@CLEAR
2  'Y_FIX'
4  'Y_FIX'
5  'ALL'
@
*
FIXBOUNDARY FACES FIXITY=ALL BODY=734
@CLEAR
2  'Y_FIX'
4  'Y_FIX'
5  'ALL'
@
*
FIXBOUNDARY POINTS FIXITY=ALL
@CLEAR
1496  'ZT'
1495  'ZYT'
504  'ZT'
503  'ZYT'
1000  'ZT'
999  'ZYT'
@
*
*Comment 12 (Temperature differentials)
*
LOAD TEMPERATURE NAME=1 MAGNITUD=10.0000000000000
*
LOAD TEMPERATURE NAME=2 MAGNITUD=-10.0000000000000
*
LOAD MASS-PROPORTIONAL NAME=1 MAGNITUD=1.00000000000000,
    AX=0.00000000000000 AY=0.00000000000000 AZ=-1.00000000000000,
    INTERPRE=BODY-FORCE
*
APPLY-LOAD BODY=1
@CLEAR
1  'TEMPERATURE' 1  'FACE' 1 0 1 0.00000000000000 0 -1 0 146 0  'NO',
    0.00000000000000 0.00000000000000 1 0  'BOTH'
2  'TEMPERATURE' 2  'FACE' 5 0 1 0.00000000000000 0 -1 0 147 0  'NO',
    0.00000000000000 0.00000000000000 1 0  'BOTH'
3  'TEMPERATURE' 1  'FACE' 1 0 1 0.00000000000000 0 -1 0 293 0  'NO',
    0.00000000000000 0.00000000000000 1 0  'BOTH'
4  'TEMPERATURE' 1  'FACE' 1 0 1 0.00000000000000 0 -1 0 440 0  'NO',
    0.00000000000000 0.00000000000000 1 0  'BOTH'
5  'TEMPERATURE' 2  'FACE' 5 0 1 0.00000000000000 0 -1 0 294 0  'NO',
    0.00000000000000 0.00000000000000 1 0  'BOTH'
6  'TEMPERATURE' 2  'FACE' 5 0 1 0.00000000000000 0 -1 0 441 0  'NO',
    0.00000000000000 0.00000000000000 1 0  'BOTH'
```

```
7  'MASS-PROPORTIONAL' 1  'MODEL' 0 0 1 0.00000000000000 0 -1 0 0 0  ,
'NO' 0.00000000000000 0.00000000000000 1 0  'MID'
@
*
***----------Tire Load----------
*Comment 11 (Tire load) ? Pressure (psi)
*
SET EGROUP NAME=1
LOADS-ELEMEN SUBSTRUC=0 REUSE=1 GROUP=1 THERMOST=0
@CLEAR
7427 3 115.000000000000 115.000000000000 115.000000000000,
    115.000000000000 1 0.00000000000000 0 -1
7428 3 115.000000000000 115.000000000000 115.000000000000,
    115.000000000000 1 0.00000000000000 0 -1
7487 3 115.000000000000 115.000000000000 115.000000000000,
    115.000000000000 1 0.00000000000000 0 -1
7488 3 115.000000000000 115.000000000000 115.000000000000,
    115.000000000000 1 0.00000000000000 0 -1
7547 3 115.000000000000 115.000000000000 115.000000000000,
    115.000000000000 1 0.00000000000000 0 -1
7548 3 115.000000000000 115.000000000000 115.000000000000,
    115.000000000000 1 0.00000000000000 0 -1
7607 3 115.000000000000 115.000000000000 115.000000000000,
    115.000000000000 1 0.00000000000000 0 -1
7608 3 115.000000000000 115.000000000000 115.000000000000,
    115.000000000000 1 0.00000000000000 0 -1
6287 3 115.000000000000 115.000000000000 115.000000000000,
    115.000000000000 1 0.00000000000000 0 -1
6288 3 115.000000000000 115.000000000000 115.000000000000,
    115.000000000000 1 0.00000000000000 0 -1
6347 3 115.000000000000 115.000000000000 115.000000000000,
    115.000000000000 1 0.00000000000000 0 -1
6348 3 115.000000000000 115.000000000000 115.000000000000,
    115.000000000000 1 0.00000000000000 0 -1
6407 3 115.000000000000 115.000000000000 115.000000000000,
    115.000000000000 1 0.00000000000000 0 -1
6408 3 115.000000000000 115.000000000000 115.000000000000,
    115.000000000000 1 0.00000000000000 0 -1
6467 3 115.000000000000 115.000000000000 115.000000000000,
    115.000000000000 1 0.00000000000000 0 -1
6468 3 115.000000000000 115.000000000000 115.000000000000,
    115.000000000000 1 0.00000000000000 0 -1
@
*
```

APPENDIX E
CRCP: SAMPLE INPUT FILE

```
*
* Command file created from session file information stored within AUI database
*
*------------------------------------Set the analysis environmental----------------------------------------
DATABASE NEW SAVE=NO PROMPT=NO
FEPROGRAM ADINA
CONTROL FILEVERSION=V89
*
FEPROGRAM PROGRAM=ADINA
*
CONTROL PLOTUNIT=PERCENT VERBOSE=YES ERRORLIM=0 LOGLIMIT=0 UNDO=5,
    PROMPTDE=UNKNOWN AUTOREPA=YES DRAWMATT=YES DRAWTEXT=EXACT,
    DRAWLINE=EXACT DRAWFILL=EXACT AUTOMREB=YES ZONECOPY=NO,
    SWEEPCOI=YES SESSIONS=YES DYNAMICT=YES UPDATETH=YES AUTOREGE=NO,
    ERRORACT=CONTINUE FILEVERS=V89 INITFCHE=NO SIGDIGIT=6,
    AUTOZONE=YES PSFILEVE=V0
*
FEPROGRAM PROGRAM=ADINA
*
CONTROL PLOTUNIT=PERCENT VERBOSE=YES ERRORLIM=0 LOGLIMIT=0 UNDO=5,
    PROMPTDE=UNKNOWN AUTOREPA=YES DRAWMATT=YES DRAWTEXT=EXACT,
    DRAWLINE=EXACT DRAWFILL=EXACT AUTOMREB=YES ZONECOPY=NO,
    SWEEPCOI=YES SESSIONS=YES DYNAMICT=YES UPDATETH=YES AUTOREGE=NO,
    ERRORACT=CONTINUE FILEVERS=V89 INITFCHE=NO SIGDIGIT=6,
    AUTOZONE=YES PSFILEVE=V0
*
FEPROGRAM PROGRAM=ADINA
*
CONTROL PLOTUNIT=PERCENT VERBOSE=YES ERRORLIM=0 LOGLIMIT=0 UNDO=5,
    PROMPTDE=UNKNOWN AUTOREPA=YES DRAWMATT=YES DRAWTEXT=EXACT,
    DRAWLINE=EXACT DRAWFILL=EXACT AUTOMREB=YES ZONECOPY=NO,
    SWEEPCOI=YES SESSIONS=YES DYNAMICT=YES UPDATETH=YES AUTOREGE=NO,
    ERRORACT=CONTINUE FILEVERS=V89 INITFCHE=NO SIGDIGIT=6,
    AUTOZONE=YES PSFILEVE=V0
*
FEPROGRAM PROGRAM=ADINA
*
CONTROL PLOTUNIT=PERCENT VERBOSE=YES ERRORLIM=0 LOGLIMIT=0 UNDO=5,
    PROMPTDE=UNKNOWN AUTOREPA=YES DRAWMATT=YES DRAWTEXT=EXACT,
    DRAWLINE=EXACT DRAWFILL=EXACT AUTOMREB=YES ZONECOPY=NO,
    SWEEPCOI=YES SESSIONS=YES DYNAMICT=YES UPDATETH=YES AUTOREGE=NO,
    ERRORACT=CONTINUE FILEVERS=V89 INITFCHE=NO SIGDIGIT=6,
    AUTOZONE=YES PSFILEVE=V0
*
FEPROGRAM PROGRAM=ADINA
*
CONTROL PLOTUNIT=PERCENT VERBOSE=YES ERRORLIM=0 LOGLIMIT=0 UNDO=5,
    PROMPTDE=UNKNOWN AUTOREPA=YES DRAWMATT=YES DRAWTEXT=EXACT,
    DRAWLINE=EXACT DRAWFILL=EXACT AUTOMREB=YES ZONECOPY=NO,
    SWEEPCOI=YES SESSIONS=YES DYNAMICT=YES UPDATETH=YES AUTOREGE=NO,
    ERRORACT=CONTINUE FILEVERS=V89 INITFCHE=NO SIGDIGIT=6,
    AUTOZONE=YES PSFILEVE=V0
```

```
*
FEPROGRAM PROGRAM=ADINA
*
CONTROL PLOTUNIT=PERCENT VERBOSE=YES ERRORLIM=0 LOGLIMIT=0 UNDO=5,
   PROMPTDE=UNKNOWN AUTOREPA=YES DRAWMATT=YES DRAWTEXT=EXACT,
   DRAWLINE=EXACT DRAWFILL=EXACT AUTOMREB=YES ZONECOPY=NO,
   SWEEPCOI=YES SESSIONS=YES DYNAMICT=YES UPDATETH=YES AUTOREGE=NO,
   ERRORACT=CONTINUE FILEVERS=V89 INITFCHE=NO SIGDIGIT=6,
   AUTOZONE=YES PSFILEVE=V0
*
FEPROGRAM PROGRAM=ADINA
*
CONTROL PLOTUNIT=PERCENT VERBOSE=YES ERRORLIM=0 LOGLIMIT=0 UNDO=5,
   PROMPTDE=UNKNOWN AUTOREPA=YES DRAWMATT=YES DRAWTEXT=EXACT,
   DRAWLINE=EXACT DRAWFILL=EXACT AUTOMREB=YES ZONECOPY=NO,
   SWEEPCOI=YES SESSIONS=YES DYNAMICT=YES UPDATETH=YES AUTOREGE=NO,
   ERRORACT=CONTINUE FILEVERS=V89 INITFCHE=NO SIGDIGIT=6,
   AUTOZONE=YES PSFILEVE=V0
*
*Comment 1(Slab dimension) - Length units are in inches
*
BODY BLOCK NAME=1 OPTION=CENTERED POSITION=VECTOR ORIENTAT=SYSTEM,
   CX1=0.00000000000000 CX2=0.00000000000000 CX3=0.00000000000000,
   SYSTEM=0 DX1=60.0000000000000 DX2=144.000000000000,
   DX3=10.0000000000000
*
BODY BLOCK NAME=2 OPTION=CENTERED POSITION=VECTOR ORIENTAT=SYSTEM,
   CX1=60.1000000000000 CX2=0.00000000000000 CX3=0.00000000000000,
   SYSTEM=0 DX1=60.0000000000000 DX2=144.000000000000,
   DX3=10.0000000000000
*
*-------------Generate Reinforcement Steel----------------------
*
COORDINATES POINT SYSTEM=0
@CLEAR
1 30.0000000000000 -72.0000000000000 -5.00000000000000 0
2 30.0000000000000 72.0000000000000 -5.00000000000000 0
3 -30.0000000000000 -72.0000000000000 -5.00000000000000 0
4 -30.0000000000000 72.0000000000000 -5.00000000000000 0
5 30.0000000000000 -72.0000000000000 5.00000000000000 0
6 30.0000000000000 72.0000000000000 5.00000000000000 0
7 -30.0000000000000 72.0000000000000 5.00000000000000 0
8 -30.0000000000000 -72.0000000000000 5.00000000000000 0
9 90.1000000000000 -72.0000000000000 -5.00000000000000 0
10 90.1000000000000 72.0000000000000 -5.00000000000000 0
11 30.1000000000000 -72.0000000000000 -5.00000000000000 0
12 30.1000000000000 72.0000000000000 -5.00000000000000 0
13 90.1000000000000 -72.0000000000000 5.00000000000000 0
14 90.1000000000000 72.0000000000000 5.00000000000000 0
15 30.1000000000000 72.0000000000000 5.00000000000000 0
16 30.1000000000000 -72.0000000000000 5.00000000000000 0
17 -30.0000000000000 0.00000000000000 0.00000000000000 0
@
*
LINE EXTRUDED NAME=1 POINT=17 DX=60.0000000000000 DY=0.00000000000000,
   DZ=0.00000000000000 SYSTEM=0 PCOINCID=YES,
```

```
    PTOLERAN=1.00000000000000E-05
*
LINE EXTRUDED NAME=2 POINT=18 DX=0.100000000000000,
    DY=0.00000000000000 DZ=0.00000000000000 SYSTEM=0 PCOINCID=YES,
    PTOLERAN=1.00000000000000E-05
*
LINE EXTRUDED NAME=3 POINT=19 DX=60.0000000000000 DY=0.00000000000000,
    DZ=0.00000000000000 SYSTEM=0 PCOINCID=YES,
    PTOLERAN=1.00000000000000E-05
*
SUBDIVIDE LINE NAME=1 MODE=LENGTH SIZE=3.00000000000000
@CLEAR
3
@
*
SUBDIVIDE LINE NAME=2 MODE=DIVISIONS NDIV=3 RATIO=1.00000000000000,
    PROGRESS=GEOMETRIC CBIAS=NO
*
*Comment 4 (Longitudinal reinforced steel design) - Length units are in inches
*
TRANSFORMATI TRANSLATION NAME=1 MODE=SYSTEM SYSTEM=0,
    DX=0.00000000000000 DY=-6.00000000000000 DZ=0.00000000000000
*
LINE TRANSFORMED NAME=4 PARENT=1 TRANSFOR=1 PCOINCID=YES,
    PTOLERAN=1.00000000000000E-05 COUPLED=YES NCOPY=11 MESH=YES,
    EGROUP=0 NCOINCID=NO NTOLERAN=1.00000000000000E-05
@CLEAR
2
3
@
*
TRANSFORMATI TRANSLATION NAME=2 MODE=SYSTEM SYSTEM=0,
    DX=0.00000000000000 DY=6.00000000000000 DZ=0.00000000000000
*
LINE TRANSFORMED NAME=37 PARENT=1 TRANSFOR=2 PCOINCID=YES,
    PTOLERAN=1.00000000000000E-05 COUPLED=YES NCOPY=11 MESH=YES,
    EGROUP=0 NCOINCID=YES NTOLERAN=1.00000000000000E-05
@CLEAR
2
3
@
*
COORDINATES POINT SYSTEM=0
@STARTMODIFY
@APPROW      108        1
109 12.0000000000000 -72.0000000000000 0.00000000000000 0
@ENDMODIFY
*
LINE EXTRUDED NAME=70 POINT=109 DX=0.00000000000000,
    DY=144.000000000000 DZ=0.00000000000000 SYSTEM=0 PCOINCID=YES,
    PTOLERAN=1.00000000000000E-05
*
SUBDIVIDE LINE NAME=70 MODE=LENGTH SIZE=3.00000000000000
*
*Comment 5 (Transverse reinforced steel design) - Length units are in inches
*
```

```
TRANSFORMATI TRANSLATION NAME=3 MODE=SYSTEM SYSTEM=0,
   DX=-36.0000000000000 DY=0.00000000000000 DZ=0.00000000000000
*
LINE TRANSFORMED NAME=71 PARENT=70 TRANSFOR=3 PCOINCID=YES,
   PTOLERAN=1.00000000000000E-05 COUPLED=YES NCOPY=1 MESH=YES,
   EGROUP=0 NCOINCID=YES NTOLERAN=1.00000000000000E-05
*
TRANSFORMATI TRANSLATION NAME=4 MODE=SYSTEM SYSTEM=0,
   DX=36.1000000000000 DY=0.00000000000000 DZ=0.00000000000000
*
LINE TRANSFORMED NAME=72 PARENT=70 TRANSFOR=4 PCOINCID=YES,
   PTOLERAN=1.00000000000000E-05 COUPLED=YES NCOPY=1 MESH=YES,
   EGROUP=0 NCOINCID=YES NTOLERAN=1.00000000000000E-05
*
TRANSFORMATI TRANSLATION NAME=5 MODE=SYSTEM SYSTEM=0,
   DX=36.0000000000000 DY=0.00000000000000 DZ=0.00000000000000
*
LINE TRANSFORMED NAME=73 PARENT=72 TRANSFOR=5 PCOINCID=YES,
   PTOLERAN=1.00000000000000E-05 COUPLED=YES NCOPY=1 MESH=YES,
   EGROUP=0 NCOINCID=YES NTOLERAN=1.00000000000000E-05
*
SUBDIVIDE BODY NAME=1 MODE=LENGTH SIZE=3.00000000000000,
   MAX-SIZE=0.00000000000000
@CLEAR
2
@
*
SUBDIVIDE EDGE NAME=5 BODY=2 MODE=DIVISIONS NDIV=4,
   RATIO=1.00000000000000 PROGRESS=ARITHMETIC BLTABLE=0
@CLEAR
6
7
8
@
*
SUBDIVIDE EDGE NAME=5 BODY=1 MODE=DIVISIONS NDIV=4,
   RATIO=1.00000000000000 PROGRESS=ARITHMETIC BLTABLE=0
@CLEAR
6
7
8
@
*
*Comment 2 (Base layer) - Length units are in inches
*
BODY BLOCK NAME=3 OPTION=CENTERED POSITION=VECTOR ORIENTAT=SYSTEM,
   CX1=30.0500000000000 CX2=0.00000000000000 CX3=-8.00000000000000,
   SYSTEM=0 DX1=120.100000000000 DX2=192.000000000000,
   DX3=6.00000000000000
*
SUBDIVIDE BODY NAME=3 MODE=LENGTH SIZE=3.00000000000000,
   MAX-SIZE=0.00000000000000
*
*Comment 3 (Subgrade layer) - Length units are in inches
*
BODY BLOCK NAME=4 OPTION=CENTERED POSITION=VECTOR ORIENTAT=SYSTEM,
```

```
    CX1=30.0500000000000 CX2=0.00000000000000 CX3=-61.0000000000000,
    SYSTEM=0 DX1=120.100000000000 DX2=192.000000000000,
    DX3=100.000000000000
*
SUBDIVIDE BODY NAME=4 MODE=LENGTH SIZE=3.00000000000000,
    MAX-SIZE=0.00000000000000
*
SUBDIVIDE EDGE NAME=5 BODY=4 MODE=DIVISIONS NDIV=15,
    RATIO=0.100000000000000 PROGRESS=ARITHMETIC BLTABLE=0
@CLEAR
6
7
8
@
*
*-----------------------Meshing Concrete and Reinforcement----------------------
*Comment 6 (Concrete properties) - Unit: E (psi), ν (unitless), Density (lb/in3), CTE (/°F)
*
MATERIAL ELASTIC NAME=1 E=5500000.00000000 NU=0.200000000000000,
    DENSITY=0.0840000000000000 ALPHA=5.80000000000000E-06 MDESCRIP=,
'Concrete'
*
*Comment 7 (Steel properties) - Unit: E (psi), ν (unitless)
*
MATERIAL ELASTIC NAME=2 E=2.90000000000000E+07 NU=0.300000000000000,
    DENSITY=0.00000000000000 ALPHA=5.00000000000000E-06 MDESCRIP=,
'steel'
*
CROSS-SECTIO PIPE NAME=1 DIAMETER=0.750000000000000,
    THICKNES=0.375000000000000 SC=0.00000000000000,
    TC=0.00000000000000 TORFAC=1.00000000000000,
    SSHEARF=0.00000000000000 TSHEARF=0.00000000000000 SOLID=YES
*
CROSS-SECTIO PIPE NAME=2 DIAMETER=0.625000000000000,
    THICKNES=0.312500000000000 SC=0.00000000000000,
    TC=0.00000000000000 TORFAC=1.00000000000000,
    SSHEARF=0.00000000000000 TSHEARF=0.00000000000000 SOLID=YES
*
*--------------------------Set the Boundary Condition---------------------
FIXITY NAME=X_FIX
@CLEAR
 'X-TRANSLATION'
 'OVALIZATION'
@
*
FIXITY NAME=Y_FIX
@CLEAR
 'X-ROTATION'
 'Y-ROTATION'
 'Z-ROTATION'
 'OVALIZATION'
@
*
FIXITY NAME=XY_FIX
@CLEAR
 'X-TRANSLATION'
```

```
 'Y-TRANSLATION'
 'OVALIZATION'
@
*
*------------------------Generate Temperature Gradient---------------------------
*
LOAD MASS-PROPORTIONAL NAME=1 MAGNITUD=1.00000000000000,
    AX=0.00000000000000 AY=0.00000000000000 AZ=-1.00000000000000,
    INTERPRE=BODY-FORCE
*
LOAD TEMPERATURE NAME=1 MAGNITUD=10.0000000000000
*
LOAD TEMPERATURE NAME=2 MAGNITUD=-10.0000000000000
*
FIXBOUNDARY FACES FIXITY=X_FIX BODY=2
@CLEAR
6  'X_FIX'
2  'Y_FIX'
4  'Y_FIX'
@
*
FIXBOUNDARY FACES FIXITY=ALL BODY=1
@CLEAR
3  'X_FIX'
2  'Y_FIX'
4  'Y_FIX'
@
*
FIXBOUNDARY FACES FIXITY=ALL BODY=3
@CLEAR
3  'X_FIX'
6  'X_FIX'
2  'Y_FIX'
4  'Y_FIX'
@
*
*----------------------Create Interface Between Slab and Subgrade----------------------
*
CGROUP CONTACT3 NAME=1 FORCES=YES TRACTION=YES NODETONO=NO,
    FRICTION=0.00000000000000 EPSN=1.00000000000000E-12,
    EPST=0.00000000000000 DIRECTIO=NORMAL CONTINUO=YES,
    INITIAL-=ALLOWED PENETRAT=ONE DEPTH=0.00000000000000,
    OFFSET=0.00000000000000 OFFSET-T=CONSTANT CORNER-C=NO,
    TBIRTH=0.00000000000000 TDEATH=0.00000000000000 TIED=NO,
    TIED-OFF=0.00000000000000 HHATTMC=0.00000000000000,
    FCTMC=0.500000000000000 FTTMC=0.500000000000000 RIGID-TA=NO,
    NORMAL-S=1.00000000000000E+11 TANGENTI=0.00000000000000,
    PTOLERAN=1.00000000000000E-08 RESIDUAL=0.00100000000000000,
    LIMIT-FO=1.00000000000000 ITERATIO=2 TIME-PEN=0.00000000000000,
    CONSISTE=DEFAULT USER-FRI=NO DESCRIPT='NONE',
    CFACTOR1=0.00000000000000 CS-EXTEN=0.00100000000000000,
    ALGORITH=DEFAULT RTP-CHEC=NO RTP-MAX=0.00100000000000000,
    XDAMP=NO XNDAMP=0.100000000000000 SLIDING-=1.00000000000000E-10,
    TENSILE-=0.00100000000000000 OSCILLAT=5,
    GAP-BIAS=0.00000000000000 OFFSET-D=AUTOMATIC DISPLACE=DEFAULT,
    FRIC-DEL=NO GAP-VALU=0.00000000000000 TENS-CON=YES FREE-OVE=NO,
```

```
   GAP-PUSH=0.00000000000000 EKTMC=0.00000000000000
*
CONTACTSURFA NAME=1 PRINT=DEFAULT SAVE=DEFAULT SOLID=YES BODY=1,
   ORIENTAT=AUTOMATIC MARQUEEB=0 DESCRIPT='NONE'
@CLEAR
6 1 0
@
*
CONTACTSURFA NAME=2 PRINT=DEFAULT SAVE=DEFAULT SOLID=YES BODY=2,
   ORIENTAT=AUTOMATIC MARQUEEB=0 DESCRIPT='NONE'
@CLEAR
3 1 0
@
*
CONTACTPAIR NAME=1 TARGET=2 CONTACTO=1 FRICTION=1.50000000000000,
   TBIRTH=0.00000000000000 TDEATH=0.00000000000000,
   HHATTMC=0.00000000000000 FCTMC=0.00000000000000,
   FTTMC=0.00000000000000 NX=0 NY=0 NZ=0 OFFSETCO=BOTH,
   EKTMC=0.00000000000000
*
CONTACTSURFA NAME=3 PRINT=DEFAULT SAVE=DEFAULT SOLID=MULT BODY=4,
   ORIENTAT=AUTOMATIC MARQUEEB=0 DESCRIPT='NONE'
@CLEAR
5 1 1
5 1 2
@
*
CONTACTSURFA NAME=4 PRINT=DEFAULT SAVE=DEFAULT SOLID=YES BODY=3,
   ORIENTAT=AUTOMATIC MARQUEEB=0 DESCRIPT='NONE'
@CLEAR
1 1 0
@
*
*Comment 10 (Frictional interface condition)
*
CONTACTPAIR NAME=2 TARGET=3 CONTACTO=4 FRICTION=1.50000000000000,
   TBIRTH=0.00000000000000 TDEATH=0.00000000000000,
   HHATTMC=0.00000000000000 FCTMC=0.00000000000000,
   FTTMC=0.00000000000000 NX=0 NY=0 NZ=0 OFFSETCO=BOTH,
   EKTMC=0.00000000000000
*
EGROUP THREEDSOLID NAME=1 DISPLACE=DEFAULT STRAINS=DEFAULT MATERIAL=1,
   RSINT=DEFAULT TINT=DEFAULT RESULTS=STRESSES DEGEN=DEFAUL,
   FORMULAT=0 STRESSRE=GLOBAL INITIALS=NONE FRACTUR=NO,
   CMASS=DEFAULT STRAIN-F=0 UL-FORMU=DEFAULT LVUS1=0 LVUS2=0 SED=NO,
   RUPTURE=ADINA INCOMPAT=DEFAULT TIME-OFF=0.00000000000000,
   POROUS=NO WTMC=1.00000000000000 OPTION=NONE DESCRIPT='NONE',
   PRINT=DEFAULT SAVE=DEFAULT TBIRTH=0.00000000000000,
   TDEATH=0.00000000000000 TMC-MATE=1 RUPTURE-=0 EM=NO JOULE=NO,
   BOLT-NUM=0 BOLT-PLA=0 BOLT-LOA=0.00000000000000,
   BOLT-TOL=0.00000000000000
*
EGROUP THREEDSOLID NAME=2 DISPLACE=DEFAULT STRAINS=DEFAULT MATERIAL=1,
   RSINT=DEFAULT TINT=DEFAULT RESULTS=STRESSES DEGEN=DEFAUL,
   FORMULAT=0 STRESSRE=GLOBAL INITIALS=NONE FRACTUR=NO,
   CMASS=DEFAULT STRAIN-F=0 UL-FORMU=DEFAULT LVUS1=0 LVUS2=0 SED=NO,
```

```
    RUPTURE=ADINA INCOMPAT=DEFAULT TIME-OFF=0.00000000000000,
    POROUS=NO WTMC=1.00000000000000 OPTION=NONE DESCRIPT='NONE',
    PRINT=DEFAULT SAVE=DEFAULT TBIRTH=0.00000000000000,
    TDEATH=0.00000000000000 TMC-MATE=1 RUPTURE-=0 EM=NO JOULE=NO,
    BOLT-NUM=0 BOLT-PLA=0 BOLT-LOA=0.00000000000000,
    BOLT-TOL=0.00000000000000
*
EGROUP BEAM NAME=3 SUBTYPE=THREE-D DISPLACE=DEFAULT MATERIAL=2 RINT=5,
    SINT=DEFAULT TINT=DEFAULT RESULTS=STRESSES INITIALS=NONE,
    CMASS=DEFAULT RIGIDEND=NONE MOMENT-C=NO RIGIDITY=1,
    MULTIPLY=1000000.00000000 RUPTURE=ADINA OPTION=NONE,
    BOLT-TOL=0.00000000000000 DESCRIPT='NONE' SECTION=1,
    PRINT=DEFAULT SAVE=DEFAULT TBIRTH=0.00000000000000,
    TDEATH=0.00000000000000 SPOINT=4 BOLTFORC=0.00000000000000,
    BOLTNCUR=0 TMC-MATE=1 BOLT-NUM=0 BOLT-LOA=0.00000000000000,
    WARP=NO ENDRELEA=ACCURATE
*
EGROUP BEAM NAME=4 SUBTYPE=THREE-D DISPLACE=DEFAULT MATERIAL=2 RINT=5,
    SINT=DEFAULT TINT=DEFAULT RESULTS=STRESSES INITIALS=NONE,
    CMASS=DEFAULT RIGIDEND=NONE MOMENT-C=NO RIGIDITY=1,
    MULTIPLY=1000000.00000000 RUPTURE=ADINA OPTION=NONE,
    BOLT-TOL=0.00000000000000 DESCRIPT='NONE' SECTION=2,
    PRINT=DEFAULT SAVE=DEFAULT TBIRTH=0.00000000000000,
    TDEATH=0.00000000000000 SPOINT=4 BOLTFORC=0.00000000000000,
    BOLTNCUR=0 TMC-MATE=1 BOLT-NUM=0 BOLT-LOA=0.00000000000000,
    WARP=NO ENDRELEA=ACCURATE
*
*Comment 8 (Base properties) - Unit: E (psi), ν (unitless)
*
MATERIAL ELASTIC NAME=3 E=44962.0000000000 NU=0.300000000000000,
    DENSITY=0.0760000000000000 ALPHA=0.00000000000000 MDESCRIP='base'
*
*Comment 9 (Subgrade properties) - Unit: E (psi), ν (unitless)
*
MATERIAL ELASTIC NAME=4 E=4395.00000000000 NU=0.400000000000000,
    DENSITY=0.0740000000000000 ALPHA=0.00000000000000 MDESCRIP=,
'subgrade'
*
EGROUP THREEDSOLID NAME=5 DISPLACE=DEFAULT STRAINS=DEFAULT MATERIAL=3,
    RSINT=DEFAULT TINT=DEFAULT RESULTS=STRESSES DEGEN=DEFAUL,
    FORMULAT=0 STRESSRE=GLOBAL INITIALS=NONE FRACTUR=NO,
    CMASS=DEFAULT STRAIN-F=0 UL-FORMU=DEFAULT LVUS1=0 LVUS2=0 SED=NO,
    RUPTURE=ADINA INCOMPAT=DEFAULT TIME-OFF=0.00000000000000,
    POROUS=NO WTMC=1.00000000000000 OPTION=NONE DESCRIPT='base',
    PRINT=DEFAULT SAVE=DEFAULT TBIRTH=0.00000000000000,
    TDEATH=0.00000000000000 TMC-MATE=1 RUPTURE-=0 EM=NO JOULE=NO,
    BOLT-NUM=0 BOLT-PLA=0 BOLT-LOA=0.00000000000000,
    BOLT-TOL=0.00000000000000
*
EGROUP THREEDSOLID NAME=6 DISPLACE=DEFAULT STRAINS=DEFAULT MATERIAL=4,
    RSINT=DEFAULT TINT=DEFAULT RESULTS=STRESSES DEGEN=DEFAUL,
    FORMULAT=0 STRESSRE=GLOBAL INITIALS=NONE FRACTUR=NO,
    CMASS=DEFAULT STRAIN-F=0 UL-FORMU=DEFAULT LVUS1=0 LVUS2=0 SED=NO,
    RUPTURE=ADINA INCOMPAT=DEFAULT TIME-OFF=0.00000000000000,
    POROUS=NO WTMC=1.00000000000000 OPTION=NONE DESCRIPT='subgrade',
    PRINT=DEFAULT SAVE=DEFAULT TBIRTH=0.00000000000000,
```

```
    TDEATH=0.00000000000000 TMC-MATE=1 RUPTURE-=0 EM=NO JOULE=NO,
    BOLT-NUM=0 BOLT-PLA=0 BOLT-LOA=0.00000000000000,
    BOLT-TOL=0.00000000000000
*
MASTER ANALYSIS=STATIC MODEX=EXECUTE TSTART=0.00000000000000 IDOF=111,
    OVALIZAT=NONE FLUIDPOT=AUTOMATIC CYCLICPA=1 IPOSIT=STOP,
    REACTION=YES INITIALS=NO FSINTERA=NO IRINT=DEFAULT CMASS=NO,
    SHELLNDO=AUTOMATIC AUTOMATI=OFF SOLVER=SPARSE,
    CONTACT-=CONSTRAINT-FUNCTION TRELEASE=0.00000000000000,
    RESTART-=NO FRACTURE=NO LOAD-CAS=NO LOAD-PEN=NO SINGULAR=YES,
    STIFFNES=0.000100000000000000 MAP-OUTP=NONE MAP-FORM=NO,
    NODAL-DE=" POROUS-C=NO ADAPTIVE=0 ZOOM-LAB=1 AXIS-CYC=0,
    PERIODIC=NO VECTOR-S=GEOMETRY EPSI-FIR=NO STABILIZ=NO,
    STABFACT=1.00000000000000E-10 RESULTS=PORTHOLE FEFCORR=NO,
    BOLTSTEP=1 EXTEND-S=YES CONVERT-=NO DEGEN=YES TMC-MODE=NO,
    ENSIGHT-=NO IRSTEPS=1 INITIALT=NO TEMP-INT=NO ESINTERA=NO,
    OP2GEOM=NO INSITU-D=NO
*
FIXITY NAME=Y_FIX
@CLEAR
 'Y-TRANSLATION'
 'X-ROTATION'
 'Y-ROTATION'
 'Z-ROTATION'
 'OVALIZATION'
@
*
FIXBOUNDARY FACES FIXITY=ALL BODY=4
@CLEAR
3  'X_FIX'
6  'X_FIX'
5  'ALL'
2  'Y_FIX'
4  'Y_FIX'
@
*
COPY ZONE NAME1=WHOLE_MODEL NAME2=MESHPLOT00001 POSITION=1
*
ZONE NAME=MESHPLOT00001 NODEATTA=YES GEOMATTA=YES
@CLEAR
 'whole model'
 'CONTACT GROUP 1 OF REUSE 1 OF SUBSTRUCTURE 0 OF PROGRAM ADINA'
@
*
ZONE NAME=MESHPLOT00001 NODEATTA=YES GEOMATTA=YES
@CLEAR
 'whole model'
 'contact group 1'
 'CONTACT GROUP 1 OF REUSE 1 OF SUBSTRUCTURE 0 OF PROGRAM ADINA'
@
*
ZONE NAME=MESHPLOT00001 NODEATTA=YES GEOMATTA=YES
@CLEAR
 'whole model'
 'contact group 1'
 'contact group 1'
```

```
 'CONTACT GROUP 1 OF REUSE 1 OF SUBSTRUCTURE 0 OF PROGRAM ADINA'
@
*
ZONE NAME=MESHPLOT00001 NODEATTA=YES GEOMATTA=YES
@CLEAR
 'whole model'
 'contact group 1'
 'contact group 1'
 'contact group 1'
 'CONTACT GROUP 1 OF REUSE 1 OF SUBSTRUCTURE 0 OF PROGRAM ADINA'
@
*
GBODY NODES=8 NCOINCID=BOUNDARIES NCTOLERA=1.00000000000000E-05,
    SUBSTRUC=0 GROUP=1 PREFSHAP=AUTOMATIC COLLAPSE=NO SIZE-FUN=0,
    DELETE-S=NO ANGLE-MI=5.00000000000000 MIDNODES=CURVED,
    METHOD=DELAUNAY PATTERN=0 MESHING=MAPPED DEGENERA=NO,
    BOUNDARY=ADVFRONT DEG-EDGE=0 GEO-ERRO=0.00000000000000,
    SAMPLING=20 MIN-SIZE=0.00000000000000 NLAYER=1 NLTABL=0,
    AUTO-GRA=NO SIMULATE=NO PYRAMIDS=NO DANGMAXB=80.0000000000000,
    DANGMAXC=60.0000000000000 DANGMAXD=80.0000000000000 HEXALAYE=NO,
    AUTO-REF=YES EVEN=SUM DENSITY=1.20000000000000 MIDFACEN=QUAD,
    REFINE=ALONG-EDGE GRID=NO BREFINE=ALONG-EDGE BLTABL=0,
    PREFSHA2=QUADRILATERAL NOPTI=1
@CLEAR
1 0
@
*
GBODY NODES=8 NCOINCID=BOUNDARIES NCTOLERA=1.00000000000000E-05,
    SUBSTRUC=0 GROUP=2 PREFSHAP=AUTOMATIC COLLAPSE=NO SIZE-FUN=0,
    DELETE-S=NO ANGLE-MI=5.00000000000000 MIDNODES=CURVED,
    METHOD=DELAUNAY PATTERN=0 MESHING=MAPPED DEGENERA=NO,
    BOUNDARY=ADVFRONT DEG-EDGE=0 GEO-ERRO=0.00000000000000,
    SAMPLING=20 MIN-SIZE=0.00000000000000 NLAYER=1 NLTABL=0,
    AUTO-GRA=NO SIMULATE=NO PYRAMIDS=NO DANGMAXB=80.0000000000000,
    DANGMAXC=60.0000000000000 DANGMAXD=80.0000000000000 HEXALAYE=NO,
    AUTO-REF=YES EVEN=SUM DENSITY=1.20000000000000 MIDFACEN=QUAD,
    REFINE=ALONG-EDGE GRID=NO BREFINE=ALONG-EDGE BLTABL=0,
    PREFSHA2=QUADRILATERAL NOPTI=1
@CLEAR
2 0
@
*
GLINE NODES=2 AUXPOINT=0 NCOINCID=ENDS NCENDS=12,
    NCTOLERA=1.00000000000000E-05 SUBSTRUC=0 GROUP=3 MIDNODES=CURVED,
    XO=0.00000000000000 YO=1.00000000000000 ZO=0.00000000000000,
    XYZOSYST=SKEW
@CLEAR
1
2
3
4
5
6
7
8
9
```

```
66
67
68
69
@
*
GLINE NODES=2 AUXPOINT=0 NCOINCID=ENDS NCENDS=12,
    NCTOLERA=1.00000000000000E-05 SUBSTRUC=0 GROUP=4 MIDNODES=CURVED,
    XO=1.00000000000000 YO=0.00000000000000 ZO=0.00000000000000,
    XYZOSYST=SKEW
@CLEAR
70
71
72
73
@
*
ZONE NAME=MESHPLOT00001 NODEATTA=YES GEOMATTA=YES
@CLEAR
 'whole model'
 'contact group 1'
 'contact group 1'
 'contact group 1'
 'contact group 1'
 ,
'SUBTRACT CONTACT GROUP 1 OF REUSE 1 OF SUBSTRUCTURE 0 OF PROG
RAM ADINA'
@
*
ZONE NAME=MESHPLOT00001 NODEATTA=YES GEOMATTA=YES
@CLEAR
 'whole model'
 'contact group 1'
 'contact group 1'
 'contact group 1'
 ,
'SUBTRACT CONTACT GROUP 1 OF REUSE 1 OF SUBSTRUCTURE 0 OF PROG
RAM ADINA'
@
*
ZONE NAME=MESHPLOT00001 NODEATTA=YES GEOMATTA=YES
@CLEAR
 'whole model'
 'contact group 1'
 'contact group 1'
 ,
'SUBTRACT CONTACT GROUP 1 OF REUSE 1 OF SUBSTRUCTURE 0 OF PROG
RAM ADINA'
@
*
GBODY NODES=8 NCOINCID=NO SUBSTRUC=0 GROUP=5 PREFSHAP=AUTOMATIC,
    COLLAPSE=NO SIZE-FUN=0 DELETE-S=NO ANGLE-MI=5.00000000000000,
    MIDNODES=CURVED METHOD=DELAUNAY PATTERN=0 MESHING=MAPPED,
    DEGENERA=NO BOUNDARY=ADVFRONT DEG-EDGE=0,
    GEO-ERRO=0.00000000000000 SAMPLING=20 MIN-SIZE=0.00000000000000,
    NLAYER=1 NLTABL=0 AUTO-GRA=NO SIMULATE=NO PYRAMIDS=NO,
```

```
    DANGMAXB=80.0000000000000 DANGMAXC=60.0000000000000,
    DANGMAXD=80.0000000000000 HEXALAYE=NO AUTO-REF=YES EVEN=SUM,
    DENSITY=1.20000000000000 MIDFACEN=QUAD REFINE=ALONG-EDGE GRID=NO,
    BREFINE=ALONG-EDGE BLTABL=0 PREFSHA2=QUADRILATERAL NOPTI=1
@CLEAR
3 0
@
*
COPY ZONE NAME1=WHOLE_MODEL NAME2=MESHPLOT00001 POSITION=1
*
ZONE NAME=MESHPLOT00001 NODEATTA=YES GEOMATTA=YES
@CLEAR
 'whole model'
 ,
'SUBTRACT CONTACT GROUP 1 OF REUSE 1 OF SUBSTRUCTURE 0 OF PROG
RAM ADINA'
@
*
GBODY NODES=8 NCOINCID=BOUNDARIES NCTOLERA=1.00000000000000E-05,
    SUBSTRUC=0 GROUP=6 PREFSHAP=AUTOMATIC COLLAPSE=NO SIZE-FUN=0,
    DELETE-S=NO ANGLE-MI=5.00000000000000 MIDNODES=CURVED,
    METHOD=DELAUNAY PATTERN=0 MESHING=MAPPED DEGENERA=NO,
    BOUNDARY=ADVFRONT DEG-EDGE=0 GEO-ERRO=0.00000000000000,
    SAMPLING=20 MIN-SIZE=0.00000000000000 NLAYER=1 NLTABL=0,
    AUTO-GRA=NO SIMULATE=NO PYRAMIDS=NO DANGMAXB=80.0000000000000,
    DANGMAXC=60.0000000000000 DANGMAXD=80.0000000000000 HEXALAYE=NO,
    AUTO-REF=YES EVEN=SUM DENSITY=1.20000000000000 MIDFACEN=QUAD,
    REFINE=ALONG-EDGE GRID=NO BREFINE=ALONG-EDGE BLTABL=0,
    PREFSHA2=QUADRILATERAL NOPTI=1
@CLEAR
4 0
@
*
*Comment 12 (Temperature differentials)
*
APPLY-LOAD BODY=4
@CLEAR
1  'MASS-PROPORTIONAL' 1  'MODEL' 0 0 1 0.00000000000000 0 -1 0 0 0  ,
'NO' 0.00000000000000 0.00000000000000 1 0  'BOTH'
2  'TEMPERATURE' 1  'FACE' 1 0 1 0.00000000000000 0 -1 0 1 0  'NO',
    0.00000000000000 0.00000000000000 1 0  'BOTH'
3  'TEMPERATURE' 1  'FACE' 1 0 1 0.00000000000000 0 -1 0 2 0  'NO',
    0.00000000000000 0.00000000000000 1 0  'BOTH'
4  'TEMPERATURE' 2  'FACE' 5 0 1 0.00000000000000 0 -1 0 1 0  'NO',
    0.00000000000000 0.00000000000000 1 0  'BOTH'
5  'TEMPERATURE' 2  'FACE' 5 0 1 0.00000000000000 0 -1 0 2 0  'NO',
    0.00000000000000 0.00000000000000 1 0  'MID'
@
*
*Comment 11 (Tire load) ? Pressure (psi)
*
LOADS-ELEMEN SUBSTRUC=0 REUSE=1 GROUP=1 THERMOST=0
@CLEAR
959 3 120.000000000000 120.000000000000 120.000000000000,
    120.000000000000 1 0.00000000000000 0 -1
960 3 120.000000000000 120.000000000000 120.000000000000,
```

120.000000000000 1 0.00000000000000 0 -1
939 3 120.000000000000 120.000000000000 120.000000000000,
120.000000000000 1 0.00000000000000 0 -1
940 3 120.000000000000 120.000000000000 120.000000000000,
120.000000000000 1 0.00000000000000 0 -1
919 3 120.000000000000 120.000000000000 120.000000000000,
120.000000000000 1 0.00000000000000 0 -1
920 3 120.000000000000 120.000000000000 120.000000000000,
120.000000000000 1 0.00000000000000 0 -1
899 3 120.000000000000 120.000000000000 120.000000000000,
120.000000000000 1 0.00000000000000 0 -1
900 3 120.000000000000 120.000000000000 120.000000000000,
120.000000000000 1 0.00000000000000 0 -1
879 3 120.000000000000 120.000000000000 120.000000000000,
120.000000000000 1 0.00000000000000 0 -1
880 3 120.000000000000 120.000000000000 120.000000000000,
120.000000000000 1 0.00000000000000 0 -1
479 3 120.000000000000 120.000000000000 120.000000000000,
120.000000000000 1 0.00000000000000 0 -1
480 3 120.000000000000 120.000000000000 120.000000000000,
120.000000000000 1 0.00000000000000 0 -1
459 3 120.000000000000 120.000000000000 120.000000000000,
120.000000000000 1 0.00000000000000 0 -1
460 3 120.000000000000 120.000000000000 120.000000000000,
120.000000000000 1 0.00000000000000 0 -1
439 3 120.000000000000 120.000000000000 120.000000000000,
120.000000000000 1 0.00000000000000 0 -1
440 3 120.000000000000 120.000000000000 120.000000000000,
120.000000000000 1 0.00000000000000 0 -1
419 3 120.000000000000 120.000000000000 120.000000000000,
120.000000000000 1 0.00000000000000 0 -1
420 3 120.000000000000 120.000000000000 120.000000000000,
120.000000000000 1 0.00000000000000 0 -1
399 3 120.000000000000 120.000000000000 120.000000000000,
120.000000000000 1 0.00000000000000 0 -1
400 3 120.000000000000 120.000000000000 120.000000000000,
120.000000000000 1 0.00000000000000 0 -1
@
*

APPENDIX F
CODES OF "AIFG" IN MATLAB PROGRAMMING LANGUAGE

```
function varargout = AIFG(varargin)
% AIFG MATLAB code for AIFG.fig
%      AIFG, by itself, creates a new AIFG or raises the existing
%      singleton*.
%
%      H = AIFG returns the handle to a new AIFG or the handle to
%      the existing singleton*.
%
%      AIFG('CALLBACK',hObject,eventData,handles,...) calls the local
%      function named CALLBACK in AIFG.M with the given input arguments.
%
%      AIFG('Property','Value',...) creates a new AIFG or raises the
%      existing singleton*.  Starting from the left, property value pairs are
%      applied to the GUI before AIFG_OpeningFcn gets called.  An
%      unrecognized property name or invalid value makes property application
%      stop.  All inputs are passed to AIFG_OpeningFcn via varargin.
%
%      *See GUI Options on GUIDE's Tools menu.  Choose "GUI allows only one
%      instance to run (singleton)".
%
% See also: GUIDE, GUIDATA, GUIHANDLES

% Edit the above text to modify the response to help AIFG

% Last Modified by GUIDE v2.5 01-Jun-2016 09:42:28

% Begin initialization code - DO NOT EDIT
gui_Singleton = 1;
gui_State = struct('gui_Name',       mfilename, ...
                   'gui_Singleton',  gui_Singleton, ...
                   'gui_OpeningFcn', @AIFG_OpeningFcn, ...
                   'gui_OutputFcn',  @AIFG_OutputFcn, ...
                   'gui_LayoutFcn',  [] , ...
                   'gui_Callback',   []);
if nargin && ischar(varargin{1})
    gui_State.gui_Callback = str2func(varargin{1});
end

if nargout
    [varargout{1:nargout}] = gui_mainfcn(gui_State, varargin{:});
else
    gui_mainfcn(gui_State, varargin{:});
end
% End initialization code - DO NOT EDIT


% --- Executes just before AIFG is made visible.
function AIFG_OpeningFcn(hObject, eventdata, handles, varargin)
% This function has no output args, see OutputFcn.
% hObject    handle to figure
% eventdata  reserved - to be defined in a future version of MATLAB
% handles    structure with handles and user data (see GUIDATA)
```

```
% varargin   command line arguments to AIFG (see VARARGIN)

% Choose default command line output for AIFG
handles.output = hObject;

% Update handles structure
guidata(hObject, handles);

% UIWAIT makes AIFG wait for user response (see UIRESUME)
% uiwait(handles.figure1);


% --- Outputs from this function are returned to the command line.
function varargout = AIFG_OutputFcn(hObject, eventdata, handles)
% varargout  cell array for returning output args (see VARARGOUT);
% hObject    handle to figure
% eventdata  reserved - to be defined in a future version of MATLAB
% handles    structure with handles and user data (see GUIDATA)

% Get default command line output from handles structure
varargout{1} = handles.output;



function title_Callback(hObject, eventdata, handles)
% hObject    handle to title (see GCBO)
% eventdata  reserved - to be defined in a future version of MATLAB
% handles    structure with handles and user data (see GUIDATA)

% Hints: get(hObject,'String') returns contents of title as text
%        str2double(get(hObject,'String')) returns contents of title as a double


% --- Executes during object creation, after setting all properties.
function title_CreateFcn(hObject, eventdata, handles)
% hObject    handle to title (see GCBO)
% eventdata  reserved - to be defined in a future version of MATLAB
% handles    empty - handles not created until after all CreateFcns called

% Hint: edit controls usually have a white background on Windows.
%       See ISPC and COMPUTER.
if ispc && isequal(get(hObject,'BackgroundColor'), get(0,'defaultUicontrolBackgroundColor'))
   set(hObject,'BackgroundColor','white');
end


% --- Executes when uipanel1 is resized.
function uipanel1_ResizeFcn(hObject, eventdata, handles)
% hObject    handle to uipanel1 (see GCBO)
% eventdata  reserved - to be defined in a future version of MATLAB
% handles    structure with handles and user data (see GUIDATA)



function length_Callback(hObject, eventdata, handles)
% hObject    handle to length (see GCBO)
```

```
% eventdata  reserved - to be defined in a future version of MATLAB
% handles    structure with handles and user data (see GUIDATA)

% Hints: get(hObject,'String') returns contents of length as text
%        str2double(get(hObject,'String')) returns contents of length as a double


% --- Executes during object creation, after setting all properties.
function length_CreateFcn(hObject, eventdata, handles)
% hObject    handle to length (see GCBO)
% eventdata  reserved - to be defined in a future version of MATLAB
% handles    empty - handles not created until after all CreateFcns called

% Hint: edit controls usually have a white background on Windows.
%       See ISPC and COMPUTER.
if ispc && isequal(get(hObject,'BackgroundColor'), get(0,'defaultUicontrolBackgroundColor'))
    set(hObject,'BackgroundColor','white');
end



function ydiv_Callback(hObject, eventdata, handles)
% hObject    handle to ydiv (see GCBO)
% eventdata  reserved - to be defined in a future version of MATLAB
% handles    structure with handles and user data (see GUIDATA)

% Hints: get(hObject,'String') returns contents of ydiv as text
%        str2double(get(hObject,'String')) returns contents of ydiv as a double


% --- Executes during object creation, after setting all properties.
function ydiv_CreateFcn(hObject, eventdata, handles)
% hObject    handle to ydiv (see GCBO)
% eventdata  reserved - to be defined in a future version of MATLAB
% handles    empty - handles not created until after all CreateFcns called

% Hint: edit controls usually have a white background on Windows.
%       See ISPC and COMPUTER.
if ispc && isequal(get(hObject,'BackgroundColor'), get(0,'defaultUicontrolBackgroundColor'))
    set(hObject,'BackgroundColor','white');
end



function zdiv_Callback(hObject, eventdata, handles)
% hObject    handle to zdiv (see GCBO)
% eventdata  reserved - to be defined in a future version of MATLAB
% handles    structure with handles and user data (see GUIDATA)

% Hints: get(hObject,'String') returns contents of zdiv as text
%        str2double(get(hObject,'String')) returns contents of zdiv as a double


% --- Executes during object creation, after setting all properties.
function zdiv_CreateFcn(hObject, eventdata, handles)
% hObject    handle to zdiv (see GCBO)
```

```
% eventdata  reserved - to be defined in a future version of MATLAB
% handles    empty - handles not created until after all CreateFcns called

% Hint: edit controls usually have a white background on Windows.
%       See ISPC and COMPUTER.
if ispc && isequal(get(hObject,'BackgroundColor'), get(0,'defaultUicontrolBackgroundColor'))
   set(hObject,'BackgroundColor','white');
end



function xdiv_Callback(hObject, eventdata, handles)
% hObject    handle to xdiv (see GCBO)
% eventdata  reserved - to be defined in a future version of MATLAB
% handles    structure with handles and user data (see GUIDATA)

% Hints: get(hObject,'String') returns contents of xdiv as text
%        str2double(get(hObject,'String')) returns contents of xdiv as a double


% --- Executes during object creation, after setting all properties.
function xdiv_CreateFcn(hObject, eventdata, handles)
% hObject    handle to xdiv (see GCBO)
% eventdata  reserved - to be defined in a future version of MATLAB
% handles    empty - handles not created until after all CreateFcns called

% Hint: edit controls usually have a white background on Windows.
%       See ISPC and COMPUTER.
if ispc && isequal(get(hObject,'BackgroundColor'), get(0,'defaultUicontrolBackgroundColor'))
   set(hObject,'BackgroundColor','white');
end



function width_Callback(hObject, eventdata, handles)
% hObject    handle to width (see GCBO)
% eventdata  reserved - to be defined in a future version of MATLAB
% handles    structure with handles and user data (see GUIDATA)

% Hints: get(hObject,'String') returns contents of width as text
%        str2double(get(hObject,'String')) returns contents of width as a double


% --- Executes during object creation, after setting all properties.
function width_CreateFcn(hObject, eventdata, handles)
% hObject    handle to width (see GCBO)
% eventdata  reserved - to be defined in a future version of MATLAB
% handles    empty - handles not created until after all CreateFcns called

% Hint: edit controls usually have a white background on Windows.
%       See ISPC and COMPUTER.
if ispc && isequal(get(hObject,'BackgroundColor'), get(0,'defaultUicontrolBackgroundColor'))
   set(hObject,'BackgroundColor','white');
end
```

```
function depth_Callback(hObject, eventdata, handles)
% hObject    handle to depth (see GCBO)
% eventdata  reserved - to be defined in a future version of MATLAB
% handles    structure with handles and user data (see GUIDATA)

% Hints: get(hObject,'String') returns contents of depth as text
%        str2double(get(hObject,'String')) returns contents of depth as a double


% --- Executes during object creation, after setting all properties.
function depth_CreateFcn(hObject, eventdata, handles)
% hObject    handle to depth (see GCBO)
% eventdata  reserved - to be defined in a future version of MATLAB
% handles    empty - handles not created until after all CreateFcns called

% Hint: edit controls usually have a white background on Windows.
%       See ISPC and COMPUTER.
if ispc && isequal(get(hObject,'BackgroundColor'), get(0,'defaultUicontrolBackgroundColor'))
   set(hObject,'BackgroundColor','white');
end


% --- Executes on button press in checkbox1.
function checkbox1_Callback(hObject, eventdata, handles)
% hObject    handle to checkbox1 (see GCBO)
% eventdata  reserved - to be defined in a future version of MATLAB
% handles    structure with handles and user data (see GUIDATA)

% Hint: get(hObject,'Value') returns toggle state of checkbox1


% --- Executes on button press in checkbox2.
function checkbox2_Callback(hObject, eventdata, handles)
% hObject    handle to checkbox2 (see GCBO)
% eventdata  reserved - to be defined in a future version of MATLAB
% handles    structure with handles and user data (see GUIDATA)

% Hint: get(hObject,'Value') returns toggle state of checkbox2


% --- Executes on button press in checkbox3.
function checkbox3_Callback(hObject, eventdata, handles)
% hObject    handle to checkbox3 (see GCBO)
% eventdata  reserved - to be defined in a future version of MATLAB
% handles    structure with handles and user data (see GUIDATA)

% Hint: get(hObject,'Value') returns toggle state of checkbox3



function submodulus_Callback(hObject, eventdata, handles)
% hObject    handle to submodulus (see GCBO)
% eventdata  reserved - to be defined in a future version of MATLAB
% handles    structure with handles and user data (see GUIDATA)
```

```
% Hints: get(hObject,'String') returns contents of submodulus as text
%        str2double(get(hObject,'String')) returns contents of submodulus as a double


% --- Executes during object creation, after setting all properties.
function submodulus_CreateFcn(hObject, eventdata, handles)
% hObject    handle to submodulus (see GCBO)
% eventdata  reserved - to be defined in a future version of MATLAB
% handles    empty - handles not created until after all CreateFcns called

% Hint: edit controls usually have a white background on Windows.
%       See ISPC and COMPUTER.
if ispc && isequal(get(hObject,'BackgroundColor'), get(0,'defaultUicontrolBackgroundColor'))
    set(hObject,'BackgroundColor','white');
end



% Hint: place code in OpeningFcn to populate axes1



function edit100_Callback(hObject, eventdata, handles)
% hObject    handle to edit100 (see GCBO)
% eventdata  reserved - to be defined in a future version of MATLAB
% handles    structure with handles and user data (see GUIDATA)

% Hints: get(hObject,'String') returns contents of edit100 as text
%        str2double(get(hObject,'String')) returns contents of edit100 as a double


% --- Executes during object creation, after setting all properties.
function edit100_CreateFcn(hObject, eventdata, handles)
% hObject    handle to edit100 (see GCBO)
% eventdata  reserved - to be defined in a future version of MATLAB
% handles    empty - handles not created until after all CreateFcns called

% Hint: edit controls usually have a white background on Windows.
%       See ISPC and COMPUTER.
if ispc && isequal(get(hObject,'BackgroundColor'), get(0,'defaultUicontrolBackgroundColor'))
    set(hObject,'BackgroundColor','white');
end



function bottomtemp_Callback(hObject, eventdata, handles)
% hObject    handle to bottomtemp (see GCBO)
% eventdata  reserved - to be defined in a future version of MATLAB
% handles    structure with handles and user data (see GUIDATA)

% Hints: get(hObject,'String') returns contents of bottomtemp as text
%        str2double(get(hObject,'String')) returns contents of bottomtemp as a double


% --- Executes during object creation, after setting all properties.
function bottomtemp_CreateFcn(hObject, eventdata, handles)
```

```
% hObject    handle to bottomtemp (see GCBO)
% eventdata  reserved - to be defined in a future version of MATLAB
% handles    empty - handles not created until after all CreateFcns called

% Hint: edit controls usually have a white background on Windows.
%       See ISPC and COMPUTER.
if ispc && isequal(get(hObject,'BackgroundColor'), get(0,'defaultUicontrolBackgroundColor'))
   set(hObject,'BackgroundColor','white');
end



function modulus_Callback(hObject, eventdata, handles)
% hObject    handle to modulus (see GCBO)
% eventdata  reserved - to be defined in a future version of MATLAB
% handles    structure with handles and user data (see GUIDATA)

% Hints: get(hObject,'String') returns contents of modulus as text
%        str2double(get(hObject,'String')) returns contents of modulus as a double


% --- Executes during object creation, after setting all properties.
function modulus_CreateFcn(hObject, eventdata, handles)
% hObject    handle to modulus (see GCBO)
% eventdata  reserved - to be defined in a future version of MATLAB
% handles    empty - handles not created until after all CreateFcns called

% Hint: edit controls usually have a white background on Windows.
%       See ISPC and COMPUTER.
if ispc && isequal(get(hObject,'BackgroundColor'), get(0,'defaultUicontrolBackgroundColor'))
   set(hObject,'BackgroundColor','white');
end



function cte_Callback(hObject, eventdata, handles)
% hObject    handle to cte (see GCBO)
% eventdata  reserved - to be defined in a future version of MATLAB
% handles    structure with handles and user data (see GUIDATA)

% Hints: get(hObject,'String') returns contents of cte as text
%        str2double(get(hObject,'String')) returns contents of cte as a double


% --- Executes during object creation, after setting all properties.
function cte_CreateFcn(hObject, eventdata, handles)
% hObject    handle to cte (see GCBO)
% eventdata  reserved - to be defined in a future version of MATLAB
% handles    empty - handles not created until after all CreateFcns called

% Hint: edit controls usually have a white background on Windows.
%       See ISPC and COMPUTER.
if ispc && isequal(get(hObject,'BackgroundColor'), get(0,'defaultUicontrolBackgroundColor'))
   set(hObject,'BackgroundColor','white');
end
```

```
function density_Callback(hObject, eventdata, handles)
% hObject    handle to density (see GCBO)
% eventdata  reserved - to be defined in a future version of MATLAB
% handles    structure with handles and user data (see GUIDATA)

% Hints: get(hObject,'String') returns contents of density as text
%        str2double(get(hObject,'String')) returns contents of density as a double


% --- Executes during object creation, after setting all properties.
function density_CreateFcn(hObject, eventdata, handles)
% hObject    handle to density (see GCBO)
% eventdata  reserved - to be defined in a future version of MATLAB
% handles    empty - handles not created until after all CreateFcns called

% Hint: edit controls usually have a white background on Windows.
%       See ISPC and COMPUTER.
if ispc && isequal(get(hObject,'BackgroundColor'), get(0,'defaultUicontrolBackgroundColor'))
    set(hObject,'BackgroundColor','white');
end



function poisson_Callback(hObject, eventdata, handles)
% hObject    handle to poisson (see GCBO)
% eventdata  reserved - to be defined in a future version of MATLAB
% handles    structure with handles and user data (see GUIDATA)

% Hints: get(hObject,'String') returns contents of poisson as text
%        str2double(get(hObject,'String')) returns contents of poisson as a double


% --- Executes during object creation, after setting all properties.
function poisson_CreateFcn(hObject, eventdata, handles)
% hObject    handle to poisson (see GCBO)
% eventdata  reserved - to be defined in a future version of MATLAB
% handles    empty - handles not created until after all CreateFcns called

% Hint: edit controls usually have a white background on Windows.
%       See ISPC and COMPUTER.
if ispc && isequal(get(hObject,'BackgroundColor'), get(0,'defaultUicontrolBackgroundColor'))
    set(hObject,'BackgroundColor','white');
end


% --- Executes on button press in checkbox4.
function checkbox4_Callback(hObject, eventdata, handles)
% hObject    handle to checkbox4 (see GCBO)
% eventdata  reserved - to be defined in a future version of MATLAB
% handles    structure with handles and user data (see GUIDATA)


function load_Callback(hObject, eventdata, handles)
% hObject    handle to load (see GCBO)
```

```
% eventdata  reserved - to be defined in a future version of MATLAB
% handles    structure with handles and user data (see GUIDATA)

% Hints: get(hObject,'String') returns contents of load as text
%        str2double(get(hObject,'String')) returns contents of load as a double


% --- Executes during object creation, after setting all properties.
function load_CreateFcn(hObject, eventdata, handles)
% hObject    handle to load (see GCBO)
% eventdata  reserved - to be defined in a future version of MATLAB
% handles    empty - handles not created until after all CreateFcns called

% Hint: edit controls usually have a white background on Windows.
%       See ISPC and COMPUTER.
if ispc && isequal(get(hObject,'BackgroundColor'), get(0,'defaultUicontrolBackgroundColor'))
   set(hObject,'BackgroundColor','white');
end



function L_Callback(hObject, eventdata, handles)
% hObject    handle to L (see GCBO)
% eventdata  reserved - to be defined in a future version of MATLAB
% handles    structure with handles and user data (see GUIDATA)

% Hints: get(hObject,'String') returns contents of L as text
%        str2double(get(hObject,'String')) returns contents of L as a double


% --- Executes during object creation, after setting all properties.
function L_CreateFcn(hObject, eventdata, handles)
% hObject    handle to L (see GCBO)
% eventdata  reserved - to be defined in a future version of MATLAB
% handles    empty - handles not created until after all CreateFcns called

% Hint: edit controls usually have a white background on Windows.
%       See ISPC and COMPUTER.
if ispc && isequal(get(hObject,'BackgroundColor'), get(0,'defaultUicontrolBackgroundColor'))
   set(hObject,'BackgroundColor','white');
end



function W_Callback(hObject, eventdata, handles)
% hObject    handle to W (see GCBO)
% eventdata  reserved - to be defined in a future version of MATLAB
% handles    structure with handles and user data (see GUIDATA)

% Hints: get(hObject,'String') returns contents of W as text
%        str2double(get(hObject,'String')) returns contents of W as a double


% --- Executes during object creation, after setting all properties.
function W_CreateFcn(hObject, eventdata, handles)
% hObject    handle to W (see GCBO)
```

```
% eventdata  reserved - to be defined in a future version of MATLAB
% handles    empty - handles not created until after all CreateFcns called

% Hint: edit controls usually have a white background on Windows.
%       See ISPC and COMPUTER.
if ispc && isequal(get(hObject,'BackgroundColor'), get(0,'defaultUicontrolBackgroundColor'))
   set(hObject,'BackgroundColor','white');
end



function B_Callback(hObject, eventdata, handles)
% hObject    handle to B (see GCBO)
% eventdata  reserved - to be defined in a future version of MATLAB
% handles    structure with handles and user data (see GUIDATA)

% Hints: get(hObject,'String') returns contents of B as text
%        str2double(get(hObject,'String')) returns contents of B as a double


% --- Executes during object creation, after setting all properties.
function B_CreateFcn(hObject, eventdata, handles)
% hObject    handle to B (see GCBO)
% eventdata  reserved - to be defined in a future version of MATLAB
% handles    empty - handles not created until after all CreateFcns called

% Hint: edit controls usually have a white background on Windows.
%       See ISPC and COMPUTER.
if ispc && isequal(get(hObject,'BackgroundColor'), get(0,'defaultUicontrolBackgroundColor'))
   set(hObject,'BackgroundColor','white');
end


function edit19_Callback(hObject, eventdata, handles)
% hObject    handle to edit19 (see GCBO)
% eventdata  reserved - to be defined in a future version of MATLAB
% handles    structure with handles and user data (see GUIDATA)

% Hints: get(hObject,'String') returns contents of edit19 as text
%        str2double(get(hObject,'String')) returns contents of edit19 as a double


% --- Executes during object creation, after setting all properties.
function edit19_CreateFcn(hObject, eventdata, handles)
% hObject    handle to edit19 (see GCBO)
% eventdata  reserved - to be defined in a future version of MATLAB
% handles    empty - handles not created until after all CreateFcns called

% Hint: edit controls usually have a white background on Windows.
%       See ISPC and COMPUTER.
if ispc && isequal(get(hObject,'BackgroundColor'), get(0,'defaultUicontrolBackgroundColor'))
   set(hObject,'BackgroundColor','white');
end
```

```
function edit20_Callback(hObject, eventdata, handles)
% hObject    handle to edit20 (see GCBO)
% eventdata  reserved - to be defined in a future version of MATLAB
% handles    structure with handles and user data (see GUIDATA)

% Hints: get(hObject,'String') returns contents of edit20 as text
%        str2double(get(hObject,'String')) returns contents of edit20 as a double


% --- Executes during object creation, after setting all properties.
function edit20_CreateFcn(hObject, eventdata, handles)
% hObject    handle to edit20 (see GCBO)
% eventdata  reserved - to be defined in a future version of MATLAB
% handles    empty - handles not created until after all CreateFcns called

% Hint: edit controls usually have a white background on Windows.
%       See ISPC and COMPUTER.
if ispc && isequal(get(hObject,'BackgroundColor'), get(0,'defaultUicontrolBackgroundColor'))
   set(hObject,'BackgroundColor','white');
end


% --- Executes when entered data in editable cell(s) in uitable1.
function uitable1_CellEditCallback(hObject, eventdata, handles)
% hObject    handle to uitable1 (see GCBO)
% eventdata  structure with the following fields (see UITABLE)
%   Indices: row and column indices of the cell(s) edited
%   PreviousData: previous data for the cell(s) edited
%   EditData: string(s) entered by the user
%   NewData: EditData or its converted form set on the Data property. Empty if Data was not changed
%   Error: error string when failed to convert EditData to appropriate value for Data
% handles    structure with handles and user data (see GUIDATA)
% ssdata=get(handles.uitable1,'Data');



% --- Executes on button press in pushbutton1.
function pushbutton1_Callback(hObject, eventdata, handles)
% hObject    handle to pushbutton1 (see GCBO)
% eventdata  reserved - to be defined in a future version of MATLAB
% handles    structure with handles and user data (see GUIDATA)

[file,path] = uiputfile('*.in','Save data As');
if (file ~=0)
   fname=sprintf('%s%s',path,file);
   fileID=fopen(fname,'w');

%fileID = fopen('ADINA-Input-File.in','w');
fprintf(fileID,'%6s\r\n','*-----------------------------------------------------------------------------------------------');
fprintf(fileID,'%6s\r\n','*Concrete Pavement Analysis with Temperature and Tire Load');
fprintf(fileID,'%6s\r\n','*-----------------------------------------------------------------------------------------------');
fprintf(fileID,'%1s\r\n','*');
fprintf(fileID,'%6s\r\n','*Command file created by ADINA Input File Generator developed by Kukjoo Kim,
University of Florida');
fprintf(fileID,'%1s\r\n','*');
fprintf(fileID,'%6s\r\n','*-----------------------------------------------------------------------------------------------');
```

```
fprintf(fileID,'%6s','*Project Name: ');
fprintf(fileID,'%6s\r\n',get(handles.title,'String'));
fprintf(fileID,'%6s\r\n','*----------------------------------------------------------------------------------------------------');
fprintf(fileID,'%1s\r\n','*');
fprintf(fileID,'%6s\r\n','*--- by ADINA Input File Generator: AIFG Version 2.1.0 ---');
fprintf(fileID,'%6s\r\n','master analysis=static, load-case=yes, idof=000111');
fprintf(fileID,'%6s\r\n','*idof codes: idof=xt, yt,zt,xr,yr,zr; 1=dof deleted, 0=dof not deleted');
fprintf(fileID,'%6s\r\n','printout volume=maximum');
fprintf(fileID,'%6s\r\n','coordinates point');
fprintf(fileID,'%6s\r\n','entries name x y z');
fprintf(fileID,'%6s\r\n','*name      x      y      z');
a=str2num(get(handles.length,'String')); %read length value
b=str2num(get(handles.width,'String')); %read width value
c=str2num(get(handles.depth,'String')); %read depth value
A=[1 0 0 0;2 a 0 0;3 a 0 c;4 0 0 c;5 0 b 0;6 a b 0;7 a b c;8 0 b c];
%use transpose A to write the matrix A
fprintf(fileID,'%6.0f %6.2f %6.2f %6.2f\r\n',A');
fprintf(fileID,'%1s\r\n','@');
fprintf(fileID,'%1s\r\n','*');
fprintf(fileID,'%6s\r\n','*---geometric entities---');
fprintf(fileID,'%1\r\n','*');
fprintf(fileID,'%6s\r\n','line straight name=1 p1=1 p2=2');
fprintf(fileID,'%6s\r\n','line straight name=2 p1=2 p2=3');
fprintf(fileID,'%6s\r\n','line straight name=3 p1=4 p2=3');
fprintf(fileID,'%6s\r\n','line straight name=4 p1=1 p2=4');
fprintf(fileID,'%1s\r\n','*');
fprintf(fileID,'%6s\r\n','line straight name=5 p1=5 p2=6');
fprintf(fileID,'%6s\r\n','line straight name=6 p1=6 p2=7');
fprintf(fileID,'%6s\r\n','line straight name=7 p1=8 p2=7');
fprintf(fileID,'%6s\r\n','line straight name=8 p1=5 p2=8');
fprintf(fileID,'%1s\r\n','*');
fprintf(fileID,'%6s\r\n','line straight name=9 p1=1 p2=5');
fprintf(fileID,'%6s\r\n','line straight name=10 p1=2 p2=6');
fprintf(fileID,'%6s\r\n','line straight name=11 p1=4 p2=8');
fprintf(fileID,'%6s\r\n','line straight name=12 p1=3 p2=7');
fprintf(fileID,'%1s\r\n','*');
%specify the mesh density
dd=str2num(get(handles.xdiv,'String'));
ee=str2num(get(handles.ydiv,'String'));
ff=str2num(get(handles.zdiv,'String'));
fprintf(fileID,'%6s %6.0f\r\n','subdivide line name=1 mode=divisions ndiv=',dd);
fprintf(fileID,'%6s %6.0f\r\n','subdivide line name=3 mode=divisions ndiv=',dd);
fprintf(fileID,'%6s %6.0f\r\n','subdivide line name=5 mode=divisions ndiv=',dd);
fprintf(fileID,'%6s %6.0f\r\n','subdivide line name=7 mode=divisions ndiv=',dd);
fprintf(fileID,'%1\r\n','*');
fprintf(fileID,'%6s %6.0f\r\n','subdivide line name=2 mode=divisions ndiv=',ff);
fprintf(fileID,'%6s %6.0f\r\n','subdivide line name=4 mode=divisions ndiv=',ff);
fprintf(fileID,'%6s %6.0f\r\n','subdivide line name=6 mode=divisions ndiv=',ff);
fprintf(fileID,'%6s %6.0f\r\n','subdivide line name=8 mode=divisions ndiv=',ff);
fprintf(fileID,'%1\r\n','*');
fprintf(fileID,'%6s %6.0f\r\n','subdivide line name=9 mode=divisions ndiv=',ee);
fprintf(fileID,'%6s %6.0f\r\n','subdivide line name=10 mode=divisions ndiv=',ee);
fprintf(fileID,'%6s %6.0f\r\n','subdivide line name=11 mode=divisions ndiv=',ee);
fprintf(fileID,'%6s %6.0f\r\n','subdivide line name=12 mode=divisions ndiv=',ee);
fprintf(fileID,'%1s\r\n','*');
fprintf(fileID,'%6s\r\n','surface patch name=1 edge1=3 edge2=12 edge3=7 edge4=11');
```

```
fprintf(fileID,'%6s\r\n','surface patch name=2 edge1=1 edge2=2 edge3=3 edge4=4');
fprintf(fileID,'%6s\r\n','surface patch name=3 edge1=10 edge2=6 edge3=12 edge4=2');
fprintf(fileID,'%6s\r\n','surface patch name=4 edge1=5 edge2=8 edge3=7 edge4=6');
fprintf(fileID,'%6s\r\n','surface patch name=5 edge1=9 edge2=4 edge3=11 edge4=8');
fprintf(fileID,'%6s\r\n','surface patch name=6 edge1=5 edge2=10 edge3=1 edge4=9');
fprintf(fileID,'%1s\r\n','*');
fprintf(fileID,'%6s\r\n','volume patch name=1 shape=hex,');
fprintf(fileID,'%6s\r\n','face1=1 face2=2 face3=3 face4=4 face5=5 face6=6');
fprintf(fileID,'%1s\r\n','*');
fprintf(fileID,'%6s\r\n','*----------Material----------');
fprintf(fileID,'%1s\r\n','*');
gg=str2num(get(handles.modulus,'String'));
hh=str2num(get(handles.poisson,'String'));
kk=str2num(get(handles.density,'String'));
mm=str2num(get(handles.cte,'String'));
multi=get(handles.checkbox4,'Value');
if multi==1
   fprintf(fileID,'%6s\r\n','MATERIAL PLASTIC-MULTILINEAR NAME=1 HARDENIN=ISOTROPIC,');
   fprintf(fileID,'%1s %1.8f %6s %1.10f %6s\r\n','E=',gg,'NU=',hh,'STRAINRA=0,');
   fprintf(fileID,'%6s %10.8f %6s %20.15f %6s\r\n','DENSITY=',kk,'ALPHA=',mm,',');
   fprintf(fileID,'%6s\r\n','TREF=0.00000000000000 DCURVE=0 DEPENDEN=NO,');
   fprintf(fileID,'%6s\r\n','TRANSITI=0.000100000000000000 EP-STRAI=0.00000000000000 BCURVE=0,');
   fprintf(fileID,'%6s\r\n','BVALUE=0.00000000000000 MDESCRIP=RAPCONCRETE');
   fprintf(fileID,'%6s\r\n','@CLEAR');
   ssdata=get(handles.uitable1,'Data');
   %c1=ssdata(:,1)   % the first column
   %c2=ssdata(:,2)
   ssdata=[ssdata{1:6,1:2}];
   %ssdata=[ssdata]
   c1=ssdata(1:6);
   c2=ssdata(7:12);
   ctotal=[c1;c2];
   fprintf(fileID,'%6.12f %6.2f\r\n',ctotal);
   fprintf(fileID,'%1s\r\n','@');

else
   fprintf(fileID,'%6s %1.2f %6s %1.2f %1s\r\n','material elastic name=1 e=',gg,'nu=',hh,',');
   fprintf(fileID,'%6s %10.8f %6s %1.15f\r\n','density=',kk,'alpha=',mm);

end
fprintf(fileID,'%1s\r\n','*');
fprintf(fileID,'%1s\r\n','*----------element---------');
fprintf(fileID,'%1s\r\n','*');
fprintf(fileID,'%6s\r\n','egroup threedsolid name=1 material=1 incompatible-modes=no');
fprintf(fileID,'%1s\r\n','*');
fprintf(fileID,'%6s\r\n','gvolume nodes=8 group=1 meshing=mapped');
fprintf(fileID,'%1s\r\n','1');
fprintf(fileID,'%1s\r\n','@');
fprintf(fileID,'%1s\r\n','*');
fprintf(fileID,'%1s\r\n','*----------boundary conditions---------');
fprintf(fileID,'%1s\r\n','*');
fprintf(fileID,'%1s\r\n','fixity name=zt');
fprintf(fileID,'%1s\r\n','X-TRANSLATION');
fprintf(fileID,'%1s\r\n','Y-TRANSLATION');
fprintf(fileID,'%1s\r\n','@');
fprintf(fileID,'%1s\r\n','*');
```

```
fprintf(fileID,'%1s\r\n','fixity name=zyt');
fprintf(fileID,'%1s\r\n','X-TRANSLATION');
fprintf(fileID,'%1s\r\n','@');
fprintf(fileID,'%1s\r\n','*');
fprintf(fileID,'%1s\r\n','FIXBOUNDARY POINTS FIXITY=ALL');
fprintf(fileID,'%1s\r\n','@CLEAR');
fprintf(fileID,'%1s\r\n','2  ZYT');
fprintf(fileID,'%1s\r\n','6  ZT');
fprintf(fileID,'%1s\r\n','@');
fprintf(fileID,'%1s\r\n','*');
subm=str2num(get(handles.submodulus,'String')); %read subgrade modulus
subm=subm*1000*(a/dd)*(b/ee);
aaa=(dd+1)*(ee+1);
aaaa=1:1:aaa;
node=((dd+1)*(ee+1)*ff+1):1:((dd+1)*(ee+1)*(ff+1));
subone=ones(1,length(aaaa)).*3;
subzero=zeros(2,length(aaaa));
spg=[aaaa;node;subone;subzero];
fprintf(fileID,'%1s\r\n','*');
bond=get(handles.checkbox3,'Value'); %define bonding condition
if bond==1
   fprintf(fileID,'%1s\r\n','PROPERTY NONLINEAR-K NAME=1 RUPTURE=NO');
   fprintf(fileID,'%1s\r\n','@CLEAR');
   nlin=[-1 0 1];
   nlin2=[-subm 0 0.01];
   nonlinear=[nlin; nlin2];
   fprintf(fileID,'%1.6f %5.6f\r\n',nonlinear);
   fprintf(fileID,'%1s\r\n','@');
   fprintf(fileID,'%1s\r\n','*');
   fprintf(fileID,'%1s\r\n','PROPERTYSET NAME=1 K=0.00000000000000 M=0.00000000000000,');
   fprintf(fileID,'%1s\r\n','C=0.00000000000000 NONLINEA=YES NK=1 NM=0 NC=0');
   fprintf(fileID,'%1s\r\n','*');
   fprintf(fileID,'%1s\r\n','EGROUP SPRING NAME=2 PROPERTY=1 RESULTS=FORCES NONLINEA=NO,');
   fprintf(fileID,'%1s\r\n','SKEWSYST=NO OPTION=NONE DESCRIPT=NONE PRINT=DEFAULT,');
   fprintf(fileID,'%1s\r\n','SAVE=DEFAULT TBIRTH=0.00000000000000 TDEATH=0.00000000000000,');
   fprintf(fileID,'%1s\r\n','6DOF-SPR=NO');
   fprintf(fileID,'%1s\r\n','*');
   %fprintf(fileID,'%1s\r\n','PROPERTYSET NAME=1 K=0.00000000000000 M=0.00000000000000,');
   %fprintf(fileID,'%1s\r\n','C=0.00000000000000 NONLINEA=YES NK=1 NM=0 NC=0');
   fprintf(fileID,'%1s\r\n','*');
   fprintf(fileID,'%1s\r\n','ENODES SUBSTRUC=0 GROUP=2 NNODES=32');
   fprintf(fileID,'%1.0f %5.0f %1.0f %1.0f %1.0f\r\n',spg);

else
   fprintf(fileID,'%1s %1s %1.8f %6s\r\n','PROPERTYSET NAME=1','K=',subm,'M=0.00000000000000,');
   fprintf(fileID,'%1s\r\n','C=0.00000000000000 S=0.00000000000000 NONLINEA=NO');
   fprintf(fileID,'%1s\r\n','*');
   fprintf(fileID,'%1s\r\n','EGROUP SPRING NAME=2 PROPERTY=1 RESULTS=FORCES NONLINEA=NO,');
   fprintf(fileID,'%1s\r\n','SKEWSYST=NO OPTION=NONE DESCRIPT=NONE PRINT=DEFAULT,');
   fprintf(fileID,'%1s\r\n','SAVE=DEFAULT TBIRTH=0.00000000000000 TDEATH=0.00000000000000,');
   fprintf(fileID,'%1s\r\n','6DOF-SPR=NO');
   fprintf(fileID,'%1s\r\n','*');
   fprintf(fileID,'%1s\r\n','NODESET NAME=1 ALL-EXT=NO DESCRIPT=NONE OPTION=SURFA GROUP=0
ZONE=``,');
   fprintf(fileID,'%1s\r\n','ELSET=0 TARGET=0 ANGLE=0.00000000000000,');
   fprintf(fileID,'%1s\r\n','DISTANCE=0.00000000000000');
```

```
    fprintf(fileID,'%1s\r\n','@CLEAR');
    fprintf(fileID,'%1s\r\n','6 0 1');
    fprintf(fileID,'%1s\r\n','@');
    fprintf(fileID,'%1s\r\n','*');
    fprintf(fileID,'%1s\r\n','ENODES SUBSTRUC=0 GROUP=2 NNODES=32');
    fprintf(fileID,'%1.0f %5.0f %1.0f %1.0f %1.0f\r\n',spg);
end
fprintf(fileID,'%1s\r\n','@');
fprintf(fileID,'%1s\r\n','*');
ttemp=str2num(get(handles.edit100,'String')); %read top temperature
btemp=str2num(get(handles.bottomtemp,'String')); %read bottom temperature
fprintf(fileID,'%1s\r\n','*-------load-------');
fprintf(fileID,'%1s\r\n','*');
fprintf(fileID,'%1s\r\n','load-case name=1');
fprintf(fileID,'%1s\r\n','*');
fprintf(fileID,'%1s %3.2f\r\n','load temperature name=1 magnitude=',ttemp);
fprintf(fileID,'%1s %3.2f\r\n','load temperature name=2 magnitude=',btemp);
fprintf(fileID,'%1s\r\n','*');
fprintf(fileID,'%1s\r\n','apply-load');
fprintf(fileID,'%1s\r\n','entries name ltype lname stype sname idirn');
fprintf(fileID,'%1s\r\n','1 temperature 1 surface 1 11');
fprintf(fileID,'%1s\r\n','2 temperature 2 surface 6 11');
fprintf(fileID,'%1s\r\n','@');
fprintf(fileID,'%1s\r\n','load mass-proportional name=3 magnitude=1 ax=0.0 ay=0.0 az=-1.0');
fprintf(fileID,'%1s\r\n','apply-load');
fprintf(fileID,'%1s\r\n','entries name ltype lname stype');
fprintf(fileID,'%1s\r\n','3 mass-proportional 3 model');
fprintf(fileID,'%1s\r\n','*');
fprintf(fileID,'%1s\r\n','@');
fprintf(fileID,'%1s\r\n','SET EGROUP NAME=1');
fprintf(fileID,'%1s\r\n','*');
fprintf(fileID,'%1s\r\n','LOADS-ELEMEN SUBSTRUC=0 REUSE=1 GROUP=1 THERMOST=0');
fprintf(fileID,'%1s\r\n','@CLEAR');
%tire loading code start here
trep=str2num(get(handles.load,'String')); %read tire pressure
trel=str2num(get(handles.L,'String')); %read tire width
trew=str2num(get(handles.W,'String')); %read tire length
treb=str2num(get(handles.B,'String')); %read tire axle length
trex=str2num(get(handles.edit19,'String')); %read tire x-location
trey=str2num(get(handles.edit20,'String')); %read tire y-location
xelsize=round(a/dd);
yelsize=round(b/ee);
%------------------------------------------------------------------------
loczro=dd*ee;%initial tire location(0,0)
%n1=(loczro-(trex/xelsize)):-1:(loczro-(trex/xelsize)-(round(trel/xelsize))+1);
n1=(loczro-(trex/xelsize))-round(trey/yelsize)*dd;
m=round(trel/xelsize);
n=(trew/yelsize);
for i=1:n
   for j=1:m
      mtx(i,j)=(n1-(j-1))-(i-1)*dd;
   end
end
n2=n1-(treb/yelsize)*dd;
for i=1:n
   for j=1:m
```

```
        mtx2(i,j)=(n2-(j-1))-(i-1)*dd;
    end
end
mtx=mtx(:);
mtx2=mtx2(:);
matrix=[mtx;mtx2];
matrix=sort(matrix(:))';
sthree=ones(1,length(matrix)).*3;
sloadm=ones(4,length(matrix)).*trep;
ftrepr=[matrix;sthree;sloadm];
fprintf(fileID,'%5.0f %1.0f %4.2f %4.2f %4.2f %4.2f\r\n',ftrepr);
%fprintf(fileID,'%1.0f %5.0f %1.0f %1.0f %1.0f\r\n',spg);
%tire loading code end
fprintf(fileID,'%1s\r\n','@');
fprintf(fileID,'%1s\r\n','*-----------------------------------------------');
fprintf(fileID,'%1s\r\n','meshplot');
fprintf(fileID,'%1s\r\n','loadplot');

    fclose(fileID);
end



% --- Executes on button press in pushbutton2.
function pushbutton2_Callback(hObject, eventdata, handles)
% hObject    handle to pushbutton2 (see GCBO)
% eventdata  reserved - to be defined in a future version of MATLAB
% handles    structure with handles and user data (see GUIDATA)
close(gcf);


% --- Executes during object creation, after setting all properties.
function axes1_CreateFcn(hObject, eventdata, handles)
% hObject    handle to axes1 (see GCBO)
% eventdata  reserved - to be defined in a future version of MATLAB
% handles    empty - handles not created until after all CreateFcns called
geo=imread('structure.jpg');
imshow(geo);

% Hint: place code in OpeningFcn to populate axes1


% --- Executes during object creation, after setting all properties.
function axes2_CreateFcn(hObject, eventdata, handles)
% hObject    handle to axes2 (see GCBO)
% eventdata  reserved - to be defined in a future version of MATLAB
% handles    empty - handles not created until after all CreateFcns called
LL=imread('loading.png');
imshow(LL);

% Hint: place code in OpeningFcn to populate axes2


% --- Executes during object creation, after setting all properties.
function axes3_CreateFcn(hObject, eventdata, handles)
% hObject    handle to axes3 (see GCBO)
```

```
% eventdata  reserved - to be defined in a future version of MATLAB
% handles    empty - handles not created until after all CreateFcns called
Stress=imread('stress.png');
imshow(Stress);

% Hint: place code in OpeningFcn to populate axes3
```

APPENDIX G
PEAK RECORDED STRAINS FROM HVS LOADING ON WHEEL PATH 1

This appendix presents the peak strain values recorded by the strain gauges when the test slabs were loaded by the HVS on Wheel Path 1. The layout of the strain gauges on the test slabs and the location of Wheel Path 1 are shown in Figure G-1. Each test slab was loaded by the HVS for a minimum of 24 hours for each Wheel Path. During HVS loading, strain readings were taken every hour for a period of 200 seconds each. Each recording period is referred to as a trial. Each recording period allowed for a minimum of 20 passes of the HVS load. The times for each recording period are shown in Table G-1. The peak strain values recorded by the strain gauges at the various trials and test slabs are presented in Tables G-2 through G-94.

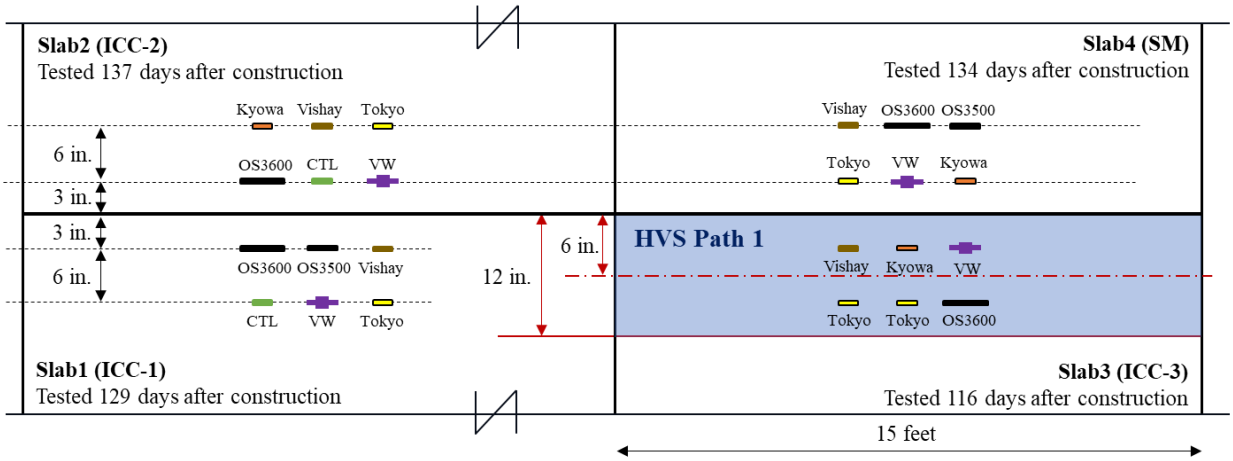

Figure G-1. Layout of strain sensors and location of HVS wheel path 1

Table G-1. The time and date for each trial (strain recording period)

Trial No.	**Slab 1_ICC-1** (Constructed 10/24/16)	**Slab 2_ICC-2** (Constructed 10/31/16)	**Slab 3_ICC-3** (Constructed 10/31/16)	**Slab 4_SM** (Constructed 10/24/16)
1	2/20/17 11:23	3/9/17 11:46	2/16/17 15:46	3/6/17 09:30
2	2/20/17 12:23	3/9/17 12:46	2/16/17 16:46	3/6/17 10:30
3	2/20/17 13:23	3/9/17 13:46	2/16/17 17:46	3/6/17 11:30
4	2/20/17 14:23	3/9/17 14:46	2/16/17 18:46	3/6/17 12:30
5	2/20/17 15:23	3/9/17 15:46	2/16/17 19:46	3/6/17 13:30
6	2/20/17 16:23	3/9/17 16:46	2/16/17 20:46	3/6/17 14:30
7	2/20/17 17:23	3/9/17 17:46	2/16/17 21:46	3/6/17 15:30
8	2/20/17 18:43	3/9/17 18:46	2/16/17 22:46	3/6/17 16:30
9	2/20/17 19:43	3/9/17 19:46	2/16/17 23:46	3/6/17 17:30
10	2/20/17 20:43	3/9/17 20:46	2/16/17 24:46	3/6/17 18:30
11	2/20/17 21:43	3/9/17 21:46	2/17/17 01:46	3/6/17 19:30
12	2/20/17 22:43	3/9/17 22:46	2/17/17 02:46	3/6/17 20:30
13	2/20/17 23:43	3/9/17 23:46	2/17/17 03:46	3/6/17 21:30
14	2/20/17 24:43	3/9/17 24:46	2/17/17 04:46	3/6/17 22:30
15	2/21/17 01:43	3/10/17 01:46	2/17/17 05:46	3/6/17 23:30
16	2/21/17 02:43	3/10/17 02:46	2/17/17 06:46	3/6/17 24:30
17	2/21/17 03:43	3/10/17 03:46	2/17/17 07:46	3/7/17 01:30
18	2/21/17 04:43	3/10/17 04:46	2/17/17 08:46	3/7/17 02:30
19	2/21/17 05:43	3/10/17 05:46	2/17/17 09:46	3/7/17 03:30
20	2/21/17 06:43	3/10/17 06:46	2/17/17 10:46	3/7/17 04:30
21	2/21/17 07:43	3/10/17 07:46	2/17/17 11:46	3/7/17 05:30
22	-	3/10/17 08:46	2/17/17 12:46	3/7/17 06:30
23	-	3/10/17 09:46	2/17/17 13:46	3/7/17 07:30
24	-	3/10/17 10:46	2/17/17 14:46	3/7/17 08:30

Table G-2. Peak strain data from HVS loading on wheel path 1, trial 1, slab 1

Load	OS3600 (Top)	OS3600 (Bottom)	OS3500 (Top)	OS3500 (Bottom)	Vishay (Top)	Vishay (Bottom)	Tokyo (Top)	Tokyo (Bottom)	CTL (Top)	CTL (Bottom)
1	-33.5	23.0	-30.2	30.2	-16.1	24.1	-18.7	21.4	-13.5	13.1
2	-34.0	23.4	-30.1	30.2	-15.9	24.0	-18.5	21.4	-13.3	13.1
3	-33.8	23.6	-30.4	30.2	-15.8	23.9	-18.8	21.4	-13.5	13.2
4	-34.3	23.3	-30.1	29.7	-16.3	24.3	-18.9	21.2	-13.4	13.1
5	-34.2	23.7	-29.9	30.4	-16.1	24.1	-18.4	21.2	-13.4	13.2
6	-34.0	23.7	-30.2	30.9	-15.7	24.1	-18.1	21.4	-13.5	13.1
7	-34.3	23.6	-30.1	30.3	-15.7	24.2	-18.7	21.6	-13.3	13.1
8	-34.2	23.2	-29.9	30.3	-16.1	24.1	-18.5	21.4	-13.4	13.2
9	-33.9	23.5	-30.0	29.8	-16.0	23.8	-18.7	21.5	-13.4	13.1
10	-34.3	23.6	-31.0	30.6	-16.0	23.5	-18.4	21.8	-13.3	13.1
11	-34.8	24.0	-29.8	30.8	-15.8	23.5	-18.4	21.4	-13.4	13.1
12	-33.8	23.3	-29.7	30.4	-15.8	23.8	-18.5	21.3	-13.3	13.2
13	-34.6	24.0	-29.4	30.8	-16.0	23.9	-18.4	21.4	-13.4	13.1
14	-34.5	23.5	-29.1	30.2	-15.9	24.1	-18.5	21.4	-13.3	13.1
15	-33.9	23.3	-29.9	30.6	-15.6	24.2	-18.4	21.7	-13.3	13.2
16	-34.0	23.5	-29.6	30.3	-	-	-	-	-	-
17	-34.6	23.3	-30.1	30.2	-	-	-	-	-	-
18	-34.0	23.2	-29.9	31.0	-	-	-	-	-	-
19	-34.6	23.6	-29.6	30.7	-	-	-	-	-	-
20	-33.9	23.6	-30.2	30.3	-	-	-	-	-	-
Aver.	-34.2	23.5	-30.0	30.4	-15.9	24.0	-18.5	21.4	-13.4	13.1

Table G-3. Peak strain data from HVS loading on wheel path 1, trial 2, slab 1

Load	OS3600 (Top)	OS3600 (Bottom)	OS3500 (Top)	OS3500 (Bottom)	Vishay (Top)	Vishay (Bottom)	Tokyo (Top)	Tokyo (Bottom)	CTL (Top)	CTL (Bottom)
1	-37.8	24.5	-29.9	31.3	-15.8	23.5	-18.4	21.0	-13.4	13.3
2	-37.8	23.6	-29.3	31.0	-15.4	23.9	-19.0	21.2	-13.4	13.2
3	-37.5	23.9	-29.7	30.8	-15.3	23.6	-18.4	20.5	-13.4	13.2
4	-37.4	23.5	-29.7	31.3	-15.9	23.1	-18.7	20.7	-13.5	13.4
5	-37.0	24.2	-29.9	30.9	-15.5	23.9	-18.5	21.0	-13.4	13.3
6	-37.7	23.9	-29.4	30.4	-16.0	23.6	-19.0	20.8	-13.4	13.1
7	-37.4	24.2	-29.2	30.4	-15.7	23.6	-18.9	21.1	-13.4	13.3
8	-37.0	23.6	-29.5	30.8	-15.6	23.4	-18.3	21.0	-13.4	13.3
9	-37.5	24.1	-29.6	30.8	-15.7	23.5	-18.8	20.7	-13.2	13.4
10	-37.5	23.8	-30.1	31.3	-15.8	23.8	-18.6	21.0	-13.2	13.2
11	-37.9	23.3	-29.7	30.8	-15.9	23.8	-17.9	21.0	-13.3	13.3
12	-37.5	24.0	-29.4	30.1	-16.0	23.8	-18.8	20.8	-13.4	13.3
13	-37.0	23.9	-29.7	30.6	-15.7	23.3	-19.1	20.3	-13.2	13.3
14	-37.6	24.2	-29.4	30.3	-15.7	23.6	-18.8	20.4	-13.3	13.2
15	-37.8	23.6	-29.9	30.6	-15.5	23.5	-19.0	20.7	-13.3	13.3
16	-38.0	23.8	-29.5	30.9	-	-	-	-	-	-
17	-37.4	23.7	-29.6	31.0	-	-	-	-	-	-
18	-37.5	23.8	-29.3	30.4	-	-	-	-	-	-
19	-37.6	23.9	-29.4	30.6	-	-	-	-	-	-
20	-37.1	23.4	-29.7	30.4	-	-	-	-	-	-
Aver.	-37.5	23.8	-29.6	30.7	-15.7	23.6	-18.7	20.8	-13.3	13.3

Table G-4. Peak strain data from HVS loading on wheel path 1, trial 3, slab 1

Load	**OS3600** (Top)	**OS3600** (Bottom)	**OS3500** (Top)	**OS3500** (Bottom)	**Vishay** (Top)	**Vishay** (Bottom)	**Tokyo** (Top)	**Tokyo** (Bottom)	**CTL** (Top)	**CTL** (Bottom)
1	-37.8	23.1	-29.7	30.2	-15.5	22.7	-17.6	20.1	-13.0	13.3
2	-37.7	23.9	-29.4	30.2	-15.4	22.3	-17.8	20.1	-13.2	13.3
3	-37.6	23.7	-29.8	30.9	-15.2	22.9	-18.0	20.1	-13.1	13.3
4	-37.6	23.8	-29.6	30.4	-15.1	22.7	-18.2	20.2	-13.1	13.2
5	-37.4	23.8	-29.0	29.9	-15.5	22.3	-18.4	19.9	-13.0	13.2
6	-38.0	23.2	-29.4	30.4	-15.3	22.6	-18.4	19.7	-13.1	13.4
7	-37.8	23.3	-29.7	30.4	-15.4	22.4	-18.5	19.7	-13.1	13.2
8	-37.5	23.9	-29.5	30.0	-15.2	22.4	-18.0	19.8	-13.1	13.3
9	-38.1	22.7	-29.5	30.4	-15.2	22.7	-18.8	19.7	-13.1	13.2
10	-37.8	23.7	-29.3	30.1	-15.3	22.3	-17.9	19.9	-13.1	13.4
11	-37.3	23.2	-29.3	30.6	-15.0	22.1	-17.9	19.7	-12.9	13.3
12	-37.7	23.6	-29.5	30.0	-15.4	22.3	-17.7	20.1	-13.1	13.3
13	-38.1	24.3	-29.4	30.4	-15.5	22.4	-18.0	19.8	-13.2	13.3
14	-37.4	23.8	-29.8	30.6	-15.2	22.3	-17.7	19.7	-13.1	13.1
15	-37.4	23.2	-29.1	30.2	-15.2	22.0	-17.7	19.6	-13.0	13.4
16	-37.7	23.8	-28.8	29.7	-	-	-	-	-	-
17	-37.6	23.0	-29.6	30.1	-	-	-	-	-	-
18	-37.6	23.6	-29.2	29.9	-	-	-	-	-	-
19	-37.8	23.6	-30.1	29.9	-	-	-	-	-	-
20	-37.7	23.4	-29.4	29.7	-	-	-	-	-	-
Aver.	-37.7	23.5	-29.5	30.2	-15.3	22.4	-18.0	19.9	-13.1	13.3

Table G-5. Peak strain data from HVS loading on wheel path 1, trial 4, slab 1

Load	**OS3600** (Top)	**OS3600** (Bottom)	**OS3500** (Top)	**OS3500** (Bottom)	**Vishay** (Top)	**Vishay** (Bottom)	**Tokyo** (Top)	**Tokyo** (Bottom)	**CTL** (Top)	**CTL** (Bottom)
1	-37.7	22.3	-29.0	28.9	-14.7	21.7	-18.5	20.1	-12.9	13.7
2	-38.4	22.7	-28.7	29.4	-14.9	21.4	-18.6	19.5	-13.1	13.6
3	-37.2	22.2	-29.2	28.8	-14.7	21.3	-18.0	19.9	-13.2	13.6
4	-37.8	22.9	-28.6	29.4	-14.7	21.8	-18.4	19.5	-13.1	13.8
5	-37.6	23.0	-28.7	29.3	-14.2	21.4	-18.2	19.7	-13.1	13.6
6	-37.6	23.0	-28.5	28.4	-15.0	21.6	-18.0	19.7	-13.0	13.6
7	-37.1	22.6	-28.7	28.9	-15.0	21.7	-18.0	20.1	-13.1	13.6
8	-37.0	23.0	-28.9	29.3	-14.9	21.1	-18.3	19.9	-13.2	13.7
9	-37.6	23.2	-29.2	28.5	-14.8	21.5	-17.8	20.1	-13.1	13.6
10	-37.8	22.9	-29.0	29.0	-14.9	21.2	-17.8	20.0	-13.0	13.6
11	-37.3	23.0	-28.9	29.0	-15.2	21.5	-18.0	20.0	-13.1	13.7
12	-37.6	23.0	-28.5	28.3	-15.1	21.4	-18.1	19.9	-13.1	13.6
13	-38.1	23.0	-29.3	29.2	-14.8	21.6	-18.5	19.8	-13.2	13.6
14	-37.4	22.5	-29.3	28.7	-14.7	21.1	-18.2	19.6	-13.1	13.7
15	-37.7	22.5	-29.2	29.3	-14.8	21.4	-18.2	19.4	-13.0	13.7
16	-37.5	22.4	-28.8	28.7	-	-	-	-	-	-
17	-36.7	22.1	-29.0	29.0	-	-	-	-	-	-
18	-37.3	23.3	-28.7	28.1	-	-	-	-	-	-
19	-37.3	22.9	-29.0	28.7	-	-	-	-	-	-
20	-37.5	22.7	-28.8	29.0	-	-	-	-	-	-
Aver.	-37.5	22.8	-28.9	28.9	-14.8	21.5	-18.2	19.8	-13.1	13.6

Table G-6. Peak strain data from HVS loading on wheel path 1, trial 5, slab 1

Load	**OS3600** (Top)	**OS3600** (Bottom)	**OS3500** (Top)	**OS3500** (Bottom)	**Vishay** (Top)	**Vishay** (Bottom)	**Tokyo** (Top)	**Tokyo** (Bottom)	**CTL** (Top)	**CTL** (Bottom)
1	-38.2	22.8	-29.0	28.2	-16.0	22.2	-18.8	20.4	-13.2	13.9
2	-38.0	22.4	-28.5	28.0	-16.0	22.1	-19.1	20.0	-13.4	13.9
3	-37.9	22.1	-28.8	28.2	-15.8	22.7	-19.0	20.2	-13.3	14.0
4	-37.9	22.4	-28.7	28.3	-15.8	22.2	-19.7	20.3	-13.3	13.9
5	-37.7	22.7	-28.8	28.4	-15.9	22.5	-19.2	19.6	-13.2	13.9
6	-37.6	22.5	-28.9	28.0	-16.1	21.9	-19.8	19.9	-13.3	13.9
7	-38.0	22.9	-28.9	28.3	-15.7	22.1	-19.1	19.8	-13.4	13.8
8	-38.0	22.7	-28.3	28.7	-16.1	22.0	-19.3	19.9	-13.3	13.8
9	-38.2	23.0	-28.6	28.7	-15.9	22.0	-19.2	19.6	-13.1	13.8
10	-38.1	22.6	-28.8	28.0	-16.2	21.6	-19.1	20.0	-13.4	13.9
11	-38.2	22.4	-28.6	28.7	-16.6	22.0	-18.8	20.0	-13.3	13.8
12	-38.3	22.9	-28.6	28.3	-16.4	22.0	-18.8	19.7	-13.4	13.9
13	-38.1	22.3	-28.9	28.8	-15.8	22.1	-19.2	19.7	-13.3	13.8
14	-38.4	22.5	-28.5	28.2	-16.2	22.1	-18.7	20.0	-13.2	13.9
15	-37.5	23.0	-28.5	28.9	-16.3	22.0	-19.1	20.1	-13.4	13.8
16	-37.7	22.4	-28.1	28.4	-	-	-	-	-	-
17	-38.2	22.9	-28.1	28.6	-	-	-	-	-	-
18	-38.1	23.0	-28.4	28.1	-	-	-	-	-	-
19	-38.3	23.2	-28.2	28.4	-	-	-	-	-	-
20	-37.3	22.9	-27.8	28.4	-	-	-	-	-	-
Aver.	-38.0	22.7	-28.5	28.4	-16.1	22.1	-19.1	19.9	-13.3	13.9

Table G-7. Peak strain data from HVS loading on wheel path 1, trial 6, slab 1

Load	**OS3600** (Top)	**OS3600** (Bottom)	**OS3500** (Top)	**OS3500** (Bottom)	**Vishay** (Top)	**Vishay** (Bottom)	**Tokyo** (Top)	**Tokyo** (Bottom)	**CTL** (Top)	**CTL** (Bottom)
1	-36.4	23.0	-30.8	29.0	-16.2	22.6	-20.4	20.4	-13.5	13.9
2	-36.4	22.3	-30.5	28.9	-15.7	22.7	-20.3	20.4	-13.4	13.9
3	-36.8	23.1	-30.6	29.2	-15.8	22.5	-20.3	20.3	-13.3	14.0
4	-36.3	23.4	-30.7	28.8	-16.2	22.7	-20.2	20.5	-13.4	13.9
5	-36.9	23.0	-30.6	29.6	-16.1	22.6	-20.1	20.4	-13.4	14.0
6	-36.7	22.6	-30.7	29.2	-16.1	22.8	-19.8	20.6	-13.5	13.9
7	-36.3	22.4	-30.9	29.6	-16.1	23.0	-20.4	20.5	-13.4	13.9
8	-36.8	22.9	-31.1	29.2	-16.3	22.9	-20.0	20.6	-13.4	13.9
9	-36.1	22.7	-30.8	29.4	-16.4	22.7	-20.4	20.3	-13.3	14.0
10	-36.9	22.8	-30.7	29.4	-16.1	22.5	-20.1	20.5	-13.4	14.1
11	-35.8	23.1	-31.5	29.7	-16.3	22.6	-20.2	20.3	-13.3	13.9
12	-36.6	23.1	-31.0	29.3	-15.8	22.9	-20.4	20.9	-13.5	14.1
13	-37.2	23.1	-31.1	29.5	-16.3	22.9	-20.2	20.9	-13.4	14.1
14	-36.5	22.4	-31.1	29.7	-15.8	22.8	-20.3	20.3	-13.5	13.9
15	-36.4	23.0	-31.1	29.8	-16.1	22.4	-20.4	20.5	-13.4	14.1
16	-37.0	22.9	-31.6	29.4	-	-	-	-	-	-
17	-36.9	23.4	-31.0	29.2	-	-	-	-	-	-
18	-36.1	22.9	-30.9	29.4	-	-	-	-	-	-
19	-36.3	23.4	-30.7	29.8	-	-	-	-	-	-
20	-36.5	23.0	-30.9	29.5	-	-	-	-	-	-
Aver.	-36.5	22.9	-30.9	29.4	-16.1	22.7	-20.2	20.5	-13.4	14.0

Table G-8. Peak strain data from HVS loading on wheel path 1, trial 7, slab 1

Load	**OS3600** (Top)	**OS3600** (Bottom)	**OS3500** (Top)	**OS3500** (Bottom)	**Vishay** (Top)	**Vishay** (Bottom)	**Tokyo** (Top)	**Tokyo** (Bottom)	**CTL** (Top)	**CTL** (Bottom)
1	-38.6	22.4	-30.4	29.3	-15.9	22.8	-19.7	20.1	-13.0	13.8
2	-37.8	22.7	-30.9	30.0	-16.1	22.9	-19.8	20.1	-13.3	13.5
3	-37.9	23.3	-30.6	30.1	-16.4	23.4	-19.7	20.5	-13.6	13.9
4	-38.1	23.1	-30.7	29.7	-16.2	22.8	-19.8	20.1	-13.7	13.9
5	-37.5	22.7	-30.7	30.0	-16.3	23.3	-20.0	20.8	-13.7	14.2
6	-37.7	23.1	-30.5	30.2	-16.2	23.3	-19.7	20.8	-13.7	14.2
7	-37.9	23.5	-30.2	29.7	-16.3	23.2	-19.9	20.5	-13.6	14.2
8	-38.1	23.4	-30.3	29.5	-16.3	23.8	-19.5	20.9	-13.6	14.2
9	-38.1	23.6	-30.4	29.8	-16.0	23.8	-19.6	20.7	-13.7	14.1
10	-38.5	23.1	-30.6	29.5	-15.7	23.6	-19.3	21.3	-13.6	14.2
11	-38.2	23.4	-30.8	29.3	-16.0	23.7	-19.2	21.0	-13.4	14.2
12	-38.2	23.4	-31.1	29.8	-15.8	23.8	-19.5	20.9	-13.7	14.2
13	-37.9	23.0	-30.6	29.7	-15.8	23.7	-19.3	21.4	-13.5	14.2
14	-37.7	23.1	-30.5	30.0	-15.8	23.9	-19.3	21.1	-13.7	14.2
15	-37.3	22.9	-30.6	29.5	-15.6	23.5	-19.5	21.1	-13.5	14.1
16	-38.2	23.4	-31.0	30.1	-	-	-	-	-	-
17	-38.4	22.9	-30.7	29.6	-	-	-	-	-	-
18	-38.2	23.7	-30.5	30.5	-	-	-	-	-	-
19	-38.3	22.7	-30.5	29.9	-	-	-	-	-	-
20	-38.0	23.0	-30.4	30.1	-	-	-	-	-	-
Aver.	-38.0	23.1	-30.6	29.8	-16.0	23.4	-19.6	20.8	-13.6	14.1

Table G-9. Peak strain data from HVS loading on wheel path 1, trial 8, slab 1

Load	**OS3600** (Top)	**OS3600** (Bottom)	**OS3500** (Top)	**OS3500** (Bottom)	**Vishay** (Top)	**Vishay** (Bottom)	**Tokyo** (Top)	**Tokyo** (Bottom)	**CTL** (Top)	**CTL** (Bottom)
1	-38.4	23.7	-30.3	30.5	-15.6	23.2	-18.9	20.9	-12.8	13.4
2	-39.0	23.3	-29.8	30.3	-16.1	24.0	-19.3	21.4	-13.2	13.7
3	-38.4	23.3	-31.1	30.6	-15.6	24.0	-19.1	21.3	-13.4	13.7
4	-38.5	24.0	-31.0	30.3	-16.1	24.3	-19.6	21.8	-13.4	13.9
5	-38.7	23.7	-30.8	30.8	-16.2	24.0	-19.6	21.7	-13.4	13.9
6	-39.0	23.6	-30.5	30.5	-16.1	24.3	-19.7	21.3	-13.6	13.9
7	-38.5	23.2	-30.2	30.4	-16.0	24.6	-19.0	21.8	-13.6	13.9
8	-38.3	23.0	-30.6	30.3	-15.7	24.3	-19.2	21.6	-13.6	13.9
9	-38.8	23.6	-30.7	30.2	-15.9	24.1	-19.6	21.4	-13.6	13.9
10	-38.6	23.4	-30.8	30.7	-15.7	24.5	-19.3	21.4	-13.6	14.0
11	-38.9	24.2	-30.8	30.2	-15.9	24.6	-18.9	21.8	-13.4	13.8
12	-38.8	23.7	-30.4	30.7	-15.7	24.5	-18.9	21.7	-13.6	13.9
13	-38.6	23.5	-30.5	30.1	-16.2	24.9	-18.7	21.9	-13.7	13.9
14	-39.1	24.4	-30.5	30.7	-16.1	24.7	-18.5	22.2	-13.6	13.7
15	-38.1	23.3	-30.9	29.8	-15.5	24.6	-18.4	21.6	-13.6	13.7
16	-38.5	23.6	-30.9	30.4	-	-	-	-	-	-
17	-38.8	23.2	-30.8	30.4	-	-	-	-	-	-
18	-38.1	23.1	-30.6	29.9	-	-	-	-	-	-
19	-38.6	23.4	-30.6	30.2	-	-	-	-	-	-
20	-38.6	23.5	-30.7	30.4	-	-	-	-	-	-
Aver.	-38.6	23.5	-30.6	30.4	-15.9	24.3	-19.1	21.6	-13.5	13.8

Table G-10. Peak strain data from HVS loading on wheel path 1, trial 9, slab 1

Load	**OS3600** (Top)	**OS3600** (Bottom)	**OS3500** (Top)	**OS3500** (Bottom)	**Vishay** (Top)	**Vishay** (Bottom)	**Tokyo** (Top)	**Tokyo** (Bottom)	**CTL** (Top)	**CTL** (Bottom)
1	-41.5	24.8	-30.1	30.8	-16.2	24.6	-19.4	21.7	-14.1	14.1
2	-41.9	24.7	-30.0	31.6	-16.0	24.7	-19.5	21.9	-14.1	14.1
3	-41.9	24.5	-29.9	30.8	-15.9	24.5	-19.4	22.0	-14.1	14.0
4	-41.9	24.1	-29.2	31.3	-15.9	24.5	-19.3	22.1	-14.0	14.1
5	-41.4	24.1	-30.0	31.0	-16.2	24.2	-19.4	22.1	-14.1	14.1
6	-41.8	24.4	-30.2	30.8	-16.1	24.7	-19.5	21.9	-14.0	14.0
7	-41.7	24.7	-30.2	31.3	-16.2	24.6	-19.6	22.0	-14.0	13.9
8	-42.2	24.0	-29.8	31.3	-16.0	24.3	-19.0	21.9	-14.0	13.9
9	-41.8	24.7	-30.2	31.0	-16.5	24.6	-19.5	21.8	-13.9	13.9
10	-41.7	24.3	-29.6	31.4	-16.0	24.8	-19.1	22.4	-14.0	14.0
11	-41.9	24.8	-30.0	31.7	-16.2	24.8	-19.7	22.0	-14.0	14.0
12	-41.7	24.4	-29.8	31.5	-16.1	24.4	-19.3	22.0	-14.0	13.9
13	-41.9	24.5	-30.1	31.3	-15.5	23.9	-19.5	22.1	-14.0	14.0
14	-41.9	24.3	-30.1	30.8	-15.8	24.3	-19.4	22.2	-14.0	14.0
15	-41.9	24.7	-29.9	31.0	-15.9	24.5	-19.4	22.1	-14.0	14.0
16	-41.7	25.1	-30.0	31.4	-	-	-	-	-	-
17	-42.0	25.2	-29.8	31.2	-	-	-	-	-	-
18	-42.5	24.2	-30.0	31.0	-	-	-	-	-	-
19	-41.7	24.5	-30.1	30.7	-	-	-	-	-	-
20	-41.6	24.4	-29.7	31.0	-	-	-	-	-	-
Aver.	-41.8	24.5	-29.9	31.1	-16.0	24.5	-19.4	22.0	-14.0	14.0

Table G-11. Peak strain data from HVS loading on wheel path 1, trial 10, slab 1

Load	**OS3600** (Top)	**OS3600** (Bottom)	**OS3500** (Top)	**OS3500** (Bottom)	**Vishay** (Top)	**Vishay** (Bottom)	**Tokyo** (Top)	**Tokyo** (Bottom)	**CTL** (Top)	**CTL** (Bottom)
1	-42.4	24.9	-30.2	31.0	-16.0	24.8	-18.6	22.8	-14.3	14.0
2	-42.8	24.5	-30.0	31.8	-16.0	24.9	-18.9	22.2	-14.2	13.9
3	-42.8	24.9	-30.2	31.4	-15.8	24.9	-19.5	22.3	-14.2	14.0
4	-42.7	25.3	-30.4	30.7	-15.5	25.1	-19.1	22.5	-14.2	13.9
5	-43.4	24.6	-29.8	31.1	-15.6	24.9	-18.6	22.5	-14.1	13.9
6	-42.6	24.9	-30.5	31.7	-16.0	25.1	-18.3	22.2	-14.1	14.0
7	-42.4	25.0	-29.7	31.6	-15.9	24.9	-18.7	22.1	-14.2	14.1
8	-42.6	24.9	-30.6	31.4	-16.1	25.1	-18.7	22.7	-14.1	14.0
9	-42.6	25.1	-30.5	31.5	-15.6	25.0	-18.9	22.2	-14.0	14.1
10	-42.9	24.8	-30.3	31.1	-16.0	24.9	-18.6	22.0	-14.2	13.9
11	-42.9	25.4	-29.9	30.6	-15.8	25.3	-19.0	22.2	-14.2	14.0
12	-42.5	24.7	-30.2	31.2	-15.8	25.3	-18.7	22.3	-14.1	14.1
13	-43.0	24.8	-29.7	31.2	-15.9	24.6	-18.7	22.4	-14.1	14.0
14	-43.3	24.5	-30.8	31.5	-15.7	25.3	-18.7	22.3	-14.1	13.9
15	-43.3	24.9	-30.4	31.2	-15.7	25.2	-18.4	22.3	-14.2	14.0
16	-42.9	24.5	-30.4	31.1	-	-	-	-	-	-
17	-42.8	24.5	-30.0	31.6	-	-	-	-	-	-
18	-42.8	24.6	-30.4	31.9	-	-	-	-	-	-
19	-43.3	24.5	-30.0	31.8	-	-	-	-	-	-
20	-42.7	24.6	-30.3	31.2	-	-	-	-	-	-
Aver.	-42.8	24.8	-30.2	31.3	-15.8	25.0	-18.8	22.3	-14.2	14.0

Table G-12. Peak strain data from HVS loading on wheel path 1, trial 11, slab 1

Load	**OS3600** (Top)	**OS3600** (Bottom)	**OS3500** (Top)	**OS3500** (Bottom)	**Vishay** (Top)	**Vishay** (Bottom)	**Tokyo** (Top)	**Tokyo** (Bottom)	**CTL** (Top)	**CTL** (Bottom)
1	-43.3	24.9	-30.0	31.5	-15.6	25.3	-19.1	22.6	-14.1	14.1
2	-42.6	24.1	-30.2	31.7	-15.5	25.6	-18.8	22.6	-14.2	14.0
3	-42.9	24.2	-29.7	31.3	-15.7	25.1	-19.0	22.8	-14.2	14.0
4	-43.2	24.5	-29.4	31.3	-15.8	25.0	-18.9	22.8	-14.2	14.0
5	-42.1	24.1	-30.0	31.5	-15.4	25.6	-18.9	22.9	-14.1	14.1
6	-42.7	24.4	-30.0	31.3	-15.8	25.5	-18.7	22.6	-14.2	14.0
7	-42.8	24.9	-30.5	31.4	-15.8	25.6	-18.7	22.7	-14.2	13.9
8	-42.6	24.9	-29.8	31.7	-15.6	25.6	-18.5	22.9	-14.2	13.9
9	-42.8	24.1	-29.5	31.0	-15.4	25.2	-19.1	22.8	-14.2	14.1
10	-42.7	25.3	-29.7	30.8	-15.5	25.1	-18.8	22.9	-14.0	14.1
11	-42.8	24.7	-30.0	31.2	-15.5	25.6	-18.8	22.5	-14.2	14.2
12	-42.9	24.1	-29.9	31.5	-15.6	25.3	-18.6	22.7	-14.3	14.0
13	-43.0	24.6	-29.7	31.6	-15.6	25.5	-18.4	23.0	-14.2	13.8
14	-43.2	25.3	-29.7	31.4	-15.6	24.8	-18.7	22.8	-14.2	14.0
15	-43.1	24.4	-29.3	30.6	-15.8	24.9	-18.7	22.6	-14.2	13.9
16	-42.9	25.0	-30.0	31.7	-	-	-	-	-	-
17	-42.9	24.4	-29.8	31.9	-	-	-	-	-	-
18	-43.0	24.9	-29.8	31.6	-	-	-	-	-	-
19	-42.8	24.5	-30.2	31.2	-	-	-	-	-	-
20	-43.2	24.7	-29.6	30.8	-	-	-	-	-	-
Aver.	-42.9	24.6	-29.8	31.4	-15.6	25.3	-18.8	22.7	-14.2	14.0

Table G-13. Peak strain data from HVS loading on wheel path 1, trial 12, slab 1

Load	**OS3600** (Top)	**OS3600** (Bottom)	**OS3500** (Top)	**OS3500** (Bottom)	**Vishay** (Top)	**Vishay** (Bottom)	**Tokyo** (Top)	**Tokyo** (Bottom)	**CTL** (Top)	**CTL** (Bottom)
1	-43.5	24.9	-29.8	31.1	-15.6	25.4	-18.2	22.4	-14.2	13.9
2	-43.1	25.7	-29.9	31.9	-15.4	25.6	-17.9	22.6	-14.2	13.7
3	-43.4	25.2	-29.5	31.8	-15.5	25.4	-18.1	22.5	-14.2	13.8
4	-43.5	24.9	-29.1	31.4	-15.4	25.8	-18.3	22.5	-14.1	13.9
5	-42.7	25.4	-29.0	31.0	-15.5	25.4	-18.1	22.7	-14.1	13.9
6	-42.9	24.9	-29.4	31.6	-15.4	25.4	-18.0	22.6	-14.0	13.8
7	-43.1	25.1	-29.0	31.6	-15.5	25.7	-17.9	22.7	-14.2	13.8
8	-43.0	25.4	-28.9	31.7	-15.4	25.4	-18.0	22.6	-14.2	13.7
9	-43.3	25.2	-29.6	31.0	-15.4	25.6	-18.4	22.5	-14.2	13.8
10	-42.8	25.5	-29.0	31.3	-15.7	25.5	-18.1	22.5	-14.2	13.9
11	-42.9	25.3	-28.7	31.8	-15.7	25.7	-18.3	22.5	-14.1	13.8
12	-43.5	24.7	-29.5	31.2	-15.5	25.5	-18.0	22.3	-14.3	13.9
13	-42.9	25.2	-29.5	31.7	-15.4	25.2	-17.9	22.6	-14.2	13.8
14	-42.7	25.2	-29.3	31.6	-15.4	25.1	-18.0	22.3	-14.3	13.8
15	-42.9	25.3	-29.0	31.2	-15.5	25.3	-18.2	22.1	-14.4	13.7
16	-43.1	25.3	-29.4	31.4	-	-	-	-	-	-
17	-43.2	24.6	-29.3	31.4	-	-	-	-	-	-
18	-43.3	25.6	-29.1	31.6	-	-	-	-	-	-
19	-43.1	25.0	-29.6	31.4	-	-	-	-	-	-
20	-42.9	25.0	-29.5	31.3	-	-	-	-	-	-
Aver.	-43.1	25.2	-29.3	31.4	-15.5	25.5	-18.1	22.5	-14.2	13.8

Table G-14. Peak strain data from HVS loading on wheel path 1, trial 13, slab 1

Load	OS3600 (Top)	OS3600 (Bottom)	OS3500 (Top)	OS3500 (Bottom)	Vishay (Top)	Vishay (Bottom)	Tokyo (Top)	Tokyo (Bottom)	CTL (Top)	CTL (Bottom)
1	-43.1	24.5	-28.9	31.4	-15.5	25.3	-18.0	23.1	-14.1	13.6
2	-43.2	25.2	-28.7	31.2	-15.2	25.0	-18.0	22.5	-14.1	13.5
3	-43.0	25.0	-28.9	30.9	-15.1	25.6	-17.7	22.3	-14.1	13.7
4	-43.7	24.8	-29.2	31.1	-15.1	25.3	-17.9	22.4	-14.0	13.6
5	-43.1	25.2	-28.9	31.1	-15.5	25.3	-17.7	22.7	-14.0	13.6
6	-43.7	25.1	-29.6	31.8	-15.2	25.3	-17.8	22.4	-14.0	13.6
7	-43.6	24.5	-28.9	31.0	-15.4	25.6	-18.1	22.8	-14.0	13.7
8	-44.0	24.8	-28.6	31.4	-15.2	25.2	-17.8	22.2	-14.1	13.6
9	-43.6	25.4	-28.8	30.8	-15.6	25.1	-17.8	22.5	-14.1	13.6
10	-43.7	24.9	-29.3	30.5	-15.0	25.0	-17.6	22.3	-14.1	13.6
11	-43.1	25.0	-28.7	30.8	-15.1	25.3	-18.2	22.3	-14.1	13.7
12	-43.4	24.8	-29.1	31.3	-15.0	25.0	-17.7	22.4	-14.0	13.7
13	-43.2	25.3	-28.8	31.7	-15.3	24.9	-18.0	22.7	-14.0	13.7
14	-43.8	25.5	-29.3	31.1	-15.1	25.0	-17.5	22.3	-13.9	13.6
15	-43.5	25.8	-29.0	31.6	-14.7	25.3	-17.8	22.8	-14.0	13.8
16	-43.7	24.9	-29.0	30.5	-	-	-	-	-	-
17	-43.4	25.2	-29.1	31.4	-	-	-	-	-	-
18	-42.0	25.3	-28.8	31.6	-	-	-	-	-	-
19	-43.2	25.7	-29.0	30.9	-	-	-	-	-	-
20	-43.2	25.5	-29.1	31.4	-	-	-	-	-	-
Aver.	-43.4	25.1	-29.0	31.2	-15.2	25.2	-17.8	22.5	-14.0	13.6

Table G-15. Peak strain data from HVS loading on wheel path 1, trial 14, slab 1

Load	OS3600 (Top)	OS3600 (Bottom)	OS3500 (Top)	OS3500 (Bottom)	Vishay (Top)	Vishay (Bottom)	Tokyo (Top)	Tokyo (Bottom)	CTL (Top)	CTL (Bottom)
1	-43.7	25.3	-28.6	31.0	-14.7	25.7	-17.5	23.0	-14.1	13.6
2	-43.8	25.4	-29.2	31.4	-14.8	25.3	-17.8	22.9	-14.1	13.6
3	-43.6	25.0	-29.6	31.1	-15.1	25.5	-17.9	22.8	-14.0	13.5
4	-43.1	25.4	-29.0	31.3	-14.8	25.2	-17.3	22.6	-14.2	13.3
5	-43.6	25.3	-28.6	31.7	-14.7	25.2	-17.5	22.7	-14.1	13.5
6	-43.8	25.8	-28.9	31.1	-14.9	25.3	-17.6	22.8	-14.1	13.6
7	-43.6	25.3	-29.4	31.2	-14.9	25.1	-18.2	22.5	-14.0	13.5
8	-43.8	25.0	-28.6	31.6	-14.9	25.5	-17.9	22.7	-14.1	13.5
9	-43.4	25.1	-29.1	31.3	-14.8	25.6	-17.8	22.7	-14.1	13.6
10	-43.7	25.2	-28.9	31.1	-14.9	25.0	-17.6	22.7	-14.2	13.5
11	-43.9	25.7	-28.5	31.0	-14.9	25.3	-17.8	22.9	-14.2	13.5
12	-43.9	25.1	-28.8	31.1	-14.9	25.4	-17.5	22.6	-14.2	13.6
13	-42.9	25.0	-29.1	31.1	-15.2	25.1	-17.9	22.4	-14.1	13.6
14	-43.1	25.5	-28.8	31.4	-15.1	25.5	-17.8	22.8	-14.1	13.6
15	-43.6	25.4	-29.0	31.2	-15.0	25.5	-17.9	23.1	-14.1	13.4
16	-43.4	25.2	-28.7	30.3	-	-	-	-	-	-
17	-43.8	25.9	-28.7	31.2	-	-	-	-	-	-
18	-43.6	24.7	-28.7	30.6	-	-	-	-	-	-
19	-43.7	25.4	-29.2	31.7	-	-	-	-	-	-
20	-43.1	25.1	-29.3	31.1	-	-	-	-	-	-
Aver.	-43.6	25.3	-28.9	31.2	-14.9	25.4	-17.7	22.7	-14.1	13.5

Table G-16. Peak strain data from HVS loading on wheel path 1, trial 15, slab 1

Load	OS3600 (Top)	OS3600 (Bottom)	OS3500 (Top)	OS3500 (Bottom)	Vishay (Top)	Vishay (Bottom)	Tokyo (Top)	Tokyo (Bottom)	CTL (Top)	CTL (Bottom)
1	-43.0	25.7	-28.5	31.5	-14.5	25.7	-17.2	22.4	-13.9	13.4
2	-44.3	26.0	-29.1	31.1	-14.8	25.8	-17.3	23.1	-14.0	13.3
3	-43.5	25.1	-29.0	31.1	-14.9	25.5	-17.4	22.8	-14.0	13.4
4	-43.9	25.5	-28.9	31.4	-15.4	25.5	-17.8	22.5	-14.0	13.4
5	-44.3	24.8	-28.7	31.6	-14.9	25.6	-17.4	22.7	-14.0	13.5
6	-44.1	25.4	-29.6	31.1	-14.6	25.2	-16.9	22.4	-14.0	13.4
7	-43.6	24.9	-28.8	31.1	-14.3	26.0	-17.3	21.8	-14.0	13.3
8	-43.9	25.5	-29.0	31.0	-14.3	25.8	-17.0	22.6	-13.9	13.3
9	-44.1	25.2	-28.4	31.4	-15.1	25.7	-16.7	22.6	-14.0	13.4
10	-43.8	25.5	-28.7	31.3	-15.0	25.6	-16.7	22.7	-14.0	13.5
11	-44.1	25.2	-29.4	30.4	-15.0	25.7	-17.0	22.7	-14.0	13.4
12	-44.0	25.6	-28.6	30.9	-15.3	25.7	-17.2	22.6	-14.0	13.4
13	-44.0	25.0	-28.5	31.4	-14.6	25.5	-17.3	22.4	-14.0	13.4
14	-44.1	25.0	-28.8	31.1	-15.1	25.6	-17.0	22.7	-14.0	13.4
15	-44.1	25.7	-29.0	31.5	-15.1	25.7	-17.4	21.9	-14.0	13.5
16	-44.3	25.4	-29.1	31.8	-	-	-	-	-	-
17	-43.8	25.5	-28.9	31.2	-	-	-	-	-	-
18	-43.8	24.9	-28.7	31.2	-	-	-	-	-	-
19	-43.6	25.4	-29.2	30.8	-	-	-	-	-	-
20	-44.6	25.1	-29.0	31.5	-	-	-	-	-	-
Aver.	-43.9	25.3	-28.9	31.2	-14.9	25.6	-17.2	22.5	-14.0	13.4

Table G-17. Peak strain data from HVS loading on wheel path 1, trial 16, slab 1

Load	OS3600 (Top)	OS3600 (Bottom)	OS3500 (Top)	OS3500 (Bottom)	Vishay (Top)	Vishay (Bottom)	Tokyo (Top)	Tokyo (Bottom)	CTL (Top)	CTL (Bottom)
1	-43.6	25.2	-28.4	31.1	-14.4	26.0	-16.9	22.7	-14.1	13.4
2	-44.3	25.4	-29.2	31.5	-14.6	26.0	-17.4	22.8	-14.2	13.6
3	-44.3	25.2	-28.9	31.7	-14.2	25.8	-17.4	22.6	-14.2	13.3
4	-44.1	25.6	-28.6	31.4	-14.7	25.9	-16.8	22.4	-14.2	13.4
5	-44.4	25.3	-28.7	31.7	-14.6	26.1	-17.3	22.6	-14.2	13.4
6	-43.8	25.9	-28.7	31.3	-14.2	25.7	-17.3	22.9	-14.3	13.4
7	-43.4	25.4	-28.2	31.3	-14.8	26.0	-17.5	23.0	-14.3	13.4
8	-43.9	25.2	-29.0	31.4	-14.4	25.8	-17.0	23.0	-14.1	13.4
9	-43.4	25.5	-28.5	31.4	-14.5	25.6	-17.2	22.2	-14.2	13.3
10	-44.5	25.3	-28.4	30.8	-14.8	25.9	-17.4	22.8	-14.1	13.4
11	-44.4	25.8	-27.8	30.9	-14.8	25.7	-17.6	22.7	-14.2	13.3
12	-43.9	26.0	-28.6	31.1	-14.5	25.5	-17.0	22.1	-14.2	13.2
13	-43.7	25.2	-28.7	31.4	-14.5	25.4	-17.1	22.3	-14.2	13.3
14	-44.2	25.5	-28.3	31.4	-14.6	25.6	-17.4	22.5	-14.2	13.5
15	-44.0	25.1	-28.5	31.4	-14.5	26.0	-17.2	22.6	-14.2	13.4
16	-44.2	25.5	-27.8	30.8	-	-	-	-	-	-
17	-43.7	25.2	-28.5	31.6	-	-	-	-	-	-
18	-44.7	25.1	-28.6	31.7	-	-	-	-	-	-
19	-44.5	25.5	-28.4	31.3	-	-	-	-	-	-
20	-44.1	26.1	-28.6	31.3	-	-	-	-	-	-
Aver.	-44.0	25.4	-28.5	31.3	-14.5	25.8	-17.3	22.6	-14.2	13.4

Table G-18. Peak strain data from HVS loading on wheel path 1, trial 17, slab 1

Load	**OS3600** (Top)	**OS3600** (Bottom)	**OS3500** (Top)	**OS3500** (Bottom)	**Vishay** (Top)	**Vishay** (Bottom)	**Tokyo** (Top)	**Tokyo** (Bottom)	**CTL** (Top)	**CTL** (Bottom)
1	-43.9	25.9	-28.4	31.7	-14.1	25.5	-17.4	22.6	-14.3	13.2
2	-44.4	25.4	-28.7	31.4	-14.3	25.5	-17.5	22.6	-14.3	13.2
3	-44.2	25.1	-28.5	30.5	-14.1	25.8	-17.1	22.5	-14.2	13.2
4	-44.4	25.0	-29.0	31.9	-14.5	25.7	-16.7	22.5	-14.1	13.3
5	-44.5	25.5	-28.4	31.4	-14.8	25.6	-17.0	22.5	-14.3	13.3
6	-44.4	25.6	-29.0	32.0	-14.7	25.1	-17.0	22.7	-14.2	13.2
7	-44.7	25.0	-28.6	31.6	-14.7	25.8	-16.8	22.5	-14.3	13.2
8	-43.9	25.2	-28.3	31.6	-14.3	25.4	-17.1	22.8	-14.3	13.2
9	-44.2	25.1	-28.3	31.8	-14.3	25.3	-17.3	22.7	-14.3	13.2
10	-44.1	25.4	-29.1	31.3	-14.4	25.5	-17.1	22.7	-14.2	13.3
11	-43.9	24.6	-28.3	32.0	-14.7	25.4	-17.2	22.6	-14.2	13.2
12	-44.2	24.9	-28.8	31.0	-14.7	25.6	-17.4	23.0	-14.2	13.1
13	-44.5	25.1	-28.4	31.8	-14.7	25.8	-17.2	22.5	-14.2	13.1
14	-44.3	25.4	-28.5	31.2	-14.7	25.8	-17.3	23.1	-14.3	13.1
15	-44.4	25.5	-28.6	31.5	-14.6	25.7	-16.9	22.7	-14.2	13.1
16	-44.4	24.9	-28.6	31.8	-	-	-	-	-	-
17	-44.6	24.9	-28.8	31.8	-	-	-	-	-	-
18	-43.9	25.5	-28.4	31.7	-	-	-	-	-	-
19	-44.2	25.5	-29.2	31.2	-	-	-	-	-	-
20	-44.5	25.2	-28.3	31.7	-	-	-	-	-	-
Aver.	-44.3	25.2	-28.6	31.5	-14.5	25.6	-17.1	22.7	-14.2	13.2

Table G-19. Peak strain data from HVS loading on wheel path 1, trial 18, slab 1

Load	**OS3600** (Top)	**OS3600** (Bottom)	**OS3500** (Top)	**OS3500** (Bottom)	**Vishay** (Top)	**Vishay** (Bottom)	**Tokyo** (Top)	**Tokyo** (Bottom)	**CTL** (Top)	**CTL** (Bottom)
1	-44.9	25.2	-28.0	31.4	-14.1	25.5	-17.5	22.7	-14.4	13.3
2	-44.5	25.5	-28.7	30.9	-14.1	25.6	-17.2	22.9	-14.4	13.1
3	-44.2	25.3	-28.7	31.6	-13.7	25.7	-17.0	23.0	-14.3	13.3
4	-44.5	25.6	-28.7	30.9	-14.3	25.1	-17.4	22.7	-14.3	13.4
5	-44.3	25.6	-28.4	31.7	-14.2	25.4	-17.4	23.0	-14.2	13.3
6	-44.8	25.7	-28.1	31.7	-14.0	25.8	-17.4	22.8	-14.3	13.3
7	-44.5	25.4	-28.2	31.1	-13.9	25.4	-17.2	22.9	-14.3	13.2
8	-44.4	25.6	-28.8	31.1	-14.4	25.3	-17.5	22.9	-14.4	13.2
9	-45.1	25.1	-28.2	31.5	-14.5	25.5	-17.2	22.4	-14.1	13.3
10	-44.4	25.9	-28.1	31.5	-14.4	25.8	-17.2	22.8	-14.3	13.4
11	-44.8	25.4	-29.0	31.1	-14.4	25.9	-17.5	22.7	-14.3	13.3
12	-43.7	25.5	-28.5	31.2	-14.3	25.6	-17.2	23.1	-14.3	13.2
13	-44.8	25.7	-28.2	31.7	-14.4	25.5	-17.5	22.8	-14.4	13.3
14	-44.5	26.1	-28.1	31.4	-14.6	25.4	-17.8	22.7	-14.3	13.3
15	-43.8	25.4	-28.7	31.3	-14.3	25.8	-17.3	22.8	-14.2	13.3
16	-44.2	25.6	-28.0	31.6	-	-	-	-	-	-
17	-44.5	25.3	-28.2	31.7	-	-	-	-	-	-
18	-44.8	25.7	-28.5	31.2	-	-	-	-	-	-
19	-44.1	25.6	-28.8	31.1	-	-	-	-	-	-
20	-44.4	25.7	-28.4	31.4	-	-	-	-	-	-
Aver.	-44.5	25.5	-28.4	31.4	-14.3	25.5	-17.4	22.8	-14.3	13.3

Table G-20. Peak strain data from HVS loading on wheel path 1, trial 19, slab 1

Load	**OS3600** (Top)	**OS3600** (Bottom)	**OS3500** (Top)	**OS3500** (Bottom)	**Vishay** (Top)	**Vishay** (Bottom)	**Tokyo** (Top)	**Tokyo** (Bottom)	**CTL** (Top)	**CTL** (Bottom)
1	-44.2	25.2	-29.0	31.8	-14.4	25.7	-16.9	22.9	-14.2	13.3
2	-43.4	25.8	-28.6	31.2	-14.6	25.2	-17.6	22.5	-14.1	13.2
3	-44.7	25.5	-28.4	31.5	-13.9	25.5	-17.0	22.7	-14.2	13.1
4	-43.8	25.4	-29.1	31.7	-14.5	25.3	-17.2	22.6	-14.1	13.2
5	-44.6	25.9	-28.1	31.9	-14.3	25.6	-17.4	22.8	-14.2	13.2
6	-43.8	25.7	-28.8	31.0	-14.3	25.7	-17.4	22.6	-14.1	13.3
7	-44.2	25.4	-28.2	30.8	-14.4	25.0	-17.2	22.8	-14.0	13.2
8	-43.7	25.4	-28.4	31.4	-14.6	25.5	-17.6	22.5	-14.1	13.2
9	-44.5	25.1	-28.8	31.3	-14.6	25.6	-17.1	22.5	-14.0	13.2
10	-44.6	25.8	-28.8	31.6	-14.6	25.4	-16.8	22.3	-14.2	13.0
11	-44.5	25.8	-28.4	31.5	-14.7	25.5	-17.4	22.4	-14.2	13.3
12	-43.9	25.5	-28.3	31.7	-14.7	25.8	-17.2	22.8	-14.1	13.2
13	-44.2	25.3	-28.3	31.5	-14.2	25.6	-17.0	22.4	-14.1	13.2
14	-44.4	25.5	-28.6	31.5	-14.5	26.0	-17.1	22.9	-14.1	13.2
15	-44.2	25.6	-28.9	31.7	-14.5	25.6	-16.8	22.4	-14.2	13.2
16	-44.5	25.1	-28.5	31.4	-	-	-	-	-	-
17	-44.6	26.1	-28.7	31.5	-	-	-	-	-	-
18	-44.2	25.9	-28.4	31.5	-	-	-	-	-	-
19	-43.9	25.1	-27.5	31.6	-	-	-	-	-	-
20	-44.4	25.0	-28.9	31.8	-	-	-	-	-	-
Aver.	-44.2	25.5	-28.5	31.5	-14.4	25.5	-17.2	22.6	-14.1	13.2

Table G-21. Peak strain data from HVS loading on wheel path 1, trial 20, slab 1

Load	**OS3600** (Top)	**OS3600** (Bottom)	**OS3500** (Top)	**OS3500** (Bottom)	**Vishay** (Top)	**Vishay** (Bottom)	**Tokyo** (Top)	**Tokyo** (Bottom)	**CTL** (Top)	**CTL** (Bottom)
1	-43.9	25.5	-28.6	31.7	-14.2	25.6	-17.5	23.0	-14.2	13.3
2	-44.6	25.4	-27.9	31.3	-14.1	25.8	-17.4	23.0	-14.2	13.2
3	-44.1	26.2	-28.1	31.6	-14.4	25.7	-17.5	23.1	-14.2	13.2
4	-44.2	25.7	-28.2	31.5	-14.3	25.6	-17.9	22.8	-14.1	13.3
5	-44.5	25.3	-28.3	31.4	-14.4	25.5	-17.5	22.7	-14.2	13.3
6	-44.6	25.7	-28.3	31.6	-14.0	25.7	-17.2	22.7	-14.2	13.3
7	-44.9	25.7	-28.5	31.7	-14.0	25.1	-17.4	22.7	-14.2	13.2
8	-45.2	25.2	-28.2	31.7	-13.8	25.5	-17.3	23.0	-14.3	13.3
9	-44.4	25.6	-28.5	31.6	-14.0	25.4	-17.4	22.5	-14.1	13.3
10	-44.0	26.1	-28.2	31.8	-14.1	25.7	-17.0	22.5	-14.2	13.3
11	-43.9	26.1	-28.4	31.9	-14.3	25.8	-17.3	22.5	-14.1	13.3
12	-44.8	25.5	-28.3	31.1	-14.4	26.0	-17.2	22.7	-14.1	13.4
13	-44.8	25.9	-28.6	31.9	-14.2	25.6	-17.3	22.7	-14.1	13.3
14	-45.0	26.0	-28.5	31.8	-14.2	25.7	-17.1	22.7	-14.2	13.4
15	-44.8	26.0	-28.3	31.1	-14.2	25.6	-17.1	22.3	-14.2	13.4
16	-44.5	25.6	-28.5	31.2	-	-	-	-	-	-
17	-44.4	25.0	-28.6	31.6	-	-	-	-	-	-
18	-44.9	26.3	-28.4	31.7	-	-	-	-	-	-
19	-44.4	26.0	-28.7	31.5	-	-	-	-	-	-
20	-44.9	25.7	-29.3	31.7	-	-	-	-	-	-
Aver.	-44.5	25.7	-28.4	31.6	-14.2	25.6	-17.3	22.7	-14.2	13.3

Table G-22. Peak strain data from HVS loading on wheel path 1, trial 21, slab 1

Load	**OS3600** (Top)	**OS3600** (Bottom)	**OS3500** (Top)	**OS3500** (Bottom)	**Vishay** (Top)	**Vishay** (Bottom)	**Tokyo** (Top)	**Tokyo** (Bottom)	**CTL** (Top)	**CTL** (Bottom)
1	-43.9	25.4	-28.0	31.6	-14.2	25.5	-18.0	23.0	-14.3	13.3
2	-44.3	25.2	-28.6	30.8	-14.1	25.2	-17.5	22.6	-14.1	13.2
3	-44.2	25.8	-28.3	31.8	-14.1	25.2	-17.8	23.2	-14.3	13.2
4	-43.5	25.1	-28.5	31.5	-14.1	25.3	-17.6	23.1	-14.2	13.1
5	-44.1	25.9	-28.5	31.9	-14.5	25.3	-17.8	22.9	-14.3	13.2
6	-43.6	26.0	-28.8	31.7	-14.1	25.2	-18.0	23.1	-14.2	13.2
7	-43.8	25.8	-28.4	31.9	-14.2	25.5	-17.8	23.1	-14.2	13.3
8	-44.5	25.5	-28.6	31.7	-14.0	25.3	-17.7	23.4	-14.2	13.2
9	-43.7	26.0	-28.4	31.6	-14.4	25.4	-18.0	22.9	-14.2	13.2
10	-44.2	25.9	-28.0	31.4	-14.6	25.1	-17.6	22.8	-14.2	13.3
11	-43.6	25.2	-28.4	31.9	-14.5	25.5	-17.6	23.3	-14.3	13.2
12	-44.2	25.5	-27.8	31.7	-14.5	25.3	-17.9	22.5	-14.2	13.2
13	-43.7	25.7	-28.7	31.8	-14.1	25.1	-18.0	22.8	-14.3	13.2
14	-43.9	26.0	-28.3	31.8	-14.3	25.2	-17.5	22.8	-14.3	13.3
15	-43.6	25.8	-28.4	31.6	-14.1	25.0	-17.4	22.9	-14.3	13.2
16	-44.0	25.3	-28.2	31.1	-	-	-	-	-	-
17	-42.9	25.5	-28.1	31.7	-	-	-	-	-	-
18	-44.3	25.4	-27.9	31.6	-	-	-	-	-	-
19	-44.0	25.1	-28.4	31.2	-	-	-	-	-	-
20	-44.0	25.4	-28.0	32.1	-	-	-	-	-	-
Aver.	-43.9	25.6	-28.3	31.6	-14.2	25.3	-17.8	23.0	-14.2	13.2

Table G-23. Peak strain data under HVS wheel path 1, trial 1, slab 2

Load	**OS3600** (Top)	**OS3600** (Bottom)	**Tokyo** (Top)	**Tokyo** (Bottom)	**Vishay** (Top)	**Vishay** (Bottom)	**Kyowa** (Top)	**Kyowa** (Bottom)	**CTL** (Top)	**CTL** (Bottom)
1	-104.5	50.9	-47.4	34.2	-66.8	29.7	-65.5	33.1	-28.5	38.5
2	-104.9	52.8	-47.4	34.2	-66.8	29.7	-65.5	33.1	-28.5	38.5
3	-104.5	53.5	-46.8	35.9	-69.2	30.5	-67.2	34.7	-29.1	39.3
4	-104.3	54.2	-47.9	37.2	-71.5	31.6	-70.2	34.8	-30.4	40.8
5	-103.5	53.7	-48.9	38.3	-74.7	32.5	-72.0	36.2	-31.4	42.4
6	-104.0	53.0	-49.1	39.0	-77.4	34.0	-73.8	36.9	-31.9	43.4
7	-104.4	53.9	-49.0	39.4	-77.0	34.1	-73.7	37.3	-32.2	43.2
8	-104.5	54.5	-49.2	39.3	-76.0	34.2	-72.3	37.5	-31.9	42.9
9	-104.2	53.9	-49.3	39.7	-75.6	34.2	-72.7	37.9	-32.0	43.1
10	-104.4	53.9	-49.5	39.9	-75.5	34.5	-73.4	37.6	-32.1	43.5
11	-105.8	54.0	-49.9	39.7	-77.9	33.8	-74.0	36.7	-32.3	43.7
12	-105.8	54.2	-49.6	40.1	-82.5	33.7	-74.4	36.7	-32.5	43.6
13	-105.4	54.0	-49.6	40.2	-82.2	34.3	-73.9	37.2	-32.5	43.8
14	-106.3	54.6	-50.4	40.5	-83.0	34.0	-74.0	36.8	-32.6	44.0
15	-106.3	54.6	-49.8	41.1	-82.4	34.5	-74.4	37.1	-32.8	43.9
16	-107.0	54.3	-	-	-	-	-	-	-	-
17	-107.2	54.6	-	-	-	-	-	-	-	-
18	-107.2	54.4	-	-	-	-	-	-	-	-
19	-107.4	54.1	-	-	-	-	-	-	-	-
20	-106.8	54.7	-	-	-	-	-	-	-	-
Aver.	-105.4	53.9	-49.0	38.9	-76.6	33.2	-72.3	36.5	-31.6	42.6

Table G-24. Peak strain data under HVS wheel path 1, trial 2, slab 2

Load	**OS3600** (Top)	**OS3600** (Bottom)	**Tokyo** (Top)	**Tokyo** (Bottom)	**Vishay** (Top)	**Vishay** (Bottom)	**Kyowa** (Top)	**Kyowa** (Bottom)	**CTL** (Top)	**CTL** (Bottom)
1	-116.9	61.5	-57.8	45.6	-89.7	42.2	-82.9	42.4	-41.2	49.8
2	-119.4	62.3	-57.2	45.4	-89.1	42.1	-82.5	41.8	-41.1	49.4
3	-118.6	62.8	-56.8	45.4	-91.1	41.5	-83.0	41.1	-41.1	49.3
4	-117.8	62.3	-57.2	45.6	-90.9	41.6	-82.8	41.5	-41.0	49.5
5	-117.6	61.8	-57.2	45.5	-91.4	42.0	-82.2	41.6	-41.0	49.6
6	-117.6	61.6	-57.0	45.4	-92.6	42.3	-82.7	42.5	-41.2	49.9
7	-119.5	62.5	-56.9	45.7	-91.5	42.6	-82.1	42.0	-41.1	49.5
8	-118.5	61.0	-57.1	45.5	-92.3	41.8	-83.0	41.9	-41.3	49.6
9	-118.6	61.7	-56.8	45.3	-92.5	42.1	-82.9	41.5	-41.0	49.6
10	-118.7	61.7	-57.1	45.4	-93.1	40.9	-82.9	40.7	-40.8	49.5
11	-118.2	62.1	-57.2	45.9	-93.4	41.7	-84.2	42.1	-41.2	50.0
12	-119.8	62.3	-57.1	45.4	-92.5	42.2	-82.6	41.7	-41.1	49.5
13	-119.3	61.7	-56.8	45.5	-92.9	42.1	-82.9	42.0	-41.1	49.6
14	-118.2	61.3	-56.5	45.6	-92.4	42.0	-82.1	42.2	-41.2	49.3
15	-118.4	61.2	-57.3	45.4	-92.5	42.5	-82.0	41.8	-41.2	49.6
16	-118.9	61.8	-	-	-	-	-	-	-	-
17	-118.6	61.8	-	-	-	-	-	-	-	-
18	-118.8	61.7	-	-	-	-	-	-	-	-
19	-117.2	61.8	-	-	-	-	-	-	-	-
20	-116.9	61.4	-	-	-	-	-	-	-	-
Aver.	-118.4	61.8	-57.1	45.5	-91.9	42.0	-82.7	41.8	-41.1	49.6

Table G-25. Peak strain data under HVS wheel path 1, trial 3, slab 2

Load	**OS3600** (Top)	**OS3600** (Bottom)	**Tokyo** (Top)	**Tokyo** (Bottom)	**Vishay** (Top)	**Vishay** (Bottom)	**Kyowa** (Top)	**Kyowa** (Bottom)	**CTL** (Top)	**CTL** (Bottom)
1	-119.4	77.1	-59.2	46.9	-92.9	44.8	-86.4	46.2	-42.0	50.6
2	-118.8	76.2	-59.3	47.3	-93.5	44.7	-86.7	46.6	-42.2	50.8
3	-118.3	75.9	-59.7	47.4	-94.5	44.8	-86.4	46.2	-42.0	50.6
4	-120.4	77.2	-60.0	46.8	-93.0	44.7	-86.1	46.4	-42.1	50.5
5	-118.6	77.3	-60.3	47.2	-95.9	45.0	-85.8	45.9	-42.0	50.6
6	-118.7	76.9	-60.0	46.5	-94.9	45.0	-85.0	46.1	-42.2	50.9
7	-118.7	76.8	-60.0	47.3	-95.6	45.2	-86.6	47.2	-42.2	50.8
8	-118.5	77.4	-59.6	47.1	-94.6	44.9	-85.5	45.9	-41.8	50.8
9	-117.8	77.6	-59.6	46.8	-94.5	44.7	-86.6	45.6	-42.1	50.4
10	-119.0	77.2	-59.6	46.9	-93.8	44.2	-86.1	46.0	-41.8	50.3
11	-118.7	77.1	-59.7	47.3	-94.5	44.6	-85.9	45.7	-41.8	50.7
12	-118.7	76.8	-59.7	47.2	-95.1	44.6	-87.5	46.0	-42.3	51.0
13	-119.4	77.5	-59.5	46.7	-94.7	43.8	-86.9	45.3	-42.0	50.5
14	-119.2	76.8	-59.5	47.2	-93.9	44.2	-86.9	45.1	-42.2	50.5
15	-119.3	77.1	-59.5	46.9	-93.7	44.4	-86.5	45.3	-41.9	50.5
16	-119.3	77.6	-	-	-	-	-	-	-	-
17	-119.0	77.2	-	-	-	-	-	-	-	-
18	-118.6	77.2	-	-	-	-	-	-	-	-
19	-118.2	77.6	-	-	-	-	-	-	-	-
20	-119.2	77.6	-	-	-	-	-	-	-	-
Aver.	-118.9	77.1	-59.7	47.0	-94.3	44.6	-86.3	46.0	-42.0	50.7

Table G-26. Peak strain data under HVS wheel path 1, trial 4, slab 2

Load	**OS3600** (Top)	**OS3600** (Bottom)	**Tokyo** (Top)	**Tokyo** (Bottom)	**Vishay** (Top)	**Vishay** (Bottom)	**Kyowa** (Top)	**Kyowa** (Bottom)	**CTL** (Top)	**CTL** (Bottom)
1	-118.2	92.1	-62.2	46.7	-97.1	49.0	-86.0	50.3	-43.8	51.3
2	-118.0	91.0	-62.2	46.6	-96.3	48.7	-84.9	49.5	-43.4	51.0
3	-118.6	91.3	-61.6	46.2	-95.9	47.4	-87.2	48.5	-43.6	50.9
4	-117.5	91.2	-61.8	46.3	-95.8	46.1	-86.6	47.5	-43.5	50.9
5	-119.5	92.8	-61.9	46.6	-95.9	47.4	-86.7	47.5	-43.7	51.2
6	-119.3	90.9	-62.0	46.5	-96.6	46.9	-86.8	47.7	-43.7	51.1
7	-119.5	91.9	-62.1	46.5	-95.6	46.6	-87.6	48.0	-43.6	51.1
8	-118.7	91.5	-62.3	46.6	-95.6	46.9	-86.3	48.5	-43.5	51.1
9	-118.1	90.9	-61.8	46.4	-94.9	46.6	-87.4	47.8	-43.4	50.8
10	-118.5	92.7	-62.5	46.8	-94.9	46.3	-86.8	47.8	-43.5	51.1
11	-118.5	92.0	-62.1	46.5	-96.3	46.2	-87.4	47.0	-43.6	51.1
12	-118.6	91.8	-61.4	46.6	-97.7	46.0	-87.9	47.9	-43.8	51.2
13	-118.1	91.8	-62.4	46.7	-98.1	45.4	-87.9	47.5	-43.6	51.1
14	-118.1	90.8	-62.0	46.4	-97.9	45.5	-88.0	47.4	-43.6	51.0
15	-118.3	91.0	-62.2	46.7	-97.3	45.0	-87.6	46.9	-43.5	50.9
16	-119.9	92.9	-	-	-	-	-	-	-	-
17	-120.0	91.4	-	-	-	-	-	-	-	-
18	-119.3	92.3	-	-	-	-	-	-	-	-
19	-118.5	91.2	-	-	-	-	-	-	-	-
20	-119.5	90.4	-	-	-	-	-	-	-	-
Aver.	-118.7	91.6	-62.0	46.5	-96.4	46.7	-87.0	48.0	-43.6	51.0

Table G-27. Peak strain data under HVS wheel path 1, trial 5, slab 2

Load	**OS3600** (Top)	**OS3600** (Bottom)	**Tokyo** (Top)	**Tokyo** (Bottom)	**Vishay** (Top)	**Vishay** (Bottom)	**Kyowa** (Top)	**Kyowa** (Bottom)	**CTL** (Top)	**CTL** (Bottom)
1	-115.4	103.5	-66.5	47.4	-95.6	48.8	-84.7	45.8	-44.9	52.2
2	-115.0	103.1	-65.7	46.8	-95.5	48.7	-84.9	46.3	-44.9	51.9
3	-115.6	102.7	-66.8	47.0	-96.0	49.2	-84.6	46.3	-45.0	52.2
4	-115.4	103.4	-66.0	46.6	-95.8	49.3	-85.1	45.7	-45.0	51.9
5	-115.8	103.4	-66.0	46.9	-95.5	49.2	-84.6	46.1	-44.8	52.0
6	-114.9	104.1	-66.2	47.2	-96.4	49.2	-84.4	45.4	-45.0	52.2
7	-115.4	103.7	-65.9	46.8	-97.4	48.7	-85.8	46.1	-45.0	52.1
8	-115.0	103.1	-66.4	47.0	-96.7	49.0	-84.9	45.8	-45.1	51.9
9	-115.4	104.1	-66.4	46.9	-97.3	48.9	-85.3	46.1	-45.1	52.0
10	-114.8	103.9	-66.5	47.3	-97.6	48.2	-85.2	45.1	-45.0	51.8
11	-115.5	103.2	-66.4	46.9	-99.4	48.5	-84.9	45.3	-45.1	52.4
12	-116.2	103.3	-66.4	47.3	-99.4	48.5	-85.1	46.3	-45.1	52.1
13	-115.8	102.3	-66.4	47.6	-100.0	48.3	-85.6	45.4	-45.1	52.2
14	-115.0	102.5	-66.5	47.1	-98.9	48.5	-85.4	46.1	-45.1	51.9
15	-115.9	102.5	-66.1	47.7	-99.4	48.4	-85.8	45.7	-44.8	52.1
16	-116.0	102.6	-	-	-	-	-	-	-	-
17	-115.4	102.9	-	-	-	-	-	-	-	-
18	-115.6	103.4	-	-	-	-	-	-	-	-
19	-115.7	103.2	-	-	-	-	-	-	-	-
20	-116.3	104.4	-	-	-	-	-	-	-	-
Aver.	-115.5	103.3	-66.3	47.1	-97.4	48.8	-85.1	45.8	-45.0	52.1

Table G-28. Peak strain data under HVS wheel path 1, trial 6, slab 2

Load	**OS3600** (Top)	**OS3600** (Bottom)	**Tokyo** (Top)	**Tokyo** (Bottom)	**Vishay** (Top)	**Vishay** (Bottom)	**Kyowa** (Top)	**Kyowa** (Bottom)	**CTL** (Top)	**CTL** (Bottom)
1	-119.5	108.3	-70.3	46.8	-97.2	49.3	-87.9	45.0	-46.9	52.7
2	-120.6	107.6	-70.2	46.9	-97.1	49.4	-88.4	45.0	-47.1	52.6
3	-119.3	108.9	-70.0	47.1	-97.7	48.9	-88.7	44.6	-47.1	52.8
4	-119.3	108.3	-70.0	46.8	-97.4	48.7	-88.3	44.9	-46.9	52.9
5	-118.8	107.3	-70.0	46.8	-97.9	48.9	-87.5	44.6	-47.3	52.8
6	-120.2	108.0	-70.4	46.9	-97.9	48.8	-88.7	45.3	-47.0	52.5
7	-120.2	109.0	-69.9	46.9	-97.5	48.7	-88.7	45.4	-47.1	52.5
8	-120.0	108.3	-70.0	46.4	-97.0	49.0	-88.5	45.4	-47.0	52.6
9	-119.3	108.1	-70.1	47.0	-97.3	49.1	-88.5	44.6	-47.0	52.5
10	-120.0	107.3	-69.9	46.3	-97.3	49.1	-87.7	44.6	-47.1	52.9
11	-120.4	108.7	-69.9	46.9	-97.9	49.1	-88.7	45.0	-47.0	52.7
12	-119.5	108.7	-70.7	47.0	-97.8	48.9	-88.4	44.7	-47.1	52.4
13	-118.3	108.4	-70.2	46.3	-97.7	49.1	-89.1	44.5	-47.1	52.4
14	-118.7	108.0	-70.6	46.9	-97.4	49.0	-88.0	44.5	-46.9	52.5
15	-119.0	108.9	-69.4	46.9	-97.4	48.5	-89.1	45.1	-47.0	52.6
16	-120.6	108.7	-	-	-	-	-	-	-	-
17	-120.1	108.3	-	-	-	-	-	-	-	-
18	-119.4	109.4	-	-	-	-	-	-	-	-
19	-119.1	108.4	-	-	-	-	-	-	-	-
20	-118.7	107.6	-	-	-	-	-	-	-	-
Aver.	-119.5	108.3	-70.1	46.8	-97.5	49.0	-88.4	44.9	-47.0	52.6

Table G-29. Peak strain data under HVS wheel path 1, trial 7, slab 2

Load	**OS3600** (Top)	**OS3600** (Bottom)	**Tokyo** (Top)	**Tokyo** (Bottom)	**Vishay** (Top)	**Vishay** (Bottom)	**Kyowa** (Top)	**Kyowa** (Bottom)	**CTL** (Top)	**CTL** (Bottom)
1	-122.3	112.5	-69.9	46.5	-100.3	36.5	-90.9	44.8	-49.7	53.9
2	-122.3	112.6	-70.2	46.6	-99.2	36.7	-90.1	44.7	-49.5	53.9
3	-121.6	111.3	-69.7	46.5	-99.6	36.5	-90.6	44.2	-49.5	53.9
4	-120.5	110.9	-70.6	46.3	-99.4	36.2	-90.3	43.9	-49.5	53.6
5	-123.5	113.2	-69.5	46.8	-99.1	36.7	-90.4	44.3	-49.5	53.9
6	-122.1	112.8	-70.1	46.6	-99.2	36.7	-90.1	44.7	-49.8	54.0
7	-122.4	112.7	-70.4	46.9	-100.4	36.5	-89.9	44.6	-49.8	53.9
8	-121.2	112.6	-69.2	46.7	-99.4	36.7	-89.8	44.5	-49.6	53.8
9	-120.1	112.8	-70.0	46.8	-99.5	37.1	-89.7	44.4	-49.6	54.1
10	-121.7	113.3	-69.7	46.6	-99.2	37.2	-90.7	45.3	-49.8	54.0
11	-122.1	112.5	-70.0	46.7	-99.3	36.4	-89.7	44.5	-49.6	54.0
12	-121.4	111.8	-70.3	47.0	-99.1	37.3	-90.4	44.4	-49.7	53.9
13	-121.2	111.0	-70.2	46.5	-99.0	36.9	-89.5	44.4	-49.7	53.7
14	-121.1	111.8	-69.9	46.7	-99.0	37.0	-89.3	44.2	-49.8	53.9
15	-121.9	113.0	-69.5	47.2	-99.9	37.0	-90.1	44.8	-49.8	54.0
16	-122.0	112.8	-	-	-	-	-	-	-	-
17	-122.6	113.2	-	-	-	-	-	-	-	-
18	-122.9	111.5	-	-	-	-	-	-	-	-
19	-121.2	112.2	-	-	-	-	-	-	-	-
20	-122.6	113.6	-	-	-	-	-	-	-	-
Aver.	-121.8	112.4	-69.9	46.7	-99.5	36.8	-90.1	44.5	-49.7	53.9

Table G-30. Peak strain data under HVS wheel path 1, trial 8, slab 2

Load	**OS3600** (Top)	**OS3600** (Bottom)	**Tokyo** (Top)	**Tokyo** (Bottom)	**Vishay** (Top)	**Vishay** (Bottom)	**Kyowa** (Top)	**Kyowa** (Bottom)	**CTL** (Top)	**CTL** (Bottom)
1	-127.7	114.1	-69.9	46.6	-105.4	50.0	-96.2	45.1	-53.4	55.7
2	-126.5	113.1	-70.2	46.7	-105.9	50.7	-95.6	45.0	-53.3	55.6
3	-129.0	116.2	-69.8	46.2	-105.4	50.5	-95.8	45.1	-53.3	55.6
4	-128.5	114.2	-70.3	46.3	-105.8	50.3	-95.3	44.3	-53.4	55.8
5	-127.5	113.8	-69.9	46.3	-105.2	50.7	-96.2	45.6	-53.2	55.8
6	-128.0	114.9	-69.9	46.6	-105.1	51.0	-94.9	45.3	-53.4	55.5
7	-128.0	114.3	-70.2	46.2	-106.1	50.5	-95.4	45.5	-53.5	55.6
8	-127.9	113.9	-70.1	46.2	-105.7	50.6	-95.9	45.4	-53.4	55.5
9	-129.6	113.1	-69.9	46.0	-104.7	50.7	-95.1	45.4	-53.2	55.5
10	-128.0	114.9	-69.8	46.3	-104.8	50.6	-94.9	45.4	-53.4	55.5
11	-128.0	114.7	-69.4	46.5	-104.6	50.7	-95.2	45.4	-53.4	55.6
12	-127.4	115.2	-70.4	46.3	-104.9	50.3	-95.1	45.3	-53.3	55.4
13	-128.8	115.3	-70.0	46.1	-104.5	50.7	-95.2	45.4	-53.3	55.4
14	-129.0	113.6	-69.8	46.3	-104.3	51.0	-95.4	44.9	-53.4	55.3
15	-128.2	113.9	-69.9	46.5	-105.1	50.8	-94.6	45.4	-53.5	55.7
16	-128.1	114.5	-	-	-	-	-	-	-	-
17	-127.9	114.5	-	-	-	-	-	-	-	-
18	-128.7	113.2	-	-	-	-	-	-	-	-
19	-129.0	114.7	-	-	-	-	-	-	-	-
20	-129.1	114.7	-	-	-	-	-	-	-	-
Aver.	-128.3	114.3	-70.0	46.3	-105.2	50.6	-95.4	45.2	-53.4	55.6

Table G-31. Peak strain data under HVS wheel path 1, trial 9, slab 2

Load	**OS3600** (Top)	**OS3600** (Bottom)	**Tokyo** (Top)	**Tokyo** (Bottom)	**Vishay** (Top)	**Vishay** (Bottom)	**Kyowa** (Top)	**Kyowa** (Bottom)	**CTL** (Top)	**CTL** (Bottom)
1	-132.6	115.6	-66.6	45.6	-110.4	51.2	-98.8	45.0	-56.7	55.6
2	-133.1	116.8	-66.4	45.3	-110.5	51.0	-98.9	45.0	-56.7	55.6
3	-133.6	115.6	-65.8	45.5	-109.7	50.9	-98.6	44.8	-56.6	55.8
4	-132.2	114.3	-66.4	45.4	-110.2	51.0	-98.0	44.6	-56.6	55.8
5	-134.4	115.9	-65.8	45.5	-109.6	51.3	-99.5	45.0	-56.7	55.8
6	-133.2	116.2	-66.3	45.4	-109.6	51.0	-98.7	44.5	-56.5	55.5
7	-133.2	115.5	-65.9	45.3	-109.4	50.9	-98.6	44.3	-56.5	55.2
8	-132.1	116.2	-65.9	45.4	-108.9	51.3	-98.2	44.9	-56.4	55.5
9	-133.3	115.3	-66.1	45.4	-109.6	51.3	-97.5	44.6	-56.6	55.5
10	-132.2	115.2	-65.4	45.3	-109.1	51.3	-98.3	45.2	-56.2	55.3
11	-133.1	116.0	-65.7	45.1	-109.0	51.1	-98.4	44.8	-56.4	55.5
12	-134.0	115.8	-66.0	45.1	-108.9	50.8	-98.1	44.3	-56.4	55.3
13	-132.6	114.8	-65.9	45.0	-109.3	51.4	-98.2	45.2	-56.5	55.8
14	-132.9	115.8	-66.3	45.6	-108.7	50.7	-97.9	45.1	-56.4	55.4
15	-132.3	114.7	-65.7	45.2	-109.5	51.2	-98.1	44.8	-56.5	55.3
16	-129.9	115.4	-	-	-	-	-	-	-	-
17	-133.8	116.6	-	-	-	-	-	-	-	-
18	-132.7	115.7	-	-	-	-	-	-	-	-
19	-132.8	116.4	-	-	-	-	-	-	-	-
20	-130.9	115.7	-	-	-	-	-	-	-	-
Aver.	-132.7	115.7	-66.0	45.4	-109.5	51.1	-98.4	44.8	-56.5	55.5

Table G-32. Peak strain data under HVS wheel path 1, trial 10, slab 2

Load	**OS3600** (Top)	**OS3600** (Bottom)	**Tokyo** (Top)	**Tokyo** (Bottom)	**Vishay** (Top)	**Vishay** (Bottom)	**Kyowa** (Top)	**Kyowa** (Bottom)	**CTL** (Top)	**CTL** (Bottom)
1	-133.5	117.8	-62.6	44.9	-111.3	51.4	-98.0	44.8	-58.1	55.3
2	-134.9	116.1	-62.3	44.9	-110.7	51.3	-98.0	44.9	-58.1	54.9
3	-131.7	117.3	-62.9	44.9	-112.1	51.8	-97.3	44.7	-58.4	55.6
4	-132.2	117.8	-62.3	44.7	-111.8	51.3	-98.5	44.9	-58.1	55.2
5	-133.6	118.1	-62.6	44.5	-110.4	51.6	-98.5	44.4	-58.0	54.9
6	-134.2	117.1	-62.0	44.9	-110.9	51.2	-98.5	44.9	-58.3	55.3
7	-132.8	117.4	-62.6	45.1	-111.7	51.3	-98.7	44.8	-58.4	55.2
8	-132.5	115.4	-62.0	44.6	-111.5	51.3	-98.8	44.7	-58.2	55.2
9	-131.6	117.4	-61.8	44.8	-111.2	52.0	-98.0	44.8	-58.2	54.8
10	-134.4	117.8	-62.4	45.3	-111.5	51.8	-98.2	45.3	-58.2	55.1
11	-133.9	117.6	-62.1	45.5	-111.6	52.2	-97.6	44.7	-58.5	55.4
12	-132.3	118.0	-61.9	44.9	-111.2	51.6	-98.8	44.9	-58.2	55.0
13	-132.8	117.1	-62.0	44.9	-110.5	50.9	-98.0	44.8	-58.0	54.7
14	-133.5	117.8	-62.5	45.1	-111.7	52.0	-98.4	44.7	-58.3	55.3
15	-133.6	115.5	-62.7	44.9	-112.0	51.6	-99.0	44.5	-58.3	55.4
16	-134.3	117.0	-	-	-	-	-	-	-	-
17	-133.0	117.3	-	-	-	-	-	-	-	-
18	-131.9	116.5	-	-	-	-	-	-	-	-
19	-134.7	117.0	-	-	-	-	-	-	-	-
20	-133.7	117.6	-	-	-	-	-	-	-	-
Aver.	-133.3	117.2	-62.3	44.9	-111.3	51.6	-98.3	44.8	-58.2	55.2

Table G-33. Peak strain data under HVS wheel path 1, trial 11, slab 2

Load	**OS3600** (Top)	**OS3600** (Bottom)	**Tokyo** (Top)	**Tokyo** (Bottom)	**Vishay** (Top)	**Vishay** (Bottom)	**Kyowa** (Top)	**Kyowa** (Bottom)	**CTL** (Top)	**CTL** (Bottom)
1	-132.8	118.3	-58.6	45.6	-111.5	52.3	-98.1	45.1	-59.5	55.0
2	-133.1	116.6	-58.8	45.5	-111.2	51.8	-97.7	44.4	-59.6	54.7
3	-131.7	116.6	-59.3	45.8	-111.4	51.9	-98.0	44.4	-59.6	54.8
4	-132.5	117.4	-59.7	46.0	-111.7	51.8	-97.7	44.7	-59.6	55.1
5	-132.9	118.7	-58.9	45.7	-111.4	51.6	-98.3	45.2	-59.5	54.8
6	-132.4	118.7	-59.2	45.7	-111.8	52.0	-97.9	45.2	-59.8	54.9
7	-130.6	119.5	-59.6	45.8	-111.7	51.9	-98.3	44.9	-59.8	54.9
8	-132.2	118.2	-59.0	45.4	-111.8	52.1	-97.8	45.2	-59.6	54.9
9	-132.4	117.9	-59.9	45.5	-111.1	51.9	-97.5	45.1	-59.6	54.9
10	-132.9	115.4	-58.8	45.3	-111.1	51.9	-97.5	45.1	-59.5	54.6
11	-134.0	117.5	-59.3	45.5	-111.5	52.2	-97.8	44.8	-59.8	55.1
12	-132.7	118.2	-59.1	45.5	-112.5	52.1	-98.2	45.0	-59.8	54.9
13	-133.3	116.1	-59.3	45.6	-112.7	51.9	-97.2	45.3	-59.6	55.0
14	-133.2	117.9	-59.1	45.3	-112.2	52.1	-96.9	44.3	-59.7	54.7
15	-132.0	117.5	-58.6	45.6	-111.0	51.4	-97.7	44.9	-59.5	54.7
16	-132.2	117.1	-	-	-	-	-	-	-	-
17	-131.9	116.8	-	-	-	-	-	-	-	-
18	-133.0	117.3	-	-	-	-	-	-	-	-
19	-132.4	117.3	-	-	-	-	-	-	-	-
20	-133.4	117.1	-	-	-	-	-	-	-	-
Aver.	-132.6	117.5	-59.1	45.6	-111.6	51.9	-97.8	44.9	-59.6	54.9

Table G-34. Peak strain data under HVS wheel path 1, trial 12, slab 2

Load	**OS3600** (Top)	**OS3600** (Bottom)	**Tokyo** (Top)	**Tokyo** (Bottom)	**Vishay** (Top)	**Vishay** (Bottom)	**Kyowa** (Top)	**Kyowa** (Bottom)	**CTL** (Top)	**CTL** (Bottom)
1	-133.8	119.6	-55.6	45.9	-111.8	52.7	-97.1	45.3	-60.9	54.4
2	-133.3	119.6	-55.9	45.5	-111.9	52.8	-97.7	45.3	-60.9	54.7
3	-131.1	120.0	-56.4	46.4	-112.5	52.9	-97.4	45.5	-61.1	54.7
4	-135.4	119.4	-56.5	46.0	-112.2	52.5	-98.5	45.3	-61.1	54.8
5	-133.5	119.6	-56.1	46.1	-112.0	52.5	-97.5	45.2	-61.0	54.4
6	-133.5	120.5	-55.9	45.8	-112.1	52.5	-97.4	45.1	-61.1	54.4
7	-134.6	119.6	-56.6	46.1	-112.6	52.6	-97.0	44.8	-60.9	54.8
8	-135.5	120.3	-56.4	45.7	-112.8	52.8	-96.5	44.4	-61.2	54.9
9	-133.1	119.4	-55.5	46.1	-111.5	52.4	-96.9	45.9	-60.9	54.3
10	-132.2	118.0	-56.1	45.9	-112.2	52.4	-97.3	45.6	-61.0	54.6
11	-135.4	119.0	-56.2	46.1	-112.8	52.7	-97.0	45.5	-61.1	54.5
12	-134.1	119.1	-56.4	46.0	-112.8	52.1	-97.4	45.6	-61.0	54.7
13	-134.0	119.0	-56.3	46.0	-112.6	52.6	-98.1	44.8	-61.1	54.7
14	-134.1	118.5	-56.4	46.0	-111.5	52.4	-97.7	45.2	-61.1	54.3
15	-132.7	117.4	-56.2	46.1	-112.3	52.3	-96.9	45.5	-61.0	54.9
16	-133.3	120.5	-	-	-	-	-	-	-	-
17	-135.0	120.2	-	-	-	-	-	-	-	-
18	-133.5	119.5	-	-	-	-	-	-	-	-
19	-132.7	119.2	-	-	-	-	-	-	-	-
20	-132.7	117.7	-	-	-	-	-	-	-	-
Aver.	-133.7	119.3	-56.2	46.0	-112.2	52.6	-97.4	45.3	-61.0	54.6

Table G-35. Peak strain data under HVS wheel path 1, trial 13, slab 2

Load	**OS3600** (Top)	**OS3600** (Bottom)	**Tokyo** (Top)	**Tokyo** (Bottom)	**Vishay** (Top)	**Vishay** (Bottom)	**Kyowa** (Top)	**Kyowa** (Bottom)	**CTL** (Top)	**CTL** (Bottom)
1	-133.9	120.4	-53.1	47.0	-112.1	52.7	-97.1	43.8	-62.5	54.2
2	-134.2	120.4	-52.5	46.9	-112.0	52.2	-96.9	43.8	-62.3	53.8
3	-133.8	120.6	-52.5	46.5	-111.2	52.1	-96.7	43.3	-62.2	53.6
4	-132.5	119.6	-52.9	47.1	-111.7	52.3	-97.2	43.3	-62.3	54.0
5	-134.3	119.1	-51.9	45.9	-111.5	51.9	-96.9	43.6	-62.1	53.5
6	-134.4	121.2	-53.2	46.4	-112.7	52.7	-97.1	43.8	-62.7	54.2
7	-134.7	119.4	-53.2	46.4	-111.9	52.2	-97.1	43.3	-62.5	53.9
8	-133.7	120.9	-53.2	46.8	-111.8	52.5	-96.6	43.6	-62.4	54.0
9	-133.3	120.3	-52.8	46.6	-112.3	52.2	-96.4	43.7	-62.3	54.1
10	-132.2	120.4	-52.0	45.9	-111.1	52.4	-96.4	44.0	-62.2	53.5
11	-134.2	120.8	-52.7	46.6	-111.4	52.5	-96.6	43.7	-62.3	53.9
12	-134.3	120.5	-52.3	47.2	-111.4	52.5	-96.3	43.6	-62.4	53.7
13	-135.2	118.9	-52.5	46.7	-112.1	52.6	-96.8	43.5	-62.6	54.0
14	-133.9	120.4	-52.7	46.6	-111.7	52.7	-95.8	43.3	-62.5	54.0
15	-133.8	120.6	-52.0	46.5	-111.5	52.3	-96.8	43.7	-62.2	53.5
16	-133.6	120.8	-	-	-	-	-	-	-	-
17	-133.3	120.6	-	-	-	-	-	-	-	-
18	-133.3	120.0	-	-	-	-	-	-	-	-
19	-133.4	121.1	-	-	-	-	-	-	-	-
20	-134.6	121.0	-	-	-	-	-	-	-	-
Aver.	-133.8	120.4	-52.6	46.6	-111.8	52.4	-96.7	43.6	-62.4	53.9

Table G-36. Peak strain data under HVS wheel path 1, trial 14, slab 2

Load	**OS3600** (Top)	**OS3600** (Bottom)	**Tokyo** (Top)	**Tokyo** (Bottom)	**Vishay** (Top)	**Vishay** (Bottom)	**Kyowa** (Top)	**Kyowa** (Bottom)	**CTL** (Top)	**CTL** (Bottom)
1	-133.3	119.4	-50.6	46.9	-112.2	52.7	-96.6	42.2	-64.0	53.5
2	-131.1	118.7	-50.9	46.9	-111.8	52.9	-96.5	42.6	-63.9	53.2
3	-133.7	119.2	-50.5	46.5	-112.0	52.6	-96.9	42.3	-63.9	53.3
4	-133.6	119.4	-50.6	47.1	-111.6	53.3	-96.5	42.0	-64.0	53.1
5	-132.9	119.3	-50.5	47.0	-111.9	52.7	-95.9	42.2	-63.9	53.4
6	-134.0	119.6	-50.0	46.6	-111.3	52.4	-96.7	42.4	-63.7	53.2
7	-133.5	120.0	-50.0	47.1	-111.7	52.8	-96.8	42.3	-64.0	53.4
8	-133.6	119.2	-51.0	47.2	-112.5	52.9	-96.4	42.5	-64.0	53.5
9	-132.5	118.6	-49.9	46.5	-111.3	52.4	-96.5	42.0	-64.0	52.9
10	-133.7	119.5	-50.4	46.9	-111.7	52.8	-95.7	42.4	-64.1	53.4
11	-135.0	118.9	-50.9	47.4	-111.5	52.9	-96.4	42.1	-63.8	53.2
12	-135.5	118.5	-50.2	47.1	-111.5	52.6	-95.9	41.7	-63.8	53.0
13	-133.0	119.6	-50.3	47.0	-111.9	52.9	-97.0	42.5	-64.0	53.3
14	-134.2	119.3	-51.1	46.8	-112.3	52.6	-96.6	42.2	-64.0	53.2
15	-133.1	118.7	-50.5	46.8	-111.9	52.5	-96.6	42.4	-63.9	53.1
16	-132.3	118.5	-	-	-	-	-	-	-	-
17	-132.7	117.7	-	-	-	-	-	-	-	-
18	-135.1	119.4	-	-	-	-	-	-	-	-
19	-134.3	119.9	-	-	-	-	-	-	-	-
20	-134.3	120.0	-	-	-	-	-	-	-	-
Aver.	-133.6	119.2	-50.5	46.9	-111.8	52.7	-96.5	42.3	-63.9	53.2

Table G-37. Peak strain data under HVS wheel path 1, trial 15, slab 2

Load	**OS3600** (Top)	**OS3600** (Bottom)	**Tokyo** (Top)	**Tokyo** (Bottom)	**Vishay** (Top)	**Vishay** (Bottom)	**Kyowa** (Top)	**Kyowa** (Bottom)	**CTL** (Top)	**CTL** (Bottom)
1	-134.3	117.8	-46.8	46.1	-111.1	52.6	-94.7	40.8	-64.3	53.5
2	-133.3	117.5	-47.1	45.8	-110.6	52.4	-95.0	41.0	-64.3	53.4
3	-134.9	116.7	-47.1	46.1	-110.8	52.8	-95.7	40.8	-64.5	53.3
4	-134.4	116.7	-46.9	45.7	-111.2	52.4	-95.1	40.8	-64.2	53.3
5	-133.4	116.4	-46.3	46.5	-110.7	52.7	-94.8	41.0	-64.2	53.1
6	-135.2	115.9	-46.7	46.0	-110.7	52.5	-94.6	41.3	-64.2	53.1
7	-132.5	117.3	-46.9	46.5	-111.0	53.1	-94.8	41.0	-64.4	53.3
8	-133.9	117.5	-47.0	46.0	-111.4	52.8	-95.0	40.7	-64.4	53.4
9	-135.0	116.3	-46.7	46.2	-111.0	52.4	-94.5	40.8	-64.3	53.2
10	-132.6	117.1	-47.0	46.2	-111.2	52.8	-94.8	40.7	-64.3	53.4
11	-131.4	115.9	-46.7	46.1	-110.8	52.5	-95.4	41.5	-64.1	53.2
12	-134.6	115.9	-47.1	46.0	-110.6	52.5	-95.0	40.9	-64.3	53.1
13	-134.3	117.1	-47.1	46.2	-110.8	52.9	-94.9	41.0	-64.5	53.3
14	-133.7	117.0	-46.5	45.9	-110.9	52.4	-94.7	40.9	-64.3	53.0
15	-131.2	117.6	-46.6	45.9	-111.3	52.9	-94.1	40.7	-64.4	53.5
16	-132.4	116.5	-	-	-	-	-	-	-	-
17	-133.9	117.9	-	-	-	-	-	-	-	-
18	-132.5	117.4	-	-	-	-	-	-	-	-
19	-133.7	117.4	-	-	-	-	-	-	-	-
20	-134.1	115.9	-	-	-	-	-	-	-	-
Aver.	-133.6	116.9	-46.8	46.1	-110.9	52.6	-94.9	40.9	-64.3	53.3

Table G-38. Peak strain data under HVS wheel path 1, trial 16, slab 2

Load	**OS3600** (Top)	**OS3600** (Bottom)	**Tokyo** (Top)	**Tokyo** (Bottom)	**Vishay** (Top)	**Vishay** (Bottom)	**Kyowa** (Top)	**Kyowa** (Bottom)	**CTL** (Top)	**CTL** (Bottom)
1	-134.7	116.7	-43.6	45.7	-109.9	51.8	-94.4	39.7	-64.5	52.8
2	-133.6	115.1	-43.4	46.2	-110.3	53.0	-94.4	39.7	-64.7	53.1
3	-133.2	117.0	-43.4	46.3	-109.3	52.4	-95.3	40.2	-64.6	53.0
4	-135.1	117.8	-44.0	46.5	-109.8	52.8	-94.9	40.5	-64.7	52.9
5	-135.4	116.0	-42.9	45.9	-109.4	52.4	-94.2	40.7	-64.6	52.8
6	-132.5	116.6	-43.5	46.4	-109.1	52.6	-94.2	40.0	-64.7	53.0
7	-133.2	116.0	-42.9	45.9	-109.8	52.7	-93.8	39.6	-64.5	53.0
8	-130.6	118.7	-43.1	46.1	-109.5	52.9	-94.5	40.4	-64.5	52.9
9	-134.4	116.7	-43.8	46.5	-110.7	52.9	-94.6	40.4	-64.6	53.1
10	-134.5	118.0	-43.4	46.0	-109.5	52.6	-94.6	40.6	-64.6	52.9
11	-134.8	117.0	-43.6	46.0	-109.7	52.8	-94.0	40.4	-64.6	52.9
12	-133.0	116.3	-43.5	46.2	-109.2	52.9	-93.9	40.3	-64.7	52.9
13	-133.9	116.9	-43.2	46.3	-109.6	53.1	-94.8	40.5	-64.6	52.9
14	-134.0	116.7	-43.4	46.2	-110.1	53.1	-94.4	40.3	-64.7	53.1
15	-133.3	116.9	-43.5	46.1	-109.8	53.1	-93.7	40.6	-64.6	53.2
16	-133.5	116.3	-	-	-	-	-	-	-	-
17	-132.5	117.1	-	-	-	-	-	-	-	-
18	-134.4	117.1	-	-	-	-	-	-	-	-
19	-132.5	117.7	-	-	-	-	-	-	-	-
20	-133.8	116.5	-	-	-	-	-	-	-	-
Aver.	-133.6	116.9	-43.4	46.2	-109.7	52.7	-94.4	40.3	-64.6	53.0

Table G-39. Peak strain data under HVS wheel path 1, trial 17, slab 2

Load	**OS3600** (Top)	**OS3600** (Bottom)	**Tokyo** (Top)	**Tokyo** (Bottom)	**Vishay** (Top)	**Vishay** (Bottom)	**Kyowa** (Top)	**Kyowa** (Bottom)	**CTL** (Top)	**CTL** (Bottom)
1	-134.2	118.4	-39.7	45.7	-110.3	52.9	-94.4	39.3	-65.6	52.9
2	-132.8	118.7	-39.9	45.8	-110.0	53.5	-93.8	39.6	-65.8	53.2
3	-134.1	116.2	-39.7	46.1	-110.1	53.0	-94.4	40.2	-65.7	52.9
4	-132.6	116.7	-40.3	46.0	-109.9	53.4	-93.9	40.1	-65.5	53.2
5	-133.7	117.8	-40.2	46.2	-110.3	53.5	-94.6	39.8	-65.6	53.0
6	-133.6	118.3	-40.5	45.8	-109.8	53.0	-93.7	39.2	-65.6	52.9
7	-134.1	118.3	-39.8	45.4	-109.4	53.0	-93.7	39.5	-65.5	52.6
8	-133.3	116.9	-39.8	46.4	-110.2	53.3	-94.3	39.9	-65.7	53.2
9	-134.1	116.8	-40.6	46.2	-109.9	53.3	-94.3	39.6	-65.8	52.9
10	-135.0	117.7	-40.1	46.1	-109.5	53.4	-94.7	39.9	-65.7	52.8
11	-133.6	118.8	-39.5	46.2	-109.8	53.1	-93.6	39.5	-65.6	53.1
12	-135.3	118.6	-40.0	45.9	-110.2	53.6	-93.1	39.6	-65.8	53.2
13	-134.7	117.6	-39.9	45.8	-109.8	53.2	-94.2	40.1	-65.6	52.9
14	-131.0	117.5	-40.2	46.2	-110.4	53.1	-94.2	39.9	-65.6	53.3
15	-133.2	117.2	-40.1	45.5	-110.6	53.3	-94.3	39.5	-65.8	52.9
16	-132.7	117.4	-	-	-	-	-	-	-	-
17	-132.1	118.4	-	-	-	-	-	-	-	-
18	-132.9	118.5	-	-	-	-	-	-	-	-
19	-132.8	118.9	-	-	-	-	-	-	-	-
20	-133.1	117.2	-	-	-	-	-	-	-	-
Aver.	-133.4	117.8	-40.0	46.0	-110.0	53.2	-94.1	39.7	-65.7	53.0

Table G-40. Peak strain data under HVS wheel path 1, trial 18, slab 2

Load	**OS3600** (Top)	**OS3600** (Bottom)	**Tokyo** (Top)	**Tokyo** (Bottom)	**Vishay** (Top)	**Vishay** (Bottom)	**Kyowa** (Top)	**Kyowa** (Bottom)	**CTL** (Top)	**CTL** (Bottom)
1	-132.8	117.8	-36.3	46.6	-109.0	54.4	-93.5	39.5	-66.8	52.8
2	-132.9	118.5	-36.4	47.2	-108.6	53.8	-93.6	39.1	-66.7	52.8
3	-132.5	117.2	-36.4	47.1	-109.0	54.0	-93.7	39.2	-66.7	52.6
4	-133.5	118.8	-37.0	46.7	-108.9	53.6	-93.2	39.8	-66.8	52.9
5	-134.3	119.4	-36.6	46.8	-109.4	54.2	-93.6	39.8	-66.9	52.7
6	-134.1	118.9	-36.1	47.2	-108.9	54.3	-93.0	39.4	-66.8	52.5
7	-132.9	118.5	-36.6	46.8	-109.6	54.5	-93.4	39.6	-66.9	53.0
8	-133.6	116.8	-36.4	47.5	-109.0	54.1	-94.5	39.9	-66.8	52.9
9	-131.9	117.4	-37.3	46.9	-109.6	53.8	-93.5	40.3	-66.9	52.7
10	-134.0	118.2	-36.6	47.0	-108.7	54.2	-93.7	39.6	-66.8	52.7
11	-132.6	118.7	-37.2	47.4	-108.5	54.5	-93.2	39.2	-66.7	52.7
12	-133.0	118.4	-36.9	47.2	-108.7	54.0	-93.8	40.1	-66.6	52.8
13	-131.8	118.2	-37.4	46.8	-108.7	54.3	-93.6	39.5	-66.9	53.1
14	-133.3	117.1	-36.8	47.1	-109.1	54.2	-94.2	39.9	-66.9	52.8
15	-133.9	118.3	-37.0	46.8	-108.5	54.0	-93.5	39.3	-66.8	52.8
16	-133.7	118.4	-	-	-	-	-	-	-	-
17	-133.3	119.1	-	-	-	-	-	-	-	-
18	-132.7	117.9	-	-	-	-	-	-	-	-
19	-130.1	118.0	-	-	-	-	-	-	-	-
20	-133.8	118.6	-	-	-	-	-	-	-	-
Aver.	-133.0	118.2	-36.7	47.0	-108.9	54.1	-93.6	39.6	-66.8	52.8

Table G-41. Peak strain data under HVS wheel path 1, trial 19, slab 2

Load	**OS3600** (Top)	**OS3600** (Bottom)	**Tokyo** (Top)	**Tokyo** (Bottom)	**Vishay** (Top)	**Vishay** (Bottom)	**Kyowa** (Top)	**Kyowa** (Bottom)	**CTL** (Top)	**CTL** (Bottom)
1	-132.1	119.6	-35.9	47.1	-107.6	54.5	-91.4	39.0	-68.1	52.4
2	-133.0	120.5	-35.7	47.6	-108.4	55.0	-90.9	39.2	-68.4	52.6
3	-130.8	119.4	-35.1	47.2	-107.5	54.1	-91.4	39.3	-68.0	52.3
4	-134.2	119.6	-36.0	47.3	-107.8	54.3	-91.2	39.3	-68.0	52.7
5	-133.0	119.3	-36.1	47.6	-108.2	54.9	-91.5	39.6	-68.4	52.5
6	-132.2	120.0	-36.1	47.2	-107.9	54.2	-91.4	39.3	-68.1	52.5
7	-131.9	119.4	-36.3	47.2	-107.9	54.7	-90.9	39.3	-68.1	52.6
8	-130.7	119.3	-35.6	47.3	-107.5	54.8	-91.1	40.0	-68.1	52.3
9	-133.4	120.2	-36.2	47.1	-107.8	54.6	-90.8	39.5	-68.3	52.7
10	-132.4	120.2	-36.1	47.8	-107.9	54.9	-91.9	39.5	-68.3	52.6
11	-132.3	119.6	-36.0	47.5	-107.7	54.7	-91.1	39.5	-68.3	52.5
12	-132.1	120.2	-35.5	47.3	-107.9	54.8	-91.1	39.1	-68.2	52.3
13	-132.8	120.4	-35.5	47.2	-107.9	55.0	-90.9	39.2	-68.2	52.5
14	-132.5	119.2	-36.0	47.3	-107.9	54.8	-91.1	39.6	-68.3	52.5
15	-132.1	119.7	-35.6	47.7	-108.1	54.7	-91.1	39.5	-68.4	52.5
16	-133.8	119.1	-	-	-	-	-	-	-	-
17	-131.3	118.3	-	-	-	-	-	-	-	-
18	-133.3	120.9	-	-	-	-	-	-	-	-
19	-131.6	120.4	-	-	-	-	-	-	-	-
20	-132.7	119.9	-	-	-	-	-	-	-	-
Aver.	-132.4	119.8	-35.8	47.4	-107.9	54.7	-91.2	39.4	-68.2	52.5

Table G-42. Peak strain data under HVS wheel path 1, trial 20, slab 2

Load	**OS3600** (Top)	**OS3600** (Bottom)	**Tokyo** (Top)	**Tokyo** (Bottom)	**Vishay** (Top)	**Vishay** (Bottom)	**Kyowa** (Top)	**Kyowa** (Bottom)	**CTL** (Top)	**CTL** (Bottom)
1	-131.0	121.2	-34.8	48.2	-106.9	55.9	-91.1	39.0	-70.1	52.0
2	-130.3	121.1	-35.3	47.5	-106.5	55.5	-90.8	38.0	-70.0	52.1
3	-132.5	120.5	-35.0	47.8	-106.7	56.1	-91.0	38.7	-70.1	52.2
4	-130.8	120.4	-35.2	48.0	-107.1	55.9	-91.0	38.8	-70.2	52.2
5	-130.3	119.6	-35.4	48.2	-107.0	55.8	-91.7	38.5	-70.2	52.4
6	-133.2	120.4	-35.1	48.0	-106.7	55.4	-90.9	38.6	-70.0	52.1
7	-132.0	120.5	-35.1	47.8	-106.5	55.6	-90.5	38.4	-69.9	51.8
8	-130.8	121.5	-34.6	47.9	-106.4	55.8	-90.9	38.5	-69.9	52.0
9	-132.2	120.5	-35.3	47.6	-106.9	55.5	-91.2	38.5	-70.3	52.4
10	-130.9	120.5	-35.7	47.9	-106.8	55.8	-91.2	38.7	-70.2	52.1
11	-130.6	120.7	-35.3	47.7	-106.7	55.5	-91.3	38.4	-70.1	52.2
12	-132.1	119.3	-35.0	48.3	-106.9	55.6	-90.9	38.4	-70.1	52.1
13	-131.8	121.0	-35.0	47.9	-107.2	55.8	-91.3	38.8	-69.9	52.3
14	-132.3	122.2	-35.3	47.9	-106.9	55.5	-91.5	38.6	-70.2	52.2
15	-131.8	120.4	-35.2	48.0	-107.0	55.7	-90.8	38.4	-70.2	52.1
16	-131.1	120.3	-	-	-	-	-	-	-	-
17	-132.5	120.1	-	-	-	-	-	-	-	-
18	-129.9	119.5	-	-	-	-	-	-	-	-
19	-131.4	120.4	-	-	-	-	-	-	-	-
20	-131.5	119.5	-	-	-	-	-	-	-	-
Aver.	-131.5	120.5	-35.2	47.9	-106.8	55.7	-91.1	38.5	-70.1	52.2

Table G-43. Peak strain data under HVS wheel path 1, trial 21, slab 2

Load	**OS3600** (Top)	**OS3600** (Bottom)	**Tokyo** (Top)	**Tokyo** (Bottom)	**Vishay** (Top)	**Vishay** (Bottom)	**Kyowa** (Top)	**Kyowa** (Bottom)	**CTL** (Top)	**CTL** (Bottom)
1	-129.0	122.0	-	-	-	-	-	-	-	-
2	-130.3	120.5	-	-	-	-	-	-	-	-
3	-128.8	120.3	-	-	-	-	-	-	-	-
4	-131.8	121.3	-	-	-	-	-	-	-	-
5	-131.3	120.9	-	-	-	-	-	-	-	-
6	-130.5	120.4	-	-	-	-	-	-	-	-
7	-128.5	121.4	-	-	-	-	-	-	-	-
8	-129.7	120.2	-	-	-	-	-	-	-	-
9	-131.3	121.9	-	-	-	-	-	-	-	-
10	-132.8	121.7	-	-	-	-	-	-	-	-
11	-130.8	121.7	-	-	-	-	-	-	-	-
12	-130.8	120.0	-	-	-	-	-	-	-	-
13	-129.3	121.2	-	-	-	-	-	-	-	-
14	-129.7	119.2	-	-	-	-	-	-	-	-
15	-131.9	120.5	-	-	-	-	-	-	-	-
16	-130.1	121.2	-	-	-	-	-	-	-	-
17	-131.3	120.6	-	-	-	-	-	-	-	-
18	-129.0	121.1	-	-	-	-	-	-	-	-
19	-129.2	120.7	-	-	-	-	-	-	-	-
20	-128.1	122.7	-	-	-	-	-	-	-	-
Aver.	-130.2	121.0	-	-	-	-	-	-	-	-

Table G-44. Peak strain data under HVS wheel path 1, trial 22, slab 2

Load	**OS3600** (Top)	**OS3600** (Bottom)	**Tokyo** (Top)	**Tokyo** (Bottom)	**Vishay** (Top)	**Vishay** (Bottom)	**Kyowa** (Top)	**Kyowa** (Bottom)	**CTL** (Top)	**CTL** (Bottom)
1	-128.4	121.9	-36.8	48.8	-105.9	55.5	-88.8	38.2	-73.5	51.7
2	-128.9	123.6	-36.7	48.5	-105.9	55.7	-89.2	38.3	-73.5	51.6
3	-129.5	122.4	-36.4	48.7	-106.0	56.1	-88.8	38.1	-73.4	51.6
4	-128.3	124.3	-36.1	48.7	-105.6	56.2	-88.8	38.4	-73.5	51.8
5	-128.9	124.2	-36.0	49.4	-105.2	56.3	-89.0	38.6	-73.5	51.8
6	-128.2	123.1	-36.4	48.9	-105.4	56.1	-88.6	38.6	-73.5	51.4
7	-127.9	122.6	-36.4	48.4	-105.4	55.6	-88.8	38.6	-73.3	51.6
8	-128.1	123.4	-36.6	49.1	-105.8	55.5	-88.4	38.0	-73.5	51.9
9	-128.4	124.7	-36.1	49.0	-105.3	55.4	-89.1	39.2	-73.5	51.6
10	-128.9	124.1	-36.7	49.0	-105.5	55.9	-88.8	38.3	-73.6	51.6
11	-128.4	124.9	-37.0	49.4	-105.6	56.2	-89.0	38.2	-73.7	51.5
12	-128.1	123.5	-36.3	49.1	-105.3	55.6	-88.8	38.6	-73.5	51.6
13	-127.2	123.2	-36.2	49.2	-106.1	56.3	-88.6	38.1	-73.8	51.9
14	-127.2	124.1	-36.2	48.7	-105.3	55.9	-88.9	39.0	-73.5	51.6
15	-130.2	123.5	-36.4	49.1	-105.9	55.9	-89.0	38.4	-73.8	51.6
16	-128.8	123.6	-	-	-	-	-	-	-	-
17	-128.8	124.0	-	-	-	-	-	-	-	-
18	-127.8	123.1	-	-	-	-	-	-	-	-
19	-127.7	123.5	-	-	-	-	-	-	-	-
20	-126.9	122.6	-	-	-	-	-	-	-	-
Aver.	-128.3	123.5	-36.4	48.9	-105.6	55.9	-88.8	38.4	-73.5	51.6

Table G-45. Peak strain data under HVS wheel path 1, trial 23, slab 2

Load	**OS3600** (Top)	**OS3600** (Bottom)	**Tokyo** (Top)	**Tokyo** (Bottom)	**Vishay** (Top)	**Vishay** (Bottom)	**Kyowa** (Top)	**Kyowa** (Bottom)	**CTL** (Top)	**CTL** (Bottom)
1	-123.2	125.5	-40.6	49.8	-102.0	56.8	-84.5	37.9	-77.1	50.5
2	-123.2	128.1	-41.1	50.5	-102.0	57.0	-85.1	37.9	-77.0	50.3
3	-123.5	128.2	-41.6	50.0	-102.5	56.7	-85.1	38.3	-77.2	50.6
4	-124.0	128.5	-41.3	50.4	-102.7	56.5	-85.4	38.4	-77.3	50.6
5	-124.6	128.0	-41.0	49.8	-101.6	56.3	-85.5	38.3	-77.1	50.2
6	-123.1	126.6	-40.9	50.0	-101.9	56.6	-85.1	37.8	-77.1	50.1
7	-122.5	126.7	-41.0	50.1	-101.9	56.5	-84.5	38.2	-77.0	50.3
8	-123.7	126.7	-40.4	50.0	-101.9	56.2	-85.2	38.6	-77.2	50.2
9	-125.1	127.5	-40.4	50.6	-101.5	56.3	-85.3	38.0	-77.2	50.3
10	-124.0	128.2	-40.4	50.5	-102.3	57.0	-85.0	38.6	-77.4	50.4
11	-123.0	128.1	-39.6	49.8	-101.7	56.4	-84.8	38.0	-77.2	50.1
12	-121.1	127.9	-40.4	50.0	-102.1	56.4	-85.7	37.7	-77.2	49.9
13	-123.0	127.5	-40.9	50.3	-101.7	56.5	-84.9	38.1	-77.4	50.1
14	-123.8	128.0	-40.6	49.5	-102.3	56.8	-84.7	37.7	-77.5	50.5
15	-124.0	129.7	-40.0	49.9	-101.6	56.6	-85.0	38.1	-77.1	50.1
16	-123.3	128.4	-	-	-	-	-	-	-	-
17	-123.0	127.8	-	-	-	-	-	-	-	-
18	-123.4	127.3	-	-	-	-	-	-	-	-
19	-123.1	128.8	-	-	-	-	-	-	-	-
20	-122.7	128.0	-	-	-	-	-	-	-	-
Aver.	-123.4	127.8	-40.7	50.1	-102.0	56.6	-85.1	38.1	-77.2	50.3

Table G-46. Peak strain data under HVS wheel path 1, trial 24, slab 2

Load	**OS3600** (Top)	**OS3600** (Bottom)	**Tokyo** (Top)	**Tokyo** (Bottom)	**Vishay** (Top)	**Vishay** (Bottom)	**Kyowa** (Top)	**Kyowa** (Bottom)	**CTL** (Top)	**CTL** (Bottom)
1	-126.5	131.6	-53.6	52.1	-104.1	58.3	-88.3	38.1	-84.4	51.5
2	-127.8	130.6	-52.9	52.0	-104.1	57.8	-88.3	37.8	-84.5	51.5
3	-127.8	131.5	-52.9	51.8	-103.9	58.1	-87.7	37.6	-84.2	51.2
4	-127.0	131.9	-53.0	52.2	-103.8	58.4	-87.6	37.3	-84.6	51.7
5	-126.1	131.8	-52.6	51.9	-103.6	58.0	-88.2	38.1	-84.3	51.4
6	-127.1	130.0	-53.4	52.4	-103.6	58.3	-88.5	38.3	-84.5	51.4
7	-126.8	130.6	-53.1	51.9	-103.8	58.2	-88.5	37.8	-84.4	51.2
8	-125.9	131.7	-53.4	52.2	-103.5	58.2	-87.9	37.8	-84.4	51.4
9	-126.8	131.3	-53.1	51.9	-104.1	58.3	-87.7	37.8	-84.7	51.7
10	-127.3	131.0	-52.9	52.0	-103.9	58.6	-88.0	37.8	-84.7	51.4
11	-127.0	132.2	-53.4	51.8	-104.7	57.8	-88.3	38.3	-84.7	51.5
12	-126.4	131.3	-52.3	51.7	-104.1	57.5	-88.2	37.9	-84.5	51.1
13	-126.1	131.9	-52.9	51.7	-104.3	58.1	-87.8	37.6	-84.5	51.5
14	-124.9	131.3	-52.8	51.6	-104.4	57.7	-88.1	37.2	-84.6	51.6
15	-126.6	132.0	-53.1	52.1	-104.1	58.1	-88.3	37.4	-84.5	51.4
16	-127.6	132.5	-	-	-	-	-	-	-	-
17	-127.0	133.4	-	-	-	-	-	-	-	-
18	-127.1	131.2	-	-	-	-	-	-	-	-
19	-126.3	131.9	-	-	-	-	-	-	-	-
20	-126.7	131.5	-	-	-	-	-	-	-	-
Aver.	-126.7	131.6	-53.0	52.0	-104.0	58.1	-88.1	37.8	-84.5	51.4

Table G-47. Peak strain data under HVS wheel path 1, trial 1, slab 3

Load	**OS3600** (Top)	**OS3600** (Bottom)	**Vishay** (Top)	**Vishay** (Bottom)	**Kyowa** (Top)	**Kyowa** (Bottom)	**Tokyo** (Top)	**Tokyo** (Bottom)	**Tokyo** (Top)	**Tokyo** (Bottom)
1	-78.6	34.2	-46.7	36.7	-84.5	24.1	-43.8	26.9	-68.0	30.8
2	-78.6	34.6	-50.6	37.1	-84.5	24.3	-44.2	27.3	-67.8	30.3
3	-78.5	34.1	-47.7	36.9	-84.6	24.0	-43.6	27.4	-68.1	30.7
4	-79.5	34.5	-46.5	36.6	-85.1	23.6	-43.7	26.9	-68.3	30.6
5	-78.6	34.1	-46.0	36.8	-84.5	24.2	-43.5	26.9	-67.3	30.8
6	-79.0	34.1	-45.7	36.7	-84.9	24.5	-43.3	26.9	-67.8	30.9
7	-78.4	34.0	-50.7	36.7	-85.1	24.2	-44.0	27.0	-67.7	30.8
8	-78.7	34.6	-47.1	36.8	-84.6	24.5	-43.8	27.1	-67.5	30.9
9	-78.8	34.3	-49.2	36.8	-85.0	24.2	-43.9	27.0	-67.6	30.6
10	-79.0	34.6	-48.0	36.7	-84.9	24.3	-44.0	26.6	-68.1	30.8
11	-79.1	34.1	-47.0	36.6	-84.9	24.3	-44.1	26.8	-67.8	30.6
12	-78.1	34.2	-46.3	36.7	-85.2	24.4	-43.6	26.6	-67.8	30.7
13	-78.8	34.1	-45.2	36.7	-85.5	23.9	-43.6	26.5	-68.1	30.7
14	-79.5	34.2	-46.8	36.9	-85.5	23.8	-43.3	27.2	-67.4	30.9
15	-79.3	35.2	-47.1	37.1	-85.9	24.0	-43.5	27.0	-68.1	30.8
16	-79.7	34.1	-46.4	37.1	-85.8	24.3	-43.6	27.2	-68.2	30.8
17	-79.8	34.4	-46.0	36.7	-85.6	24.1	-43.8	26.9	-67.9	30.6
18	-80.0	34.9	-45.9	36.8	-85.5	24.1	-43.2	26.9	-68.4	31.0
19	-78.7	34.0	-45.0	36.9	-85.3	24.1	-44.0	26.5	-68.2	31.0
20	-79.5	34.8	-44.8	36.7	-85.5	24.1	-44.0	26.6	-67.6	30.4
Aver.	-79.0	34.3	-46.9	36.8	-85.1	24.2	-43.7	26.9	-67.9	30.7

Table G-48. Peak strain data under HVS wheel path 1, trial 2, slab 3

Load	**OS3600** (Top)	**OS3600** (Bottom)	**Vishay** (Top)	**Vishay** (Bottom)	**Kyowa** (Top)	**Kyowa** (Bottom)	**Tokyo** (Top)	**Tokyo** (Bottom)	**Tokyo** (Top)	**Tokyo** (Bottom)
1	-81.4	33.8	-47.7	36.4	-87.9	21.2	-45.9	27.0	-70.8	27.8
2	-82.1	33.6	-47.6	36.7	-87.8	21.2	-45.4	27.5	-71.0	28.1
3	-81.5	33.9	-47.4	36.9	-87.4	21.4	-45.7	27.2	-70.8	27.7
4	-81.5	34.5	-47.9	36.6	-87.4	21.0	-45.6	27.0	-71.0	27.7
5	-81.9	34.0	-48.9	36.3	-87.6	21.5	-45.7	27.1	-70.8	27.6
6	-81.5	33.9	-49.8	36.4	-88.0	21.5	-45.4	26.7	-71.2	27.6
7	-81.5	34.0	-49.8	36.2	-87.1	21.4	-45.5	26.9	-70.5	27.7
8	-82.1	34.9	-49.5	36.3	-87.5	21.4	-45.9	26.9	-70.5	27.8
9	-81.7	34.5	-47.9	36.9	-87.9	21.7	-45.3	26.7	-70.6	27.7
10	-82.7	33.8	-47.0	36.7	-88.2	21.3	-45.9	27.3	-70.9	27.7
11	-81.8	34.2	-46.9	36.6	-87.1	21.2	-45.5	27.1	-70.6	28.1
12	-81.7	33.8	-49.0	36.4	-87.7	21.4	-45.9	27.0	-71.0	28.3
13	-81.5	33.2	-48.6	36.6	-87.5	21.5	-45.7	26.9	-70.8	27.7
14	-81.4	34.9	-48.1	36.8	-87.7	21.2	-45.3	27.3	-70.8	27.7
15	-81.5	34.3	-52.0	36.1	-87.4	21.5	-45.7	27.2	-70.6	28.2
16	-81.7	34.1	-50.5	36.3	-88.0	21.4	-45.7	27.2	-71.3	27.4
17	-81.6	33.7	-50.6	36.3	-87.9	21.5	-45.7	26.9	-71.4	27.9
18	-82.0	34.0	-55.6	36.7	-87.4	21.5	-45.4	26.9	-71.2	27.5
19	-81.7	34.1	-53.8	36.2	-87.1	21.7	-45.0	26.9	-70.9	27.7
20	-82.1	33.2	-49.4	36.2	-88.1	21.0	-45.8	26.9	-71.1	27.6
Aver.	-81.8	34.0	-49.4	36.5	-87.6	21.4	-45.6	27.0	-70.9	27.8

Table G-49. Peak strain data under HVS wheel path 1, trial 3, slab 3

Load	**OS3600** (Top)	**OS3600** (Bottom)	**Vishay** (Top)	**Vishay** (Bottom)	**Kyowa** (Top)	**Kyowa** (Bottom)	**Tokyo** (Top)	**Tokyo** (Bottom)	**Tokyo** (Top)	**Tokyo** (Bottom)
1	-83.3	34.7	-61.0	35.0	-89.7	20.2	-46.4	26.5	-72.4	25.4
2	-82.8	34.6	-60.9	35.5	-89.3	20.3	-46.5	26.7	-72.5	26.0
3	-82.9	34.3	-59.9	35.5	-89.1	20.1	-45.3	26.8	-72.2	25.9
4	-83.7	33.4	-62.2	35.6	-88.9	20.5	-45.9	26.5	-72.3	25.8
5	-83.5	34.6	-62.2	35.5	-88.6	20.4	-46.3	27.1	-72.9	26.0
6	-83.2	34.1	-59.7	35.6	-89.2	20.5	-46.0	27.1	-72.4	25.9
7	-84.2	33.0	-58.7	35.5	-88.8	20.9	-46.2	27.0	-72.3	26.1
8	-82.7	34.5	-59.0	35.6	-88.8	20.8	-46.0	27.2	-72.4	26.2
9	-83.2	34.6	-56.0	35.8	-88.6	20.6	-45.5	27.4	-72.0	25.9
10	-83.1	33.6	-53.6	35.5	-88.7	20.8	-45.3	27.4	-72.4	26.1
11	-83.7	34.5	-48.7	36.1	-88.3	21.0	-45.3	27.4	-72.1	26.6
12	-83.4	34.7	-47.7	35.7	-87.8	20.9	-45.8	27.1	-72.5	26.2
13	-82.8	34.3	-47.6	36.0	-88.5	21.0	-45.5	27.2	-72.3	26.5
14	-83.7	34.0	-46.7	35.8	-88.9	21.0	-45.4	27.6	-71.6	26.4
15	-83.5	34.3	-46.2	36.3	-88.1	21.1	-44.7	27.4	-71.1	26.8
16	-83.7	34.3	-47.4	36.1	-88.2	21.2	-45.0	27.5	-71.6	26.8
17	-83.6	33.9	-47.7	36.1	-88.2	21.4	-46.0	27.7	-71.5	26.9
18	-82.4	34.7	-46.3	36.0	-88.5	21.4	-44.8	28.2	-71.5	27.1
19	-83.6	35.2	-47.0	36.2	-87.8	21.2	-45.0	28.0	-71.8	27.6
20	-83.1	34.2	-46.0	36.7	-87.8	21.8	-44.6	28.1	-71.2	26.6
Aver.	-83.3	34.3	-53.2	35.8	-88.6	20.9	-45.6	27.3	-72.1	26.3

Table G-50. Peak strain data under HVS wheel path 1, trial 4, slab 3

Load	**OS3600** (Top)	**OS3600** (Bottom)	**Vishay** (Top)	**Vishay** (Bottom)	**Kyowa** (Top)	**Kyowa** (Bottom)	**Tokyo** (Top)	**Tokyo** (Bottom)	**Tokyo** (Top)	**Tokyo** (Bottom)
1	-83.3	35.9	-47.3	34.5	-90.1	20.0	-44.4	27.1	-72.3	26.0
2	-83.3	34.5	-48.4	34.7	-89.2	19.8	-44.7	27.1	-72.6	25.7
3	-83.6	33.7	-48.3	34.4	-89.1	19.9	-44.5	27.1	-72.1	25.8
4	-83.6	35.7	-48.4	34.6	-89.6	20.0	-44.6	27.1	-72.6	26.4
5	-84.1	36.9	-49.1	34.4	-89.4	20.4	-44.2	26.6	-72.0	25.9
6	-83.3	36.4	-47.1	34.9	-89.4	19.7	-45.3	26.8	-72.3	26.2
7	-84.3	35.1	-47.2	34.6	-89.5	19.7	-44.8	27.2	-72.2	26.0
8	-84.4	34.9	-47.2	34.7	-89.8	20.0	-45.1	27.0	-73.2	26.2
9	-83.0	36.6	-47.4	34.8	-89.8	20.2	-44.2	26.7	-72.3	26.2
10	-83.8	35.8	-46.9	34.8	-88.9	20.0	-44.2	27.4	-72.7	25.8
11	-83.3	35.6	-46.6	34.8	-89.3	20.4	-43.8	26.9	-72.1	26.2
12	-83.5	37.7	-48.2	34.7	-89.3	20.1	-44.7	27.0	-72.0	26.3
13	-84.1	35.4	-49.8	34.6	-89.3	20.0	-44.4	27.0	-72.0	26.2
14	-83.5	34.6	-48.6	34.6	-89.3	20.2	-44.5	26.9	-71.8	26.3
15	-84.4	35.2	-51.2	34.9	-89.5	20.3	-44.7	27.0	-72.2	26.1
16	-82.9	34.7	-51.8	34.6	-89.8	19.9	-44.4	27.1	-72.4	26.4
17	-83.3	34.4	-48.5	34.6	-89.2	20.2	-44.2	26.9	-72.0	26.3
18	-83.7	34.5	-48.1	34.9	-89.1	20.2	-44.6	27.0	-71.6	26.4
19	-83.6	34.2	-49.5	34.8	-89.7	20.4	-44.4	27.2	-71.9	26.7
20	-83.6	33.8	-48.9	34.9	-89.5	20.0	-44.6	27.2	-71.8	26.3
Aver.	-83.6	35.3	-48.4	34.7	-89.4	20.1	-44.5	27.0	-72.2	26.2

Table G-51. Peak strain data under HVS wheel path 1, trial 5, slab 3

Load	**OS3600** (Top)	**OS3600** (Bottom)	**Vishay** (Top)	**Vishay** (Bottom)	**Kyowa** (Top)	**Kyowa** (Bottom)	**Tokyo** (Top)	**Tokyo** (Bottom)	**Tokyo** (Top)	**Tokyo** (Bottom)
1	-83.5	34.0	-43.8	33.9	-89.0	19.0	-42.3	26.3	-71.4	26.0
2	-83.8	34.4	-42.8	34.2	-89.1	19.4	-42.2	26.1	-71.2	26.3
3	-83.9	34.3	-43.1	33.7	-88.8	19.0	-42.0	26.2	-71.0	26.0
4	-83.8	33.0	-42.7	33.9	-89.2	18.5	-42.4	26.4	-71.5	26.2
5	-83.2	34.2	-42.8	34.0	-88.7	19.0	-42.5	25.9	-71.3	26.1
6	-83.5	34.7	-44.5	34.1	-88.5	19.1	-42.4	27.0	-70.8	26.4
7	-83.6	33.6	-44.0	34.4	-89.0	19.2	-41.9	26.8	-71.1	25.9
8	-83.4	34.1	-46.9	33.8	-88.9	19.1	-42.4	26.1	-71.3	25.9
9	-83.2	34.3	-45.1	34.0	-88.8	19.1	-42.4	26.5	-71.2	25.8
10	-84.1	33.8	-44.1	34.1	-88.7	19.3	-42.2	26.6	-71.2	26.1
11	-82.8	33.7	-44.2	34.1	-88.5	19.0	-41.9	26.3	-70.9	25.8
12	-82.7	34.5	-46.3	34.3	-88.6	19.0	-41.4	26.7	-70.8	26.3
13	-83.7	34.9	-46.1	34.0	-88.6	19.2	-42.1	26.6	-70.7	25.8
14	-82.7	34.9	-45.4	33.8	-89.1	19.3	-42.2	26.5	-71.2	26.0
15	-83.1	38.0	-46.2	34.0	-88.5	19.1	-42.4	26.4	-70.7	25.7
16	-82.6	35.6	-43.1	34.1	-88.5	19.3	-42.5	27.0	-70.7	26.1
17	-83.5	33.6	-43.0	34.0	-88.9	19.2	-41.8	26.5	-70.9	26.5
18	-83.5	32.2	-43.2	34.3	-88.7	19.0	-42.3	26.5	-70.7	26.0
19	-83.3	35.5	-42.8	34.2	-88.6	19.1	-42.5	26.8	-71.0	26.2
20	-82.7	36.4	-43.3	34.1	-89.2	18.9	-42.8	26.0	-70.7	25.7
Aver.	-83.3	34.5	-44.2	34.0	-88.8	19.1	-42.2	26.5	-71.0	26.0

Table G-52. Peak strain data under HVS wheel path 1, trial 6, slab 3

Load	**OS3600** (Top)	**OS3600** (Bottom)	**Vishay** (Top)	**Vishay** (Bottom)	**Kyowa** (Top)	**Kyowa** (Bottom)	**Tokyo** (Top)	**Tokyo** (Bottom)	**Tokyo** (Top)	**Tokyo** (Bottom)
1	-83.0	33.7	-41.3	33.4	-88.6	18.2	-39.0	26.5	-69.0	25.7
2	-82.5	34.3	-41.5	33.5	-88.6	18.2	-39.4	26.1	-69.3	25.5
3	-82.3	33.1	-41.5	33.2	-88.5	18.9	-39.5	26.1	-68.9	25.8
4	-82.2	35.0	-41.6	33.3	-88.1	18.5	-39.8	26.2	-69.1	25.5
5	-83.0	34.2	-59.5	33.2	-88.5	18.6	-39.2	26.4	-69.3	25.7
6	-83.1	33.6	-59.2	33.2	-88.4	18.6	-40.1	26.3	-68.8	25.3
7	-82.3	33.3	-57.9	33.2	-88.5	18.7	-39.6	26.0	-69.2	26.3
8	-82.2	35.5	-55.5	33.2	-88.4	18.7	-39.4	26.1	-69.3	25.9
9	-83.3	36.4	-51.3	33.4	-89.2	18.8	-39.6	26.3	-69.2	25.7
10	-82.7	34.9	-44.0	33.5	-88.7	18.4	-39.7	25.9	-69.3	25.6
11	-82.5	33.7	-42.8	33.5	-88.8	18.3	-39.5	26.2	-69.1	25.7
12	-81.6	34.4	-44.2	33.5	-88.7	18.3	-39.6	25.8	-69.0	25.3
13	-81.7	35.6	-43.5	33.2	-88.3	18.5	-39.4	26.3	-69.2	25.4
14	-82.5	33.7	-42.8	33.4	-88.3	18.6	-39.6	26.2	-69.2	25.5
15	-82.8	34.4	-43.6	33.3	-88.7	18.7	-39.7	26.0	-69.1	25.4
16	-83.4	33.3	-42.3	33.5	-88.4	18.8	-39.9	26.6	-68.9	25.5
17	-82.6	34.0	-42.5	33.5	-88.7	18.6	-39.5	26.4	-68.7	25.4
18	-83.1	34.5	-42.2	33.3	-88.5	18.5	-39.2	26.0	-69.1	25.3
19	-82.6	34.9	-42.1	33.3	-87.6	18.8	-40.0	26.0	-69.4	25.9
20	-81.8	34.5	-41.7	33.6	-88.1	18.9	-39.8	26.0	-68.9	25.9
Aver.	-82.6	34.3	-46.1	33.4	-88.5	18.6	-39.6	26.2	-69.1	25.6

Table G-53. Peak strain data under HVS wheel path 1, trial 7, slab 3

Load	**OS3600** (Top)	**OS3600** (Bottom)	**Vishay** (Top)	**Vishay** (Bottom)	**Kyowa** (Top)	**Kyowa** (Bottom)	**Tokyo** (Top)	**Tokyo** (Bottom)	**Tokyo** (Top)	**Tokyo** (Bottom)
1	-82.1	37.5	-39.4	32.5	-87.6	17.9	-36.2	25.9	-66.0	25.3
2	-82.9	34.5	-43.9	32.7	-87.3	18.3	-35.2	25.9	-65.2	24.9
3	-83.0	31.9	-41.4	33.1	-87.7	17.9	-36.1	25.9	-65.9	25.0
4	-81.9	35.7	-41.0	32.8	-87.4	18.0	-36.4	26.0	-66.1	25.4
5	-82.6	34.6	-43.7	32.7	-87.2	18.0	-36.5	25.9	-66.3	25.2
6	-82.2	33.8	-44.1	33.0	-87.2	18.0	-36.0	25.8	-66.2	25.6
7	-82.6	33.9	-44.0	33.1	-87.1	18.3	-35.7	25.8	-65.5	25.4
8	-82.7	34.1	-42.0	32.7	-86.7	18.6	-35.8	26.0	-65.8	25.3
9	-82.6	33.8	-41.3	32.9	-87.2	18.3	-36.1	26.0	-66.0	25.0
10	-82.9	33.7	-41.5	32.8	-87.1	17.8	-35.9	25.8	-65.5	25.1
11	-82.8	35.2	-41.1	32.7	-86.9	18.3	-35.8	25.6	-65.6	25.3
12	-82.4	33.9	-40.7	33.1	-87.5	18.3	-35.6	25.7	-66.2	25.5
13	-82.8	34.0	-41.2	33.1	-87.0	18.3	-36.1	25.8	-66.1	25.6
14	-82.5	34.2	-40.2	33.0	-87.2	18.5	-35.6	26.1	-65.6	25.4
15	-82.1	34.6	-40.3	33.1	-87.2	18.5	-36.6	25.7	-65.5	25.3
16	-82.9	33.4	-40.2	32.9	-87.2	18.2	-36.3	26.1	-65.3	25.4
17	-82.5	34.5	-40.0	32.8	-87.4	18.4	-36.4	25.7	-65.4	25.4
18	-82.1	34.3	-39.5	33.1	-87.2	18.1	-35.9	25.9	-66.1	25.3
19	-82.7	33.6	-39.8	32.5	-87.6	18.8	-36.5	26.1	-65.5	25.5
20	-83.1	33.2	-39.2	32.9	-87.2	18.4	-35.7	26.0	-65.5	26.2
Aver.	-82.6	34.2	-41.2	32.9	-87.2	18.2	-36.0	25.9	-65.8	25.3

Table G-54. Peak strain data under HVS wheel path 1, trial 8, slab 3

Load	**OS3600** (Top)	**OS3600** (Bottom)	**Vishay** (Top)	**Vishay** (Bottom)	**Kyowa** (Top)	**Kyowa** (Bottom)	**Tokyo** (Top)	**Tokyo** (Bottom)	**Tokyo** (Top)	**Tokyo** (Bottom)
1	-80.4	33.3	-40.5	32.9	-86.9	17.8	-32.8	26.3	-62.1	24.3
2	-80.7	33.4	-40.4	32.8	-86.8	18.0	-32.8	25.9	-61.7	24.7
3	-81.5	34.6	-40.3	33.1	-86.8	17.8	-33.3	25.7	-61.6	24.6
4	-80.6	34.4	-40.5	32.7	-87.0	18.1	-33.2	25.9	-61.6	24.6
5	-81.1	32.9	-46.6	33.0	-87.4	17.8	-33.0	25.8	-62.3	24.2
6	-80.8	34.0	-42.9	32.6	-87.5	17.8	-32.9	25.7	-62.2	24.6
7	-80.6	34.1	-43.1	32.6	-86.8	17.9	-33.0	25.7	-62.3	24.4
8	-81.2	34.1	-41.9	32.6	-87.0	17.6	-32.8	25.7	-62.1	24.7
9	-81.4	34.2	-42.9	32.4	-86.8	17.7	-32.5	25.6	-62.0	24.5
10	-81.1	33.6	-41.9	32.3	-87.3	17.8	-33.2	26.2	-62.3	24.3
11	-80.5	33.9	-41.1	32.9	-86.4	17.7	-33.0	26.3	-62.0	24.5
12	-80.9	33.1	-40.5	33.2	-87.4	18.0	-33.0	26.0	-62.3	24.7
13	-79.8	35.4	-40.3	32.7	-86.9	18.1	-33.3	25.6	-62.5	24.3
14	-80.3	33.9	-40.3	32.9	-86.8	18.2	-33.4	25.8	-62.4	24.6
15	-81.1	34.4	-40.4	32.6	-86.7	17.9	-32.7	25.7	-62.0	25.1
16	-80.5	33.2	-40.5	32.7	-86.7	17.8	-33.8	25.5	-62.1	24.5
17	-81.7	34.9	-40.6	32.9	-86.8	17.9	-33.6	25.9	-62.4	24.3
18	-81.3	33.5	-41.0	32.6	-86.9	18.0	-33.3	25.5	-62.5	24.5
19	-81.3	33.7	-40.8	32.7	-87.2	18.0	-33.6	25.6	-62.5	24.4
20	-80.0	33.7	-40.2	32.6	-87.0	17.7	-33.1	25.9	-62.8	24.6
Aver.	-80.8	33.9	-41.3	32.7	-87.0	17.9	-33.1	25.8	-62.2	24.5

Table G-55. Peak strain data under HVS wheel path 1, trial 9, slab 3

Load	**OS3600** (Top)	**OS3600** (Bottom)	**Vishay** (Top)	**Vishay** (Bottom)	**Kyowa** (Top)	**Kyowa** (Bottom)	**Tokyo** (Top)	**Tokyo** (Bottom)	**Tokyo** (Top)	**Tokyo** (Bottom)
1	-81.3	35.0	-41.0	32.3	-86.6	17.8	-29.1	26.2	-58.9	23.7
2	-82.1	32.0	-40.5	32.5	-86.3	17.6	-29.4	25.7	-58.9	24.2
3	-81.0	34.0	-41.1	32.5	-86.4	17.6	-29.6	25.6	-58.9	24.0
4	-81.2	33.8	-39.8	32.1	-85.9	17.3	-28.7	25.5	-58.9	24.3
5	-81.7	33.6	-39.3	32.2	-86.0	17.5	-29.4	25.6	-58.2	24.3
6	-81.5	34.9	-39.2	32.1	-86.3	17.5	-29.4	25.8	-58.7	24.0
7	-81.2	33.8	-39.9	32.1	-86.4	17.5	-29.4	25.6	-59.3	23.8
8	-80.9	33.1	-39.1	32.0	-86.0	17.8	-29.6	25.5	-58.6	23.7
9	-80.6	33.9	-39.0	32.4	-85.9	17.9	-29.2	25.3	-58.6	24.2
10	-81.2	34.2	-56.5	32.3	-86.6	17.7	-29.6	25.7	-58.9	24.0
11	-81.1	34.9	-50.4	32.2	-86.4	17.5	-29.5	25.4	-58.8	24.0
12	-81.8	33.1	-46.8	31.8	-86.0	17.8	-29.6	25.4	-58.9	24.6
13	-81.1	34.6	-43.1	31.9	-86.3	17.4	-29.7	25.7	-58.9	24.0
14	-81.5	33.4	-41.3	32.0	-86.9	17.6	-29.4	25.4	-59.0	24.0
15	-80.9	33.7	-45.6	31.9	-86.5	17.4	-29.5	25.7	-58.8	24.1
16	-81.4	33.8	-42.0	31.9	-86.3	17.3	-29.7	25.3	-58.7	24.3
17	-81.1	34.0	-39.3	32.2	-86.3	17.5	-29.5	25.7	-58.9	24.0
18	-80.5	34.8	-39.1	32.1	-86.5	17.5	-29.8	25.3	-58.4	24.4
19	-81.5	34.2	-39.5	32.0	-86.0	17.2	-29.5	25.5	-58.9	24.3
20	-81.6	34.3	-38.6	32.5	-86.8	17.5	-29.9	25.8	-58.9	24.3
Aver.	-81.3	34.0	-42.1	32.2	-86.3	17.6	-29.5	25.6	-58.8	24.1

Table G-56. Peak strain data under HVS wheel path 1, trial 10, slab 3

Load	**OS3600** (Top)	**OS3600** (Bottom)	**Vishay** (Top)	**Vishay** (Bottom)	**Kyowa** (Top)	**Kyowa** (Bottom)	**Tokyo** (Top)	**Tokyo** (Bottom)	**Tokyo** (Top)	**Tokyo** (Bottom)
1	-80.5	32.9	-41.5	32.0	-86.6	18.3	-26.1	24.3	-56.1	23.7
2	-81.1	34.7	-39.4	31.9	-86.2	18.0	-26.2	24.5	-55.9	23.8
3	-80.7	34.8	-38.1	32.1	-86.5	17.8	-26.6	24.5	-56.4	23.7
4	-80.4	34.3	-40.3	32.0	-86.3	18.2	-26.2	24.7	-56.2	23.6
5	-81.5	35.0	-39.8	31.8	-86.7	18.3	-25.9	24.8	-56.0	23.7
6	-80.8	35.1	-38.7	31.7	-86.5	18.2	-26.0	24.5	-55.8	23.5
7	-79.7	35.2	-39.2	32.1	-86.6	18.3	-26.5	24.6	-55.7	23.5
8	-81.3	35.7	-38.7	32.1	-86.7	18.0	-25.9	24.3	-56.0	23.7
9	-80.5	33.6	-39.8	32.1	-86.6	18.2	-26.3	24.8	-56.0	23.7
10	-80.9	35.2	-39.8	31.8	-86.6	17.6	-26.3	24.9	-56.6	23.4
11	-81.0	32.9	-38.4	32.1	-86.3	18.4	-26.3	24.7	-56.4	23.6
12	-79.8	36.7	-38.7	31.7	-86.4	18.6	-26.5	24.5	-55.8	23.8
13	-81.1	34.3	-44.3	31.9	-86.8	18.0	-26.3	24.9	-56.0	23.3
14	-81.4	34.3	-44.2	32.3	-86.5	18.2	-25.6	25.1	-55.7	23.8
15	-81.3	34.5	-44.0	31.8	-87.0	18.2	-26.6	24.9	-56.3	23.5
16	-81.7	35.1	-40.9	32.1	-86.0	18.3	-26.5	25.1	-56.3	23.5
17	-80.7	33.3	-38.3	32.1	-86.2	18.1	-26.0	24.7	-56.0	23.4
18	-80.6	32.9	-37.2	31.7	-86.5	18.6	-26.2	24.7	-56.0	24.0
19	-80.6	33.1	-37.3	31.9	-86.5	18.0	-26.6	24.4	-55.9	23.7
20	-81.3	33.5	-38.2	31.9	-86.3	18.2	-26.1	24.9	-55.9	23.4
Aver.	-80.9	34.4	-39.8	32.0	-86.5	18.2	-26.2	24.7	-56.0	23.6

Table G-57. Peak strain data under HVS wheel path 1, trial 11, slab 3

Load	**OS3600** (Top)	**OS3600** (Bottom)	**Vishay** (Top)	**Vishay** (Bottom)	**Kyowa** (Top)	**Kyowa** (Bottom)	**Tokyo** (Top)	**Tokyo** (Bottom)	**Tokyo** (Top)	**Tokyo** (Bottom)
1	-79.3	32.7	-39.2	31.5	-86.0	18.3	-23.9	24.6	-54.6	23.5
2	-79.4	33.1	-38.8	31.8	-85.3	18.5	-24.1	24.3	-54.3	23.3
3	-79.0	32.8	-39.5	31.4	-85.5	18.4	-23.5	24.6	-53.8	23.0
4	-79.4	33.0	-40.2	31.7	-85.4	18.4	-23.3	24.8	-54.2	23.4
5	-79.4	33.4	-41.0	31.7	-85.3	18.2	-23.7	24.5	-54.3	23.0
6	-79.9	33.4	-40.5	31.7	-85.5	18.3	-23.9	24.2	-54.5	23.2
7	-79.5	33.5	-40.1	31.8	-85.7	18.2	-23.8	24.9	-54.8	23.3
8	-79.7	35.1	-39.3	31.5	-85.8	18.8	-23.7	24.2	-54.0	23.7
9	-79.9	34.4	-39.0	31.4	-85.7	18.5	-24.2	24.4	-54.3	23.3
10	-78.4	32.8	-39.2	31.9	-85.6	18.2	-23.6	24.6	-53.8	23.3
11	-79.3	36.6	-39.3	31.4	-85.2	18.3	-23.6	24.8	-54.0	23.1
12	-80.4	33.7	-39.0	31.5	-86.2	18.4	-23.7	24.8	-53.9	23.2
13	-79.7	35.2	-39.8	32.1	-85.7	18.4	-24.3	24.4	-54.1	23.0
14	-79.7	34.3	-39.2	31.6	-85.6	18.3	-24.5	25.2	-54.1	22.8
15	-79.7	33.4	-41.1	32.0	-85.4	18.4	-24.1	24.6	-53.8	23.1
16	-79.5	34.4	-40.8	31.8	-85.7	18.7	-24.3	24.9	-53.6	23.1
17	-79.0	33.0	-39.6	31.6	-85.3	18.6	-24.1	24.5	-54.0	23.2
18	-79.6	31.9	-39.4	31.8	-85.4	18.8	-24.3	24.5	-54.2	23.2
19	-79.8	32.6	-38.9	31.8	-85.3	18.4	-24.1	24.7	-54.4	23.2
20	-79.8	34.0	-38.7	32.1	-85.3	19.0	-23.9	24.9	-54.2	23.2
Aver.	-79.5	33.7	-39.6	31.7	-85.5	18.4	-23.9	24.6	-54.2	23.2

Table G-58. Peak strain data under HVS wheel path 1, trial 12, slab 3

Load	**OS3600** (Top)	**OS3600** (Bottom)	**Vishay** (Top)	**Vishay** (Bottom)	**Kyowa** (Top)	**Kyowa** (Bottom)	**Tokyo** (Top)	**Tokyo** (Bottom)	**Tokyo** (Top)	**Tokyo** (Bottom)
1	-81.2	33.1	-37.3	31.7	-85.9	18.5	-20.7	24.0	-51.2	22.8
2	-80.6	32.1	-43.3	31.3	-86.3	18.3	-20.9	24.2	-51.5	22.7
3	-81.6	32.9	-39.4	31.3	-85.5	18.5	-21.6	24.5	-51.1	22.4
4	-81.0	32.7	-39.0	31.4	-86.3	17.8	-21.5	24.5	-52.0	22.5
5	-81.9	32.6	-40.7	31.5	-85.9	18.2	-21.1	24.1	-51.7	22.7
6	-81.3	32.8	-39.4	31.6	-85.7	18.0	-20.7	24.4	-51.6	22.7
7	-80.6	33.3	-39.9	31.4	-86.0	18.2	-21.0	24.1	-51.7	22.5
8	-81.5	31.5	-40.2	31.4	-85.7	18.3	-21.2	24.1	-51.7	22.6
9	-80.9	33.7	-39.5	31.6	-85.9	18.4	-21.1	24.2	-51.8	22.6
10	-81.2	32.5	-39.3	31.6	-85.7	18.4	-21.4	24.0	-52.0	22.6
11	-81.9	33.1	-40.0	31.4	-85.7	18.3	-21.1	23.9	-51.8	22.8
12	-81.1	34.1	-38.9	31.6	-85.8	18.2	-21.6	24.4	-51.5	22.8
13	-80.8	33.2	-39.1	31.6	-85.8	18.4	-21.1	25.2	-51.3	23.1
14	-80.9	33.5	-38.1	31.9	-85.8	18.4	-21.3	24.4	-51.5	22.7
15	-81.8	32.8	-37.5	32.1	-85.5	18.7	-21.4	24.4	-51.5	22.9
16	-81.5	32.5	-36.6	31.9	-85.4	18.6	-20.9	24.6	-51.9	22.8
17	-81.0	33.9	-37.9	31.7	-85.6	18.1	-21.8	24.6	-51.7	22.6
18	-81.5	32.8	-39.5	31.8	-85.8	18.1	-21.6	24.2	-51.5	22.5
19	-82.0	33.0	-38.8	31.7	-86.0	18.1	-21.5	24.0	-51.4	22.9
20	-81.1	33.8	-38.2	31.5	-85.8	18.4	-21.4	24.0	-51.8	22.8
Aver.	-81.3	33.0	-39.1	31.6	-85.8	18.3	-21.2	24.3	-51.6	22.7

Table G-59. Peak strain data under HVS wheel path 1, trial 13, slab 3

Load	**OS3600** (Top)	**OS3600** (Bottom)	**Vishay** (Top)	**Vishay** (Bottom)	**Kyowa** (Top)	**Kyowa** (Bottom)	**Tokyo** (Top)	**Tokyo** (Bottom)	**Tokyo** (Top)	**Tokyo** (Bottom)
1	-79.8	32.9	-37.7	31.6	-85.8	18.4	-17.6	24.1	-46.6	22.6
2	-80.8	32.1	-38.5	31.6	-86.7	18.1	-17.8	23.7	-47.0	22.6
3	-80.4	32.9	-37.5	31.2	-86.0	19.2	-17.5	24.1	-46.7	23.0
4	-80.9	31.4	-37.4	31.3	-86.1	18.1	-17.8	24.0	-46.7	23.1
5	-80.6	33.4	-36.8	31.1	-86.2	18.3	-18.0	23.6	-47.1	22.7
6	-80.8	32.9	-36.4	31.4	-86.3	18.6	-18.5	24.0	-47.1	23.0
7	-80.3	32.6	-36.4	31.0	-86.7	18.6	-18.3	24.0	-46.9	22.6
8	-79.9	33.1	-36.6	31.9	-86.1	18.3	-18.3	23.9	-47.1	22.9
9	-79.9	33.4	-37.8	31.5	-86.3	18.7	-18.1	23.9	-47.0	22.5
10	-80.4	32.9	-38.1	31.2	-86.0	18.7	-17.9	24.2	-47.1	22.9
11	-80.0	33.4	-41.6	31.4	-85.6	18.7	-18.0	23.8	-46.9	22.9
12	-80.4	33.3	-41.1	31.0	-86.5	18.4	-18.5	23.8	-47.4	22.6
13	-80.1	33.5	-40.5	31.2	-86.4	18.3	-17.9	24.0	-47.3	22.3
14	-80.1	32.8	-39.6	31.6	-86.1	18.5	-18.2	24.0	-46.8	22.4
15	-80.9	32.8	-39.2	31.2	-85.9	18.2	-18.4	24.0	-47.1	22.7
16	-79.3	32.4	-39.3	31.8	-86.7	18.5	-18.5	23.7	-47.2	22.6
17	-80.0	33.8	-40.3	31.6	-86.1	18.0	-18.5	24.0	-47.7	22.6
18	-79.9	32.6	-39.2	31.0	-85.9	18.5	-18.6	23.9	-46.6	22.9
19	-79.7	31.8	-39.1	31.4	-86.1	18.7	-18.7	24.1	-46.9	22.1
20	-81.0	34.1	-39.5	31.2	-86.1	18.7	-19.1	24.1	-47.6	22.6
Aver.	-80.3	32.9	-38.6	31.4	-86.2	18.5	-18.2	23.9	-47.0	22.7

Table G-60. Peak strain data under HVS wheel path 1, trial 14, slab 3

Load	**OS3600** (Top)	**OS3600** (Bottom)	**Vishay** (Top)	**Vishay** (Bottom)	**Kyowa** (Top)	**Kyowa** (Bottom)	**Tokyo** (Top)	**Tokyo** (Bottom)	**Tokyo** (Top)	**Tokyo** (Bottom)
1	-79.8	34.5	-36.0	31.1	-86.9	18.1	-15.5	24.3	-40.3	22.3
2	-80.4	33.0	-37.1	31.5	-87.0	17.9	-15.3	24.2	-40.3	22.2
3	-80.1	33.4	-38.1	31.2	-86.1	18.7	-15.8	24.2	-40.0	22.5
4	-80.2	32.7	-41.0	31.6	-86.5	18.1	-16.0	23.7	-40.3	22.2
5	-80.2	32.4	-40.4	31.3	-86.3	18.4	-15.3	24.4	-40.0	22.6
6	-80.0	32.6	-40.5	31.0	-87.1	18.2	-15.9	23.9	-40.3	22.2
7	-80.4	33.7	-40.6	30.9	-86.4	18.1	-16.2	24.1	-40.1	22.5
8	-79.4	32.7	-39.9	31.1	-87.0	18.1	-16.7	23.7	-40.4	22.5
9	-79.8	32.3	-39.7	31.7	-86.4	18.2	-16.0	23.9	-40.1	22.9
10	-80.1	33.3	-39.2	31.2	-86.6	18.0	-15.9	24.0	-40.1	22.3
11	-79.5	33.4	-38.8	31.4	-86.6	18.3	-16.1	24.1	-40.2	22.7
12	-80.3	32.3	-38.2	31.1	-86.0	18.7	-16.0	23.9	-40.3	22.4
13	-79.9	34.1	-38.0	31.2	-86.2	18.0	-16.5	23.9	-40.0	22.5
14	-80.2	32.8	-38.1	31.3	-86.5	18.1	-16.3	24.5	-40.4	22.2
15	-80.0	33.3	-38.1	31.1	-86.6	18.4	-16.8	24.0	-40.2	22.6
16	-78.3	32.9	-38.8	31.2	-86.3	18.4	-16.3	24.6	-39.8	22.3
17	-80.0	32.3	-38.7	31.3	-86.1	18.4	-16.8	24.1	-40.5	22.4
18	-80.0	32.5	-40.3	31.2	-86.4	18.6	-16.7	24.0	-40.5	22.5
19	-79.8	34.2	-40.2	31.1	-86.4	18.5	-16.9	24.0	-40.6	22.5
20	-79.5	34.4	-46.0	31.2	-86.2	18.2	-17.2	23.8	-40.4	22.1
Aver.	-79.9	33.1	-39.4	31.2	-86.5	18.3	-16.2	24.1	-40.2	22.4

Table G-61. Peak strain data under HVS wheel path 1, trial 15, slab 3

Load	**OS3600** (Top)	**OS3600** (Bottom)	**Vishay** (Top)	**Vishay** (Bottom)	**Kyowa** (Top)	**Kyowa** (Bottom)	**Tokyo** (Top)	**Tokyo** (Bottom)	**Tokyo** (Top)	**Tokyo** (Bottom)
1	-79.8	33.6	-37.7	31.1	-87.9	18.5	-15.2	23.6	-31.6	22.6
2	-79.8	32.5	-38.1	31.1	-88.0	18.6	-14.9	23.7	-31.8	22.5
3	-79.6	33.8	-39.0	31.1	-87.6	18.6	-15.1	23.8	-32.0	22.1
4	-79.7	33.8	-40.6	31.0	-87.6	18.6	-15.1	23.6	-31.7	22.0
5	-80.6	33.0	-37.9	31.3	-87.8	18.6	-14.3	23.7	-31.7	22.2
6	-80.5	33.2	-37.4	31.2	-88.1	18.3	-15.0	23.7	-31.7	22.4
7	-80.1	33.8	-38.7	30.9	-88.0	18.5	-14.8	23.6	-32.5	22.4
8	-80.3	34.2	-39.5	31.4	-87.5	18.6	-15.1	23.5	-32.2	21.9
9	-80.1	33.6	-38.7	31.3	-87.3	18.6	-14.9	23.9	-32.1	22.4
10	-80.0	32.3	-39.8	30.8	-87.2	18.5	-14.9	23.5	-31.9	22.6
11	-80.0	32.0	-38.9	30.9	-87.4	18.6	-15.5	23.5	-31.8	22.7
12	-80.1	33.3	-39.2	31.4	-87.2	18.6	-15.0	23.5	-31.7	22.4
13	-80.5	32.5	-46.7	31.1	-87.8	18.5	-15.4	23.2	-32.3	22.4
14	-80.0	33.5	-45.8	31.0	-87.8	18.5	-15.4	24.0	-32.2	22.5
15	-80.3	32.3	-46.4	30.9	-88.0	18.8	-16.1	24.1	-32.3	22.3
16	-80.1	33.1	-48.7	31.1	-88.0	18.4	-15.8	23.6	-32.1	22.3
17	-80.4	32.5	-48.9	30.9	-87.3	18.6	-15.8	24.0	-32.1	22.2
18	-80.2	35.1	-52.5	30.9	-87.4	18.7	-16.2	23.2	-32.4	22.3
19	-79.1	34.2	-51.1	30.8	-87.8	18.8	-15.9	23.5	-32.4	22.1
20	-79.7	33.5	-51.5	30.5	-88.0	18.8	-16.2	24.1	-32.3	22.2
Aver.	-80.0	33.3	-42.9	31.0	-87.7	18.6	-15.3	23.7	-32.0	22.3

Table G-62. Peak strain data under HVS wheel path 1, trial 16, slab 3

Load	**OS3600** (Top)	**OS3600** (Bottom)	**Vishay** (Top)	**Vishay** (Bottom)	**Kyowa** (Top)	**Kyowa** (Bottom)	**Tokyo** (Top)	**Tokyo** (Bottom)	**Tokyo** (Top)	**Tokyo** (Bottom)
1	-80.4	33.8	-40.5	30.7	-88.1	18.1	-15.1	23.5	-26.0	22.3
2	-80.7	33.1	-40.2	30.8	-88.3	18.0	-15.2	23.5	-26.0	22.0
3	-81.0	33.2	-40.1	31.0	-88.5	18.4	-15.1	23.1	-25.6	22.6
4	-80.3	32.9	-39.5	30.7	-88.6	18.1	-15.1	23.6	-25.4	22.6
5	-80.4	33.1	-39.6	31.0	-88.5	18.3	-14.4	23.8	-26.0	22.6
6	-80.9	33.3	-40.0	31.1	-88.8	18.2	-14.9	23.7	-25.8	22.2
7	-81.0	33.0	-39.7	30.9	-88.3	18.4	-15.1	23.6	-25.7	22.2
8	-80.3	33.5	-39.0	30.9	-88.4	18.5	-14.9	23.2	-26.1	22.3
9	-80.2	34.1	-38.8	30.9	-88.3	18.3	-14.8	23.9	-26.0	22.4
10	-81.9	32.7	-38.8	30.9	-88.0	18.4	-15.6	23.6	-26.4	22.4
11	-81.2	35.6	-38.8	30.7	-88.3	18.5	-15.7	23.4	-25.8	22.4
12	-80.0	36.2	-38.9	30.8	-88.2	18.1	-15.4	23.5	-26.2	22.4
13	-81.5	33.8	-38.4	30.9	-87.9	18.5	-15.6	23.6	-26.2	22.6
14	-80.3	34.6	-44.4	31.1	-88.3	18.2	-15.4	23.5	-26.4	22.5
15	-80.1	34.0	-47.9	30.9	-88.2	18.3	-16.0	23.4	-26.2	22.3
16	-79.8	36.1	-54.2	30.6	-88.0	18.8	-15.8	23.9	-26.2	22.1
17	-80.9	32.0	-59.2	31.1	-88.2	18.4	-15.7	23.6	-26.8	22.0
18	-80.4	32.9	-60.3	31.0	-88.4	18.5	-16.1	23.4	-26.3	22.2
19	-80.4	33.2	-60.8	30.9	-88.6	18.7	-16.2	23.7	-26.2	22.2
20	-81.0	32.5	-60.2	31.2	-88.1	18.2	-15.8	23.2	-27.0	22.5
Aver.	-80.6	33.7	-45.0	30.9	-88.3	18.3	-15.4	23.5	-26.1	22.3

Table G-63. Peak strain data under HVS wheel path 1, trial 17, slab 3

Load	**OS3600** (Top)	**OS3600** (Bottom)	**Vishay** (Top)	**Vishay** (Bottom)	**Kyowa** (Top)	**Kyowa** (Bottom)	**Tokyo** (Top)	**Tokyo** (Bottom)	**Tokyo** (Top)	**Tokyo** (Bottom)
1	-81.1	32.4	-38.9	31.2	-87.6	18.5	-15.5	23.6	-24.2	22.3
2	-80.5	33.0	-39.1	30.6	-88.1	18.3	-15.4	23.3	-24.8	22.1
3	-80.8	33.5	-38.9	30.9	-88.3	18.7	-15.5	23.5	-24.5	22.5
4	-81.9	32.9	-39.0	30.6	-88.1	18.2	-15.1	23.6	-24.7	22.0
5	-81.3	33.7	-38.7	30.9	-88.3	18.5	-15.4	23.3	-24.5	22.2
6	-81.2	36.1	-38.7	31.1	-87.4	18.4	-15.6	23.4	-24.3	22.5
7	-80.6	32.9	-39.0	30.8	-87.9	18.6	-15.9	23.4	-24.1	22.3
8	-81.2	32.6	-39.2	30.9	-88.2	18.7	-15.3	23.4	-24.8	22.2
9	-81.1	34.4	-38.1	30.6	-87.6	18.4	-15.7	23.3	-24.6	22.2
10	-80.9	35.9	-38.7	30.9	-88.0	18.6	-15.4	23.2	-24.4	22.1
11	-81.1	33.3	-39.0	30.6	-88.4	18.3	-15.3	22.9	-24.8	22.1
12	-80.9	36.4	-40.4	30.8	-87.7	18.3	-15.6	23.3	-24.2	22.1
13	-80.6	34.0	-39.5	30.9	-87.9	18.2	-15.9	23.0	-24.4	22.3
14	-81.1	36.1	-39.3	30.8	-88.1	18.2	-15.6	23.4	-24.7	21.9
15	-80.7	32.4	-39.4	30.9	-88.1	18.1	-15.9	23.4	-24.7	22.3
16	-81.2	33.0	-39.0	30.5	-88.1	18.2	-15.8	23.1	-25.2	22.1
17	-81.2	32.4	-39.3	30.9	-88.2	18.5	-16.3	23.4	-24.4	22.4
18	-81.4	33.7	-39.1	30.8	-88.1	18.1	-16.0	23.1	-24.8	22.5
19	-81.9	33.6	-38.9	30.4	-87.9	18.5	-16.3	23.0	-24.7	22.4
20	-81.2	34.0	-39.4	30.7	-88.2	18.1	-15.6	23.2	-24.9	22.3
Aver.	-81.1	33.8	-39.1	30.8	-88.0	18.4	-15.7	23.3	-24.6	22.2

Table G-64. Peak strain data under HVS wheel path 1, trial 18, slab 3

Load	**OS3600** (Top)	**OS3600** (Bottom)	**Vishay** (Top)	**Vishay** (Bottom)	**Kyowa** (Top)	**Kyowa** (Bottom)	**Tokyo** (Top)	**Tokyo** (Bottom)	**Tokyo** (Top)	**Tokyo** (Bottom)
1	-78.8	33.3	-40.2	30.8	-81.7	17.5	-15.4	24.0	-24.1	21.8
2	-78.3	33.1	-39.4	30.8	-81.9	17.8	-15.6	24.0	-24.1	21.5
3	-78.8	33.3	-38.1	30.3	-82.2	17.5	-15.8	23.6	-23.2	21.7
4	-78.8	33.1	-38.6	30.3	-82.6	17.3	-15.4	23.4	-23.6	21.9
5	-79.0	32.9	-38.1	30.5	-82.0	18.1	-15.6	23.2	-23.0	21.6
6	-78.7	32.9	-38.3	30.4	-82.5	17.8	-15.4	23.6	-23.6	21.9
7	-78.4	34.8	-37.7	30.6	-82.3	17.5	-14.6	23.5	-23.1	21.5
8	-79.2	37.0	-37.4	30.5	-82.1	17.5	-14.8	23.3	-23.2	21.3
9	-79.8	35.5	-38.3	30.5	-82.1	18.0	-14.7	23.6	-22.9	21.6
10	-78.8	35.4	-38.0	30.5	-81.9	17.6	-15.0	23.5	-22.8	21.0
11	-79.7	32.2	-37.7	30.4	-82.2	17.9	-14.1	23.5	-22.6	21.9
12	-79.1	34.8	-38.1	30.3	-82.6	17.5	-14.0	23.5	-22.6	21.4
13	-79.2	35.2	-38.6	30.9	-82.2	17.8	-14.2	23.7	-22.0	21.6
14	-78.4	33.6	-38.0	30.8	-82.3	17.7	-13.9	23.7	-22.1	21.6
15	-79.2	32.6	-37.7	30.6	-82.4	17.4	-13.8	23.8	-21.9	21.6
16	-79.2	32.4	-38.1	30.5	-82.1	17.5	-13.8	23.6	-21.7	21.9
17	-79.5	33.4	-37.8	30.5	-82.3	17.8	-13.4	23.9	-21.7	21.3
18	-78.9	34.9	-37.6	30.6	-82.2	17.8	-12.9	24.0	-21.8	21.6
19	-79.4	33.5	-37.7	30.6	-82.8	17.6	-12.7	23.6	-21.4	21.5
20	-79.7	35.6	-37.7	30.6	-82.9	17.6	-12.7	23.2	-21.2	21.3
Aver.	-79.1	34.0	-38.2	30.6	-82.3	17.6	-14.4	23.6	-22.6	21.6

Table G-65. Peak strain data under HVS wheel path 1, trial 19, slab 3

Load	**OS3600** (Top)	**OS3600** (Bottom)	**Vishay** (Top)	**Vishay** (Bottom)	**Kyowa** (Top)	**Kyowa** (Bottom)	**Tokyo** (Top)	**Tokyo** (Bottom)	**Tokyo** (Top)	**Tokyo** (Bottom)
1	-73.0	32.2	-43.5	29.9	-76.9	15.7	-21.6	23.5	-39.3	19.7
2	-73.5	30.3	-43.9	30.3	-76.5	15.6	-20.9	23.4	-39.2	19.4
3	-73.6	32.5	-42.9	29.8	-76.2	15.8	-20.7	23.2	-39.3	19.4
4	-73.9	33.2	-42.3	29.7	-76.2	15.5	-20.4	23.0	-38.8	19.6
5	-73.6	33.0	-41.3	29.6	-76.5	15.9	-20.3	23.6	-38.9	19.5
6	-74.0	30.7	-41.7	29.7	-76.2	15.3	-19.9	23.2	-39.3	19.8
7	-74.5	32.4	-40.4	30.0	-76.8	16.0	-19.5	23.6	-39.1	19.7
8	-74.7	31.7	-41.2	30.0	-76.4	15.9	-19.1	23.0	-38.4	19.4
9	-74.4	33.4	-40.1	30.1	-76.5	15.7	-18.9	23.3	-38.6	19.0
10	-74.6	31.8	-39.4	30.1	-76.8	15.8	-18.8	23.2	-38.4	19.4
11	-74.1	32.5	-39.1	30.3	-76.2	15.8	-18.1	23.1	-39.0	19.5
12	-74.1	33.0	-39.0	30.1	-76.2	16.1	-17.8	23.3	-38.7	19.4
13	-74.5	32.0	-38.5	30.0	-76.5	15.7	-17.7	23.0	-38.5	19.7
14	-74.8	32.1	-38.9	29.7	-76.4	15.8	-17.8	23.3	-38.4	19.1
15	-75.0	32.1	-37.3	30.2	-77.0	15.5	-17.2	23.2	-38.2	19.6
16	-74.8	32.2	-37.8	29.9	-76.6	15.7	-16.8	23.0	-37.6	19.6
17	-74.7	32.9	-36.7	30.3	-76.7	15.6	-16.6	23.5	-38.3	19.5
18	-74.8	32.5	-45.8	29.8	-77.0	15.5	-16.1	23.0	-37.8	19.8
19	-74.7	32.4	-40.4	29.6	-77.1	15.7	-15.7	22.9	-38.0	19.3
20	-74.8	32.6	-37.4	29.7	-76.3	15.5	-15.9	23.1	-37.9	19.5
Aver.	-74.3	32.3	-40.4	29.9	-76.6	15.7	-18.5	23.2	-38.6	19.5

Table G-66. Peak strain data under HVS wheel path 1, trial 20, slab 3

Load	**OS3600** (Top)	**OS3600** (Bottom)	**Vishay** (Top)	**Vishay** (Bottom)	**Kyowa** (Top)	**Kyowa** (Bottom)	**Tokyo** (Top)	**Tokyo** (Bottom)	**Tokyo** (Top)	**Tokyo** (Bottom)
1	-70.5	31.2	-46.6	28.9	-72.0	12.5	-36.9	23.4	-56.1	17.0
2	-70.9	32.7	-45.1	29.3	-71.8	12.7	-37.3	23.1	-56.0	16.6
3	-71.1	31.9	-45.3	29.4	-71.9	13.0	-37.5	22.8	-56.2	17.5
4	-70.8	31.3	-45.7	29.2	-71.9	12.8	-37.2	23.3	-55.4	17.2
5	-70.7	31.8	-44.5	29.1	-71.7	13.2	-37.2	22.7	-56.1	17.0
6	-70.7	32.5	-44.3	28.9	-71.8	13.4	-37.0	22.8	-55.4	17.0
7	-70.8	32.2	-44.6	29.1	-71.8	13.4	-37.2	23.1	-56.1	16.6
8	-71.5	32.7	-44.4	29.1	-72.3	13.5	-37.0	23.4	-56.0	16.8
9	-70.7	33.1	-45.4	29.5	-72.0	13.5	-37.3	23.2	-56.0	17.2
10	-71.0	32.0	-46.5	29.0	-72.1	13.3	-37.1	23.1	-56.3	16.9
11	-70.7	30.6	-45.7	29.3	-72.2	13.2	-37.0	23.2	-55.8	16.8
12	-70.9	31.4	-45.8	28.7	-72.1	13.0	-37.2	23.2	-55.9	17.1
13	-70.3	34.2	-46.9	29.1	-71.8	13.0	-36.7	23.4	-55.5	16.8
14	-70.4	32.8	-45.9	29.3	-72.6	13.2	-37.4	23.3	-56.1	16.8
15	-70.7	32.3	-45.8	29.3	-72.1	13.0	-37.2	23.3	-55.8	16.7
16	-70.9	29.7	-45.6	29.1	-72.9	12.8	-37.2	23.4	-55.8	16.9
17	-71.1	33.6	-45.2	29.3	-72.0	13.3	-37.2	23.1	-55.5	16.6
18	-70.7	32.2	-45.6	29.2	-72.4	13.0	-37.3	23.2	-56.0	17.0
19	-71.0	33.1	-45.2	29.2	-72.6	13.1	-37.1	23.6	-55.6	16.8
20	-70.1	32.7	-45.1	28.9	-72.2	12.9	-37.3	23.3	-55.7	17.1
Aver.	-70.8	32.2	-45.4	29.1	-72.1	13.1	-37.2	23.2	-55.9	16.9

Table G-67. Peak strain data under HVS wheel path 1, trial 21, slab 3

Load	**OS3600** (Top)	**OS3600** (Bottom)	**Vishay** (Top)	**Vishay** (Bottom)	**Kyowa** (Top)	**Kyowa** (Bottom)	**Tokyo** (Top)	**Tokyo** (Bottom)	**Tokyo** (Top)	**Tokyo** (Bottom)
1	-74.9	32.0	-46.6	29.6	-78.4	13.6	-37.7	24.0	-60.5	17.3
2	-74.5	32.2	-46.1	29.6	-78.3	13.7	-37.8	23.8	-60.7	17.1
3	-74.1	31.8	-46.1	29.4	-78.5	13.4	-37.8	23.5	-60.6	16.9
4	-74.0	31.8	-46.6	29.4	-78.5	13.8	-37.8	24.0	-60.5	17.6
5	-74.5	31.9	-47.3	29.7	-78.5	13.6	-37.8	24.0	-60.8	17.3
6	-74.0	32.4	-47.9	29.5	-78.9	13.5	-37.8	23.5	-60.8	17.2
7	-74.0	31.6	-50.8	29.4	-78.2	13.6	-37.4	23.6	-60.2	16.7
8	-74.5	31.6	-51.6	29.2	-78.2	13.6	-38.5	23.9	-60.8	16.6
9	-74.5	31.3	-54.3	29.6	-79.1	13.7	-38.0	23.4	-60.8	16.7
10	-74.3	31.8	-48.4	29.2	-78.4	13.7	-38.4	23.3	-60.6	17.2
11	-74.2	31.3	-46.1	29.8	-77.8	13.8	-37.9	23.5	-60.8	17.1
12	-74.5	31.1	-45.2	29.9	-78.2	13.6	-37.2	24.3	-60.7	16.5
13	-74.0	31.8	-44.4	29.1	-78.5	13.5	-37.4	23.7	-60.8	16.5
14	-74.2	32.5	-44.3	29.6	-78.0	13.4	-37.9	23.7	-60.0	16.9
15	-74.2	31.9	-43.6	29.9	-78.1	13.2	-37.9	23.7	-60.8	16.7
16	-74.8	31.7	-43.6	29.6	-78.5	13.5	-37.2	23.9	-60.7	16.7
17	-73.8	31.7	-43.0	29.8	-78.1	13.6	-37.4	24.2	-60.3	17.1
18	-74.6	31.9	-42.7	30.0	-78.1	13.8	-37.4	24.4	-60.7	16.8
19	-74.1	32.7	-43.0	29.0	-78.0	13.8	-37.4	23.8	-60.6	17.0
20	-74.5	31.8	-43.7	29.7	-77.7	13.8	-37.3	23.9	-60.3	17.0
Aver.	-74.3	31.8	-46.3	29.5	-78.3	13.6	-37.7	23.8	-60.6	17.0

Table G-68. Peak strain data under HVS wheel path 1, trial 22, slab 3

Load	**OS3600** (Top)	**OS3600** (Bottom)	**Vishay** (Top)	**Vishay** (Bottom)	**Kyowa** (Top)	**Kyowa** (Bottom)	**Tokyo** (Top)	**Tokyo** (Bottom)	**Tokyo** (Top)	**Tokyo** (Bottom)
1	-75.8	32.9	-44.5	30.4	-80.9	14.7	-40.2	25.0	-64.2	18.1
2	-75.0	33.4	-44.4	30.6	-81.4	14.7	-39.9	24.6	-64.1	18.5
3	-75.1	32.6	-44.4	30.2	-80.6	15.0	-40.2	25.3	-64.0	18.3
4	-75.1	33.5	-45.7	30.1	-81.0	14.7	-40.2	25.0	-64.1	18.1
5	-75.2	33.8	-45.5	30.7	-79.9	15.0	-39.3	24.9	-63.9	18.4
6	-75.8	33.4	-44.8	30.6	-80.3	14.7	-39.6	24.9	-63.9	18.6
7	-75.3	33.3	-45.1	30.4	-80.9	14.9	-39.5	24.5	-64.2	18.2
8	-75.0	33.4	-44.5	30.8	-80.8	14.8	-39.9	24.5	-64.0	18.2
9	-74.8	33.3	-44.8	30.4	-80.6	15.4	-39.9	24.5	-64.3	18.6
10	-75.3	34.0	-45.2	30.6	-81.1	15.2	-39.5	24.3	-63.3	18.3
11	-74.9	33.4	-45.2	30.2	-80.7	15.1	-39.4	24.5	-63.7	18.0
12	-75.3	32.4	-45.2	30.5	-80.9	14.8	-39.9	24.6	-64.0	18.3
13	-74.8	32.7	-45.1	30.3	-80.5	15.1	-39.6	24.9	-63.6	18.2
14	-75.3	33.2	-45.2	30.7	-80.7	14.7	-40.1	24.7	-63.8	18.7
15	-75.2	33.2	-45.1	30.4	-80.8	14.7	-39.8	24.4	-64.4	18.4
16	-74.8	33.2	-44.7	30.6	-80.9	15.1	-40.3	24.8	-64.1	18.1
17	-74.8	32.8	-44.5	30.6	-81.1	15.0	-40.0	25.4	-63.9	18.2
18	-75.8	32.4	-44.7	30.4	-80.7	14.7	-39.6	24.4	-64.2	18.1
19	-75.2	33.8	-46.7	30.5	-80.9	14.8	-38.8	25.2	-63.6	18.6
20	-75.3	32.6	-46.9	30.1	-81.1	15.1	-39.7	25.0	-64.2	18.2
Aver.	-75.2	33.2	-45.1	30.5	-80.8	14.9	-39.8	24.8	-64.0	18.3

Table G-69. Peak strain data under HVS wheel path 1, trial 23, slab 3

Load	**OS3600** (Top)	**OS3600** (Bottom)	**Vishay** (Top)	**Vishay** (Bottom)	**Kyowa** (Top)	**Kyowa** (Bottom)	**Tokyo** (Top)	**Tokyo** (Bottom)	**Tokyo** (Top)	**Tokyo** (Bottom)
1	-77.7	33.8	-41.0	32.9	-82.9	17.5	-42.3	26.0	-67.0	21.0
2	-77.3	34.8	-41.2	32.4	-83.3	17.1	-41.8	25.8	-67.2	20.4
3	-77.2	34.4	-40.4	32.3	-83.1	17.3	-42.2	25.9	-67.3	20.7
4	-77.1	33.9	-40.7	32.5	-82.6	17.1	-41.9	25.8	-66.5	20.7
5	-77.8	34.5	-40.4	32.1	-83.6	16.8	-42.3	25.9	-67.2	20.2
6	-78.0	34.6	-41.3	32.2	-83.1	17.0	-42.2	26.3	-67.6	20.5
7	-77.5	33.3	-40.7	32.4	-83.1	16.9	-42.1	26.0	-67.6	20.6
8	-77.8	34.5	-43.3	32.4	-83.0	16.7	-41.7	25.9	-67.7	20.5
9	-77.7	34.3	-43.4	32.1	-83.3	16.8	-41.6	25.6	-66.9	19.9
10	-77.9	34.3	-44.4	32.4	-83.5	16.9	-41.6	25.8	-67.2	20.0
11	-77.7	34.3	-47.0	32.3	-82.8	17.0	-41.3	25.9	-67.4	20.5
12	-77.7	34.5	-46.2	32.4	-82.7	16.7	-41.8	26.1	-66.8	20.0
13	-77.5	34.5	-45.9	32.4	-83.6	16.9	-41.3	25.9	-66.9	20.0
14	-76.8	34.6	-46.9	32.4	-83.0	16.8	-41.9	25.8	-67.4	20.4
15	-77.8	34.1	-47.3	32.3	-83.5	16.9	-41.9	25.8	-67.6	20.7
16	-76.8	34.9	-48.3	32.1	-83.4	16.6	-41.4	25.9	-67.4	20.4
17	-78.0	35.3	-48.8	32.4	-83.2	16.5	-41.7	26.1	-67.4	20.0
18	-77.4	35.0	-49.8	32.3	-83.8	16.6	-41.5	25.7	-66.9	20.0
19	-77.6	34.1	-49.9	32.3	-83.3	17.0	-41.7	25.6	-67.2	20.4
20	-78.0	34.4	-49.1	32.5	-83.2	16.7	-41.7	25.7	-67.0	20.5
Aver.	-77.6	34.4	-44.8	32.4	-83.2	16.9	-41.8	25.9	-67.2	20.4

Table G-70. Peak strain data under HVS wheel path 1, trial 24, slab 3

Load	**OS3600** (Top)	**OS3600** (Bottom)	**Vishay** (Top)	**Vishay** (Bottom)	**Kyowa** (Top)	**Kyowa** (Bottom)	**Tokyo** (Top)	**Tokyo** (Bottom)	**Tokyo** (Top)	**Tokyo** (Bottom)
1	-78.5	34.4	-48.5	32.4	-84.1	15.9	-42.9	26.5	-68.7	19.9
2	-77.9	34.5	-47.6	32.3	-83.7	16.3	-43.0	26.0	-68.0	20.1
3	-78.0	34.0	-47.9	32.4	-83.8	16.7	-42.7	26.1	-68.9	20.0
4	-78.5	34.9	-47.5	32.6	-84.2	16.6	-43.2	25.9	-69.1	19.8
5	-78.1	34.7	-47.6	32.6	-84.2	16.2	-43.3	25.8	-68.8	19.9
6	-77.3	34.1	-47.6	32.6	-84.2	16.2	-42.6	26.1	-68.9	19.6
7	-78.3	34.2	-47.5	32.6	-83.8	16.5	-43.3	26.1	-68.9	19.6
8	-78.4	34.1	-47.5	32.2	-83.8	16.5	-42.6	26.1	-68.9	20.0
9	-78.0	34.2	-47.8	32.9	-84.1	16.2	-42.9	26.2	-68.7	19.7
10	-78.8	34.4	-47.8	32.5	-83.8	16.3	-43.0	26.1	-68.7	19.7
11	-78.6	34.8	-47.6	32.2	-84.0	16.6	-43.2	25.5	-68.8	19.8
12	-78.8	34.4	-47.3	32.6	-84.2	16.0	-43.1	25.8	-69.4	20.0
13	-77.6	33.9	-47.4	32.2	-83.9	16.3	-42.9	25.8	-68.7	20.3
14	-77.9	34.3	-47.4	31.8	-83.9	16.6	-43.2	25.9	-68.6	19.7
15	-77.8	34.2	-47.1	32.4	-83.8	16.5	-42.7	25.7	-68.4	19.9
16	-78.1	35.1	-47.2	31.9	-83.8	16.6	-43.4	25.8	-69.3	19.5
17	-78.6	34.5	-47.2	32.3	-84.0	16.5	-42.8	25.5	-68.8	19.3
18	-78.2	35.7	-47.0	32.4	-84.8	16.3	-43.3	25.7	-68.6	19.5
19	-78.1	34.8	-47.3	32.5	-84.3	16.0	-43.2	26.0	-69.3	19.6
20	-78.1	33.7	-47.3	32.0	-84.3	16.0	-43.1	26.0	-69.2	19.4
Aver.	-78.2	34.4	-47.5	32.4	-84.0	16.3	-43.0	25.9	-68.8	19.8

Table G-71. Peak strain data under HVS wheel path 1, trial 1, slab 4

Load	**OS3500** (Top)	**OS3500** (Bottom)	**OS3600** (Top)	**OS3600** (Bottom)	**Kyowa** (Top)	**Kyowa** (Bottom)	**Tokyo** (Top)	**Tokyo** (Bottom)	**Vishay** (Top)	**Vishay** (Bottom)
1	-22.4	26.5	-24.9	22.4	-20.6	26.6	-25.6	24.8	-15.4	20.7
2	-22.5	26.3	-25.5	22.3	-20.8	26.5	-25.2	25.0	-15.4	20.9
3	-22.8	26.7	-24.5	22.3	-20.8	26.5	-25.7	25.0	-15.6	21.1
4	-22.6	26.8	-24.7	22.6	-20.5	26.8	-25.7	25.0	-15.5	21.1
5	-22.1	26.3	-24.6	22.5	-20.4	26.4	-25.4	24.8	-15.5	21.1
6	-22.5	26.5	-25.0	22.4	-20.2	26.5	-25.7	24.9	-15.6	21.2
7	-21.8	26.7	-24.9	22.4	-20.9	27.0	-25.4	24.6	-15.3	21.1
8	-22.3	26.8	-24.8	22.6	-20.4	26.4	-25.3	24.7	-15.5	21.0
9	-22.4	26.4	-24.9	22.4	-20.9	26.9	-25.2	24.8	-15.2	20.8
10	-22.4	26.7	-24.0	22.7	-20.5	26.3	-25.8	24.8	-15.2	20.9
11	-22.0	26.8	-24.4	22.5	-	-	-	-	-	-
12	-22.1	26.7	-24.7	22.4	-	-	-	-	-	-
13	-21.9	26.5	-24.1	22.9	-	-	-	-	-	-
14	-21.7	26.0	-25.1	22.3	-	-	-	-	-	-
15	-21.8	25.9	-24.3	22.8	-	-	-	-	-	-
16	-21.8	26.2	-24.5	22.6	-	-	-	-	-	-
17	-21.3	26.1	-24.5	22.2	-	-	-	-	-	-
18	-21.9	26.1	-24.4	22.8	-	-	-	-	-	-
19	-21.6	26.4	-24.5	22.7	-	-	-	-	-	-
20	-22.1	26.8	-24.3	22.5	-	-	-	-	-	-
Aver.	-22.1	26.5	-24.6	22.5	-20.6	26.6	-25.5	24.8	-15.4	21.0

Table G-72. Peak strain data under HVS wheel path 1, trial 2, slab 4

Load	**OS3500** (Top)	**OS3500** (Bottom)	**OS3600** (Top)	**OS3600** (Bottom)	**Kyowa** (Top)	**Kyowa** (Bottom)	**Tokyo** (Top)	**Tokyo** (Bottom)	**Vishay** (Top)	**Vishay** (Bottom)
1	-24.3	26.5	-26.1	22.9	-22.8	29.6	-27.7	27.0	-17.2	23.0
2	-24.0	26.6	-26.3	22.7	-22.3	29.3	-27.5	27.0	-17.1	23.2
3	-23.9	26.7	-26.1	22.9	-22.7	29.7	-28.0	26.9	-17.3	22.9
4	-23.7	26.5	-26.0	23.0	-22.3	29.4	-28.2	27.1	-17.0	22.6
5	-23.9	26.5	-26.6	23.0	-22.6	29.2	-27.5	26.9	-17.4	23.0
6	-24.1	26.3	-25.9	22.5	-22.8	29.3	-27.5	26.9	-17.1	22.7
7	-23.9	26.3	-25.8	23.0	-22.9	29.3	-27.8	26.6	-17.5	23.0
8	-23.6	26.4	-26.5	22.6	-22.7	29.2	-27.9	26.9	-17.4	22.7
9	-23.4	26.2	-26.2	22.8	-22.7	29.8	-27.8	27.3	-17.2	23.3
10	-23.1	26.2	-25.9	22.9	-22.6	29.9	-27.2	27.0	-17.1	22.8
11	-23.8	26.3	-25.6	22.8	-	-	-	-	-	-
12	-24.0	27.0	-25.5	23.3	-	-	-	-	-	-
13	-23.6	26.5	-25.7	23.2	-	-	-	-	-	-
14	-23.9	26.7	-25.6	23.3	-	-	-	-	-	-
15	-23.8	27.0	-26.2	22.8	-	-	-	-	-	-
16	-23.4	26.6	-26.2	23.3	-	-	-	-	-	-
17	-23.9	26.4	-26.1	23.1	-	-	-	-	-	-
18	-23.3	26.5	-26.1	23.1	-	-	-	-	-	-
19	-24.1	26.5	-26.2	23.4	-	-	-	-	-	-
20	-23.7	26.9	-25.8	22.9	-	-	-	-	-	-
Aver.	-23.8	26.5	-26.0	23.0	-22.6	29.5	-27.7	27.0	-17.2	22.9

Table G-73. Peak strain data under HVS wheel path 1, trial 3, slab 4

Load	**OS3500** (Top)	**OS3500** (Bottom)	**OS3600** (Top)	**OS3600** (Bottom)	**Kyowa** (Top)	**Kyowa** (Bottom)	**Tokyo** (Top)	**Tokyo** (Bottom)	**Vishay** (Top)	**Vishay** (Bottom)
1	-25.3	26.9	-27.2	23.6	-23.0	29.8	-29.1	26.9	-16.7	23.0
2	-24.4	26.4	-27.3	23.7	-23.0	29.5	-28.1	27.1	-17.0	23.5
3	-24.6	27.2	-27.4	23.9	-23.0	29.7	-28.4	26.9	-17.1	23.1
4	-24.8	26.7	-27.5	23.1	-22.8	29.1	-28.9	26.8	-17.3	22.8
5	-25.1	26.8	-27.2	23.8	-22.9	29.6	-28.7	26.9	-17.4	22.7
6	-24.6	26.9	-27.2	23.7	-22.8	29.3	-28.5	27.1	-16.9	23.2
7	-24.6	26.3	-27.1	23.2	-22.8	29.8	-28.6	27.1	-17.1	23.3
8	-24.5	27.2	-27.3	23.4	-23.0	29.4	-28.6	27.2	-17.3	23.4
9	-24.8	27.1	-26.5	23.7	-22.6	29.6	-28.8	26.6	-16.9	23.3
10	-24.6	26.7	-26.9	23.6	-22.6	29.3	-28.3	26.7	-17.2	23.0
11	-24.5	27.4	-26.7	23.3	-	-	-	-	-	-
12	-24.8	26.7	-27.0	23.2	-	-	-	-	-	-
13	-24.7	27.4	-26.5	23.3	-	-	-	-	-	-
14	-24.4	27.2	-27.2	23.7	-	-	-	-	-	-
15	-25.1	26.9	-27.2	23.7	-	-	-	-	-	-
16	-24.5	26.8	-27.4	23.6	-	-	-	-	-	-
17	-24.4	27.0	-27.5	24.0	-	-	-	-	-	-
18	-24.6	27.5	-26.7	23.3	-	-	-	-	-	-
19	-24.9	27.5	-27.8	23.5	-	-	-	-	-	-
20	-25.4	27.3	-27.3	23.7	-	-	-	-	-	-
Aver.	-24.7	27.0	-27.1	23.5	-22.8	29.5	-28.6	26.9	-17.1	23.1

Table G-74. Peak strain data under HVS wheel path 1, trial 4, slab 4

Load	**OS3500** (Top)	**OS3500** (Bottom)	**OS3600** (Top)	**OS3600** (Bottom)	**Kyowa** (Top)	**Kyowa** (Bottom)	**Tokyo** (Top)	**Tokyo** (Bottom)	**Vishay** (Top)	**Vishay** (Bottom)
1	-24.9	27.8	-28.2	25.0	-22.9	29.6	-29.3	26.8	-17.0	23.1
2	-25.6	28.0	-27.8	24.7	-23.1	29.3	-28.8	27.3	-16.9	23.3
3	-25.9	28.5	-27.8	25.3	-22.5	29.6	-28.6	26.8	-16.7	22.9
4	-25.5	28.2	-28.1	24.8	-23.2	29.3	-28.4	27.3	-16.8	23.3
5	-25.4	28.0	-27.8	25.2	-22.9	29.5	-28.5	26.7	-17.1	23.0
6	-25.7	28.0	-27.7	24.8	-22.8	29.7	-28.4	26.9	-16.6	23.3
7	-25.1	27.9	-28.0	25.0	-22.9	29.7	-28.9	27.2	-17.2	23.3
8	-25.1	27.5	-27.4	24.9	-22.8	29.5	-29.1	27.0	-17.2	23.0
9	-25.6	28.1	-27.9	25.5	-22.8	29.1	-28.5	27.2	-16.8	23.0
10	-25.3	28.1	-28.1	25.0	-22.5	29.7	-28.0	27.7	-16.8	23.1
11	-25.7	28.1	-28.0	25.0	-	-	-	-	-	-
12	-25.3	27.7	-27.7	25.0	-	-	-	-	-	-
13	-25.7	27.8	-28.1	24.8	-	-	-	-	-	-
14	-25.5	28.0	-28.2	24.6	-	-	-	-	-	-
15	-25.8	28.2	-27.9	25.0	-	-	-	-	-	-
16	-25.4	28.4	-28.3	24.7	-	-	-	-	-	-
17	-25.3	27.6	-28.4	24.7	-	-	-	-	-	-
18	-25.9	28.1	-28.4	24.6	-	-	-	-	-	-
19	-25.9	27.6	-27.9	25.2	-	-	-	-	-	-
20	-25.4	27.6	-28.5	24.9	-	-	-	-	-	-
Aver.	-25.5	27.9	-28.0	24.9	-22.8	29.5	-28.6	27.1	-16.9	23.1

Table G-75. Peak strain data under HVS wheel path 1, trial 5, slab 4

Load	**OS3500** (Top)	**OS3500** (Bottom)	**OS3600** (Top)	**OS3600** (Bottom)	**Kyowa** (Top)	**Kyowa** (Bottom)	**Tokyo** (Top)	**Tokyo** (Bottom)	**Vishay** (Top)	**Vishay** (Bottom)
1	-25.7	29.1	-27.5	25.1	-22.8	29.3	-29.1	27.1	-17.1	22.8
2	-26.3	29.3	-27.7	25.3	-22.6	29.5	-29.0	26.7	-17.3	23.2
3	-26.0	29.8	-27.8	25.6	-23.0	29.0	-29.2	27.1	-17.5	22.7
4	-26.1	29.6	-28.2	24.9	-22.9	29.5	-29.3	27.0	-17.1	23.0
5	-26.6	29.8	-27.7	25.3	-22.9	28.9	-28.8	27.3	-17.1	23.0
6	-26.0	29.3	-27.6	25.5	-23.2	29.1	-28.7	26.9	-17.1	23.0
7	-26.0	29.4	-27.9	25.0	-22.9	28.7	-28.9	26.8	-17.2	22.9
8	-25.9	29.0	-27.8	25.7	-22.8	28.7	-29.0	26.7	-17.1	23.1
9	-26.0	29.9	-27.8	25.4	-23.1	28.9	-28.9	26.9	-17.2	22.8
10	-26.5	29.4	-27.3	25.2	-22.8	29.1	-29.0	27.1	-17.3	22.8
11	-26.1	29.8	-28.0	25.8	-	-	-	-	-	-
12	-26.1	29.1	-28.0	25.2	-	-	-	-	-	-
13	-25.8	29.4	-28.0	25.8	-	-	-	-	-	-
14	-26.6	30.1	-27.8	25.4	-	-	-	-	-	-
15	-25.8	29.7	-27.9	25.9	-	-	-	-	-	-
16	-26.1	28.9	-27.5	25.6	-	-	-	-	-	-
17	-26.1	29.7	-27.9	25.9	-	-	-	-	-	-
18	-25.9	29.6	-28.2	25.4	-	-	-	-	-	-
19	-26.0	29.3	-27.9	25.3	-	-	-	-	-	-
20	-26.0	29.6	-27.9	25.5	-	-	-	-	-	-
Aver.	-26.1	29.5	-27.8	25.4	-22.9	29.1	-29.0	27.0	-17.2	22.9

Table G-76. Peak strain data under HVS wheel path 1, trial 6, slab 4

Load	**OS3500** (Top)	**OS3500** (Bottom)	**OS3600** (Top)	**OS3600** (Bottom)	**Kyowa** (Top)	**Kyowa** (Bottom)	**Tokyo** (Top)	**Tokyo** (Bottom)	**Vishay** (Top)	**Vishay** (Bottom)
1	-20.5	29.4	-14.6	25.7	-22.8	29.4	-29.3	26.4	-17.0	22.6
2	-20.3	29.4	-14.6	26.1	-23.0	29.8	-29.7	26.8	-17.2	22.2
3	-20.4	29.8	-14.4	26.0	-22.7	29.5	-29.4	26.3	-17.1	22.8
4	-19.9	29.4	-14.5	26.0	-22.7	29.5	-29.7	26.5	-17.4	22.7
5	-20.0	29.3	-14.6	25.8	-22.7	29.1	-29.3	26.8	-17.2	22.9
6	-20.0	29.1	-14.9	25.8	-22.9	29.7	-29.9	26.2	-17.4	22.8
7	-20.0	29.7	-14.6	26.3	-22.8	29.4	-29.8	26.7	-16.9	23.0
8	-20.6	29.6	-14.9	25.7	-22.4	29.0	-29.6	26.7	-17.2	22.7
9	-19.6	29.6	-14.4	26.0	-22.1	29.2	-29.5	26.8	-17.2	23.1
10	-20.4	29.1	-13.9	26.1	-22.5	29.1	-29.5	26.4	-17.2	22.8
11	-20.0	29.4	-14.8	25.5	-	-	-	-	-	-
12	-19.9	29.4	-14.5	25.8	-	-	-	-	-	-
13	-20.0	30.2	-14.4	25.6	-	-	-	-	-	-
14	-19.9	30.0	-14.7	25.7	-	-	-	-	-	-
15	-20.0	29.4	-14.7	25.6	-	-	-	-	-	-
16	-19.9	29.7	-14.5	25.3	-	-	-	-	-	-
17	-20.1	29.7	-14.1	26.2	-	-	-	-	-	-
18	-20.5	29.2	-14.5	25.5	-	-	-	-	-	-
19	-20.0	29.3	-14.3	26.3	-	-	-	-	-	-
20	-20.1	29.5	-14.5	25.8	-	-	-	-	-	-
Aver.	-20.5	29.4	-14.6	25.7	-22.7	29.4	-29.6	26.6	-17.2	22.8

Table G-77. Peak strain data under HVS wheel path 1, trial 7, slab 4

Load	**OS3500** (Top)	**OS3500** (Bottom)	**OS3600** (Top)	**OS3600** (Bottom)	**Kyowa** (Top)	**Kyowa** (Bottom)	**Tokyo** (Top)	**Tokyo** (Bottom)	**Vishay** (Top)	**Vishay** (Bottom)
1	-26.8	29.7	-28.0	26.4	-20.4	26.2	-22.9	23.9	-13.9	19.5
2	-26.4	29.7	-28.0	26.3	-19.4	25.6	-23.5	23.7	-13.6	19.4
3	-26.3	29.3	-27.9	26.0	-19.7	25.9	-23.5	23.9	-14.0	19.4
4	-26.3	29.5	-27.9	26.7	-19.9	26.7	-23.4	23.8	-14.3	20.0
5	-26.3	29.8	-28.4	26.4	-20.0	26.1	-23.5	24.6	-13.9	20.2
6	-26.0	29.2	-28.2	26.1	-20.0	26.0	-23.3	24.1	-14.2	19.9
7	-26.3	30.2	-28.4	26.3	-19.7	26.5	-23.7	24.7	-14.0	20.2
8	-26.7	29.4	-28.3	26.0	-20.3	26.2	-23.5	23.9	-13.7	19.8
9	-26.5	29.5	-28.1	26.1	-20.0	26.3	-23.4	24.2	-13.6	20.1
10	-26.6	29.5	-28.4	26.0	-20.1	26.6	-23.2	24.5	-13.8	19.9
11	-26.2	29.1	-28.1	26.3	-	-	-	-	-	-
12	-26.9	29.6	-28.1	26.4	-	-	-	-	-	-
13	-26.4	29.4	-27.9	26.4	-	-	-	-	-	-
14	-26.6	29.6	-28.2	26.2	-	-	-	-	-	-
15	-26.7	29.5	-28.0	26.2	-	-	-	-	-	-
16	-27.0	29.7	-28.5	26.7	-	-	-	-	-	-
17	-26.9	29.5	-28.2	26.5	-	-	-	-	-	-
18	-26.4	29.7	-28.6	26.4	-	-	-	-	-	-
19	-26.8	29.5	-28.2	26.0	-	-	-	-	-	-
20	-27.0	29.8	-28.6	25.9	-	-	-	-	-	-
Aver.	-26.6	29.6	-28.2	26.3	-19.9	26.2	-23.4	24.1	-13.9	19.8

Table G-78. Peak strain data under HVS wheel path 1, trial 8, slab 4

Load	**OS3500** (Top)	**OS3500** (Bottom)	**OS3600** (Top)	**OS3600** (Bottom)	**Kyowa** (Top)	**Kyowa** (Bottom)	**Tokyo** (Top)	**Tokyo** (Bottom)	**Vishay** (Top)	**Vishay** (Bottom)
1	-26.5	29.5	-28.5	26.0	-23.3	28.8	-29.8	26.7	-16.8	22.3
2	-26.4	29.0	-28.0	25.5	-23.1	29.3	-29.6	26.6	-16.5	22.4
3	-26.4	30.3	-28.0	26.0	-23.4	28.7	-30.0	26.9	-16.8	23.3
4	-26.3	29.7	-28.2	25.6	-23.7	28.8	-29.6	26.8	-16.9	22.7
5	-26.3	29.6	-28.0	25.9	-23.5	29.2	-29.4	26.9	-16.9	22.8
6	-26.8	29.8	-28.3	26.2	-23.5	29.4	-29.1	27.0	-16.5	22.8
7	-26.5	29.9	-28.2	25.6	-23.5	28.9	-29.3	27.1	-17.1	22.6
8	-26.5	30.0	-28.5	26.0	-22.9	29.2	-29.4	27.3	-16.4	23.2
9	-27.1	29.5	-28.8	25.5	-23.3	29.1	-29.4	27.2	-16.8	22.5
10	-26.3	29.1	-28.0	26.0	-23.4	28.7	-29.5	26.8	-17.1	22.7
11	-26.5	30.0	-28.3	25.6	-	-	-	-	-	-
12	-26.4	29.8	-28.5	25.6	-	-	-	-	-	-
13	-26.5	30.0	-28.4	25.7	-	-	-	-	-	-
14	-26.6	29.8	-28.3	25.8	-	-	-	-	-	-
15	-26.4	29.3	-28.4	26.1	-	-	-	-	-	-
16	-26.3	29.7	-28.2	25.5	-	-	-	-	-	-
17	-26.1	29.5	-28.6	26.0	-	-	-	-	-	-
18	-26.3	29.3	-28.3	25.3	-	-	-	-	-	-
19	-26.5	29.6	-28.3	25.5	-	-	-	-	-	-
20	-26.1	29.2	-28.0	25.4	-	-	-	-	-	-
Aver.	-26.4	29.6	-28.3	25.7	-23.4	29.0	-29.5	26.9	-16.8	22.7

Table G-79. Peak strain data under HVS wheel path 1, trial 9, slab 4

Load	**OS3500** (Top)	**OS3500** (Bottom)	**OS3600** (Top)	**OS3600** (Bottom)	**Kyowa** (Top)	**Kyowa** (Bottom)	**Tokyo** (Top)	**Tokyo** (Bottom)	**Vishay** (Top)	**Vishay** (Bottom)
1	-26.4	30.1	-27.8	25.9	-23.5	29.0	-30.1	26.6	-16.8	22.9
2	-26.8	30.5	-28.1	25.9	-23.0	29.2	-30.0	26.9	-16.6	23.5
3	-26.7	29.9	-27.7	25.5	-23.3	29.4	-30.2	26.7	-16.7	23.4
4	-26.7	29.7	-27.9	25.9	-23.6	29.2	-29.7	26.5	-16.8	23.2
5	-26.4	29.1	-28.1	25.4	-23.3	29.3	-30.1	26.5	-16.8	23.2
6	-26.8	29.7	-27.9	25.6	-23.8	28.9	-29.9	27.1	-16.3	23.2
7	-26.4	29.7	-27.9	25.7	-24.1	29.2	-30.0	27.0	-16.4	23.4
8	-26.4	29.4	-28.3	25.6	-23.6	29.4	-29.9	26.8	-16.3	23.1
9	-26.3	29.8	-27.7	25.4	-23.5	29.7	-30.3	26.5	-16.5	22.9
10	-26.6	29.4	-28.0	25.6	-23.4	29.5	-29.8	26.8	-16.6	22.8
11	-26.4	30.0	-28.3	25.6	-	-	-	-	-	-
12	-26.6	29.6	-28.2	25.8	-	-	-	-	-	-
13	-26.1	29.8	-27.9	25.9	-	-	-	-	-	-
14	-26.6	29.9	-28.7	25.4	-	-	-	-	-	-
15	-26.6	29.4	-28.1	25.5	-	-	-	-	-	-
16	-26.5	29.6	-28.2	25.8	-	-	-	-	-	-
17	-26.1	29.6	-27.8	25.4	-	-	-	-	-	-
18	-26.5	29.5	-27.9	25.4	-	-	-	-	-	-
19	-26.7	29.8	-27.8	25.7	-	-	-	-	-	-
20	-26.0	30.1	-28.0	26.0	-	-	-	-	-	-
Aver.	-26.5	29.7	-28.0	25.7	-23.5	29.3	-30.0	26.7	-16.6	23.2

Table G-80. Peak strain data under HVS wheel path 1, trial 10, slab 4

Load	**OS3500** (Top)	**OS3500** (Bottom)	**OS3600** (Top)	**OS3600** (Bottom)	**Kyowa** (Top)	**Kyowa** (Bottom)	**Tokyo** (Top)	**Tokyo** (Bottom)	**Vishay** (Top)	**Vishay** (Bottom)
1	-25.8	30.4	-27.6	25.7	-23.4	29.4	-30.4	27.0	-16.4	22.6
2	-25.9	30.1	-27.9	25.5	-22.8	29.3	-30.3	26.7	-16.8	22.2
3	-25.6	29.9	-27.9	25.4	-22.6	29.3	-30.1	26.5	-16.8	22.4
4	-25.7	29.8	-27.8	25.9	-23.0	29.4	-30.2	26.5	-16.8	22.7
5	-26.2	29.8	-28.0	25.4	-22.8	29.2	-30.1	26.5	-16.7	22.7
6	-26.3	30.0	-28.3	25.4	-23.3	29.5	-30.4	26.6	-16.8	22.9
7	-25.8	30.7	-27.7	25.8	-22.8	29.6	-30.5	26.5	-16.6	22.7
8	-25.9	30.0	-27.6	25.5	-22.8	29.5	-30.8	26.7	-16.6	22.5
9	-26.0	29.9	-27.9	25.8	-23.1	29.5	-30.7	27.1	-16.6	22.6
10	-26.2	29.9	-27.4	26.2	-22.9	29.4	-30.3	27.1	-16.9	22.3
11	-25.8	29.9	-28.3	25.9	-	-	-	-	-	-
12	-26.2	30.0	-27.6	25.8	-	-	-	-	-	-
13	-25.2	29.9	-27.7	25.8	-	-	-	-	-	-
14	-26.1	29.9	-28.1	25.6	-	-	-	-	-	-
15	-25.2	29.9	-27.8	25.4	-	-	-	-	-	-
16	-25.2	29.5	-28.0	25.5	-	-	-	-	-	-
17	-25.8	29.5	-27.9	25.2	-	-	-	-	-	-
18	-25.7	29.7	-28.1	26.1	-	-	-	-	-	-
19	-25.9	29.9	-27.4	26.0	-	-	-	-	-	-
20	-25.9	29.8	-27.9	25.6	-	-	-	-	-	-
Aver.	-25.8	29.9	-27.8	25.7	-23.0	29.4	-30.4	26.7	-16.7	22.6

Table G-81. Peak strain data under HVS wheel path 1, trial 11, slab 4

Load	**OS3500** (Top)	**OS3500** (Bottom)	**OS3600** (Top)	**OS3600** (Bottom)	**Kyowa** (Top)	**Kyowa** (Bottom)	**Tokyo** (Top)	**Tokyo** (Bottom)	**Vishay** (Top)	**Vishay** (Bottom)
1	-25.6	30.2	-27.1	25.1	-23.3	29.9	-30.9	27.2	-17.0	23.5
2	-25.6	29.5	-27.5	25.2	-23.5	29.9	-30.3	27.2	-16.8	23.4
3	-25.3	29.3	-27.7	25.4	-23.7	29.8	-30.4	27.4	-17.0	22.9
4	-25.3	30.3	-28.0	25.8	-23.6	30.0	-30.5	27.3	-17.3	22.8
5	-25.0	29.5	-27.9	25.0	-22.9	30.2	-30.0	27.1	-17.1	23.1
6	-25.7	30.1	-27.0	25.6	-23.3	29.8	-30.8	27.3	-17.2	22.9
7	-25.3	29.4	-27.5	24.8	-23.9	29.9	-30.6	27.0	-17.0	22.7
8	-25.6	30.3	-27.7	25.0	-23.3	29.7	-30.0	27.2	-17.2	23.0
9	-25.4	29.7	-27.9	25.6	-23.4	29.5	-30.2	26.8	-16.9	23.3
10	-25.4	30.3	-27.9	25.7	-23.6	29.3	-30.2	27.2	-17.1	23.0
11	-25.7	30.5	-27.6	25.4	-	-	-	-	-	-
12	-26.0	29.8	-27.7	25.1	-	-	-	-	-	-
13	-25.5	29.9	-27.9	25.6	-	-	-	-	-	-
14	-25.3	29.8	-27.9	25.3	-	-	-	-	-	-
15	-25.5	30.5	-27.5	26.3	-	-	-	-	-	-
16	-25.5	30.6	-27.6	26.0	-	-	-	-	-	-
17	-25.8	29.5	-27.8	25.4	-	-	-	-	-	-
18	-25.7	30.5	-27.8	25.3	-	-	-	-	-	-
19	-25.9	30.1	-27.9	25.7	-	-	-	-	-	-
20	-25.8	29.9	-28.2	25.7	-	-	-	-	-	-
Aver.	-25.5	30.0	-27.7	25.4	-23.4	29.8	-30.4	27.2	-17.1	23.1

Table G-82. Peak strain data under HVS wheel path 1, trial 12, slab 4

Load	**OS3500** (Top)	**OS3500** (Bottom)	**OS3600** (Top)	**OS3600** (Bottom)	**Kyowa** (Top)	**Kyowa** (Bottom)	**Tokyo** (Top)	**Tokyo** (Bottom)	**Vishay** (Top)	**Vishay** (Bottom)
1	-25.7	29.8	-27.7	25.0	-21.7	26.8	-26.7	25.2	-16.2	21.9
2	-26.0	29.1	-26.4	26.9	-21.5	26.6	-27.0	25.5	-16.4	21.5
3	-25.4	30.1	-27.4	25.9	-21.5	26.6	-26.5	25.4	-16.2	21.5
4	-25.4	30.1	-27.5	25.8	-21.6	26.9	-26.7	25.3	-16.2	21.3
5	-25.7	29.9	-27.3	25.7	-21.9	26.7	-27.5	25.6	-16.4	21.4
6	-25.8	29.8	-27.8	25.8	-21.8	26.9	-26.8	25.6	-16.4	21.5
7	-25.5	30.1	-27.4	26.0	-21.8	26.9	-27.1	25.6	-16.5	21.7
8	-25.4	30.3	-27.7	25.8	-21.5	26.7	-27.4	25.2	-16.1	21.5
9	-25.7	29.4	-27.0	26.0	-21.8	26.6	-27.0	25.0	-16.5	21.8
10	-25.1	30.0	-27.7	25.4	-21.7	26.8	-27.7	25.1	-16.6	21.6
11	-25.1	29.5	-27.2	26.7	-	-	-	-	-	-
12	-25.6	29.4	-27.8	26.0	-	-	-	-	-	-
13	-25.7	30.4	-27.0	26.0	-	-	-	-	-	-
14	-25.0	29.8	-27.3	26.2	-	-	-	-	-	-
15	-25.3	29.3	-27.4	24.9	-	-	-	-	-	-
16	-25.2	29.5	-27.2	26.2	-	-	-	-	-	-
17	-25.6	29.6	-27.7	25.9	-	-	-	-	-	-
18	-25.5	29.1	-27.0	25.7	-	-	-	-	-	-
19	-25.5	29.5	-27.7	25.7	-	-	-	-	-	-
20	-25.1	29.9	-27.2	26.2	-	-	-	-	-	-
Aver.	-25.5	29.7	-27.4	25.9	-21.7	26.8	-27.0	25.3	-16.3	21.6

Table G-83. Peak strain data under HVS wheel path 1, trial 13, slab 4

Load	**OS3500** (Top)	**OS3500** (Bottom)	**OS3600** (Top)	**OS3600** (Bottom)	**Kyowa** (Top)	**Kyowa** (Bottom)	**Tokyo** (Top)	**Tokyo** (Bottom)	**Vishay** (Top)	**Vishay** (Bottom)
1	-26.0	30.0	-27.9	25.6	-23.6	29.4	-30.7	26.4	-16.7	22.8
2	-25.0	29.5	-27.1	26.5	-23.8	29.3	-31.0	26.5	-16.8	22.4
3	-24.9	29.4	-27.4	25.8	-23.8	29.0	-31.2	26.8	-16.9	22.8
4	-25.3	30.3	-27.8	25.7	-24.3	29.5	-30.7	26.4	-16.8	22.7
5	-25.6	29.5	-27.7	25.3	-23.8	29.6	-31.0	26.3	-16.9	22.9
6	-25.9	29.2	-28.5	25.1	-23.7	29.6	-30.9	26.5	-17.1	22.7
7	-25.5	29.3	-28.5	26.2	-24.2	29.6	-31.1	27.0	-16.8	22.7
8	-25.1	30.5	-28.6	24.7	-24.2	29.6	-30.9	26.5	-16.7	22.7
9	-25.2	29.6	-27.5	26.2	-23.8	29.1	-30.5	26.4	-17.0	22.6
10	-25.1	30.1	-28.0	25.2	-23.6	29.4	-30.2	26.8	-16.7	22.6
11	-25.3	29.1	-28.1	25.4	-	-	-	-	-	-
12	-25.2	29.2	-27.7	26.3	-	-	-	-	-	-
13	-25.6	29.7	-28.7	25.4	-	-	-	-	-	-
14	-25.3	29.4	-27.3	25.6	-	-	-	-	-	-
15	-25.2	30.0	-27.7	26.2	-	-	-	-	-	-
16	-25.6	30.1	-27.7	25.6	-	-	-	-	-	-
17	-25.5	30.4	-27.2	26.0	-	-	-	-	-	-
18	-25.9	29.7	-28.4	25.8	-	-	-	-	-	-
19	-25.3	29.8	-27.8	26.7	-	-	-	-	-	-
20	-25.5	29.6	-28.2	25.7	-	-	-	-	-	-
Aver.	-25.4	29.7	-27.9	25.7	-23.9	29.4	-30.8	26.6	-16.8	22.7

Table G-84. Peak strain data under HVS wheel path 1, trial 14, slab 4

Load	**OS3500** (Top)	**OS3500** (Bottom)	**OS3600** (Top)	**OS3600** (Bottom)	**Kyowa** (Top)	**Kyowa** (Bottom)	**Tokyo** (Top)	**Tokyo** (Bottom)	**Vishay** (Top)	**Vishay** (Bottom)
1	-25.0	29.9	-27.6	26.4	-23.8	29.3	-30.6	26.8	-16.7	23.2
2	-24.6	29.0	-27.7	25.1	-23.5	29.1	-30.7	26.6	-16.7	22.9
3	-25.1	29.5	-27.4	25.7	-23.9	29.3	-30.6	26.6	-16.6	23.4
4	-25.0	29.4	-28.0	25.9	-24.0	29.5	-30.7	26.2	-16.9	23.0
5	-25.4	29.0	-27.7	26.3	-23.8	29.1	-30.7	26.6	-16.6	22.8
6	-25.1	29.6	-28.1	25.9	-23.8	29.1	-31.0	26.4	-16.9	22.7
7	-25.1	29.6	-28.1	25.4	-24.2	29.1	-31.0	26.4	-16.9	23.0
8	-24.7	30.1	-27.3	25.7	-24.2	29.1	-31.0	26.8	-16.6	23.3
9	-25.4	29.2	-27.6	26.0	-23.9	29.5	-30.9	26.6	-16.9	23.0
10	-25.3	30.3	-27.6	26.2	-23.9	29.5	-30.9	26.6	-16.9	23.0
11	-25.0	29.9	-27.8	25.7	-	-	-	-	-	-
12	-25.5	29.7	-27.4	25.9	-	-	-	-	-	-
13	-25.5	29.3	-27.5	25.7	-	-	-	-	-	-
14	-25.5	29.7	-27.3	25.6	-	-	-	-	-	-
15	-25.1	29.8	-27.8	25.2	-	-	-	-	-	-
16	-25.2	29.7	-27.3	25.9	-	-	-	-	-	-
17	-25.9	29.6	-28.1	25.4	-	-	-	-	-	-
18	-25.3	29.5	-27.6	25.6	-	-	-	-	-	-
19	-25.5	29.9	-27.1	25.4	-	-	-	-	-	-
20	-25.4	30.0	-27.2	25.4	-	-	-	-	-	-
Aver.	-25.2	29.6	-27.6	25.7	-23.9	29.3	-30.8	26.6	-16.8	23.0

Table G-85. Peak strain data under HVS wheel path 1, trial 15, slab 4

Load	**OS3500** (Top)	**OS3500** (Bottom)	**OS3600** (Top)	**OS3600** (Bottom)	**Kyowa** (Top)	**Kyowa** (Bottom)	**Tokyo** (Top)	**Tokyo** (Bottom)	**Vishay** (Top)	**Vishay** (Bottom)
1	-25.0	29.7	-28.3	26.1	-24.2	28.9	-31.5	26.7	-16.6	22.7
2	-25.1	29.5	-28.5	25.1	-24.1	29.0	-31.8	26.6	-16.6	22.3
3	-24.6	29.4	-28.3	25.8	-23.9	29.1	-31.5	26.9	-16.9	22.4
4	-25.0	30.0	-28.3	25.9	-24.0	29.2	-31.4	26.7	-16.7	22.5
5	-24.5	29.4	-28.6	25.8	-23.9	29.0	-31.2	26.6	-17.0	22.4
6	-24.9	29.8	-27.8	25.9	-24.2	28.7	-31.7	26.8	-17.0	22.1
7	-25.1	28.9	-28.5	26.7	-24.5	29.0	-31.3	26.7	-17.0	22.3
8	-24.8	29.3	-28.4	25.9	-23.8	28.9	-31.6	26.5	-16.6	22.6
9	-24.5	29.8	-28.3	25.3	-23.9	28.7	-31.3	26.6	-16.8	22.1
10	-24.9	29.6	-28.9	24.7	-24.0	28.7	-31.1	26.9	-16.9	22.3
11	-24.6	29.2	-27.0	26.1	-	-	-	-	-	-
12	-24.9	30.2	-27.5	26.6	-	-	-	-	-	-
13	-25.1	30.2	-27.3	26.2	-	-	-	-	-	-
14	-24.5	29.3	-27.9	26.2	-	-	-	-	-	-
15	-24.9	30.0	-29.2	25.2	-	-	-	-	-	-
16	-25.2	30.0	-28.2	25.4	-	-	-	-	-	-
17	-24.9	30.5	-27.8	25.8	-	-	-	-	-	-
18	-24.7	30.8	-28.0	25.6	-	-	-	-	-	-
19	-24.7	29.3	-28.2	25.4	-	-	-	-	-	-
20	-24.7	29.4	-27.8	25.7	-	-	-	-	-	-
Aver.	-24.8	29.7	-28.1	25.8	-24.0	28.9	-31.4	26.7	-16.8	22.4

Table G-86. Peak strain data under HVS wheel path 1, trial 16, slab 4

Load	**OS3500** (Top)	**OS3500** (Bottom)	**OS3600** (Top)	**OS3600** (Bottom)	**Kyowa** (Top)	**Kyowa** (Bottom)	**Tokyo** (Top)	**Tokyo** (Bottom)	**Vishay** (Top)	**Vishay** (Bottom)
1	-24.7	29.5	-27.9	25.1	-23.9	29.7	-31.7	26.2	-16.7	22.1
2	-24.9	29.7	-27.4	25.2	-24.1	29.6	-31.5	26.2	-16.5	22.1
3	-24.8	29.2	-27.6	25.5	-23.8	29.7	-31.2	26.2	-16.4	22.7
4	-24.9	29.0	-27.5	25.5	-24.2	29.5	-31.7	26.5	-16.6	22.2
5	-24.8	29.4	-27.4	24.9	-24.0	29.8	-31.5	26.7	-16.5	22.3
6	-25.2	29.8	-27.8	24.9	-24.0	29.4	-31.6	26.7	-16.3	22.6
7	-25.5	29.5	-27.9	25.3	-23.7	29.5	-31.5	26.4	-16.6	22.7
8	-25.2	29.9	-27.7	25.7	-24.0	29.5	-31.3	26.6	-16.9	22.2
9	-25.2	29.4	-27.9	25.3	-23.6	29.0	-31.7	26.7	-16.6	22.4
10	-24.6	29.5	-27.7	24.9	-23.9	29.0	-31.4	26.5	-16.7	22.1
11	-25.2	29.5	-27.8	25.3	-	-	-	-	-	-
12	-24.9	29.6	-27.9	26.1	-	-	-	-	-	-
13	-25.0	29.5	-27.1	25.7	-	-	-	-	-	-
14	-24.9	29.0	-27.4	25.8	-	-	-	-	-	-
15	-24.8	28.3	-27.7	25.8	-	-	-	-	-	-
16	-25.1	29.9	-27.1	25.8	-	-	-	-	-	-
17	-24.7	30.3	-27.7	24.8	-	-	-	-	-	-
18	-24.9	29.5	-27.7	25.5	-	-	-	-	-	-
19	-24.9	29.4	-27.7	26.4	-	-	-	-	-	-
20	-25.2	29.5	-28.4	24.6	-	-	-	-	-	-
Aver.	-25.0	29.5	-27.7	25.4	-23.9	29.5	-31.5	26.5	-16.6	22.3

Table G-87. Peak strain data under HVS wheel path 1, trial 17, slab 4

Load	**OS3500** (Top)	**OS3500** (Bottom)	**OS3600** (Top)	**OS3600** (Bottom)	**Kyowa** (Top)	**Kyowa** (Bottom)	**Tokyo** (Top)	**Tokyo** (Bottom)	**Vishay** (Top)	**Vishay** (Bottom)
1	-24.4	29.8	-27.8	25.5	-23.4	28.5	-31.0	26.0	-16.8	22.7
2	-24.7	29.2	-28.1	25.0	-23.8	28.4	-31.0	26.1	-16.1	22.6
3	-24.7	29.7	-28.2	25.4	-23.6	28.2	-31.4	26.1	-16.4	22.2
4	-24.8	29.4	-28.3	26.0	-23.2	28.0	-31.1	25.9	-16.8	22.5
5	-25.2	29.9	-28.5	25.8	-23.9	27.9	-30.9	26.4	-16.0	22.5
6	-25.0	30.3	-28.5	25.8	-23.8	27.7	-30.7	26.3	-16.1	22.7
7	-24.6	29.9	-27.8	26.8	-23.4	28.4	-31.2	26.0	-16.3	22.6
8	-25.2	29.5	-28.5	25.9	-23.5	28.2	-30.9	26.2	-16.3	22.7
9	-24.4	30.0	-27.9	25.3	-23.6	28.3	-31.1	26.0	-16.2	22.6
10	-25.0	29.8	-27.9	25.7	-23.8	28.4	-31.1	26.1	-16.5	22.6
11	-24.7	29.9	-27.8	25.1	-	-	-	-	-	-
12	-25.0	29.9	-27.7	25.4	-	-	-	-	-	-
13	-24.7	30.3	-27.4	25.6	-	-	-	-	-	-
14	-24.3	30.1	-28.2	25.5	-	-	-	-	-	-
15	-24.9	30.0	-27.8	25.9	-	-	-	-	-	-
16	-25.0	30.3	-27.8	25.1	-	-	-	-	-	-
17	-24.9	29.7	-27.6	25.9	-	-	-	-	-	-
18	-24.6	30.1	-27.9	25.2	-	-	-	-	-	-
19	-25.3	29.6	-28.0	25.0	-	-	-	-	-	-
20	-24.7	29.9	-27.7	25.2	-	-	-	-	-	-
Aver.	-24.8	29.9	-28.0	25.6	-23.6	28.2	-31.0	26.1	-16.3	22.6

Table G-88. Peak strain data under HVS wheel path 1, trial 18, slab 4

Load	**OS3500** (Top)	**OS3500** (Bottom)	**OS3600** (Top)	**OS3600** (Bottom)	**Kyowa** (Top)	**Kyowa** (Bottom)	**Tokyo** (Top)	**Tokyo** (Bottom)	**Vishay** (Top)	**Vishay** (Bottom)
1	-24.7	29.2	-28.0	25.4	-22.1	28.0	-27.4	26.1	-17.0	22.1
2	-24.8	29.9	-28.0	25.8	-22.4	28.0	-27.4	26.5	-16.9	22.2
3	-25.1	29.9	-28.0	25.9	-22.2	28.3	-27.5	26.0	-17.2	22.5
4	-25.1	30.1	-27.9	25.8	-21.9	28.2	-26.9	26.1	-16.8	22.4
5	-24.9	30.0	-27.9	25.7	-22.2	28.1	-27.2	26.1	-16.8	22.8
6	-24.5	30.1	-27.9	26.4	-22.0	28.4	-27.5	26.4	-16.7	22.5
7	-24.6	29.7	-28.5	26.1	-22.1	27.8	-27.5	26.2	-17.0	22.2
8	-25.1	29.8	-28.1	25.3	-22.2	28.3	-27.5	26.6	-16.8	22.3
9	-25.1	29.3	-27.7	26.9	-22.2	28.1	-27.3	26.2	-16.8	22.1
10	-24.9	29.6	-28.0	26.1	-22.4	28.1	-27.7	26.6	-17.0	22.5
11	-24.6	29.6	-27.8	26.6	-	-	-	-	-	-
12	-25.0	29.7	-28.3	24.7	-	-	-	-	-	-
13	-24.6	29.2	-28.5	24.9	-	-	-	-	-	-
14	-24.6	29.2	-28.2	25.7	-	-	-	-	-	-
15	-24.7	29.7	-28.2	25.9	-	-	-	-	-	-
16	-24.4	30.1	-27.7	26.0	-	-	-	-	-	-
17	-24.7	29.7	-28.2	25.8	-	-	-	-	-	-
18	-24.1	29.5	-27.8	26.3	-	-	-	-	-	-
19	-24.4	28.8	-28.5	25.6	-	-	-	-	-	-
20	-24.5	30.1	-28.2	26.4	-	-	-	-	-	-
Aver.	-24.7	29.7	-28.1	25.9	-22.2	28.1	-27.4	26.3	-16.9	22.3

Table G-89. Peak strain data under HVS wheel path 1, trial 19, slab 4

Load	**OS3500** (Top)	**OS3500** (Bottom)	**OS3600** (Top)	**OS3600** (Bottom)	**Kyowa** (Top)	**Kyowa** (Bottom)	**Tokyo** (Top)	**Tokyo** (Bottom)	**Vishay** (Top)	**Vishay** (Bottom)
1	-24.4	28.7	-28.1	25.2	-22.2	28.6	-27.2	26.5	-17.1	22.7
2	-24.5	29.3	-28.0	25.1	-22.5	28.5	-28.2	26.6	-17.2	22.4
3	-24.5	29.9	-28.0	25.0	-22.2	29.1	-28.0	26.7	-17.2	22.6
4	-24.4	28.8	-28.3	25.7	-22.4	28.9	-27.6	26.4	-17.4	22.5
5	-24.2	28.7	-28.0	25.4	-22.7	29.0	-27.7	26.3	-17.6	22.9
6	-24.3	28.8	-27.8	25.5	-22.5	29.2	-27.5	26.2	-17.5	22.4
7	-24.9	29.2	-27.8	25.3	-22.6	28.6	-27.4	26.7	-17.1	23.0
8	-24.4	29.7	-27.7	25.1	-22.4	29.0	-28.1	26.8	-17.3	22.9
9	-24.3	28.9	-27.7	25.3	-22.1	29.1	-27.7	26.8	-16.9	23.1
10	-24.5	29.4	-28.3	25.0	-22.1	28.6	-27.5	26.7	-17.3	23.2
11	-24.8	29.4	-28.5	24.9	-	-	-	-	-	-
12	-24.7	29.1	-28.2	25.4	-	-	-	-	-	-
13	-24.5	29.0	-28.6	25.2	-	-	-	-	-	-
14	-24.8	29.4	-28.2	25.0	-	-	-	-	-	-
15	-24.7	29.2	-28.2	25.4	-	-	-	-	-	-
16	-24.9	29.4	-28.9	25.8	-	-	-	-	-	-
17	-24.7	29.4	-27.8	25.5	-	-	-	-	-	-
18	-24.7	29.2	-28.7	25.0	-	-	-	-	-	-
19	-24.8	29.5	-28.1	24.8	-	-	-	-	-	-
20	-24.9	29.7	-28.1	25.0	-	-	-	-	-	-
Aver.	-24.6	29.2	-28.1	25.2	-22.4	28.9	-27.7	26.6	-17.3	22.8

Table G-90. Peak strain data under HVS wheel path 1, trial 20, slab 4

Load	**OS3500** (Top)	**OS3500** (Bottom)	**OS3600** (Top)	**OS3600** (Bottom)	**Kyowa** (Top)	**Kyowa** (Bottom)	**Tokyo** (Top)	**Tokyo** (Bottom)	**Vishay** (Top)	**Vishay** (Bottom)
1	-24.7	29.4	-27.4	26.2	-22.8	29.1	-27.9	27.1	-17.6	22.9
2	-24.1	29.3	-28.3	26.0	-23.0	28.8	-27.5	26.6	-17.5	22.8
3	-24.9	29.6	-28.1	25.3	-22.4	29.0	-28.0	27.0	-17.7	23.0
4	-24.5	29.6	-28.6	25.1	-23.0	29.3	-28.3	26.8	-17.7	22.6
5	-24.2	29.3	-27.8	26.1	-22.5	28.8	-28.1	27.1	-17.8	22.9
6	-24.3	29.2	-28.2	25.4	-23.0	29.2	-27.9	27.2	-17.6	22.9
7	-24.4	29.4	-27.1	26.2	-22.6	29.0	-27.8	27.0	-17.5	22.9
8	-24.4	29.8	-27.6	25.6	-22.8	29.1	-27.8	26.8	-17.5	22.5
9	-24.5	29.4	-27.7	25.4	-22.9	29.1	-27.2	27.1	-17.5	22.8
10	-24.5	29.3	-28.4	25.0	-23.0	29.2	-27.3	26.9	-17.6	22.4
11	-25.1	29.4	-27.4	25.2	-	-	-	-	-	-
12	-24.8	29.9	-27.8	25.6	-	-	-	-	-	-
13	-24.7	29.7	-28.2	25.6	-	-	-	-	-	-
14	-24.7	29.8	-27.4	25.9	-	-	-	-	-	-
15	-25.1	29.3	-27.3	25.5	-	-	-	-	-	-
16	-24.7	30.1	-27.7	26.0	-	-	-	-	-	-
17	-24.5	29.0	-28.5	25.3	-	-	-	-	-	-
18	-25.2	30.3	-27.3	26.0	-	-	-	-	-	-
19	-24.8	29.3	-28.3	26.4	-	-	-	-	-	-
20	-24.5	29.2	-28.2	25.7	-	-	-	-	-	-
Aver.	-24.6	29.5	-27.9	25.7	-22.8	29.1	-27.8	27.0	-17.6	22.8

Table G-91. Peak strain data under HVS wheel path 1, trial 21, slab 4

Load	**OS3500** (Top)	**OS3500** (Bottom)	**OS3600** (Top)	**OS3600** (Bottom)	**Kyowa** (Top)	**Kyowa** (Bottom)	**Tokyo** (Top)	**Tokyo** (Bottom)	**Vishay** (Top)	**Vishay** (Bottom)
1	-23.7	29.1	-28.2	25.2	-22.7	29.4	-27.2	27.0	-17.7	22.8
2	-24.1	29.5	-28.1	25.5	-22.9	29.6	-27.4	27.6	-17.8	22.9
3	-24.2	29.3	-29.1	25.2	-23.1	29.2	-27.3	27.2	-17.7	22.8
4	-23.8	29.4	-27.9	25.2	-22.9	29.2	-27.5	27.1	-17.5	23.2
5	-23.9	28.9	-28.3	25.6	-22.8	29.1	-28.2	27.1	-17.6	22.9
6	-23.9	29.7	-28.0	25.2	-23.0	29.4	-27.8	27.4	-17.9	23.1
7	-24.2	29.2	-28.4	25.3	-23.0	29.9	-27.7	27.4	-18.0	23.5
8	-24.4	29.0	-28.2	25.4	-23.3	29.5	-28.3	27.2	-17.8	23.3
9	-24.2	29.4	-27.8	25.3	-22.8	29.9	-27.6	27.3	-17.8	23.2
10	-24.4	29.3	-28.8	25.1	-22.8	29.8	-27.4	27.6	-17.8	23.5
11	-23.8	29.4	-27.9	25.3	-	-	-	-	-	-
12	-24.8	29.9	-28.7	25.8	-	-	-	-	-	-
13	-24.4	29.5	-27.8	25.3	-	-	-	-	-	-
14	-24.4	29.0	-28.7	24.5	-	-	-	-	-	-
15	-24.0	29.2	-28.2	25.3	-	-	-	-	-	-
16	-23.7	29.3	-28.2	24.6	-	-	-	-	-	-
17	-24.5	29.5	-27.9	25.2	-	-	-	-	-	-
18	-24.4	29.7	-27.7	25.4	-	-	-	-	-	-
19	-24.9	29.3	-28.7	26.0	-	-	-	-	-	-
20	-24.4	29.4	-28.8	26.0	-	-	-	-	-	-
Aver.	-24.2	29.3	-28.3	25.3	-22.9	29.5	-27.6	27.3	-17.8	23.1

Table G-92. Peak strain data under HVS wheel path 1, trial 22, slab 4

Load	**OS3500** (Top)	**OS3500** (Bottom)	**OS3600** (Top)	**OS3600** (Bottom)	**Kyowa** (Top)	**Kyowa** (Bottom)	**Tokyo** (Top)	**Tokyo** (Bottom)	**Vishay** (Top)	**Vishay** (Bottom)
1	-24.2	29.0	-27.7	24.8	-23.0	29.7	-28.3	27.0	-17.3	23.2
2	-23.9	29.6	-28.0	25.2	-23.2	29.2	-28.0	27.1	-17.3	23.2
3	-24.4	29.1	-27.8	25.2	-23.1	29.6	-28.3	27.2	-17.4	23.2
4	-24.5	29.2	-28.2	25.0	-22.9	29.5	-28.4	27.0	-17.8	23.3
5	-24.1	28.9	-28.1	25.2	-23.1	29.5	-27.8	27.1	-17.3	23.4
6	-24.3	28.7	-27.7	25.0	-23.2	29.6	-28.4	26.9	-17.7	22.9
7	-23.9	28.9	-28.1	25.1	-23.5	29.4	-28.4	27.1	-17.7	23.3
8	-24.3	28.5	-26.8	25.2	-23.4	29.8	-28.3	27.1	-17.6	23.5
9	-24.0	29.3	-27.5	25.4	-23.0	29.6	-28.1	26.8	-17.4	23.1
10	-23.9	28.8	-28.1	25.3	-23.2	30.0	-27.9	27.5	-17.4	23.5
11	-24.3	29.5	-28.1	25.6	-	-	-	-	-	-
12	-24.0	29.3	-27.9	25.5	-	-	-	-	-	-
13	-25.9	31.2	-11.9	10.1	-	-	-	-	-	-
14	-23.9	29.0	-28.7	25.1	-	-	-	-	-	-
15	-24.4	30.2	-28.0	25.3	-	-	-	-	-	-
16	-25.3	28.8	-27.4	25.7	-	-	-	-	-	-
17	-24.8	28.5	-27.6	25.9	-	-	-	-	-	-
18	-24.0	28.8	-27.8	24.7	-	-	-	-	-	-
19	-24.7	28.9	-28.2	25.8	-	-	-	-	-	-
20	-24.1	29.0	-28.4	25.3	-	-	-	-	-	-
Aver.	-24.3	29.2	-27.1	24.5	-23.2	29.6	-28.2	27.1	-17.5	23.3

Table G-93. Peak strain data under HVS wheel path 1, trial 23, slab 4

Load	**OS3500** (Top)	**OS3500** (Bottom)	**OS3600** (Top)	**OS3600** (Bottom)	**Kyowa** (Top)	**Kyowa** (Bottom)	**Tokyo** (Top)	**Tokyo** (Bottom)	**Vishay** (Top)	**Vishay** (Bottom)
1	-24.3	29.3	-28.0	24.7	-23.4	29.9	-28.6	27.0	-18.0	23.2
2	-24.3	28.8	-28.1	24.9	-23.0	29.9	-28.7	27.1	-17.9	23.6
3	-24.5	29.1	-27.9	24.9	-23.5	29.9	-28.5	27.1	-17.9	23.3
4	-24.7	29.0	-27.8	24.9	-23.0	29.6	-28.6	27.2	-17.8	23.6
5	-24.1	28.9	-28.3	25.1	-22.9	30.0	-28.3	27.0	-17.6	23.2
6	-24.7	28.9	-28.3	25.3	-23.5	29.4	-28.8	27.3	-17.9	23.1
7	-24.1	28.6	-28.6	24.5	-23.2	29.8	-28.5	27.2	-18.2	22.9
8	-24.4	28.9	-28.2	25.1	-22.9	29.6	-28.6	26.7	-17.9	23.1
9	-24.6	29.2	-28.2	25.3	-23.0	29.9	-28.4	27.3	-17.9	23.2
10	-24.8	29.2	-28.7	24.8	-23.0	29.7	-28.1	27.1	-17.9	23.5
11	-24.0	29.1	-27.6	24.9	-	-	-	-	-	-
12	-23.7	28.6	-27.8	25.3	-	-	-	-	-	-
13	-24.4	29.1	-28.6	24.8	-	-	-	-	-	-
14	-24.4	29.4	-29.0	24.2	-	-	-	-	-	-
15	-24.3	28.2	-27.4	25.2	-	-	-	-	-	-
16	-24.3	29.3	-28.2	25.5	-	-	-	-	-	-
17	-24.3	28.6	-27.9	24.4	-	-	-	-	-	-
18	-23.9	29.2	-28.2	25.1	-	-	-	-	-	-
19	-24.4	28.9	-28.7	24.5	-	-	-	-	-	-
20	-23.8	29.4	-27.8	25.2	-	-	-	-	-	-
Aver.	-24.3	29.0	-28.2	24.9	-23.1	29.8	-28.5	27.1	-17.9	23.3

Table G-94. Peak strain data under HVS wheel path 1, trial 24, slab 4

Load	**OS3500** (Top)	**OS3500** (Bottom)	**OS3600** (Top)	**OS3600** (Bottom)	**Kyowa** (Top)	**Kyowa** (Bottom)	**Tokyo** (Top)	**Tokyo** (Bottom)	**Vishay** (Top)	**Vishay** (Bottom)
1	-24.2	28.3	-27.7	25.3	-22.8	29.6	-27.8	26.9	-18.2	23.1
2	-24.5	28.6	-27.9	25.2	-22.9	29.1	-28.0	26.8	-17.6	22.9
3	-24.3	28.7	-27.9	25.3	-23.0	29.7	-28.1	26.7	-17.7	22.6
4	-24.4	28.6	-27.7	25.4	-23.0	29.7	-27.8	26.9	-17.4	23.1
5	-23.9	28.6	-27.8	25.4	-22.9	29.5	-28.2	26.6	-17.6	23.0
6	-24.0	28.9	-27.9	25.2	-22.5	29.2	-27.7	26.7	-17.5	23.6
7	-24.0	29.1	-28.2	25.3	-22.5	29.6	-28.2	27.0	-17.5	23.0
8	-24.0	29.0	-27.9	25.4	-22.9	30.2	-27.8	27.0	-17.1	23.2
9	-24.6	28.8	-28.2	25.0	-22.8	29.9	-28.2	26.9	-17.2	23.0
10	-23.6	29.0	-27.7	25.4	-23.1	30.0	-27.9	27.1	-17.4	23.2
11	-24.4	28.8	-27.2	25.4	-	-	-	-	-	-
12	-24.0	28.8	-28.1	25.6	-	-	-	-	-	-
13	-23.9	29.1	-27.8	25.2	-	-	-	-	-	-
14	-24.0	29.4	-27.7	25.4	-	-	-	-	-	-
15	-23.9	28.2	-28.0	25.0	-	-	-	-	-	-
16	-24.0	29.2	-28.0	26.1	-	-	-	-	-	-
17	-23.9	28.4	-27.8	25.6	-	-	-	-	-	-
18	-24.1	29.1	-27.4	25.2	-	-	-	-	-	-
19	-24.5	29.6	-27.8	25.0	-	-	-	-	-	-
20	-24.0	28.9	-27.6	24.8	-	-	-	-	-	-
Aver.	-24.1	28.9	-27.8	25.3	-22.8	29.7	-28.0	26.8	-17.5	23.1

APPENDIX H
PEAK RECORDED STRAINS FROM FWD TESTS

This appendix presents the peak strain values recorded by the strain gauges when the test slabs were loaded by the Falling Weight Deflectometer (FWD). Figure H-1 shows the FWD loading locations on each test slab. For each loading location, three FWD load levels, namely 6, 9, and 12 kips, were used. For the fiber optic strain sensors, a minimum sampling rate of 500 Hz was used. For the electrical resistance strain gauges, a minimum sampling rate of 1000 Hz was used. For each of the FWD load, peak strain values were determined from the strain data recorded by the two closest pairs of strain gauges, using the methodology described in Section 8.3.8.

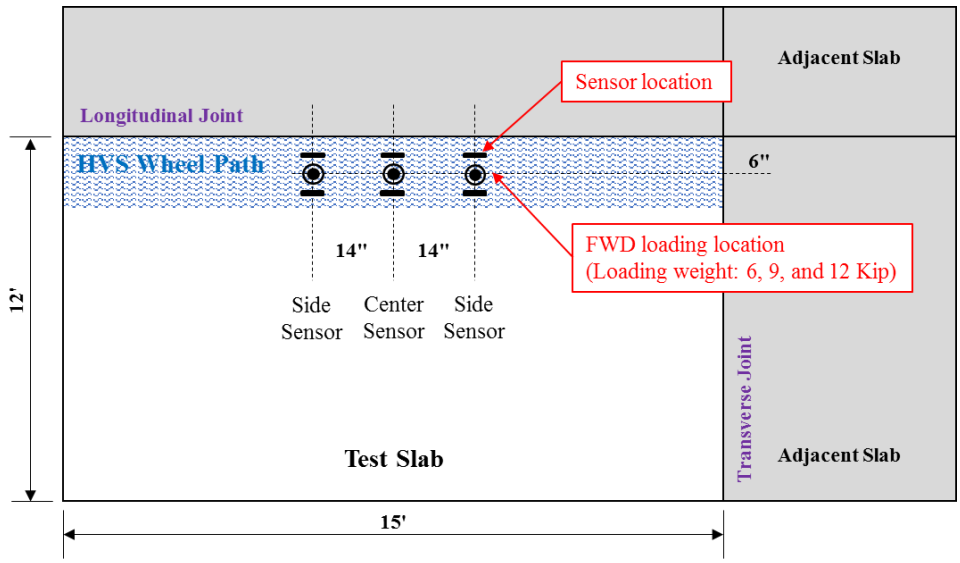

Figure H-1. Layout of the sensor locations and the locations of FWD Loads

Using the FE models developed for the test slabs, the maximum strains caused by the FWD loads at the location of the strain gauges were computed and compared with the measured values from the strain gauges. Table H-1 presents the comparison of the maximum computed strains from FE analysis and the recorded values from strain sensors due to the FWD loads on Slab 1 and Slab 4.

Table H-1. Comparison of the maximum computed strains from FE model analysis and recorded values from strain sensors due to the FWD loads on slab 1 and slab 4

FE		Center sensor		Side sensor	
		Top	Bottom	Top	Bottom
Slab1	6Kip	-11.7	14.4	-11.6	12.3
	9Kip	-18.7	23.0	-18.5	19.7
	12Kip	-25.7	31.6	-25.4	27.2
Slab4	6Kip	-11.1	12.9	-10.8	11.3
	9Kip	-17.7	20.6	-17.3	18.1
	12Kip	-24.3	28.3	-23.8	24.9

Sensor		OS3500 (center)		OS3600 (side)		Tokyo (side)		CTL (side)	
		Top	Bottom	Top	Bottom	Top	Bottom	Top	Bottom
Slab1	6Kip	-15.2	16.3	-23.3	12.5	-15.0	14.5	-6.6	6.5
	9Kip	-23.0	22.9	-32.5	18.2	-19.6	16.8	-9.9	10.0
	12Kip	-30.4	31.1	-44.0	20.6	-22.9	21.6	-12.7	13.4
Sensor		OS3500 (side)		Kyowa (side)		Tokyo (side)		Vishay (side)	
		Top	Bottom	Top	Bottom	Top	Bottom	Top	Bottom
Slab4	6Kip	-10.7	12.1	-13.3	10.3	-10.7	12.1	-13.3	10.3
	9Kip	-17.0	16.3	-18.7	14.8	-17.0	16.3	-18.7	14.8
	12Kip	-22.4	22.8	-22.8	20.2	-22.4	22.8	-22.8	20.2

Note: values are in units of micro strain (με).

APPENDIX I
PEAK RECORDED STRAINS FROM SEVEN SENSORS FOR EVALUATION OF STRAIN GAUGE CONFIGURATION

This appendix presents the peak strains recorded by the seven uniformly-spaced strain sensors caused by the 12-kip HVS load on Test Slab 4 in the evaluation of strain gauge configuration as presented in Section 8.3.9.

Table I-1. Peak recorded strains due to HVS load along wheel path 1 (center of wheel was 6 inches from slab edge)

Sensor Location and Types	**Sensor 1** (3 in.*)	**Sensor 2** (9 in.*)	**Sensor 3** (15 in.*)	**Sensor 4** (21 in.*)	**Sensor 5** (27 in.*)	**Sensor 6** (33 in.*)	**Sensor 7** (39 in.*)
	Kyowa (Top)	**OS3600** (Top)	**Kyowa** (Top)	**Kyowa** (Top)	**Kyowa** (Top)	**Kyowa** (Top)	**Kyowa** (Top)
1	-24.5	-25.5	-21.9	-15.7	-10.4	-	-6.8
2	-24.6	-24.6	-21.1	-15.2	-10.4	-	-6.6
3	-24.4	-25.0	-21.5	-15.8	-10.4	-	-6.6
4	-24.2	-25.1	-22.2	-15.2	-10.4	-	-5.9
5	-23.9	-24.6	-21.5	-15.4	-10.4	-	-5.7
6	-24.4	-25.0	-21.5	-15.2	-10.4	-	-5.5
7	-24.6	-24.4	-21.6	-15.6	-10.5	-	-5.8
8	-23.7	-24.9	-21.2	-15.4	-10.6	-	-6.1
9	-23.8	-25.1	-21.0	-15.7	-10.4	-	-6.5
10	-23.9	-24.8	-21.8	-15.6	-10.4	-	-5.8
11	-23.9	-24.5	-21.1	-15.7	-11.3	-	-6.3
12	-24.5	-24.9	-20.9	-15.9	-11.5	-	-6.0
13	-24.1	-24.6	-21.1	-15.8	-10.5	-	-5.9
14	-23.8	-24.8	-21.7	-15.3	-10.5	-	-6.6
15	-24.0	-25.0	-22.2	-15.2	-11.2	-	-5.7
16	-24.1	-24.4	-21.6	-15.3	-11.1	-	-6.2
17	-24.7	-24.9	-21.7	-15.4	-11.0	-	-5.7
18	-24.6	-25.2	-21.7	-15.7	-10.6	-	-6.5
19	-24.5	-24.8	-22.1	-15.5	-10.3	-	-5.8
20	-24.1	-24.6	-21.7	-15.5	-10.6	-	-6.3
Aver.	-24.2	-24.8	-21.6	-15.5	-10.6	-	-6.1

Note: *distance between the slab's edge and sensor's location.

Table I-2. Peak recorded strains due to HVS load along wheel path 2 (center of wheel was 15 inches from slab edge)

Sensor Location and Types	**Sensor 1** (3 in.*)	**Sensor 2** (9 in.*)	**Sensor 3** (15 in.*)	**Sensor 4** (21 in.*)	**Sensor 5** (27 in.*)	**Sensor 6** (33 in.*)	**Sensor 7** (39 in.*)
	Kyowa (Top)	**OS3600** (Top)	**Kyowa** (Top)	**Kyowa** (Top)	**Kyowa** (Top)	**Kyowa** (Top)	**Kyowa** (Top)
1	-15.0	-19.1	-19.2	-16.4	-12.0	-	-7.5
2	-15.5	-19.1	-19.2	-16.7	-12.1	-	-7.5
3	-15.0	-18.3	-19.2	-16.9	-12.2	-	-7.7
4	-14.7	-18.5	-19.1	-16.7	-11.7	-	-7.5
5	-15.1	-18.7	-19.4	-16.4	-12.1	-	-7.4
6	-15.5	-18.9	-19.1	-16.5	-11.7	-	-7.3
7	-15.3	-18.8	-19.0	-16.6	-12.2	-	-7.4
8	-15.1	-18.9	-19.0	-16.3	-11.5	-	-7.1
9	-15.2	-18.2	-19.3	-16.4	-11.9	-	-7.6
10	-14.9	-18.6	-19.1	-16.6	-12.0	-	-7.8
11	-15.1	-18.7	-19.2	-16.3	-11.7	-	-7.3
12	-15.0	-18.5	-18.9	-16.7	-11.8	-	-7.2
13	-15.0	-18.9	-18.9	-16.2	-11.8	-	-7.2
14	-14.7	-18.8	-19.2	-16.5	-11.9	-	-7.2
15	-15.1	-18.5	-19.1	-16.5	-11.8	-	-7.4
16	-15.2	-18.6	-18.8	-16.6	-11.9	-	-7.4
17	-15.0	-18.2	-19.0	-16.5	-11.7	-	-7.5
18	-15.4	-18.7	-18.8	-16.2	-11.8	-	-7.4
19	-14.9	-18.5	-18.6	-16.3	-11.9	-	-7.5
20	-14.9	-18.6	-19.4	-16.2	-11.8	-	-7.2
Aver.	-15.1	-18.7	-19.1	-16.5	-11.9	-	-7.4

Note: *distance between the slab's joint and sensor's location.

Table I-3. Peak recorded strains due to HVS load along wheel path 3 (center of wheel was 23 inches from slab edge)

Sensor Location and Types	**Sensor 1** (3 in.*)	**Sensor 2** (9 in.*)	**Sensor 3** (15 in.*)	**Sensor 4** (21 in.*)	**Sensor 5** (27 in.*)	**Sensor 6** (33 in.*)	**Sensor 7** (39 in.*)
	Kyowa (Top)	**OS3600** (Top)	**Kyowa** (Top)	**Kyowa** (Top)	**Kyowa** (Top)	**Kyowa** (Top)	**Kyowa** (Top)
1	-11.4	-13.2	-18.4	-19.5	-17.7	-	-12.4
2	-11.9	-13.2	-17.9	-18.9	-17.8	-	-12.4
3	-11.5	-13.0	-18.2	-18.9	-18.0	-	-12.4
4	-11.4	-13.2	-17.8	-19.0	-18.3	-	-12.0
5	-11.4	-12.9	-17.9	-19.2	-17.7	-	-12.1
6	-11.4	-13.0	-17.9	-18.9	-17.7	-	-12.0
7	-11.3	-13.0	-18.4	-19.3	-18.3	-	-12.0
8	-11.7	-12.7	-18.1	-18.9	-17.9	-	-12.2
9	-11.8	-13.2	-18.0	-19.1	-17.7	-	-12.3
10	-11.4	-13.0	-17.6	-19.2	-17.9	-	-12.1
11	-11.3	-13.0	-17.8	-19.0	-17.9	-	-12.4
12	-11.5	-13.0	-17.6	-18.6	-17.9	-	-12.3
13	-11.2	-13.5	-17.9	-19.1	-17.9	-	-11.9
14	-11.7	-13.0	-18.0	-18.5	-18.0	-	-12.1
15	-11.4	-12.9	-17.7	-18.9	-17.8	-	-12.1
16	-11.2	-13.3	-17.6	-18.7	-17.4	-	-12.1
17	-11.3	-12.9	-17.5	-18.3	-17.5	-	-12.2
18	-11.3	-12.7	-17.3	-18.7	-17.8	-	-12.2
19	-11.4	-13.3	-18.0	-19.0	-17.9	-	-11.9
20	-11.2	-13.3	-17.6	-18.6	-17.4	-	-11.8
Aver.	-11.4	-13.1	-17.9	-18.9	-17.8	-	-12.1

Note: *distance between the slab's joint and sensor's location.